
A

Presented to
the faculty of the School of Engineering and Applied Science
University of Virginia

in partial fulfillment
of the requirements for the degree

by

APPROVAL SHEET

This

is submitted in partial fulfillment of the requirements
for the degree of

Author:

Advisor:

Advisor:

Committee Member:

Committee Member:

Committee Member:

Committee Member:

Committee Member:

Committee Member:

Accepted for the School of Engineering and Applied Science:

A handwritten signature in black ink that reads "Jennifer L. West". The signature is written in a cursive style with a large initial 'J' and 'W'.

Jennifer L. West, School of Engineering and Applied Science

To my husband and the Richardson Wolf Pack.

Contents

List of Figures	x
List of Tables	xx
List of Acronyms	xxii
Acknowledgments	xxiv
Abstract of the Dissertation	xxvi
1 Introduction	1
1.1 Motivation	1
1.1.1 Submarining is linked to increased injury risk to nearly every body region, and its prevalence in the field is underestimated.	1
1.1.2 Submarining is predicted to become more prevalent in the field.	3
1.1.3 Submarining is affected by a multitude of factors, and their effects have not been quantified.	4
1.1.4 Computational human body models can be used to increase our understanding of the submarining phenomenon.	4
1.2 Scope of Research	5
1.2.1 Goal of dissertation.	5
1.2.2 Specific aims.	5
1.2.3 Dissertation overview.	6
2 Hypothesized Factors Affecting Submarining Occurrence: A Review	8
2.1 Executive Summary	8
2.1.1 Relevance and goal	8
2.1.2 Key conclusions	9
2.1.3 Contributions	9
2.2 Introduction	10
2.2.1 Pelvic-abdominal anatomy overview in relation to lap belt interaction	10
2.2.2 Restraint system advancement over the years	12
2.2.3 Current state-of-the-art computational HBMs	13
2.3 Methodology	14

2.3.1	Search strategy	14
2.3.2	Data extraction methods	15
2.4	Identified Factors	16
2.4.1	Extrinsic factors	17
2.4.2	Intrinsic factors	19
2.5	Discussion	20
2.6	Conclusions	24
3	The Effect of a Reclined Posture on Lap Belt-Pelvis Interaction	26
3.1	Executive Summary	26
3.1.1	Relevance and Goal	26
3.1.2	Key Conclusions	26
3.1.3	Contributions	27
3.1.4	Publications	28
3.2	Introduction	28
3.3	Material and Methods	30
3.3.1	Test Environment	30
3.3.2	PMHS Selection	33
3.3.3	PMHS Instrumentation	34
3.3.4	PMHS Positioning	34
3.3.5	Data Analysis	37
3.4	Results	40
3.4.1	Pelvis Kinematics and Injury	40
3.4.2	Lap Belt Kinematics and Kinetics	42
3.4.3	Lumbar Spine Kinematics and Injury	45
3.5	Discussion	47
3.5.1	Lumbar Spine Compliance	47
3.5.2	Lap Belt-Pelvis Interaction	50
3.6	Conclusions	54
4	Evaluation of HBM Biofidelity in a Reclined Posture	56
4.1	Executive Summary	56
4.1.1	Relevance and Goal	56
4.1.2	Key Conclusions	57
4.1.3	Contributions	57
4.2	Introduction	57
4.3	Materials and Methods	58
4.3.1	Software and Hardware Used	58
4.3.2	FE Environment	58
4.3.3	HBMs	60
4.3.4	HBM Positioning	60
4.3.5	Initial Lap Belt Placement	61
4.3.6	Data Analysis	63
4.4	Results	63
4.4.1	Pelvis Kinematics	64

4.4.2	Lap Belt Kinetics	69
4.4.3	Lumbar Spine Kinematics	71
4.5	Discussion	77
4.5.1	Lumbar Spine Compliance	77
4.5.2	Lap Belt-Pelvis Interaction	78
4.6	Conclusions	81
5	The Effect of Lap Belt-Pelvis Angle on Lap Belt-Pelvis Interaction	82
5.1	Executive Summary	82
5.1.1	Relevance and Goal	82
5.1.2	Key Conclusions	83
5.1.3	Contributions	83
5.1.4	Publication	83
5.2	Introduction	84
5.3	Materials and Methods	86
5.3.1	Test Matrix	86
5.3.2	Test Environment	86
5.3.3	PMHS Selection	89
5.3.4	Initial Positioning	89
5.3.5	Data Analysis	92
5.4	Results	93
5.4.1	Initial Positioning	93
5.4.2	Submarining Occurrence	96
5.5	Discussion	100
5.5.1	Lap Belt-Pelvis Angle	100
5.5.2	Abdominal Soft Tissue	101
5.6	Conclusions	102
6	Evaluation of HBM Submarining Sensitivity to Lap Belt-Pelvis Angle	104
6.1	Executive Summary	104
6.1.1	Relevance and Goal	104
6.1.2	Key Conclusions	105
6.1.3	Contributions	105
6.1.4	Publication	106
6.2	Introduction	106
6.3	Methodology	107
6.3.1	Software and Hardware Used	107
6.3.2	Test Matrix	107
6.3.3	FE Environment	107
6.3.4	Initial Positioning	108
6.3.5	Soft Tissue Compliance	114
6.3.6	Data Analysis	115
6.4	Results	115
6.4.1	Initial Lap Belt Placement	115
6.4.2	Submarining Occurrence	116

6.4.3	Soft Tissue Compliance	119
6.5	Discussion	121
6.5.1	Initial Lap Belt Placement	121
6.5.2	Submarining Sensitivity	122
6.5.3	Lap Belt Migration	124
6.6	Conclusions	126
7	Selection of HBM for Submarining Analysis	128
7.1	Executive Summary	128
7.1.1	Relevance and Goal	128
7.1.2	Key Conclusions	129
7.1.3	Contributions	129
7.1.4	Publications	130
7.2	Introduction	130
7.3	Methodology	131
7.3.1	Study Overview	132
7.3.2	Instrumentation	132
7.3.3	Data Analysis	135
7.4	Results	138
7.4.1	Submarining Occurrence	138
7.4.2	Lap Belt Tension to ASIS Load	140
7.5	Discussion	146
7.5.1	Submarining Occurrence	146
7.5.2	Lap Belt Tension to ASIS Load	150
7.6	Conclusions	155
8	Quantifying Effects of Factors on Submarining: Simulations	156
8.1	Executive Summary	156
8.1.1	Relevance and Goal	156
8.1.2	Key Conclusions	157
8.1.3	Contributions	157
8.2	Introduction	157
8.3	Methodology	161
8.3.1	FE Environment	161
8.3.2	Parameter Selection	162
8.3.3	Sampling	165
8.3.4	Positioning and Settling	167
8.3.5	Seatbelt Routing	168
8.3.6	Final Simulations	171
8.3.7	NN Metamodeling	174
8.4	Results	176
8.4.1	Final Simulations	176
8.4.2	Metamodeling	178
8.4.3	Data Aggregation	181
8.5	Discussion	182

8.6	Conclusions	183
9	Quantifying Effects of Factors on Submarining: Analysis	185
9.1	Executive Summary	185
9.1.1	Relevance and Goal	185
9.1.2	Key Conclusions	186
9.1.3	Contributions	186
9.1.4	Publication	186
9.2	Introduction	187
9.3	Methodology	187
9.3.1	Data Aggregation	187
9.3.2	Clustering	188
9.4	Results	191
9.4.1	Influential Parameter Ranking	191
9.4.2	Submarining Occurrence	193
9.4.3	Maximum Submarining Distance	195
9.4.4	Maximum Pelvis Forward Displacement	197
9.4.5	Maximum Pelvis Rotation (pitch)	199
9.4.6	Maximum Lap Belt Tension	201
9.5	Discussion	202
9.5.1	Exploring a Continuous Parameter Space: A Thought Exercise	202
9.5.2	Dominating Factors Affecting Submarining Risk	206
9.5.3	Applicability of FMVSS 210	210
9.5.4	Trade-Offs Resulting from Varying Lap Belt Anchorage Position	212
9.6	Conclusions	212
10	Conclusions	214
10.1	Concluding Remarks	214
10.2	Future Research and Limitations	217
10.2.1	HBM Biofidelity and Submarining Prediction	217
10.2.2	Alternative Boundary Conditions	218
10.2.3	Considerations for Occupants of Varying Anthropometry	218
10.2.4	Restraint Design Considerations	219
10.2.5	Other Considerations	220
10.3	Contributions	220
11	Publications	222
11.1	Journal Articles	222
11.2	Conference Proceedings	223
	Bibliography	225
A	Automotive Restraint Timeline	237
A.1	Timeline	237
A.2	References for Timeline	242

B	Reclined PMHS Frontal Impact Sled Test Experiments	245
B.1	Positioning Data	245
B.2	Pelvis and Sacrum Injuries	246
C	Reclined HBM Frontal Impact Simulations	248
C.1	Positioning Data	248
C.2	HBM Responses compared to PMHS Responses: Nominal Pelvis Angle	250
C.3	HBM Responses compared to PMHS Responses: 12°Posterior Pelvis Angle	264
C.4	HBM Responses compared to PMHS Responses: 12°Anterior Pelvis Angle	279
D	Belt Pull Experiments using PMHS	294
D.1	Lap Belt Anchorage Positions	294
E	Belt Pull Simulations	295
E.1	Soft Tissue Load Curve Changes	295
F	Belt-ASIS Load Transfer Simulations	296
F.1	Verification load cases for ASIS cross-sections	296
F.2	Method to flag lap belt low on ASIS cases	297
G	Pelvis Orientations of GHBMC Model	299
H	Neural Network Metamodel Development	301
H.1	AU-ROC for Monitoring Error	301
H.2	Training and Testing Progression of Model Performance	301
I	Analysis of Simulated Dataset	321
I.1	Distribution of Output Metrics	321
I.2	K-Means Clustering Analysis	322
I.2.1	Submarining Occurrence	322
I.2.2	Submarining Distance	325
I.2.3	Pelvis Forward Displacement	328
I.2.4	Pelvis Rotation	331
I.2.5	Lap Belt Tension	334
J	Analysis of Full-Factorial Generated Dataset	338
J.1	Distribution of Output Metrics	338
J.2	K-Means Clustering Analysis	339
J.2.1	Submarining Occurrence	339
J.2.2	Submarining Distance	342
J.2.3	Pelvis Forward Displacement	345
J.2.4	Pelvis Rotation (Pitch)	348
J.2.5	Lap Belt Tension	351
J.3	Additional Cut-Off Values for Continuous Output Metrics	354
J.3.1	Pelvis Forward Displacement	354
J.3.2	Pelvis Rotation	360

J.3.3	Submarining Distance	365
J.3.4	Lap Belt Tension	370
K	1M Generated Dataset (Continuous Sampling)	375

List of Figures

1.1	The submarining phenomenon, defined as the lap belt, initially placed favorably relative to the pelvic bone (t_0) translates superior to the pelvis and loads the abdominal soft tissue during the crash (t).	2
1.2	Overview of dissertation.	7
2.1	(a) Bony pelvis anatomy. (b) Proper positioning of lap belt with respect to bony pelvis anatomy.	11
2.2	(a) Abdominal organ anatomy. (b) Example of abdominal lap belt loading due to submarining.	12
2.3	Computational M50 human body models: (a) GHBMC-O M50 v.6 and (b) THUMS AM50 v.6.1.	14
2.4	Process in identified potential factor classifications and their use in the remainder of this dissertation.	15
2.5	Causality diagram depicting the three categories of factors based on four stages of the crash event, including the determination of the submarining outcome.	16
2.6	Unfavorable occupant kinematics, in which the torso is reclined and the H-Point is anterior to the S-Point	19
2.7	Free body diagram of the pelvis, illustrating lap belt-pelvis interaction.	22
3.1	(a) Sled fixture and (b) buck coordinate system.	31
3.2	Acceleration pulse used in this test series (CFC 60).	31
3.3	(a) Oblique view of the semi-rigid seat in the experimental test setup. (b) Lateral view of the semi-rigid seat.	32
3.4	(a) Pre-test CT showing the installation locations for the motion-tracking hardware. (b) Motion-tracking arrays rigidly affixed to the internal hardware at several locations on the specimen.	34
3.5	Belt-pelvis angle definition.	35
3.6	Initial position of the five subjects from the five tests. The labelled angles show the initial pitch angle (rotation about the y-axis) of the measured bones in the spinal column, where the solid arrows indicate the initial orientation of the x-axis for each vertebral body's local coordinate system. The pelvis angle is measured as the Nyquist angle.	36

3.7	Initial position of the pelvis and lap-belt in the buck coordinate system, viewed from the outboard (left column) and inboard (right column) sagittal planes.	39
3.8	Definition of local coordinate systems on the head, vertebra, and pelvis, each defined by the corresponding bone's anatomic landmarks.	39
3.9	Pelvis kinematics of the five PMHS: (a) forward (X-) displacement, (b) angular displacement. A negative pelvis angle indicates a forward pelvis rotation.	41
3.10	Video stills of Subject 5 submarining.	42
3.11	Lap belt angular displacement in the sagittal view up to 100 ms (during pelvic rebound): (a) the inboard (buckle) side of the occupant, (b) the outboard side of the occupant.	43
3.12	(a) Lap belt tension (outboard side); (b) buckle resultant force (inboard side). . . .	44
3.13	Vertebral body forward (X) and downward (Z) displacements.	46
3.14	Position of the first three subjects at the time of fracture (Subject 1: 65 ms, Subject 2: 48 ms, Subject 3: 65 ms) and Subjects 4 and 5 at 65 ms for kinematic comparison with Subjects 1 and 3, of equal mass. Kinematic tracking of the pelvis of Subject 3 was lost at 30 ms.	47
3.15	L1 vertebral body rotation relative to L3 vertebral body rotation (a). A positive value indicates a rearward rotation of L1 relative to L3, akin to lumbar extension or lordosis (b).	48
3.16	L1 vertebral body rotation (a) and L3 vertebral body rotation (b) relative to the pelvis rotation. A positive value indicates a rearward rotation of L1 or L3 relative to the pelvis, akin to lumbar extension or lordosis (c).	49
3.17	Position of the lap belt relative to the subjects' pelvises (segmented CT scans) in the initial configuration (left column) and during the pelvis forward displacement (right column). See Richardson IRCOBI paper for details on the selected times of interest in the right column. Subject 3 is omitted as pelvis motion tracking was lost. The solid line connects the motion-capture markers at the center of the lap belt and the dashed lines approximate the width of the lap belt webbing.	52
3.18	A simplified free body diagram showing the lap belt tension vector relative to the pelvis COR for two different lap belt placements, inducing two opposing moments.	53
3.19	Lap belt-pelvis angle on the inboard side. This parameter is defined in Figure 3 5. Lap belt motion tracking was lost during the subjects' forward pelvis excursion due to lack of visibility of the lap belt markers.	54
4.1	FE model of the semi-rigid seat.	59
4.2	Outlined process of HBM alignment relative to PMHS position.	62
4.3	Belt fit for the positioned HBMs relative to the pelvis orientations and abdominal curvature. Left to right are the different pelvis angles: 12° posterior rotation, nominal, and 12° anterior rotation.	63
4.4	Pelvis forward (X) displacement. A positive value indicates anterior, or forward, motion.	64
4.5	Pelvis downward (Z) displacement. A positive value indicates downward, or inferior, motion (towards ground).	65
4.6	Pelvis pitch, or rotation about the Y-axis. A positive value indicates a rearward rotation.	66

4.7	Pelvis pitch, or rotation about the Y-axis for the three THUMS models with different initial pelvis orientations. A positive value indicates a rearward rotation.	67
4.8	Pelvis pitch, or rotation about the Y-axis for the three GHBMC models with different initial pelvis orientations. A positive value indicates a rearward rotation.	67
4.9	THUMS Pos12deg model forward pelvis displacement. The flesh at the back edge of the seatpan interacts with the seatpan during the forward displacement, which affected pelvis kinematics. Top-down: 0ms, 20ms, 50ms.	68
4.10	Lap belt tension, measured on the outboard side, for the GHBMC and THUMS nominal pelvis angle models.	69
4.11	Buckle resultant force, measured beneath the buckle on the inboard side, for the GHBMC and THUMS nominal pelvis angle models.	70
4.12	Lap belt tension, measured on the outboard side, for the three GHBMC models with different initial pelvis orientations.	70
4.13	Lap belt tension, measured on the outboard side, for the three THUMS models with different initial pelvis orientations.	71
4.14	Vertebral body forward (X) displacements. Top-down: T11, L1, and L3 vertebral body displacements.	72
4.15	Vertebral body downward (Z) displacements. Top-down: T11, L1, and L3 vertebral body displacements.	73
4.16	L1 vertebral body rotation relative to L3 vertebral body rotation (a) comparisons between the PMHS and the HBMs (nominal pelvis angle). A positive value indicates a rearward rotation of L1 relative to L3, akin to lumbar extension or lordosis (b).	74
4.17	L1 vertebral body rotation (a) and L3 vertebral body rotation (b) relative to the pelvis rotation comparisons between the PMHS and the HBMs (nominal pelvis angle). A positive value indicates a rearward rotation of L1 or L3 relative to the pelvis, akin to lumbar extension or lordosis (c).	75
4.18	Left-right: GHBMC, THUMS Nominal, Ant12deg, and Pos12deg model comparisons. Top-down: L1/Pelvis, L3/Pelvis, and L1/L3 rotations.	76
4.19	THUMS Ant12deg model lumbar spine buckling during forward pelvis displacement.	77
4.20	Lumbar spine kinematics shown during forward excursion for the GHBMC (top row) and THUMS (bottom row) Nominal models. Left-right: 0ms, 30ms, 60ms, 90ms.	78
4.21	The THUMS model's flesh sliding contact permitting the anterior gathering of this tissue, which collapses the webbing.	80
4.22	Lap belt-flesh interaction during forward pelvis displacement. Left-right: GHBMC, THUMS, PMHS.	80
5.1	Test rig setup.	87
5.2	Output displacement pulse of the drive cable and lap belt for each test.	88
5.3	CT scan of subject 993M's spinal and pelvic instrumentation.	90
5.4	Lap belt-pelvis angle definition.	91
5.5	Test setup showing the lap belt routed superficial to the abdominal soft tissue.	92

5.6	Submarining definition: when the belt is positioned above (-Z) and also behind (-X) the pelvis by 25 mm (approximate half-width of lap belt webbing), as the motion tracking markers were placed on the center of the lap belt webbing. Thus, the markers moving posterior to the pelvis by a distance greater than 25 mm indicates the full width of the webbing passed over and behind the pelvis.	93
5.7	Initial lap belt midpoint (width- and lengthwise) relative to the ASIS midpoint in the global reference frame (see Figure). The colors indicate the size of the lap belt-pelvis angle: red indicates the large angle, yellow indicates mid angle, and green indicates the small angle. The shapes correspond to the torso angle: diamonds indicate the reclined torso angle and circles indicate the upright torso angle.	94
5.8	Initial position of the lap belt relative to the 3D segmented pelvis CT scans of subject 993M. The solid black line is the midline (widthwise) of the belt webbing, instrumented with 3D motion tracking markers. The dashed lines are the approximated width of the lap belt webbing.	96
5.9	Lap belt trajectory (tracked at the lap belt marker positioned closest to the left ASIS) and lap belt tension time histories of the reclined tests D1589 (left column) and D1591 (right column).	97
5.10	Lap belt trajectory (tracked at the lap belt marker positioned closest to the left ASIS) and lap belt tension time histories of the upright tests D1592 (left column) and D1594 (right column).	98
5.11	Photo of test D1594, which did not result in submarining, taken at the time of maximum lap belt displacement. The ASIS protuberance can be seen behind the lap belt webbing.	99
5.12	Lap belt interaction with abdominal soft tissue for subject 993M's test (D1592) at 55 ms, 70 ms (time of initial peak in lap belt tension), 85 ms (second peak), and 100 ms.	100
5.13	Simplified diagram describing the mechanism of abdominal adipose tissue expansion above the lap belt, which obstructs upward lap belt migration relative to the pelvis.	102
6.1	Finite-element environment for the simulations, which matches the belt pull experiments from Chapter 5. The model's upper and lower extremities were fully constrained.	108
6.2	Outline of the HBM pelvises relative to the PMHS pelvis for the four different tests (left: reclined tests; right: upright tests). The light gray outlines show the left side of the PMHS pelvis (far view) and the dark gray outlines show the right side of the PMHS pelvis (near view).	110
6.3	T1 and L1 vertebral body alignment of the two HBMs. Angle α matched the position of the reclined (45deg) or upright (22deg) torso angles from Chapter 5's experiments.	110
6.4	Total pelvis Y-rotation, or pitch, from the PMHS belt pull experiments.	111
6.5	Procedure to route the lap belts of the HBMs using the LS-PrePost manual belt routing tool	112

6.6	Initial lap belt paths relative to the pelvis in the global reference frame for each test (top-down) and for each surrogate. The left column shows the approximated belt width ($\pm 25\text{mm}$) along the centerline of the lap belt. The right column shows solely the centerline of the lap belt.	113
6.7	Soft tissue compliance modifications. (a) GHBMC pelvis and abdomen flesh parts and corresponding materials, whose load curves (LCID) were scaled (SFO) by either 50% or 200% for decreased and increased levels of stiffness. (b) THUMS internal body contact, where the friction between the internal anatomical structure and external flesh was changed through scaling the friction coefficient by either 50% or 200% for decreased and increased levels of stiffness.	114
6.8	Lap belt midpoint (length- and width-wise) relative to the midpoint of the left and right ASIS for each test and surrogate. (a) Scatter plot showing the initial lap belt midpoint position relative to the ASIS midpoint ($x = 0, z = 0$), where the colors indicate the test number and the symbols indicate the surrogate type. (b) The lap belt midpoint coordinates relative to the ASIS (tabulating the left figure's graphic).	116
6.9	Lap belt initial position, kinematics, and tension time histories for each test (top-down) and surrogate. Left-right: the lap belt centerline initial position (left column), trajectory of the point on the lap belt located nearest to the right ASIS in the sagittal plane (middle column), and the tension time history (right column).	118
6.10	Variation in lap belt-pelvis trajectory for the HBMs with the different prescribed soft tissue stiffnesses, where "Soft" indicates 50% of the nominal stiffness and "Stiff" indicates 200% of the nominal stiffness. The red dashed line indicates marks where submarining did or did not occur. Top-down: the four different tests. Left-right: GHBMC (left column) and THUMS (right column).	120
6.11	Lap belt placement of the GHBMC (a) and the THUMS (b) after stretching the belt using the LS-PrePost stretch tool.	121
6.12	Simulation results from increasing the lap belt load limit of test D1592, which resulted in submarining for both HBMs, matching the PMHS response. (a) Lap belt trajectories relative to the pelvis in the sagittal plane. (b) Lap belt tension time histories.	123
6.13	Simulation results from moving the anchorage points approximately 60mm rearward from test D1592 (same lap belt load limit): Lap belt trajectory relative to the pelvis in the sagittal plane. Both models submarined in this condition, with the THUMS showing higher sensitivity.	124
6.14	Photos from the THUMS simulation of test D1594 (at 30ms, 60ms, and 90ms), which shows the belt migrating down the pelvis as a result of the flesh sliding relative to the pelvis.	125
6.15	Simulation results from increasing the lap belt load limit of test D1594: Lap belt trajectory relative to the pelvis in the sagittal plane. The THUMS model shows increased downward displacement relative to test D1594 (nominal lap belt load limit). The GHBMC did not show downward lap belt motion.	126

7.1	(a) Keyword *DATABASE_CROSS_SECTION in LS-PrePost, where the node set, solid element set, and shell element set are what we defined to define the ASIS cross-section. (b) Difference in defining this cross-section for a mesh with hexahedral elements (top) versus a mesh with tetrahedral elements, as is used in the pelvises of the GHBMC and HBMs (bottom).	133
7.2	Submarining definition. Three nodes are selected on the bottom edge of the lap belt webbing as those closest (Euclidean distance) to the right ASIS (RASIS), ASIS midpoint (MID), and left ASIS (LASIS) (top). These are iteratively selected throughout the course of the simulation. Submarining is detected when the lap belt node moves above (+Z) and behind (+X) the corresponding pelvis node in the global reference frame.	136
7.3	Pre-submarining versus dynamic submarining example.	137
7.4	Example of output cross-plot showing peak ASIS load (measured at the cross-section) relative to peak lap belt tension.	138
7.5	Submarining occurrence resulting from the GHBMC and THUMS simulations (120 sims each). The light shading (and inset data labels) are reclined simulations. The dark shading are upright simulations. The top data labels are total simulations (combined upright and reclined). “Error” marks the simulations that error terminated prior to 80 ms.	139
7.6	Submarining occurrence resulting from the GHBMC and THUMS simulations (120 sims each). The light shading (and inset data labels) are the simulations with a shallow lap belt angle (see Section 7.3.1.2). The dark shading are simulations with the nominal and more vertical lap belt angles. The top data labels are total simulations. “Error” marks the simulations that error terminated prior to 80 ms.	139
7.7	Submarining distinction, based on the definitions from Figure 7 3. The light shading (and inset data labels) are reclined simulations. The dark shading are upright simulations. The top data labels are total simulations (combined upright and reclined).	140
7.8	Peak lap belt tension and measured ASIS load at the time of peak lap belt tension for the GHBMC (red) and THUMS (blue) HBMs in upright and recline. Inner (a and b) and outer (c and d) ASIS cross-sections. Left iliac wing (a and c) and right iliac wing (a and c).	141
7.9	Approximate time of peak pelvis forward displacement for the occupant models. Top-down: GHBMC (a and b) and THUMS (c and d). Left-right: Torso kinematics (a and c) and lap belt-pelvis kinematics (b and d).	143
7.10	Outer cross-section ASIS force vs lap belt tension: Top row: the simulations in which the lap belt remained low on the pelvis are highlighted for both the THUMS (originally in blue) and GHBMC (originally in red) (a, left ASIS and b, right ASIS). Bottom row: after removal of the highlighted cases (c, left ASIS and d, right ASIS).	144
7.11	Inner cross-section ASIS force vs lap belt tension: Top row: the simulations in which the lap belt remained low on the pelvis are highlighted for both the THUMS (originally in blue) and GHBMC (originally in red) (a, left ASIS and b, right ASIS). Bottom row: after removal of the highlighted cases (c, left ASIS and d, right ASIS).	145

7.12	(a) The number of simulations that were flagged for lap belt roping in the GHBMC (blue) and THUMS (orange), wherein the resultant distance between the upper and lower edges of the lap belt close in within 5 mm of each other. The light shading (and inset data labels) are reclined simulations. The dark shading are upright simulations. The top data labels are total simulations (combined upright and reclined). (b) An image taken of the lap belt roping in a simulation with the THUMS model.	146
7.13	Outer cross-section ASIS force vs lap belt tension: Top row: the simulations in which the lap belt roping occurred are highlighted for both the THUMS (originally in blue) and GHBMC (originally in red) (a, left ASIS and b, right ASIS). Bottom row: after removal of the highlighted cases (c, left ASIS and d, right ASIS).	147
7.14	Inner cross-section ASIS force vs lap belt tension: Top row: the simulations in which lap belt roping occurred are highlighted for both the THUMS (originally in blue) and GHBMC (originally in red) (a, left ASIS and b, right ASIS). Bottom row: after removal of the highlighted cases (c, left ASIS and d, right ASIS).	148
7.15	The collapsing of lap belt elements seen for several of the THUMS cases (in which lap belt roping was identified).	150
7.16	Matched reclined simulations between the GHBMC (circle) and THUMS (cross), after removal of cases that submarined, or where the lap belt either did not migrate up the pelvis to load the ASIS or folded over itself (i.e., roping). which are those that were suitable for the belt-ASIS load transfer analysis, for the three occupant models. The colors correspond to a given simulation condition and the shapes correspond to the computational model.	151
7.17	Cross-section ASIS force vs lap belt tension comparison between the GHBMC (circles) and THUMS (crosses) for varying lap belt angles. Top row: inner cross-section ASIS forces (a, left ASIS and b, right ASIS). Bottom row: outer cross-section ASIS forces (a, left ASIS and b, right ASIS).	154
8.1	Automated simulation cycle.	158
8.2	Generic training and testing of selected topology	161
8.3	FE Environment.	162
8.4	The three impact pulses, or crash severities, used in this study: (a) acceleration pulse; (b) delta V.	163
8.5	a) Lap belt angle measurement as defined in FMVSS 210 (NHTSA, 1999). b) The varied belt anchorage positions in this study and the corresponding lap belt angles, as measured by the method outlined in a).	163
8.6	a) Overhead lap belt angle measurement, looking at the occupant from the top view where the black semi-circle represents the lap belt. The angle was taken between the segment connecting the seat reference point to the lap belt anchorage point relative to the X-axis in the overhead view. b) The varied lateral belt anchorage positions and the corresponding overhead lap belt angles, as measured by the method outlined in a).	165
8.7	Results from the first sample iteration (for the first batch of simulations) for the lap belt angle parameters, discretized at specific levels as shown in Table. As this plot shows only two parameters, the points are not unique; however, incorporating the other parameters (in a nine-dimension domain) results in unique points (simulations).	166

8.8	Frequency of the first iteration’s sampled points for the fore-aft lap belt angle location parameter levels, showing more sampling occurring at the bounds.	167
8.9	Images from the belt fitting simulation. This example is with the GHBM positioned in recline, with the belt anchorages positioned outward from the nominal position.	169
8.10	Lap belt placements based on the five fore-aft lap belt anchorage position definitions (see Figure) used in this study. Left: Upright position. Right: Reclined position.	170
8.11	Lap belt placement (no change in fore-aft or lateral anchorage position) for different pelvis angles. Left-right: anterior (+12°), nominal, and posterior angle (-12°). See Figure for the upright orientations and Table for the pelvis angle measurements of all prescribed positions.	171
8.12	Shoulder belt placement resulting from moving the belt anchorages. a) Effect from moving the belt anchorages fore-aft (left: upright, right: reclined). b) Effect from moving the belt anchorages laterally (left: upright, right: reclined).	172
8.13	Images of an example simulation taken at 0ms, 50ms, 100ms, and 150ms.	172
8.14	Submarining distance output metric. A positive distance indicated the belt passed behind the ASIS (submarining) and a negative distance indicated the belt was in front of the ASIS (non-submarining). This measurement was taken between the initial time and the time at peak forward pelvis displacement.	174
8.15	Topology of the NN metamodel.	175
8.16	Metamodel error tracking. a) The progression of the normalized root mean square deviation (RMSD) of the four continuous output metrics. b) The progression of submarining prediction using accuracy. A value of 0 equates to 0% of the total dataset accurately predicted and a value of 1 equates to 100% of the total dataset accurately predicted. See Appendix for details on AU-ROC.	179
8.17	Predicted and actual values of the training and testing points for the output metrics. As the metamodel’s prediction of submarining occurrence was evaluated using the area under the receiver/operator curve (AUROC), the true and false positive rates are shown for this output.	180
8.18	Metamodel error tracking, showing the progression of the absolute error of the four continuous output metrics.	181
9.1	Selected submarining occurrence influential parameter plots (automated simulation dataset).	190
9.2	Selected submarining occurrence influential parameter plots (full-factorial sample). The color scale indicates the model’s predicted probability of submarining, based on the percentage of simulations that resulted in predicted submarining for given levels of those parameters (i.e., per square).	194
9.3	Selected submarining distance influential parameter plots (full-factorial sample). The color scale indicates the model’s predicted probability of the maximum submarining distance exceeding 75.1 mm, based on the percentage of simulations that were predicted to exceed this distance for given levels of those parameters (i.e., per square).	196

9.4	Selected pelvis forward displacement influential parameter plots (full-factorial sample). The color scale indicates the model's predicted probability of the maximum forward pelvis displacement exceeding 137.8 mm, based on the percentage of simulations that were predicted to exceed this distance for given levels of those parameters (i.e., per square).	198
9.5	Selected pelvis rotation influential parameter plots (full-factorial sample). The color scale indicates the model's predicted probability of the maximum pelvis rotation exceeding 8.9° (rearward), based on the percentage of simulations that were predicted to exceed this magnitude (more rearward rotation) for given levels of those parameters (i.e., per square).	200
9.6	Selected lap belt tension influential parameter plots (full-factorial sample). The color scale indicates the model's predicted probability of the maximum lap belt tension exceeding 6.2 kN, based on the percentage of simulations that were predicted to exceed this magnitude for given levels of those parameters (i.e., per square).	202
9.7	Selected submarining occurrence influential parameters plot (1M continuous sample). The color scale indicates the model's predicted probability of submarining, based on the percentage of simulations that resulted in predicted submarining for given levels of those parameters (i.e., per square).	204
9.8	Aid in how to interpret the results of the continuous 1M sample plots relative to the discrete full-factorial sample plots. The probabilities were linearly interpolated between the discrete datapoints for which the metamodel was validated for, but the model's predictions between these points were not validated. Thus, the continuous plots serve only as a gross overview of trends and exact magnitudes should not be extracted.	205
9.9	The effect of fore-aft lap belt angle and recline angle on maximum pelvis displacement. a) Full-factorial sample results, with discrete parameters. The color scale indicates the model's predicted probability of the maximum pelvis displacement exceeding 136.5mm based on the percentage of simulations that were predicted to exceed this magnitude for given levels of those parameters (i.e., per square). b) 1M sample results, with continuous parameters. The color scale indicates the model's predicted probability of the maximum pelvis displacement exceeding 118.4mm based on the percentage of simulations that were predicted to exceed this magnitude for given levels of those parameters (i.e., per square).	206
9.10	Initial lap belt-pelvis angles (see Figure 2.7) of the simulated dataset, divided by submarining outcome.	207
9.11	Lap belt placement relative to pelvis (global coordinate system): a) based on changing lap belt anchorage positions (e.g., rearward, nominal, forward) and torso recline angle. b) based on resulting submarining occurrence. The pelvis schematic is positioned to orient the viewer but is not to scale and the orientation varied based on recline angle and pelvis angle.	208

9.12	Identification of lap belts initially placed unfavorably relative to the pelvis: a) method of how these were identified (adapted from ; b) identified cases based on the method in a) looking at the lap belt midpoint wrt the ASIS. The pelvis schematic is positioned to orient the viewer but is not to scale and the orientation varied based on recline angle and pelvis angle.	209
9.13	Free-body diagram of pelvis and increase in belt slip force resulting from an increase in lap belt-pelvis angle (due to reclined seating posture and shallow fore-aft lap belt angle).	210
10.1	Overview of the dissertation.	214
D.1	Lap Belt Anchorage Positions per Test wrt Global Reference Frame.	294
F.2	The % measured load at the outer and inner ASIS cross sections (Left: GHBMC; Right: THUMS). The solid bar indicates the point load directed straight on the ASIS, the bar with the stripes angled down is the point load directed -45 deg downward, and the bar with the stripes angled up is the point load directed +45 deg upward.297	

List of Tables

2.1	The final factors chosen for further study in this dissertation.	9
2.2	Definitions for terms shown in free body diagram of Figure 2.7.	23
3.1	Initial pelvis and lap belt orientations and lap belt-pelvis angle at the time of Subject 5's submarining (55ms). The lap belt-pelvis angle is measured as angle β from Figure 2.7 and is also described in Figure 3.5	27
3.2	Specimen data for the five male PMHS used in the sled tests.	33
3.3	Initial lap belt angles.	37
3.4	Distance between the center of the lap belt and the ASIS in the X-direction (defined in the right schematic) and resulting pelvis rotation polarities.	51
5.1	Initial (template) test matrix.	86
5.2	Subject information.	89
5.3	Final test matrix.	95
6.1	Initial positioning for each test and surrogate – the PMHS measurements are from the experiments conducted in Chapter 5. Each measurement is rounded to the nearest degree.	109
6.2	Submarining occurrence, and resulting change in lap belt-pelvis angle, for each test and surrogate.	119
7.1	ASIS cross sections defined to measure ASIS load for the GHBMC and THUMS models.	134
7.2	Submarining type distinctions and definitions.	137
7.3	Belt fit of the shallowest lap belt angle (relative to horizontal), with the belt anchorages positioned 200 mm rearward (in X) from the nominal position. (Columns: posture; Rows: computational model).	149
7.4	Differences in belt-pelvis stress contours for the GHBMC (left column) and THUMS (right column). Rows: GHBMC and THUMS cross-sections (top), the first matched simulation (middle), and the second matched simulation (bottom).	152
8.1	Selected discrete parameters and their corresponding levels.	164
8.2	GHBMC model during positioning and settling in the upright and reclined torso angle.	168
8.3	Output metrics from each simulation.	173

8.4	Four example simulations with different defined input parameters, showing the wide variability in resulting kinematics.	177
8.5	Preliminary data aggregation: Non-submarining metrics.	181
8.6	Preliminary data aggregation: Submarining metrics.	182
8.7	The NN metamodel's predictions versus actual outcomes for the five output metrics for a new, unique batch of simulations. The green-shaded cells correspond to a difference between the NN's predictions and the actual values below the average difference. The orange-shaded cells correspond to a difference above the average difference.	183
9.1	Preliminary data aggregation: Non-Submarining metrics.	188
9.2	Preliminary data aggregation: Submarining metrics.	188
9.3	Influential parameter determination for submarining occurrence. The parameters in green showed an absolute distance greater than 0.1 between cluster means (negative versus positive outcome); the parameters in yellow showed an absolute distance greater than 0.05 between cluster means (negative versus positive outcome).	189
9.4	Rank of input parameter influence for the generated full-factorial simulation sample. The parameters in bold font had a substantial effect on the outcome: the parameters in green showed an absolute distance greater than 0.1 between cluster means (negative versus positive outcome); the parameters in yellow showed an absolute distance greater than 0.05 between cluster means (negative versus positive outcome).	192
9.5	Rank of input parameter influence for the generated 1M simulation sample with continuous input parameters (except for foot support). The parameters in bold font had a substantial effect on the outcome: the parameters in green showed an absolute distance greater than 0.1 between cluster means (negative versus positive outcome); the parameters in yellow showed an absolute distance greater than 0.05 between cluster means (negative versus positive outcome).	203

List of Acronyms

- ADS** Automated Driving System.
- AIS** Abbreviated Injury Scale.
- AIIS** Anterior Inferior Iliac Spines.
- ASIS** Anterior Superior Iliac Spines.
- ATD** Anthropomorphic Test Device.
- AU-ROC** Area Under Receiver Operator Curve.
- BMI** Body Mass Index.
- CPU** Central Processing Unit.
- CT** Computed Tomography.
- CV** Cross-Validation.
- DXA** Dual-energy X-ray Absorptiometry.
- FE** Finite Element.
- FMVSS** Federal Motor Vehicle Safety Standard.
- HBM** Human Body Model.
- GHBMC** Global Human Body Models Consortium.
- LASSO** Least Absolute Shrinkage and Selection Operator.
- MAIS** Maximum Abbreviated Injury Scale.
- MPP** Massively Parallel Processing.
- MVC** Motor Vehicle Collision.
- NASS** National Automotive Safety System.
- NHTSA** National Highway Traffic Safety Administration.

NN Neural Network.

NRMSD Normalized Root Mean Square Deviation.

PMHS Post-Mortem Human Surrogate.

ROM Range Of Motion.

THUMS Total HUman Model for Safety.

Acknowledgments

Thanks to my advisor, Dr. Jason Kerrigan. At the writing of this thesis, I have known Jason now for over 6 years, since first interning at the CAB in the fall of 2016. At that time, he also advised me on my undergraduate Capstone research project and allowed me to use CAB's resources to fulfill that project. I likely would not have pursued graduate school had I not met Jason at the end of my fourth year. His passion and dedication to the research at CAB was contagious and motivated me to pursue a challenging path in a challenging field of which was somewhat outside of my biomedical engineering bubble. Jason never let me doubt my ability to succeed in this field, and I'll forever be thankful for the conversations we shared in our weekly meetings - research-related and beyond.

I would also like to thank Dr. Jason Forman and Dr. Bronislaw Gepner for all of their guidance and support in several projects since I first started at CAB. Jason F. provided hands-on guidance and expertise with my early experimental work, and truly lead by example in his demonstrated thoroughness and patience during very long test days. His guidance later expanded beyond the test bay, where his knowledge of the field helped guide the quality of my analysis. Bronek has taught me everything I know related to CAE, providing on-call guidance during a massive computationally-heavy project. Despite his expertise, his humble nature and friendly manner always made me comfortable to ask him all the detailed technical questions.

A big thanks goes out to the rest of my advisory committee. I want to thank Dr. Thomas Hartka, who initially helped me in the early stages of my experimental work and, with his breadth of expertise, provided thoughtful feedback on several items in this dissertation. A big thanks to Dr. Dan Quinn for putting up with us automotive injury-focused engineers and asking the hard questions to get the wheels turning.

The CAB faculty and staff have been a big part of this journey. I can't give a big enough thank you to JP and Sara Sochor for all their technical expertise and good humor that kept me going strong during the hours/days spent in the prep room. I also want to thank Kevin Kopp, Brian Overby, Joey White, Mohan Jayathirtha, and Aida Chebbi for all of their support, patience, and effort during the conduct and analysis of the experimental work. A huge thank you to Dr. Daniel Perez-Rapela, who helped me accomplish the CAE goals of this dissertation, and whose quest to always learn more and willingness to always go to the math to help answer the difficult research questions continues to impact my approach to problem solving.

The CAB students have been a tremendous part of this journey, from which I've made many colleagues and friends. In particular, Sophie Tushak and JP Donlon not only became lifelong colleagues, but became foundational supports on my journey and lifelong friends. Thanks to Zhaonan Sun, Jacek Toczkowski, Carolyn Roberts, Brandon Perry, Kevin Kong, Kalle Chastain, Jeessoo Shin, Ben Koerber, David Moreau, Rachel Newman, Kristen Reynier, Maddy Eaton, Cody O'Cain,

Watson Spivey, Sayak Mukherjee, and Cori Espelien for their helpful discussions and friendship during the stressful times that inevitably arise during long days and nights at the lab.

Finally, my family has been the ultimate support system during this journey, always encouraging me to persevere which has only made me stronger. In particular, my husband has been a tremendous support during this process. It's an incredibly unique situation to have both of us getting PhDs in engineering and going through graduate school at the same time (I think the three words "I love you" were said equally as often as "You working tonight?"). I can't wait for what lies ahead for us, but I'll forever cherish the days we took a break from work to go for a long hike in the Blue Ridge with our dog Jake and ended with a jumbo margarita at Plaza. Here's to the rest of our lives (and more mountains) together. A huge thank you to my dad for helping foster my passion for math and physics, and for teaching me the importance of hard work and integrity, balanced with humility. My mom has been my rock from the beginning, and her support and positivity always helped me put the stress of graduate school in perspective. To my whole slew of siblings, you all are everything to me and your support and encouragement have been imperative. I love you all so much. Thank you also to my four-legged colleagues Jake, Hallie, and Bella for sitting by my side day and night the past six months as I wrote this dissertation.

Abstract of the Dissertation

Critical Factors Influencing Lap Belt-Pelvis Interaction and Submarining Occurrence for Occupants in Frontal Crashes

by

Rachel E. Richardson

Doctor of Philosophy in Mechanical and Aerospace Engineering

University of Virginia, December 2022

Jason R. Kerrigan, Advisor

Submarining is qualitatively defined as the mechanism in which the lap belt, initially positioned superficial to the anterior superior iliac spines (ASIS), fails to engage the bony pelvis during occupant forward excursion, and translates superior and posterior relative to the ASIS, loading the abdominal soft tissue. While submarining increases the likelihood of abdominal injuries due to direct lap belt loading, the resulting effects on occupant kinematics and restraint interaction increase the risk of injury to nearly every body region. A multitude of intrinsic and extrinsic factors have been hypothesized to affect lap belt-pelvis interaction and submarining occurrence in the literature, and modifications to federal safety regulations were made to improve pelvis restraint based on this research. However, further research is required to investigate how these parameters affect submarining using a restraint system equipped with modern technologies and to provide updates for safety regulations. Additionally, recent advancements in automated driving system (ADS) technologies introduce new challenges to restraint design that also need to be addressed.

The goal of this dissertation was to evaluate how parameters pertaining to the vehicle environment (extrinsic) and occupant (intrinsic) affect lap belt-pelvis interaction and submarining occurrence through experiments using post-mortem human surrogates (PMHS) and simulations using computational human body models (HBMs).

First, a comprehensive literature review was performed to identify the intrinsic and extrinsic factors that have been hypothesized to affect lap belt-pelvis interaction, particularly submarining. Of these factors, investigating the effects of a reclined torso angle and the angle of the lap belt relative to the pelvis required additional experimental research and subsequent HBM validation. This finding informed the design of the experimental and computational studies of this dissertation.

As no experimental data existed to understand how a reclined seating posture affected lap belt-pelvis interaction and submarining occurrence, an innovative methodology was developed to investigate this through experimental sled tests using PMHS. One subject that exhibited a relatively large lap belt-pelvis angle (indicating a shallow fore-aft lap belt angle) submarined. This prompted the need for further experimental study to identify a submarining threshold through variation of this parameter. The GHBM HBM was shown to exhibit better biofidelity over the THUMS in the reclined sled test condition, with more biofidelic lumbar spine compliance and lap belt-flesh-pelvis interaction.

Lap belt-pelvis angle was further investigated in belt pull experiments through systematic variation of lap belt and torso angle, which identified a submarining threshold. Additionally, this parameter was found to affect the placement of the lap belt relative to the pelvis. The GHBM HBM ranked superior relative to the THUMS HBM, as the THUMS showed a downward lap belt migration relative to the pelvis at a steeper fore-aft lap belt angle, which was not seen in the PMHS.

This dissertation's final parametric study, in which the effects of extrinsic and intrinsic factors on lap belt-pelvis interaction and submarining would be quantified, was setup using the GHBM with several varied intrinsic and extrinsic factors. These simulations were sampled to approximate the design space for a subset of 480 simulations and were used to develop, train, and test a Neural Network (NN) metamodel which predicted submarining occurrence and distance, pelvis kinematic and lap belt kinetic outputs based on these varied parameters.

From the NN metamodel's predictions, fore-aft lap belt angle and recline angle were identified as the dominating factors that affected submarining occurrence. A shallow lap belt angle, in combination with a reclined torso angle, was linked to a higher likelihood of submarining. Submarining risk was decreased for a steeper lap belt angle in both postures, however in the reclined posture this risk was only substantially mitigated at the steepest fore-aft lap belt angle (87°). Additionally, the range of permitted lap belt angles by FMVSS 210 was shown to be insufficient in mitigating submarining risk in a reclined posture with a modern restraint system (equipped with dual lap belt pretensioners). For a reclined seating posture, the lap belt anchorages must be positioned further forward relative to the occupant to reduce submarining risk. Potential trade-offs resulting from moving the lap belt anchorages further forward included increased pelvis forward displacement (from 63° to 75° in upright and from 75° to 87° in recline) and increased lap belt tension (from 46° to 75° for both postures).

This dissertation provided the automotive safety community with a wealth of data to inform restraint system design for current and future vehicles. Specifically, this improves the automotive safety field's understanding of the fundamental characteristics that influence lap belt-pelvis interaction and submarining. This research also identified limitations of current safety standards for a restraint system equipped with modern technologies, and for a reclined seating posture. Finally, the quantification identified consistencies and differences across different torso angles, providing guidance on potential vehicle environment modifications that need to be made to mitigate submarining in a reclined posture versus an upright posture.

Chapter 1

Introduction

A summary of the state of the art and research gaps is first presented to motivate the dissertation. The specific goals and aims proposed in this dissertation, which will fill these research gaps, are then presented. Finally, an overview is provided as a road map to navigate through this dissertation document.

1.1 Motivation

This section provides an overview of the state of the art and motivations for the content of this dissertation. Topics covered include (i) the complexity of the submarining phenomenon, (ii) the link between a reclined torso angle and automotive occupant injury risk, (iii) the use of computational human body models in a reclined posture, (iv) the existing evidence for lap belt-pelvis interaction to be affected by abdominal soft tissue compliance, and (v) the lack of available data quantifying the relative effects of environment- and occupant-related factors on submarining. Finally, the implications of the proposed work on the automotive safety field will be presented.

1.1.1 Submarining is linked to increased injury risk to nearly every body region, and its prevalence in the field is underestimated.

Submarining is qualitatively defined as the mechanism in which the lap belt, initially positioned superficial to the anterior superior iliac spines (ASIS), fails to engage the pelvic bone during occupant forward excursion, and translates superior and posterior relative to the ASIS, loading the abdominal soft tissue [1, 2] Figure 1.1. Submarining poses a high risk of abdominal injuries, partic-

CHAPTER 1. INTRODUCTION

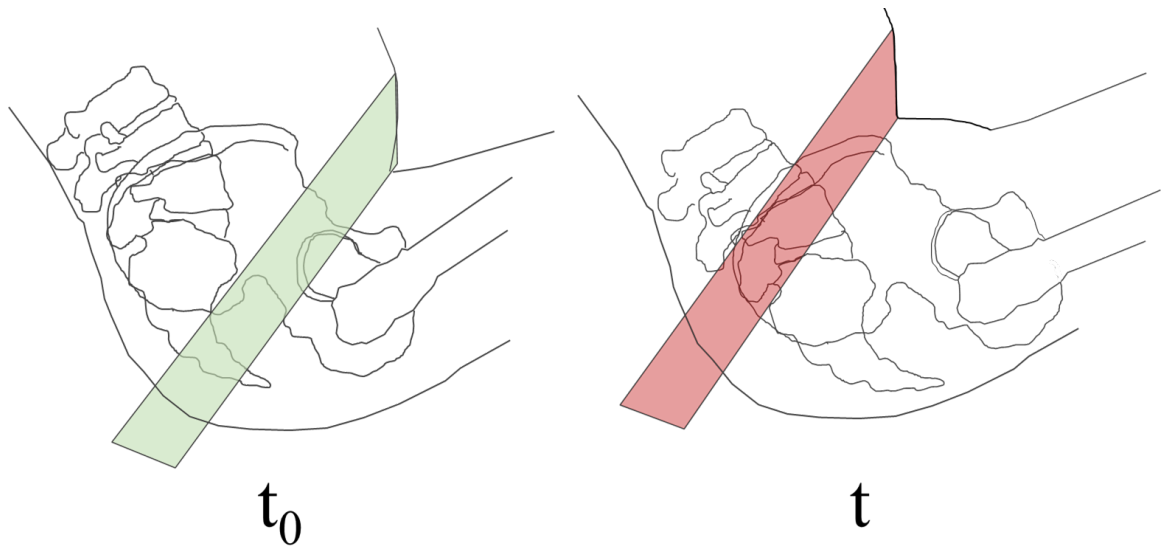


Figure 1.1: The submarining phenomenon, defined as the lap belt, initially placed favorably relative to the pelvic bone (t_0) translates superior to the pelvis and loads the abdominal soft tissue during the crash (t).

ularly for hollow organs inferior to the transumbilical plane, as these injuries are a direct result of lap belt loading [3, 4, 5, 6].

The frequency of abdominal injuries in the automotive field has historically been relatively low [2, 7, 8]; however, the majority of these injuries are severe. An analysis of frontal impact crashes from the National Highway Traffic Safety Administration's (NHTSA) National Automotive Safety System (NASS) database (1988-1994; front seat, belted, frontal impact) indicated that with increasing abbreviated injury scale (AIS) severity score, abdominal injuries became more prominent: abdominal injuries constituted 8% of all AIS 3, 16.5% of AIS 4+, and 20.5% of AIS 5+ injuries [9]. Additionally, for frontal and side impact crashes (NASS 1998-2004; front seat, belted), the risk of AIS 4+ abdominal injury ranks behind only the risk of AIS 4+ head and thorax injuries [10]. Generally, the frequency of abdominal injuries ranks low relative to other body regions [4, 11]; however, in addition to the abdomen, submarining poses a risk of injury to the skeletal thorax, cervical and lumbar spine, and lower extremities, as the mechanism affects overall occupant kinematics and subsequent interaction with the vehicle environment [12, 13, 14]. Additionally, submarining does not always result in abdominal injuries: alternative load paths, such as impact of the knees with the knee bolster, can decrease lap belt force and thus decrease likelihood of abdominal injury, while still posing risk of injury to other body regions [1]. Conversely, abdominal injuries can oc-

CHAPTER 1. INTRODUCTION

cur without submarining through interaction with the vehicle compartment (e.g., steering wheel) or initial malplacement of the belt above the ASIS, which makes the submarining diagnosis further convoluted [4, 10]. Thus, it is difficult to discern injuries resulting from submarining without a rigorous accident analysis of both the vehicle (e.g., evidence of impact with knee bolster or front seat back, markings on the seat belt webbing, seatback position, etc.) and the occupant (e.g., occupant position, initial position/placement of belt, “seat belt sign”, etc.) [15, 16]. It is therefore likely that the frequency of submarining is currently underestimated in the field. As Adomeit and Heger state: “failure to find abdominal injuries resulting from submarining in the usual sense has led to an underestimation of the problem” [1].

1.1.2 Submarining is predicted to become more prevalent in the field.

Epidemiology data shows an increase in the likelihood of injury (fatal and non-fatal) for a reclined occupant relative to an upright occupant [17, 18]. Most recently, a thorough statistical analysis of reclined position with regard to crash injury severity showed an increased odds ratio for a reclined occupant relative to an upright occupant for every body region, with high effect sizes in the head-face-neck body region (MAIS 4+), the pelvis-hip-lower extremity body region (MAIS 3+), and the thorax, abdominal, and upper extremity body regions (MAIS 2+) [14]. Case studies on reclined occupants show resulting injuries at the regions of the cervical spine [12, 19, 20], thorax [21], and abdomen [16, 20]. Four cases explicitly identified submarining as a leading injury mechanism [16, 20, 21].

Level 3 Autonomous Driving Systems (ADS) will liberate the occupant from having to control the vehicle [22]. With the introduction of ADS Level 3, a reclined posture is predicted to become more prevalent [23, 24]. Thus, the automotive industry has been researching reclined occupant kinematics such that the design of safety systems and interior compartments can mitigate potential injury [25]. Future interior compartment designs show vehicle seats will be placed further from the knee bolster and instrument panel thus placing a higher reliance on the seatbelt for restraint. However, prior to this study, no human or cadaveric studies had been performed to examine how effectively novel restraint systems can mitigate submarining for reclined occupants. Thus, it is critical that research on reclined occupants in novel restraint systems be conducted to guide the industry towards successful mitigation of submarining and resulting injuries in future vehicles.

1.1.3 Submarining is affected by a multitude of factors, and their effects have not been quantified.

Submarining is a complex problem because its occurrence is associated with several parameters, including environmental (e.g., lap belt angle, boundary conditions), crash-related (e.g., delta-V, impact direction), and occupant-related (e.g., posture, pelvic orientation) factors [8, 2]. The most comprehensive way to quantify individual and interaction effects of factors on submarining occurrence is through a sensitivity study, in which the influence of an input (e.g., lap belt angle) on an output (e.g., submarining occurrence) is quantified through controlled variation of that input. Sensitivity studies can be conducted experimentally or computationally.

A substantial amount of research in understanding the submarining mechanism and its causal factors took place during the 1970's and 1980's, prior to the advancement in computational resources. Thus, these possible submarining-causing factors were primarily identified experimentally without a rigorous, statistical quantification of parameter effects. Additionally, this research occurred prior to more recent advancements in restraint design. Restraint technologies, including pyrotechnic pretensioners and load limiters, which are now known to affect occupant kinematics and hence, occupant-restraint interaction, have substantially advanced since their industry-wide application in 1998 [26]. Thus, the understanding of submarining-causing factors originally developed from 1970-1990 requires further research using both modern restraint technologies and modern tools.

1.1.4 Computational human body models can be used to increase our understanding of the submarining phenomenon.

To enhance the safety of vehicles, the automotive industry, government, and academia use computational finite element (FE) full human body models (HBMs) as a tool to study blunt impact and injury in motor vehicle crashes. Geometry for current state-of-the-art average male (M50) seated whole-body models- based on medical imaging data (e.g. computed tomography data)- are made up of approximately two million elements [27, 28]. These HBMs, largely validated at the component and full-body model levels, have been used extensively for evaluation of kinematics in multiple automotive crash loading modes. The kinematic response of these HBMs in reclined seating posture has been investigated [29, 30, 31, 32, 33, 34]; however, the models have not been evaluated relative to post-mortem human surrogate (PMHS) data. This study aims to utilize the HBM as a tool to evaluate how parameters affect submarining. Therefore, the response of the HBMs

CHAPTER 1. INTRODUCTION

will be compared to PMHS to evaluate the HBM's ability to capture the fundamental mechanics of lap belt-pelvis interaction.

Additionally, HBMs can be used as tools to understand submarining sensitivity relative to various parameters. Experimental sensitivity studies are generally not as comprehensive as computational studies due to physical and financial limitations; though, they are useful as they provide a dataset for model validation and a hypothesis of which parameter has the greatest effect on response. Currently, sensitivity studies are most always done computationally. Several computational submarining sensitivity studies exist that investigate the effects of various parameters on submarining occurrence [29, 30, 31, 32, 35, 36, 37]. These studies are useful for evaluating HBM biofidelity; however, the variation in occupant and vehicle design parameters was limited, focusing on a small subset of simulations. Further, these studies do not contain statistical analyses to quantify the relative effects of these parameters. This research aims to conduct a robust, quantifiable analysis on a large dataset of simulations using a HBM.

1.2 Scope of Research

1.2.1 Goal of dissertation.

The current research gaps lead to the goal of this dissertation, which is to determine how vehicle environment and occupant-related characteristics affect lap belt-pelvis kinematics and submarining occurrence.

1.2.2 Specific aims.

This research was divided into four aims to evaluate and quantify the effects of various extrinsic (vehicle environment-related) and intrinsic (occupant-related) factors on lap belt-pelvis kinematics and submarining occurrence. The first aim was to identify the extrinsic and intrinsic factors that have been hypothesized to affect lap belt-pelvis interaction and submarining occurrence by performing a comprehensive review of the literature. The second aim was to determine the effect of a reclined torso angle on lap belt-pelvis interaction through dynamic sled tests using PMHS, and then to evaluate how well computational HBMs replicate the PMHS response (model biofidelity evaluation). The third aim was to determine the effect of the lap belt-pelvis angle on lap belt-pelvis interaction through seated belt pull tests using PMHS, and again, evaluate HBM biofidelity. The second and third aims used two different state-of-the-art HBMs (mid-sized, or 50th percentile, males)

CHAPTER 1. INTRODUCTION

that are frequently used in the automotive safety field to replicate and study human body response or injury. Based on the results of the biofidelity evaluations performed in the second and third aims, the model that best replicated the PMHS response (superior biofidelity) was chosen for use in the fourth aim. The fourth aim determined the relative effects of the intrinsic and extrinsic factors on lap belt-pelvis interaction and submarining occurrence through a large-scale parametric study of frontal impact simulations. Through this parametric study, the relative effect of each factor were quantified using statistical analysis, and the outcome informed the automobile safety community of potential vehicle environment modifications that could improve lap belt-pelvis engagement.

The specific aims of this research are outlined here:

- **Aim 1:** Identify intrinsic and extrinsic factors that may affect lap belt-pelvis interaction and submarining occurrence.
- **Aim 2:** Evaluate the effect of a reclined torso angle on lap belt-pelvis interaction and the ability of HBMs to predict this interaction.
- **Aim 3:** Evaluate the effect of lap belt-pelvis angle on lap belt-pelvis interaction and the ability of HBMs to predict this interaction.
- **Aim 4:** Determine the relative effects of intrinsic and extrinsic factors on lap belt-pelvis interaction and submarining occurrence.

1.2.3 Dissertation overview.

This dissertation was divided into eight chapters addressing the specific aims, in addition to an introduction and conclusion chapter Figure 1.2. Chapter 2 described the methods and results of the comprehensive literature review performed for Aim 1, which identified the intrinsic and extrinsic factors that have been hypothesized to affect lap belt-pelvis kinematics. These factors were evaluated in the remainder of this dissertation. Chapters 3 and 4 described the experimental and computational studies performed for Aim 2, which evaluated how a reclined torso angle influenced lap belt-pelvis interaction and assessed the computational model's ability to predict this interaction. Chapters 5 and 6 described the experimental and computational studies performed for Aim 3, which evaluated the effect of lap belt-pelvis angle on lap belt-pelvis interaction and assessed the computational model's ability to predict this interaction. Chapter 7 described an additional analysis which justified the selection of the computational model used in the remainder of the dissertation. Chapters 8 and 9 described the parametric study and subsequent statistical analysis performed to support

CHAPTER 1. INTRODUCTION

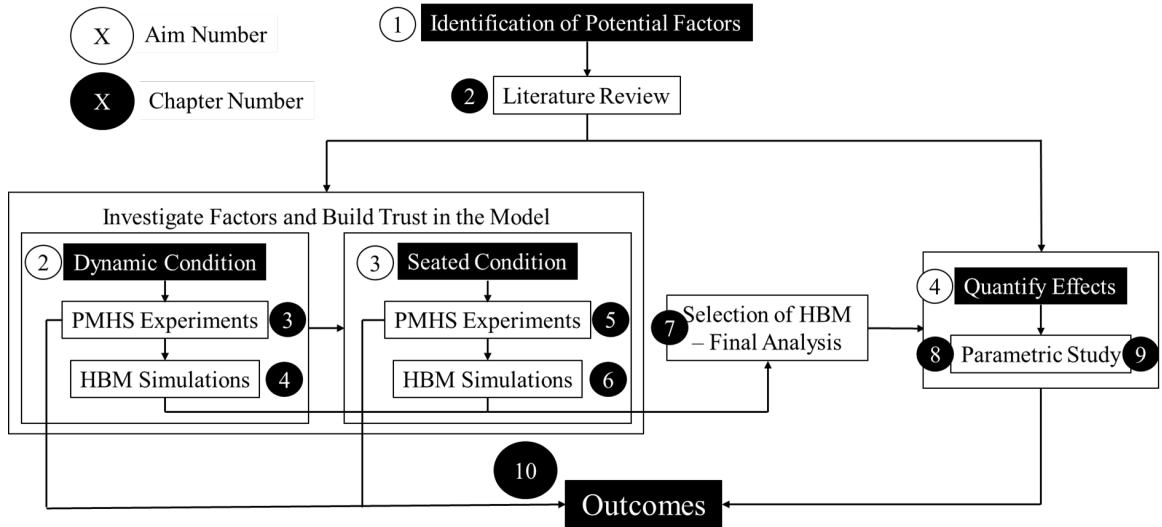


Figure 1.2: Overview of dissertation.

Aim 4, which determined the relative effects of intrinsic and extrinsic factors on lap belt-pelvis interaction and submarining occurrence.

The results from this work improved the field’s understanding of the individual and relative effects of intrinsic and extrinsic factors on lap belt-pelvis interaction, particularly in a reclined posture, and thus aided the automotive safety field in restraint design targeted at mitigating submarining in current and future vehicles. This study started with a comprehensive literature review on factors that have been predicted to affect lap belt-pelvis interaction and submarining (Chapter 2), such that the subsequent aims could be specifically tailored to address these factors and meet the goal and aims of the study.

Chapter 2

Hypothesized Factors Affecting Submarining Occurrence: A Review

2.1 Executive Summary

2.1.1 Relevance and goal

In Chapter 1, the complexity of the submarining phenomenon, identification of factors that affect lap belt-pelvis interaction, and feasibility of using computational HBMs to evaluate the effect of intrinsic and extrinsic factors on lap belt-pelvis interaction was briefly introduced. As this dissertation aimed to evaluate the effect of intrinsic and extrinsic factors on lap belt-pelvis interaction, with the ultimate goal of quantifying these effects through a parametric study using a computational HBM in Aim 4 (Chapters 8 and 9), a comprehensive literature review that identifies such potential influencing factors was required. Thus, the main objective of chapter was to survey the current knowledge of all environmental (extrinsic) and occupant-related (intrinsic) factors that have been hypothesized to affect lap belt-pelvis interaction and subsequent submarining occurrence. These factors were organized in their relationship to each other and their contribution to the submarining phenomenon, then categorized through a series of steps, which dictated whether, or how, they would be carried through the remainder of this dissertation.

The literature review consisted of nearly 220 articles, including epidemiological, analytical, experimental, and computational studies. This chapter outlines the literature search methodology and findings by first identifying the potential factors and how they were hypothesized. The main outcomes of this analysis of the literature were a free body diagram and a causal model, which

summarized these factors.

The context of this review was guided by the following research questions:

1. Which factors have been hypothesized to affect lap belt-pelvis interaction and submarining occurrence?
2. What do we currently know about how these potential factors relate to each other (e.g., dependencies, correlations, etc.)?
3. What areas require further HBM evaluation in order to use the HBM as a tool to evaluate the effect these factors have on lap belt-pelvis interaction and submarining occurrence, and to trust the HBM's predictions?

2.1.2 Key conclusions

The full list of conclusions can be found in Section 2.6 below. In summary, ten extrinsic and intrinsic factors were selected for further study in the remainder of this dissertation, as these factors were deemed the most critical and useful for understanding how they affect lap belt-pelvis interaction Table 2.1. Narrowing down to these factors also allowed for a more controlled sensitivity study that was feasible to accomplish using computational HBMs.

Table 2.1: The final factors chosen for further study in this dissertation.

Extrinsic	Intrinsic
<ul style="list-style-type: none"> • Crash severity (impact pulse) • Lap belt angle (fore-aft) • Lap belt angle (overhead) <ul style="list-style-type: none"> • Foot support • Friction between belt/occupant • Friction between seat/occupant 	<ul style="list-style-type: none"> • Torso angle • Pelvis angle • HBM type • Pelvic-abdominal soft tissue compliance/stiffness

2.1.3 Contributions

This chapter describes a comprehensive review of several factors that have been postulated to affect lap belt-pelvis interaction and submarining occurrence. This research defined the current

knowledge of the field and identified areas in which further study was required, thus providing the impetus for this dissertation.

2.2 Introduction

This section is divided into three subsections aimed to form the foundation of knowledge on pelvis anatomy, advancement in automotive restraint technology, and the current state-of-the-art computational HBMs for automotive biomechanics applications. This provides the background background knowledge which contextualizes the results of the literature review.

2.2.1 Pelvic-abdominal anatomy overview in relation to lap belt interaction

The bony pelvis is a basin-shaped complex of bones that serves a variety of functions including the support and balance of the upper torso, the motion of the legs, hips, and trunk, the containment and protection of soft, internal abdominal organs, and, for females, forms a ring which functions as the birth canal. The upper torso and lower extremities are conjoined at the bony pelvis through a multitude of muscular and ligamentous connections, all of which aim to promote bipedal mobility. The pelvis consists of bilateral coxal bones, each of which are comprised of three bones that join together in development: the ilium, the ischium, and the pubis (Figure 2.1a). These coxal bones are joined together anteriorly at the pubic symphysis and posteriorly at the sacral-iliac joint. The ilium is a blade-shaped bone, which accounts for the width of the hips (referred to as the “hip bones” in colloquial terminology). In an automotive environment, the lap belt is designed to be placed superficial to the ilium, ideally engaging the notch between the anterior inferior iliac spine (AIIS) and anterior superior iliac spine (ASIS) during the occupant’s forward displacement (Figure 2.1b). When the lap belt translates superior to the ASIS, it can load the abdominal organs just superior to the pelvis. The ischium bone, in addition to the sacrum and coccyx, provides support postero-inferiorly; this is typically where the weight falls in sitting and leaning backwards. The pubis bone provides support antero-inferiorly; this is typically where the weight falls in sitting leaning forwards. All three bones – the ilium, ischium, and pubis – join at the acetabulum, a socket that contains the femoral head.

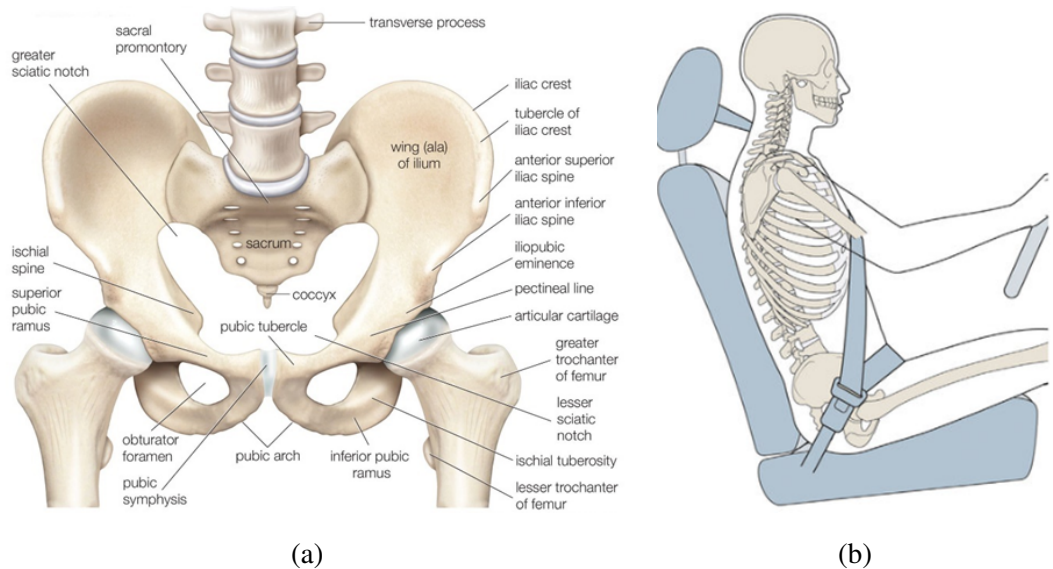


Figure 2.1: (a) Bony pelvis anatomy [38]. (b) Proper positioning of lap belt with respect to bony pelvis anatomy [39]

The abdominal cavity is a hollow space between the diaphragm and the pelvis which contains several organs (Figure 2.2a). These organs can be divided into four quadrants, where the upper quadrants are separated from the lower quadrants at the transumbilical plane, a transverse plane at the area of the umbilical, or the belly button. The solid abdominal viscera is the collective term for the organs above the transumbilical plane, which are solid in nature; these include the liver, pancreas, spleen, adrenals, and kidneys. In contrast, the hollow organs of the lower abdominal cavity encompass the large intestine, small intestine, and mesentery. The stomach, another hollow organ, is above the transumbilical plane. Injuries to these organs represent approximately 50% of abdominal organ injuries in belt-restrained occupants in frontal collisions [4]. While injuries to the organs above the transumbilical plane are often attributed to the steering wheel, door, or other internal automotive structure, injuries to the organs inferior to this plane are almost always due to loading from the lap belt [4] (e.g., Figure 2.2b). This direct loading from the lap belt is attributed to submarining, as it indicates a failure of bony pelvis engagement.

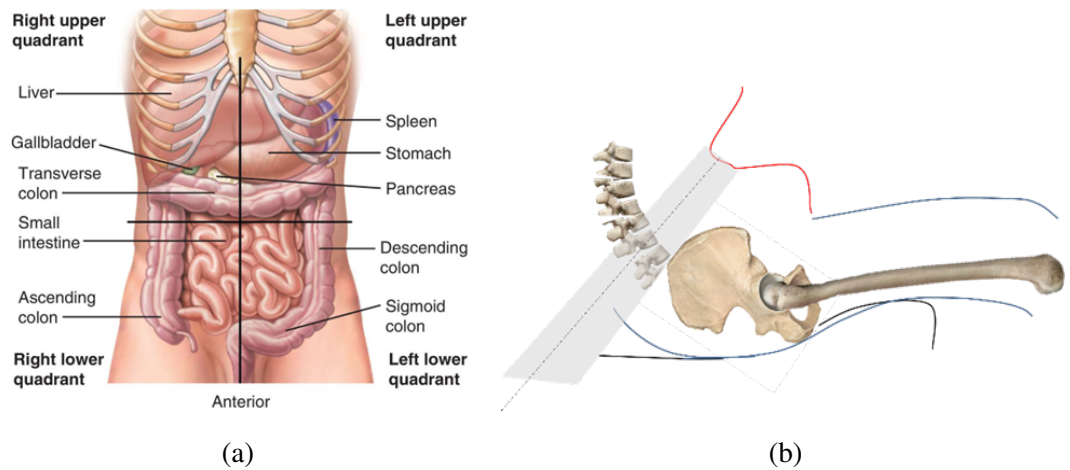


Figure 2.2: (a) Abdominal organ anatomy [40]. (b) Example of abdominal lap belt loading due to submarining.

2.2.2 Restraint system advancement over the years

A brief history of automotive seatbelt restraint system advancement, particularly the lap belt, will now be introduced to contextualize the restraints installed in the current vehicle fleet. A substantial amount of research in understanding the submarining mechanism took place during the 1970's and 1980's, after lap belts were required in U.S. vehicles in 1966 [41], and prior to the NHTSA's first mandate of Federal Motor Vehicle Safety Standard (FMVSS) 210 in 1990 [26, 42]. For a complete timeline of U.S. automotive restraints, see Appendix A. Lap belt anchorages were originally required to be installed such that the lap belt angle relative to the horizontal was between 20° and 75° ; this mandate adopted a 30° minimum. NHTSA claimed the change would "decrease the likelihood of submarining [...] even though the interrelationship of [submarining] factors [was] not yet quantified" [42]. NHTSA's 1988 study, which prompted this amendment, included a literature review of accident data and research studies using analytical and experimental models to predict several environmental and occupant-related parameters that affect submarining [43, 44].

While useful, these studies were conducted prior to the advancement in restraint design. Restraint technologies, including pyrotechnic pretensioners and load limiters, have substantially advanced since their industry-wide introduction in 1998 [26]. Pretensioners remove slack in the shoulder and/or lap belt just after the time of impact (approximately 3-10 ms), thus increasing the likelihood of engagement with the ASIS and subsequent mitigation of submarining [45, 46]. Load

limiters are effectively a yielding mechanism, as they prevent a predefined threshold of occupant load from being exceeded through a plastic deformation in the retractor mechanism (e.g., torsion bar) and/or a gradual release of the seatbelt webbing [47]. Both pretensioners and load limiters are targeted to improve injury outcomes and have a substantial effect on occupant kinematics. Additionally, early analytical models were over-simplified, not accounting for the effect of flesh compliance on belt-pelvis interaction, which has a known effect on belt-pelvis interaction [35, 48]. Thus, criteria for a vehicle's restraint system geometry (FMVSS 210), which plays a critical role in occupant kinematics, are based on research conducted prior to the advancement in restraint design and research tools.

A collection of research that encompasses both studies that occurred prior to and after the advancement in restraints was necessary to gain a clear understanding of the current knowledge of the factors proposed to have an influence on belt-pelvis interaction. The research conducted prior to restraint advancement is still useful, though the degree, or magnitude, of influence the proposed factors have on submarining occurrence may be different with modern restraints. Sensitivity studies that use modern restraints also use modern tools (i.e., computational HBMs), which likewise have their own limitations. Thus, this literature review was necessary to a) collect all factors hypothesized to influence belt-pelvis interaction and, for those proposed prior to restraint advancement, understand how these may have an influence using a modern restraint, and b) identify areas in which more recent research, which uses modern restraints and modern computational tools, required further validation in order to trust the conclusions drawn from the models.

2.2.3 Current state-of-the-art computational HBMs

From the literature review, several different surrogates were used to increase understanding of human kinematics and injury tolerance. Here, human body models are introduced as these are tools used most commonly today and were used extensively throughout this dissertation.

To enhance the safety of vehicles, the automotive industry, government, and academia use computational finite element (FE) full human body models (HBMs) as a tool to study blunt impact and injury in motor vehicle crashes. Geometry for current state-of-the-art mid-sized male (M50) seated whole-body models- based on medical imaging data (e.g. computed tomography data)- are made up of approximately two million elements [27, 28]. The two most recently developed and updated state-of-the-art HBMs are the Global Human Body Models Consortium detailed M50 seated model v.6 (GHBMC-O M50 v.6) and the Total HUman Model for Safety (THUMS AM50 v.6.1)

(Figure 2.3). These HBMs have different geometric, material, and mathematical formulations, but are both classified as an average, or mid-sized male anthropometry. The geometry of the GHBM was measured from a living male volunteer, 26 years old, 174.9 cm, and 78.6 ± 0.77 kg [28]. The THUMS geometry was designed to fit a mid-sized male occupant based on data reported by Schneider et al. [49], with a height of 179 cm and mass of 79 kg [50]. These HBMs, largely validated at the component and full-body model levels, have been used extensively for evaluation of kinematics in multiple automotive crash loading modes and have been shown to exhibit different kinematic and kinetic responses.

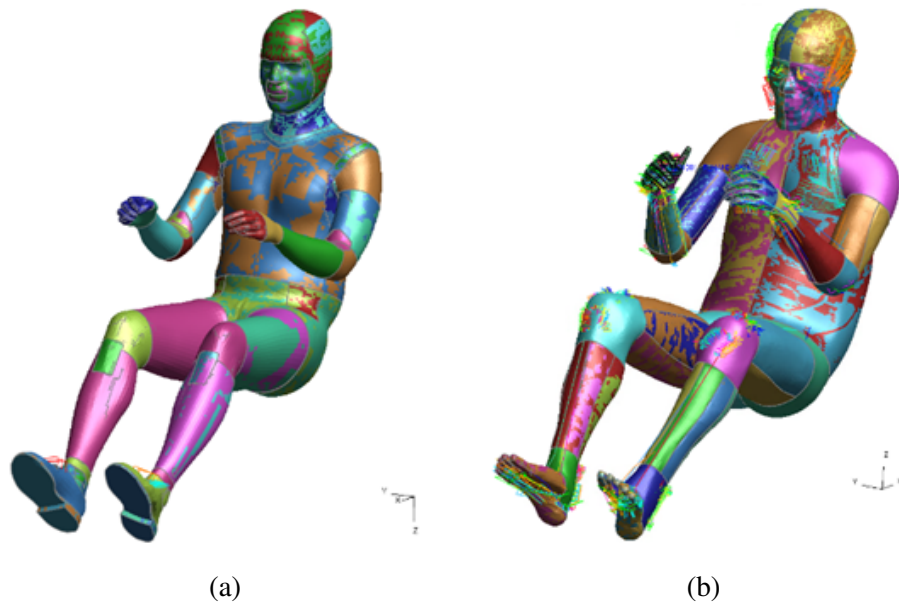


Figure 2.3: Computational M50 human body models: (a) GHBM-O M50 v.6 and (b) THUMS AM50 v.6.1.

2.3 Methodology

2.3.1 Search strategy

The search for literature articles was conducted using internal and external data sources. The internal data source, known as the Center for Applied Biomechanics (CAB) Library, which encompasses several thousand biomechanics-focused articles from various journals, conferences, theses and dissertations, textbooks, and government documents. External sources included PubMed,

Engineering Village, and Google Scholar. The following key words were used to identify relevant papers of interest: “submarining”, “lap belt pelvis interaction”, “lap belt abdomen loading”, and “pelvis kinematics”. This resulted in nearly 220 articles, including epidemiological, analytical, experimental, and computational studies.

2.3.2 Data extraction methods

The 220 articles were used to investigate the phenomenon of submarining, describe the history of automotive restraints and how modern advancements have come about, and to identify common themes and factors that have been proposed to influence belt-pelvis interaction and submarining occurrence.

Once all the factors were collected, a process was followed to specify how these factors would be used in the parametric study in Aim 4 (Figure 2.4).

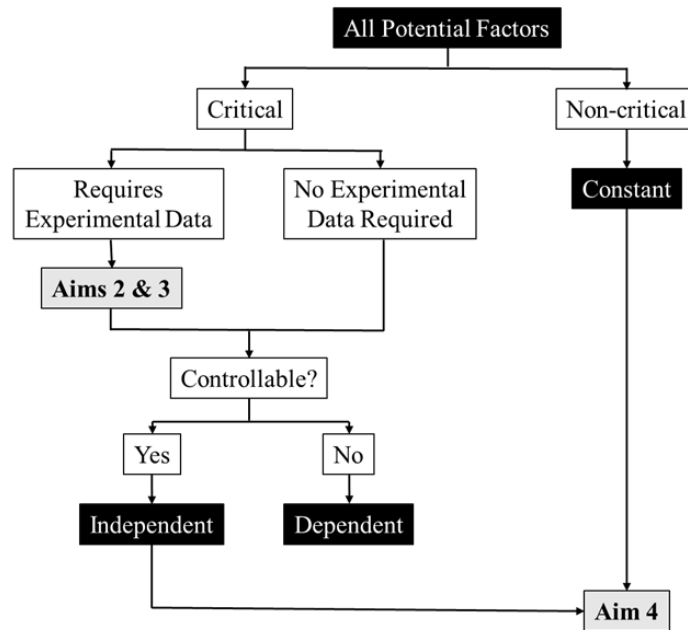


Figure 2.4: Process in identified potential factor classifications and their use in the remainder of this dissertation.

2.4 Identified Factors

Several factors that have been hypothesized to affect submarining occurrence were identified in this literature review (Figure 2.5). These were divided into three categories based on four stages of the crash event. First, the input parameters are those that set up the initial conditions of the crash event, such as those that pertain to the type of crash, the vehicle environment, the occupant, and the restraint system. Next, the parameters that arise during the crash event which are influenced by the input parameters, including occupant kinematics and seat and restraint system interaction. These kinematics and interactions affect the final stage, coined as the critical time in which submarining does or does not occur. The final factors influencing this occurrence pertain to the lap belt-pelvis geometry and surrounding boundary conditions.

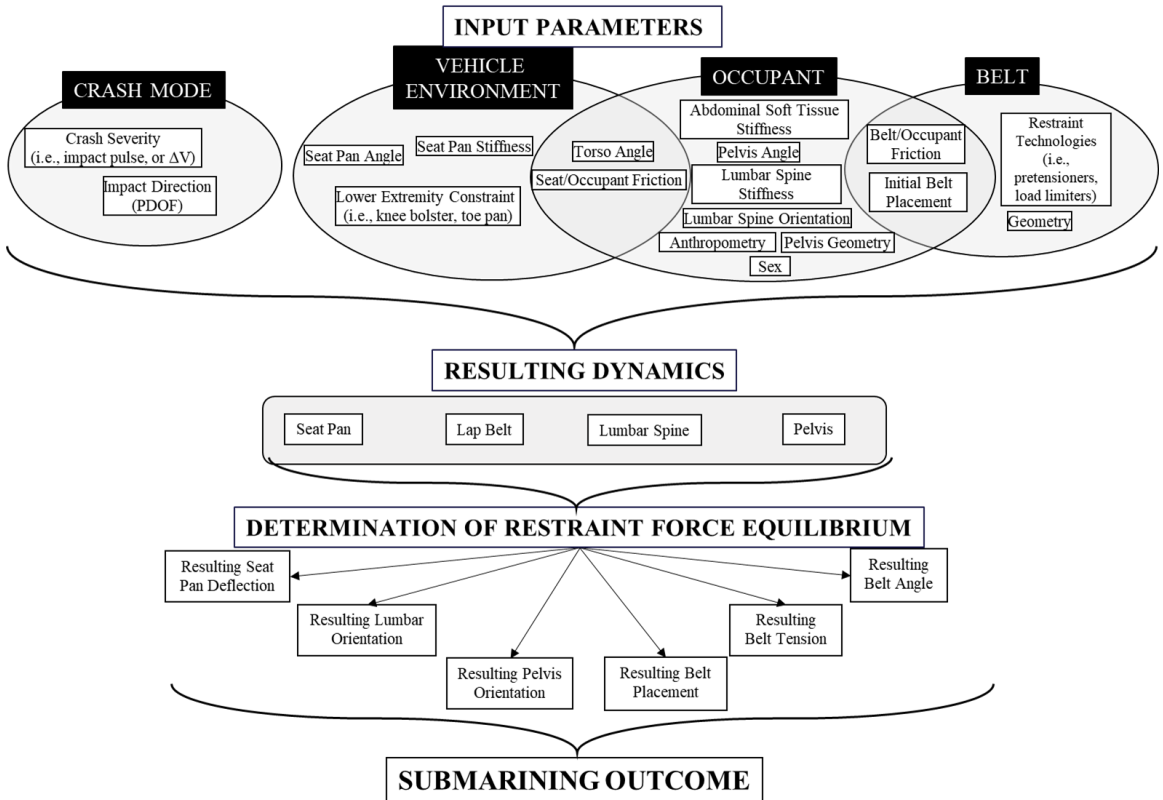


Figure 2.5: Causality diagram depicting the three categories of factors based on four stages of the crash event, including the determination of the submarining outcome.

A subset of factors was chosen from the input parameters for further study in this dissertation for two reasons. First, these factors were deemed the most critical and useful for the automotive

safety field to understand in how they affect lap belt-pelvis interaction. Second, narrowing down to these factors allowed for a more controlled sensitivity study that was feasible to accomplish using a computational HBM in Chapter 8.

To have a narrower scope on the causality of submarining, only one HBM was used in the parametric study of Chapter 8. The HBMs have been shown to exhibit different belt-pelvis interaction responses due to differences in their geometric and material formulations. Thus, Aims 2 and 3 (Chapters 3-6) will not only be used to evaluate the HBM responses relative to the PMHS data, but also to compare the biofidelity of these HBMs to each other which will aid in the choice of HBM to use in Chapter 8. Choosing a single HBM to use in Chapter 8 eliminated many occupant variables, as they are dependent on the occupant model.

To further simplify the parametric study, the surrounding boundary conditions, including the seat, impact direction, and restraint, will also be held constant. As mentioned, it is important to evaluate the effect these factors have on submarining using a modern restraint system, as much of this research was conducted prior to restraint advancement. Thus, a novel restraint system, incorporating dual lap belt pretensioners which are targeted to mitigate submarining, was used in Chapter 8's parametric study. This restraint system is discussed in Section 3.3.1. Additionally, a semi-rigid seat that is simple to model physically and computationally and is repeatable was used and is also discussed in Section 3.3.1. Finally, only a frontal impact is studied, as this causes forward motion of the pelvis relative to the seat and lap belt, and is thus most relevant to the submarining phenomenon.

After eliminating factors pertaining to occupant sex and anthropometry, crash mode, restraint type, and seat, ten were chosen for further study in this dissertation (Table 2.1). These are discussed in the following sections.

2.4.1 Extrinsic factors

Extrinsic factors pertain to the restraint, vehicle, and crash environment; namely, all factors that do not pertain to the occupant.

2.4.1.1 Lap belt angle

One identified potential extrinsic parameter was fore-aft lap belt angle, or the angle of the lap belt relative to the horizontal, which FMVSS 210 requires to be between 30-75° in U.S. vehicles [51]. A more horizontal lap belt angle fails to provide sufficient downward force to resist upward motion of the belt which occurs prior to submarining and is thus less likely to engage the notch

between the ASIS and the AIIS [2, 8]. Several other studies have hypothesized a more horizontal lap belt will increase likelihood of submarining [2, 8, 46, 52, 53, 54, 55, 56, 57, 58, 59, 60, 61]. A more vertical lap belt angle was predicted to not provide adequate restraint of the torso; however, this hypothesis was geared toward lap belt-only restraints and was developed prior to invention and integration of pretensioners and thus, needs further evaluation [1, 43]. Additionally, the angle of the lap belt relative to the seat structure in the overhead view, or the lateral lap belt angle, was also hypothesized to affect submarining outcome: as the notch between the ASIS and AIIS is a 3D structure, anchorage attachment from both the fore-aft and lateral directions affect restraint interaction [8, 62].

2.4.1.2 Lower extremity support

Support of the lower extremities, through either a knee bolster or toe pan, has been shown to affect submarining, as this affects the inertial force of the lower extremities: unconstrained lower extremities have been linked to rearward pelvis rotation due to the increased inertial force of the lower extremities, thus increasing submarining risk [63, 54, 64]. Details on how a rearward pelvis rotation increases submarining risk is discussed below.

2.4.1.3 Crash severity

While impact speed, or crash severity, has not been explicitly linked to increased risk of submarining, a higher acceleration increases the inertial force of the occupant and subsequent reaction forces of the restraint; risk of abdominal injury, a potential consequence of submarining, increases for a higher crash severity [65].

2.4.1.4 Friction

Frictional forces between the occupant and the seat structure and the lap belt (e.g., due to occupant clothing) have been hypothesized to affect effective lap belt restraint, and subsequent submarining outcome [62, 63, 54].

2.4.2 Intrinsic factors

2.4.2.1 Torso angle

Occupant-related factors include all those directly associated with the occupant. Occupant torso angle has been shown to affect belt-pelvis interaction and subsequent submarining occurrence [1, 44, 43, 46, 20, 36, 57]. Adomeit and Heger [1] defined torso angle as the line connecting the occupant's hip-point (H-point) and shoulder-point (S-point) relative to the positive horizontal (anterior to the occupant). "Unfavorable occupant kinematics" results in the H-point displacing further forward than the S-point (Figure 2.6). These kinematics describe the initial position of an occupant seated in recline. Additionally, a reclined position initially pitches the pelvis rearward relative to the lap belt, which further increases the likelihood of submarining as the lap belt cannot effectively engage the ASIS protuberance during occupant forward excursion [29, 32]. Chapter 3.2 discusses additional details pertaining to submarining risk for reclined occupants. As mentioned in Section 1.1.2, reclined seating is predicted to become more prevalent with the advancement of ADS [22]; however, no experimental data exists to investigate the effect of a reclined posture on submarining. As this posture is predicted to increase submarining likelihood, investigating this effect through experiments is critical.

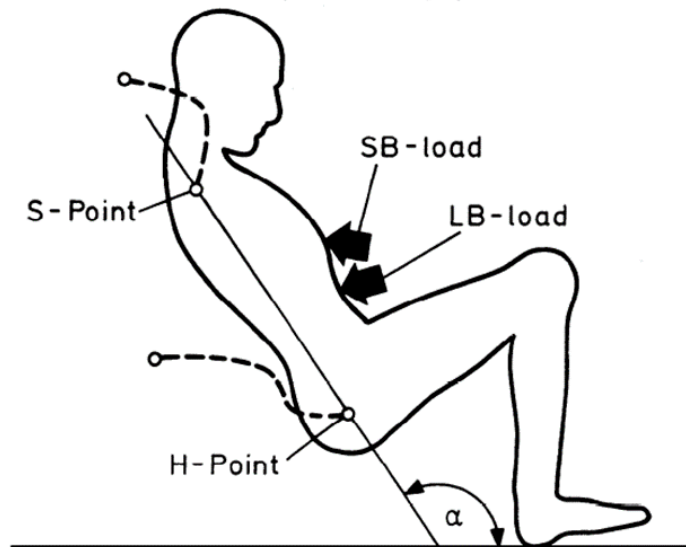


Figure 2.6: Unfavorable occupant kinematics, in which the torso is reclined and the H-Point is anterior to the S-Point [1].

2.4.2.2 Abdominal soft tissue compliance

Another factor is the compliance, or stiffness, of abdominal tissue in the ASIS region, which has been shown to affect belt-pelvis interaction [35, 48, 62, 55]. Soft tissue affects belt engagement with the ASIS due to the material's incompressibility and low shear stiffness, which allows the belt to move over the ASIS more easily than it would without this barrier as a result of the soft tissue's shear deformation. Human adipose tissue has been shown to have a wide range of inter- and intra-subject variability in stiffness under compression and shear loading [66]. A high variability of flesh stiffness response results in variable belt-pelvis interaction and submarining occurrence: preliminary results comparing belt-pelvis motion using varying soft tissue stiffnesses show this influences submarining outcome [48]. A higher shear stiffness of abdominal soft tissue may prevent upward lap belt migration relative to the pelvis, while a lower stiffness may promote submarining.

2.4.2.3 Computational human body models

Additionally, different computational HBMs have been shown to vary in belt-pelvis kinematic and kinetic responses. Most HBMs have been developed to study overall occupant responses in severe crashes and loads on the skeletal structure, with less focus on the detailed mechanism of belt-flesh interaction [67]. The Global Human Body Models Consortium HBM (obese GHBM version 4.4) was evaluated against the belt pull experiments of Kim et al. [68] and was unable to replicate the submarining exhibited by the PMHS due to the tissue's over-stiff response in shear, which restricted the belt from translating superiorly over the pelvis [35]. The Total HUMAN Model for Safety HBM (THUMS) flesh material model is also limited, since the model was calibrated against experimental tests that did not include shear loading of the soft tissue [50]. In order to utilize the HBM as a tool to evaluate how parameters affect submarining, a comparison of HBM and PMHS submarining sensitivities and subsequent evaluation of the HBM's ability to capture the submarining mechanism is critical.

2.5 Discussion

One way to graphically illustrate the critical time prior to possible submarining occurrence (shown in Figure 2.5) in addition to summarizing the factors outlined in Sections 2.4.1 and 2.4.2, is through a free body diagram which illustrates the belt-pelvis geometry as well as the applied

CHAPTER 2. HYPOTHESIZED FACTORS AFFECTING SUBMARINING OCCURRENCE: A REVIEW

forces, moments, and resulting reactions for a given occupant (Figure 2.6). Submarining can result when the restraining forces acting on the pelvis are not in equilibrium, resulting in a rearward pelvis rotation and/or an upward translation of the belt relative to the ASIS. The components and features of this diagram and their associated dependencies are defined in Table 2.2.

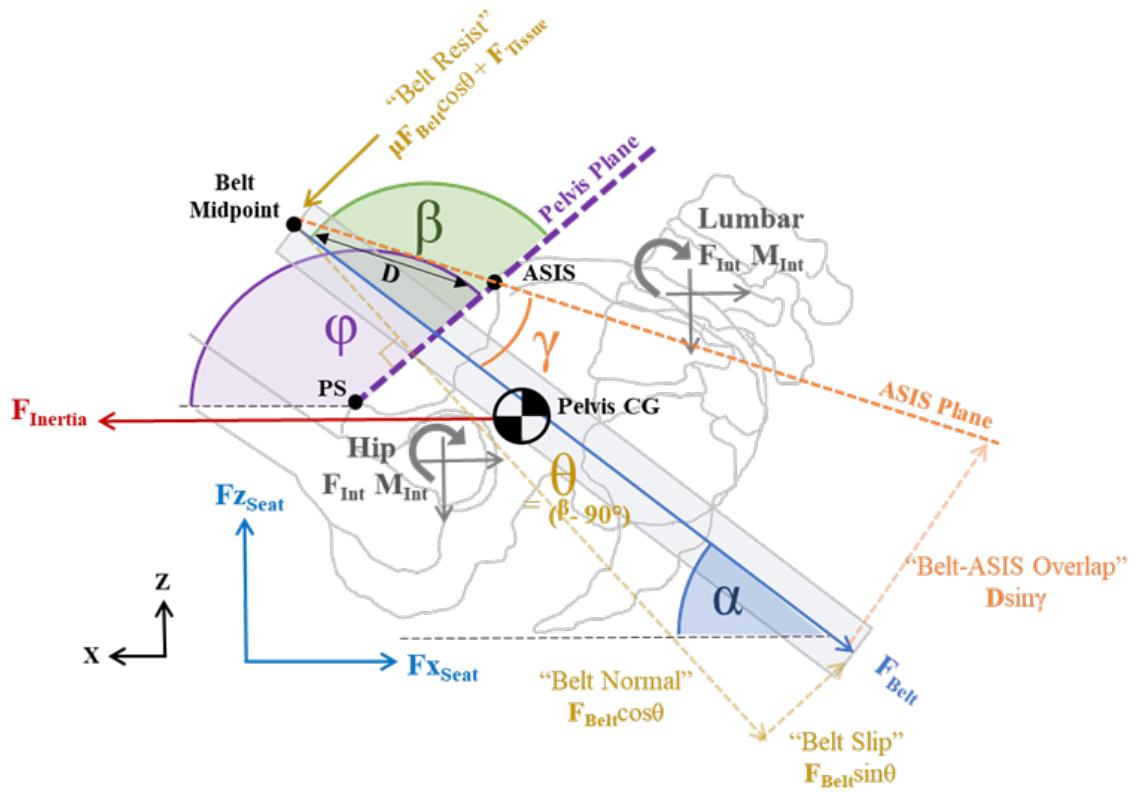


Figure 2.7: Free body diagram of the pelvis, illustrating lap belt-pelvis interaction. (Adapted from [2, 69, 70, 71])

Table 2.2: Definitions for terms shown in free body diagram of Figure 2.7.

Metric	Definition	Dependencies
ASIS	Anterior Superior Iliac Spines	NA (see Belt-ASIS Distance)
PS	Pubic Symphysis	NA
Belt Midpoint	Midpoint (length- and width-wise) of lap belt	NA (see Belt-ASIS Distance)
Pelvis Plane	Orientation of pelvis, defined along the Nyquist plane	<ul style="list-style-type: none"> Occupant (Lumbar Internal Forces and Moment) Occupant torso angle
$F_{Inertia}$	Inertial force	<ul style="list-style-type: none"> Crash severity (ΔV) Impact direction Lower extremity constraint Occupant mass
F_{Seat}	Seat force	<ul style="list-style-type: none"> Seat pan angle Seat stiffness Seat/occupant friction
F_{Belt}	Belt tension	<ul style="list-style-type: none"> $F_{Inertia}$, $F_{X_{Seat}}$ ($F_{Inertia} - F_{X_{Seat}}$) Restraint technology
α	Lap belt angle	<ul style="list-style-type: none"> Lap belt geometry
φ	Pelvis angle	<ul style="list-style-type: none"> Pelvis orientation
β	Angle of lap belt relative to angle of pelvis: connecting the belt midline and the Pelvis Plane	<ul style="list-style-type: none"> α φ
θ	Angle of lap belt relative to angle of pelvis: connecting the belt midline and normal component of F_{Belt} w.r.t. the Pelvis Plane	<ul style="list-style-type: none"> α φ β
γ	Angle of lap belt relative to ASIS segment (measured between the lap belt midpoint and the ASIS)	<ul style="list-style-type: none"> α φ
“Belt Normal” Force	Normal component of F_{Belt} w.r.t. the Pelvis Plane	<ul style="list-style-type: none"> F_{Belt} θ
“Belt Slip” Force	Tangent component of F_{Belt} w.r.t. the Pelvis Plane	<ul style="list-style-type: none"> F_{Belt} θ
“Belt Resist” Force	“Friction” force preventing belt from translating over ASIS combined with the force resulting from the stiffness of the abdominal soft tissue	<ul style="list-style-type: none"> F_{Belt} θ Belt/occupant friction Abdominal soft tissue shear stiffness
“Belt-ASIS Overlap”	Measure of an effective interaction of the lap belt force with the anterior edge of the pelvis	<ul style="list-style-type: none"> D γ
D	Distance of lap belt midpoint relative to ASIS	<ul style="list-style-type: none"> θ Lap belt placement Occupant abdominal soft tissue curvature and depth
Lumbar and Hip F_{int} , M_{int}	Lumbar and hip internal forces and moments	<ul style="list-style-type: none"> Occupant (i.e., lumbar stiffness)

Seat pan angle and compliance, combined with the inertial force and lumbar spine compliance, will affect resulting pelvis kinematics as these forces act above and below the pelvis center of gravity. A more compliant seat pan (smaller F_{Seat}) and/or a more compliant lumbar spine (smaller My_{Lumbar}) relative to the magnitude of the lap belt force (F_{Belt}) will promote rearward pelvis rotation, which increases submarining likelihood.

As mentioned, the lap belt angle relative to the horizontal has been predicted to affect submarining, where a more horizontal lap belt angle increases submarining likelihood. Similarly, the angle of the lap belt relative to the pelvis (angles α and β , Figure 2.7) will also dictate submarining occurrence. A large angle θ , indicating a large angle between the normal component of the belt tension (“Belt Normal”) and the pelvis (or “Pelvis Plane”), will increase the “Belt Slip” force, which promotes upward translation of the lap belt. If this force is larger than the opposing “Belt Resist” force, upward translation of the belt occurs. This “Belt Resist” force is affected by belt-occupant friction in addition to the shear stiffness of the abdominal soft tissue.

Additionally, initial lap belt placement relative to the ASIS (“Belt-ASIS Overlap”) affects submarining likelihood, as a belt located more superior to the ASIS will have a lesser likelihood of engaging the ASIS during occupant forward excursion. The “Belt-ASIS Overlap” is likewise affected by abdominal soft tissue depth - an occupant of higher BMI is typically associated with larger abdominal soft tissue depth, which places the belt further anterior and superior relative to the ASIS (larger D and γ , Figure 2.7). This unfavorable position decreases the likelihood of sufficient belt-pelvis engagement, meaning occupants with a higher BMI are generally at a higher risk of submarining [72, 73].

2.6 Conclusions

The following conclusions were drawn from this chapter’s analysis:

1. Several factors, and their associated relationships, were identified from this literature review (Table 2.1). Of these factors, ten were selected for further study in the remainder of this dissertation, as these factors were deemed the most critical and useful for the automotive safety researchers to determine how they affect lap belt-pelvis interaction. These factors included: crash severity, fore-aft lap belt angle, overhead lap belt angle, occupant-to-seat friction, occupant-to-belt friction, HBM type, torso angle, recline angle, pelvis angle, and pelvic-abdominal soft tissue stiffness. Narrowing down to these factors also allowed for a

CHAPTER 2. HYPOTHESIZED FACTORS AFFECTING SUBMARINING OCCURRENCE: A REVIEW

more controlled sensitivity study that was feasible to accomplish using computational HBMs.

2. Much of the research behind the identification of these factors took place prior to the advancement of restraint systems. As restraint systems which play a key role in occupant kinematics and associated occupant-restraint interaction, understanding how these factors affect submarining using a modern restraint system is still required.
3. No experimental PMHS data exists to investigate the influence of a reclined seating posture on lap belt-pelvis interaction and submarining occurrence and to evaluate the HBM's response relative to the PMHS data. These tests were conducted, and the methodology and results are described in Chapter 3. The HBMs were then evaluated relative to the experiments, which is described in Chapter 4.

Chapter 3

The Effect of a Reclined Posture on Lap Belt-Pelvis Interaction

3.1 Executive Summary

3.1.1 Relevance and Goal

In Chapter 2, the comprehensive literature review identified occupant posture, namely, torso angle, as a potential factor that could affect lap belt-pelvis interaction and submarining occurrence. Prior to this dissertation, no reclined occupant kinematic data existed with which to investigate reclined occupant kinematics, particularly lap belt-pelvis interaction. Further, while computational HBMs have been evaluated in a reclined posture [33, 34], it was unclear whether the kinematic and kinetic responses predicted by the HBMs could be trusted as the models were not validated. Thus, this chapter aims to evaluate the kinematic and kinetic responses of reclined PMHS in a frontal impact through dynamic sled tests. An additional goal was to generate kinematic and kinetic data of the PMHS responses for HBM comparison and evaluation in chapter 4. These experiments utilized a modern restraint system and both the PMHS and surrounding environment were instrumented to acquire detailed measurement of occupant kinematics, restraint interaction, and boundary condition loading.

3.1.2 Key Conclusions

The full list of conclusions can be found in Section 3.6 below. In summary, the five PMHS exhibited variation in lumbar spine and pelvis kinematics which dictated injury and submarining

CHAPTER 3. THE EFFECT OF A RECLINED POSTURE ON LAP BELT-PELVIS INTERACTION

outcomes. One of five subjects submarined and exhibited the largest lap belt-pelvis angle (angle β from Figure 2.7) at the time of submarining onset despite having an initial pelvis and lap belt orientation within the range of the other subjects (Table 3.1). All subjects exhibited combined compression and flexion of the lumbar spine during forward torso excursion, though the initial lumbar spine kinematics (prior to peak pelvis forward displacement) varied based on each subject's initial lumbar spine curvature, orientation, and compliance, as well as initial pelvis orientation and kinematics. These initial kinematics dictated lumbar spine injury outcomes. Finally, in addition to other factors, initial lap belt placement may have contributed to the direction of pelvis rotation, which varied among subjects.

Table 3.1: Initial pelvis and lap belt orientations and lap belt-pelvis angle at the time of Subject 5's submarining (55ms). The lap belt-pelvis angle is measured as angle β from Figure 2.7 and is also described in Figure 3.5

Subject No.	Pelvis Angle (deg)	Inboard Lap Belt Angle (deg)	Lap Belt-Pelvis Angle - Initial	Lap Belt-Pelvis Angle – Time of Sub
1	165	57	108	116
2	179	64	115	117
3	168	56	112	NA
4	160	66	94	112
5	170	62	108	124

The biggest difference between the submarining subject and the non-submarining subjects was the lap belt-pelvis angle at the time of submarining, where the submarining subject exhibited the largest angle. As a result, this parameter was explored through experiments and simulations in Chapters 5 and 6. Evaluating the ability of the HBMs to replicate fundamental mechanisms exhibited by the PMHS pertaining to lumbar spine compliance and lap belt-pelvis interaction was conducted in Chapter 4.

3.1.3 Contributions

This work produced the first dataset of mid-sized male PMHS responses to frontal impact in a reclined environment, with the first ever analysis of lumbar spine kinematics, lap belt-pelvis interaction, and submarining resulting from this posture. Additionally, several sources of kinematic

CHAPTER 3. THE EFFECT OF A RECLINED POSTURE ON LAP BELT-PELVIS INTERACTION

and kinetic data were generated from the PMHS responses, which can be used for evaluation of computational HBMs, physical anthropomorphic test devices (ATDs, or crash test dummies), and PMHS of other sex and anthropometry.

3.1.4 Publications

The detailed methods and results of these experiments were published in the open literature. While the complete methods and results are described in these publications, the details deemed most critical to this dissertation were included in this chapter.

Richardson R, Donlon J-P, Jayathirtha M, Forman J, Shaw G, Gepner B, Kerrigan J, Ostling M, Mroz K, Pipkorn B. (2020). Kinematic and Injury Response of Reclined PMHS in Frontal Impacts. *Stapp Car Crash Journal*, 64, 85-153.

Richardson, R., Jayathirtha, M., Chastain, K., Donlon, J. P., Forman, J., Gepner, B., ... & Kerrigan, J. (2020). Thoracolumbar spine kinematics and injuries in frontal impacts with reclined occupants. *Traffic injury prevention*, 21(sup1), S66-S71.

Richardson R, Jayathirtha M, Donlon JP, Forman JL, Gepner B, Ostling M, Mroz K, Pipkorn B, Kerrigan JR. (2020). Pelvis Kinematics and Injuries of Reclined Occupants in Frontal Impacts. *Proceedings of the 2020 IRCOBI Conference*, IRC-20-60 (499-515).

Richardson, R., Donlon, J. P., Chastain, K., Shaw, G., Forman, J., Sochor, S., ... & Pipkorn, B. (2019). Test methodology for evaluating the reclined seating environment with human surrogates. *In Proceedings of the 26th International Technical Conference on the Enhanced Safety of Vehicles, ESV*, Eindhoven, Netherlands, 10th June–13th June.

3.2 Introduction

In Chapter 2, a comprehensive literature review found a reclined torso angle to be a potential factor that affects occupant lap belt-pelvis interaction and submarining occurrence. Crashes with reclined occupants are relatively rare but can have severe consequences. Only 0.3% of occupants in NASS-CDS frontal crashes (1995-2005) were fully reclined, however these occupants had a 77% higher fatality rate than occupants seated in upright or partially reclined postures (Dissanaike et al., 2008). A similar incidence (0.1%) of belted reclined occupants was found in more recent crashes (2000-2015), with a 21% greater risk of MAIS 2+ and a 69% greater risk of MAIS 3+ injuries. (McMurry et al., 2018).

CHAPTER 3. THE EFFECT OF A RECLINED POSTURE ON LAP BELT-PELVIS INTERACTION

The absence of evidence for reclined occupants in car crashes does not demonstrate that there is evidence of absence: in NASS-CDS, pre-crash occupant posture is assessed based on the crash investigator's vehicle inspection, and supported by occupant interviews; in many cases, this variable is not recorded during crash investigations. For instance, in the aforementioned studies, cases that had an occupant posture left unrecorded made up 24% and 17.6% of the total, respectively. Further, non-traditional seating postures (e.g., not seated upright and/or not facing forward) are predicted to increase with the introduction of highly automated or "self-driving" vehicles. The self-driving technology of these vehicles may liberate the driver from controlling the vehicle. A reclined seating position in particular is predicted to become more prevalent with the introduction of highly automated or "self-driving" vehicles [23, 24].

The limited field data on reclined occupants in frontal crashes suggests that unfavorable seatbelt engagement may contribute to the increased risk of injury and fatality [17, 18]. Indeed, in 1988, the National Transportation Safety Board (NTSB) conducted a study on the danger of reclined seats, stating that the protection offered by a three-point pillar-mounted seat belt is compromised when the seat is reclined, presenting a "potentially dangerous combination in a moving vehicle" [21]. In particular, a reclined posture may increase the risk of submarining. Likewise, computational simulations predict unfavorable occupant kinematics, including both submarining and the combined loading of the lumbar spine in compression and flexion, due to seatback recline angle and altered seatbelt loading paths [36, 20].

Several vehicle design countermeasures have been investigated to mitigate submarining, including the use of a seat-pan airbag, knee bolster, and a combination pretensioners and force limiting retractors [29, 74, 75]. However, with the introduction of Level 3 Automated Driving Systems (ADS), prototype interior vehicle environment setups show front-seat occupants positioned away from the knee bolster and airbag, toward the rear of the vehicle [22]. This position increases the reliance of restraint on the seat and seatbelt. The addition of pretensioners to the seat belts has been shown to tie the occupant to the deceleration of the car early in an accident, which will reduce the peak load experienced by the occupant by more than 20% [45]. Additionally, novel restraint systems that include dual lap belt pretensioners have been investigated [34, 46, 36]. Sled tests conducted on the reclined THOR anthropomorphic test device (ATD) compared the effectiveness of different restraint systems on occupant submarining [46]. It was shown that, in comparison to tests run using a restraint system with either solely a retractor pretensioner or both a retractor pretensioner and a single lap belt pretensioner (both of which resulted in occupant submarining), a restraint system that integrated dual lap belt pretensioners resulted in no submarining. Similarly, reclined

HBM simulations show a restraint system with dual lap belt pretensioning mitigated submarining in the GHBMC-OS M50 model (v.1.8.4), THUMS SAFER AM50 model (v9), and THUMS AM50 model (v5) [34], even in the absence of a knee bolster. In contrast, the GHBMC-O M50 model (v4.5) resulted in submarining [34].

Previous simulation studies comparing different HBMs have observed important differences in lumbar kinematics and pelvis engagement in a reclined seating posture [34]. Further, no validation dataset exists to verify HBMs in a reclined seating configuration. Therefore, post-mortem human subject (PMHS) reference data was needed to not only serve as a basis for model evaluation and improvement, but to investigate the predicted risks associated with this posture. Further, the restraint system's effectiveness in mitigating submarining in PMHS must be evaluated, as it has shown proven effectiveness in submarining mitigation for ATDs and HBMs.

The goal of this study was to describe the response of mid-sized male PMHS in a reclined seating environment by generating kinematic response and kinetic boundary condition data captured during the tests. This data was used for HBM validation in Chapter 4. Additionally, injury outcomes and analyses resulting from this study are reported.

3.3 Material and Methods

3.3.1 Test Environment

The tests were performed on a Seattle Safety (Kent, WA) 1.4 MN ServoSled® (Figure 3.1a). A 35-g ($\Delta V = 50$ km/h) pulse was used, which has been used in previous sled tests to assess PMHS submarining [76] (Figure 3.2).

3.3.1.1 Semi-rigid seat

The subjects were seated on a semi-rigid seat designed to reproduce the behavior of a real vehicle seat, in a front passenger configuration (Figure 3.3). This semi-rigid seat has been used in previous PMHS studies [76, 77] and consists of both a seat pan and an anti-submarining ramp, each of which individually articulate as a function of the stiffness and position of corresponding springs. The orientations of the seat pan and anti-submarining pan were set to 15° and 30° , respectively; the same orientation has been used in previous sled tests [76, 77]. The maximum allowable seat pan deflection was set to 50 mm. The stiffness of the springs was tuned to that of a real frontal vehicle seat; the same stiffness has been used in previous sled tests [76, 77].

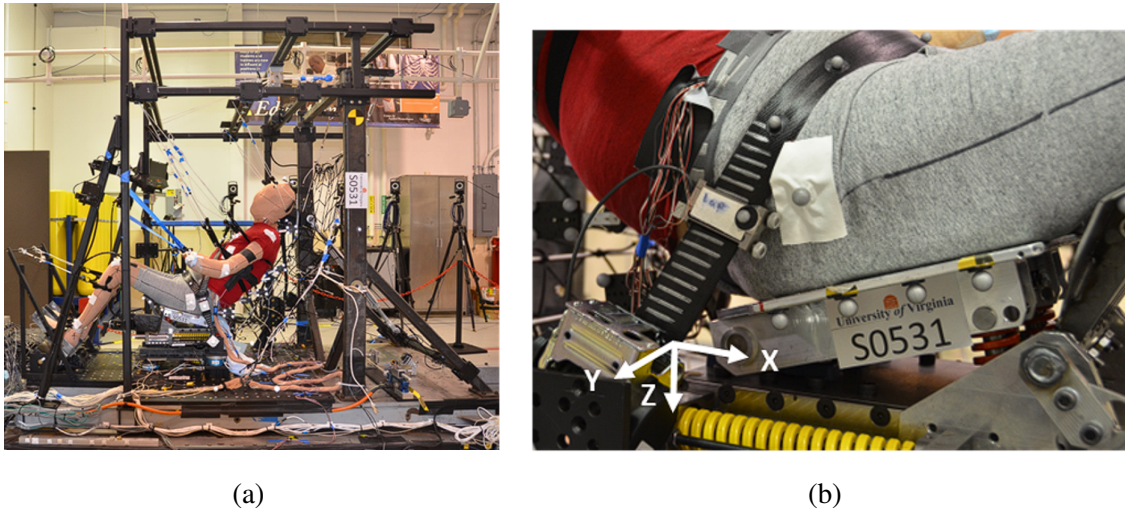


Figure 3.1: (a) Sled fixture and (b) buck coordinate system.

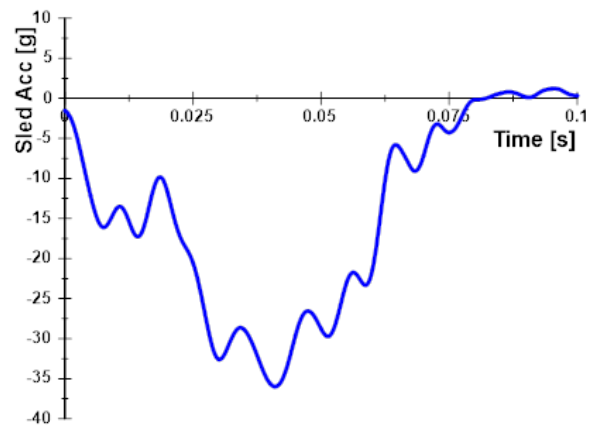
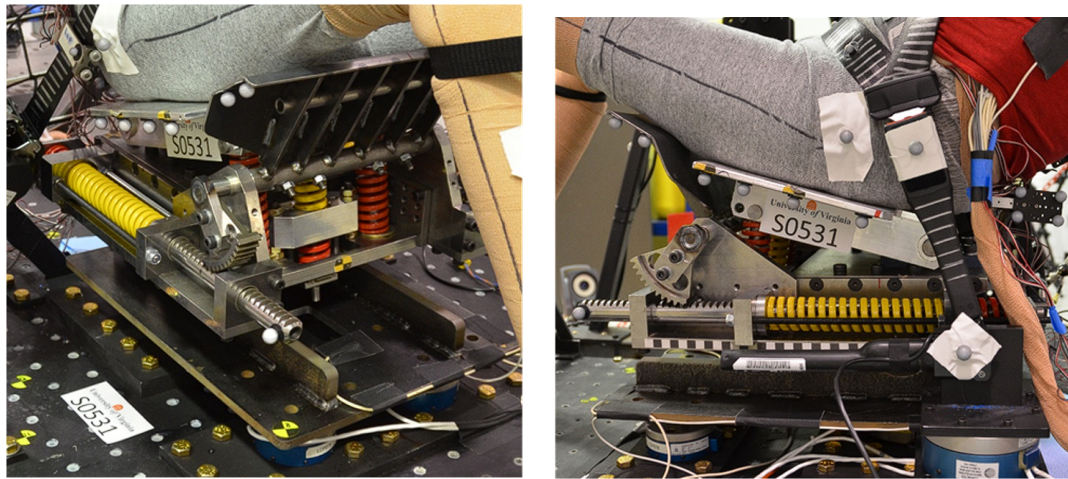


Figure 3.2: Acceleration pulse used in this test series (CFC 60).

A simplified seatback supported the subjects while permitting visibility of posterior motion-capture instrumentation [78]. The simplified seatback consisted of support straps behind the head, upper torso, and lower torso (Figure 3.1a). The straps were released by a pyrotechnic mechanism at the start of the test.



(a)

(b)

Figure 3.3: (a) Oblique view of the semi-rigid seat in the experimental test setup. (b) Lateral view of the semi-rigid seat.

3.3.1.2 Restraint system

The seatbelt concept was developed to reduce the risk of submarining in reclined seating [46]. The subjects were restrained by a seat-integrated three-point belt equipped with dual lap belt pretensioners, and a shoulder belt pretensioner and shoulder belt load limiter of 3.5 kN (constant force). The inboard lap belt pretensioner, located at the buckle, activated at 3 ms. The outboard lap belt pretensioner, located within the outboard retractor, as well as the shoulder-belt retractor pretensioner, simultaneously fired at 10 ms. The belt system also included a crash locking tongue that mitigated webbing transfer from shoulder-belt to lap belt. The D-ring in each test was positioned to approximate the position of a seatback-integrated D-ring. The lap belt was positioned by routing it anterior to the subject's ASIS landmarks, which were estimated by palpation.

3.3.1.3 External instrumentation and data acquisition

The tests were recorded using several off-board and on-board high-speed cameras. Additional single 3D tracking markers were located on the seat pan and anti-submarining ramp, seat-belt webbing, seat-belt D-ring (positioned to mimic a belt-integrated seat), and lap belt anchorage locations. The seat-belt webbing was instrumented with two tension gauges located at the upper shoulder-belt between the subject's shoulder and the D-ring, and at the lap belt between the subject's right hip and the lap belt anchor. Load cells were installed beneath the seat, buckle, and toe pan.

3.3.2 PMHS Selection

Five male PMHS were tested (Table 3.2). The specimens were selected targeting the 50th percentile male; Subject 2 (test 530) was of lighter mass but similar stature of a mid-sized male. All tissue donation, testing, and handling procedures were approved by the University of Virginia Institutional Review Board – Human Surrogate Use (IRB-HSU) Committee. The subjects were preserved by freezing and confirmed free of infectious diseases including HIV and Hepatitis B and C. Full body Computed Tomography (CT) scans were taken of each subject prior to testing to confirm the absence of bony trauma. Dual-energy X-ray absorptiometry (DXA) was performed to assess bone quality. All subjects' upper extremities were amputated mid-forearm bilaterally to allow for full visibility of the occupant's lap belt and pelvis during the forward excursion.

Table 3.2: Specimen data for the five male PMHS used in the sled tests.

Subject No.	Age	BMD (g/cm ²); Bone Quality	Cause of Death	Weight [kg]	Stature [cm]
1	66	1.065; Osteopenia	Dementia	74	175
2	53	1.357; Normal	Glioblastoma	57	175
3	72	1.133; Osteopenia	Sepsis	74	185
4	25	1.221; Normal	Gun-shot wound to head	75	174
5	55	1.009; Osteopenia	Myocardial infarction	74	180

3.3.3 PMHS Instrumentation

A 3D tracking array was mounted to the head, T1, T8, T11, L1 (in Subjects 1, 2, and 3), L3, pelvis, and sternum (Figure 3.4b). Multiple 3D tracking markers were located on the surface of the thorax, shoulders, upper and lower limbs. Pressure transducers were inserted in the intervertebral discs targeting three locations: T12/L1, L2/L3, and L4/L5 (Richardson et al., 2020b). Strain gauge rosettes were affixed to the lateral aspect of the left and right iliac wings (two rosettes per wing) (Richardson et al., 2020a).

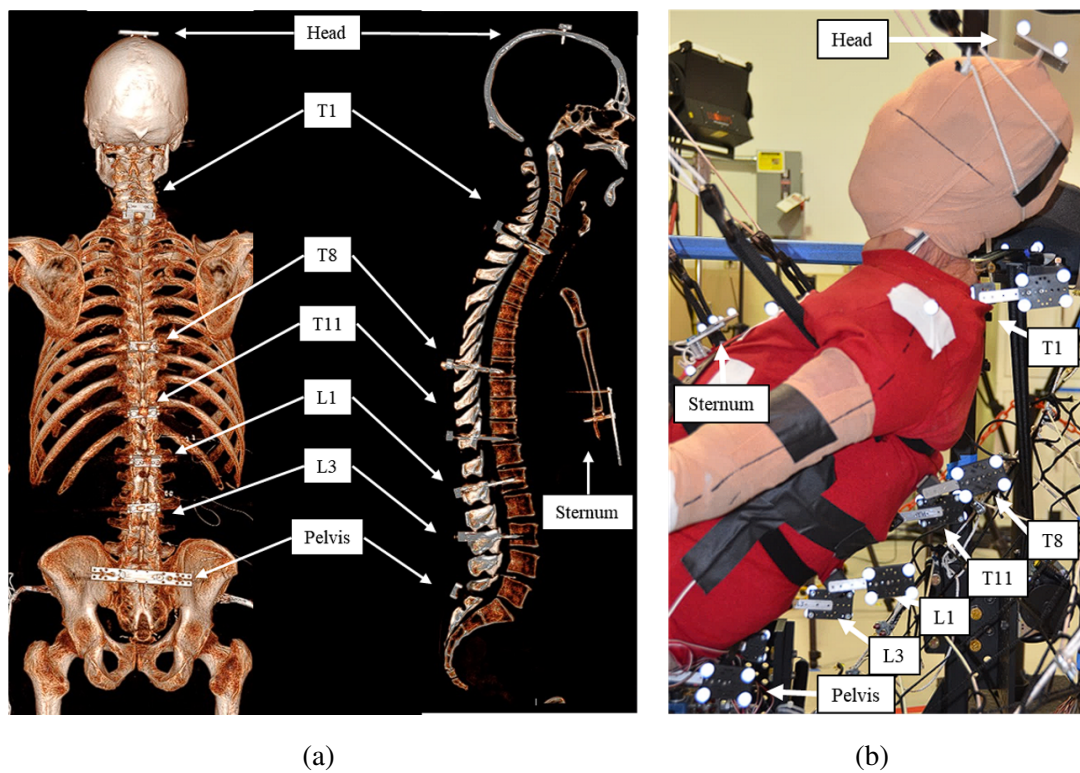


Figure 3.4: (a) Pre-test CT showing the installation locations for the motion-tracking hardware. (b) Motion-tracking arrays rigidly affixed to the internal hardware at several locations on the specimen.

3.3.4 PMHS Positioning

The subjects were seated in a simulated right front passenger position with the feet fully constrained (Richardson et al., 2019). The subjects were reclined to a torso angle of approximately 50° relative to the vertical by measuring the angle between the segment connecting the H-point to the acromion and the vertical in the sagittal plane. The initial positions of the local coordinate

systems for each of the body segments that were tracked with 3D motion tracking are tabulated in Table B.1.

3.3.4.1 Initial lumbar spine and pelvis orientation

The pelvis angle was not controlled but rather dictated by both the torso recline angle and the subject's natural lumbar orientation and curvature. The pelvis angle was defined as the angle between the segment connecting the midpoint of the left and right ASIS and the center of the pubic symphysis (PS) relative to the horizontal axis (X-axis) in the sagittal plane, referred to as the "Nyquist angle" in the literature [79] (Figure 3.5). A typical upright occupant's seated pelvis (Nyquist) angle is generally just greater than 90° , and a greater pelvis angle corresponds to a reclined, rearward-rotated pelvis [52]. The lap belt angle was defined as the angle between the segment connecting the anchorage point and the approximate center of the lap belt relative to the horizontal in the sagittal plane. The belt-pelvis angle was defined as the difference between these angles (pelvis angle – lap belt-pelvis angle) (same as angle β , Figure 2.7).

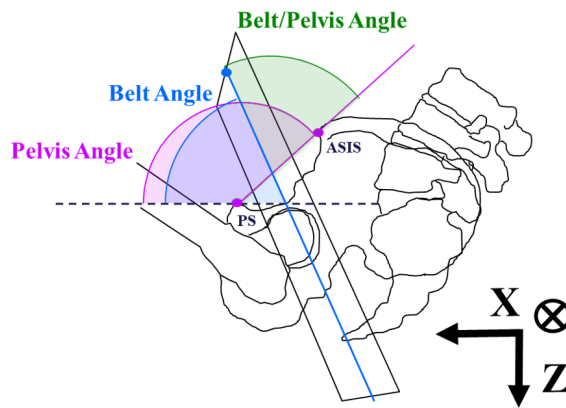


Figure 3.5: Belt-pelvis angle definition.

Initial orientations of the bony local coordinate systems relative to the crash direction were calculated using reconstructed CT scans from each subject (Figure 3.6). This provided a detailed representation of the vertebral and pelvic alignment in their pre-test position using each subject's specific bony geometry measured in the global coordinate system.

Subject 1's lumbar spine exhibited an initial lordotic curvature (lumbar extension): T11 was pitched 7° upward relative to L3 (Figure 3.6). In contrast, Subjects 2, 3, and 5 exhibited initial lumbar flexion, indicated by a downward pitch of T11 toward L3 (11° average). Subject 4 exhibited

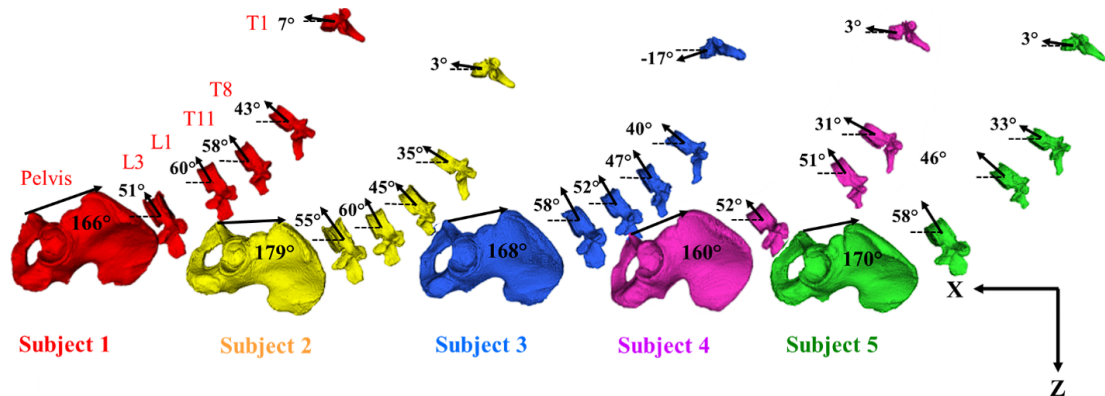


Figure 3.6: Initial position of the five subjects from the five tests. The labelled angles show the initial pitch angle (rotation about the y-axis) of the measured bones in the spinal column, where the solid arrows indicate the initial orientation of the x-axis for each vertebral body’s local coordinate system. The pelvis angle is measured as the Nyquist angle.

minimal initial relative rotation between T11 and L3, indicating a neutral lumbar alignment (neither flexed nor extended).

The subjects exhibited initial pelvis (Nyquist) angles from 160-179° with Subjects 2 and 5 pitched most rearward (179° and 170°) and Subject 4 pitched most forward (160°) (Figure 3.6). The initial pelvis angles of all subjects were found to lie within the standard deviation developed from data on volunteers [80].

3.3.4.2 Initial lap belt positioning

Initial lap-belt angles (defined in Figure 3.5) were 56-66° (inboard) and 60-74° (outboard) (Table 3.3) and were measured using 3D motion tracking. The buckle was initially positioned more rearward than the outboard anchorage point, which resulted in a smaller angle at the inboard side.

Table 3.3: Initial lap belt angles.

Subject	Inboard Belt Angle (deg)	Outboard Belt Angle (deg)
1	57	65
2	64	74
3	56	60
4	66	71
5	62	66

The subjects' abdominal tissue curvature and pelvic orientation dictated the natural placement of the lap belt relative to the pelvis (Figure 3.7). In this figure, the solid black line connects the motion-capture markers placed in the center (width-wise) of the lap-belt. The dashed line approximates the edges of the lap-belt. The grey pelvis outline represents each subject's corresponding pelvis, reconstructed from the subject's CT-scan. Subjects 1, 2, and 3 had initial low lap belt placements, where the lap belt center is closer to the pubic symphysis. In contrast, Subjects 4 and 5 show higher initial lap belt placements, where the lap belt center was closer to the ASIS and the webbing is also further up the pelvis. While all subjects exhibit slight asymmetry in lap belt placement, wherein the inboard side (right column) is initially positioned higher relative to the pelvis than the outboard side (left column), this is exaggerated for Subject 5. On the inboard side, this Subject's lap belt webbing is just below the ASIS.

3.3.5 Data Analysis

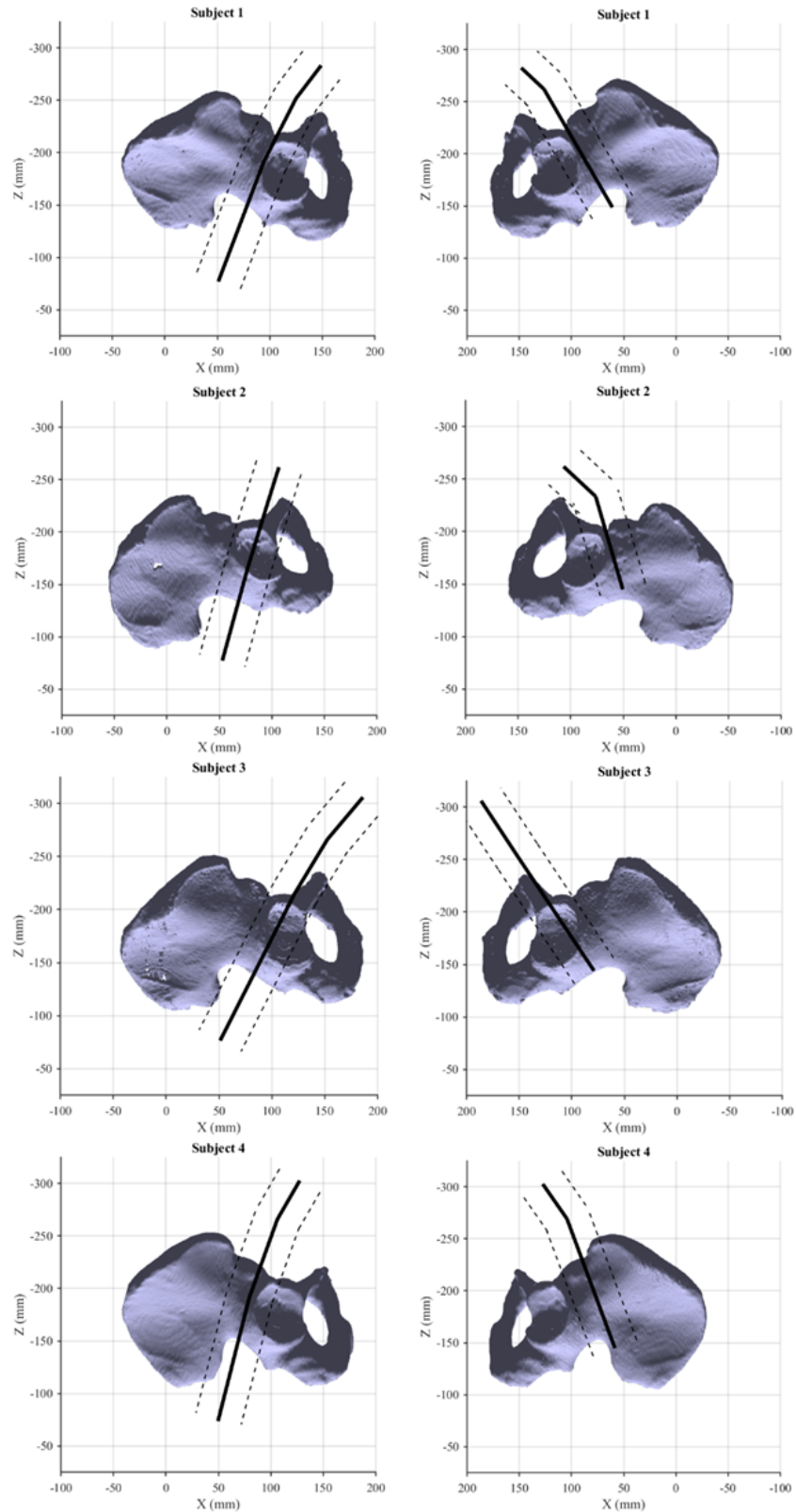
3.3.5.1 Motion-capture data

The motions of local coordinate systems (Figure 3.8) defined on the head, vertebrae, and pelvis were calculated relative to the global coordinate system defined on the buck (Figure 3.1b) using pre-test CT scans, hardware schematics, and digitization of hardware assemblies (Shaw et al., 2009). Thus, a positive X-value indicates a forward motion; a positive Y-value indicates motion towards the occupant's right; and a positive Z-value indicates a downward motion.

3.3.5.2 Restraint Instrumentation

Uniaxial belt tension gauges were installed both on the shoulder belt, between the subject's shoulder and the D-ring, and on the lap belt, between the subject's right hip and the outboard

CHAPTER 3. THE EFFECT OF A RECLINED POSTURE ON LAP BELT-PELVIS INTERACTION



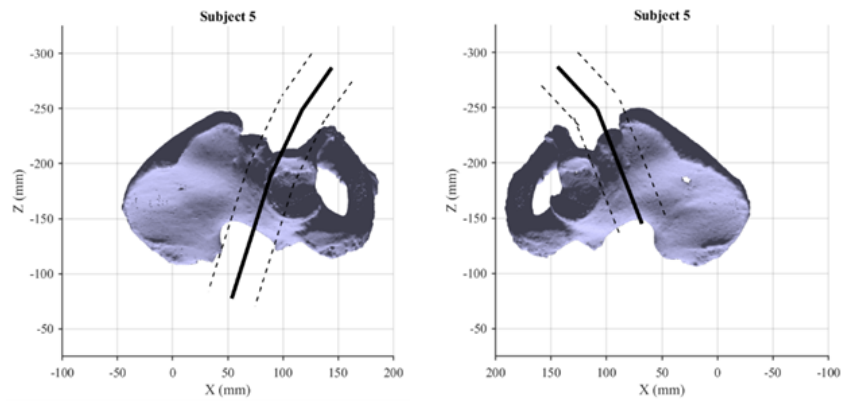


Figure 3.7: Initial position of the pelvis and lap-belt in the buck coordinate system, viewed from the outboard (left column) and inboard (right column) sagittal planes.

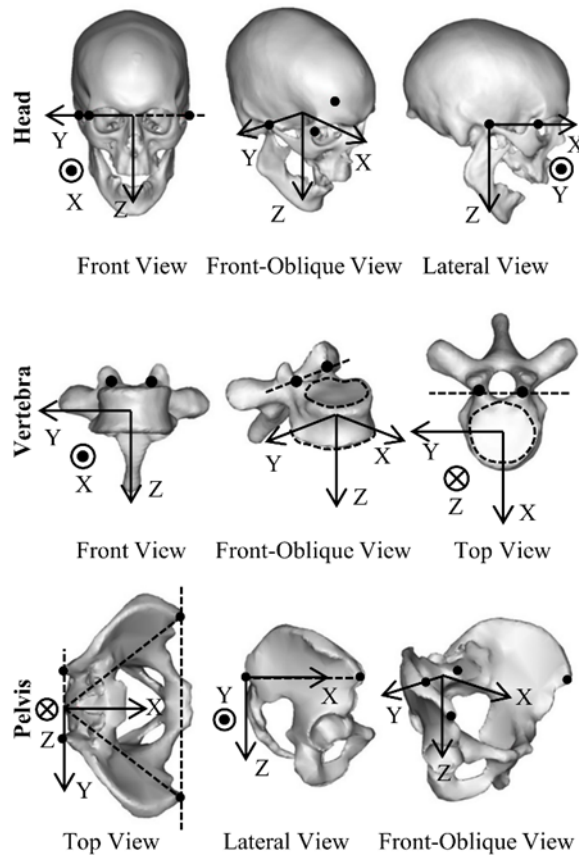


Figure 3.8: Definition of local coordinate systems on the head, vertebra, and pelvis, each defined by the corresponding bone's anatomic landmarks.

retractor. A six-axis load cell was installed beneath the buckle on the subject's inboard side.

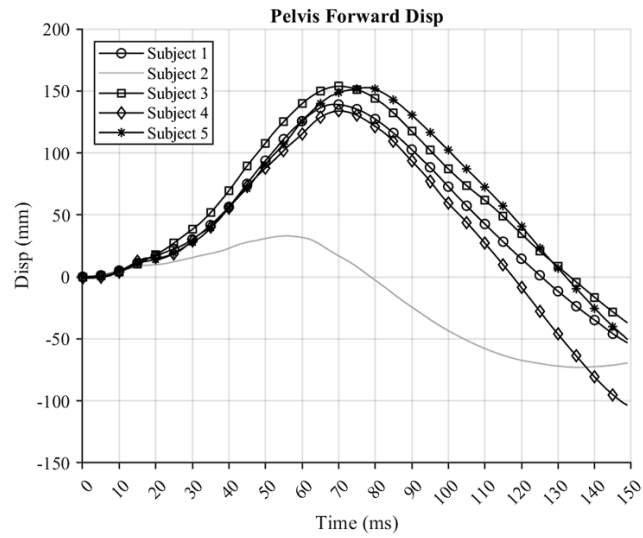
3.4 Results

The resulting kinematic measurements of the five reclined PMHS show a biphasic response of the occupant's pelvis and upper torso. The sequence of kinematics occurred in the following order: (i) pelvis initial forward displacement (5-7ms, pelvis X-dir), (ii) upper torso initial forward pitch (17-47ms, T8 Z-dir), (iii) pelvis peak forward displacement followed by pelvis rebound (57-76ms, pelvis X-dir), (iv) upper torso peak forward displacement followed by upper torso rebound (104-115ms, head X-dir). The times of maximum force in the lap belt, shoulder belt, and seat occurred consistently across all five subjects. Maximum lap belt force and seat forces occurred near the time of maximum forward pelvis displacement (57-76ms). Maximum shoulder belt force occurred near the time of maximum forward torso (T1) displacement (97-109ms) and remained near the nominal force-limit value (3.5-3.8kN actual vs. 3.5kN nominal). The kinematic and kinetic measurements from the test with the lighter mass Subject 2 were smaller in magnitude compared to the four midsized subjects.

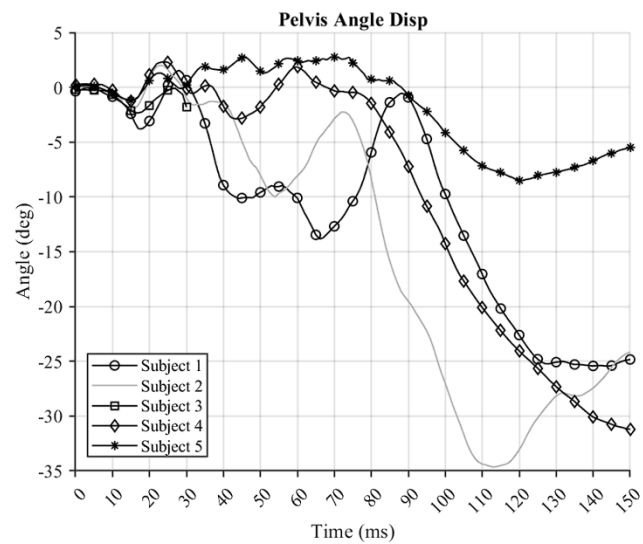
Injuries to the sacrum/coccyx, iliac wing, lumbar spine, and ribcage were identified in post-test dissections [81, 82]. No injuries to the head, extremities, and viscera were observed. No injuries to the integumentary system were observed, apart from abrasions attributable to the seatbelt at the ASIS and clavicle.

3.4.1 Pelvis Kinematics and Injury

The four midsize subjects showed consistent pelvis forward displacement with an average maximum of 148mm, which occurred between 70ms (Subject 1) and 77ms (Subject 5) (Figure 3.9a). The magnitude of pelvis forward displacement is similar to sled tests conducted at 56 km/h with a pelvic-restraint cushion (100-133 mm) [74]. Similar to the dual lap belt pretensioners, which has been shown to mitigate submarining in four of the five tests, the pelvic-restraint cushion has been proposed as an avenue for mitigating submarining in the reclined position [46]. In previous tests that did not use a pelvis-restraint cushion or double lap belt pretensioning, the pelvis reached a higher magnitude of displacement (200-300 mm) [74, 76]. Subject 2 of lighter mass exhibited a peak pelvis displacement of 33mm at 58ms. In all tests, the pelvis rotated forward (negative direction, per Figure 3 5) except Subject 5 which exhibited a rearward rotation of 2-3° (Figure 3.9b).



(a)



(b)

Figure 3.9: Pelvis kinematics of the five PMHS: (a) forward (X-) displacement, (b) angular displacement. A negative pelvis angle indicates a forward pelvis rotation.

CHAPTER 3. THE EFFECT OF A RECLINED POSTURE ON LAP BELT-PELVIS INTERACTION

Subject 5 submarined at the inboard (buckle) side (left iliac wing) at approximately 55ms. High-speed video was focused on Subject 5's pelvis during the submarining event (Figure 3.10).

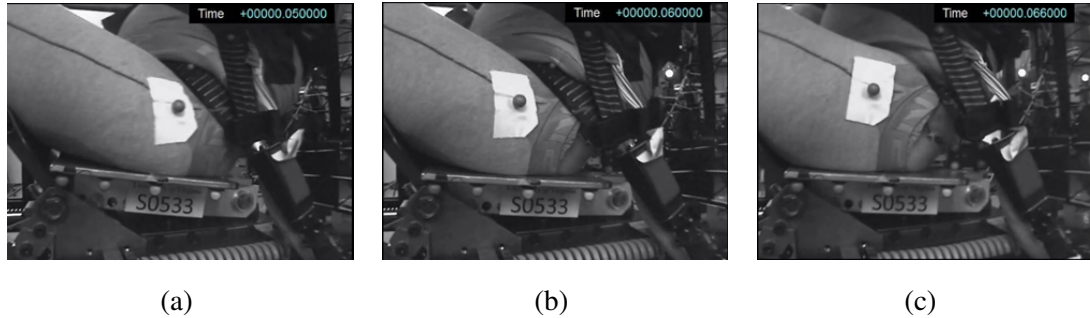
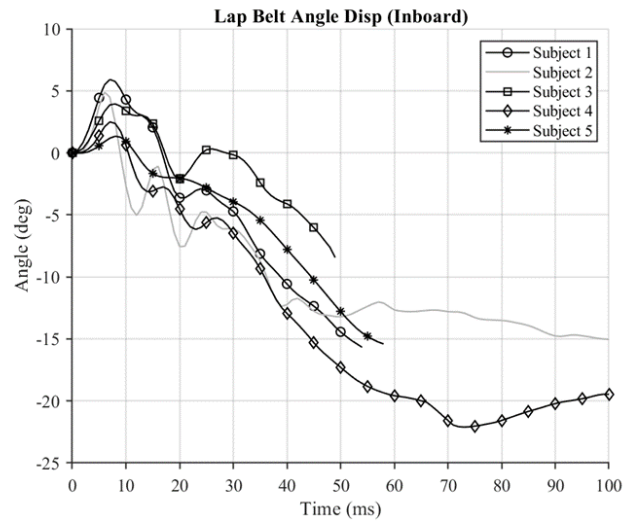


Figure 3.10: Video stills of Subject 5 submarining.

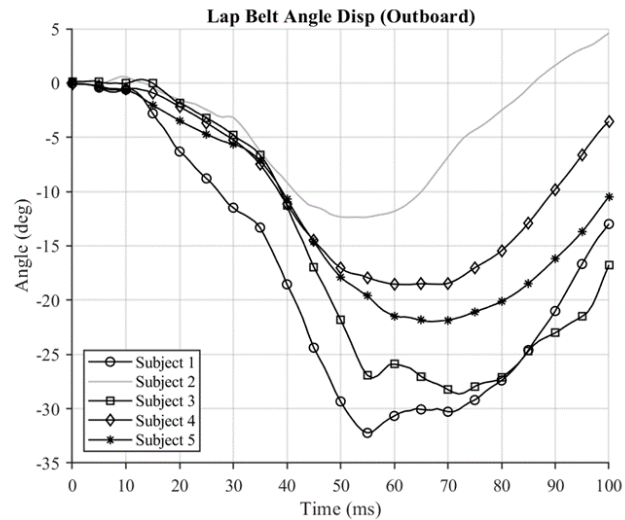
Subjects 1 and 3 sustained pelvis fractures at the right iliac wing between the ASIS and AIIS landmarks at approximately 60ms and 53ms, respectively B.2. Subjects 1, 2, 3, and 5 all sustained injuries at the lower-level sacrum.

3.4.2 Lap Belt Kinematics and Kinetics

The five subjects showed consistent trends in lap-belt angle time-history, with a decreasing lap belt angle (indicating a shallower lap belt angle) that peaked around the time of peak pelvis forward excursion (Figure 3.11). Lap belt motion tracking on the inboard side was lost (due to lack of visibility) just prior to peak pelvis forward displacement for Subjects 1, 3, and 4. On the outboard side, Subjects 1 and 3 exhibited the most horizontal lap belt angle at the time of peak pelvis forward excursion, followed by Subjects 4 and 5. Subject 2's lap belt rotated approximately 15° less than the other subjects as this subject exhibited far less pelvis displacement (Figure 3.9a).



(a)

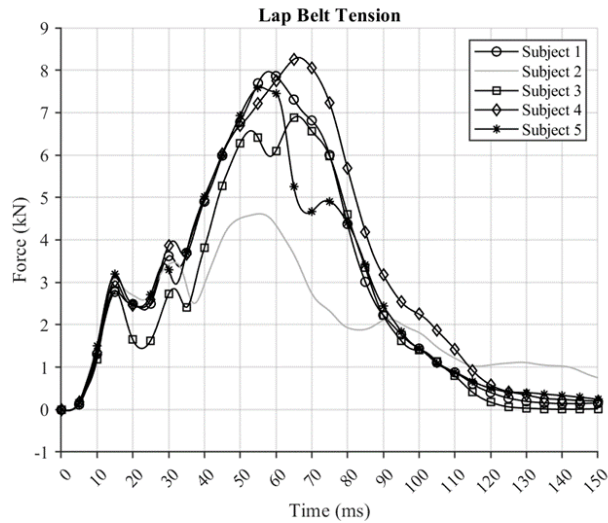


(b)

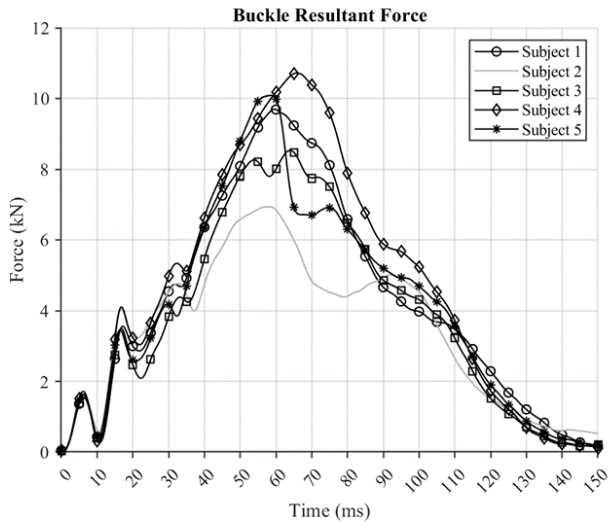
Figure 3.11: Lap belt angular displacement in the sagittal view up to 100 ms (during pelvic rebound): (a) the inboard (buckle) side of the occupant, (b) the outboard side of the occupant. A negative trend indicates a shallower lap belt angle, or a lap belt angle oriented closer to the horizontal axis.

CHAPTER 3. THE EFFECT OF A RECLINED POSTURE ON LAP BELT-PELVIS INTERACTION

Maximum lap belt tension and resultant buckle force occurred near the time of maximum forward pelvis displacement (56-75 ms) (Figure 3.12). Peak lap belt tension ranged from 4.6kN (Subject 2) to 8.3kN (Subject 4) and peak resultant buckle force ranged from 6.9kN (Subject 2) to 10.7 kN (Subject 4). The reduction in lap belt tension for Subjects 3 and 5 correspond to iliac wing fracture timing and submarining, respectively.



(a)



(b)

Figure 3.12: (a) Lap belt tension (outboard side); (b) buckle resultant force (inboard side).

3.4.3 Lumbar Spine Kinematics and Injury

The four midsized subjects showed similar forward displacements (X-dir) of the T11 (190-240mm, 95-105ms), L1 (165-183mm, 75ms), and L3 (140-187mm, 65-80ms) vertebral bodies (Figure 3.13). Subject 2 exhibited less forward displacement which occurred earlier than the midsized subjects. While the T11 vertebral body Z-displacements were grossly similar for these subjects (all trending in the negative direction, indicating an upward motion per Figure 3.8), differences were seen in the L1 and L3 vertebral body Z-displacements. Subject 1 exhibited more upright behavior for both L1 and L3, with the spinal column oriented closer to the vertical axis and the corresponding vertebral bodies displacing up more vertically, whereas the other subjects showed more lumbar spine compliance, exhibiting a downward behavior at these vertebral body locations.

Subjects 1, 2, and 3 sustained L1 vertebral body fractures, which occurred at 65ms for Subjects 1 and 3 and 48ms for Subject 2 (Figure 3.14 shows the spine orientation at the time of fracture). These L1 fractures occurred just prior to peak forward pelvis displacement for the corresponding subjects and were attributed to combined compression and flexion loading of the lumbar vertebral column due to both the arrested motion of the pelvis (by the lap belt) and the forward flexion of the torso. Subject 1 exhibited an aligned spinal column at the time of injury, with no relative pitch between the T11 and L1 vertebrae and the L3 vertebra pitched downward relative to L1. This aligned lumbar column resulted in a more distributed load across the L1 vertebral body and a three-column burst fracture occurred. This subject exhibited flexion immediately following time of injury. In contrast, Subjects 2 and 3 exhibited flexion at the time of injury. Subject 2 sustained a single column compression fracture (concentrated anterior loading of the vertebral body) and Subject 3 sustained a two-column burst fracture (less concentrated anterior loading of the vertebral body).

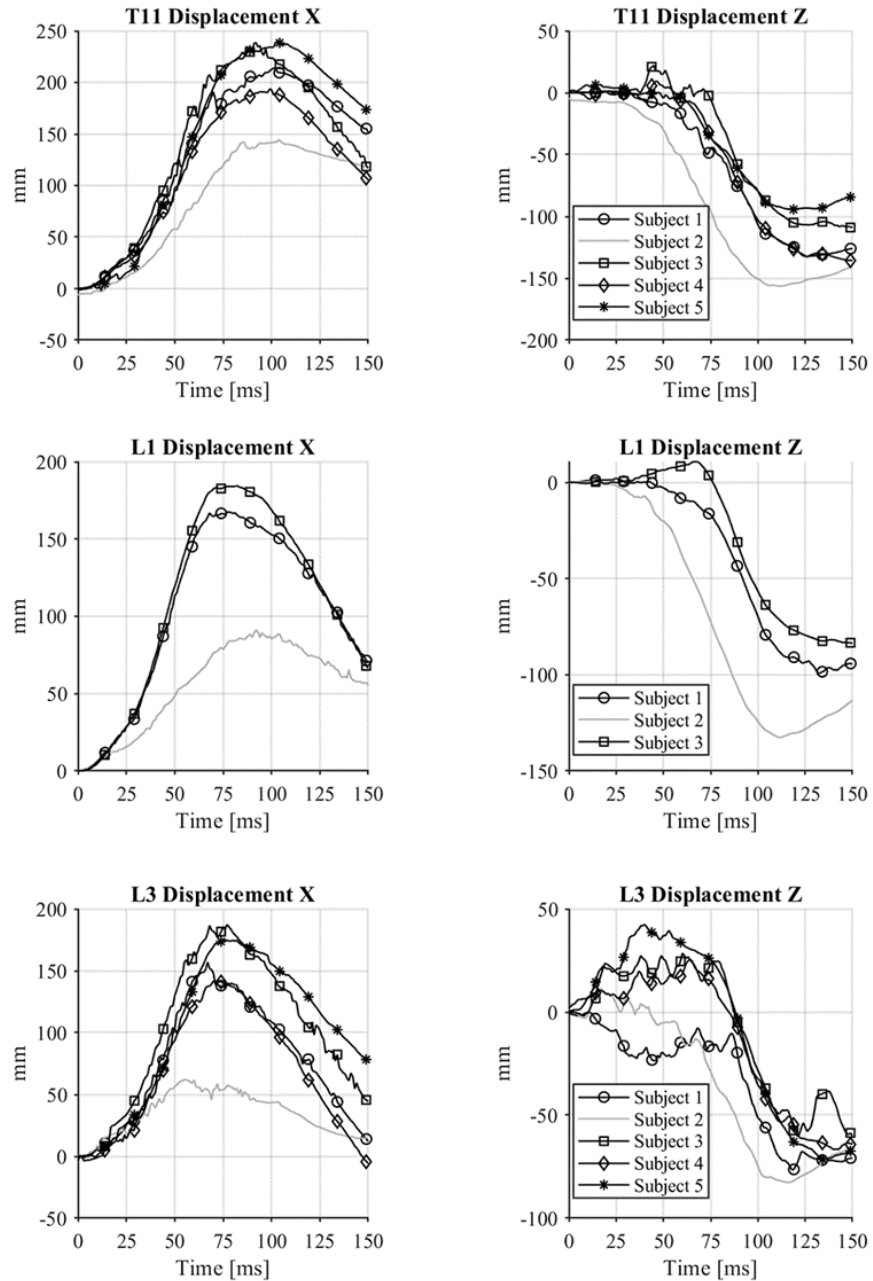


Figure 3.13: Vertebral body forward (X) and downward (Z) displacements.

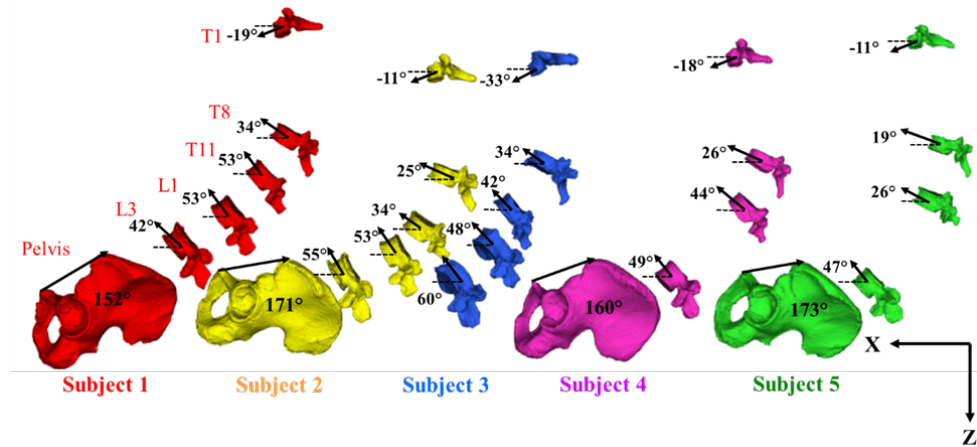


Figure 3.14: Position of the first three subjects at the time of fracture (Subject 1: 65 ms, Subject 2: 48 ms, Subject 3: 65 ms) and Subjects 4 and 5 at 65 ms for kinematic comparison with Subjects 1 and 3, of equal mass. Kinematic tracking of the pelvis of Subject 3 was lost at 30 ms.

3.5 Discussion

The test results gave insight into the responses of PMHS in a reclined seating configuration subjected to a frontal impact. The PMHS showed variation in lumbar spine and pelvis kinematics, which dictated injury and submarining outcomes. This variation resulted in a wide range of responses for HBM comparison in the biofidelity assessment of Chapter 4. However, it is critical to first understand how these kinematics inform the underlying fundamental mechanisms of lumbar spine compliance and lap belt-pelvis interaction in the PMHS and ensure the HBM can capture these mechanisms, as they have a direct effect on submarining occurrence.

3.5.1 Lumbar Spine Compliance

The kinematics of the lumbar spine were influenced by both the subject's initial spinal curvature in relation to the pelvis and the pelvis kinematics (Richardson et al., 2020b). While the subjects were positioned to a similar gross torso angle (50° in the sagittal plane), the lumbar spinal columns showed varying levels of kyphosis or lordosis initially due to subject-specific characteristics (Figure 3 7). Recall, motion tracking hardware was installed on the vertebral bodies of Subjects 1, 2, and 3. Thus, information on lumbar spine flexion and extension kinematics can be obtained by plotting the relative rotations of the L1 vertebral body to the L3 vertebral body (Figure 3 13) and, for Subjects 1 and 2, relative to the pelvis (recall pelvis motion tracking was lost for Subject 3)

(Figure 3.14). For Subjects 1, 2, 4, and 5, flexion/extension kinematics can be obtained by plotting the L3 rotation relative to the pelvis rotation (Figure 3.14).

Subject 1, who exhibited forward pelvis rotation during forward excursion, exhibited a more vertically-oriented spinal column than the other subjects at the time of injury (Figure 3.14). While there was distributed loading across the L1 vertebral body superiorly and inferiorly, resulting in a three-column burst fracture, L1 was pitched upwards relative to L3 and the pelvis, indicating extension (Figures 3.15 and 3.16). In contrast, Subjects 2 and 3 exhibited pure flexion of L1 relative to L3 (Figure 3.15a). However, prior to peak forward pelvis displacement, Subject 2 showed extension of the L1 vertebral body relative to the pelvis (Figure 3.16a) and Subjects 2 and 4 showed extension of the L3 vertebral body relative to the pelvis (Figure 3.16b). Subject 5, who submarined exhibited pure flexion of L3 relative to the pelvis.

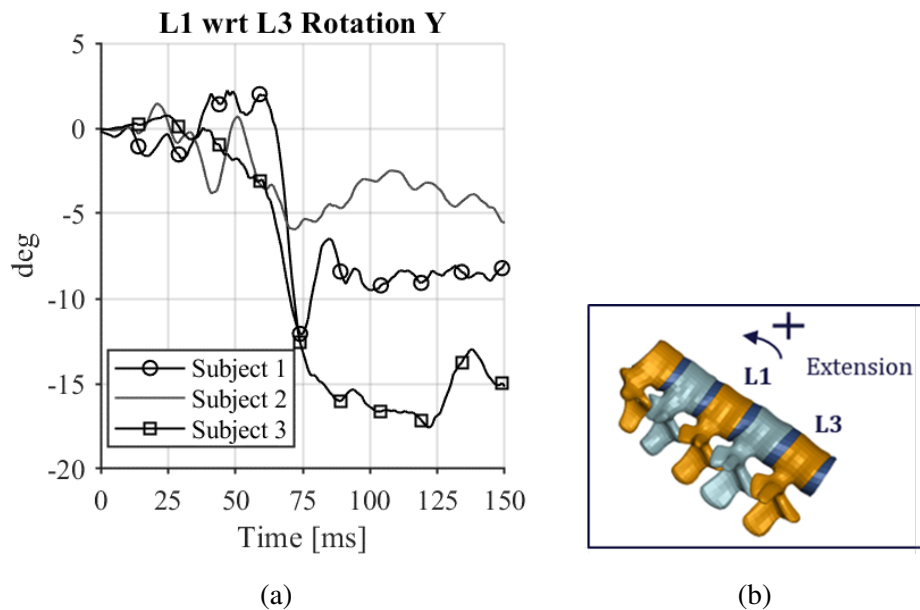


Figure 3.15: L1 vertebral body rotation relative to L3 vertebral body rotation (a). A positive value indicates a rearward rotation of L1 relative to L3, akin to lumbar extension or lordosis (b).

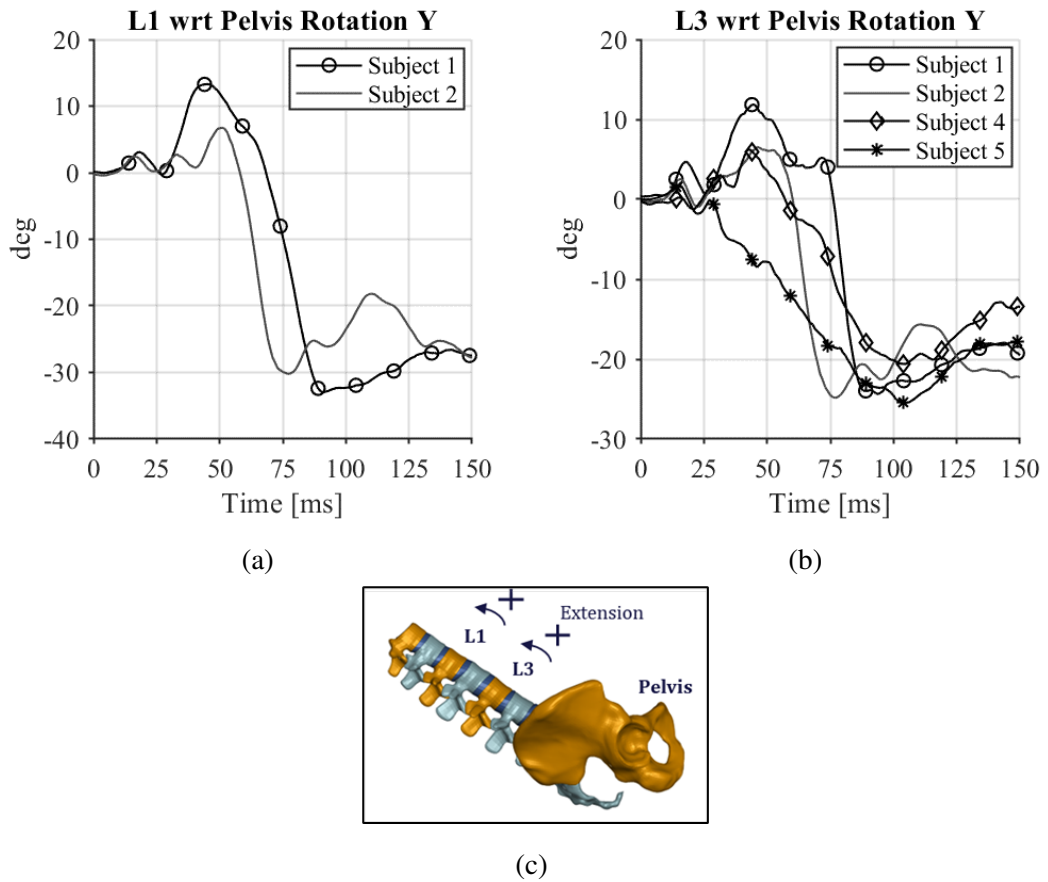


Figure 3.16: L1 vertebral body rotation (a) and L3 vertebral body rotation (b) relative to the pelvis rotation. A positive value indicates a rearward rotation of L1 or L3 relative to the pelvis, akin to lumbar extension or lordosis (c).

3.5.2 Lap Belt-Pelvis Interaction

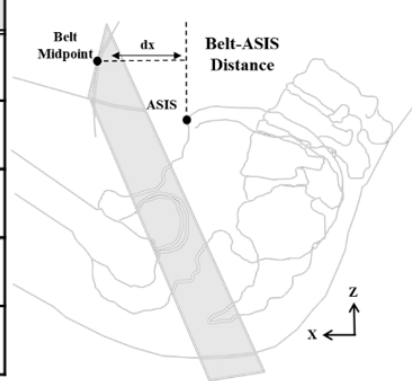
3.5.2.1 Lap belt placement and pelvis rotation

Prior to peak forward pelvis displacement, the PMHS exhibited different pelvis rotation polarities. Subjects 1 and 2 exhibited approximately 10-15° of forward pelvis rotation (Figure 3.9b). Subject 4 exhibited less forward pelvis rotation ($< 3^\circ$) until just before peak pelvis forward excursion (60-70ms) when this subject exhibited a slight rearward pelvis rotation. Subject 5, who submarined, exhibited rearward rotation through the entire duration of pelvis forward excursion. All subjects exhibited different initial pelvis and lumbar spine orientations based on the subject's natural seating posture, however, there are no clear links between these differences in initial position and the subsequent differences in pelvis rotation polarity.

One clear difference among PMHS was the initial lap belt fit, which was largely dictated by the subject-specific shape of the abdomen. Subjects 4 and 5, who exhibited a neutral or slightly rearward pelvis rotation, had the lap belt initially positioned closer to the ASIS (dx) than Subjects 1 and 2, who exhibited a forward pelvis rotation (Table 3.4). This was also seen by looking at the lap belt webbing relative to the subject-specific pelvises, where Subjects 1 and 2 had the lap belts positioned lower, below the AIIS, and Subjects 4 and 5 had the lap belts positioned higher, closer to the notch between the AIIS and ASIS (Figure 3.17, left column). There was also a difference in subsequent lap belt-pelvis engagement between Subjects 1 and 2 and Subjects 4 and 5, where again Subjects 1 and 2 had a lower lap belt placement relative to the pelvis (Figure 3.17, right column).

Table 3.4: Distance between the center of the lap belt and the ASIS in the X-direction (defined in the right schematic) and resulting pelvis rotation polarities.

Subject No.	dx (mm)	Pelvis rotation polarity
1	73.8	Forward
2	79.2	Forward
3	129.7	Unknown
4	56	Neutral
5	69.5	Rearward



Linking the difference in pelvis rotation solely to the lap belt placement relative to the pelvis is a large simplification. In reality, there are several factors that contribute to pelvis kinematics, as Chapter 2 demonstrated (Figure 2.7). However, lap belt placement may be one factor that contributed to the differences in pelvis rotation. Neglecting all other factors and isolating the lap belt tension vector relative to the pelvis, the resulting pelvis rotation can be visualized by summing the components of the lap belt tension in relation to the pelvis center-of-rotation (COR) (Figure 3.18). From this simplified diagram, the lap belt placed anterior relative to the pelvis COR (F_{Belt1}) will result in a moment that promotes a forward rotation(positive X-component), whereas the lap belt placed posterior to the pelvis COR (F_{Belt1}) will result in a moment that promotes a rearward rotation (negative X-component). Thus, the more anterior initial position of the lap belt relative to the pelvis COR seen for Subjects 1 and 2 may be a partial cause for the resulting forward pelvis rotation. Likewise, the more posterior initial position of the lap belts relative to the pelvis COR seen for Subjects 4 and 5 may be a partial cause for the resulting rearward pelvis rotation

3.5.2.2 Lap belt-pelvis angle and submarining

Subject 5 was near the average initial pelvis angle for the four midsize male subjects (170° vs. 166° avg.) (Figure 3.7), inboard lap belt angle (62° vs. 60° avg) (Table 3.3), and thus, initial lap belt-pelvis angle for the midsize PMHS (108° vs 108° avg); however, this subject submarined on the inboard side starting at approximately 55ms. Chapter 2’s literature search originally revealed

CHAPTER 3. THE EFFECT OF A RECLINED POSTURE ON LAP BELT-PELVIS INTERACTION

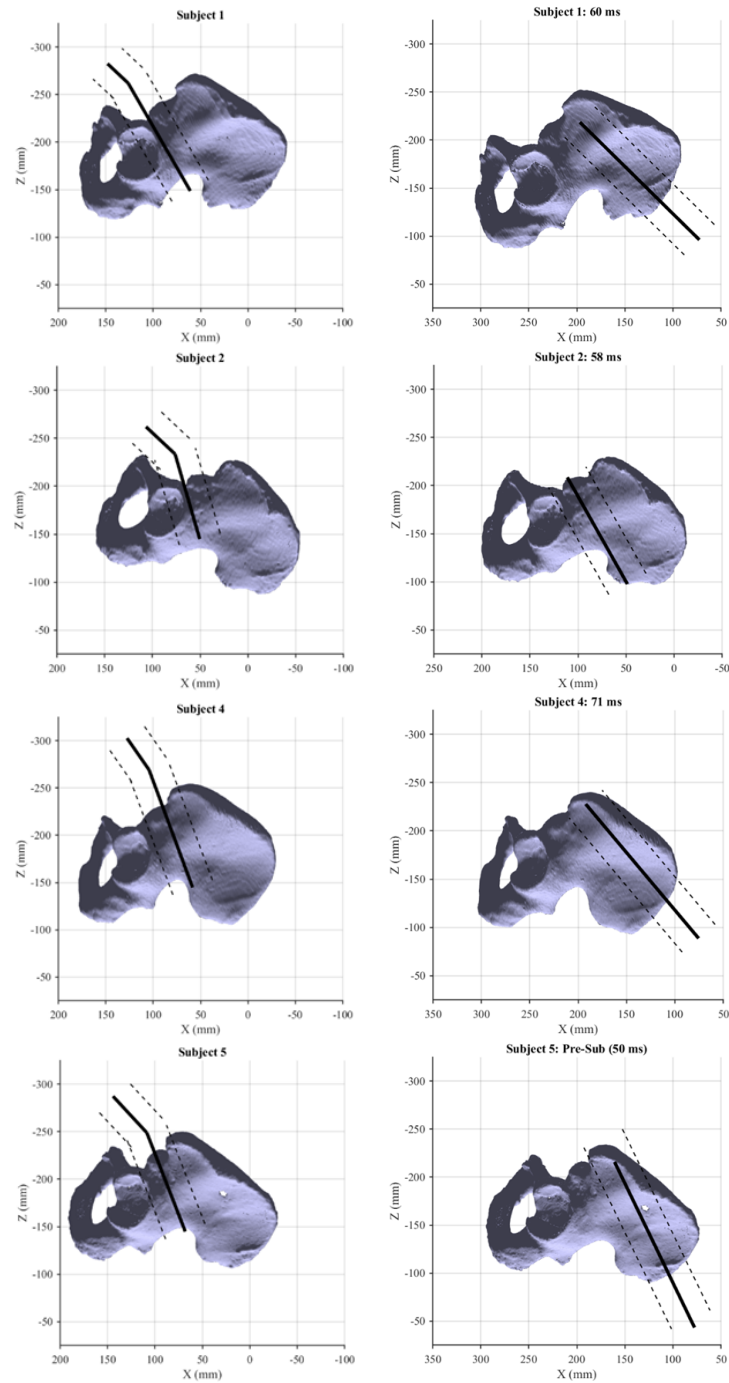


Figure 3.17: Position of the lap belt relative to the subjects' pelvises (segmented CT scans) in the initial configuration (left column) and during the pelvis forward displacement (right column). See Richardson IRCOBI paper for details on the selected times of interest in the right column. Subject 3 is omitted as pelvis motion tracking was lost. The solid line connects the motion-capture markers at the center of the lap belt and the dashed lines approximate the width of the lap belt webbing.

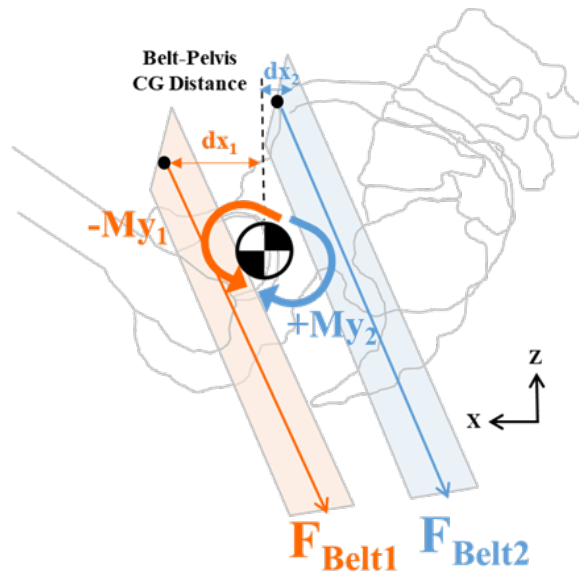


Figure 3.18: A simplified free body diagram showing the lap belt tension vector relative to the pelvis COR for two different lap belt placements, inducing two opposing moments.

lap belt-pelvis angle as a potential factor that influences submarining occurrence. The inter-subject differences in lap belt-pelvis angle at the time of Subject 5's submarining shows that this as an important parameter for investigating submarining threshold. At the onset of submarining ($t= 55$ ms), Subject 5 exhibited a relatively high magnitude of lap belt tension (Figure ??) and the largest lap belt-pelvis angle of the mid-sized subjects (124° vs 117° avg), indicating the most horizontally-oriented lap belt angle relative to the pelvis (Figure 3.19, angle β in Figure 2.7). This suggested a threshold for which, at a given lap belt-pelvis angle, submarining would occur. Evaluating the submarining sensitivity to this parameter was further investigated in Chapter 5.

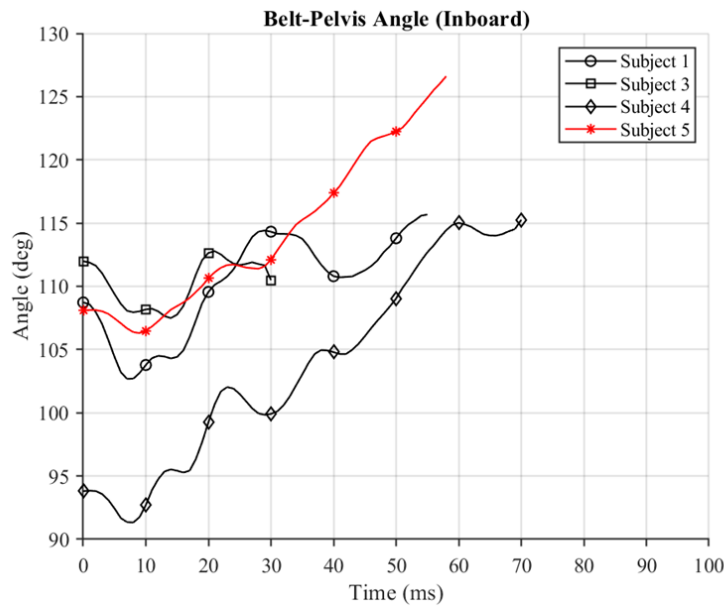


Figure 3.19: Lap belt-pelvis angle on the inboard side. This parameter is defined in Figure 3.5 and is angle β in Figure 2.7. Lap belt motion tracking was lost during the subjects' forward pelvis excursion due to lack of visibility of the lap belt markers.

3.6 Conclusions

The following conclusions were drawn from this chapter's analysis:

1. Lap belt-pelvis angle was shown as a potential parameter that affected submarining occurrence, as the subject who submarined exhibited the largest lap belt-pelvis angle (indicating a more horizontally-oriented lap belt relative to the pelvis) at the time of submarining. This parameter was further studied in Chapters 5 and 6.
2. In addition to several other factors, the initial lap belt placement relative to the bony pelvis may have played a role in the resulting direction of pelvis rotation, which varied among subjects.
3. The PMHS exhibited varying responses in lumbar spine kinematics, particularly flexion and extension, due to the subject-specific variation in initial lumbar spine alignment and compliance and initial pelvis orientation and kinematics. Some subjects exhibited slight extension of the lumbar spine during pelvis forward excursion. All subjects exhibited combined compression and flexion loading of the lumbar spine during forward torso excursion.

CHAPTER 3. THE EFFECT OF A RECLINED POSTURE ON LAP BELT-PELVIS INTERACTION

Ensuring the models can capture the fundamental mechanisms of lumbar spine compliance and belt-pelvis interaction resulting from this test series is paramount. Several signals will be compared in the HBM biofidelity evaluation in Chapter 4. These signals were deemed as those that most comprehensibly illustrate important similarities and discrepancies between the HBMs and PMHS. These include all boundary kinetic signals (belt, seat, and toe pan forces), seat pan and anti-submarining pan rotation, restraint system responses (belt pay-in/pay-out), and surrogate kinematic response.

Chapter 4

Evaluation of HBM Biofidelity in a Reclined Posture

4.1 Executive Summary

4.1.1 Relevance and Goal

Prior to executing the parametric study in which a computational model (e.g., HBMs) was used to draw conclusions for an physical model (e.g., humans), it was critical to first perform a benchmark biofidelity evaluation, in which the computational model's kinematic and kinetic responses are compared to the physical model, to understand existing differences between these models [83]. Prior to this dissertation, HBMs had not been evaluated in their ability to predict belt-pelvis interaction exhibited by PMHS in a reclined posture.

Thus, the goal of this chapter was to evaluate the biofidelity of the GHBMC and THUMS HBMs by comparing their kinematic and kinetic responses to those exhibited by the PMHS from Chapter 3. This evaluation allows for the assessment of the HBMs' capabilities and limitations in a reclined posture, with particular focus on pelvis and lumbar spine kinematics and restraint interaction. This chapter, in combination with Chapter 6, informed the selection of the HBM for the evaluation of lap belt-pelvis interaction and submarining occurrence in Chapter 8's parametric study.

4.1.2 Key Conclusions

The full list of conclusions can be found in Section 4.6 below. In summary, the GHBM was identified as the more suitable choice for detailed study of lap belt-pelvis interaction as the lap belt shell elements collapsed in the THUMS simulations during the model's forward torso flexion. This phenomenon in the THUMS simulation may be due to either the sliding contact between the model's flesh and pelvis, or due to the material stiffness of the flesh itself. The collapse of the webbing elements affected lap belt-pelvis loading and resulting pelvis kinematics. Additionally, the THUMS exhibited more lumbar spine compliance than both the GHBM and the PMHS.

These conclusions, in addition to those drawn from Chapter 6's simulation study, will be used to inform the selection of the HBM to use in Chapter 8's parametric study.

4.1.3 Contributions

This chapter provides the first biofidelity evaluation of HBMs in a reclined seating environment through a comprehensive comparison of kinematic and kinetic data traces. This signal comparison, in addition to visual (i.e., video) analysis, allowed for a deeper understanding of the HBMs' limitations in this posture, with particular emphasis on lap belt-pelvis interaction and lumbar spine compliance. Understanding these limitations informs the field of potential body regions in which further data and/or research is required to improve HBM biofidelity, which expands beyond the reclined posture.

4.2 Introduction

In Chapter 2, a comprehensive literature review identified a reclined torso angle to be a potential factor that affects occupant lap belt-pelvis interaction and submarining occurrence. A reclined posture is predicted to increase in prevalence with the introduction of Level 3 ADS, so investigating the mechanism of how this posture may increase risk of submarining is critical. Current HBM simulations reveal an increased risk of submarining for a reclined posture due to the initial rearward pitch of the pelvis. However, prior to this dissertation, no PMHS data existed to investigate reclined occupant kinematics and associated submarining risk or to validate computational HBM responses in this posture. Thus, Chapter 3 described the methods and results of reclined midsized male PMHS sled test experiments using a restraint system designed to mitigate occupant submarining, though one of five subjects submarined. These tests revealed mechanisms in both the

CHAPTER 4. EVALUATION OF HBM BIOFIDELITY IN A RECLINED POSTURE

lumbar spine and lap belt-pelvis regions which were found critical for a computational HBM to be able to replicate, as these mechanisms influenced pelvis kinematics and subsequent submarining outcomes.

The two most recently developed and updated state-of-the-art mid-sized male (M50) HBMs are the Global Human Body Models Consortium detailed M50 seated model v.6 (GHBMC-O M50 v.6) and the Total Human Model for Safety (THUMS AM50 v.6.1). These HBMs have different geometric, material, and mathematical formulations, but are both classified as representing the average, or mid-sized, male anthropometry. Geometry for these whole-body models is based on medical imaging data (e.g. computed tomography data) and each model is comprised of approximately two million elements [27, 28]. These HBMs, largely validated at the component and full-body model levels, have been used extensively for evaluation of kinematics and injury prediction in multiple automotive crash loading modes and have been shown to exhibit different kinematic and kinetic responses.

As the final aim of this dissertation is to use a computational HBM to evaluate the effect of extrinsic and intrinsic factors, including a reclined seating posture, on lap belt-pelvis interaction and submarining occurrence (Chapters 8 and 9), it is critical to use a model that exhibits biofidelity in representing these mechanisms. Neither the GHBMC nor the THUMS model have been evaluated in a reclined seating posture. Thus, this chapter performed the biofidelity evaluation necessary to assess the performance of both models relative to the PMHS responses, and, in combination with Chapter 6, aided in determining the superior model to select for the final parametric study in Chapter 8.

4.3 Materials and Methods

4.3.1 Software and Hardware Used

The simulations in this chapter were performed using LS-DYNA (R11) Massively Parallel Processing (MPP) explicit FE solver. The simulations were performed on the high-performance computational cluster (Intel Xeon64/sse2). All jobs were run on two nodes.

4.3.2 FE Environment

The simulation environment matched the setup used in the tests presented in Chapter 3, featuring a semi-rigid simplified seat, a 50° torso recline angle, and a prototype 3-point restraint

CHAPTER 4. EVALUATION OF HBM BIOFIDELITY IN A RECLINED POSTURE

system. No knee bolster was used. The semi-rigid seat was based on a design developed by [76] which was used in Chapter 3. The FE model of the semi-rigid seat was developed by Laboratory of Accidentology and Biomechanics/Centre Européen d'Etudes de Sécurité et d'Analyse des Risques (LAB/CEESAR) in cooperation with Partnership for Dummy Technology and Biomechanics (PDB) and was further improved by Autoliv Development AB in Sweden (Figure 4.1). The gravity was applied to all parts of the model through the *LOAD_BODY_Z keyword and no global damping was used.

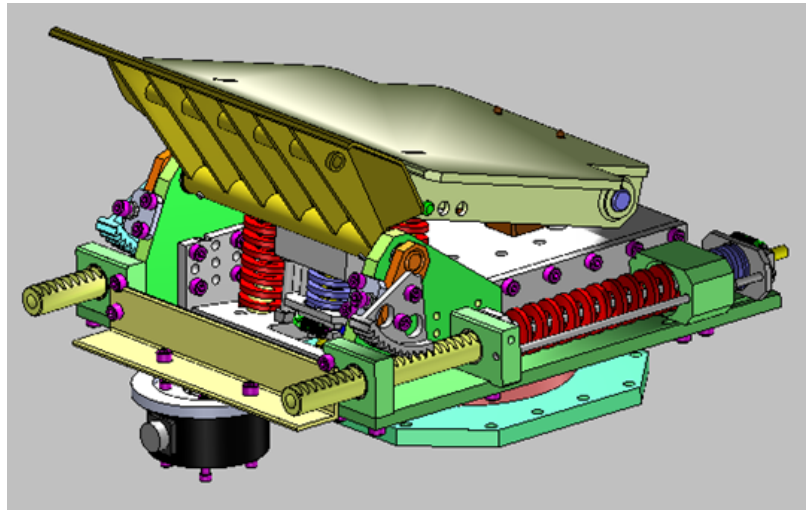


Figure 4.1: FE model of the semi-rigid seat.

As in Chapter 3, the restraint system used consisted of a three-point belt equipped with dual lap belt pretensioners, a shoulder belt retractor pretensioner, a crash locking tongue, and a shoulder belt load limiter of 3.5 kN. Anchorage points geometry was designed to represent a seatback-integrated belt configuration. Belt webbing was created using shell seatbelt elements and a 2D slip-ring formulation to facilitate stable and unobstructed belt payout. The FE model of the restraint system, which was developed by Autoliv Development AB and used with permission here, comprised of validated component models of production parts. System model was validated by means of sled tests using THOR-50M. The occupant to the environment contact was modelled with the static and dynamic friction coefficient of 0.35 for the seat pan and 0.30 for the belt, which are default friction values for automotive impact simulations and have been used in similar studies using this seat and restraint system [34].

4.3.3 HBMs

Two mid-sized male HBMs – the GHBMC v.6.0 and the THUMS v.6.1 – were used in this chapter. These HBMs represented gross 50th male anthropometry, however they differed in specific local geometry, e.g., pelvic shape and lumbar spine alignment. The GHBMC v.6.0 is the newest iteration of the GHBMC mid-sized male occupant model, made publicly available in late 2021. It features, among other updates, new softer definition for the adipose tissue and detailed ligamentous lumbar spine model [84]. THUMS v.6.1, released in early 2019, was developed based on previously developed THUMS v.4 model. It features internal organ model and an implementation of active musculature [85]. Both HBMs were validated by means of component tests, table-top experiments and whole-body sled tests. All models feature injury prediction capabilities in several body regions [84, 85].

4.3.4 HBM Positioning

The HBMs were positioned based on the initial positions of the four mid-sized PMHS (Subjects 1, 3, 4, and 5) from the tests described in Chapter 3 (Appendix C.1). The rigid body positioning was carried out in three sequential steps (Figure 4.2). In the first step, the HBMs were initially aligned by their hip points (or H-points) relative to the PMHS average, defined based on the center of the acetabulum (note that the THUMS v.6.1's acetabulum needed to be shifted forward 25mm to account for an apparent smoothing in the local curvature of the acetabulum) (Figure 4.2, Step 1). Recall that Chapter 2 introduced both initial lumbar spine and pelvis orientation as potential factors that affect lap belt-pelvis interaction. From positioning the PMHS relative to two different pelvis angles measured at different locations on the pelvis geometry (the Nyquist angle and the Notch angle or the segment connecting the ASIS and anterior inferior iliac spines relative to the horizontal as in [86]), the resulting lumbar column orientation differed between the two HBMs (Figure 4.2, Intermediate Step). Thus, the HBMs were positioned to effectively split the difference between both the lumbar spine and pelvis alignment by aligning the vector passing between the center of the sacrum and the L5 superior endplate (Figure 4.2, Step 2). Finally, the HBMs were reclined and aligned with the PMHS using average PMHS: L1, L3 and pelvis H-point and iliac crest positions (Figure 4.2, Step 3). To have a better approximation of the range in initial pelvis and lumbar orientations observed in the PMHS tests, the HBMs were also positioned at pelvis orientations $\pm 12^\circ$ relative to this nominal angle. These steps were achieved using rigid body transformations of the HBMs.

CHAPTER 4. EVALUATION OF HBM BIOFIDELITY IN A RECLINED POSTURE

The 12° value was derived based off the difference in the two different pelvis angles explored in the Intermediate Step. Thus, the end result was three pelvis angles per model for a total of six positioned HBMs (three GHBMC and three THUMS). In this Chapter, these positioned models will be coined as the “Nominal”, “Ant12deg”, and “Pos12deg” models based on their corresponding pelvis orientations.

Following the rigid body transformations, the models were positioned with respect to the average PMHS position of L3, L1, T11, T8, T1, head, knee, and calcaneus obtained from Chapter 3’s experiments. Throughout this process, the pelvis was constrained to maintain its rigid body alignment from previous steps. Positioning was carried out using the Oasys PRIMER HBM positioning module (Arup, London, England), using a displacement-based cable approach. Finally, the HBMs were settled onto the seat by driving a positioned model into the seat to the desired depth of posterior flesh compression (matching top of the iliac crest with the PMHS), with the skeleton constrained so that the bones could not move relative to each other. Gravity settling was initially attempted but was ultimately not used since it resulted in HBM H-point positions above the average PMHS position (presumably due to the stiffness of the posterior pelvis flesh). Consequently, initial stress and strain in posterior flesh tissue that resulted from the settling procedure was not considered. The final posture and its comparison with PMHS targets are found in Appendix C.1.

4.3.5 Initial Lap Belt Placement

The belts were individually routed across each HBM using an automated belt routing program developed in-house. The purpose of this seatbelt routing was to generate a natural or realistic seatbelt position using pre-defined anchorage points. This automated method was stress-tested in this chapter prior to being used in Chapter 8, in which multiple belt anchorage positions were defined for both reclined and upright postures. More details on this method can be found in Chapter 8. Both the lap and chest belt sections were stretched across each HBM individually to form the shortest belt path. Even though the same restraint anchorage points were used for all simulations, the lap belt routing differed across the models due to differences in external body shape. The abdominal tissue curvatures were the main driving factor behind observed differences. The GHBMC had a higher initial lap belt placement relative to the pelvis than the THUMS for all pelvis orientations (Figure 4 3).

CHAPTER 4. EVALUATION OF HBM BIOFIDELITY IN A RECLINED POSTURE

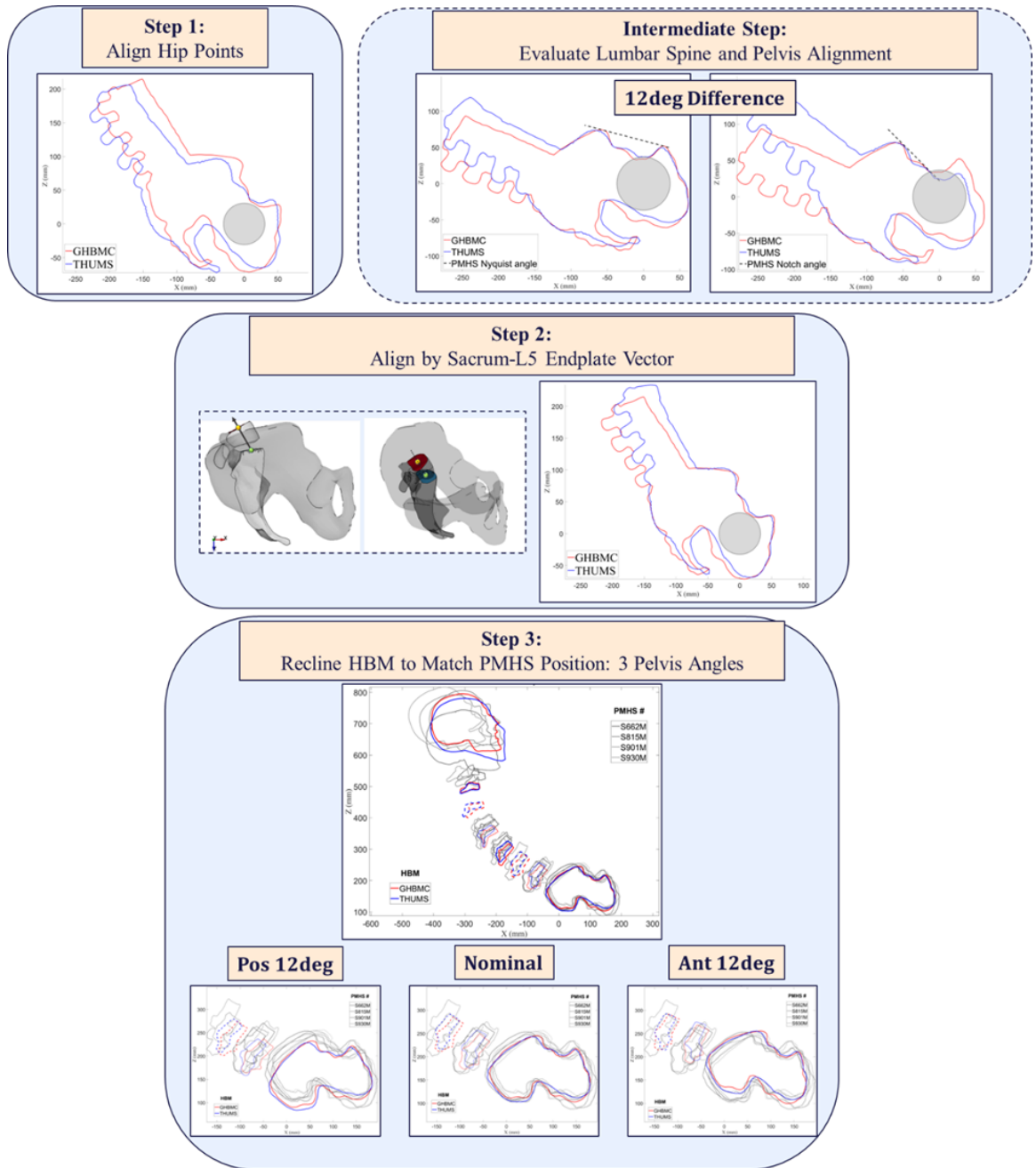


Figure 4.2: Outlined process of HBM alignment relative to PMHS position.

CHAPTER 4. EVALUATION OF HBM BIOFIDELITY IN A RECLINED POSTURE

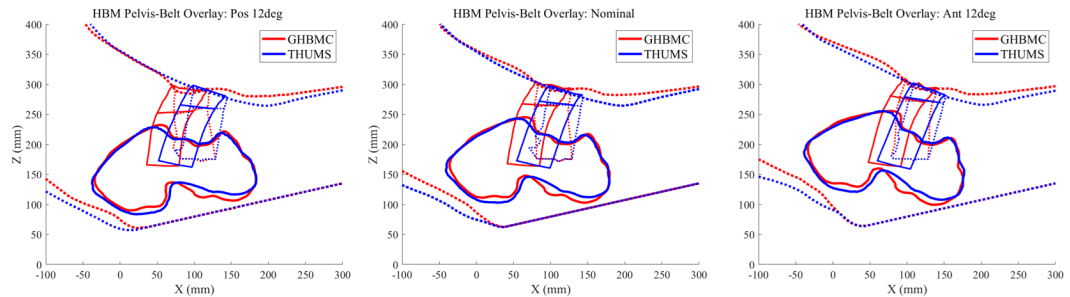


Figure 4.3: Belt fit for the positioned HBMs relative to the pelvis orientations and abdominal curvature. Left to right are the different pelvis angles: 12° posterior rotation, nominal, and 12° anterior rotation.

4.3.6 Data Analysis

Of all the kinematic and kinetic data acquired from the PMHS experiments in Chapter 3, specific signals were chosen as those that most comprehensively illustrate the important similarities and discrepancies between the HBMs and PMHS. These included the head (X,Y,Z), T1 (X,Y,Z), T8 (X,Y,Z), T11 (X,Z), L1 (X,Z), L3 (X,Z) and pelvis (X,Z) displacement time histories; head (Y) and pelvis (Y) rotation time histories; L1, L3 and pelvis relative rotation time histories (to understand lumbar spine flexion and extension kinematics); semi-rigid seat and foot pan boundary forces and deflections; and restraint system forces and displacements. This chapter discusses those signals pertaining to lumbar spine compliance and lap belt-pelvis interaction specifically; however, all signal comparisons between the PMHS and the HBMs (nominal pelvis angle) can be found in Appendix C.2. The HBM responses were compared to the PMHS signals qualitatively to ensure the HBM captured the fundamental mechanisms exhibited by the PMHS in this condition. Additionally, video time-stills were used for qualitative evaluation.

4.4 Results

All signal comparisons between the PMHS and the HBMs (nominal pelvis angle) can be found in Appendix C.2. This section highlights the signals found most important both in their contribution to lap belt-pelvis interaction and in identifying differences among models: pelvis kinematics, lap belt kinetics, and lumbar spine kinematics. The HBMs initially positioned with the nominal pelvis orientation are first compared to the PMHS signals, followed by a discussion of how the modified initial pelvis orientations affected the responses.

4.4.1 Pelvis Kinematics

Neither HBM, including all three initial pelvis orientations, submarined in the simulation. As discussed in Chapter 3, one PMHS submarined (Subject 5).

The pelvis forward displacements (X) of both the GHBMC and THUMS were of similar magnitude to the PMHS (approximately 150mm), with the time of peak occurring slightly later (2-4ms) than Subjects 1, 3, and 4 (70ms) but prior to Subject 5 who submarined (77ms) (Figure 4.4). Around the time of peak pelvis displacement and early pelvis rebound (60-80ms), both HBMs exhibited an upward pelvis displacement (Z), whereas the PMHS exhibited a downward pelvis displacement at this time (Figure 4.5).

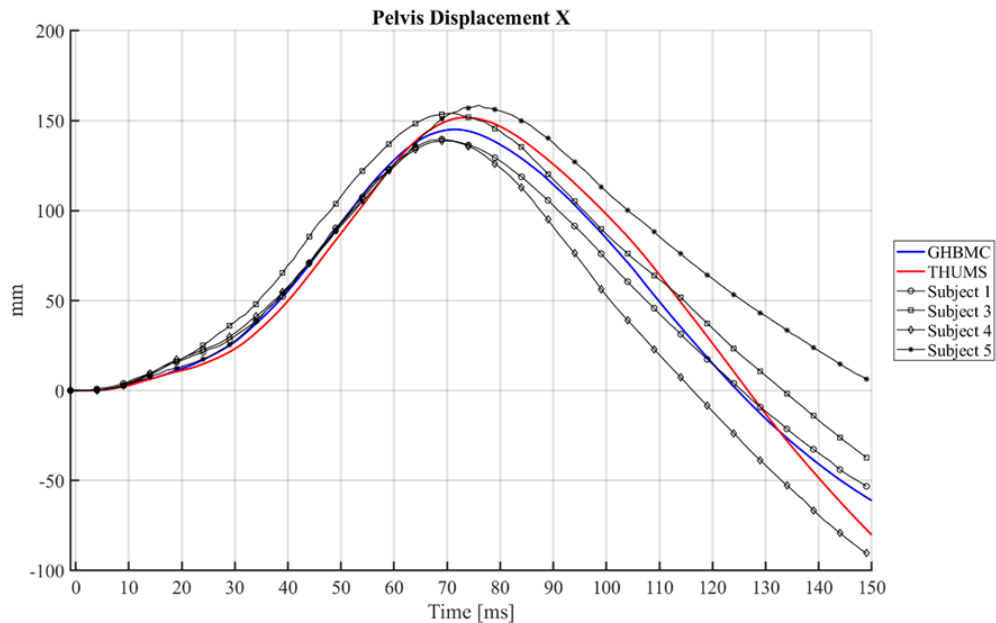


Figure 4.4: Pelvis forward (X) displacement. A positive value indicates anterior, or forward, motion.

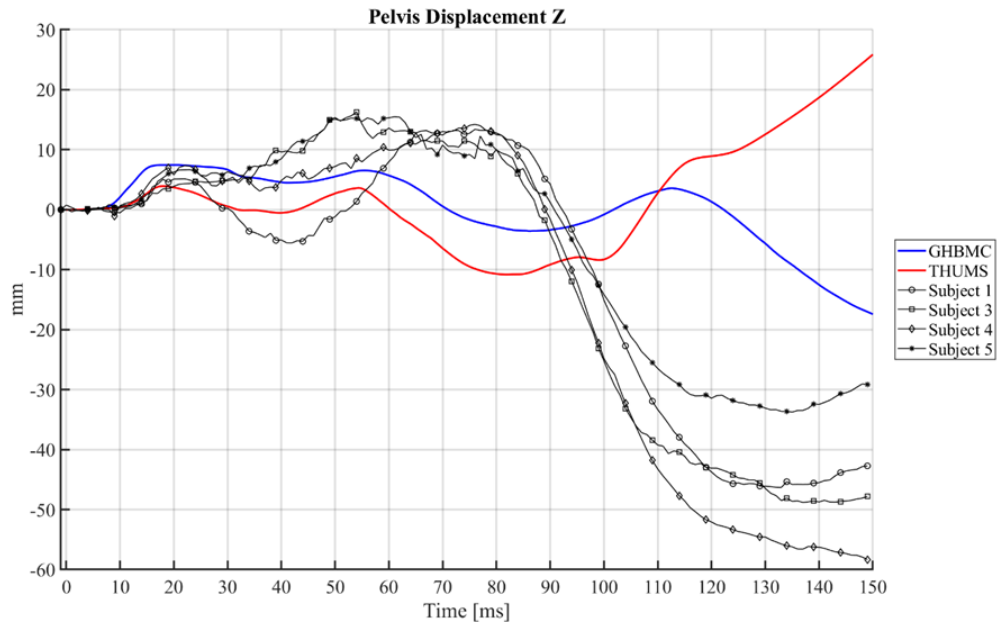


Figure 4.5: Pelvis downward (Z) displacement. A positive value indicates downward, or inferior, motion (towards ground).

Prior to peak forward pelvis displacement, the THUMS exhibited a more forward pelvis rotation which is consistent with Subjects 1 and 4 (Figure 4 6). In contrast, the GHBMC exhibited a rearward rotation which was of similar magnitude as Subject 5 who submarined ($2\text{-}3^\circ$) prior to approximately 60ms, when the GHBMC's pelvis increased in rearward rotation. Both models exhibited a rearward rotation at the time of peak pelvis forward displacement (7° for GHBMC; 3° for THUMS). At this time, Subject 1's pelvis began to pitch rearward, though the pelvis was still oriented forward, and Subject 4's pelvis exhibited nearly no change in pitch relative to the initial orientation. Subject 5 exhibited approximately 3° rearward pelvis rotation. Like the PMHS, both models exhibited forward rotation during pelvis rebound (after approximately 70ms).

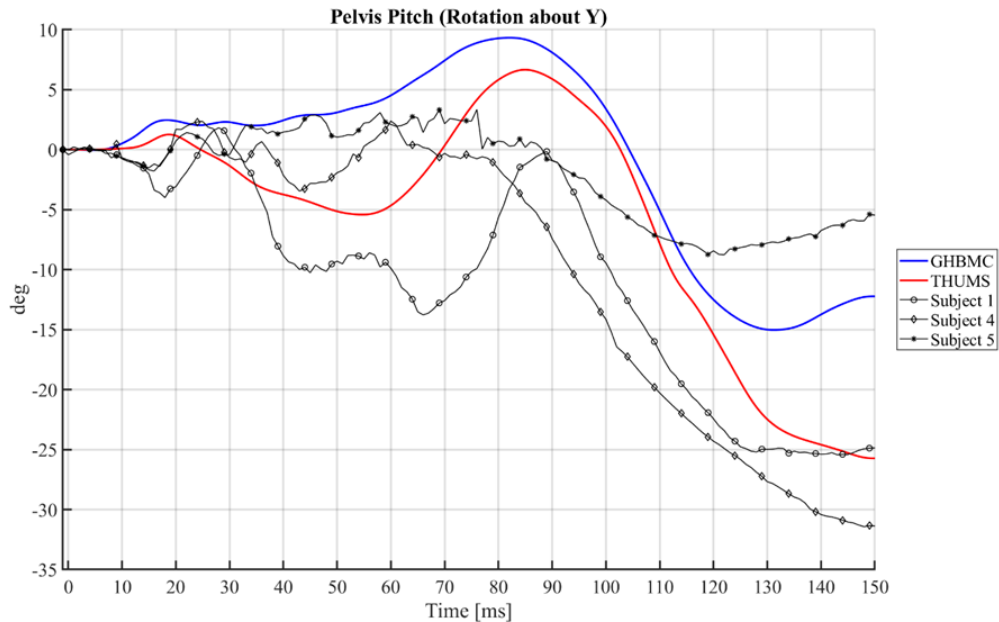


Figure 4.6: Pelvis pitch, or rotation about the Y-axis. A positive value indicates a rearward rotation.

Early in the simulation, the THUMS exhibited a forward pelvis rotation for the three pelvis angle positions, which better aligns with Subjects 1 and 4 (Figure 4.7). In contrast, only the GHBMC Pos 12° model exhibited this forward rotation (Figure 4.8). However, upon closer look at the THUMS Ant12deg model simulation, the flesh behind and below the pelvis interacted with the seatpan during the forward pelvis displacement (Figure 4.9). This artifact affected total body kinematics for the THUMS Ant12deg model (Appendix C.4). All models exhibited a rearward pelvis rotation during pelvis rebound (after 70ms), though the THUMS Ant12deg model exhibited less than the others.

CHAPTER 4. EVALUATION OF HBM BIOFIDELITY IN A RECLINED POSTURE

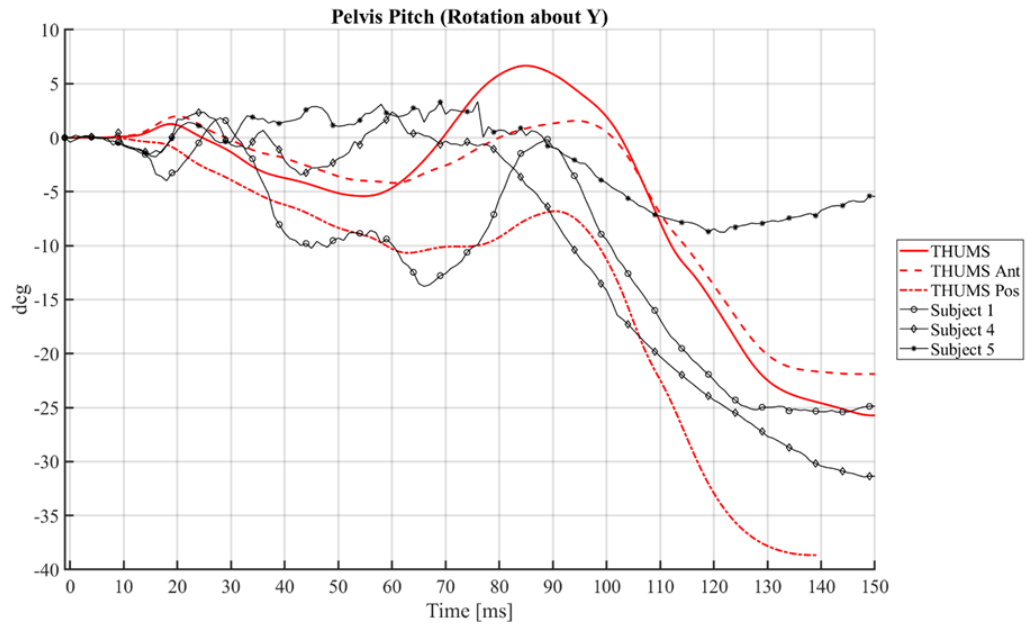


Figure 4.7: Pelvis pitch, or rotation about the Y-axis for the three THUMS models with different initial pelvis orientations. A positive value indicates a rearward rotation.

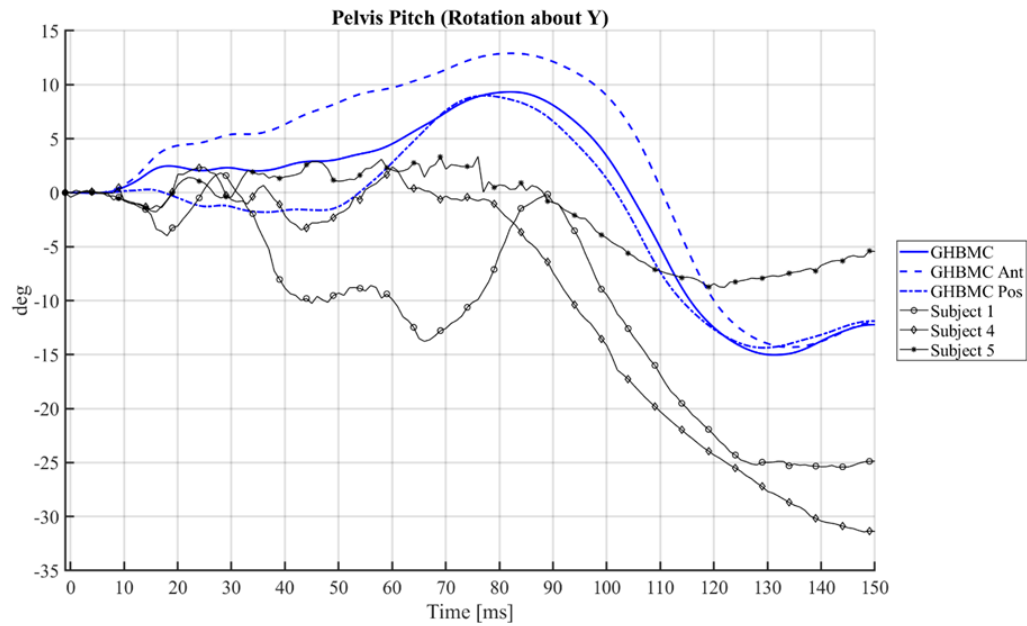


Figure 4.8: Pelvis pitch, or rotation about the Y-axis for the three GHBMC models with different initial pelvis orientations. A positive value indicates a rearward rotation.

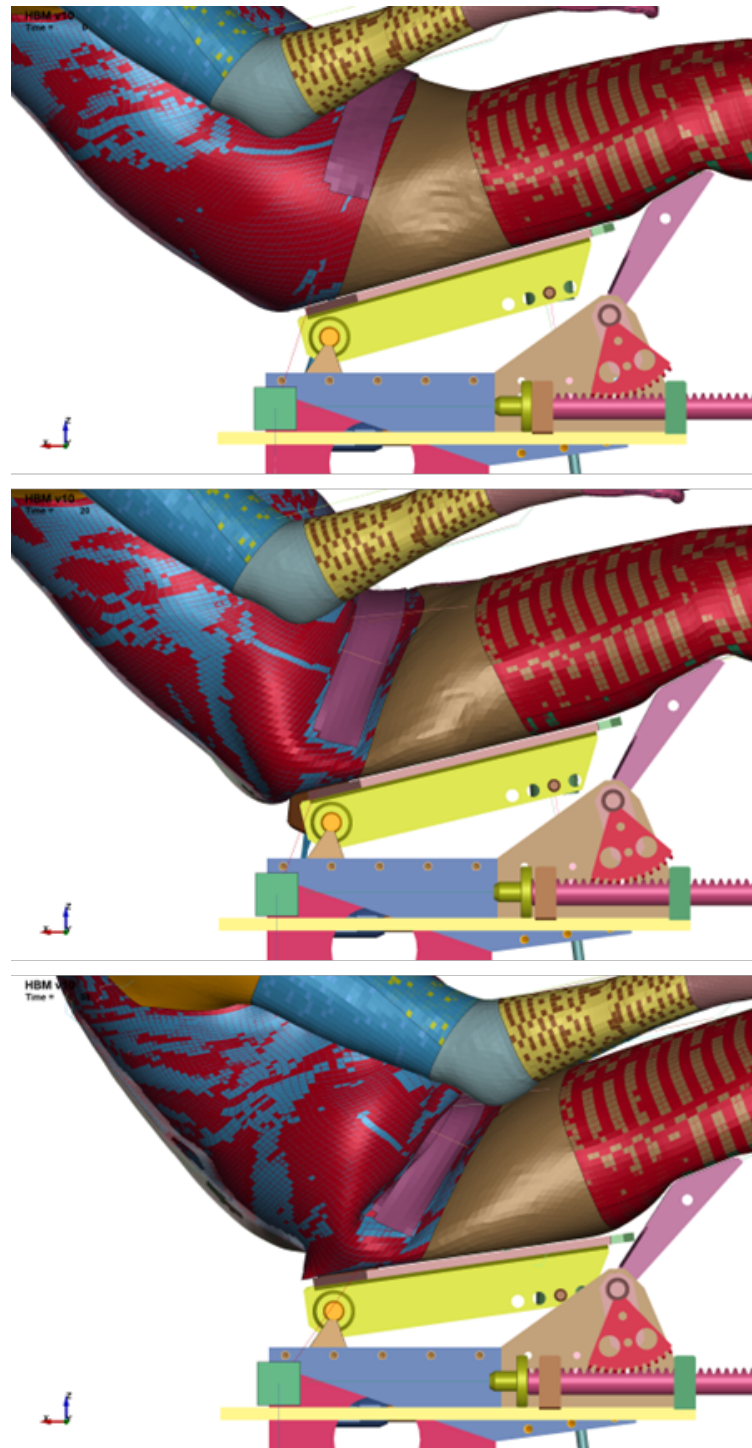


Figure 4.9: THUMS Pos12deg model forward pelvis displacement. The flesh at the back edge of the seatpan interacts with the seatpan during the forward displacement, which affected pelvis kinematics. Top-down: 0ms, 20ms, 50ms.

4.4.2 Lap Belt Kinetics

Peak lap belt tension was similar for both HBMs (approximately 7kN), which was approximately the same magnitude as Subject 3, which had lower lap belt tension due to iliac wing fracture (Figure 4.10). The THUMS exhibited a sharp reduction in lap belt tension between 50-60ms. This occurred for the THUMS models with all three pelvis positions (Figure 4.13) and was also noticeable in the buckle resultant force time history (Figure 4.11). The THUMS's peak lap belt tension and buckle resultant force also occurred approximately 10ms later than both the GHBMC and the PMHS (approximately 62ms).

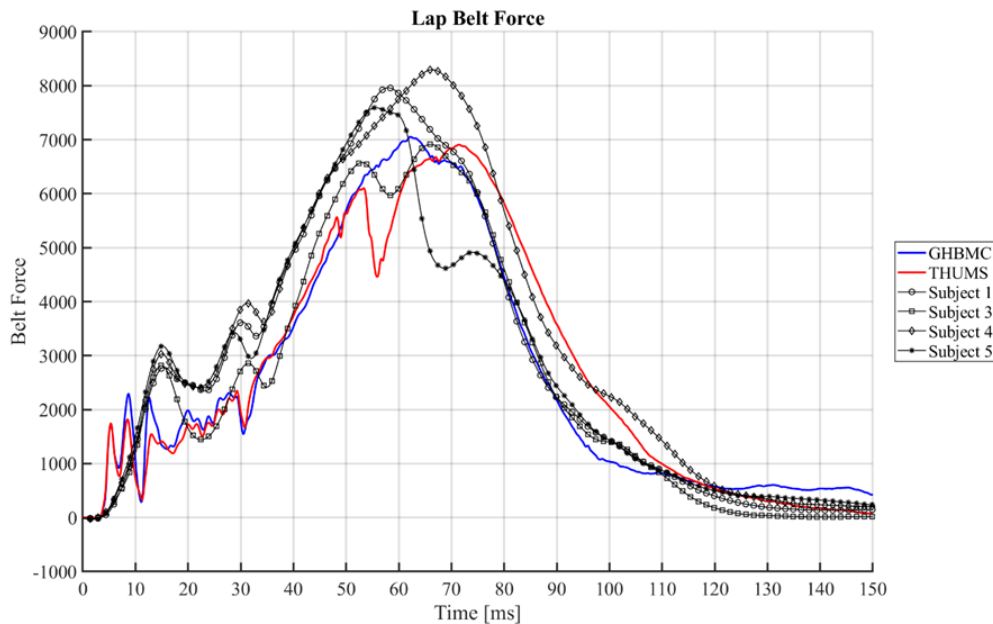


Figure 4.10: Lap belt tension, measured on the outboard side, for the GHBMC and THUMS nominal pelvis angle models.

The different pelvis orientations did not have a substantial effect on resulting lap belt tension for the GHBMC (Figure 4.12). In the THUMS however, the alternative pelvis orientations (Ant12deg and Pos12deg) resulted in lower magnitudes (1kN) of peak lap belt tension (Figure 4.13). The sharp decrease in lap belt tension was also seen for the THUMS positioned with alternative pelvis orientations.

CHAPTER 4. EVALUATION OF HBM BIOFIDELITY IN A RECLINED POSTURE

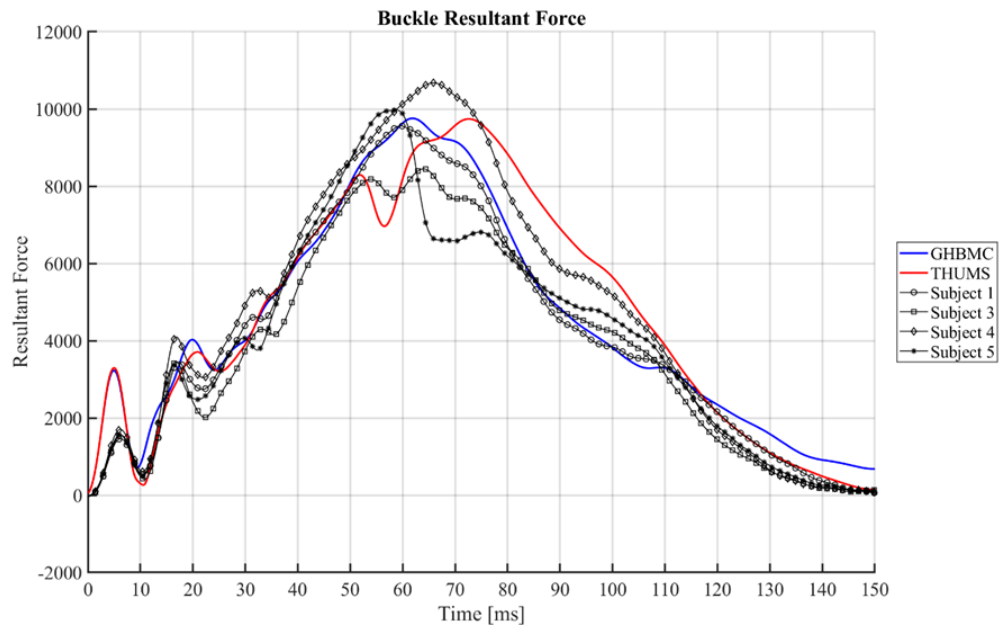


Figure 4.11: Buckle resultant force, measured beneath the buckle on the inboard side, for the GHBMC and THUMS nominal pelvis angle models.

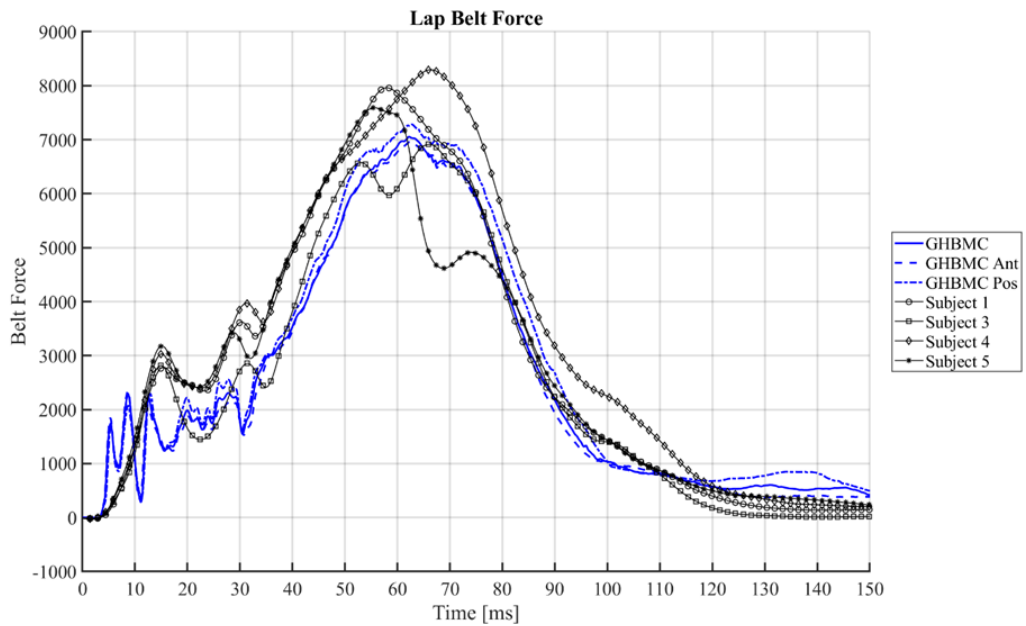


Figure 4.12: Lap belt tension, measured on the outboard side, for the three GHBMC models with different initial pelvis orientations.

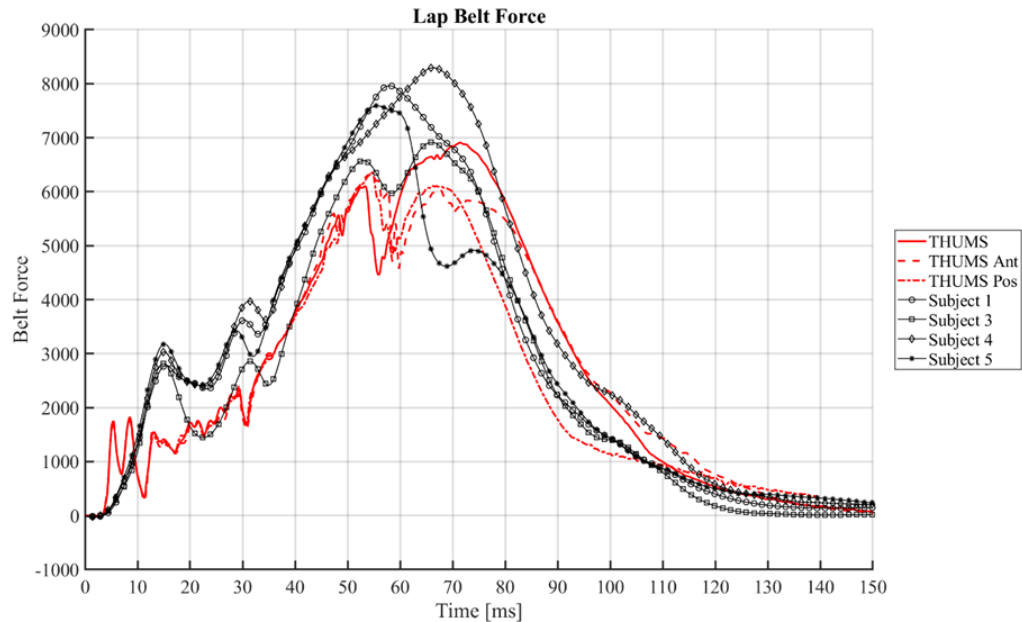


Figure 4.13: Lap belt tension, measured on the outboard side, for the three THUMS models with different initial pelvis orientations.

4.4.3 Lumbar Spine Kinematics

Generally, both HBMs exhibited less forward displacement (X) of the T11, L1, and L3 vertebral bodies than the PMHS, with the GHBMC exhibiting less forward displacement than the THUMS (Figure 4.14). This is most evident for the L1 vertebra forward displacement. Additionally, both HBMs generally exhibited more downward (Z) displacement than the PMHS, with the GHBMC exhibiting more downward displacement than the THUMS (Figure 4.15). The alternative pelvis orientations bounded the nominal response, where the Ant12deg models exhibited less forward displacement (X) and more downward displacement (Z) than the nominal pelvis position (Appendix C.4), and vice versa for the Pos12deg models (Appendix C.3).

Prior to peak pelvis forward displacement (approx. 70ms), the GHBMC and THUMS lumbar spine flexion and extension responses bounded the PMHS responses, where the THUMS exhibited a higher degree of lumbar spine extension and the GHBMC exhibited a higher degree of flexion (Figures 4.16 and 4.17). During torso forward excursion (approx. 70-100ms), the HBMs exhibited approximately 15-30° more lumbar spine flexion than the PMHS.

CHAPTER 4. EVALUATION OF HBM BIOFIDELITY IN A RECLINED POSTURE

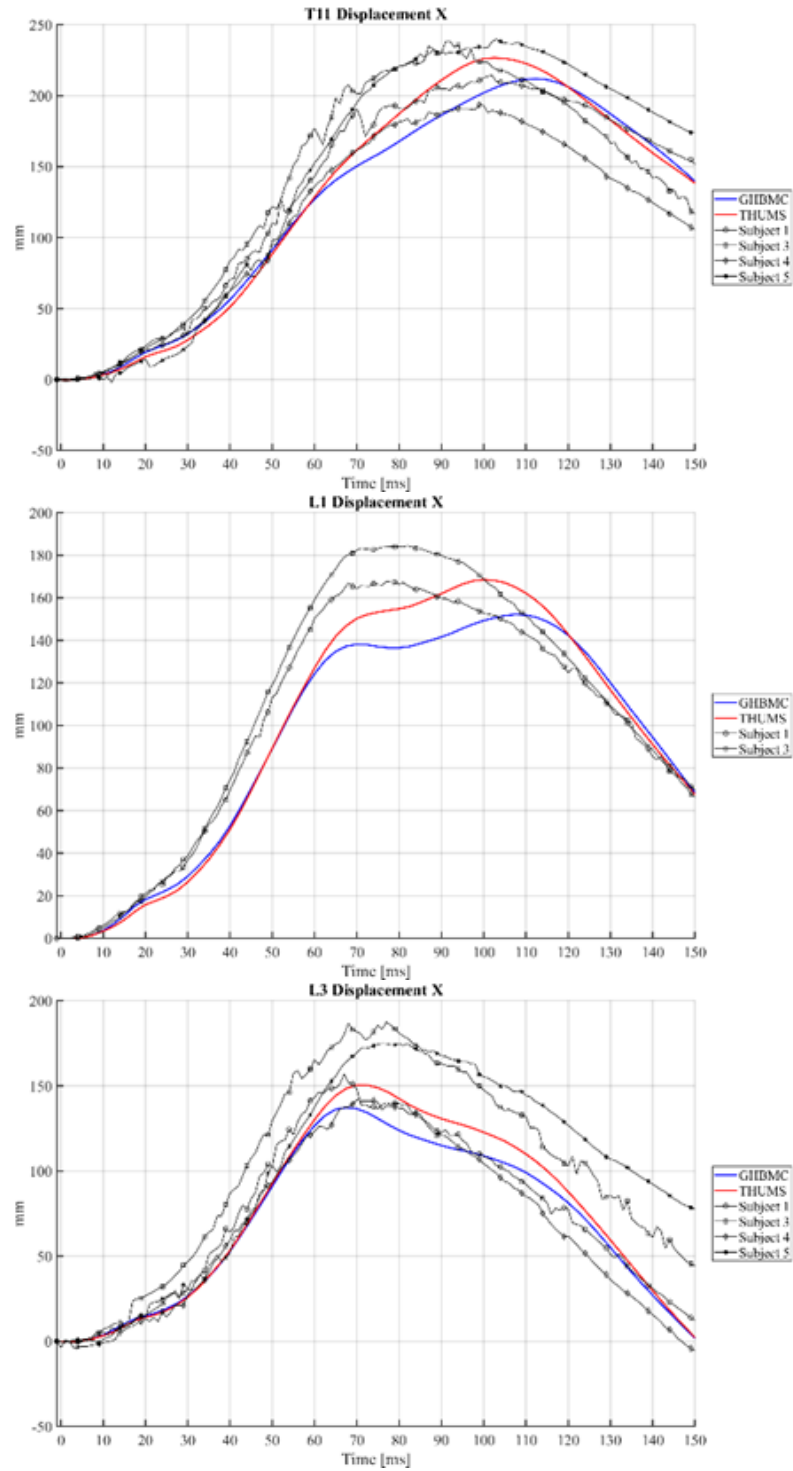


Figure 4.14: Vertebral body forward (X) displacements. Top-down: T11, L1, and L3 vertebral body displacements.

CHAPTER 4. EVALUATION OF HBM BIOFIDELITY IN A RECLINED POSTURE

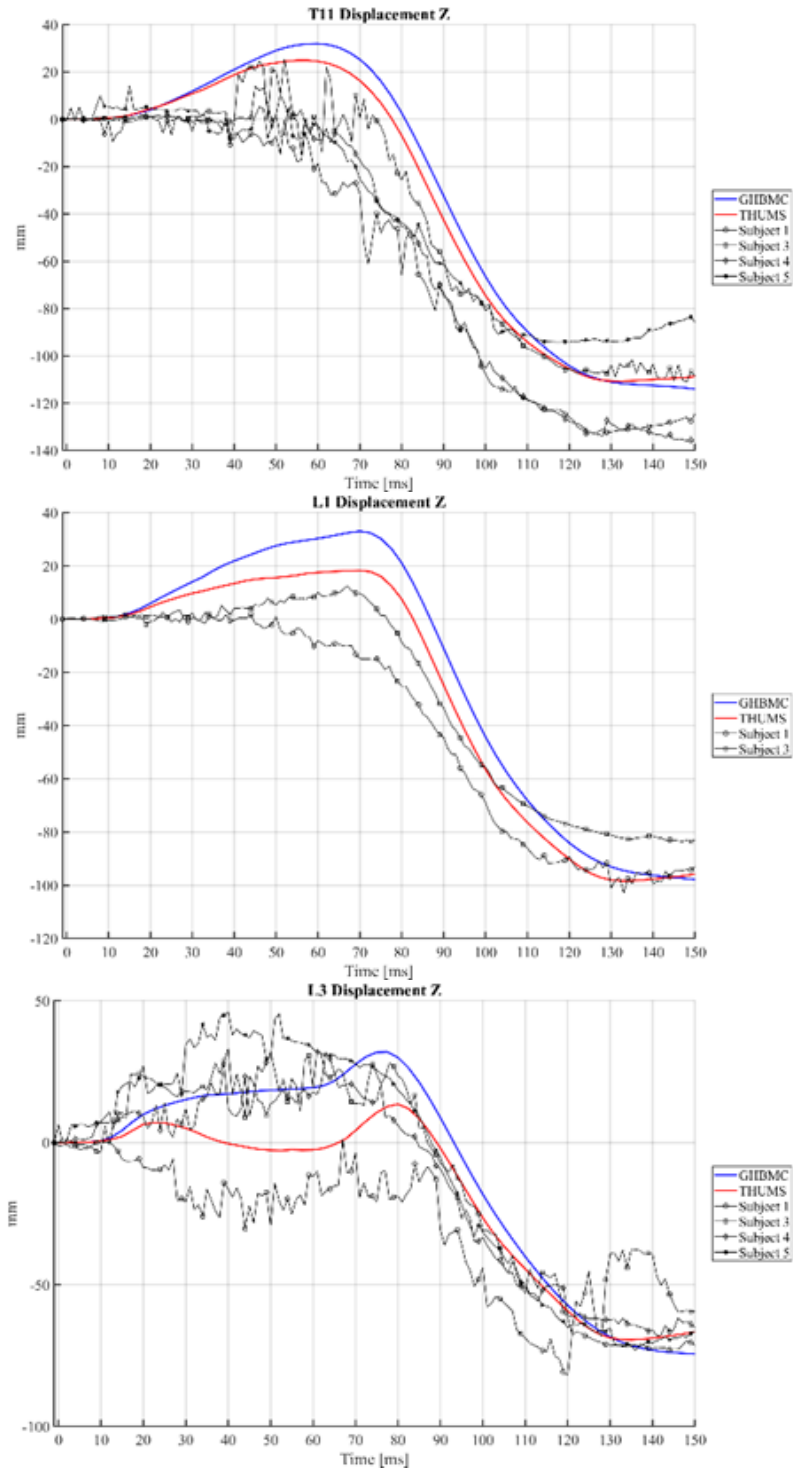


Figure 4.15: Vertebral body downward (Z) displacements. Top-down: T11, L1, and L3 vertebral body displacements.

CHAPTER 4. EVALUATION OF HBM BIOFIDELITY IN A RECLINED POSTURE

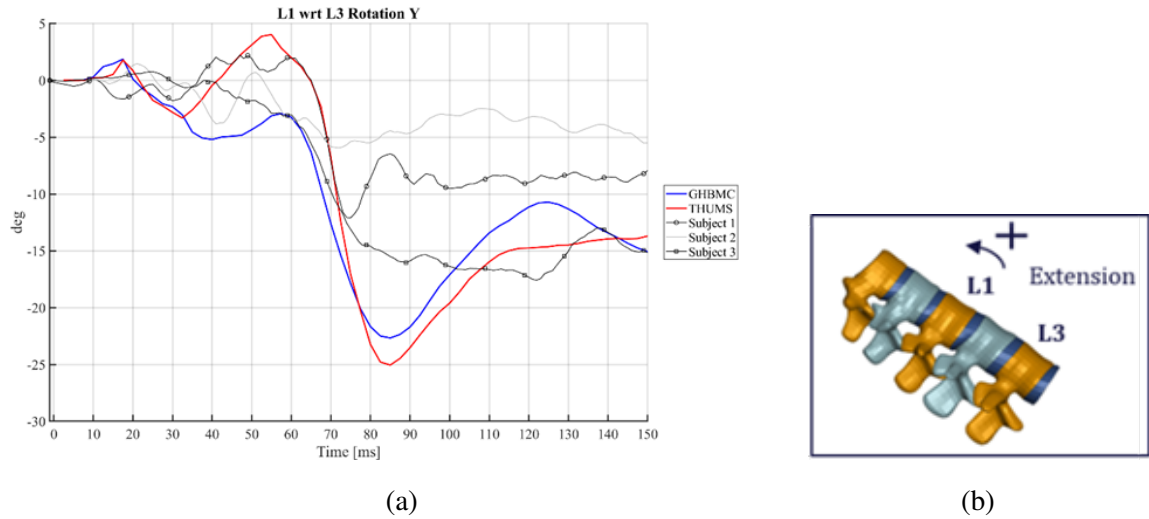


Figure 4.16: L1 vertebral body rotation relative to L3 vertebral body rotation (a) comparisons between the PMHS and the HBMs (nominal pelvis angle). A positive value indicates a rearward rotation of L1 relative to L3, akin to lumbar extension or lordosis (b).

For both HBMs, the Ant12deg and Pos12deg model flexion and extension responses bounded the Nominal model’s response (Figure 4.18). In all cases for the GHBMC, the Pos12deg model exhibited more lumbar extension prior to peak pelvis displacement whereas the Ant12deg model exhibited more lumbar flexion. This pattern held for the THUMS’s L1/Pelvis and L3/Pelvis rotations; however, in the L1/L3 rotation, the Pos12deg model exhibited more flexion prior to peak pelvis displacement and the Ant12deg model exhibited more extension. The time of peak forward flexion also varied in the THUMS model, unlike the GHBMC model, likely as a result of lumbar “buckling” (Figure 4.19).

CHAPTER 4. EVALUATION OF HBM BIOFIDELITY IN A RECLINED POSTURE

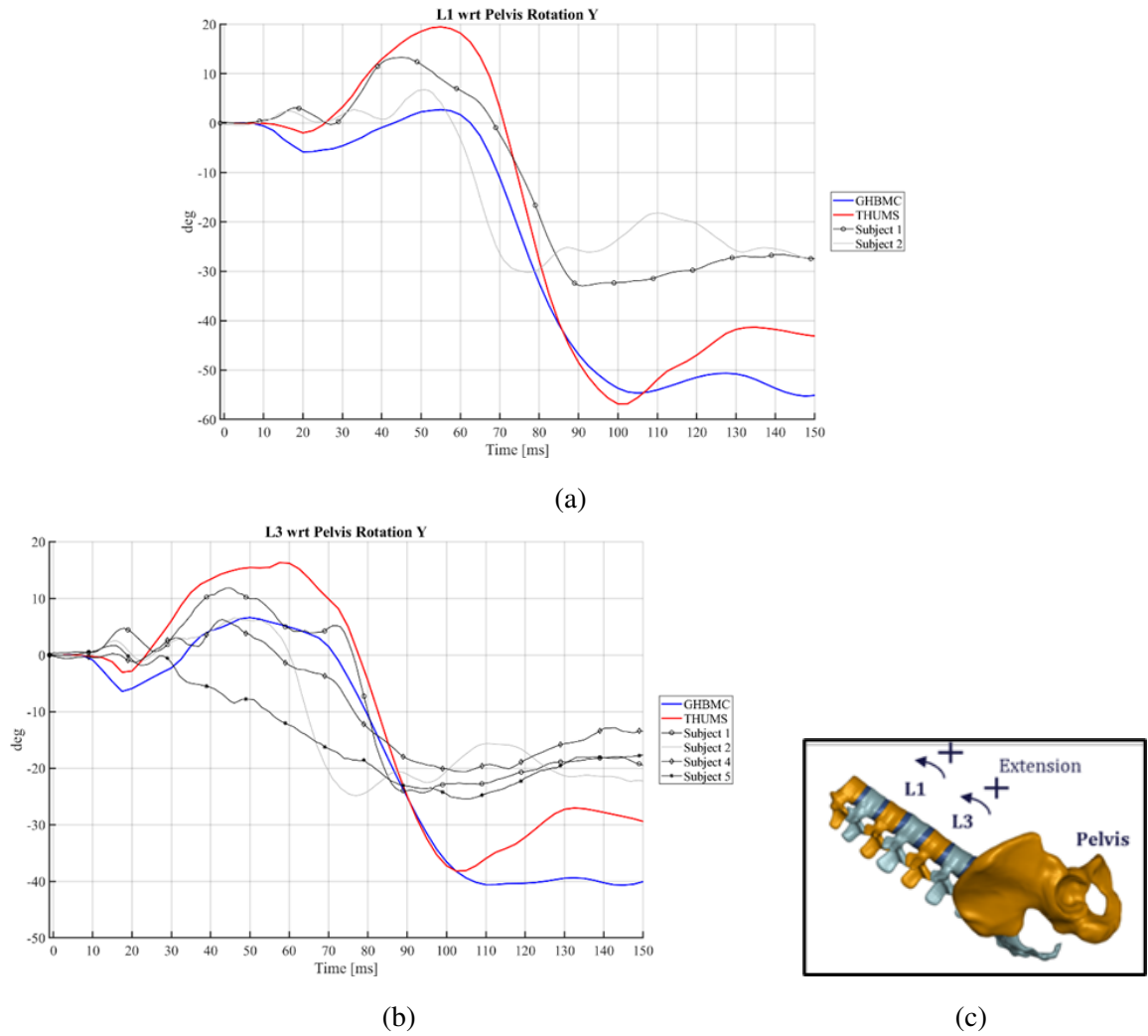


Figure 4.17: L1 vertebral body rotation (a) and L3 vertebral body rotation (b) relative to the pelvis rotation comparisons between the PMHS and the HBMs (nominal pelvis angle). A positive value indicates a rearward rotation of L1 or L3 relative to the pelvis, akin to lumbar extension or lordosis (c).

CHAPTER 4. EVALUATION OF HBM BIOFIDELITY IN A RECLINED POSTURE

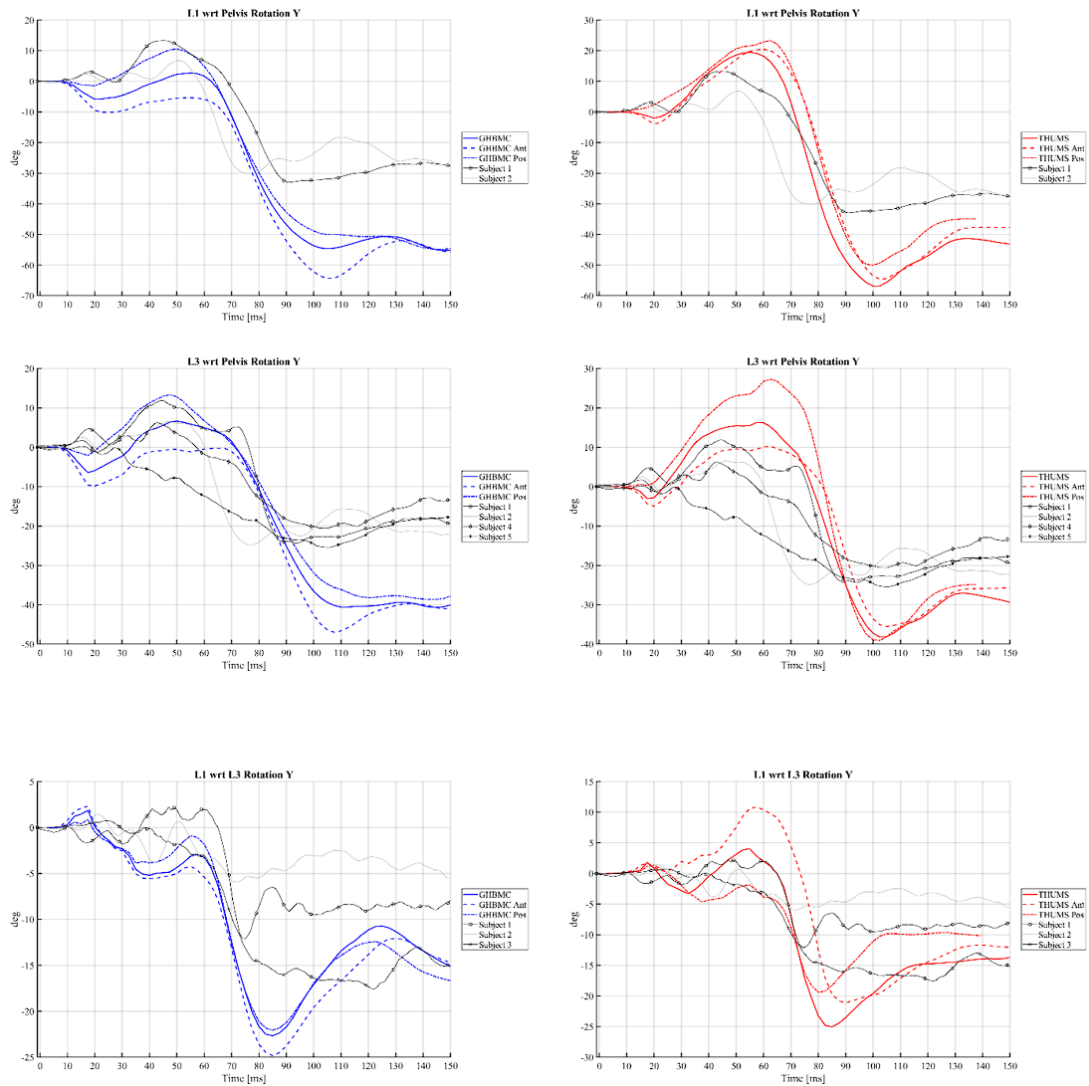


Figure 4.18: Left-right: GHBM, THUMS Nominal, Ant12deg, and Pos12deg model comparisons. Top-down: L1/Pelvis, L3/Pelvis, and L1/L3 rotations.

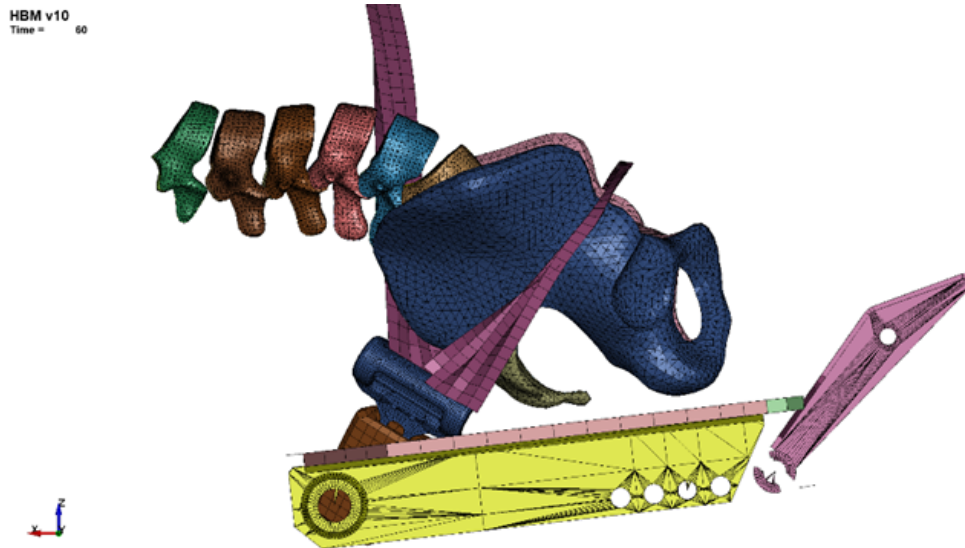


Figure 4.19: THUMS Ant12deg model lumbar spine buckling during forward pelvis displacement.

4.5 Discussion

4.5.1 Lumbar Spine Compliance

As discussed in Chapter 2, the compliance and orientation of the lumbar spine are hypothesized to influence lap belt-pelvis interaction. Thus, it is important to understand how the HBM lumbar spine compliance compares to the PMHS. Assuming equal load is being applied to the lumbar column, both the GHBMC and the THUMS showed more compliance than the PMHS, generally exhibiting less forward and more downward motion in the sagittal plane (Figures 4.14 and 4.15). From these signals, the GHBMC exhibited more lumbar spine compliance, with less forward displacement and increased downward displacement of the vertebral bodies, than the THUMS and the PMHS.

However, interpreting solely the vertebral body X- and Z-displacements is limiting as lumbar spine flexion and extension, which are key mechanisms that describe lumbar spine stiffness or compliance, cannot be discerned. The flexion and extension responses were better interpreted through the relative vertebral body rotation responses (Figures 4.16 and 4.17) in addition to the video stills of the simulation (Figure 4.20). This data confirmed the HBM lumbar spines sustained more deformation than the PMHS, exhibiting a higher degree of lumbar spine flexion (in the GHBMC) or extension (in the THUMS) prior to peak pelvis forward displacement (Figure 4.18). Additionally,

at peak forward torso excursion, both models exhibited more lumbar spine flexion than the PMHS.

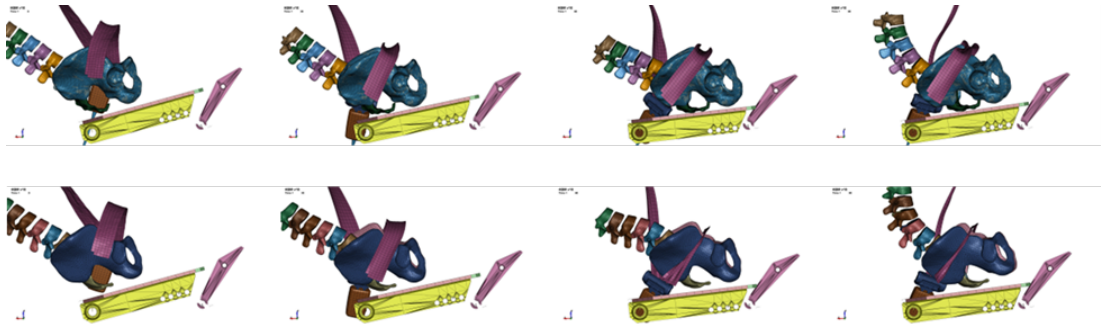


Figure 4.20: Lumbar spine kinematics shown during forward excursion for the GHBMC (top row) and THUMS (bottom row) Nominal models. Left-right: 0ms, 30ms, 60ms, 90ms.

Of the five PMHS subjects, Subject 1 exhibited more extension than the other PMHS prior to peak pelvis forward displacement and prior to sustaining a three-column burst fracture at the L1 vertebral body. However, this extension was of less magnitude than the THUMS and also transitioned into forward flexion at an earlier time. The GHBMC showed more forward flexion than the PMHS prior to peak pelvis displacement for the L1/L3 and L1/Pelvis rotations but exhibited a similar flexion response for L3/Pelvis rotation.

During forward torso excursion, both models exhibited more lumbar spine flexion than the PMHS. However, the GHBMC showed a magnitude of bending (range of motion, or ROM) that was generally more similar to the PMHS than the THUMS. Measuring the change in angle from peak extension to peak flexion, the GHBMC had on average approximately 10-15° more ROM than the PMHS, whereas the THUMS had approximately 15-30° more ROM. Thus, while the formulation of both HBMs' lumbar spines showed more ROM than the PMHS, the GHBMC exhibited a more biofidelic lumbar spine flexion and extension response than the THUMS .

4.5.2 Lap Belt-Pelvis Interaction

One conclusion drawn from Chapter 3 was that the initial lap belt fit may have partially contributed to resulting pelvis rotation polarity: Subjects 1 and 2 had lower initial lap belt placements relative to the pelvis and exhibited forward pelvis rotation, and Subjects 4 and 5 had higher initial lap belt placements relative to the pelvis and exhibited a neutral and slight rearward pelvis rotation, respectively. In this chapter, the GHBMC had a higher initial lap belt placement relative to the pelvis than the THUMS as a result of the subject's abdomen shape (Figure 4.3), and also

CHAPTER 4. EVALUATION OF HBM BIOFIDELITY IN A RECLINED POSTURE

exhibited a rearward pelvis rotation during pelvis forward displacement (Figure 4.6). In contrast, the THUMS had a lower initial lap belt placement and exhibited a forward pelvis rotation. Thus, it is possible that, in addition to the initial orientation and compliance of the HBMs' lumbar spines, the initial lap belt fit may also have affected the resulting pelvis rotation exhibited by these models.

In the THUMS simulations, the lap belt roped substantially, which effectively collapsed the belt webbing shell elements and resulted in a reduction in lap belt tension that occurred at the time of roping. This roping did not occur in the PMHS tests and the resulting reduction in tension is an artifact of the simulation that would not occur in reality. This artifact will substantially affect submarining occurrence, as the lap belt migration relative to the pelvis may not be possible with the collapsing of the lap belt webbing elements. This is likely attributed to both the compliance and mechanical nature of the THUMS's flesh, which is disconnected from the internal musculoskeletal structure of the model and thus fits over the model as a glove would over one's hand. One likely resulting mechanism is that, during the model's forward pelvis displacement, the flesh is sliding relative to the internal structure, resulting in a non-realistic gathering of this tissue anteriorly, which crimps down on the lap belt (Figure 4.21). Curiously, while this disconnect between the flesh and musculoskeletal system is inherently non-biofidelic, a gross comparison of the flesh-belt interaction between the THUMS model and the PMHS looks more similar than the GHBMC model and the PMHS, as the PMHS's flesh also protrudes out anteriorly and folds over the lap belt during forward torso flexion (Figure 4.22). This is interesting since the GHBMC's tied contact between the flesh and the musculoskeletal structure is inherently more biofidelic. It is also worth mentioning that no substantial migration of the lap belt relative to the pelvis occurred for either HBM, which is consistent with what was seen in the PMHS tests other than the inboard side of Subject 5 who submarined.

Chapter 2 introduced the compliance of the adipose tissue as a potential factor that affects lap belt-pelvis interaction. The non-realistic lap belt roping seen in the THUMS simulations, the visible differences of belt-flesh interaction between the HBMs, and the lack of lap belt-pelvis migration all point to this flesh compliance as a factor affecting the belt-pelvis interaction. This factor will be further explored in Chapter 6.

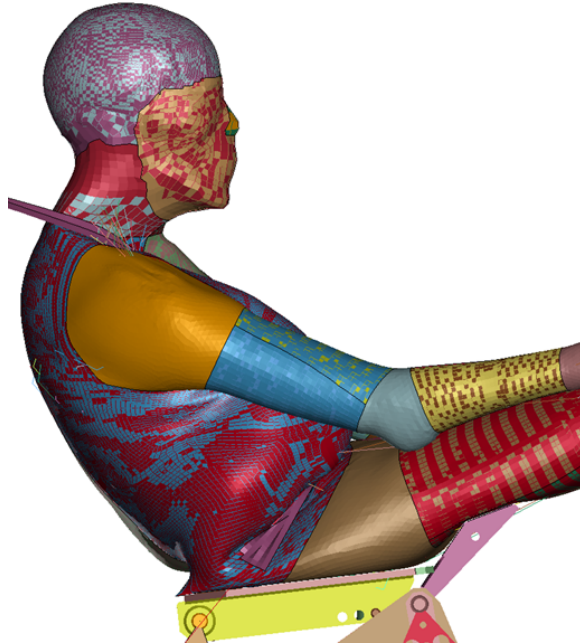


Figure 4.21: The THUMS model's flesh sliding contact permitting the anterior gathering of this tissue, which collapses the webbing (See Figure 4.20).



Figure 4.22: Lap belt-flesh interaction during forward pelvis displacement. Left-right: GHMBC, THUMS, PMHS.

4.6 Conclusions

The following conclusions were drawn from this chapter's analysis:

1. The GHBMC and THUMS HBMs exhibited more range of motion in the lumbar column than the PMHS, resulting in increased downward vertebral body displacements, decreased forward vertebral body displacements, and increased flexion during forward torso excursion.
2. Prior to peak forward pelvis displacement, the THUMS lumbar spine exhibited more extension than the PMHS, whereas the GHBMC exhibited more flexion than the PMHS. Both models exhibited increased flexion after peak pelvis displacement, during forward torso excursion.
3. While both HBMs exhibited more lumbar spine ROM, the GHBMC showed a level of compliance that was more like the PMHS than the THUMS, where the GHBMC exhibited an average of 10-15° more range of motion than the PMHS and the THUMS exhibited 15-30° more range of motion.
4. The THUMS's flesh interaction with the lap belt resulted in lap belt roping not seen in the PMHS tests, with a subsequent decrease in lap belt tension which would not occur in reality. This artificially affected the lap belt-pelvis interaction and resulting pelvis kinematics.
5. Abdominal soft tissue compliance was again found to be a potential factor that affected lap belt-pelvis interaction as the belt-flesh interaction is visibly different between HBMs. This will be further explored in Chapter 6.

The results from this chapter show the THUMS as the less biofidelic HBM in this condition. These results, combined with the results of Chapter 6, will be used to inform the selection of which HBM to use in Chapter 8's parametric study.

Chapter 5

The Effect of Lap Belt-Pelvis Angle on Lap Belt-Pelvis Interaction

5.1 Executive Summary

5.1.1 Relevance and Goal

Chapter 2 first introduced the lap belt-pelvis angle (Figure 2.7), which encompasses both the pelvis and lap belt angle parameters, as a factor that was hypothesized to affect submarining occurrence. This factor was identified in the reclined frontal impact sled test experiments of Chapter 3, in which the subject who submarined exhibited the largest lap belt-pelvis angle (indicating a shallow lap belt angle relative to the pelvis) at the time of submarining (Figure 3.19). This finding suggested a threshold at which, for a given lap belt-pelvis angle, submarining would occur. While this mechanism has been described as lap belt “unhooking” from the ASIS, this underplays the contribution of soft tissue, of which the curvature has been shown to dictate initial lap belt position (Figure 4.3) and the material formulation has been shown to influence lap belt-pelvis interaction (Figure 4.22). Thus, the goal of this chapter was to evaluate the effect of lap belt-pelvis angle on submarining occurrence in both an upright and reclined posture. As the soft tissue curvature will change for a given torso angle, investigation of the contribution of abdomen shape on initial lap belt fit and submarining occurrence will also be performed.

5.1.2 Key Conclusions

The full list of conclusions can be found in Section 5.6 below. In summary, both torso angle and lap belt-pelvis angle affected initial lap belt placement. Generally, the lap belts were positioned higher and further forward in the upright condition versus the reclined condition due to the forward protrusion of the abdominal soft tissue in the upright posture. A smaller lap belt-pelvis angle also positioned the lap belt further forward from the pelvis. One of four tests, with an upright torso angle and a small lap belt-pelvis angle (indicating a more vertical lap belt angle with respect to ground) did not result in submarining. In this test, the lap belt was also positioned most forward relative to the pelvis, and the additional abdominal soft tissue between the belt and the pelvis may have aided in mitigating submarining for this subject as the tissue's volumetric expansion (resulting from the belt pull) formed a physical barricade above the lap belt that prevented upward lap belt migration.

The results of these tests provided a wealth of information, including how varying lap belt-pelvis and torso angle contribute to initial lap belt fit and submarining occurrence, as well as highlighting potential contributions of abdominal soft tissue stiffness on these outcomes. Chapter 6 evaluated the response of the HBMs relative to these outcomes and aid in determining a model that demonstrates better biofidelity, which was used in Chapter 9.

5.1.3 Contributions

This chapter presents the first experiments conducted to examine the effect of lap belt-pelvis angle on submarining occurrence for both upright and reclined posture. This dataset can be used for validating the response of the HBM's abdominal soft tissue during lap belt-pelvis interaction of the HBM, as HBMs have been shown to exhibit differences in these responses based on differences in abdominal soft tissue compliance [35].

5.1.4 Publication

Richardson, R., Donlon, J. P., Forman, J., Gepner, B., Kerrigan, J. (2022). The Effect of Recline Angle and Restraint Geometry on Lap Belt-Pelvis Interaction for Automotive Occupants of High BMI. *Annals of Biomedical Engineering*. (Submitted).

5.2 Introduction

Chapter 2 first introduced the lap belt-pelvis angle (Figure 2.7) as a factor that was hypothesized to affect submarining occurrence in the literature. The lap belt-pelvis angle is at the intersection of an intrinsic and an extrinsic parameter hypothesized to influence submarining occurrence and thus may serve as a useful metric in understanding submarining compared to lap belt or pelvis angle alone. The results of the experimental sled tests discussed in Chapter 3 indicated the influence of lap belt-pelvis angle as a factor that affected submarining occurrence: the subject that submarined exhibited the largest lap belt-pelvis angle at the time of submarining (Figure 3.19). A larger magnitude of the belt-pelvis angle metric indicates a more rearward pitch of the pelvis and/or a shallower lap belt angle in the global reference frame. This finding suggested a threshold at which, for a given lap belt-pelvis angle, submarining will occur.

The most comprehensive way to quantify individual and interaction effects of factors on belt-pelvis interaction is through a sensitivity study, in which the influence of an input (e.g., torso recline angle and belt-pelvis angle) on an output (e.g., resulting belt fit and submarining occurrence) is quantified through controlled variation of that input. Sensitivity studies can be conducted experimentally or computationally; however, they are most always conducted computationally due to the physical, ethical, and financial limitations of experiments. To perform a computational sensitivity study, one must use a model that has been validated for the evaluated conditions, meaning the model has been validated relative to experimental (e.g., PMHS) data and has shown sufficient biofidelity. Most HBMs have been developed to study overall occupant responses in severe crashes and loads on the skeletal structure, with less focus on the detailed mechanism of belt-flesh interaction. In comparing to belt-pelvis kinematic response data obtained from seated belt pull tests using PMHS, a state-of-the-art HBM lacked biofidelity due to the pelvic-abdominal tissue's over-stiff response in shear, which restricted the belt from translating superiorly [35]. Thus, understanding the role of torso angle and lap belt-pelvis angle on submarining occurrence via a sensitivity study was best understood through experiments using PMHS prior to evaluating how well the HBMs predict the PMHS response.

Furthermore, understanding the role of soft tissue curvature and compliance on lap belt-pelvis interaction remains to be understood. In a frontal motor vehicle collision (MVC), the lap belt loading the abdomen can occur due to two different conditions: 1) initial lap belt malplacement or 2) submarining. The first case is when the lap belt is originally (unfavorably) placed superior to the occupant's ASIS and fails to engage with the pelvis during the occupant's forward excursion.

CHAPTER 5. THE EFFECT OF LAP BELT-PELVIS ANGLE ON LAP BELT-PELVIS INTERACTION

Studies on occupant-related factors that contribute to seatbelt fit show that obesity is one of the predominant reasons that proper lap belt fit is altered [61, 59, 60, 87]. For obese occupants, the lap belt is initially positioned further anterior-superior to the ASIS compared to non-obese occupants [59, 55]. In the second case, submarining, the lap belt is originally favorably placed inferior to the occupant's ASIS but translates superior and posterior to the ASIS during the occupant's forward excursion, loading the abdominal soft tissues. In lap belt-pelvis interaction tests conducted on different cadavers wherein the lap belt was initially positioned favorably, a lack of belt "hooking" by the pelvis was observed in cases for pelvises that had a relatively thick layer of soft tissue over the iliac crests [52]. One proposed reason for this mechanism is that the soft tissue covering the ASIS is more compliant in shear rather than in compression when engaged with the lap belt, which leads to the upward translation of the lap belt and eventually its disengagement from the ASIS [35]. One resulting physical indicator of lap belt motion relative to the occupant's pelvis during an MVC is the "seat belt sign": contusion and ecchymosis seen on the surface of the occupant's abdomen due to the high force of the belt in restraining the occupant during the crash [88]. One study, which examined real-world MVC case studies with corresponding CT scans of the automotive occupant's abdomen, found that the lap belt, as indicated by the "seat belt sign", was located further anterior to the ASIS for occupants of higher body mass index (BMI), as abdominal girth typically increases with BMI [16]. However, other factors were also hypothesized to contribute to lap belt position (and thus, submarining risk) during an MVC, including lap belt pretensioners, occupant pelvis pitch, and lap belt angle [16].

Seated belt pull tests can be used to investigate the potential contribution of soft tissue curvature and compliance on a submarining threshold through controlled variation of lap belt-pelvis angle, as these tests remove the complex factors of a dynamic sled test environment. In belt pull tests, the lap belt is dynamically pulled over the fixed surrogate's pelvis and thus, isolates the deformation response of the soft tissue. Such tests have been conducted and published in the open literature [68, 86, 89]. This chapter not only evaluated how lap belt-pelvis angle and soft tissue curvature affected initial belt fit and submarining occurrence in the PMHS, but also provided a dataset to evaluate the biofidelity of the HBM response in Chapter 6.

5.3 Materials and Methods

5.3.1 Test Matrix

To achieve this study’s aim, a test matrix was designed *a priori* with the intention of investigating intra-subject differences in initial lap belt fit and submarining occurrence (Table 5.1). Four tests were conducted in both recline (two tests) and upright (two tests) conditions at varying lap belt-pelvis angles. The lap belt-pelvis angle varied from “large”, indicating a more horizontal or shallower belt angle (first test), to “small”, indicating a more vertical or steeper belt angle (fourth test). The large lap belt-pelvis angle was predicted to increase submarining risk, which was reduced with decreasing angle. A lap belt-pelvis angle between the large and small bounds, coined “mid”, was held constant for both torso angles (second and third tests), permitting intra-subject comparison of torso angle effect.

Table 5.1: Initial (template) test matrix.

Test No.	Torso Angle	Lap belt-Pelvis Angle
D1589	Recline	Large
D1591		Mid
D1592	Upright	Mid
D1594		Small

5.3.2 Test Environment

5.3.2.1 Test rig

Seated belt pull tests were conducted using a combined pneumatic-hydraulic system (Dr. Steffan Datentechnik Advanced Side Impact System, Linz, Austria) (Figure 5.1). This system, which dynamically pulls a lap belt over a fixed surrogate and thus, isolates the kinematics of the lap belt relative to the pelvis, has been used in previous research [86].

An acceleration pulse displacement was input into a feedback-controlled air over hydraulic impactor software to generate a similar lap belt displacement relative to the pelvis as was seen in the dynamic tests of Chapter 3. This was done by analyzing the 3-D motion of the lap belt (tracked with motion tracking markers) relative to the pelvis local coordinate system from these tests. The impactor was then attached to a drive cable wrapped around two sheaves to transfer the

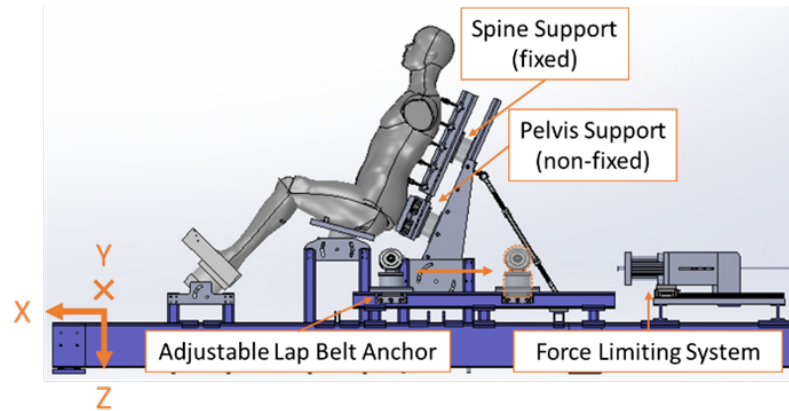


Figure 5.1: Test rig setup.

pushing force into a pulling force. The impactor system attempts to match the acceleration of the impactor as well as the hydraulic brake pressure pulse; it is not force controlled. Each end of the lap belt was connected to a steel cable which attached to the main drive cable. The generated acceleration pulse was a 120 mm nominal displacement over 80 ms (1.5 m/s), tuned at a low force limit (2 kN total, 1 kN per side of the lap belt). As a result of this impactor's feedback-loop learning system to tune the system's output to the target acceleration pulse, the resulting displacement of the drive cable (output pulse) varied among tests (Figure 5.2).

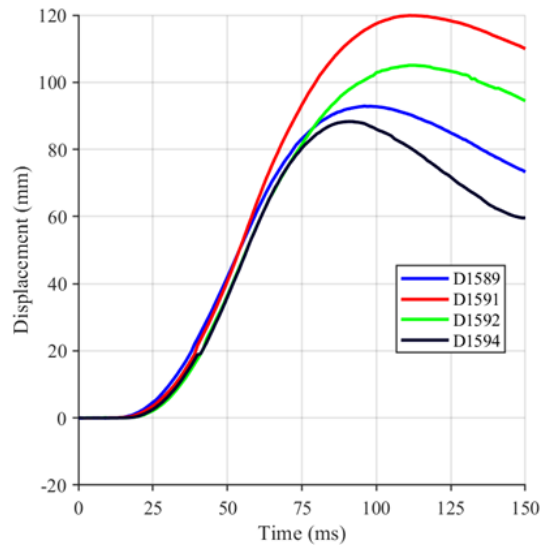


Figure 5.2: Output displacement pulse of the drive cable and lap belt for each test.

5.3.2.2 Kinematic motion tracking

Kinematic data were collected at 1000Hz using an optoelectronic motion capture system consisting of 20 cameras (Vicon MXTM, Centennial, CO, USA). These cameras tracked the positions of retroreflective spherical markers in a calibrated 3D space lying within the cameras' collective field of view. Single markers were affixed to several points on the surrounding test rig, the belt, and the spine support (seat back) attached to the subject. A mount containing four-marker clusters was rigidly installed to the pelvis posteriorly at the location of the posterior superior iliac spines (PSIS) to measure the initial pelvis orientation and track any pelvis motion, as the pelvis was not rigidly constrained. All motion was measured in the global reference frame (Figure 5.1). Initial lap belt position was measured in the local pelvis coordinate system (Figure A1). High-speed video (500Hz) recorded the full duration of the test.

5.3.2.3 Kinetic data acquisition

To measure lap belt tension, uniaxial belt tension gauges were installed on the belt webbing between the subject and the belt anchorage on both sides of the subject. Due to the viscoelastic properties of the abdominal soft tissue, a prescribed initial belt force was not possible: the measured belt force returned to zero after manually tightening the belt cables. Thus, the belt cables were tight-

ened enough to remove visible slack in the webbing and maintain initial belt placement, but without causing substantial initial deformation of the soft tissue.

5.3.3 PMHS Selection

These tests were conducted on an obese male PMHS (Table 5.2). All tissue donation, testing, and handling procedures were approved by the University of Virginia Institutional Review Board – Human Surrogate Use (IRB-HSU) Committee. The subject was frozen until testing and screened for blood-borne pathogens including HIV and Hepatitis B and C. A full body computed tomography (CT) scan confirmed the absence of bone injury, and dual-energy X-ray absorptiometry (DXA) was used to measure bone mineral density (BMD), an indicator of bone quality.

Table 5.2: Subject information.

Subject ID	Sex	Age	Cause of Death	Mass (kg)	Stature (cm)	BMI (kg/m ²)
993	M	72	Chronic obstructive pulmonary disease (COPD)	104	183	31.2

5.3.4 Initial Positioning

5.3.4.1 PMHS positioning

The subject was seated on a rigid seat pan (angled at 15°) with the feet constrained. The height and position (fore-aft) of the seat pan, seat back, and toe pan were adjustable. The belt anchors (pulleys) were adjustable in the fore-aft direction to allow for varying lap belt angles. A spinal fixation technique was implemented to rigidly fix the thoracic (four vertebrae) and lumbar (two vertebrae) spines to an aluminum bar, which was connected to the seatback (Figure 5.3). This fixation technique has been used in previous studies [68, 86]. The pelvis was supported posteriorly to restrict pelvis motion and was independent from the spine support.

The subject was positioned in a semi-reclined (45°) or upright (23°) posture, defined as the segment connecting the center-points of the first thoracic vertebra (T1) and first lumbar vertebra (L1) relative to the vertical. After torso positioning, the lower extremities were positioned such that the femurs were at 15° (parallel to the seat pan), tibias at 50°, and the feet constrained to the toe pan angled at 45° (all relative to the horizontal). The pelvis was permitted to move orientation as the

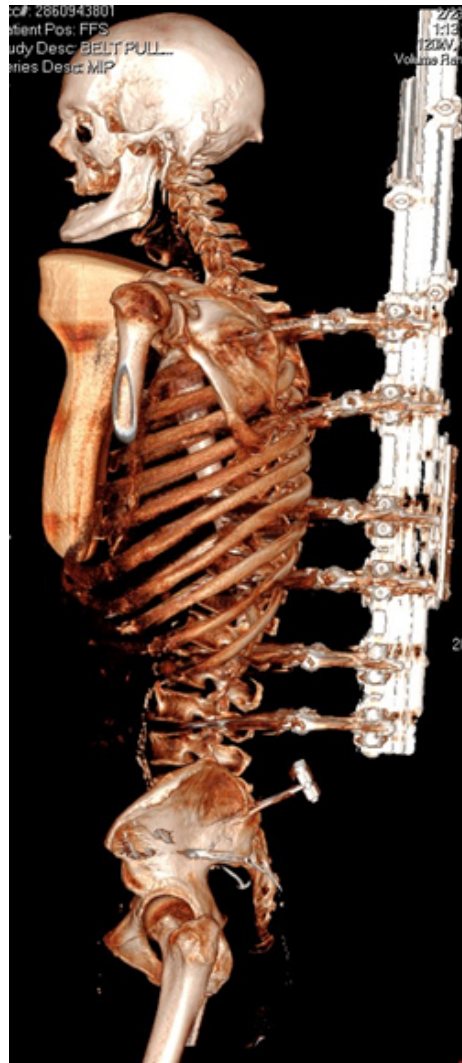


Figure 5.3: CT scan of subject 993M's spinal and pelvic instrumentation.

subject was positioned on the seat. This was the natural pelvis orientation for that subject, but was partially pre-determined by the level of lordosis present in the lumbar spine after spinal fixation.

The lap belt-pelvis angle definition is the same as that defined in Chapter 2 (Figure 2.7). The pelvis angle was defined as the angle between the segment connecting the midpoint of the left and right ASIS and the center of the pubic symphysis (PS) relative to the horizontal in the sagittal plane, referred to as the Nyquist angle in the literature [79] (Figure 5.4). The lap belt angle was defined as the angle between the segment connecting the end of the lap belt webbing to the center of the lap belt relative to the horizontal in the sagittal plane (average of left and right). Thus, the lap belt-pelvis angle was defined as the difference between these two angles (pelvis angle – lap belt angle).

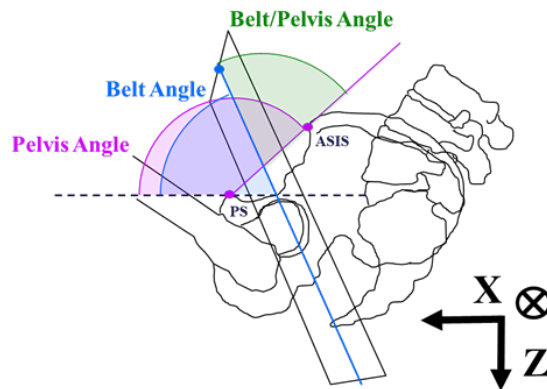


Figure 5.4: Lap belt-pelvis angle definition.

5.3.4.2 Lap belt positioning

The lap belt anchorage points were moved fore-aft to modify lap belt angle (see Appendix D.1). The target initial lap belt placement was a balance between a favorable position, such that the top edge of the belt webbing was just inferior to the ASIS (identified through palpation), and a position ensuring both the motion tracking of the lap belt and the deformation response of the soft tissue were captured. Thus, the belt was routed superficial to the pelvic-abdominal soft tissue and, where applicable, superior to the abdominal fold (Figure 5.5).

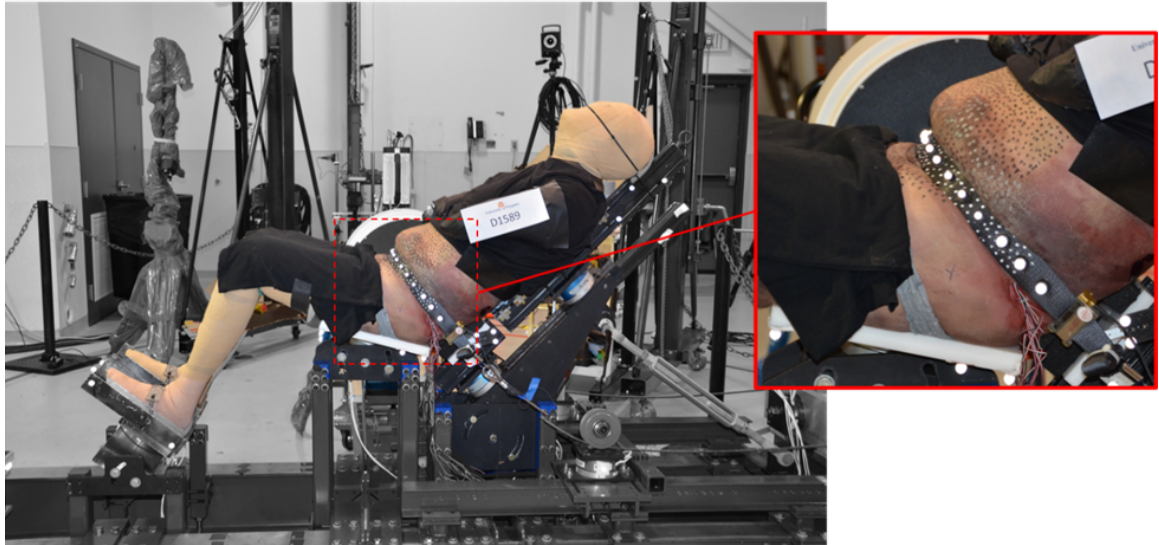


Figure 5.5: Test setup showing the lap belt routed superficial to the abdominal soft tissue.

5.3.5 Data Analysis

5.3.5.1 Coordinate System

The global reference frame was positioned anterior to the subject (origin at subject's lateral midline), with the X-axis pointing anterior and parallel to ground, Y-axis pointing right of the subject and parallel to ground, and Z-axis pointing inferior (Figure 5.1).

5.3.5.2 Submarining detection

Submarining was determined through 3D motion tracking of the markers located on the lap belt and corroborated by a sharp decrease in lap belt tension. In this study, submarining was defined as the lap belt marker (positioned along the midline of the belt webbing, widthwise) closest to the left or right ASIS passing posterior to the corresponding ASIS by more than 25 mm (half the width of the lap belt webbing) in the global reference frame (Figure 5.6). This would indicate the full width of the belt webbing moved posterior to the ASIS (since the markers were in the middle of the lap belt webbing). In the submarining cases, a sharp decrease in belt tension occurred prior to the time at which the lap belt markers passed posterior to the ASIS, as the latter measurement occurred when half of the webbing already surpassed the ASIS. Thus, the time at which the tension in the lap belt decreased was used as the time of submarining onset.

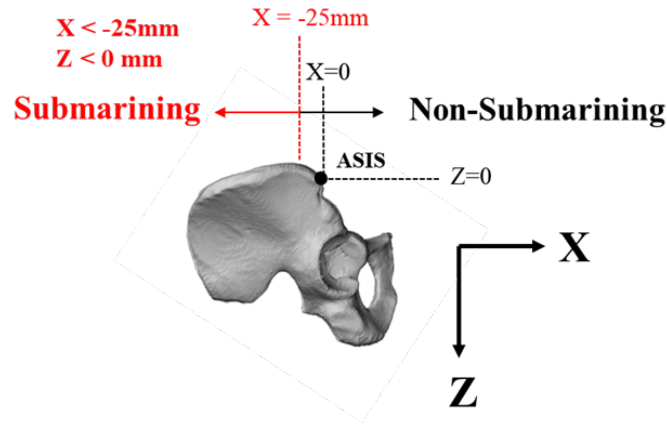


Figure 5.6: Submarining definition: when the belt is positioned above ($-Z$) and also behind ($-X$) the pelvis by 25 mm (approximate half-width of lap belt webbing), as the motion tracking markers were placed on the center of the lap belt webbing. Thus, the markers moving posterior to the pelvis by a distance greater than 25 mm indicates the full width of the webbing passed over and behind the pelvis.

5.4 Results

5.4.1 Initial Positioning

The lap belt anchorages were positioned such that the resulting LBP angle followed the target test matrix (Table 5.3), where test D1589 had a large lap belt-pelvis angle; tests D1591 and D1592 had mid lap belt-pelvis angles of approximately the same value ($\pm 5^\circ$ tolerance); and test D1594 had a small lap belt-pelvis angle (Table 5.1). The large lap belt-pelvis angle of 109° was decided upon as an initial target postulated to induce submarining as this was approximately the initial lap belt-pelvis angle of the subject who submarined in the reclined dynamic sled tests (Table 3.1).

The lap belt-pelvis and torso angle influenced the initial position of the lap belt midpoint relative to the pelvis (Figure 5.7). The fore-aft lap belt distance relative to the pelvis (dx) increased with decreasing lap belt-pelvis angle (large to small angles); thus, a smaller lap belt-pelvis angle, indicating a more vertical lap belt angle relative to the horizontal, placed the lap belt further away (in X) from the pelvis. Additionally, the fore-aft lap belt distance relative to the pelvis was larger in an upright posture.

For the same lap belt-pelvis angle (mid angle), the lap belt was initially placed higher

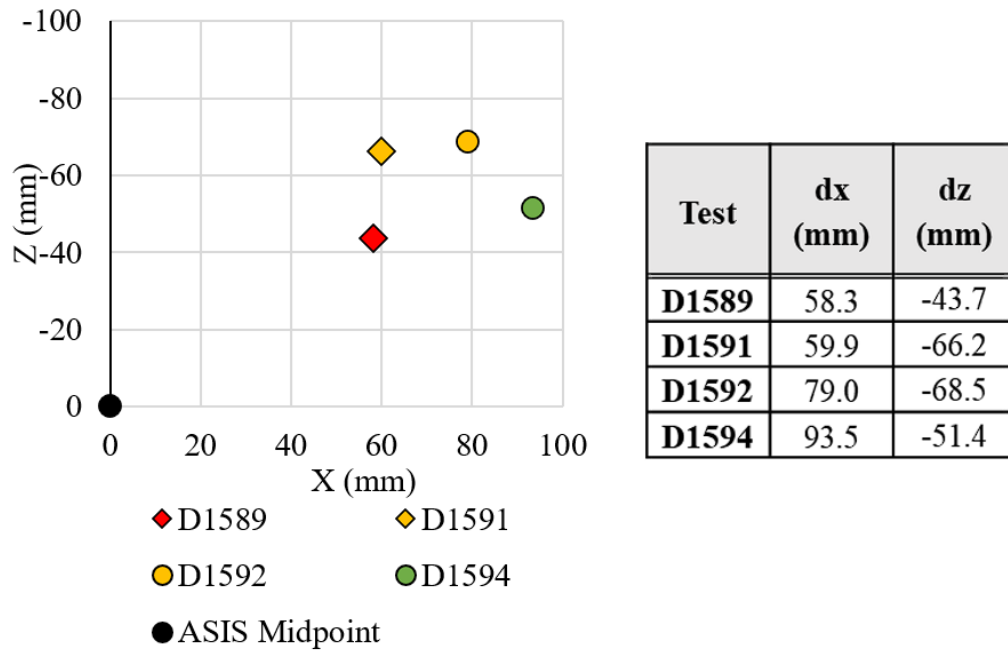


Figure 5.7: Initial lap belt midpoint (width- and lengthwise) relative to the ASIS midpoint in the global reference frame (see Figure 5.1). The colors indicate the size of the lap belt-pelvis angle: red indicates the large angle, yellow indicates mid angle, and green indicates the small angle. The shapes correspond to the torso angle: diamonds indicate the reclined torso angle and circles indicate the upright torso angle.

CHAPTER 5. THE EFFECT OF LAP BELT-PELVIS ANGLE ON LAP BELT-PELVIS INTERACTION

Table 5.3: Final test matrix.

Test	Torso Angle	Torso Angle (deg)	Pelvis Angle (deg)	Lap Belt Angle (deg)	Lap Belt-Pelvis Angle	Lap Belt-Pelvis Angle (deg)	Submarining	Time of Submarining (ms)	Lap Belt-Pelvis Angle at Submarining (deg)
D1589	Recline	45	160	51	Large	109	Yes	61	112
D1591			160	61		99	Yes	70	111
D1592	Upright	22	140	44	Mid	96	Yes	67	104
D1594			141	50		Small	90	No	X

(-dz) in the upright posture than in the reclined posture (Figure 5.7). The effect of lap belt-pelvis angle on vertical lap belt placement was dependent on the torso angle. In the reclined condition, a larger lap belt-pelvis angle (mid versus small) positioned the belt higher relative to the pelvis; however, in the upright condition, a larger lap belt-pelvis angle (large versus mid) positioned the belt lower relative to the pelvis.

Accounting for the full width of the lap belt webbing, the top edge of the webbing was at the location of the ASIS in the sagittal plane (Figure 5.8).

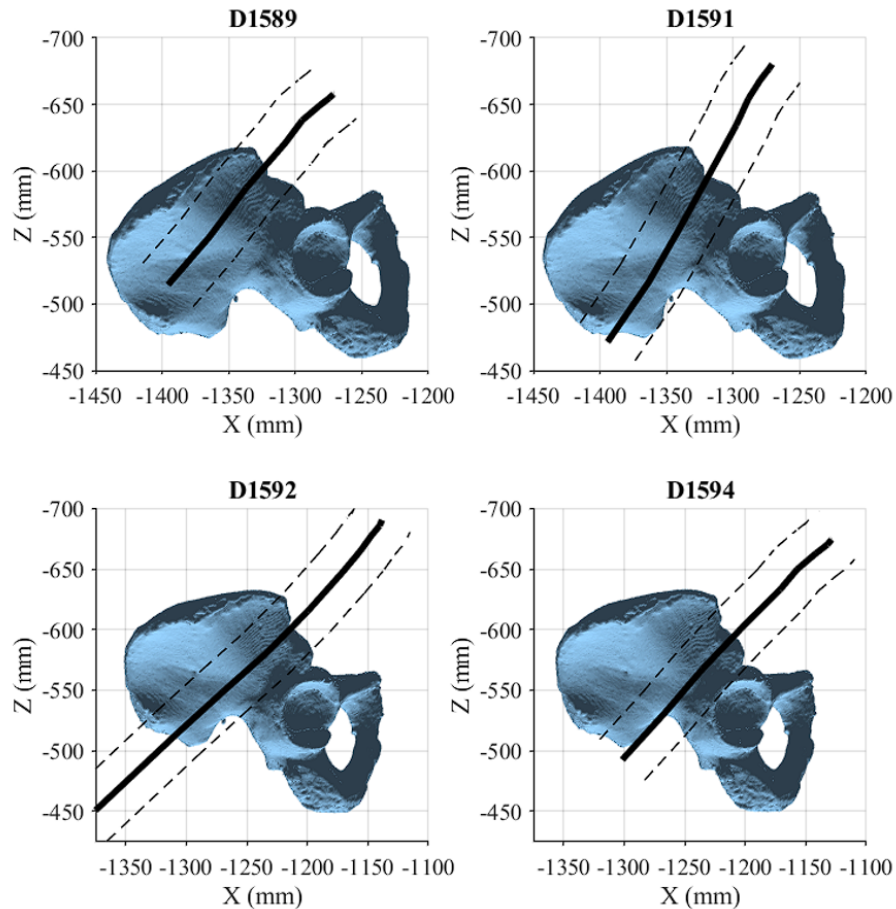


Figure 5.8: Initial position of the lap belt relative to the 3D segmented pelvis CT scans of subject 993M. The solid black line is the midline (widthwise) of the belt webbing, instrumented with 3D motion tracking markers. The dashed lines are the approximated width of the lap belt webbing.

5.4.2 Submarining Occurrence

Submarining occurred in all tests except D1594, which had an upright torso angle and small lap belt-pelvis angle, indicating a lap belt angle oriented more upright relative to ground (Figures 5.9 and 5.10). Test D1594 showed a higher magnitude of lap belt tension than the other tests (1.5-1.6 kN relative to 0.9-1.4 kN) with a peak occurring approximately 10 ms later than the other tests. While the approximated lower belt webbing edge was near the submarining threshold ($X = -25$ mm), the higher magnitude and delayed peak lap belt tension, combined with the high-speed video, resolved that the belt did not pass posterior to the ASIS (Figure 5.11).

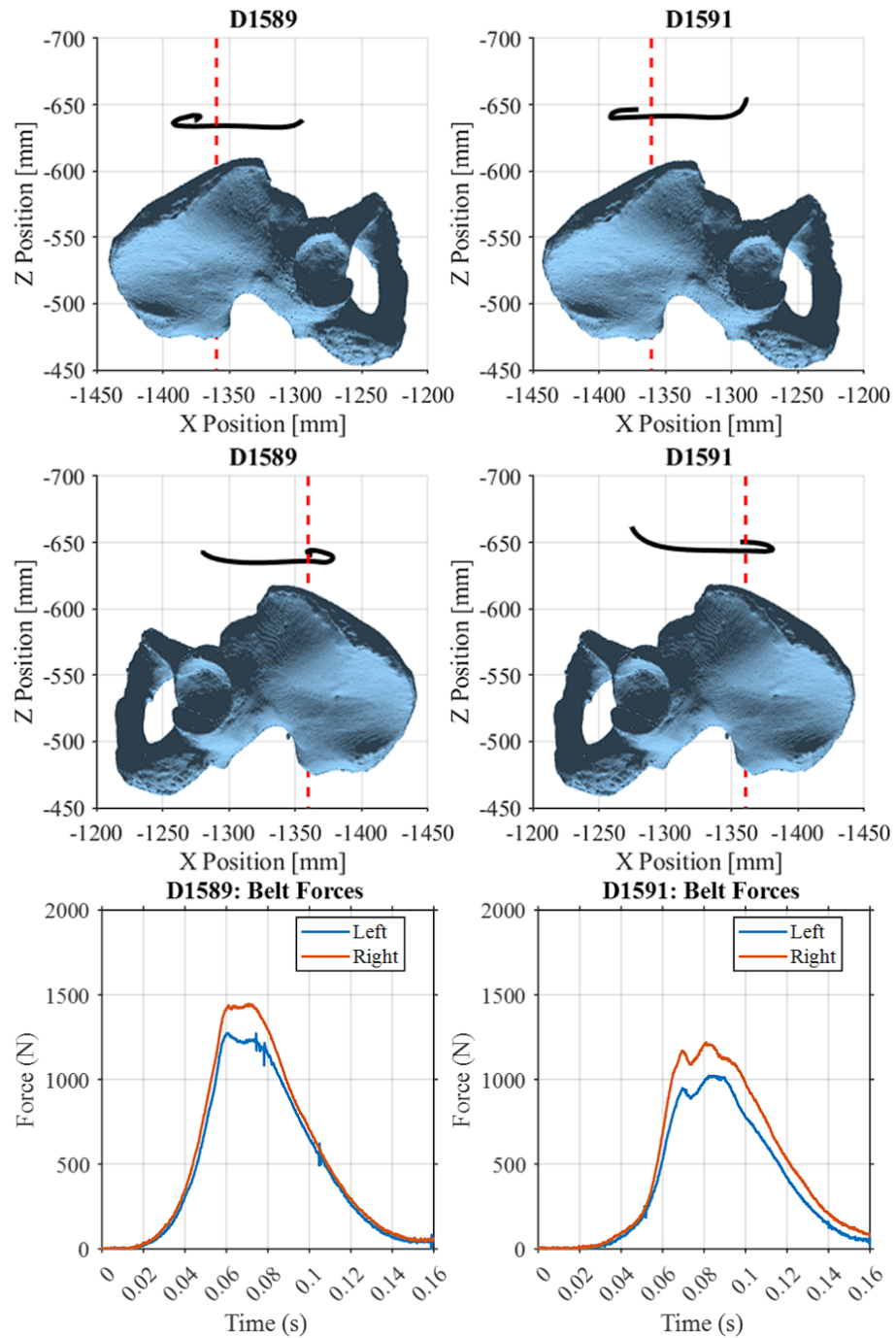


Figure 5.9: Lap belt trajectory (tracked at the lap belt marker positioned closest to the left ASIS) and lap belt tension time histories of the reclined tests D1589 (left column) and D1591 (right column).

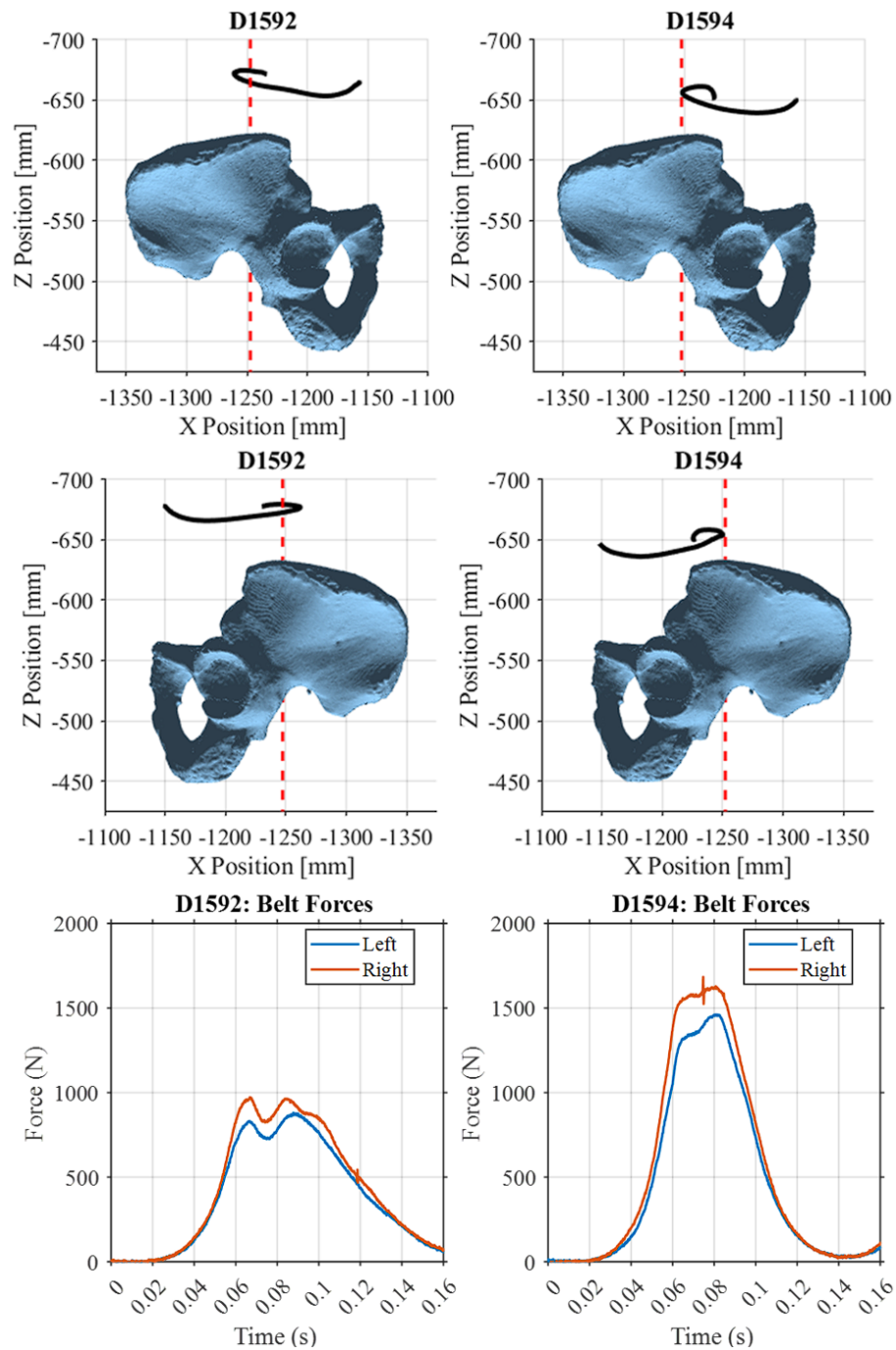


Figure 5.10: Lap belt trajectory (tracked at the lap belt marker positioned closest to the left ASIS) and lap belt tension time histories of the upright tests D1592 (left column) and D1594 (right column).

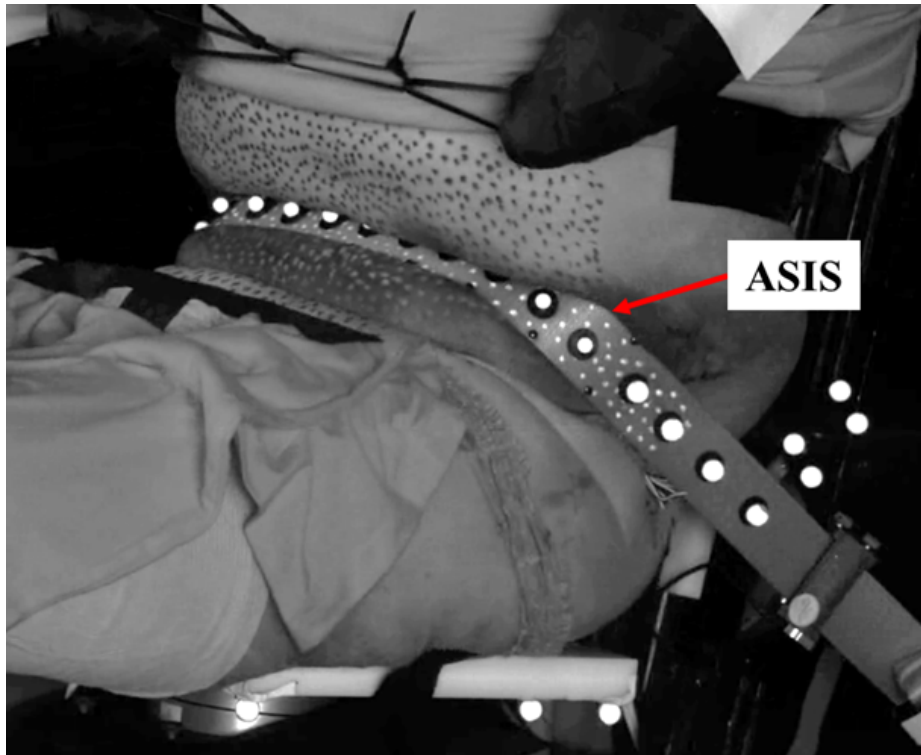


Figure 5.11: Photo of test D1594, which did not result in submarining, taken at the time of maximum lap belt displacement. The ASIS protuberance can be seen behind the lap belt webbing.

The lap belt-pelvis angle changed during the belt pulling as a result of increased lap belt tension combined with the interaction between the lap belt and the abdominal soft tissue curvature. For tests D1589, D1591, and D1592, submarining occurred at a larger lap belt-pelvis angle than the initial lap belt-pelvis angle by 3-12°, indicating a more horizontal belt relative to the pelvis and the ground (Table 5.3). Submarining occurred at nearly the same lap belt-pelvis angle for both reclined tests.

Submarining occurred between 61-70 ms, prior to peak lap belt displacement, which occurred at approximately 100 ms (Figure 5.2). The belt force-time histories showed a bimodal behavior in many instances (Figures 5.9 and 5.10). This is due to the lap belt interacting with (compressing) the subject's abdominal soft tissue (first peak) followed by contact with the pelvic bone (second peak) (Figure 5.12). This response has been seen in other belt pull tests conducted on obese cadavers [89], and is likely a result of the low force limit (1 kN) in the lap belt. For all tests, the lap belt tension on the right side of the subject was higher (by approximately 200 N) than the left side. As this trend is consistent for all tests, this may be a result of the lap belt gauge insensitivity at low

levels of belt tension.



Figure 5.12: Lap belt interaction with abdominal soft tissue for subject 993M's test (D1592) at 55 ms, 70 ms (time of initial peak in lap belt tension), 85 ms (second peak), and 100 ms.

5.5 Discussion

5.5.1 Lap Belt-Pelvis Angle

5.5.1.1 Lap belt-pelvis angle and initial lap belt placement

In addition to the subject's abdominal soft tissue, the lap belt-pelvis angle influenced initial lap belt placement; however, how lap belt-pelvis angle affected lap belt placement was dependent on the torso angle. In the upright condition, the belt was placed more anterior-inferior for a decreasing lap belt-pelvis angle (mid to small). This same effect has been seen in upright volunteer tests for varying lap belt angles, where a more vertical belt angle (indicating a corresponding smaller lap belt-pelvis angle) placed the belt more anterior-inferior relative to the ASIS [59]. However, in recline, the lap belt was positioned 23 mm higher for the smaller lap belt-pelvis angle (mid versus large). In recline, the subject's natural soft tissue curvature may have played a more dominant role in dictating belt placement relative to the ASIS than the lap belt-pelvis angle (see Section 5.5.2 below).

5.5.1.2 Lap belt-pelvis angle and submarining occurrence

Lap belt-pelvis angle was the primary factor that affected the submarining outcome in these experiments, as the test that did not result in submarining (D1594) was prescribed the smallest initial lap belt-pelvis angle. This confirms the findings of the studies identified in Chapter 2 which claimed a more vertical lap belt-angle and/or a more upright pelvis will decrease the likelihood of

submarining. This also confirms the finding from the reclined frontal impact sled test experiments discussed in Chapter 3, which showed a larger lap belt-pelvis angle for the subject who submarined.

5.5.2 Abdominal Soft Tissue

5.5.2.1 Soft tissue curvature and initial lap belt placement

The subject's high BMI resulted in a substantial amount of soft tissue in the pelvic-abdominal region, and the distribution (or curvature) of this tissue was affected by the torso angle. Since the lap belt was placed anterior to this tissue (rather than beneath an existing fold), the exterior curvature affected the initial belt placement. The upright condition caused the abdominal soft tissue to protrude out more anteriorly, which forced the belt to be positioned more anterior-superior relative to the ASIS (Figure 5.7). A more anterior-superior position of the belt with respect to the ASIS has been seen in obese volunteers relative to volunteers of normal BMI, which is likely due to this increased amount of soft tissue between the belt and pelvis [59, 60]. Similarly, an increase in seatback recline angle positioned the belt closer relative to the ASIS in the horizontal direction (dx) which has also been seen in volunteer studies [80].

5.5.2.2 Soft tissue compliance and lap belt-pelvis interaction

As mentioned in Section 5.5.2, the non-submarining test (D1594) had the most anterior (+X) initial belt placement relative to the ASIS out of all other tests; thus, for this test, there was an increased depth of abdominal soft tissue between the pelvis and the belt. This increased depth has been associated with a decreased likelihood of the belt "hooking" the pelvis in other experiments [52]; however, in an analysis of rear-world MVCs with obese occupants, the belt was shown to be able to potentially "hook" the pelvis during a forward collision, even if the belt was initially placed anterior-superior relative to the ASIS [16]. This resulting pelvis engagement was attributed to a combination of potential factors. In this study, the increased abdominal soft tissue depth between the pelvis and the belt may have aided in maintaining a low belt position in test D1594, thereby mitigating submarining.

The belt-flesh-pelvis interaction has been described as a combination of both compression and shear force, where the lap belt compresses the flesh inward toward the pelvis then shears the flesh superior relative to the pelvis [35]. A high shear stiffness resists the belt from migrating upward and submarining. In the non-submarining cases of this study, with the belt initially positioned more anterior and inferior relative to both the pelvis and abdominal soft tissue, there is a larger volume

of tissue (with increased depth) undergoing compression and shear both beneath the surface of and superior to the lap belt. The lap belt's compression of this tissue results in an anterior expansion of the flesh volume above the lap belt as a result of the incompressible nature of adipose tissue (Figure 5.12). This anterior expansion forms a physical barrier above the belt and prevents the belt from migrating up the pelvis and submarining. While a lower belt placement is typically seen as more favorable in mitigating submarining due to the increased likelihood of lap belt-ASIS engagement as the belt migrates upward, in this test series it is likely that the lower belt placement also positioned the flesh (through combined compression and shearing) to form a physical barrier which prevented upward belt-pelvis migration (Figure 5.13). Such “barrier-like” behavior of adipose tissue has been seen in other belt pull studies using obese cadavers [89], though likely to a lesser extent than in dynamic experiments with the presence of higher inertial forces.

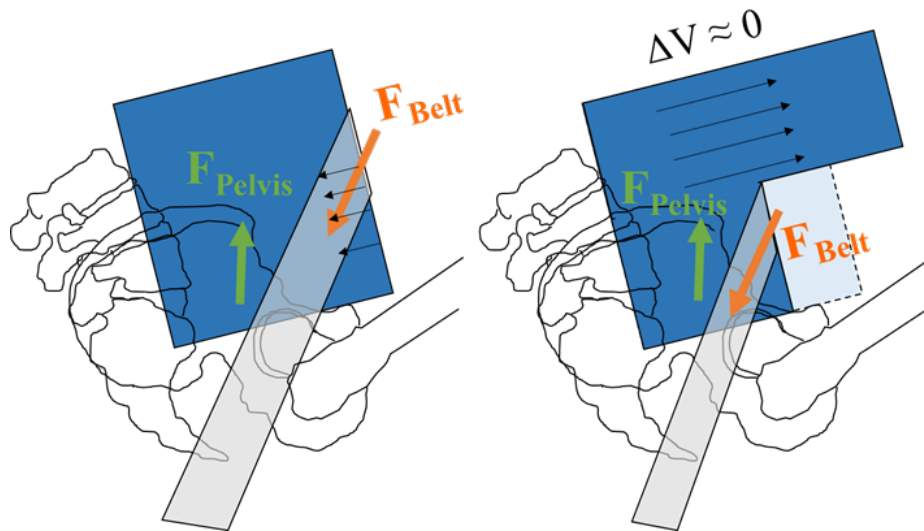


Figure 5.13: Simplified diagram describing the mechanism of abdominal adipose tissue expansion above the lap belt, which obstructs upward lap belt migration relative to the pelvis.

5.6 Conclusions

The following conclusions were drawn from this chapter's analysis:

1. The test with the subject seated in an upright torso angle and with the smallest lap belt-pelvis angle did not result in submarining, whereas the other three tests with larger lap belt-pelvis

CHAPTER 5. THE EFFECT OF LAP BELT-PELVIS ANGLE ON LAP BELT-PELVIS INTERACTION

angles, two of which had reclined torso angles, resulted in submarining. This further clarifies the lap belt-pelvis angle and recline angle as parameters that influence submarining occurrence, though their relative effects have not been quantified. In order to quantify these effects in Chapter 8's parametric study, the HBM must demonstrate similar submarining sensitivity as the PMHS to lap belt-pelvis and torso angle. Exploring this sensitivity is included in Chapter 8.

2. Both lap belt-pelvis angle and soft tissue curvature (which varied based on torso angle) influenced initial lap belt placement. In the upright condition, the lap belt was positioned further forward (+dx) from the pelvis than in the reclined condition. Additionally, a smaller lap belt-pelvis angle positioned the belt further forward (+dx) than a larger lap belt-pelvis angle. For the same lap belt-pelvis angle (mid angle), the lap belt was initially placed higher (-dz) in the upright posture than in the reclined posture (Figure 5.7). The effect of lap belt-pelvis angle on vertical lap belt placement was dependent on the torso angle. In the reclined condition, a larger lap belt-pelvis angle (mid versus small) positioned the belt higher relative to the pelvis; however, in the upright condition, a larger lap belt-pelvis angle (large versus mid) positioned the belt lower relative to the pelvis. As Chapter 2 highlighted initial lap belt placement as a potential factor that affects submarining, understanding the HBM sensitivities regarding the effect of lap belt-pelvis and torso angle on initial lap belt placement relative to the PMHS sensitivities is critical. This was evaluated in Chapter 6.
3. In the test that did not result in submarining, the additional soft tissue between the lap belt and the pelvis (dx) may have aided in submarining as the tissue's volumetric expansion formed a physical barricade that prevented upward lap belt migration. It is unknown to what extent this "barricade-like" behavior has for occupants of normal BMI or in dynamic conditions. The stiffness of soft tissue was first identified as a potential submarining-affecting factor in the literature review discussed in Chapter 2 and identified in the sled test simulations in Chapter 4, where the THUMS's abdomen flesh motion affected the resulting belt-flesh-pelvis interaction. Understanding the role of abdominal soft tissue compliance on submarining occurrence will be evaluated in Chapter 6.

Chapter 6

Evaluation of HBM Submarining Sensitivity to Lap Belt-Pelvis Angle

6.1 Executive Summary

6.1.1 Relevance and Goal

In the literature described in Chapter 2, lap belt-pelvis angle was identified as a factor that affects submarining occurrence, where a larger lap belt-pelvis angle (shallower lap belt angle) increases submarining likelihood (Figure 2.7). This factor was then investigated in the dynamic reclined sled test experiments described in Chapter 3, in which the subject that submarined exhibited the largest lap belt-pelvis angle at the time of submarining (Figure 3.19). The effect of lap belt-pelvis angle on submarining occurrence in both a reclined and seated condition was investigated through a controlled experimental sensitivity study described in Chapter 5. The test which had the smallest lap belt-pelvis angle (steeper lap belt angle) resulted in no submarining, again confirming the hypothesis of a large lap belt-pelvis angle increasing submarining risk (Figure 5.10). Additionally, lap belt-pelvis angle was found to affect initial lap belt placement, which was identified as another factor that contributes to submarining risk in the literature.

The effect of lap belt-pelvis angle on initial lap belt placement and submarining occurrence has been investigated experimentally, but it is unknown whether computational HBMs exhibit similar submarining sensitivity to this parameter. As Chapter 8 aimed to evaluate the effect of several parameters, including lap belt and pelvis angle, on submarining using an HBM in a dynamic sled test condition, ensuring the HBMs follow the similar trend as the PMHS in a controlled seated

condition was critical. Thus, the goal of this chapter was to evaluate the sensitivities exhibited by the HBM regarding lap belt pelvis angle's effect on initial lap belt fit and submarining occurrence compared to the PMHS. This chapter, in addition to Chapter 4, compared the responses of two different mid-sized HBMs and together present the analysis which determined the choice in model for the parametric study in Chapter 8.

6.1.2 Key Conclusions

The full list of conclusions can be found in Section 6.6 below. In summary, both HBMs exhibited grossly similar sensitivities to the effects of torso and lap belt-pelvis angle on initial lap belt placement; however, the HBMs showed a more favorable (lower) lap belt placement in the upright condition compared to the reclined condition for the same lap belt-pelvis angle. Additionally, the HBMs exhibited similar submarining sensitivity to lap belt-pelvis and torso angle, though compared to the PMHS, more force was required to pull the lap belt over the ASIS in the upright condition due to the difference in anthropometry between the models and the PMHS. Variation in soft tissue compliance had negligible effect on lap belt-pelvis motion. Finally, the THUMS showed a higher sensitivity to lap belt-pelvis angle than the GHBMC, exhibiting a bifurcation effect at the ASIS: a larger lap belt-pelvis angle resulted in increased lap belt penetration into the abdomen and a smaller lap belt-pelvis angle resulted in downward lap belt motion relative to the bony pelvis. Additionally, the THUMS model's lap belt-pelvis angle was more vertical at the time of submarining than the PMHS and the GHBMC. Both the increased sensitivity and change in lap belt-pelvis angle were attributed to the model's flesh - either the compliance of the material or the sliding contact relative to the pelvis.

These conclusions, in addition to Chapter 4's conclusions, were summarized in Chapter 7, which included additional analysis to verify the choice in model for the parametric study described in Chapter 8.

6.1.3 Contributions

This chapter presented the first simulation sensitivity study that investigated and compared computational HBM submarining thresholds (i.e., submarining or no submarining) to PMHS data for varying lap belt and torso angles. This analysis identified important model-specific outcomes that aided in HBM biofidelity evaluation.

6.1.4 Publication

Richardson, R., Gepner, B., Kerrigan, J. (2023). Evaluating the Effect of Recline Angle and Restraint Geometry on Lap Belt-Pelvis Interaction for Computational Human Body Models. *Traffic injury prevention*. (Planned).

6.2 Introduction

Chapter 5 described the results of the seated belt pull test, in which the lap belt-pelvis angle was found to dictate initial lap belt placement and submarining occurrence. A larger lap belt-pelvis angle, obtained by a lap belt oriented more horizontal relative to the ground and/or a pelvis pitched rearward, increases the likelihood of submarining as the lap belt is less likely to engage the ASIS. This parameter's affect on submarining was investigated in the parametric study presented in Chapter 8, in which the lap belt angle (achieved by lap belt anchorage positioning) and pelvis angle (achieved through model positioning) were separately evaluated in a dynamic sled test condition using a computational HBM. Thus, it was critical to ensure that the models demonstrated similar sensitivity to lap belt-pelvis angle as the PMHS.

Comparing the HBM and PMHS sensitivities to lap belt-pelvis angle is best done in a controlled seated condition as it removes the complexity and potential confounding factors of a dynamic condition. Computational studies have investigated the effect of varying lap belt angle on lap belt-pelvis interaction in a dynamic environment [37, 29, 30, 31, 32]; however, the HBM responses were not evaluated relative to PMHS data. Other computational studies have investigated the effect of varying lap belt angle on submarining occurrence in a seated condition using morphed obese HBMs and compared the responses to PMHS data [35, 68]. These studies showed that the models' abdominal soft tissue compliance plays a critical role in dictating submarining occurrence. The adipose tissue of the obese GHBM v4.4., in particular, was shown to exhibit a stiffer response in compression and shear than human adipose tissue [35, 48]. When the pelvis flesh is overly stiff in shear, the belt is more likely to remain below the ASIS and will not replicate submarining seen in PMHS [35].

Abdominal soft tissue compliance was identified as a potential factor that influences submarining in the literature review of Chapter 2. Additionally, abdominal soft tissue compliance was qualitatively observed to affect lap belt-pelvis interaction in the dynamic simulations (Section 4.5.2) and seated experiments (Section 5.5.2). Evaluating how different levels of abdominal soft

tissue compliance in computational HBMs was important as it may address HBM biofidelity issues. Additionally, this may also help explain how lap belt-pelvis interaction varies across a more diverse population, as experimental studies on human tissue show a wide range of inter- and intra-subject variability in stiffness under compression and shear loading [48].

This chapter describes the evaluation and comparison of the submarining sensitivities exhibited by the HBMs, for varying lap belt-pelvis and torso angles, to the PMHS sensitivities described in Chapter 5. Additionally, soft tissue compliance was investigated to understand how this variation affected lap belt-pelvis interaction and model biofidelity. This chapter, with Chapter 4, aided in the selection of the HBM to use in the parametric study of Chapter 8.

6.3 Methodology

6.3.1 Software and Hardware Used

The simulations in this chapter were performed using LS-DYNA (R11) Massively Parallel Processing (MPP) explicit FE solver. The simulations were performed on the high-performance computational cluster (Intel Xeon64/sse2). All jobs were run on the same number of nodes (2).

6.3.2 Test Matrix

Four simulations per HBM were performed to match the four experimental tests described in Chapter 5 (Table 5.1). This included two tests with a reclined torso angle (D1589 and D1591), and two tests with an upright torso angle (D1592 and D1594). Three different levels of lap belt-pelvis angle were evaluated, including a large lap belt-pelvis angle (D1589), a mid lap belt-pelvis angle (D1591 and D1592) and a small lap belt-pelvis angle (D1594).

6.3.3 FE Environment

The FE environment mimicked that of the experiments documented in Chapter 5 (Figure6.1). The global reference frame matched that of the PMHS tests: positioned anterior to the subject (origin at subject's lateral midline), with the X-axis pointing anterior and parallel to ground, Y-axis pointing right of the subject and parallel to ground, and Z-axis pointing inferior (Figure5.1). An FE model of the test fixtures used in the tests was developed using 3D computer-aided design (CAD) drawings of the original test fixture. All parts were modeled as rigid bodies. A belt pulling

piston along with the 1D belt routed through a series of sliprings was connected to the 2D belt webbing positioned on the occupant. The lap belt anchorage points (sliprings) were positioned fore-aft to match each test-specific position from the experiments documented in Chapter 5. The length of lap belt webbing was prescribed based on the length measured in each of the tests.

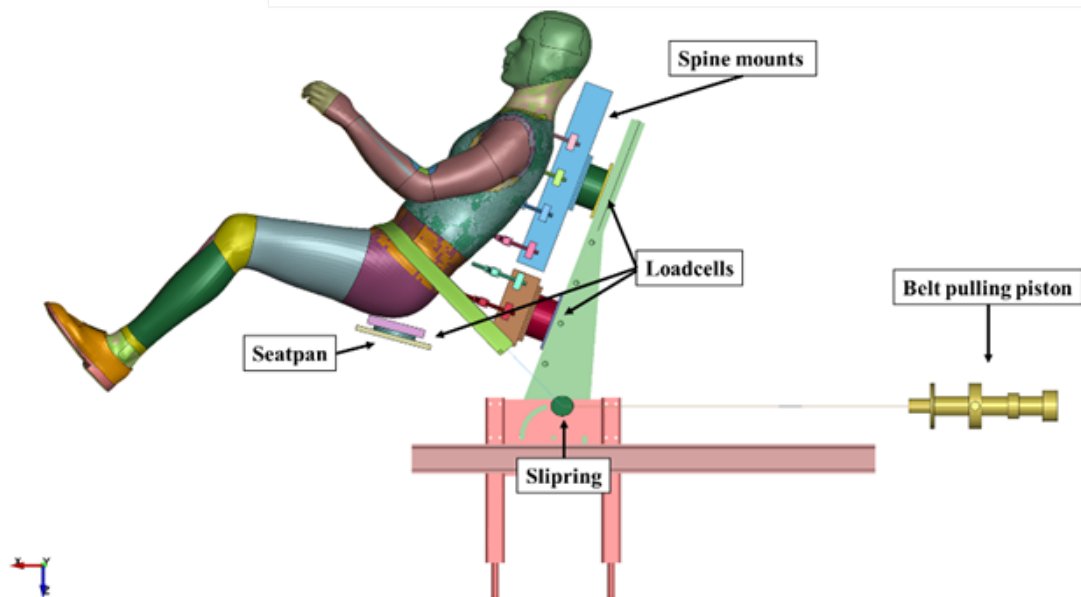


Figure 6.1: Finite-element environment for the simulations, which matches the belt pull experiments from Chapter 5. The model's upper and lower extremities were fully constrained.

While not graphically illustrated, the HBM was fully constrained using the `CONSTRAINED_EXTRA_NODES_SET` material card in LS-PrePost. Every other vertebral body and the sacrum were constrained to the spine mounts. The upper extremities and lower extremities were also fully constrained. A prescribed displacement time history, recorded from each experiment, was applied to the belt pulling piston in order to force the belt into the model's abdomen (Figure 5.2). As the experiments incorporated a mechanical lap belt load limiter (honeycomb), a load limit was also prescribed based on the peak lap belt load recorded from each test (0.9-1.6 kN).

6.3.4 Initial Positioning

6.3.4.1 HBM positioning

As in Chapter 4, two mid-sized male computational HBMs – the THUMS v.6.1 and GHBM v6.0 – were used in this chapter. These HBMs were positioned to closely match the torso

CHAPTER 6. EVALUATION OF HBM SUBMARINING SENSITIVITY TO LAP BELT-PELVIS ANGLE

recline angle and pelvis angle from the experiments documented in Chapter 5 (Table 6.1), though differences in anthropometry (mass and stature) resulted in some variability. As the goal was to investigate lap belt-pelvis angle and its effect on submarining occurrence, matching the pelvis angle (defined as the Nyquist angle, see Figure 5.4) was a priority.

Table 6.1: Initial positioning for each test and surrogate – the PMHS measurements are from the experiments conducted in Chapter 5. Each measurement is rounded to the nearest degree.

Surrogate	Test	Torso Angle	Lap Belt-Pelvis Angle	Torso Angle (deg)	Pelvis Angle (deg)	Lap Belt Angle (deg)	Lap Belt-Pelvis Angle (deg)	
PMHS	D1589	Recline	Large	45	160	51	109	
GHBMC				47	159	46	113	
THUMS				50	160	46	114	
PMHS	D1591		Mid	45	160	61	99	
GHBMC				47	159	50	109	
THUMS				50	160	50	110	
PMHS	D1592	Upright		Small	22	140	44	96
GHBMC					25	141	38	103
THUMS					26	141	38	103
PMHS	D1594		Upright	Small	22	141	50	90
GHBMC					25	141	45	95
THUMS					26	141	45	96

The positioning procedure was similar to that which was conducted for the dynamic simulations, outlined in Section 4.3.4. First, the pelvises of the HBMs and the PMHS were aligned by aligning the H-points, then oriented to match the pelvis angle (Figure 6.2). After matching the initial pelvis position and angle, the torso angle was oriented to match the angle of the PMHS within a 5° tolerance. This was done by aligning the segment connecting the center of the T1 and L1 vertebrae relative to the vertical in the sagittal plane (Figure 6.3). The femurs were positioned to match the approximate angle of the PMHS (15° relative to horizontal, in the sagittal plane).

While the pelvis was not rigidly constrained in the PMHS experiments, the pelvis was constrained externally by foam blocks which resulted in minimal pelvis rotation during the test (Figure 6.4). Thus, in addition to the spine, the sacrum was fully constrained in these simulations

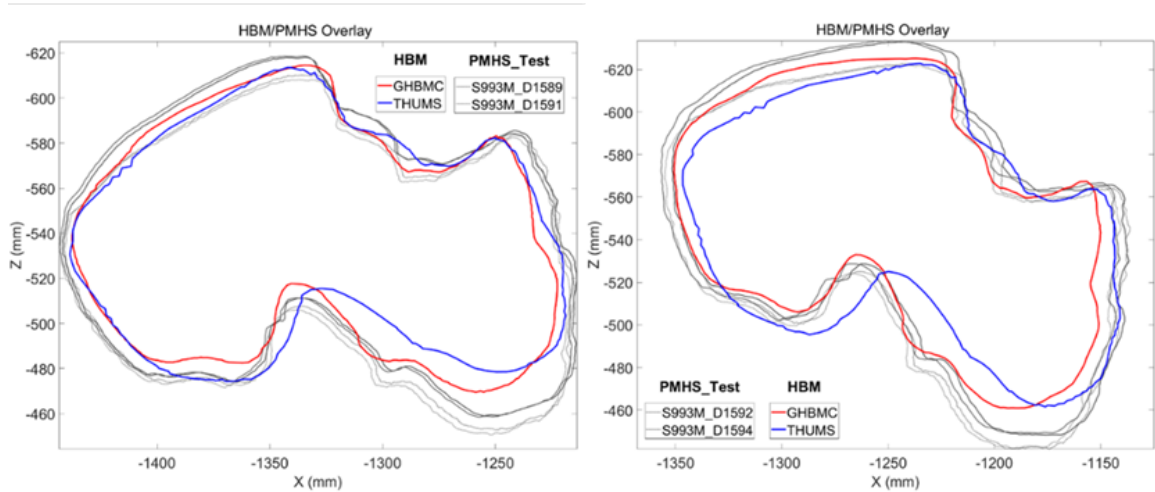


Figure 6.2: Outline of the HBM pelvises relative to the PMHS pelvis for the four different tests (left: reclined tests; right: upright tests). The light gray outlines show the left side of the PMHS pelvis (far view) and the dark gray outlines show the right side of the PMHS pelvis (near view).

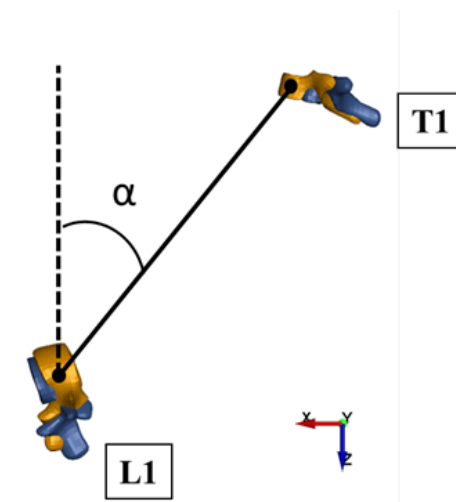


Figure 6.3: T1 and L1 vertebral body alignment of the two HBMs. Angle α matched the position of the reclined (45deg) or upright (22deg) torso angles from Chapter 5's experiments.

to improve simulation stability and allow for a more controlled analysis of the simulation results.

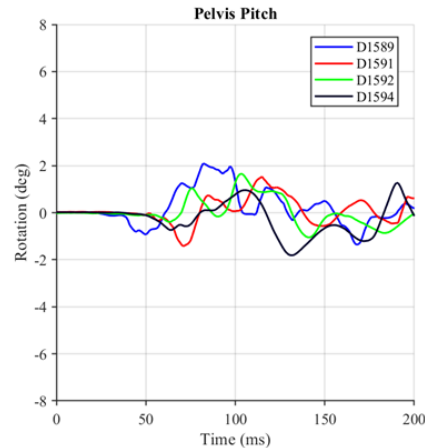


Figure 6.4: Total pelvis Y-rotation, or pitch, from the PMHS belt pull experiments.

6.3.4.2 Lap belt positioning

The belts were individually routed across the HBMs with the belt anchorage points positioned to match the fore-aft position from each PMHS test. Thus, the HBM's resulting lap belt angle (Table 6.1) and placement was dictated by the HBM's abdominal shape and anthropometry, which differed from the PMHS. As the PMHS was obese, this resulted in more soft tissue in the pelvic-abdominal region, with an increased depth between the bony pelvis and the surface of the abdomen (and lap belt) than the mid-sized HBMs. The resulting lap belt angles of the HBMs were approximately the same value for each test when rounded to the nearest degree (Table 6.1).

To route the belts, the LS-PrePost manual belt routing feature was used. Initially, the lap belt was routed across three points: the left and right anchorage points, and the node on the HBM that was closest to the center point of the lap belt from the experiments for that test in the sagittal plane (Figure 6.5, Steps 1-3). The lap belt section was then stretched across the HBM to form the shortest belt path using the LS-PrePost stretch feature (Figure 6.5, Step 4). During the stretching, the lap belt webbing takes the shortest distance from routing around the HBM's abdominal surface to connecting to the anchorage point. As a result, the lap belt migrated up the pelvis relative to the initial prescribed point. This final step was dictated by the model's abdominal shape.

The initial lap belt paths of the HBMs relative to the PMHS reflected the differences in abdominal soft tissue depth and curvature among the surrogates (Figure 6.6). As the HBMs were

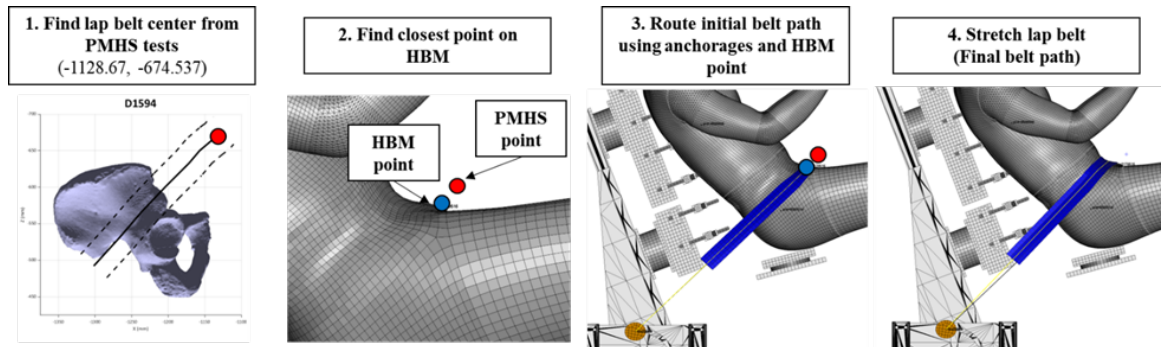


Figure 6.5: Procedure to route the lap belts of the HBMs using the LS-PrePost manual belt routing tool

mid-sized and the PMHS was obese, the lap belt center of the PMHS was generally positioned more anterior-superior relative to the pelvis than that of the HBMs due to the PMHS's excess abdominal soft tissue, which increased the depth between the bony pelvis and the lap belt. Details regarding how the lap belt placement was affected by the lap belt-pelvis and torso angle, which varied between tests, is discussed in Section 6.4.1.

6.3.4.3 Lap belt-pelvis angle

The lap belt-pelvis angle was defined as in Chapter 5 (Figure 5.4). The lap belt anchorages of the HBMs were positioned to match the anchorage positions from the PMHS tests; however, the HBMs' initial lap belt angles, and resulting lap belt-pelvis angles, differed from the PMHS due to their different anthropometries. However, the trends in target lap belt-pelvis angle size from test to test (i.e., large, mid, and small lap belt-pelvis angles) remained the same (Table 6.1). As the initial pelvis orientations and lap belt angles were approximately equal between HBMs, the resulting initial lap belt-pelvis angles were also equal between HBMs. As the lap belts of the HBMs were all oriented more horizontal relative to ground for each test's specific lap belt anchorage point location, the resulting lap belt-pelvis angles were larger than that of the PMHS for each test. Additionally, the mid lap belt-pelvis angles of the HBMs differed between the reclined (test D1591) and upright (test D1592) condition by 6-7° versus 3° for the PMHS.

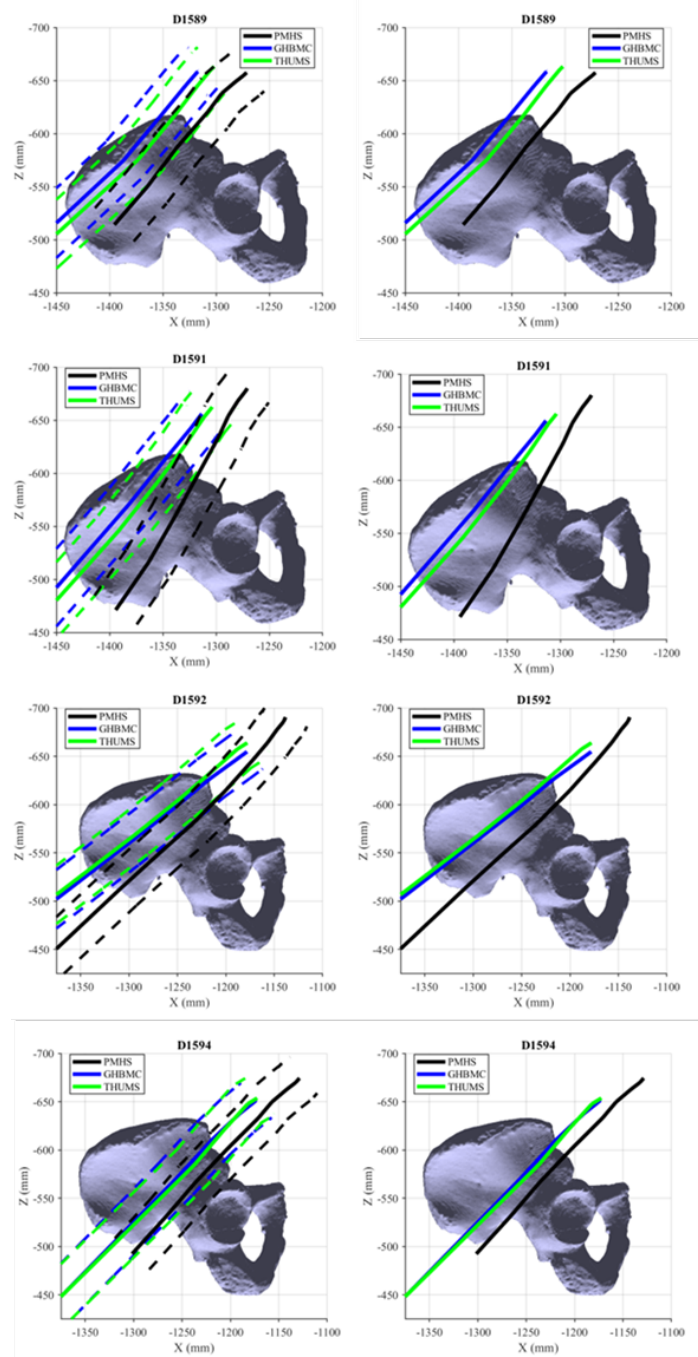


Figure 6.6: Initial lap belt paths relative to the pelvis in the global reference frame (Figure 6.1) for each test (top-down) and for each surrogate. The left column shows the approximated belt width (± 25 mm) along the centerline of the lap belt. The right column shows solely the centerline of the lap belt.

6.3.5 Soft Tissue Compliance

Modifying the soft tissue compliance required different implementation for each of the models due to the differing parts, contact definitions, and model-specific formulations. The goal was to change the stiffness of the soft tissue in the pelvic-abdominal region to represent a wider spread of subsequent lap belt-pelvis interactions. For the GHBMC, this involved scaling the material load curves (LCID) by 50% or 200% for several parts in the pelvic-abdominal region, which encompassed the gluteal tissue and the thorax (Figure 6.7a). See Appendix E.1 for additional details on the scaling of load curves. For the THUMS, as the connection between the flesh and the internal body structure is a sliding contact, the friction values of this contact were adjusted to 50% or 200% of the nominal value (0.1) 6.7b).

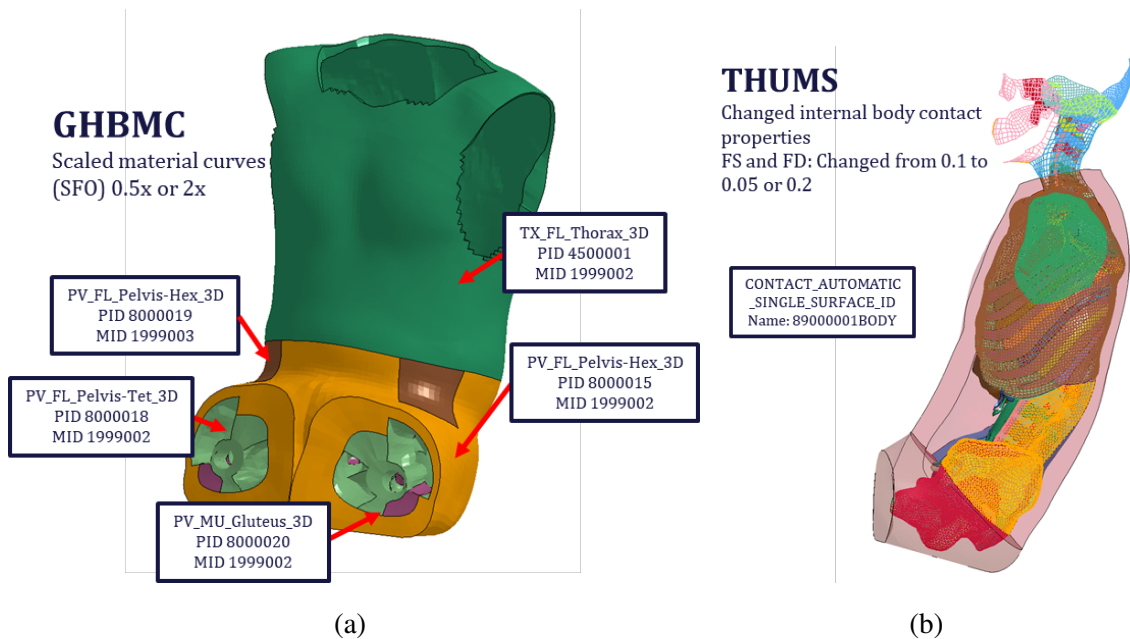


Figure 6.7: Soft tissue compliance modifications. (a) GHBMC pelvis and abdomen flesh parts and corresponding materials, whose load curves (LCID) were scaled (SFO) by either 50% or 200% for decreased and increased levels of stiffness. (b) THUMS internal body contact, where the friction between the internal anatomical structure and external flesh was changed through scaling the friction coefficient by either 50% or 200% for decreased and increased levels of stiffness.

6.3.6 Data Analysis

This chapter, with Chapter 4, aids in identifying the computational HBM that demonstrates superior biofidelity by comparing to the PMHS responses from the experiments documented in Chapter 5. Specifically, determining if the HBM can demonstrate the sensitivities of initial lap belt fit and submarining to lap belt-pelvis and torso angle, identified in the PMHS tests, is the goal.

Qualitative comparisons of initial lap belt placement, lap belt-pelvis trajectories, lap belt tension, and resulting submarining occurrence were conducted. As in Chapter 5, the global reference frame was positioned anterior to the subject (origin at subject's lateral midline), with the X-axis pointing anterior and parallel to ground, Y-axis pointing right of the subject and parallel to ground, and Z-axis pointing inferior (Figure 5.1). Additionally, comparisons were performed after modifying the soft tissue compliance to understand how this influenced biofidelity.

As in Chapter 5, submarining was determined by tracking the trajectory of the lap belt relative to the pelvis. Submarining was defined as the lap belt node (positioned along the midline of the belt webbing, widthwise) closest to the left or right ASIS passing posterior to the corresponding ASIS by more than 25 mm (half the width of the lap belt webbing) in the global reference frame (Figure 5.6). This indicated the full width of the belt webbing moved posterior to the ASIS. As the differences in HBM abdominal soft tissue compliance affect lap belt tension time histories, motion tracking of the lap belt relative to the pelvis was used as the primary measurement for submarining detection.

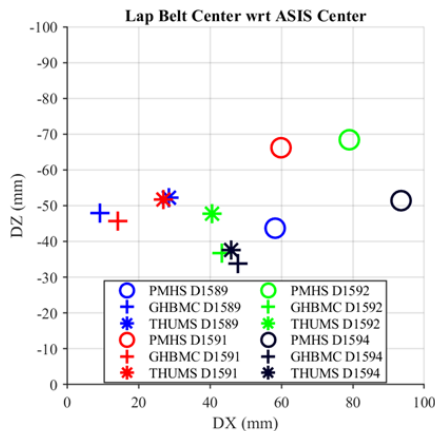
6.4 Results

6.4.1 Initial Lap Belt Placement

The lap belts were positioned in the same manner for both HBMs; thus, any differences in lap belt placement were due to the differences in abdomen shape between the two models. As mentioned in Chapter 5, the placement of the lap belt was dependent on both torso angle and lap belt-pelvis angle in the PMHS belt pull experiments (Figure 5.7). Largely, the HBMs' resulting lap belt placement in the fore-aft direction (dx) was similarly dependent on torso angle and lap belt-pelvis angle as the PMHS (Figure 6.8). The PMHS showed an increase in lap belt-pelvis distance (dx) from a reclined posture to an upright posture (e.g., from test D1591 to test D1592), and from a larger lap belt angle to a smaller lap belt angle (e.g., from test D1592 to D1594) (Figure 6.8b, also visible in Figure 6.6). The HBMs followed this trend except for the THUMS in recline, where a

smaller lap belt-pelvis angle resulted in decreased lap belt-pelvis distance (dx) (from test D1589 to D1591).

The HBMs were only able to replicate the PMHS trend in both vertical (dz) and horizontal (dx) directions in the upright condition: the smaller lap belt-pelvis angle resulted in the lap belt placed further forward (+dx) and downward (+dz) (from test D1592 to D1594) (Figure 5.7). For the HBMs, a smaller lap belt-pelvis angle also positioned the lap belt more downward (+dz) in recline (test D1589 to test D1591), which was not seen in the PMHS. Additionally, changing only the torso angle (test D1591 to test D1592) positioned the lap belt more downward (+dz), unlike the PMHS.



(a)

Test	PMHS		GHBMC		THUMS	
	dx (mm)	dz (mm)	dx (mm)	dz (mm)	dx (mm)	dz (mm)
D1589	58.3	-43.7	9.2	-48.0	28.5	-52.3
D1591	59.9	-66.2	14.2	-45.8	26.9	-51.7
D1592	79.0	-68.5	43.4	-36.7	40.6	-47.8
D1594	93.5	-51.4	47.8	-33.8	45.9	-37.5

(b)

Figure 6.8: Lap belt midpoint (length- and width-wise) relative to the midpoint of the left and right ASIS for each test and surrogate. (a) Scatter plot showing the initial lap belt midpoint position relative to the ASIS midpoint ($x = 0$, $z = 0$), where the colors indicate the test number and the symbols indicate the surrogate type. (b) The lap belt midpoint coordinates relative to the ASIS (tabulating the left figure’s graphic).

6.4.2 Submarining Occurrence

6.4.2.1 Kinematics and Kinetics

Like the PMHS, the HBMs submarined in both reclined tests (D1589 and D1591); however, neither model submarined in the upright tests (D1592 and D1594) (Figure 6.9), whereas the PMHS submarined in test D1592. For those tests that resulted in submarining, the HBMs exhibited similar lap belt penetration (into the abdomen) as the PMHS. In tests D1589 and D1591, a decrease

in lap belt tension near the time of peak magnitude, in addition to the lap belt marker passing over and behind the ASIS by 25 mm (approximately half the belt width) indicated submarining occurrence. Neither outcome (lap belt-pelvis migration or reduction in lap belt tension) occurred in tests D1592 and D1594.

6.4.2.2 Change in lap belt-pelvis angle

The lap belt-pelvis angle of the HBMs changed during the belt pull due to the increase in lap belt tension and interaction with the abdominal soft tissue during the belt pull, though not to the scale of the PMHS (0-2° change in HBMs versus 3-18° in PMHS) (Table 6.2). In part, this difference in magnitude between the PMHS and the HBMs is due to the differences in abdominal soft tissue girth and curvature. The excess abdominal soft tissue of the PMHS allows for more interference with the lap belt than the minimal abdominal soft tissue of the HBMs. Because of the greater soft tissue depth and resulting increased compliance of the PMHS soft tissue, it is possible the lap belt could more easily get wedged in between folds of soft tissue, which would decrease the rate of lap belt migration over the anterior abdominal surface relative to the lap belt migration at the lateral ends of the webbing. In contrast, the decreased abdominal soft tissue depth and higher stiffness of the HBMs' soft tissue results in less opportunity for the lap belt to get wedged anterior to the pelvis (e.g., in between folds of tissue) and thus the rate of lap belt migration on the abdominal surface and the lateral ends are better coupled. Additionally, the initial level of lap belt tension in the FE environment is more controllable than in the physical environment. Thus, it is also possible there was more initial slack in the lap belt in the experiments, which would result in a greater change in lap belt angle as the belt is being pulled due to increased tension (i.e., straightening of the webbing, permitting the shortest path).

Although the initial lap belt-pelvis angles differed between the HBMs and the PMHS (Table 6.2), the lap belt-pelvis angle at the time of submarining was within 1-3° of the PMHS.

CHAPTER 6. EVALUATION OF HBM SUBMARINING SENSITIVITY TO LAP BELT-PELVIS ANGLE

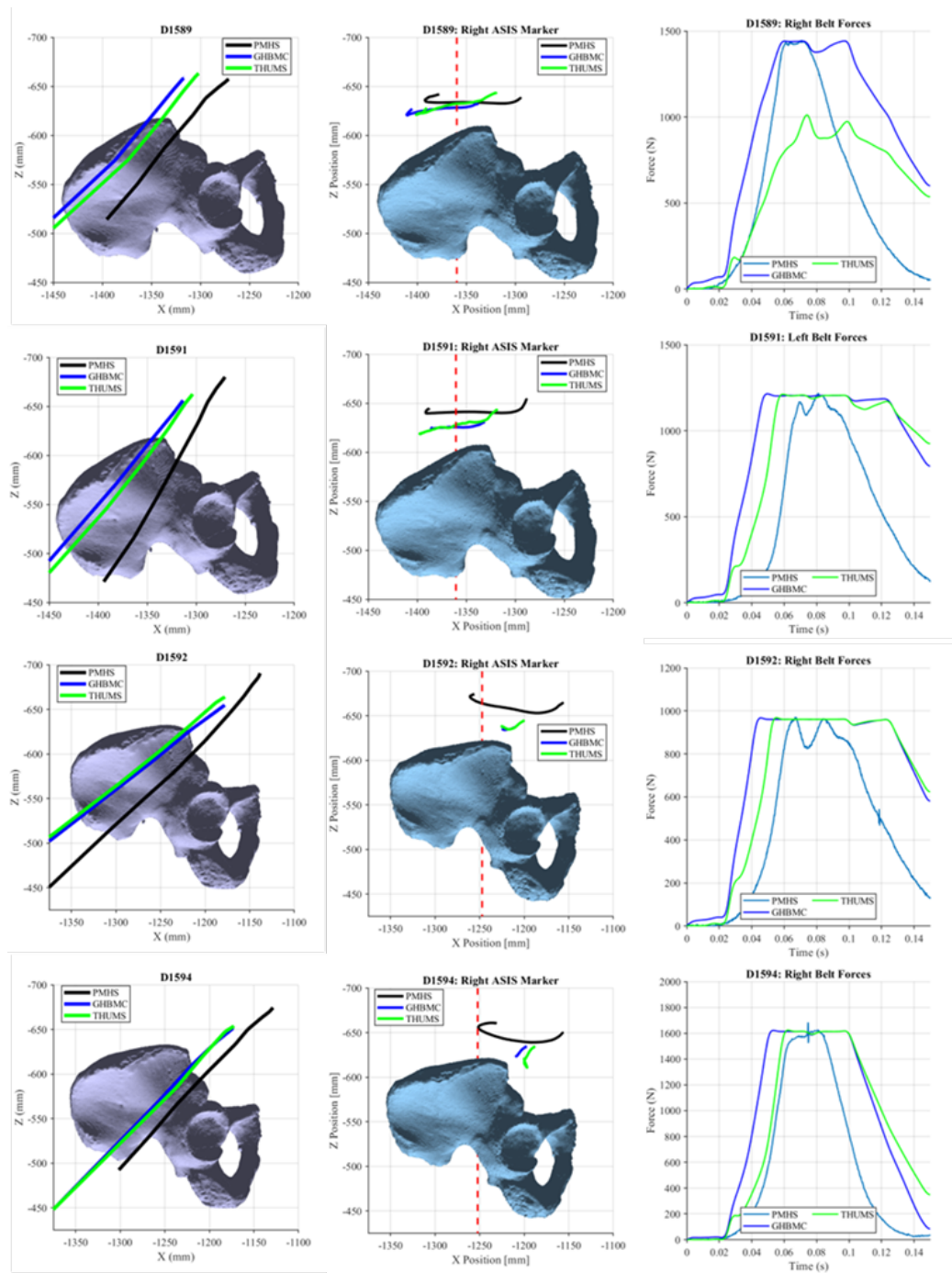


Figure 6.9: Lap belt initial position, kinematics, and tension time histories for each test (top-down) and surrogate. Left-right: the lap belt centerline initial position (left column), trajectory of the point on the lap belt located nearest to the right ASIS in the sagittal plane (middle column), and the tension time history (right column).

Table 6.2: Submarining occurrence, and resulting change in lap belt-pelvis angle, for each test and surrogate.

Surrogate	Test	Torso Angle	Lap Belt-Pelvis Angle	Sub.	Time of Sub. (ms)	Lap Belt-Pelvis Angle at Sub. (deg)	Change in Lap Belt-Pelvis Angle (deg)	
PMHS	D1589	Recline	Large	Y	61	112	3	
GHBMC				Y	41	114	1	
THUMS				Y	57	113	-1	
PMHS	D1591		Mid	Y	70	111	12	
GHBMC				Y	51	109	0	
THUMS				Y	62	108	-2	
PMHS	D1592	Upright		Mid	Y	67	114	18
GHBMC					N	X	X	X
THUMS					N	X	X	X
PMHS	D1594		Small	Small	N	X	X	X
GHBMC					N	X	X	X
THUMS					N	X	X	X

6.4.3 Soft Tissue Compliance

Modifications to soft tissue compliance resulted in no difference in submarining occurrence and negligible differences in lap belt-pelvis motion and lap belt tension (Figure 6.10). In the reclined tests (D1589 and D1591), the more compliant soft tissue condition (“Soft”, 50% nominal stiffness) resulted in approximately 3-5 mm more inward displacement (-X) relative to the pelvis than the nominal soft tissue condition (“Nominal”) for both HBMs. Additionally, the less compliant condition (“Stiff”, 200% nominal stiffness) resulted in approximately 3-5 mm less inward displacement (-X) relative to the pelvis than the nominal case in the reclined tests for both HBMs. However, these differences were not visible in the upright tests.

CHAPTER 6. EVALUATION OF HBM SUBMARINING SENSITIVITY TO LAP BELT-PELVIS ANGLE

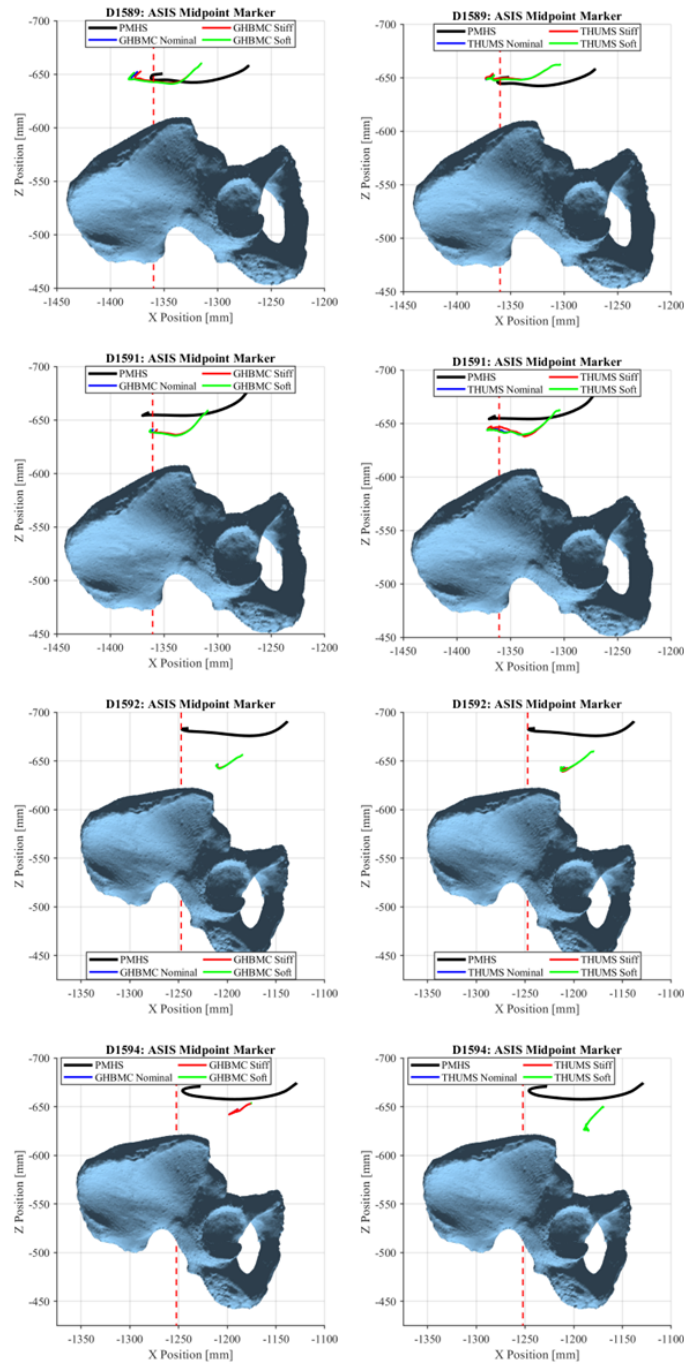


Figure 6.10: Variation in lap belt-pelvis trajectory for the HBMs with the different prescribed soft tissue stiffnesses, where “Soft” indicates 50% of the nominal stiffness and “Stiff” indicates 200% of the nominal stiffness. The red dashed line indicates marks where submarining did or did not occur. Top-down: the four different tests. Left-right: GHBMC (left column) and THUMS (right column).

6.5 Discussion

6.5.1 Initial Lap Belt Placement

The effects of torso and lap belt-pelvis angle on initial lap belt placement were similar between HBMs but differed from the PMHS in some cases. For the PMHS, a smaller lap belt-pelvis angle positioned the lap belt further anterior, which was seen in all HBM cases but the THUMS in recline, in which the lap belt was positioned 1.6 mm rearward for the smaller lap belt-pelvis angle. This is a result of the THUMS's abdominal shape, which is smoother than the GHBMC and thus the lap belt is more prone to migrating up the abdomen and rearward to the pelvis, along the abdomen slope, as it is routed and stretched (Figure 6.12).

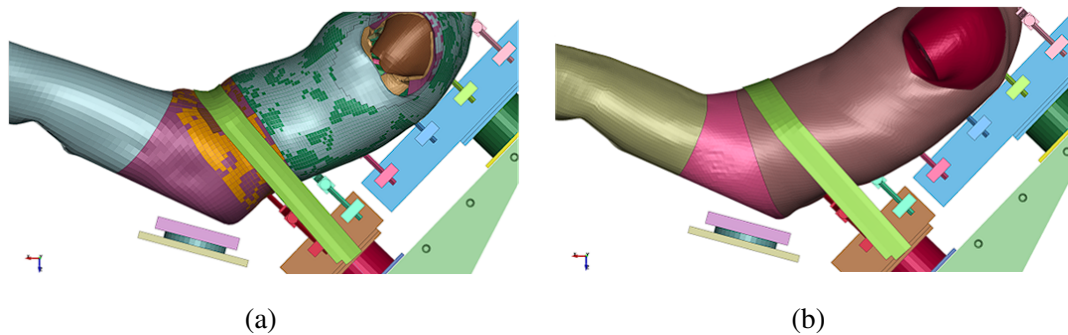


Figure 6.11: Lap belt placement of the GHBMC (a) and the THUMS (b) after stretching the belt using the LS-PrePost stretch tool.

In maintaining lap belt-pelvis angle and changing torso angle (D1591 reclined torso and mid lap belt-pelvis angle to D1592 upright torso and mid lap belt-pelvis angle), the PMHS had a 2.3 mm increase in lap belt vertical placement ($-dz$) (Table 6.2). In contrast, the HBMs had a larger decrease in lap belt vertical placement (9 mm dz for GHBMC; 4mm dz for THUMS) from recline to upright. This is a result of the differences in the amount of soft tissue between the mid-sized HBMs and the obese PMHS. Effectively, the abdominal soft tissue is better coupled to the pelvis in the HBMs, as these models have a smaller abdominal flesh depth between the surface of the abdomen and the pelvis. For the PMHS, the soft tissue is less coupled as there is an increased volume, and associated depth, of soft tissue between the surface of the abdomen and the pelvis. Thus, the PMHS pelvis angle is largely independent of the orientation of the soft tissue, and associated lap belt placement, unlike the HBMs (Figure 6.6).

This difference in vertical lap belt placement trend from test D1591 and D1592 between

the HBMs and the PMHS is worth noting, as the HBMs lower initial lap belt placement in test D1592 (relative to test D1591) placed the lap belt more favorably relative to the pelvis than the PMHS, who had a higher initial lap belt placement in test D1592. This may be a partial cause for the difference in submarining occurrence between these surrogates. The decreased abdominal depth (dx) between the HBMs and the pelvis may have also contributed to a decreased likelihood of submarining, as the lap belt could more easily engage the bony pelvis.

6.5.2 Submarining Sensitivity

Both HBMs showed similar submarining sensitivity to lap belt-pelvis and torso angle: submarining occurred in the reclined condition but not in the upright condition. The submarining occurrence in both recline tests matches the outcomes from the PMHS tests, however the PMHS also submarined in one upright test with the more horizontal lap belt-pelvis angle (D1592), which was not exhibited by the HBMs.

While the lap belt-pelvis geometry at the time of submarining is critical in dictating submarining outcome, this is not the only factor at play (Figure 2.7) - lap belt tension plays a critical role as well. While maintaining the lap belt load limit prescribed in the experiments ensures a one-to-one comparison of the experimental setup, the anthropometries between the HBMs and the PMHS are different. The obese PMHS has additional abdominal soft tissue and associated increased depth between the surface of the abdomen and the bony pelvis, whereas the mid-sized HBMs have minimal abdominal tissue depth. This results in different levels of lap belt penetration for the same load: the PMHS will have greater depth of penetration at a given load limit than the PMHS due to the increased abdominal tissue depth. As a result, the lap belt requires more force to induce submarining for the HBM than for the PMHS. Thus, an additional simulation was run to understand how increasing the lap belt load limit affected submarining outcome in the HBMs. The setup of this simulation was the same configuration as test D1592, which resulted in submarining for the PMHS and no submarining for the HBMs. The lap belt load limit was increased to 5 kN instead of the 0.9 kN peak lap belt tension achieved in the experiment, which resulted in submarining for both models (Figure 6.12). The 5 kN load limit was chosen as it is high enough to determine whether lap belt load limit plays a factor in submarining occurrence; however, the threshold load limit required to induce submarining in these models may be lower. Additionally, unlike the PMHS, who exhibited an 18° change in lap belt-pelvis angle prior to submarining in this test (Table 6.2), the models exhibited minimal change (GHBMC: 0° ; THUMS: -2°). This is again likely a result of the differences

in anthropometry, soft tissue-pelvis interaction, and initial lap belt tension, as described in Section 6.4.1. Nonetheless, the models exhibited a similar submarining to lap belt-pelvis angle as the PMHS in the upright condition; however, more force was required to induce submarining as a result of the increased stiffness in the pelvic-abdominal region.

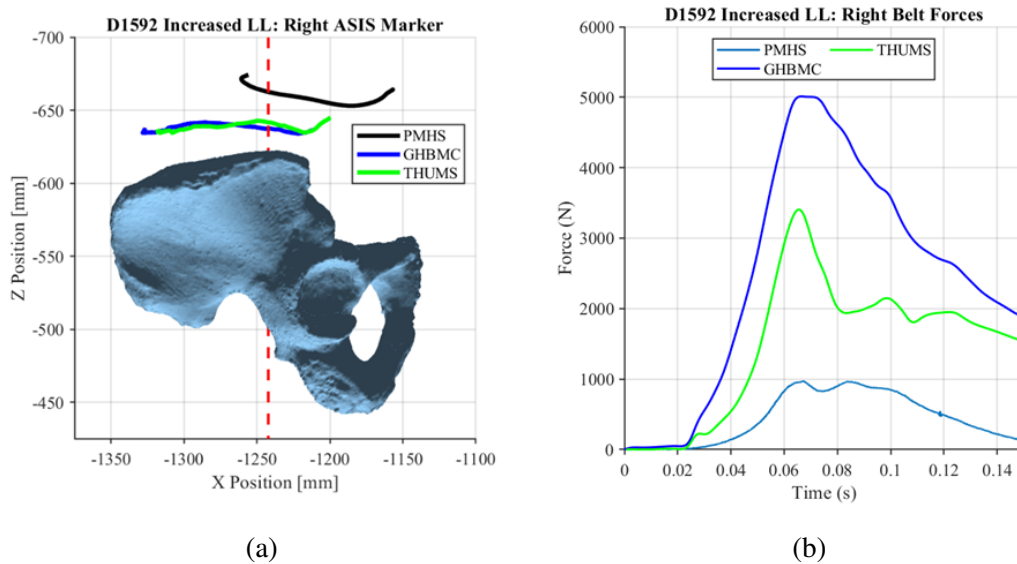


Figure 6.12: Simulation results from increasing the lap belt load limit of test D1592, which resulted in submarining for both HBMs, matching the PMHS response. (a) Lap belt trajectories relative to the pelvis in the sagittal plane. (b) Lap belt tension time histories.

As discussed in Section 6.4.3, varying the stiffness factor (via scaling of the material load curve) had no effect on submarining outcomes and negligible effects on lap belt migration. However, there are several other parameters that contribute to the model’s stiffness behavior, including the stiffness of the abdominal content (e.g., organs), flesh-pelvis friction (for THUMS), and element stiffening at large strains (for GHBMC).

Further, to ensure the models could demonstrate sensitivity to solely lap belt-pelvis angle in the upright condition, an additional case was run in which the lap belt anchorages were positioned approximately 60 mm more rearward relative to D1592 (upright torso; more horizontal lap belt-pelvis angle), which was less than the anchorage position step size between tests (Appendix D.1). This resulted in submarining for both models, though the THUMS showed more sensitivity, with increased lap belt penetration relative to the GHBMC (Figure 6.13). This demonstrated that, though these models exhibit different submarining thresholds than the PMHS when prescribed the same

load limit, the HBMs showed sensitivity to lap belt-pelvis angle in the upright condition.

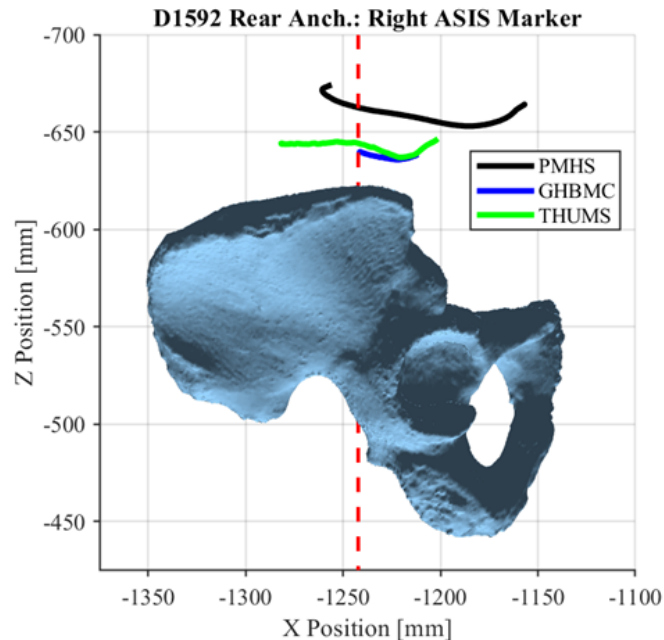


Figure 6.13: Simulation results from moving the anchorage points approximately 60mm rearward from test D1592 (same lap belt load limit): Lap belt trajectory relative to the pelvis in the sagittal plane. Both models submarined in this condition, with the THUMS showing higher sensitivity.

6.5.3 Lap Belt Migration

While there was a substantial difference in abdominal soft tissue depth between the HBMs and the PMHS, the lap belt trajectories of the HBMs generally followed a similar trend to the PMHS. However, one key difference was observed for the THUMS model in test D1594 (upright torso; vertical lap belt-pelvis angle). While the lap belt of the GHBMC maintains position after pelvis engagement, the THUMS shows a downward migration of the lap belt relative to the pelvis. Qualitative video analysis of the simulations shows this may be a result of the disconnect between the exterior soft tissue and the bony pelvis in the THUMS model, which promotes sliding of the flesh, and subsequently lap belt, relative to the pelvis (Figure 6.14). Additionally, the THUMS model was the only surrogate that exhibited a more vertical lap belt-pelvis angle at the time of submarining (Table 6.2), which shows that the abdominal soft tissue is not interacting with the

lap belt (e.g., providing resistance) in the same manner as the PMHS or GHBM. This limited resistance may again be attributed to the flesh sliding relative to the pelvis during the belt pull.

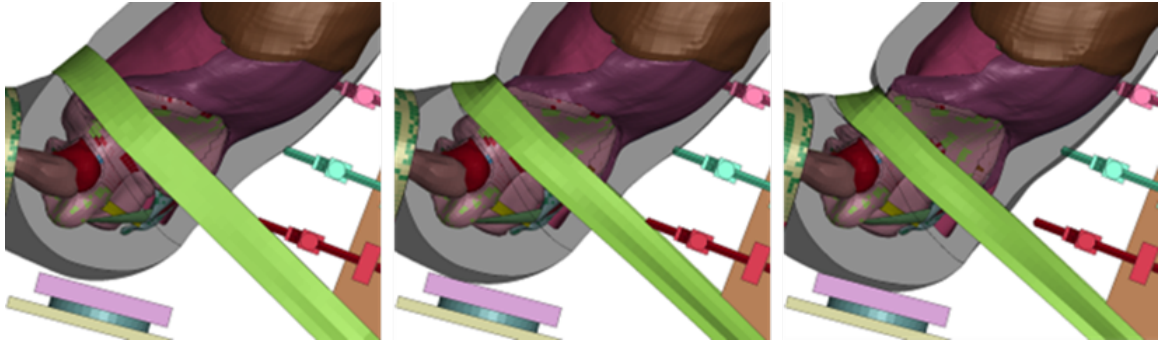


Figure 6.14: Photos from the THUMS simulation of test D1594 (at 30ms, 60ms, and 90ms), which shows the belt migrating down the pelvis as a result of the flesh sliding relative to the pelvis.

This downward lap belt displacement resulting from the abdominal soft tissue of the THUMS was also seen in Chapter 4, wherein the dynamic simulation showed the THUMS flesh “pockets” the lap belt and collapses the webbing elements (Figure 4.21). To confirm this effect is exaggerated at a higher level of belt tension, another simulation was run with the same configuration as test D1594 (upright torso; vertical lap belt-pelvis angle), but with a higher lap belt load limit of 8 kN, similar to the peak lap belt tension magnitude seen in the dynamic tests (Figure 4.10). This resulted in an increased downward displacement of the lap belt relative to the pelvis for the THUMS (Figure 6.15).

The sliding contact between the THUMS external soft tissue and the pelvis may have been the cause of the model’s higher sensitivity to lap belt-pelvis angle, where inward lap belt penetration resulted from a larger lap belt-pelvis angle (e.g., Figure 6.13), and downward lap belt migration occurred due to a smaller lap belt-pelvis angle (e.g., Figure 6.14). This bifurcation effect has been seen in other studies [55]. Although this mechanism does not necessarily pose the THUMS as a less biofidelic model, this high sensitivity may risk simulation instability in a dynamic environment with higher inertial forces.

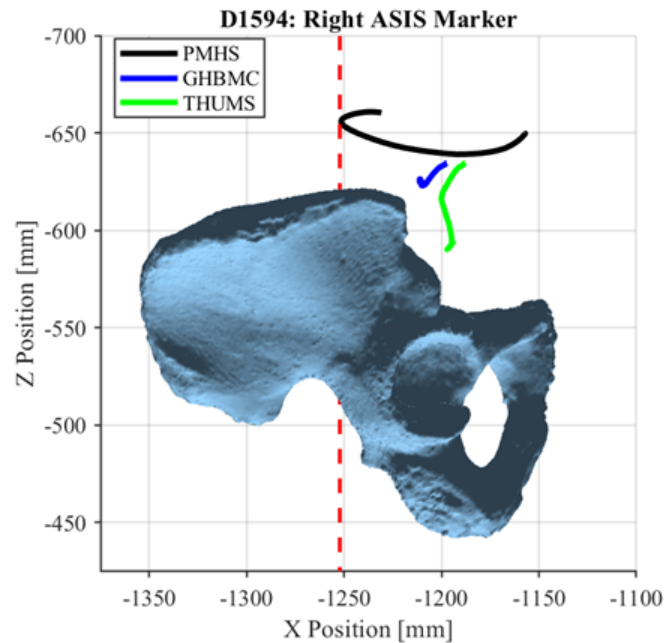


Figure 6.15: Simulation results from increasing the lap belt load limit of test D1594: Lap belt trajectory relative to the pelvis in the sagittal plane. The THUMS model shows increased downward displacement relative to test D1594 (nominal lap belt load limit). The GHBM did not show downward lap belt motion.

6.6 Conclusions

The following conclusions were drawn from this chapter's analysis:

1. The effects of torso and lap belt-pelvis angle on initial lap belt placement was similar between the GHBM and THUMS, but these differed from the PMHS in some cases:
 - (a) For the PMHS, a more vertical lap belt-pelvis angle positioned the lap belt further forward relative to the pelvis, which was also seen in all HBM cases but the THUMS in recline.
 - (b) The HBMs showed a lower lap belt placement in the upright condition relative to the reclined condition for the same lap belt-pelvis angle, unlike the PMHS tests.
2. Likewise, the submarining sensitivity to lap belt-pelvis angle and torso angle was similar between HBMs and the PMHS, though the threshold was different than the PMHS.

CHAPTER 6. EVALUATION OF HBM SUBMARINING SENSITIVITY TO LAP BELT-PELVIS ANGLE

- (a) Specifically, the HBMs were able to exhibit submarining in the upright test with a mid lap belt angle (D1592) as the PMHS did; however, an increase in force was necessary to do so as the models soft tissue depths were smaller than the PMHS.
 - (b) Positioning the anchorage points further back and maintaining the original lap belt load limit also resulted in submarining for the models.
3. Modifying abdominal soft tissue compliance resulted in negligible effects on lap belt-pelvis trajectory and no effect on submarining occurrence.
4. The THUMS showed a higher sensitivity to lap belt-pelvis angle than the GHBMC, exhibiting a bifurcation effect at the ASIS: a larger lap belt-pelvis angle resulted in increased lap belt penetration into the abdomen and a smaller lap belt-pelvis angle resulted in downward lap belt motion relative to the bony pelvis. Additionally, this model's lap belt-pelvis angle was smaller at the time of submarining relative to the initial time, whereas this angle increased between the initial time and the time of submarining for the PMHS and the GHBMC. Both the increased sensitivity and change in lap belt-pelvis angle were attributed to the model's flesh-pelvis sliding contact, though this may also be due to the model's flesh material stiffness.

The results from this chapter showed that, while both HBMs exhibited similar sensitivities regarding the effect of lap belt-pelvis angle and torso angle on initial lap belt placement and submarining occurrence, the THUMS exhibited higher lap belt migration sensitivity to lap belt-pelvis angle than the PMHS and GHBMC as a result of the model's flesh-pelvis sliding contact. This behavior may increase risk of simulation stability in dynamic test conditions. Thus, this Chapter, in addition to Chapter 4, supported using the GHBMC in the parametric study described in Chapter 8. The results from these two chapters were summarized in Chapter 7, which included an additional analysis to confirm these chapters' conclusions.

Chapter 7

Selection of HBM for Submarining Analysis

7.1 Executive Summary

7.1.1 Relevance and Goal

Chapters 4 and 6 described the biofidelity limitations and simulation stability concerns for the THUMS model, which were largely attributed to either the model's sliding interface between the flesh and the internal musculoskeletal system or the flesh material stiffness. In the dynamic reclined simulations described in Chapter 4, the anterior compression of the abdominal flesh resulting from the forward torso excursion collapsed the lap belt shell elements which would not occur in the physical world and affected belt-pelvis loading. In Chapter 6's seated belt pull tests, the migration of the lap belt in the THUMS simulations showed higher sensitivity to lap belt-pelvis angle than the PMHS and GHBM: a larger lap belt-pelvis angle (horizontally oriented lap belt relative to ground) resulted in increased lap belt penetration into the abdomen, whereas a smaller lap belt-pelvis angle resulted in downward lap belt migration relative to the pelvis. Additionally, the model exhibited a negative change in lap belt-pelvis angle at the time of submarining relative to the initial time, indicating a smaller lap belt-pelvis angle at the time of submarining. This disagrees with previous studies which link a larger lap belt-pelvis angle with increased risk of submarining, and both the GHBM and PMHS exhibited a larger lap belt-pelvis angle at the time of submarining. Both of the THUMS model's limitations described in Chapter 4 were also largely attributed to the model's sliding interface between the flesh and the pelvis.

CHAPTER 7. SELECTION OF HBM FOR SUBMARINING ANALYSIS

While the results described in Chapters 4 and 6 suggested the GHBMC as the more suitable model for detailed study of lap belt-pelvis interaction relative to the THUMS, it remained to be seen whether the concerning behaviors exhibited by the THUMS model were still visible in other configurations. This was particularly relevant as the model that was chosen for use in the final parametric study was evaluated in a dynamic condition with varying intrinsic and extrinsic parameters. Thus, the goal of this chapter was to understand if the identified limitations of the THUMS model remained in the targeted parametric study conditions. Through this analysis, the conclusions drawn from the simulations of Chapters 4 and 6 were challenged and contextualized, which provided a more robust determination of HBM choice for this dissertation's remaining analysis.

7.1.2 Key Conclusions

The full list of conclusions can be found in Section 7.6 below. In summary, the THUMS exhibited less instances of submarining than the GHBMC for varying configurations. Instead, the THUMS showed several cases in which the lap belt remained low on the pelvis (toward the pubic rami), particularly for cases with a vertically oriented lap belt. Thus, the downward lap belt migration resulting from a vertically oriented lap belt in the seated belt pull simulations of Chapter 6 was also identified in dynamic conditions with varying configurations and parameters. Additionally, the collapsing of the lap belt shell elements identified in Chapter 4's THUMS simulations was again seen for various conditions. Both of these behaviors, attributed to either the THUMS sliding interface between the flesh and the pelvis or the flesh material stiffness, confirmed that the previously identified biofidelity limitations and stability concerns for the THUMS model were relevant for the final parametric study's conditions. Thus, the GHBMC model was selected for the remaining analysis of this dissertation.

7.1.3 Contributions

This chapter advances the automotive safety field's knowledge on the consistencies and differences in lap belt-pelvis interaction - specifically, submarining occurrence and lap belt-pelvis loading - for two state-of-the-art computational HBMs under varying restraint and posture configurations. Additionally, novel HBM-specific instrumentation was developed to measure load at the ASIS/iliac wing cross-sections. In this application, this information was utilized to determine the feasibility of using a given HBM to predict kinematic and kinetic outcomes under these various conditions in addition to identifying areas of potential stability risk.

7.1.4 Publications

Richardson, R., Gepner, B., Kerrigan, J., Forman, J., (2023). Evaluation of Lap Belt-Pelvis Load Transfer in Frontal Impact Simulations. *Traffic injury prevention*. (Planned).

Gepner, B., **Richardson, R.**, Kerrigan, J., Forman, J., (2023). Modification of THOR Sacral Geometry to Improve Biofidelity in a Reclined Posture. *IRCOBI Short Communication*. (Planned).

7.2 Introduction

The dynamic reclined sled test simulations conducted and analyzed in Chapter 4 showed that both the GHBMC and THUMS computational HBMs exhibited more lumbar spine range of motion (ROM) than the PMHS. In particular, the lumbar spine of the THUMS model exhibited the most ROM, exhibiting 15-30° higher ROM (peak extension to peak flexion) than the PMHS, whereas the GHBMC exhibited 10-15° higher ROM. Additionally, due to either the sliding contact between the external flesh and the pelvis or the flesh material stiffness, the THUMS abdominal soft tissue compressed the lap belt during forward excursion, which collapsed the lap belt elements. Both models exhibited similar submarining sensitivity to the PMHS in the seated belt pull condition (Chapter 6), though it took more lap belt pulling force to submarine the HBMs for the same lap belt-pelvis angle that caused submarining in the PMHS in the upright condition. The THUMS exhibited a higher lap belt migration sensitivity to lap belt-pelvis angle, where a larger lap belt-pelvis angle increased the level of lap belt penetration into the abdomen (more than the GHBMC and the PMHS) and a smaller lap belt-pelvis angle resulted in downward lap belt migration relative to the pelvis (not seen in the GHBMC or the PMHS). Additionally, the THUMS model exhibited a negative change in lap belt-pelvis angle between the initial angle and the angle at the time of submarining, indicating the model submarined at a smaller lap belt-pelvis angle than the initial setup. In contrast, the GHBMC and PMHS submarined at a larger lap belt-pelvis angle. The high sensitivity to lap belt-pelvis angle, and the difference in lap belt-pelvis angle from the initial time to the time of submarining, were again attributed to the THUMS model's flesh - either the sliding contact between the flesh and the pelvis or the flesh material stiffness.

The areas of vulnerability described in Chapters 4 and Chapter 6 concluded that the stiffness of the THUMS model's exterior flesh, and its sliding contact with the pelvis and internal structures, resulted in choosing the GHBMC as the better choice for further study. Hence, the re-

CHAPTER 7. SELECTION OF HBM FOR SUBMARINING ANALYSIS

sults from these chapters pointed towards the GHBM model as the superior choice to proceed forward with in the parametric study in Chapter Chapter 8. However, as this parametric study was designed to vary several intrinsic and extrinsic variables, the simulation setups (e.g., configurations, boundary conditions, etc.) differed from those of Chapters 4 and 6. It was important to ensure that the conclusions deduced from these chapters' results were not solely specific to those simulation configurations but were also relevant for the parametric study.

Prior to proceeding forward with the GHBM for use in Chapter 8's parametric study, two questions first needed to be addressed:

1. Was the collapsing of the lap belt shell elements seen in the THUMS simulations (Chapter 4) solely seen in that chapter's specific configuration (i.e., reclined torso, specific restraint geometry, 51 km/h pulse, etc.)?
2. Was the downward migration of the lap belt relative to the pelvis resulting from a small lap belt-pelvis angle (test D1594 of Chapter 6) only seen for a constrained surrogate?

Thus, the goal of this chapter was to understand if the identified limitations of the THUMS model, which were concluded to result from the model's sliding flesh contact, remained in the targeted parametric study conditions. To achieve this, both HBMs would be evaluated through a pilot parametric study, in which the varying intrinsic and extrinsic parameters, previously identified in Chapter 2 (Table 2.1) and selected for the final parametric study in Chapter 8, would stress test the performance of these models. As the concerns with the THUMS model are focused on the lap belt-pelvis interaction, instrumentation was designed to quantify this interaction and understand if the limitations of Chapters 4 and 6 (i.e., the collapsing of the lap belt elements and the downward migration of the lap belt) were present under varying conditions. The quantifiable metrics of lap belt-pelvis interaction were compared across both HBMs. Through this analysis, the conclusions drawn from Chapters 4 and 6 were challenged and contextualized, which provided a more robust determination of HBM choice for this dissertation's remaining analysis.

7.3 Methodology

As this chapter's sensitivity study was a small-scale version of the study conducted in Chapter 8, the methods are briefly introduced herein. The full details on these methods can be found in Chapter 8.

7.3.1 Study Overview

As before, the GHBMC and the THUMS mid-sized male computational HBMs were used in this evaluation. For each HBM, 120 matched frontal impact simulations were setup and run, each with a unique and randomly sampled set of parameters. The lap belt-pelvis interaction was quantified as lap belt-pelvis load transfer. Specifically, the maximum amount of load measured by the pelvis (for two different cross-sections) under an applied lap belt load (see Section 7.3.2).

7.3.1.1 FE environment

The FE environment was the same as that described in Chapter 4 (see Section 4.3.2t), which included a semi-rigid seat, toe pan, and a restraint system equipped with dual lap belt pretensioners and a shoulder belt pretensioner and load limiter. The lap belt anchorage points, and corresponding lap belt geometry, was modified based upon the specified lap belt angle parameter (see next section). The lap belt routing procedure is fully described in Section 8.3.5.

7.3.1.2 Parameters

Several parameters were varied to stress test the HBMs under different restraint configurations, postures, and boundary conditions. These parameters were randomly sampled using a stochastic sampling method described in Section 8.3.3. The extrinsic parameters included impact pulse (three levels), fore-aft lap belt angle (five levels), lateral lap belt angle (three levels), torso angle (two levels), foot pan contact (two levels), pelvic-abdominal flesh stiffness (three levels), belt/occupant friction (three levels), and seat/occupant friction (three levels). The definition of these parameters, their associated levels, and the reasoning behind these levels is found in Section 8.3.2.

7.3.2 Instrumentation

7.3.2.1 ASIS load cells

As the aim of this chapter was to understand if the lap belt-pelvis interaction concerns drawn from Chapters 4 and 6 for the THUMS remained for various dynamic loading conditions, as well as compare this interaction between the GHBMC and THUMS models, a method was designed to quantify this interaction. Specifically, instrumentation was designed to measure the level of lap belt load transferred to the bony pelvis. Through this instrumentation, the quantity of load transferred from the lap belt to the pelvis provides information on differences in HBM flesh compliance

CHAPTER 7. SELECTION OF HBM FOR SUBMARINING ANALYSIS

behavior. Additionally, the location of this applied load on the bony pelvis during the simulation provided information on belt-pelvis migration, which was relevant for addressing the previously observed THUMS limitations.

To measure the section forces at the ASIS location, the LS-PrePost keyword `DATABASE_CROSS_SECTION` was used to define a 3D cross-sectional area in which force could be measured (Figure 7.1a). This keyword defines the cross section using a selected node set, with the forces measured by the elements connected to those nodes. The section force was calculated as the sum of these measured forces; thus, the section only included elements on one side of the defined cross-section.

A clean cross-section is simple for a hexahedral mesh as the sides of the elements may be aligned with the cross-section edge (Figure 7.1b). However, the pelvises of the GHBM and THUMS are composed of a tetrahedral mesh, which complicated the method of defining a cross-section, particularly for the 3D structure. Thus, a function was developed in MATLAB which selected all elements connected to the chosen node set to avoid error associated with manual selection. This automated method also permitted symmetry for the left and right sides.

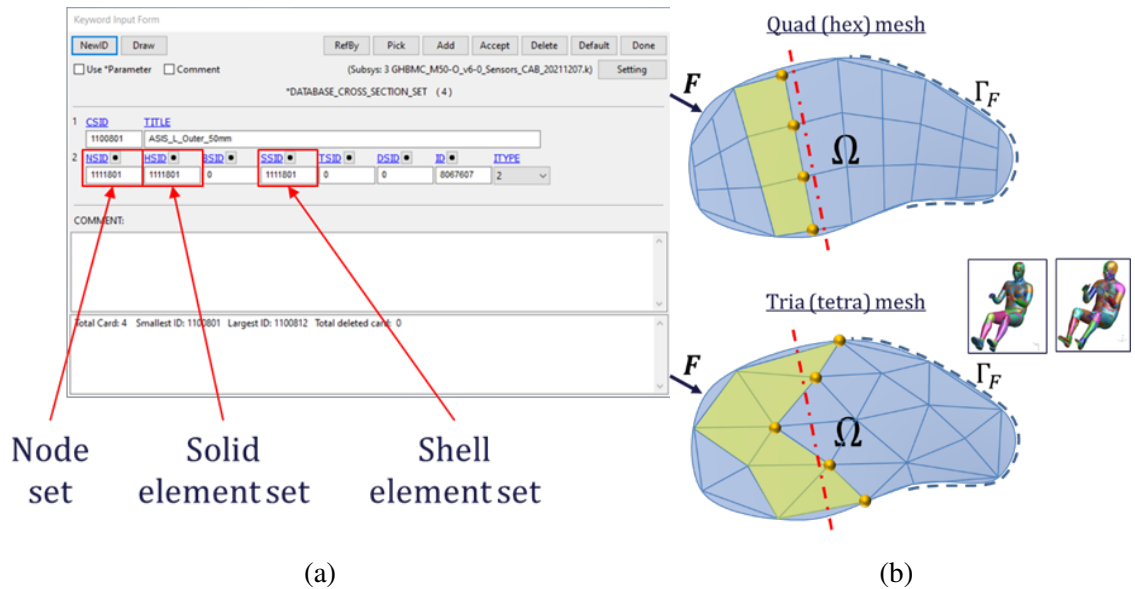


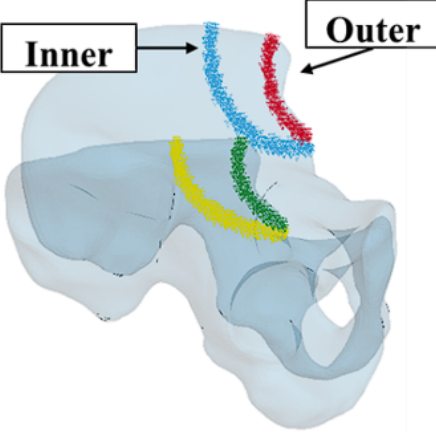
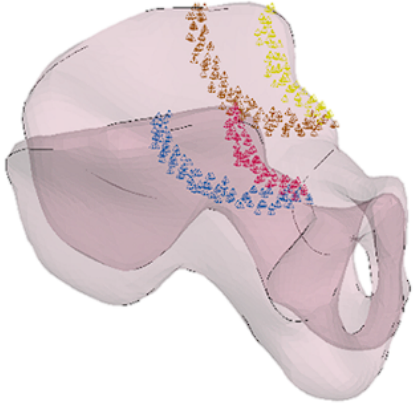
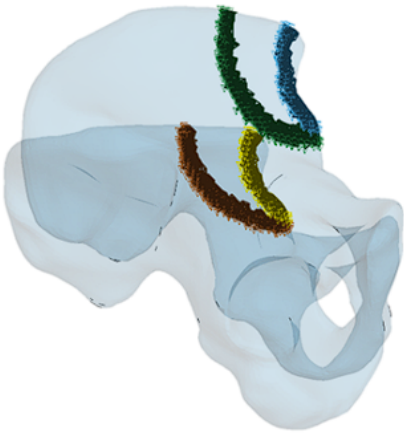
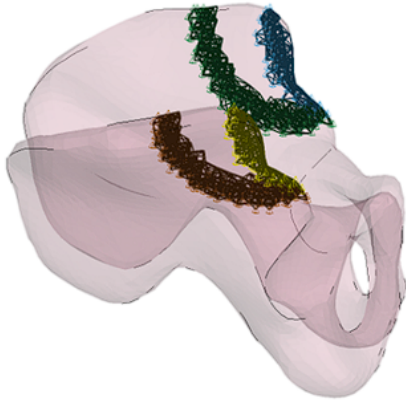
Figure 7.1: (a) Keyword `*DATABASE_CROSS_SECTION` in LS-PrePost, where the node set, solid element set, and shell element set are what we defined to define the ASIS cross-section. (b) Difference in defining this cross-section for a mesh with hexahedral elements (top) versus a mesh with tetrahedral elements, as is used in the pelvises of the GHBM and HBMs (bottom).

CHAPTER 7. SELECTION OF HBM FOR SUBMARINING ANALYSIS

Two areas were chosen in design of these cross-sections, which were defined with a cylindrical method (Table 7.1). The first area is located at the outer or anterior surface of the ASIS and is the approximate width of the lap belt webbing (50mm) ('ASIS Outer', 7.1). The second area encompassed a larger region of the iliac wing, including the upper part of the iliac wing ('ASIS Inner', 7.1). This section was defined as the inner cross-section as it is the most interior section.

Verification load cases were performed to ensure the full applied load was being captured by the ASIS cross-sections (see Appendix F.1).

Table 7.1: ASIS cross sections defined to measure ASIS load for the GHBMC and THUMS models.

	GHBMC	THUMS
Node Sets Shown Only		
Cross Section Sets (Nodes + Solids)		

7.3.3 Data Analysis

7.3.3.1 Submarining detection

Several intrinsic and extrinsic parameters were varied in the simulation sensitivity study, which were hypothesized to affect lap belt-pelvis interaction, lap belt-pelvis loading, and/or submarining outcome. As submarining results in the lap belt loading the abdomen (instead of the pelvis), simulations that resulted in submarining were flagged and removed from the lap belt-ASIS load transfer analysis.

All nodes on the upper and lower edges of the lap belt were tracked throughout the duration of the simulation, in addition to the nodes located at the left and right ASIS. With this, it was possible to identify exact timing of when the bottom edge of the lap belt translated superior and posterior to the ASIS landmarks, indicating that submarining occurred. As the model moved forward, three nodes on the bottom edge of the lap belt corresponding to the points closest (in the lateral, or Y-direction) to the left ASIS (LASIS), right ASIS (RASIS) and the ASIS midpoint, were identified (Figure 7.2). The closest nodes were iteratively calculated for each timestep. Submarining was detected if the bottom lap belt edge node passed superior and posterior to the corresponding ASIS node. Submarining was divided into two categories: pre-submarining and dynamic submarining (Table 7.2, Figure 7.3).

7.3.3.2 Output metrics

Once the simulations that resulted in submarining were removed, the peak ASIS force measured at both the inner and outer cross sections was plotted relative to the peak lap belt tension for both models (Figure 7.4). This allowed for a visual comparison of lap belt-ASIS load transfer across both models.

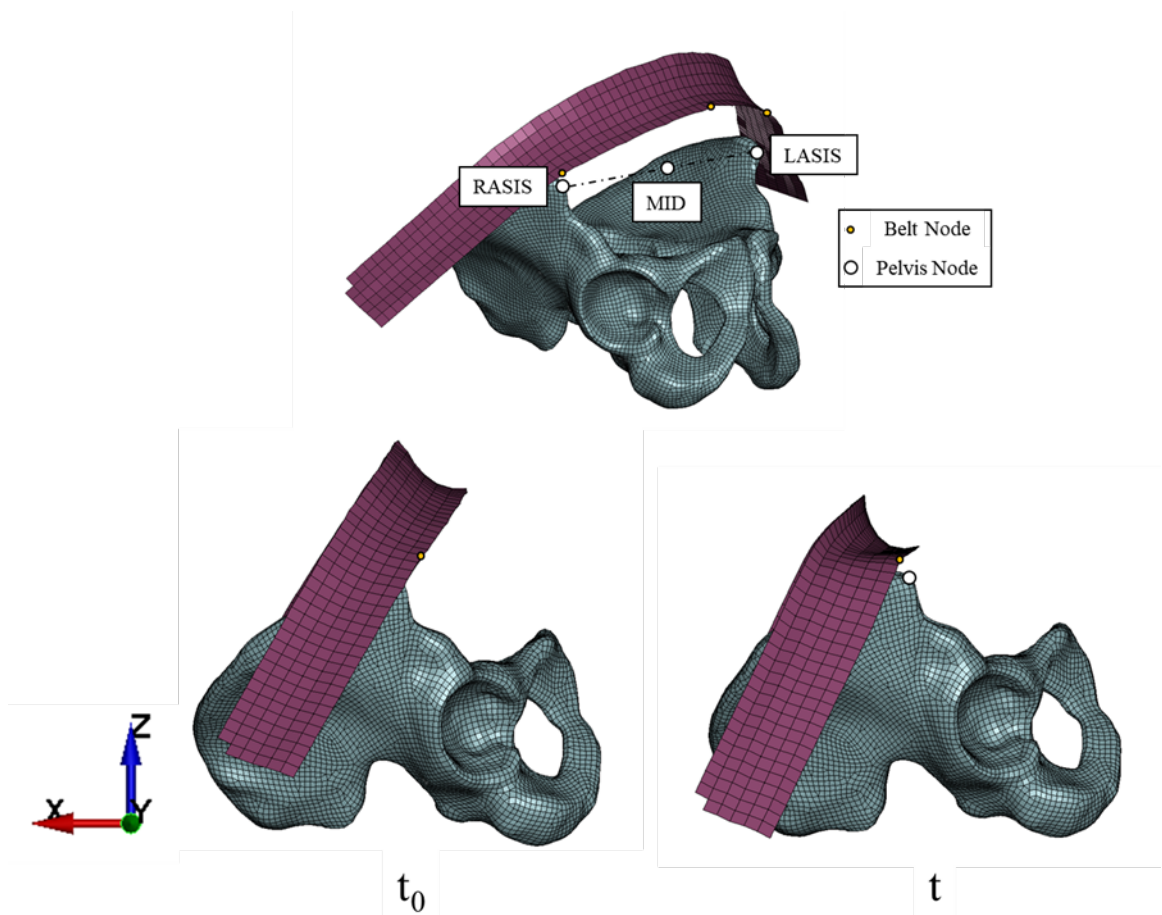


Figure 7.2: Submarining definition. Three nodes are selected on the bottom edge of the lap belt webbing as those closest (Euclidean distance) to the right ASIS (RASIS), ASIS midpoint (MID), and left ASIS (LASIS) (top). These are iteratively selected throughout the course of the simulation. Submarining is detected when the lap belt node moves above (+Z) and behind (+X) the corresponding pelvis node in the global reference frame.

CHAPTER 7. SELECTION OF HBM FOR SUBMARINING ANALYSIS

Table 7.2: Submarining type distinctions and definitions.

Submarining Type	Definition
No Submarining	Corresponding nodes on bottom edge of lap belt do not go behind (+X) and over (+Z) the LASIS point, RASIS point, or ASIS midpoint.
Pre-Submarining	Lap belt initially routed in a submarined position (due to the posture and angle of the belt). Corresponding nodes on bottom edge of lap belt are initially (at $t = 0$ <u>ms</u>) behind (+X) and over (+Z) the LASIS point, RASIS point, and ASIS midpoint.
Dynamic Submarining	Submarining on both sides. Corresponding nodes on bottom edge of lap belt pass behind (+X) and over (+Z) the LASIS point, RASIS point, and ASIS midpoint.

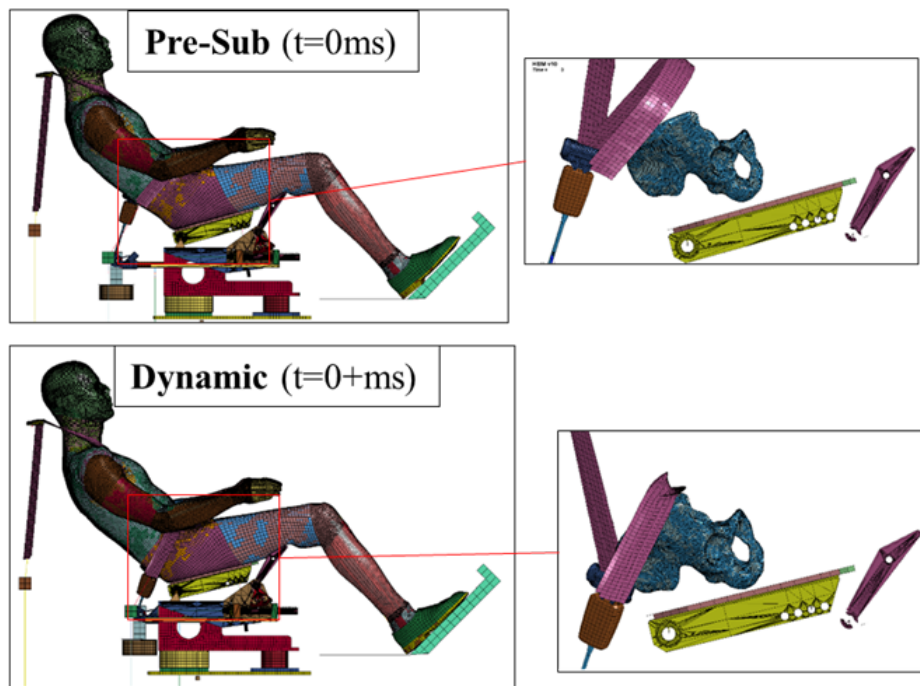


Figure 7.3: Pre-submarining versus dynamic submarining example.

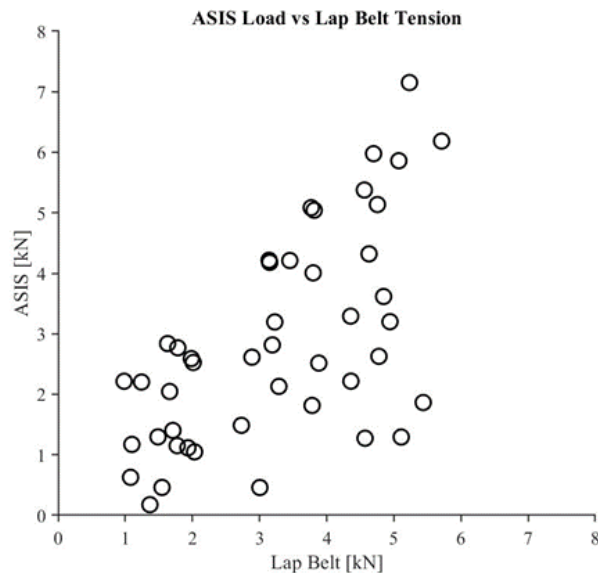


Figure 7.4: Example of output cross-plot showing peak ASIS load (measured at the cross-section) relative to peak lap belt tension.

7.4 Results

7.4.1 Submarining Occurrence

Submarining was categorized for all simulations that did not error terminate prior to 80 ms (the averaged approximated time of peak pelvis forward excursion) (Figure 7.5). Of the simulations that did not error terminate, more cases resulted in submarining for the GHBMC (45 simulations, 43% of non-error cases) than the THUMS (30 simulations, 28% of non-error cases). Additionally, nearly all (97%) of the THUMS submarining cases were in the reclined condition whereas 40% of the GHBMC submarining cases were in the upright condition.

As the THUMS exhibited high sensitivity to lap belt-pelvis angle in Chapter 6 (6.13) showing more abdomen penetration from the lap belt for a shallower lap belt angle relative to ground (or for a large lap belt-pelvis angle), comparing the model submarining sensitivities to a shallow lap belt angle was of interest (Figure 7.6). Both models showed a similar submarining sensitivity to a shallow lap belt angle: approximately 87% of the submarining cases for both models had a shallow lap belt angle. Additionally, 13-23% of the non-submarining cases for both models had a shallow lap belt angle.

As noted in Section 7.3.3, submarining was categorized into two groups: 1) pre-submarining,

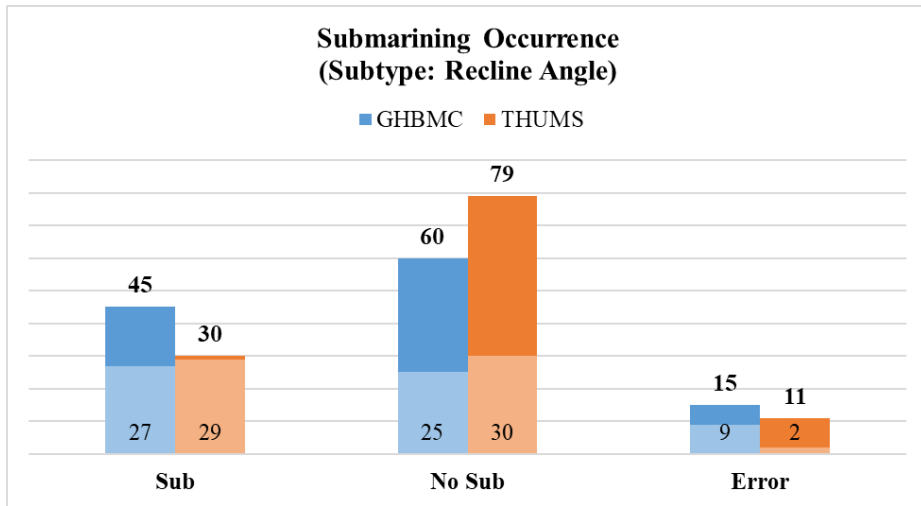


Figure 7.5: Submarining occurrence resulting from the GHBMC and THUMS simulations (120 sims each). The light shading (and inset data labels) are reclined simulations. The dark shading are upright simulations. The top data labels are total simulations (combined upright and reclined). “Error” marks the simulations that error terminated prior to 80 ms.

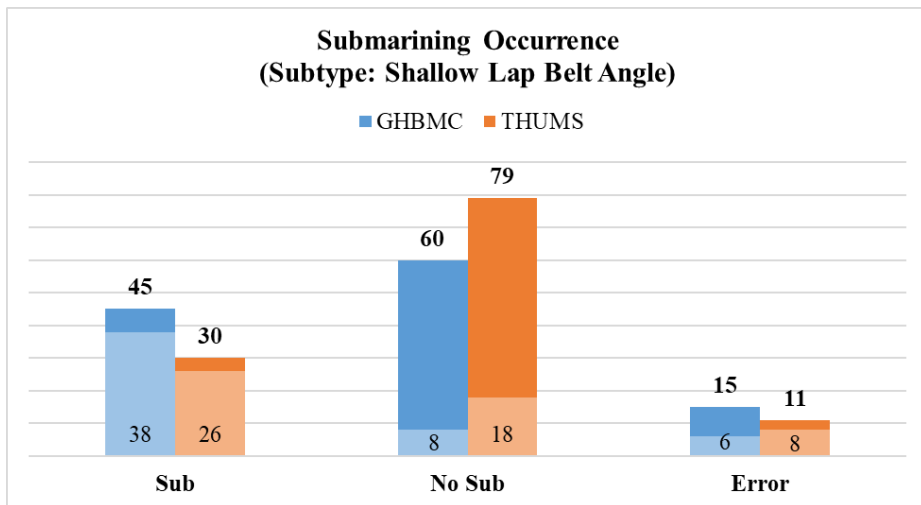


Figure 7.6: Submarining occurrence resulting from the GHBMC and THUMS simulations (120 sims each). The light shading (and inset data labels) are the simulations with a shallow lap belt angle (see Section 7.3.1.2). The dark shading are simulations with the nominal and more vertical lap belt angles. The top data labels are total simulations. “Error” marks the simulations that error terminated prior to 80 ms.

in which the lap belt is initially above and behind the ASIS (resulting from lap belt routing), and 2) dynamic submarining, in which the lap belt moves above and behind both the left and right ASIS during the simulation. In categorizing the total submarining cases, most of the THUMS submarining cases (83%) were pre-submarining cases with only 17% of submarining cases showing true submarining behavior (Figure 7.7). In contrast, 47% of the GHBMC submarining simulations were categorized as pre-submarining cases, with 53% of submarining cases showing true submarining behavior.

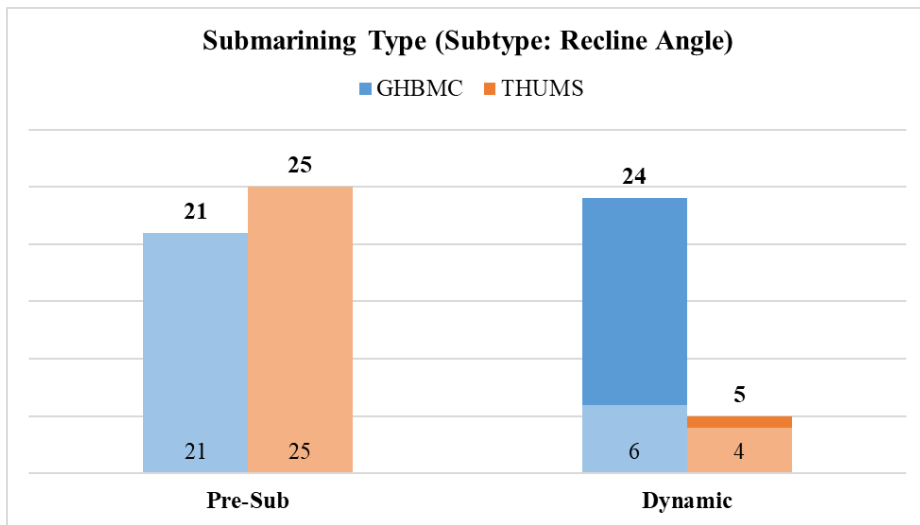


Figure 7.7: Submarining distinction, based on the definitions from Figure 7.3. The light shading (and inset data labels) are reclined simulations. The dark shading are upright simulations. The top data labels are total simulations (combined upright and reclined).

7.4.2 Lap Belt Tension to ASIS Load

For both models, the inner ASIS cross-section measured higher lap belt tension than the outer ASIS cross-section, likely due to additional shear force transferred through the pelvis-flesh attachment (for the GHBMC), or the sliding friction interface (for the THUMS), which contributed traction force to the inner cross-sections (Figure 7.8). The ASIS cross-sections of the GHBMC measured more load for a given level of lap belt tension than the THUMS. For the THUMS, there were several cases in which the lap belt measured a relatively high magnitude of lap belt tension with negligible load measured at the ASIS. This was particularly apparent in the outer ASIS cross-section of the THUMS (Figures 7.8c and 7.8d).

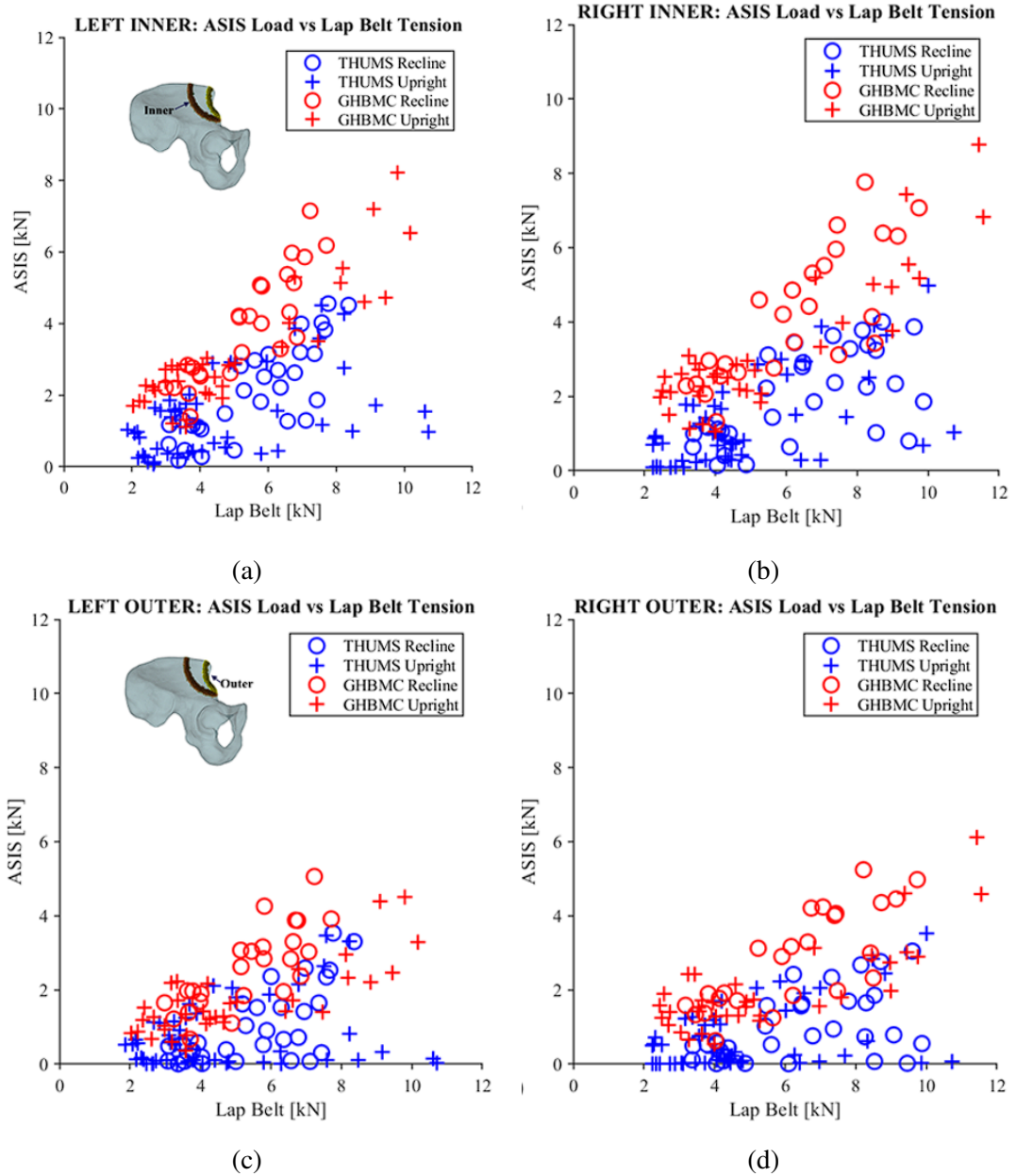


Figure 7.8: Peak lap belt tension and measured ASIS load at the time of peak lap belt tension for the GHBMC (red) and THUMS (blue) HBMs in upright and recline. Inner (a and b) and outer (c and d) ASIS cross-sections. Left iliac wing (a and c) and right iliac wing (a and c).

CHAPTER 7. SELECTION OF HBM FOR SUBMARINING ANALYSIS

Further investigation was conducted on several of the THUMS cases which measured relatively high magnitudes of lap belt tension with negligible measured ASIS load. From this investigation, the lap belt of the THUMS was found to stay generally low relative to the bony pelvis (closer towards the AIIS) versus the GHBMC (Figure 7.9). As a result, the lap belt was not migrating high enough along the iliac wing to load the ASIS cross-sections, of which the boundaries were located at the AIIS (Table 7.1). Thus, no lap belt load was being measured by the ASIS of the THUMS in these conditions as the lap belt effectively bypassed the instrumentation.

A method to flag the cases in which the lap belt never migrated up the bony pelvis was developed (Appendix F.2). This mechanism was present in 24% of the THUMS non-submarining cases and 17% of the GHBMC non-submarining cases, with the vast majority occurring in the upright posture. These flagged simulations were removed from further belt-ASIS load transfer analysis, as they resulted in a substantial portion of the lap belt load transferring through the lower pelvis and thighs rather than the ASIS (Figure 7.10 and Figure 7.11).

After removing the cases in which the lap belt remained low on the pelvis, there were still several cases in which the THUMS measured a negligible level of ASIS force for a high level of lap belt tension. Further examining cases revealed that lap belt roping occurred frequently in the THUMS (Figure 7.12). These cases were quantified by measuring the resultant distance of the nodes on the top and bottom edges of the lap belt webbing and flagging when this distance was under 5 mm. The THUMS exhibited this behavior four times as frequently as the GHBMC.

Removing these cases from the cross-plot removed several outliers that were present in the data, in addition to cases in the lower right quadrant of the plot, wherein the lap belt tension increased with minimal increase in measured ASIS load (Figure 7.13 and 7.14). However, a number of THUMS cases still showed negligible low being measured at the ASIS cross-section for a relatively high lap belt load.

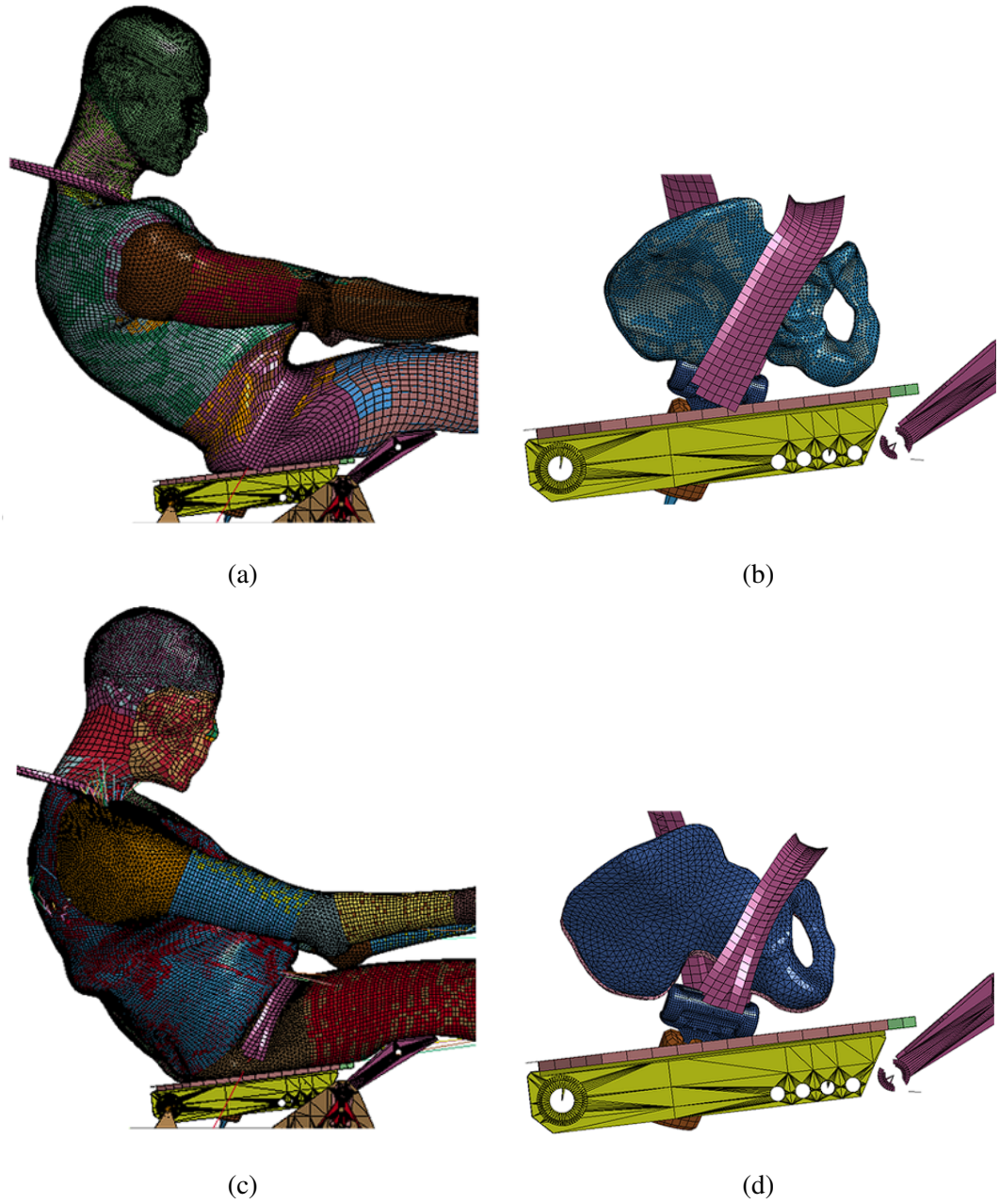


Figure 7.9: Approximate time of peak pelvis forward displacement for the occupant models. Top-down: GHBM (a and b) and THUMS (c and d). Left-right: Torso kinematics (a and c) and lap belt-pelvis kinematics (b and d).

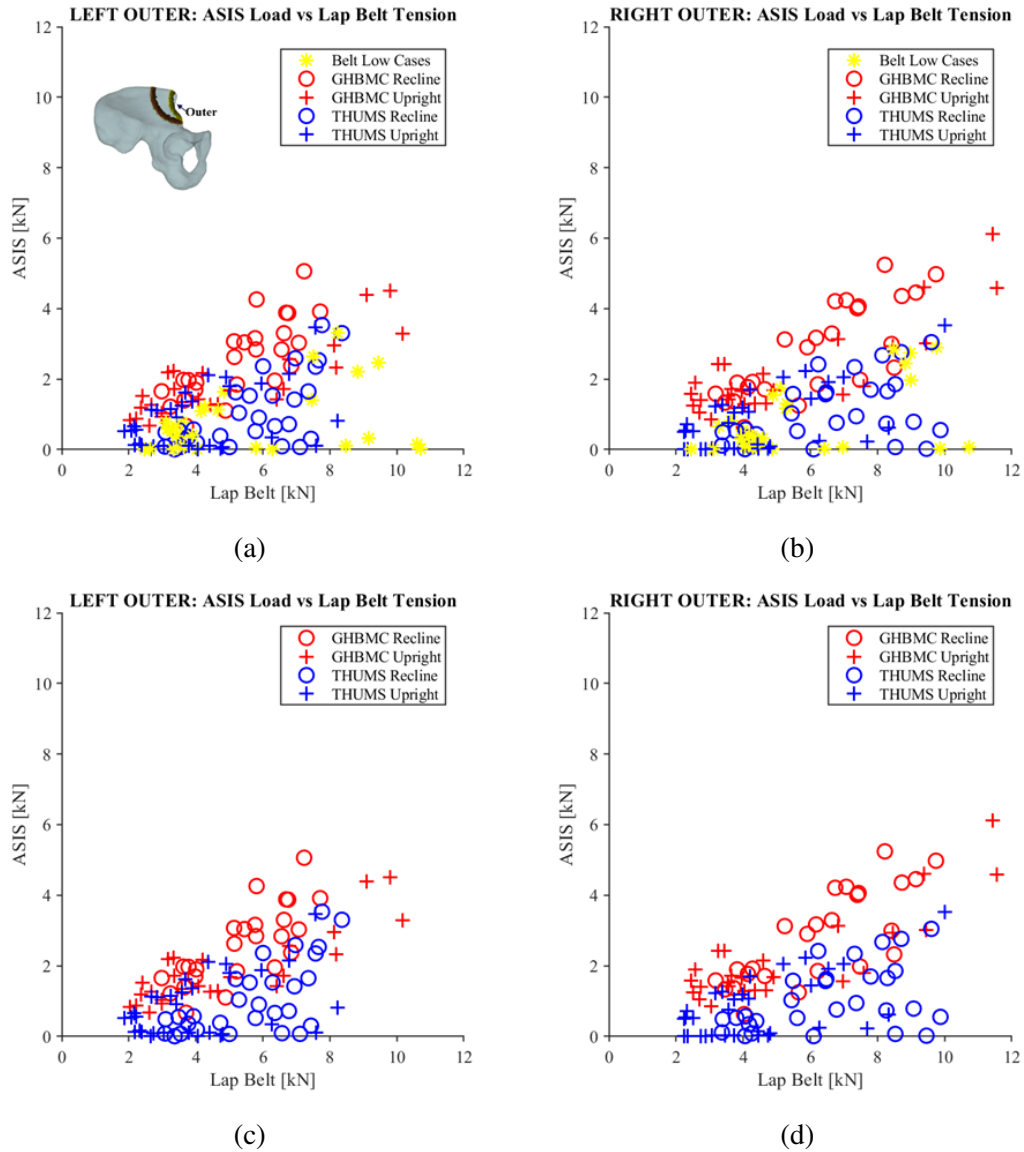


Figure 7.10: Outer cross-section ASIS force vs lap belt tension: Top row: the simulations in which the lap belt remained low on the pelvis are highlighted for both the THUMS (originally in blue) and GHBMC (originally in red) (a, left ASIS and b, right ASIS). Bottom row: after removal of the highlighted cases (c, left ASIS and d, right ASIS).

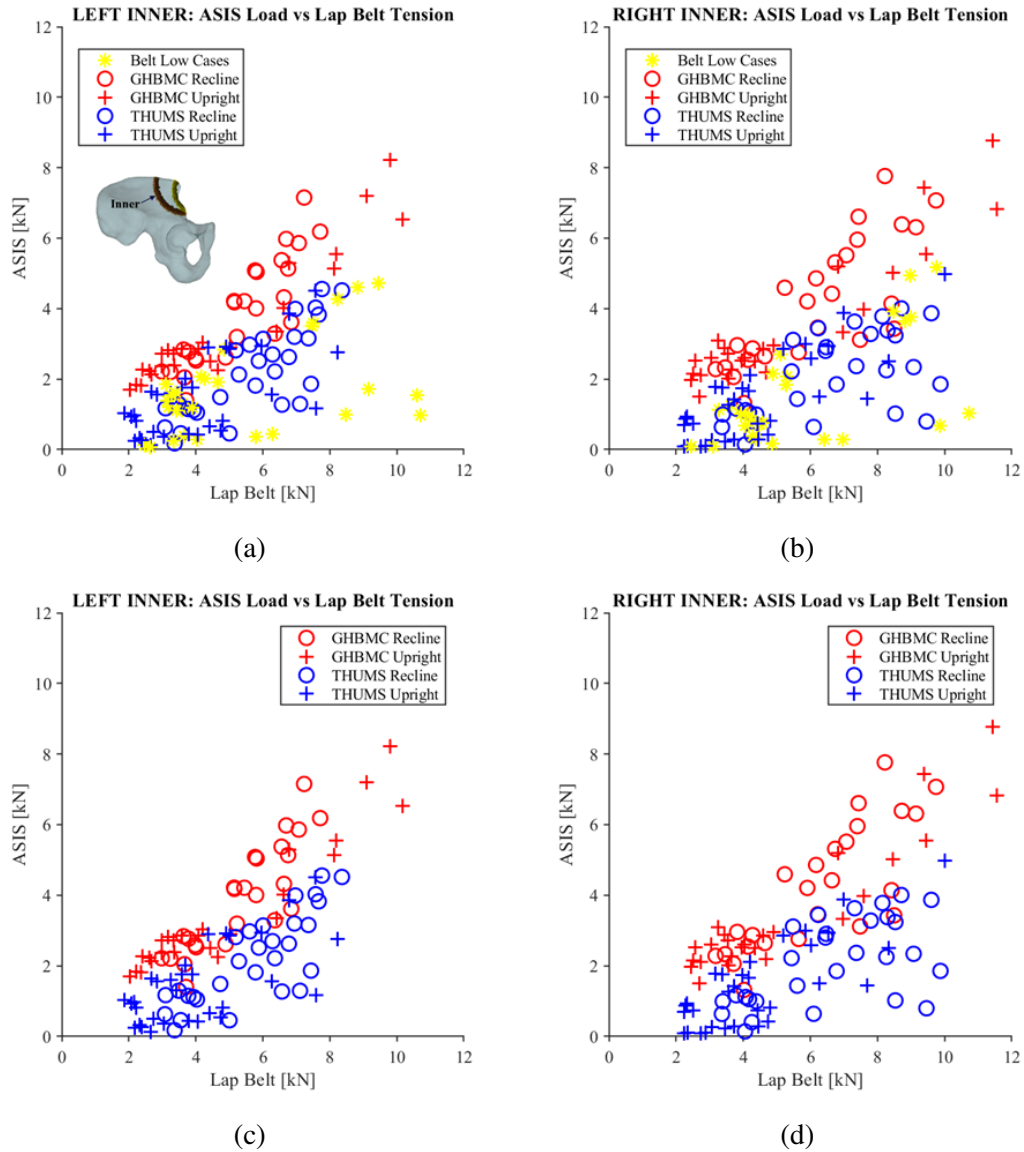


Figure 7.11: Inner cross-section ASIS force vs lap belt tension: Top row: the simulations in which the lap belt remained low on the pelvis are highlighted for both the THUMS (originally in blue) and GHBMC (originally in red) (a, left ASIS and b, right ASIS). Bottom row: after removal of the highlighted cases (c, left ASIS and d, right ASIS).

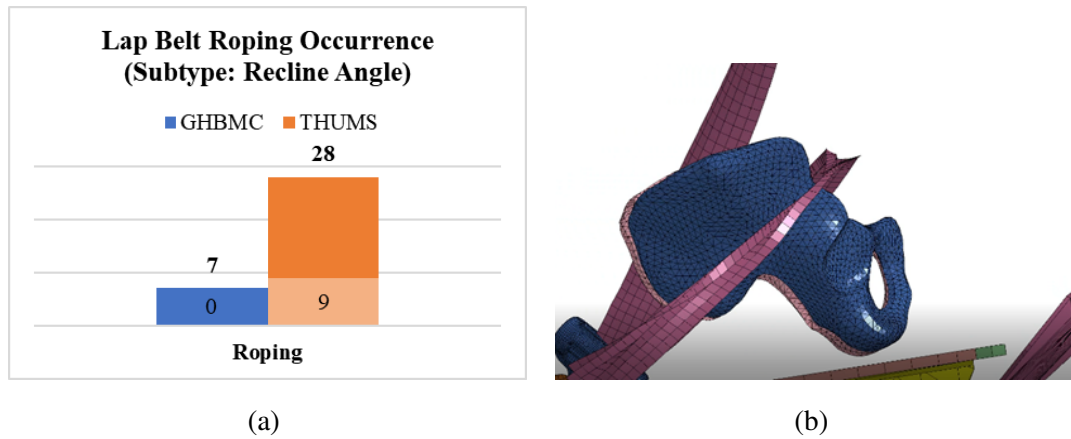


Figure 7.12: (a) The number of simulations that were flagged for lap belt roping in the GHBMC (blue) and THUMS (orange), wherein the resultant distance between the upper and lower edges of the lap belt close in within 5 mm of each other. The light shading (and inset data labels) are reclined simulations. The dark shading are upright simulations. The top data labels are total simulations (combined upright and reclined). (b) An image taken of the lap belt roping in a simulation with the THUMS model.

7.5 Discussion

7.5.1 Submarining Occurrence

In the seated belt pull simulations described in Chapter 6, the THUMS exhibited a higher sensitivity to a shallow lap belt-pelvis angle, showing more abdominal penetration from the lap belt than what was seen for the GHBMC in the same condition. In contrast, this chapter’s dynamic simulations showed both models were equally sensitive to a shallow lap belt angle, with a similar distribution of shallow lap belt angle simulations resulting in submarining (Figure 7.6). Thus, it seemed likely that the identifications described in Chapter 6 regarding THUMS’s higher submarining sensitivity to a shallow lap belt angle was specific to the seated test configuration, with a constrained surrogate (e.g., lap belt load limit, displacement rate, etc.). Additionally, the THUMS had less overall submarining cases than the GHBMC (Figure 7.5), with most of these cases being pre-submarining cases versus dynamic, or true, submarining cases (Figure 7.7). All of the pre-submarining cases occurred in recline for both models. As pre-submarining specifies the case in which the lap belt is already above and behind the ASIS initially, it was a direct result of both the lap belt routing and the HBM-specific abdomen shape. For a very shallow lap belt angle, the lap

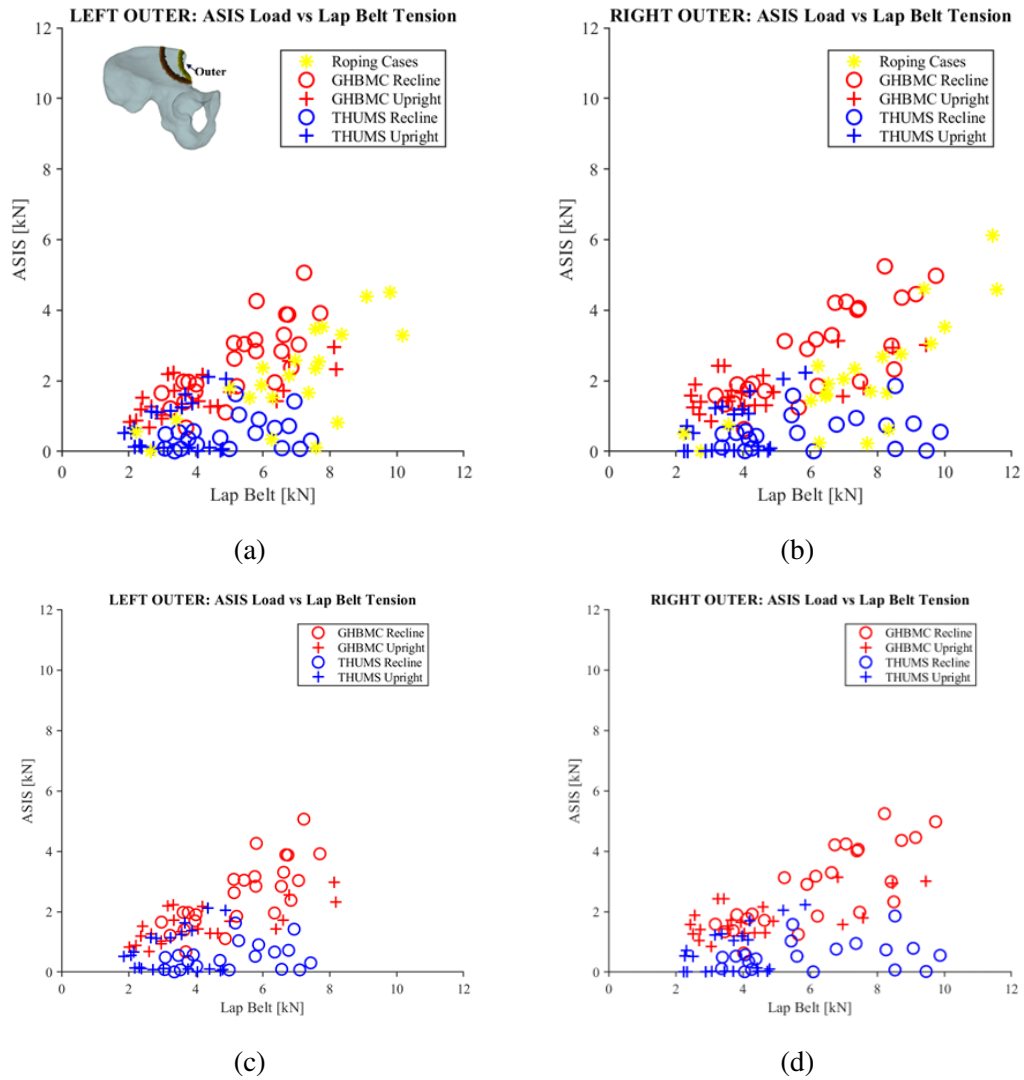


Figure 7.13: Outer cross-section ASIS force vs lap belt tension: Top row: the simulations in which the lap belt roping occurred are highlighted for both the THUMS (originally in blue) and GHBMC (originally in red) (a, left ASIS and b, right ASIS). Bottom row: after removal of the highlighted cases (c, left ASIS and d, right ASIS).

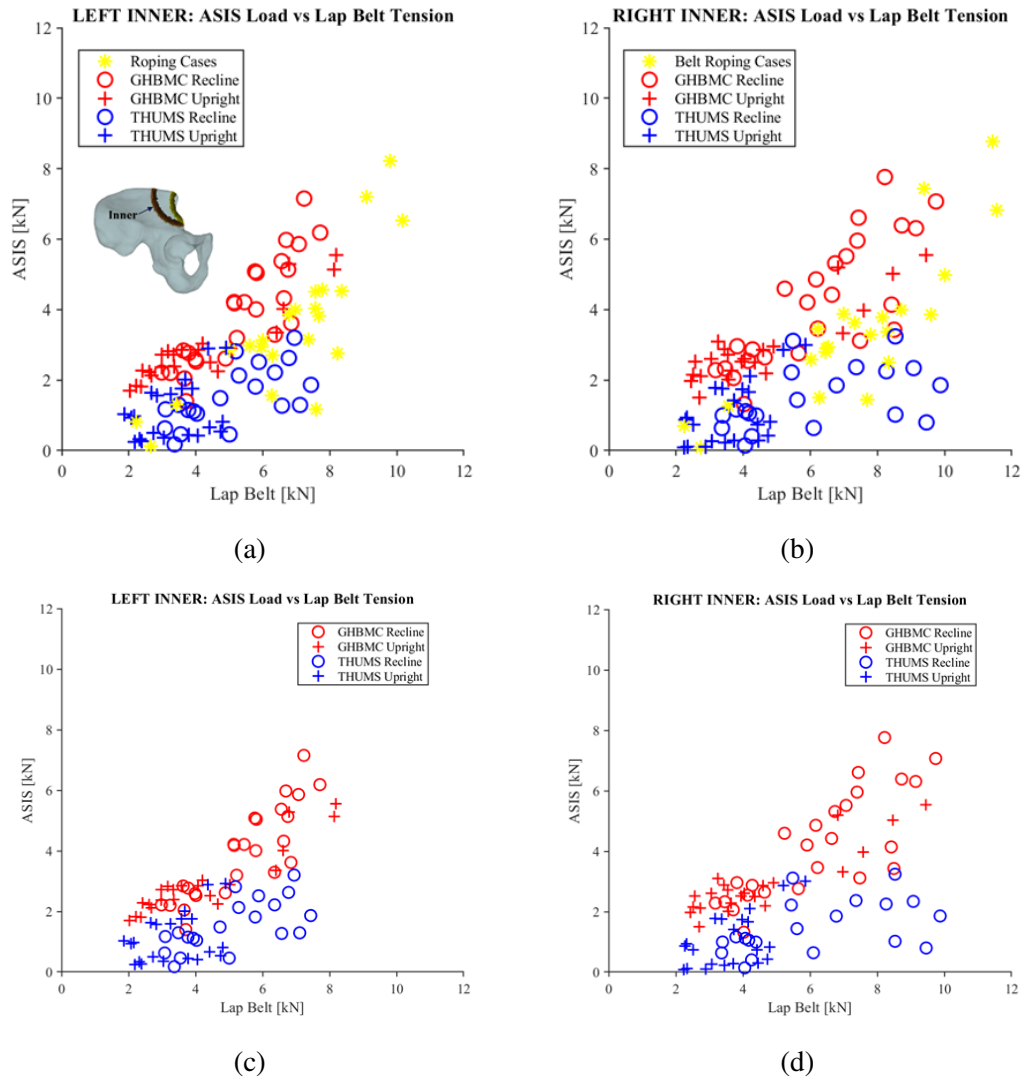
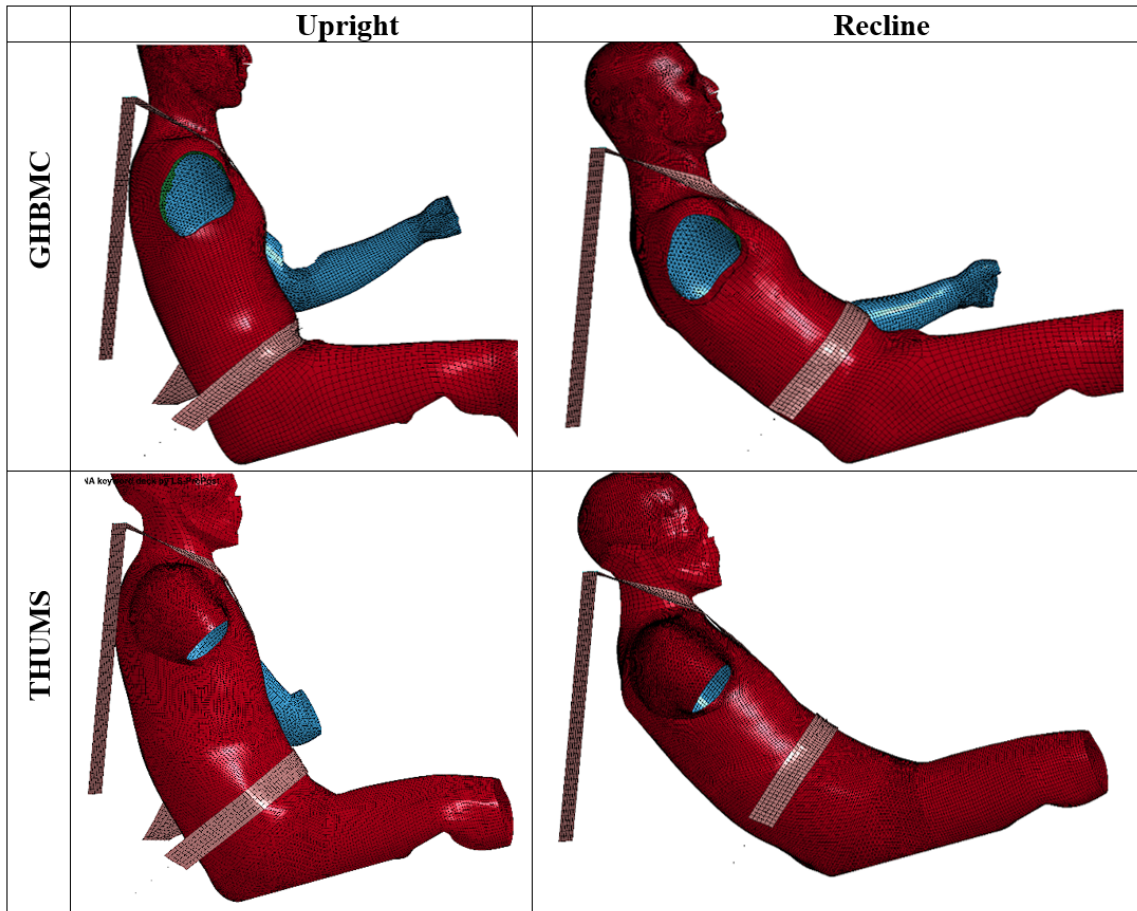


Figure 7.14: Inner cross-section ASIS force vs lap belt tension: Top row: the simulations in which lap belt roping occurred are highlighted for both the THUMS (originally in blue) and GHBMC (originally in red) (a, left ASIS and b, right ASIS). Bottom row: after removal of the highlighted cases (c, left ASIS and d, right ASIS).

CHAPTER 7. SELECTION OF HBM FOR SUBMARINING ANALYSIS

belt was positioned higher on the abdomen of the THUMS model versus the GHBMC model in both upright and reclined cases (Table 7.2). During the belt routing, the occupant was modeled as a rigid body and the lap belt is modeled as a deformable membrane structure which wraps around the occupant model with a predefined level of friction. Consequently, the lap belt is routed and stretched over the abdomen by using the shortest path. As the THUMS model has a shallower abdominal slope with smoother curvature relative to the GHBMC, the belt migrates up the abdomen more easily on the THUMS model during the lap belt routing and stretching.

Table 7.3: Belt fit of the shallowest lap belt angle (relative to horizontal), with the belt anchorages positioned 200 mm rearward (in X) from the nominal position. (Columns: posture; Rows: computational model).



Only 17% of the submarining cases for the THUMS were true submarining, which occurs

CHAPTER 7. SELECTION OF HBM FOR SUBMARINING ANALYSIS

dynamically as the belt migrates above and behind the pelvis during the impact. In contrast, the GHBMC had 53% of cases that resulted in dynamic submarining. This suggested that the belt more easily migrated up the bony pelvis of the GHBMC than it did for the THUMS. Additionally, 24% of the THUMS cases without submarining resulted in the lap belt not migrating up the pelvis (and loading the ASIS cross-section) whereas 17% of such instances resulted in the GHBMC non-submarining cases. This observation was further expanded upon in the following section.

7.5.2 Lap Belt Tension to ASIS Load

Lap belt roping occurred in several of the THUMS simulations, including the same behavior first identified in Chapter 4, in which the lap belt elements collapsed due to either the THUMS's sliding contact between the flesh and the pelvis or the flesh material stiffness (Figure 7.15). Thus, the limitation first identified in Chapter 4 was not solely attributed to that given configuration but was also seen in several other cases with varying parameters.

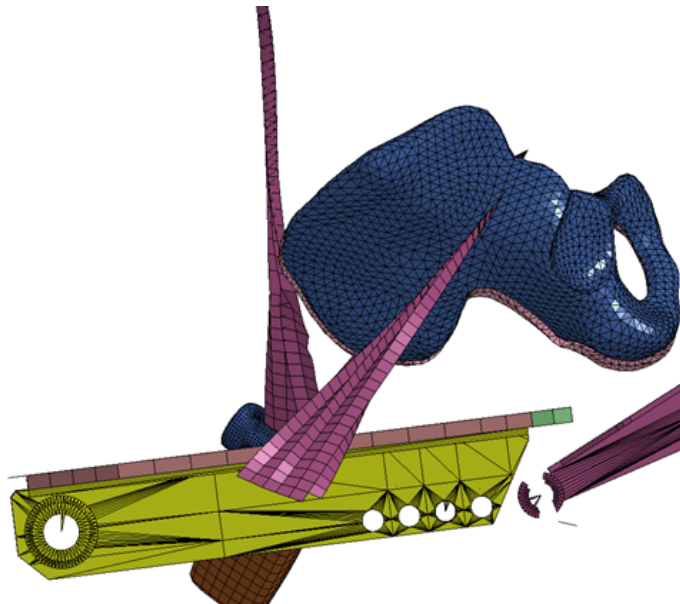


Figure 7.15: The collapsing of lap belt elements seen for several of the THUMS cases (in which lap belt roping was identified).

Simulations with the THUMS model resulted in more cases in which the lap belt either did not migrate far enough up the pelvis to load the ASIS cross-section instrumentation or folded over upon itself (i.e., roping). Despite removing these cases, several THUMS cases still showed negligible ASIS loading for a relatively high level of lap belt tension (Figure 7.13 and 7.14). In

CHAPTER 7. SELECTION OF HBM FOR SUBMARINING ANALYSIS

order to thoroughly understand this difference in measured ASIS load between models, matched cases between the GHBMC and THUMS were identified (Figure 7.16). In most cases, the GHBMC and THUMS showed comparable levels of lap belt tension, but the THUMS was still measuring low ASIS load relative to the GHBMC.

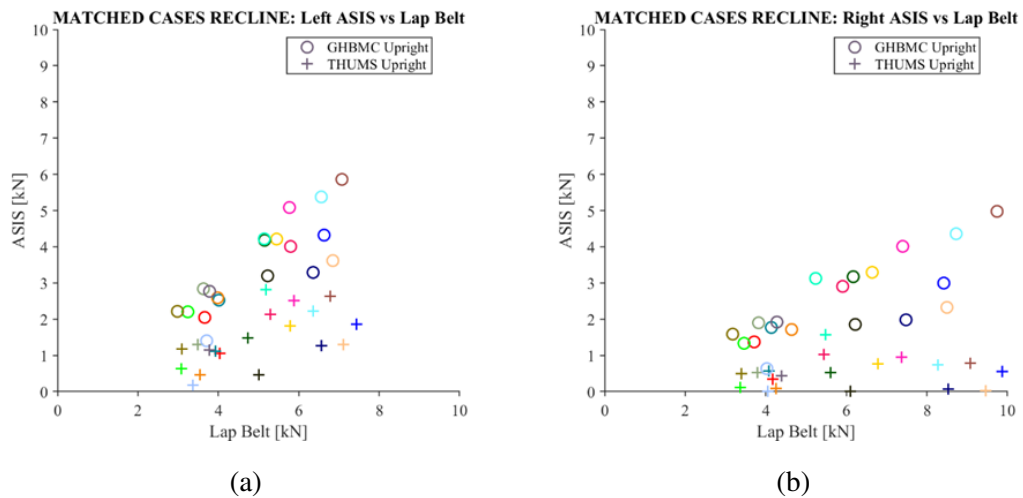


Figure 7.16: Matched reclined simulations between the GHBMC (circle) and THUMS (cross), after removal of cases that submarined, or where the lap belt either did not migrate up the pelvis to load the ASIS or folded over itself (i.e., roping). which are those that were suitable for the belt-ASIS load transfer analysis, for the three occupant models. The colors correspond to a given simulation condition and the shapes correspond to the computational model.

To understand the mechanism behind the THUMS consistently measuring less ASIS load relative to the GHBMC, two specific simulations were investigated to compare the kinematics and lap belt interaction. The first simulation (in magenta in Figure 7.16) showed that both the GHBMC and THUMS measured the same level of lap belt tension (approximately 6 kN on the left and right), but with differing measured ASIS load (3-4 kN for the GHBMC, 1-2 kN for the THUMS). The second simulation (in brown in Figure 7.16) showed the same pattern: both the GHBMC and THUMS measure approximately the same lap belt tension (approximately 7 kN on the left and 8-9 kN on the right), but with differing measured ASIS load (5-6 kN for the GHBMC, 1-3 kN for the THUMS).

Further investigating these simulations showed that the lap belt still remains relatively low on the pelvis of the THUMS relative to the GHBMC (Table 7.4). While the top edge of the lap belt webbing was still located at the AIIS, and thus did not meet the threshold to be flagged as a

CHAPTER 7. SELECTION OF HBM FOR SUBMARINING ANALYSIS

simulation in which the lap belt remained low on the pelvis for the entire simulation, a substantial portion of the internal stresses (resulting from the lap belt loading) were below the AIIS. Thus, only a small portion of the lap belt webbing passed through the ASIS cross-sections. In contrast, the internal stresses of the GHBMC were located on the ASIS.

Table 7.4: Differences in belt-pelvis stress contours for the GHBMC (left column) and THUMS (right column). Rows: GHBMC and THUMS cross-sections (top), the first matched simulation (middle), and the second matched simulation (bottom).

	GHBMC	THUMS
Cross-Sections		
First matched simulation	<p>HBM v10 Time = 85 Contours of Effective Stress (v-m) reference shell surface min=1.13581e-07, at elem# 60000057 max=0.160655, at elem# 8614544</p> <p>Effective Stress (v-m) 3.000e-02 2.700e-02 2.400e-02 2.100e-02 1.800e-02 1.500e-02 1.200e-02 9.000e-03 6.000e-03 3.000e-03 0.000e+00</p>	<p>HBM v10 Time = 85 Contours of Effective Stress (v-m) reference shell surface min=0, at elem# 7232101 max=0.0729125, at elem# 83517571</p> <p>Effective Stress (v-m) 3.000e-02 2.700e-02 2.400e-02 2.100e-02 1.800e-02 1.500e-02 1.200e-02 9.000e-03 6.000e-03 3.000e-03 0.000e+00</p>
Second matched simulation	<p>HBM v10 Time = 67.5 Contours of Effective Stress (v-m) reference shell surface min=2.05826e-07, at elem# 60001965 max=0.190498, at elem# 8600928</p> <p>Effective Stress (v-m) 3.000e-02 2.700e-02 2.400e-02 2.100e-02 1.800e-02 1.500e-02 1.200e-02 9.000e-03 6.000e-03 3.000e-03 0.000e+00</p>	<p>HBM v10 Time = 67.5 Contours of Effective Stress (v-m) reference shell surface min=0, at elem# 7232201 max=0.0761274, at elem# 83018081</p> <p>Effective Stress (v-m) 3.000e-02 2.700e-02 2.400e-02 2.100e-02 1.800e-02 1.500e-02 1.200e-02 9.000e-03 6.000e-03 3.000e-03 0.000e+00</p>

Thus, the belt consistently remained low on the pelvis of the THUMS, with little upwards

CHAPTER 7. SELECTION OF HBM FOR SUBMARINING ANALYSIS

migration. This was again likely a result of the sliding contact interface between the flesh and the skeleton of this model, allowing the belt to migrate downwards as the flesh slides over the pelvis. While there is an absence of data to validate the lap belt-pelvis interaction behavior in either the GHBMC or THUMS in these cases, this finding backs the biofidelity limitation identified in Chapter 6, in which a small lap belt-pelvis angle resulted in a downward lap belt-pelvis trajectory. Indeed, several of the THUMS cases in which negligible ASIS load was measured for a given level of lap belt tension had a lap belt angle oriented more vertical relative to ground (or a small lap belt-pelvis angle) (Figure 7.17). In contrast, the GHBMC measured a higher ASIS load for a vertically oriented lap belt angle. Thus, the biofidelity limitation for the THUMS identified in the belt pull experiments in Chapter 6, in which the lap belt angle oriented more vertically (small lap belt-pelvis angle) resulted in a downward migration of the lap belt relative to the pelvis, was also seen in the dynamic condition under varying conditions.

CHAPTER 7. SELECTION OF HBM FOR SUBMARINING ANALYSIS

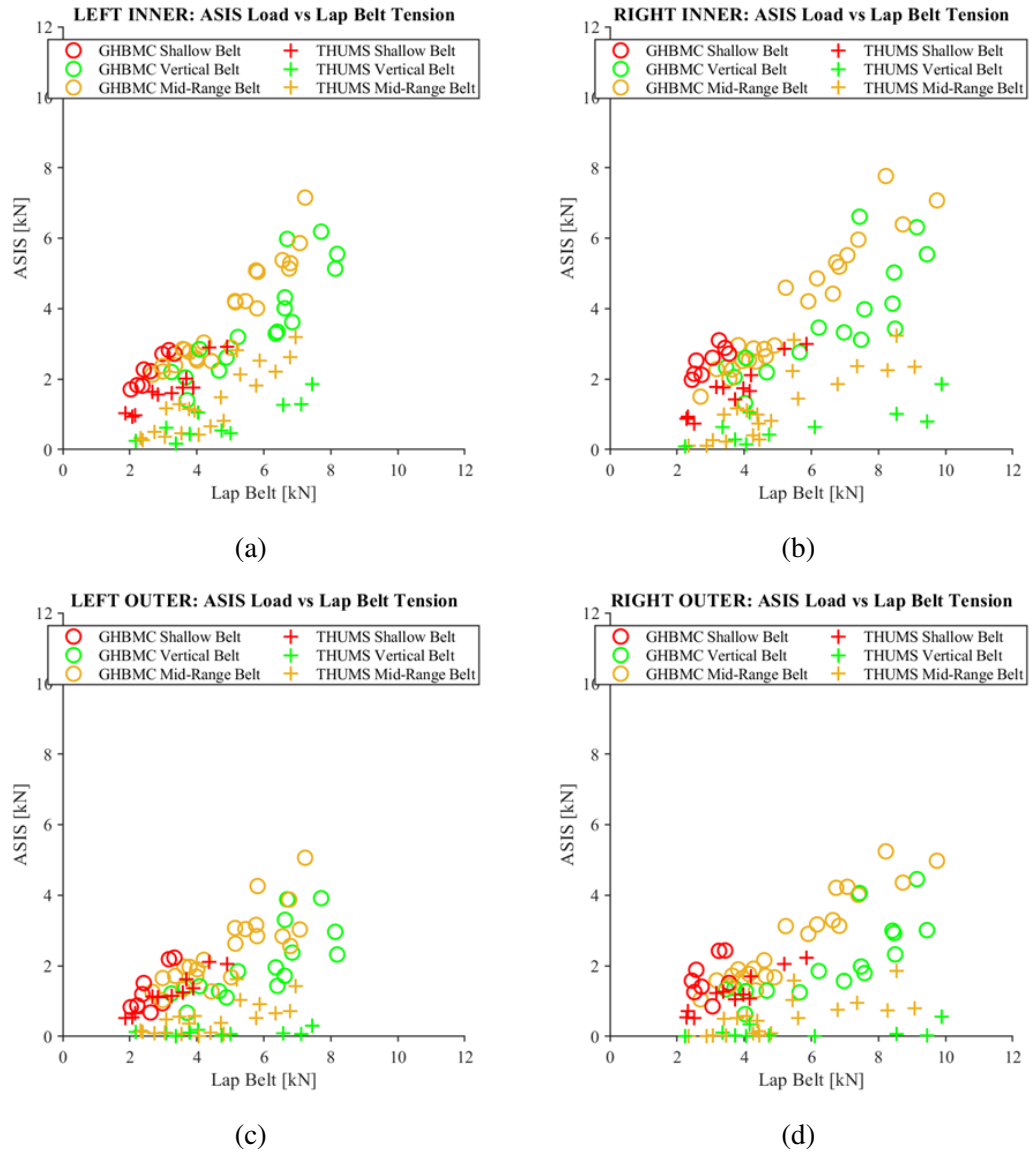


Figure 7.17: Cross-section ASIS force vs lap belt tension comparison between the GHBM (circles) and THUMS (crosses) for varying lap belt angles. Top row: inner cross-section ASIS forces (a, left ASIS and b, right ASIS). Bottom row: outer cross-section ASIS forces (a, left ASIS and b, right ASIS).

7.6 Conclusions

The following conclusions were drawn from this chapter's analysis:

1. Despite the THUMS exhibiting more lap belt penetration for a more horizontally oriented belt (large lap belt-pelvis angle) in the belt pull tests described in 6, the model exhibited less submarining behavior than the GHBMC. In particular, the majority of the submarining cases for the THUMS were pre-submarining cases, which resulted from the lap belt routing but not from the lap belt-pelvis kinematics.
2. The collapsing of the lap belt elements first identified in the THUMS simulation of Chapter 4 was seen in other configurations with varying parameters. Additionally, the THUMS exhibited more lap belt roping behavior than the GHBMC. This behavior affected lap belt-pelvis loading and was attributed to the sliding interface between the flesh and the pelvis.
3. The downward migration of the lap belt relative to the pelvis for a vertically oriented lap belt angle (small lap belt-pelvis angle) which was first identified in the belt pull tests described in Chapter 6, was also seen in the dynamic condition with varying parameters. Additionally, the lap belt loading lower on the pelvis was seen for other lap belt angles. This behavior affected lap belt-pelvis loading and was again attributed to the sliding interface between the flesh and the pelvis.

This sensitivity study confirmed that the THUMS limitations drawn from the simulations described in Chapters 4 and 6 were not specific to those configurations but were also present for several configurations and varying intrinsic and extrinsic parameters. As the GHBMC did not show problematic behavior regarding lap belt-pelvis interaction (i.e., loading) under varying conditions, this model was selected for use in the final parametric study of this dissertation (Chapter 8).

Chapter 8

Quantifying Effects of Factors on Submarining: Simulations

8.1 Executive Summary

8.1.1 Relevance and Goal

The results of the simulations conducted in Chapters 4, 6, and 7 informed the selection of the GHBMC HBM to use in the execution of the final parametric study and to inform conclusions on how various intrinsic and extrinsic parameters affect submarining occurrence, pelvis kinematics, and lap belt kinetics. This parametric study had to have enough data to draw meaningful conclusions. As conducting a full factorial study comes at a high computational cost, metamodeling was used to interpolate conclusions for a dataset of this size. Thus, an automated cycle was developed in which batches of simulations were run, neural network metamodels were iteratively trained, and the model's prediction error was progressively monitored until convergence was reached. These batches of simulations were sampled such that they were distributed throughout the full design space. This chapter discusses the development of this automation cycle and a resulting neural network metamodels that could predict submarining occurrence in addition to continuous outputs, including pelvis kinematics and lap belt kinetics. The developed metamodels were used for further analysis described in Chapter 9.

8.1.2 Key Conclusions

The full list of conclusions can be found in Section 8.6. In summary, the developed automation cycle proved to be an effective way of simulating 480 full-scale frontal impact simulations. This simulation dataset, with several semi-stochastically sampled input parameters (i.e., impact pulse, lap belt angle, etc.), was proven sufficient to optimize the NN metamodels' predictions of several outputs (i.e., submarining occurrence, pelvis kinematics, etc.). An additional sensitivity analysis performed using the NNs showed the models exhibited excellent sensitivity, where the predicted magnitudes of the output metrics correlated with the actual magnitudes. In-depth analysis of the NN metamodels' predictions was conducted within the simulated dataset dataset and beyond, which is described in Chapter 9.

8.1.3 Contributions

The developed automation pipeline is an effective way of simulating large numbers of frontal impact simulations. While the design and implementation of the automation suite was a significant investment of time and resources, the result is that the human interaction bottleneck was removed from the process. Using this method, study size is limited only by the available computational resources. Future studies with hundreds or thousands of simulations can utilize the methods outlined herein to draw conclusions on how sampled input parameters affect a given outcome.

8.2 Introduction

The results of the simulations described in Chapters 4, 6, and 7 were used to select the GHBM HBM in the execution of the final parametric study and to inform conclusions on how various intrinsic and extrinsic parameters affect submarining occurrence, pelvis kinematics, and lap belt kinetics. To inform the relationship between input parameters and lap belt-pelvis interaction, metamodels were developed and trained based on the results of the parametric study, which consisted of several unique simulations with varying parameters. The parametric study must consist of enough simulations to explore the entirety of the parameter space and subsequently train the metamodels to predict outcomes in this space. Manually progressing through each step in the FE model setup, which includes parameter sampling, HBM positioning, settling, seatbelt routing, and parameter modification, is unfeasible. Thus, an algorithm was adapted from previous studies [90, 91] to automate each step in the process, from the initial parameter sampling to post-processing the

CHAPTER 8. QUANTIFYING EFFECTS OF FACTORS ON SUBMARINING: SIMULATIONS

simulation results. This automated process allowed for a much larger number of simulations to be executed than could be executed manually, which resulted in a greater understanding of how these parameters affect lap belt-pelvis interaction and submarining occurrence.

The automation process was designed to work in a cyclical manner, with the results of each step acting as the inputs for the following step (Figure 8.1). In this manner, the metamodels could be iteratively trained after each batch of simulations was executed and post-processed (after each cycle), and the models' resulting prediction errors could be used to inform when sufficient simulations have been run to draw accurate predictions. The individual steps of the process were executed using MATLAB, LS Dyna, and LS PrePost. Steps 1, 2, and 6 utilized local computer resources, while steps 3, 4, and 5 were executed on computing clusters. The later sections in this chapter describe the details of each step.

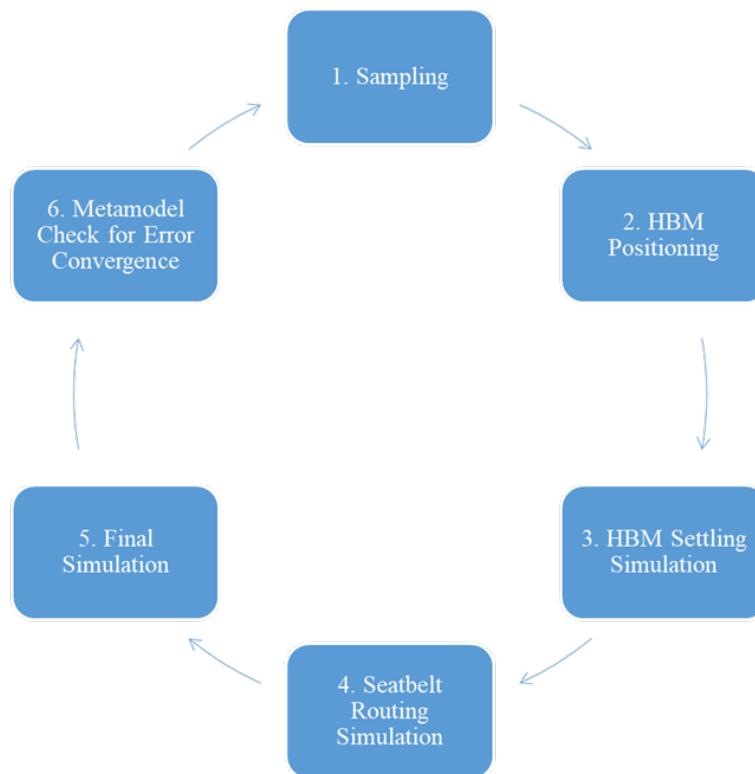


Figure 8.1: Automated simulation cycle.

An FE model response surface, or metamodel, consists of generating a continuous response based on a discrete sample of simulations in a multidimension (i.e., multiparameter) space. Thus, a successful metamodel will predict the entire response surface based on a finite number of

datapoints, or simulations. In the field of biomechanics, metamodels range in complexity. The choice in metamodel depends on the complexity of the relationship among input parameters (e.g., co-dependencies) and the relationship between the input and output parameters (e.g., linearity or nonlinearity).

While ordinary linear regressions have been used in the field of biomechanics [92, 93, 94] to directly quantify the effect that different input factors have on a particular response (through coefficients), this technique has limitations for its use in the generation of multidimensional response surfaces. First, they require the identification and definition of the underlying mathematical response (i.e., $y = mx + b$). The choice in model is critical as low-order models may overlook nonlinearities in the data, and a high-order model could lead to over-fitting. This is an issue for this application as the underlying mathematical response is unknown and the relationship between the predictors and the response cannot be observed due to the multidimensionality of the problem. In this case, the approach used to explore the domain needs to be able to converge to the underlying mathematical model response with no a priori knowledge of the system. Second, as the order of the regression increases to represent a non-linear or non-continuous response (i.e., a binary output such as submarining or no submarining), it becomes difficult to interpret the meaning of each regression coefficient [95].

In addition to Neural Networks, another technique that has been used to estimate regression coefficients is Least Absolute Shrinkage and Selection Operator (LASSO) regularization [96, 97]. This method is able to reduce the complexity of the model in order to optimize out-of-sample prediction by eliminating predictors if they do not contribute to a substantial improvement of the error. This method has been used in the field of biomechanics [98]; however, this method has recently been shown to rank inferior to the NN model in its ability to predict kinematic outcomes from a series of intrinsic and extrinsic predictors [90, 91, 99].

NN models have only recently been used in the field of injury biomechanics to quantify the effects of various inputs on a kinematic output for a large batch of FE HBM simulations [99]; however, this technique has been available for decades. The primary criterion for the evaluation of model performance is its predictive accuracy on out-of-sample data, rather than goodness of fit on training data [100]. Thus, correctly trained NNs are able to represent the underlying mathematical model response of the system. Unlike ordinary regressions or interpolation methods, NNs avoid under- or over-fitting by varying their complexity (e.g., number of neurons) to optimize out-of-sample prediction. One of the most used techniques for this optimization is cross-validation (CV) [101, 102].

CHAPTER 8. QUANTIFYING EFFECTS OF FACTORS ON SUBMARINING: SIMULATIONS

Prior to the CV phase, the dataset of a given iteration is divided into a training subset (e.g., 67% of the data) and a testing subset (e.g., 33% of the data) (Figure 8.2). During the CV phase, the training data is divided into k groups, hence the name k -fold CV. Once the groups are created, a number of NNs with different topologies (i.e., number of neurons, their connectivity and activation functions) and learning algorithms (e.g., backpropagation algorithms) are trained using $k-1$ groups as a training set. The resulting NN performance is based on its error in predicting the responses in the remaining group (validation set). This process is repeated k times using each group once as a validation set. At the end of this process, the network with the minimum average validation error is selected as the final network topology. This procedure generates a NN that generalizes well, as it's been rigorously trained with a bulk of the data. The final topology is trained with the totality of the training set and its prediction error measured using the testing set. This error, as mentioned before, is the primary criterion for the evaluation of model performance. This training process is conducted in an iterative manner, where the main dataset is progressively increased. Thus, this process minimizes the number of simulations run since the prediction error can be checked after each iteration and the process stopped once the error converges. All these characteristics and methods for NN make very robust regression techniques, which can manage noisy systems and, with sufficient training data, converge to the true underlying model response.

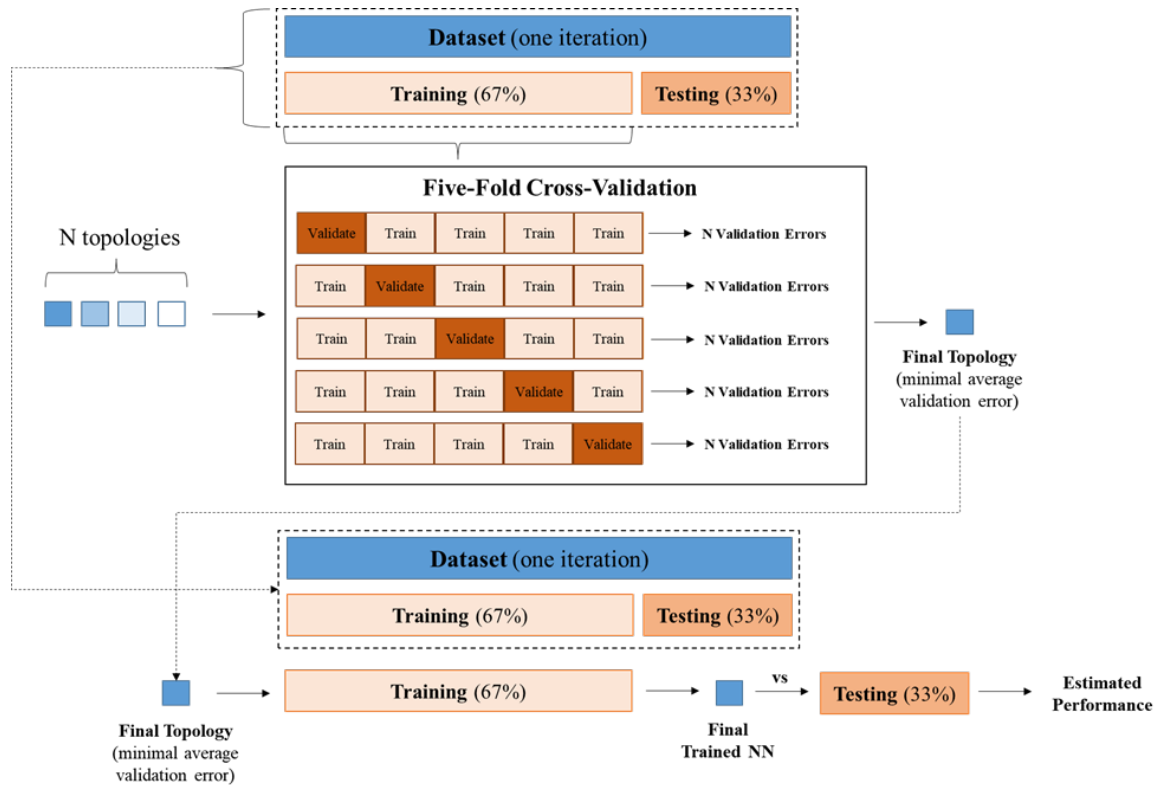


Figure 8.2: Generic training and testing of selected topology (adapted from [90, 100]).

8.3 Methodology

8.3.1 FE Environment

Similar to Chapters 4 and 7, the FE environment consisted of a semi-rigid seat, toe pan, and restraint system (Figure 8.3). The GHBMCM50-O v.6.0 occupant model was used in this parametric study. The restraint system, used in Chapter 3's reclined sled test experiments and Chapter 4's matched simulations, included novel technology designed to mitigate submarining and control overall kinematics. This included a seat-integrated D-Ring, dual lap belt pretensioners, a shoulder belt pretensioner, and a shoulder belt load limiter. The geometry of this restraint system (i.e., D-Ring and lap belt anchorage point locations) was modified based on the sampled lap belt angle (fore-aft and lateral anchorage position modifications) and torso angle (upright or reclined) parameters. The semi-rigid seat, also used in Chapters 3 and 4, was comprised of an independently articulated aluminum seat pan and anti-submarining pan.

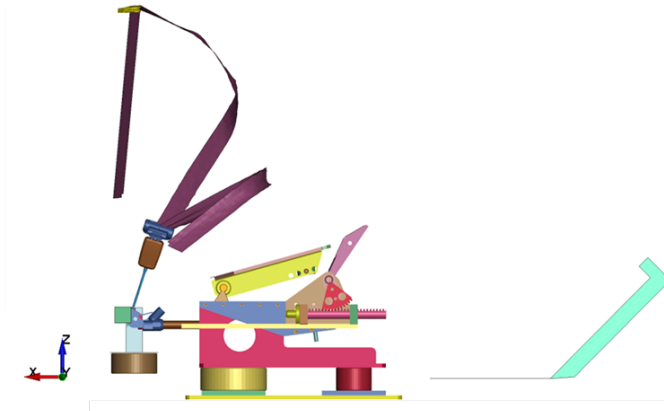


Figure 8.3: FE Environment.

8.3.2 Parameter Selection

The parameters selected were those that were identified in the literature (Chapter 2) as having a potential effect on lap belt-pelvis interaction and submarining (Table 8.1). Discrete levels were chosen for each parameter and the justification behind these values is discussed below.

The impact pulse, or crash severity, was discretized at three levels of delta-V. A simplified trapezoidal 12 g (40 km/h) and a 16 g (56 km/h) pulse were selected based on generic pulses from exemplar full-frontal crash test simulations for unbelted and belted tests (per FMVSS 208 regulations), respectively (Figure 8.4). The 51 km/h (35 g) pulse was used in the reclined frontal sled test experiments and simulations described in Chapters 3 and 4.

The geometry of the lap belt was varied by moving the position of the lap belt anchorage points fore-aft, thus changing the angle of the belt in the sagittal plane, and outward laterally, which changed the angle of the belt in the overhead view. The fore-aft anchorage positions were varied relative to the nominal position used in Chapters 3 and 4, which corresponded to a lap belt angle of approximately 63° relative to the horizontal, as measured by the method described in FMVSS 210: the angle between the segment connecting the anchorage point to the designated H-point position on the vehicle seat, relative to the horizontal [103] (Figure 8.5a). As of 1990, the bounds of this angle, set by FMVSS 210's standard, is $30\text{--}75^\circ$. The selected anchorage positions were chosen to explore the bounds of this range, as well as to explore the potential effects of a more vertical lap belt anchor outside of this range (87°) (Figure 8.5b).

Laterally, the belt anchorage positions were adjusted to 50 and 100 mm further outward from the occupant such that the angle in the overhead view was changed (Figure 8.6). Part of this

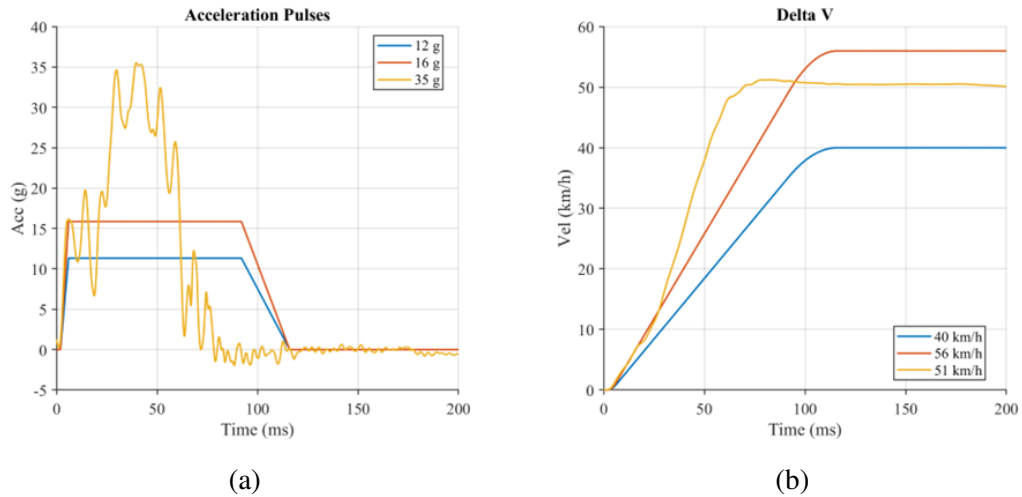


Figure 8.4: The three impact pulses, or crash severities, used in this study: (a) acceleration pulse; (b) delta V.

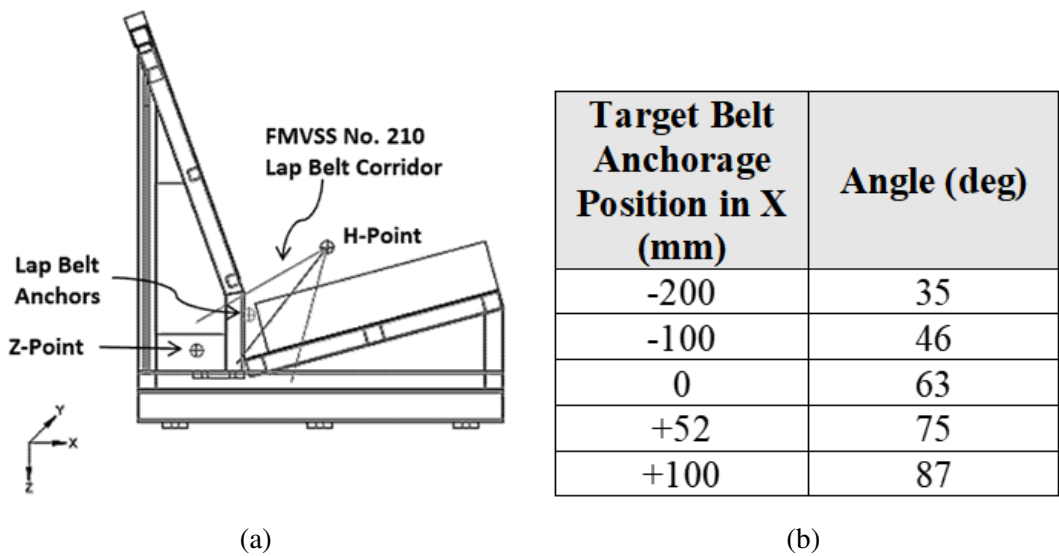


Figure 8.5: a) Lap belt angle measurement as defined in FMVSS 210 [103]. b) The varied belt anchorage positions in this study and the corresponding lap belt angles, as measured by the method outlined in a).

Table 8.1: Selected discrete parameters and their corresponding levels.

Category	Parameter	Levels	Values
Extrinsic	Impact Pulse (g)	3	[12, 16, 35]
	Fore-Aft Lap Belt Angle (mm)	5	Relative to nominal: + [-200, -100, 0, 52, 100]
	Lateral Lap Belt Angle (mm)	3	Relative to nominal: + [0, 50, 100]
	Foot Support	2	Contact on/off
	Belt/Occupant Friction	3	Relative to nominal: μ + [-0.2, 0, 0.2]
	Seat/Occupant Friction	3	Relative to nominal: μ + [-0.2, 0, 0.2]
Intrinsic	Recline Angle (deg)	2	[25 (upright), 50 (reclined)]
	Pelvis Angle (deg)	3	Relative to nominal: + [-12, 0, 12]
	Pelvis Flesh Stiffness (Scale Factor – SFO)	3	Relative to nominal: \times [0.5, 1, 2]

decision was based off early research conducted in the 1980's, which introduced this variable as one that, in combination with the fore-aft angle, affects submarining occurrence [8]. This research predicted an increase in submarining risk for lap belt anchorages moved further outward from the seat and occupant. The lateral belt anchorage position also affected how the pelvis was loaded, as the iliac wing is a 3D structure.

The foot constraint was varied by either including or excluding the contact definition between the occupant and the toe pan, which was positioned at the front of the setup. The belt/occupant and seat/occupant friction levels were varied ± 0.2 relative to the nominal friction level of these contacts ($\mu_{Seat} = 0.35$; $\mu_{Belt} = 0.30$) which has been used in similar studies [104].

Torso angle was varied through occupant positioning (see Section 8.3.4). This intrinsic parameter included a reclined torso angle of 50° relative to the vertical axis, as in the dynamic reclined sled test simulations described in Chapter 4 which matched the experiments described in Chapter 3. Additionally, an upright torso angle of 25° was investigated. Thus, the effects of a reclined posture, which was previously predicted to increase submarining risk [29, 30, 31], could be evaluated.

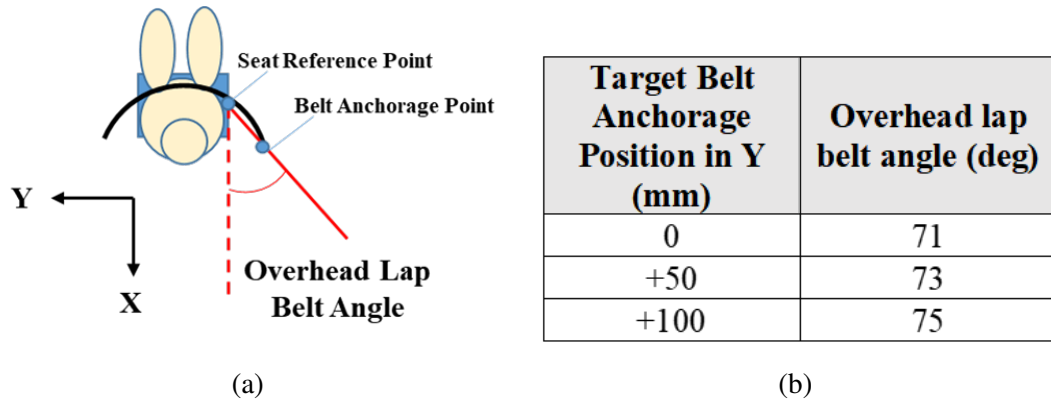


Figure 8.6: a) Overhead lap belt angle measurement, looking at the occupant from the top view where the black semi-circle represents the lap belt. The angle was taken between the segment connecting the seat reference point (see Figure 8.5a) to the lap belt anchorage point relative to the X-axis in the overhead view. b) The varied lateral belt anchorage positions and the corresponding overhead lap belt angles, as measured by the method outlined in a).

The pelvic-abdominal flesh stiffness was varied based on the methods described in Section 6.3.5. This involved scaling the material (*MAT_SIMPLIFIED_RUBBER/FOAM) load curves (LCIDs) by 50% or 200% for several of the GHBM model parts, which encompassed the gluteal tissue and the thorax (Figure 6.7a and Appendix E.1).

Finally, the pelvis angles were varied through HBM positioning based on the methods described in Section 4.3.4, which involved a forward or rearward tilt of 12° relative to the nominal orientation for a given posture. For the reclined posture, these pelvis orientations directly matched those of Chapter 4. For the upright posture, the pelvis was oriented $\pm 12^\circ$ the natural orientation for the model in that posture.

8.3.3 Sampling

Sampling the parameter space required exploration of a nine-dimensional domain. A distance-based algorithm that sought to maximize the space between individual data points was developed by adapting previous methodologies [99]. This algorithm uses a distance-based sampling method known as Simulated Annealing [105, 106]. Simulated Annealing takes random initial guesses for a set of parameters, then iterates them to minimize a distance-based loss function. Through this method, each iteration of points maximizes the approximation of the nine-dimensional parameter space by maximizing the distance between points (Figure 8.7), thus oversampling the

bounds (Figure 8.8). The result is a unique set of nine parameters per simulation. Each of the parameter ranges were normalized prior to sampling to remove biases created by larger values.

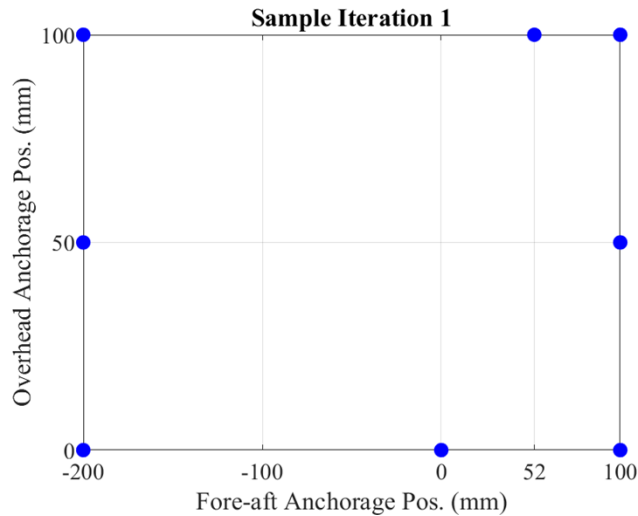


Figure 8.7: Results from the first sample iteration (for the first batch of simulations) for the lap belt angle parameters, discretized at specific levels as shown in Table 9.1. As this plot shows only two parameters, the points are not unique; however, incorporating the other parameters (in a nine-dimension domain) results in unique points (simulations).

The end result of this sampling process was several sample sets (i.e., iterations or batches) of simulations with nine parameters uniquely defined for each simulation. Each batch consisted of 15 simulations. As this algorithm maximizes the distance among points in the parameter space, the bounds of certain parameters are sampled more frequently than the center point. For example, the most extreme fore-aft lap belt anchorage positions (i.e., -200mm and +100mm relative to nominal) were sampled more frequently than the mid-points (i.e., -100mm, 0mm, +52mm relative to nominal). Using MATLAB, the list of parameters for a simulation were used to modify the keyword files as well as to identify and allocate the appropriate input files into that simulation’s execution folder.

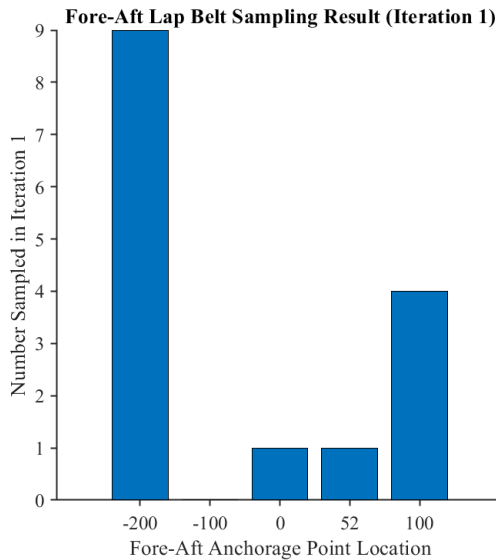

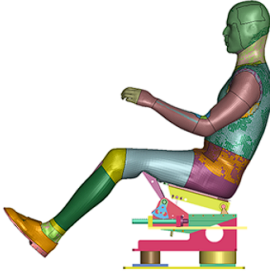




Figure 8.8: Frequency of the first iteration’s sampled points for the fore-aft lap belt angle location parameter levels, showing more sampling occurring at the bounds.

8.3.4 Positioning and Settling

The GHBMC was positioned in both an upright (25° relative to vertical) and reclined (50° relative to vertical) posture (Table 8.2). The hip-points (H-points) between the upright and reclined position were aligned. As the flesh of the HBM is not validated under gravitational loading, forcing the model into the seat (thereby compressing the flesh) has been shown to improve the biofidelity of the pelvis kinematic response [104]. Thus, the GHBMC was first gravity settled then forced into the seat pan by a distance of 20 mm, with the initial stress and strain states removed prior to the simulation. As mentioned above, the pelvis orientations of the reclined model directly matched those of the simulations described in Chapter 4 (nominal ± 12). Comparison of the three prescribed pelvis orientations within and between postures can be found in Appendix G.

Table 8.2: GHBMC model during positioning and settling in the upright and reclined torso angle.

	Positioned	Settled
Upright		
Reclined		

8.3.5 Seatbelt Routing

The purpose of the seatbelt routing simulations was to generate natural or realistic seatbelt positions for the various sampled belt anchorage positions in the six different postures (three pelvis angles per torso angle). This seatbelt position was then added to the model prior to running the final simulation. This method was used in Chapter 7 but was different from that used in Chapters 4 and 6, which used the LS-PrePost belt fitting feature. The seatbelt routing simulations occurred over a 100 ms timeframe, with various part motions happening over that span. The settled positions of the corresponding models were used as inputs for the seatbelt routing simulations. The model's torso, thighs, left arm, head, and neck were rigidized and used in the simulation (Figure 8.9). The seatbelt routing pre-positioning consisted of translating the model's left arm upwards from its initial position and translating the remaining portions of the model down and away from the initial positions. The seatbelt was then imported in a "stock position" (Figure 8.9, left). During the simulation, the model was moved back into the original position as the belt was being tightened (removing slack), with the slippers moving into their designated positions (Figure 8.9, middle). Moving the model into

the belt as it tightened allowed the belt to find its natural position along the torso and thighs (Figure 8.9, right).

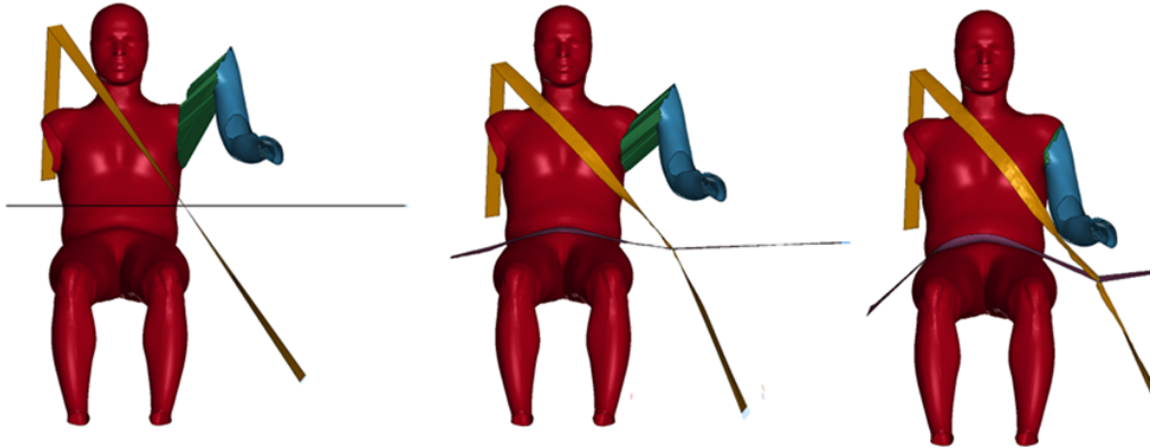


Figure 8.9: Images from the belt fitting simulation. This example is with the GHBM positioned in recline, with the belt anchorages positioned outward from the nominal position.

The seatbelt routing was affected by the lap belt anchorage positions and occupant posture. In total, given two postures (upright and reclined) \times five fore-aft belt anchor positions \times three lateral belt anchor positions \times three pelvis angles, 90 unique belts could be routed. In altering the fore-aft lap belt anchorage position, the belt placement along the abdomen also changed (Figure 8.10). For a more rearward anchorage position (shallow lap belt angle), the belt migrated further up the abdomen – this is particularly exaggerated in the reclined case. As the lap belt anchorage points were positioned more forward (steep lap belt angle), the belt tended to rest lower on the pelvis. This coupling between lap belt placement, lap belt angle, and torso angle was first identified in the seated belt pull experiments of Chapter 5.

While the seatbelts were routed independently for each pelvis angle, the change in pelvis angle had minimal effect on global lap belt placement relative to the abdomen (Figures 8.11 and G.1). Instead, the pelvis appeared to orient relative to a constant lap belt angle and placement.

The change in fore-aft position of the lap belt anchorage points not only dictated the lap belt placement but also the shoulder belt placement (Figure 8.12a). A belt anchor positioned further rearward (shallow lap belt angle) corresponded with an upward migration of the shoulder belt into the neck. A forward belt anchor position (steep lap belt angle) corresponded with a downward migration, positioned lower on the sternum, but this effect was less exaggerated. As with the lap belt migration, this effect was exaggerated in the reclined posture. Moving the belt anchorage

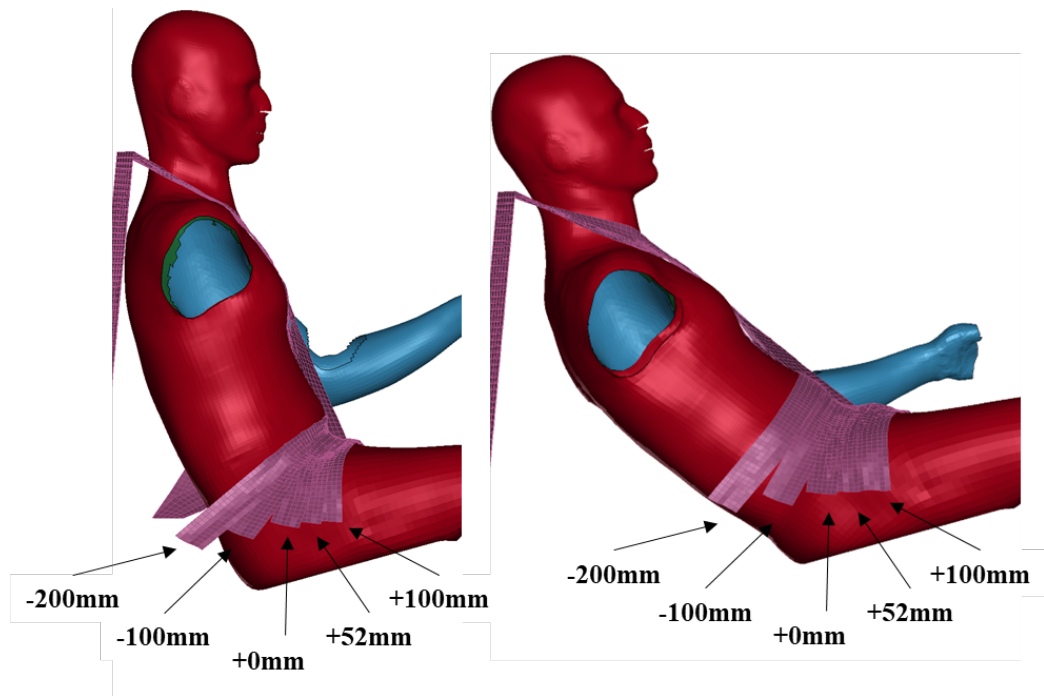


Figure 8.10: Lap belt placements based on the five fore-aft lap belt anchorage position definitions (see Figure 8.5) used in this study. Left: Upright position. Right: Reclined position.

positions fore-aft caused a visibly larger change in shoulder belt fit than moving the belt anchorages outward laterally (Figure 8.12b).

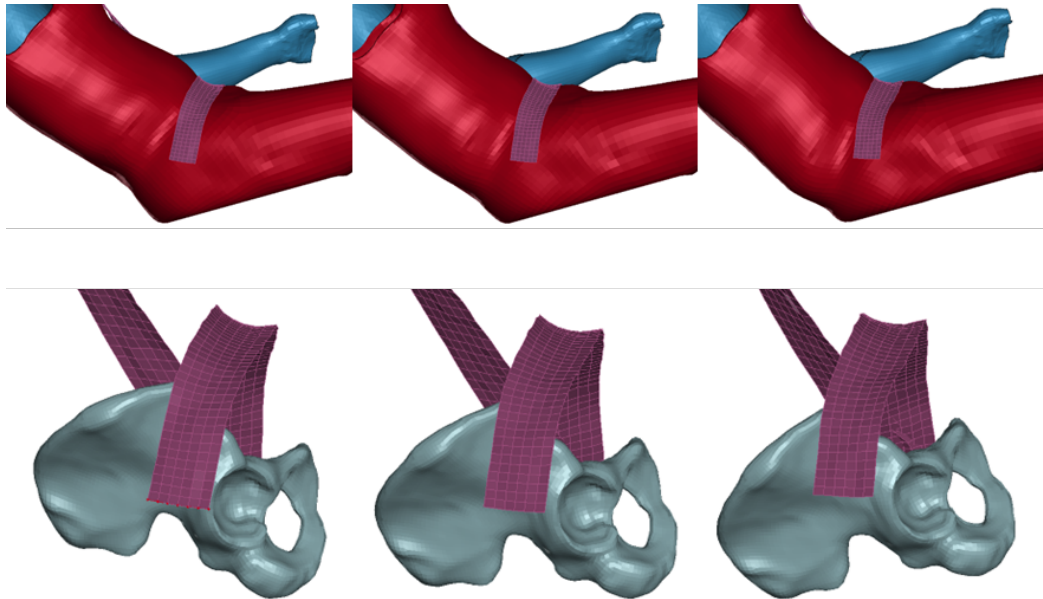


Figure 8.11: Lap belt placement (no change in fore-aft or lateral anchorage position) for different pelvis angles. Left-right: anterior ($+12^\circ$), nominal, and posterior angle (-12°). See Figure G.1 for the upright orientations and Table G.1 for the pelvis angle measurements of all prescribed positions.

8.3.6 Final Simulations

8.3.6.1 Inputs

The settled model with the initial stress/strain states removed, semi-rigid seat, toe pan, and post-processed seatbelt from Section 8.3.5 were used as the starting position for the final simulations. The remaining input parameters (shown in Table 8.1), including the impact pulse, foot contact, friction levels, and flesh stiffness scale factors, were specified in the main *INCLUDE input file. The final simulation had a run time of 150 ms (Figure 8.13).

8.3.6.2 Submarining detection

Submarining was detected using the same method as defined in Section 7.3.3, wherein three lap belt nodes (bottom edge of webbing) were tracked relative to the left and right ASIS and the ASIS midpoint (Figure 7.2). Submarining was detected when the lap belt node passed above and behind the corresponding pelvis node in the global reference frame. Submarining was coded as a binary output, wherein 0 indicated no submarining and 1 indicated submarining.

8.3.6.3 Output metrics

Data directly pertaining to the lap belt and pelvis interaction were output from the simulations. This included pelvis kinematics (displacement and rotation), lap belt tension, and submarining occurrence and distance (Table 8.3). The continuous outputs were chosen based off the results of the literature review described in Chapter 2 (Figure 2.7): pelvis displacement (a result of $F_{Inertia}$), pelvis rotation (affecting β), and lap belt tension (F_{Belt}) have all been hypothesized to contribute to the submarining phenomenon. The justification for selecting the submarining distance parameter is shown below.

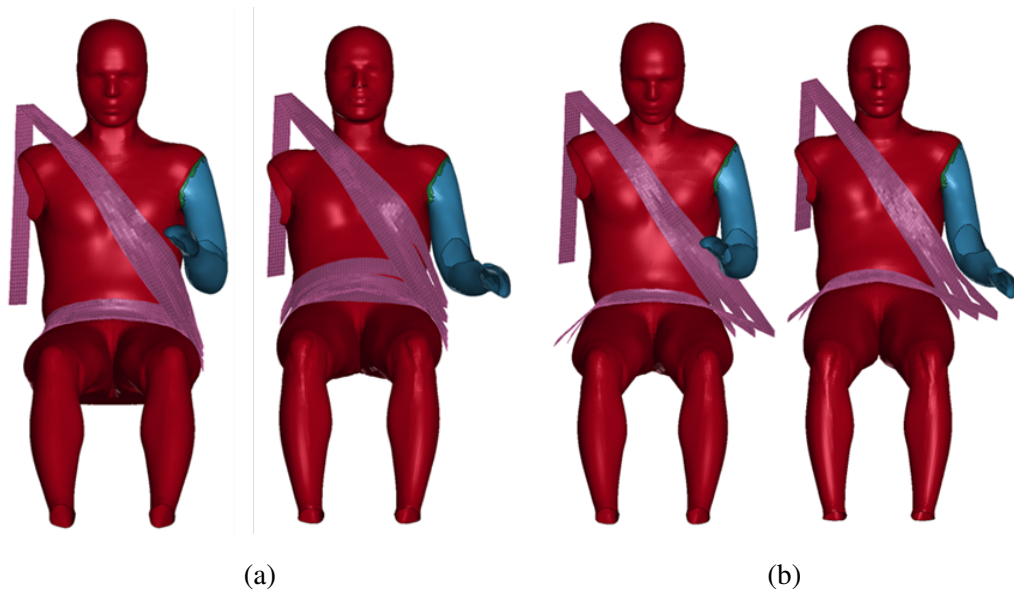


Figure 8.12: Shoulder belt placement resulting from moving the belt anchorages. a) Effect from moving the belt anchorages fore-aft (left: upright, right: reclined). b) Effect from moving the belt anchorages laterally (left: upright, right: reclined).

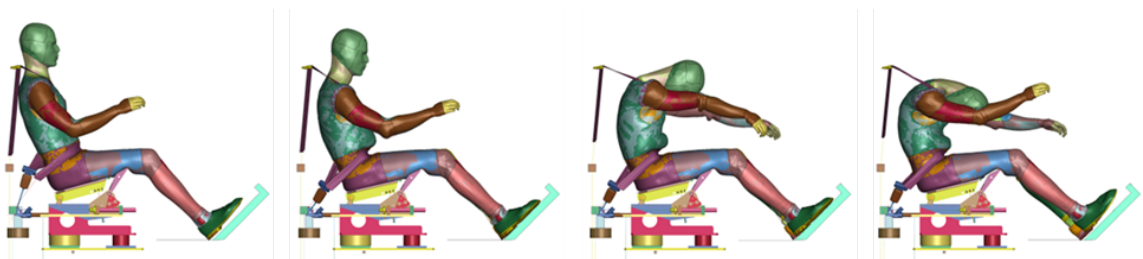


Figure 8.13: Images of an example simulation taken at 0ms, 50ms, 100ms, and 150ms.

CHAPTER 8. QUANTIFYING EFFECTS OF FACTORS ON SUBMARINING: SIMULATIONS

The submarining occurrence output metric was recorded throughout the entire 150 ms simulation run. The other continuous metrics were recorded between the initial time and the time of peak pelvis forward displacement.

Table 8.3: Output metrics from each simulation.

Output Metric	Measurement	Reference Frame
Maximum Forward Pelvis Displacement	Translation of the pelvis from its initial position	Global (X direction)
Maximum Pelvis Rotation (Pitch)	Rotation of the pelvis relative to its initial angle	Global (Y rotation)
Maximum Lap Belt Tension	Force measured at the cross-section of the lap belt webbing (average of inboard and outboard sides)	N/A
Submarining Occurrence	As defined in Section 7.3.3.1	Global (X and Z directions)
Maximum Submarining Distance	Distance between the lap belt midpoint and the midpoint between the left and right ASIS	Global (X direction)

The maximum distance between the lap belt midpoint and the midpoint of the left and right ASIS was measured to define a quantitative metric of the "severity" or magnitude of submarining (Figure 8.14). This output, submarining distance, was defined as a continuous output, in which a positive distance indicated the belt passed behind the ASIS (submarining) and a negative distance indicated the belt was in front of the ASIS (non-submarining). This measurement was taken between the initial time and the time at peak forward pelvis displacement.

8.3.6.4 Postprocessing

A MATLAB object was created for each simulation, storing both the inputs and outputs for each simulation. Information about landmark nodes, section forces, contacts, and coordinate systems were recorded for each simulation timestep. Additional output metrics could be generated from this information in future studies. In addition, images were output from each simulation and reviewed for issues such as lap belt penetration (e.g., Figure 8.13).

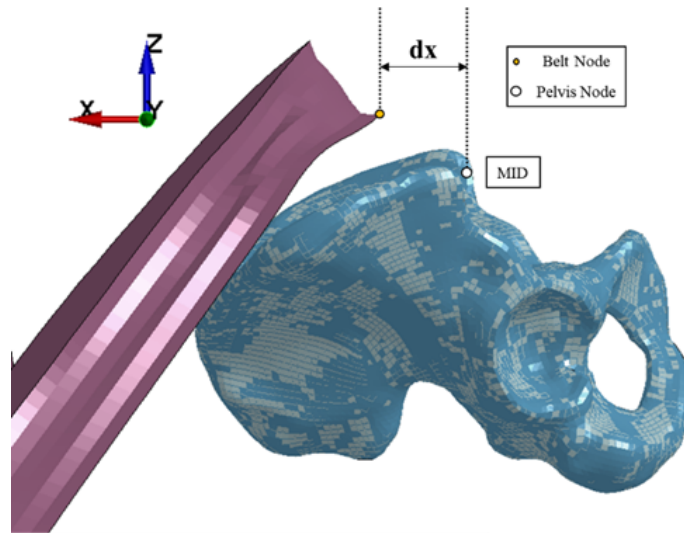


Figure 8.14: Submarining distance output metric. A positive distance indicated the belt passed behind the ASIS (submarining) and a negative distance indicated the belt was in front of the ASIS (non-submarining). This measurement was taken between the initial time and the time at peak forward pelvis displacement.

8.3.7 NN Metamodeling

The final step in the automated simulation cycle was to develop the NN metamodels and monitor error convergence. The automated simulation cycle was stopped once metamodel error convergence was achieved. A threshold for this error was not predetermined; rather, convergence was identified when there was relatively small variation in error after several sequential iterations. Error convergence was prioritized for the submarining occurrence output metric, but this error was monitored across all output metrics.

8.3.7.1 Topology

In general, the topology of NN models is made up of nodes organized into an input layer, some number of hidden layers, and an output layer (Figure 8.15). The input layer feeds information into the nodes in the hidden layers, which perform weighted calculations and pass the information on to the output layer. In this dissertation, a NN with one hidden layer and a maximum of ten neurons was selected as this specification permitted a model that was detailed enough to capture the response. Such specifications have been used in previous applications of similar size and scope

[90, 91]. The hidden layers used a sigmoid activation function, while the output layer used a linear activation function for all metrics other than submarining occurrence. A sigmoid activation function was used for the submarining occurrence activation function, with the output bounded between 0 and 1. This approach has been used in other applications of metamodeling for the purpose of predicting submarining occurrence [91]. Similarly, the output for the lap belt tension was bounded such that no negative magnitudes resulted (minimum at 0).

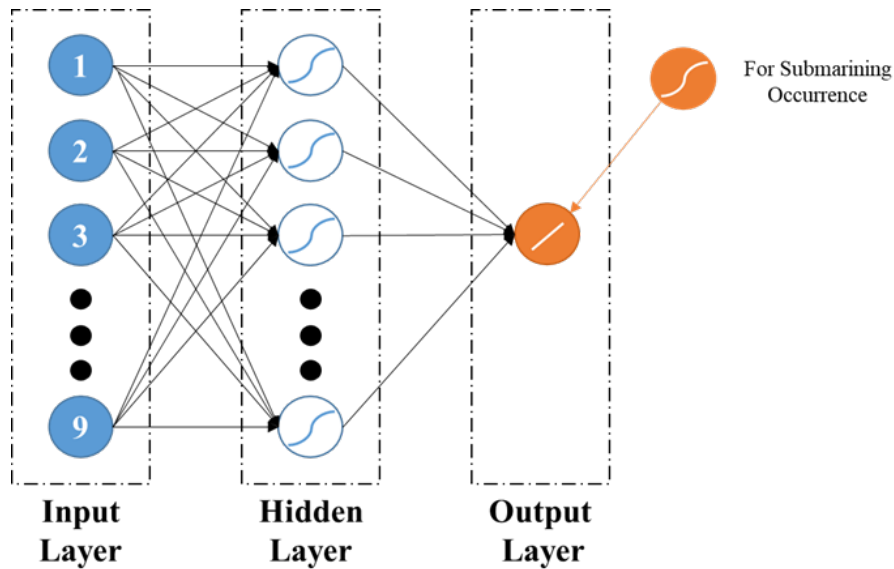


Figure 8.15: Topology of the NN metamodel.

8.3.7.2 Training and optimization

A new NN model was generated for each output metric of interest upon completion of each batch of simulations (i.e., iteration). The entire set of available data was divided into a training data set (80% of available simulations) and a testing data set (20% of available simulations) (example shown in Figure 8.2). A three-fold CV process was used, which has also been used in previous applications of similar size and scope [90, 91]. Each model was generated using the available training dataset, and then performance was evaluated using the remaining testing dataset.

8.3.7.3 Error convergence

The metamodel predictions were used to monitor error convergence. The error between the actual testing data values and the values predicted by the NNs were tracked across each batch

of simulations. The metamodels' predictions for pelvis displacement and rotation, lap belt tension, and submarining occurrence and distance were all tracked during error convergence, with the submarining occurrence error prioritized. The metamodel error was deemed to have converged when it no longer decreased as additional simulations were run. At this point, the cycle was stopped and no more automated simulations were run.

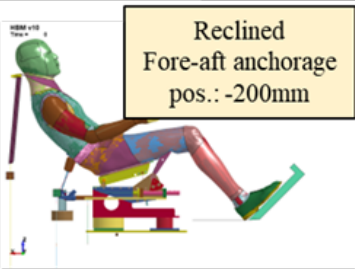
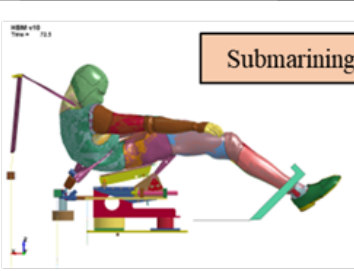

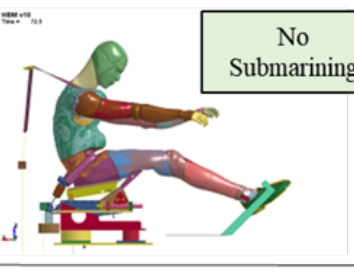

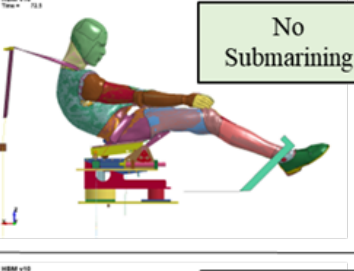
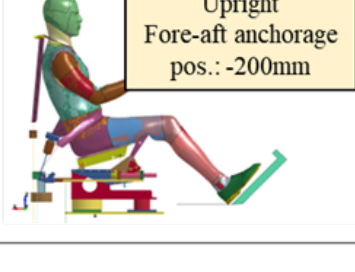
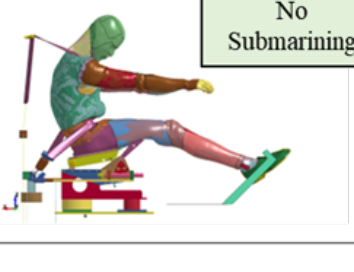
For the continuous output parameters, the model's performance was measured using the average absolute error in addition to the normalized root mean square deviation (NRMSD) resulting from the predictions of the testing dataset. The average absolute error allows for the magnitude of error to be assessed relative to that particular output metric (e.g., 20 mm of error for predicted maximum pelvis displacement). The NRMSD allows the error to be quantified as a percentage relative to that output metric's range (e.g., 20 mm of absolute error for a 100 mm range of maximum pelvis displacement = 20% NRMSD). As submarining occurrence was a binary output, the model's performance was quantified using accuracy, which identified the fraction of cases that were correctly identified as either submarining or non-submarining (true positives and true negatives) relative to the size of the dataset. Accuracy was determined if the model accurately predicted submarining (1) or non-submarining (0) within a 0.05 tolerance.

8.4 Results

8.4.1 Final Simulations

The automation pipeline resulted in a process that was far faster than a comparable manual approach. From this cycle (Figure 8.1, steps 3, 4, and 5 utilized cluster computing to allow 12 setups to be simulated in parallel using 80 CPUs per simulation for steps 3 and 5, and 40 CPUs for step 4. The finalized automation could move 36 simulations entirely through the pipeline in less than one day, with the bottleneck being the cluster capacity and not the model setup or pipeline automation itself. The responses in pelvis kinematics and submarining were variable based on the defined input parameters (Table 8.4).

Table 8.4: Four example simulations with different defined input parameters, showing the wide variability in resulting kinematics.

	0ms	80ms
Example #1	 <p>Reclined Fore-aft anchorage pos.: -200mm</p>	 <p>Submarining</p>
Example #2	 <p>Upright Fore-aft anchorage pos.: -100mm</p>	 <p>No Submarining</p>
Example #3	 <p>Reclined Fore-aft anchorage pos.: +52mm</p>	 <p>No Submarining</p>
Example #4	 <p>Upright Fore-aft anchorage pos.: -200mm</p>	 <p>No Submarining</p>

8.4.2 Metamodeling

Error convergence, determined when relatively no variation or change in error occurred after several sequential run batches, was achieved after 36 batches of simulations were executed (15 simulations per batch). Out of these 36 batches, 480 simulations completed successfully (exceeding 80 ms). The metamodels' error decreased as additional simulations were fed into the models, and eventually plateaued to steady, low level of error (below 10%, Figure 8.16). The metamodels captured the lap belt tension responses for the entirety of the range and the pelvis kinematic responses for most of the range; however, it was less accurate for substantially high magnitudes of forward pelvis displacement (>300 mm) and submarining distance (>200 mm), and substantially low magnitudes of pelvis rotation ($<-25^\circ$ forward rotation) (Figure 8.16). At these extremes, the kinematics are uncontrolled and nonlinear. The absolute error for the four continuous output metrics converged at approximately: 25 mm for pelvis displacement, 3.8° for pelvis rotation, 0.3 kN for lap belt tension, and 28 mm for submarining distance (Figure 8.17). When normalized relative to the range of these respective outputs, the error converged at a similar level (approximately 8% error) (Figure 8.18). Appendix H.2 shows the progression of metamodel performance throughout the 36 batches. The model's error resulting from prediction of submarining occurrence was also quantified using AU-ROC (Appendix H.1).

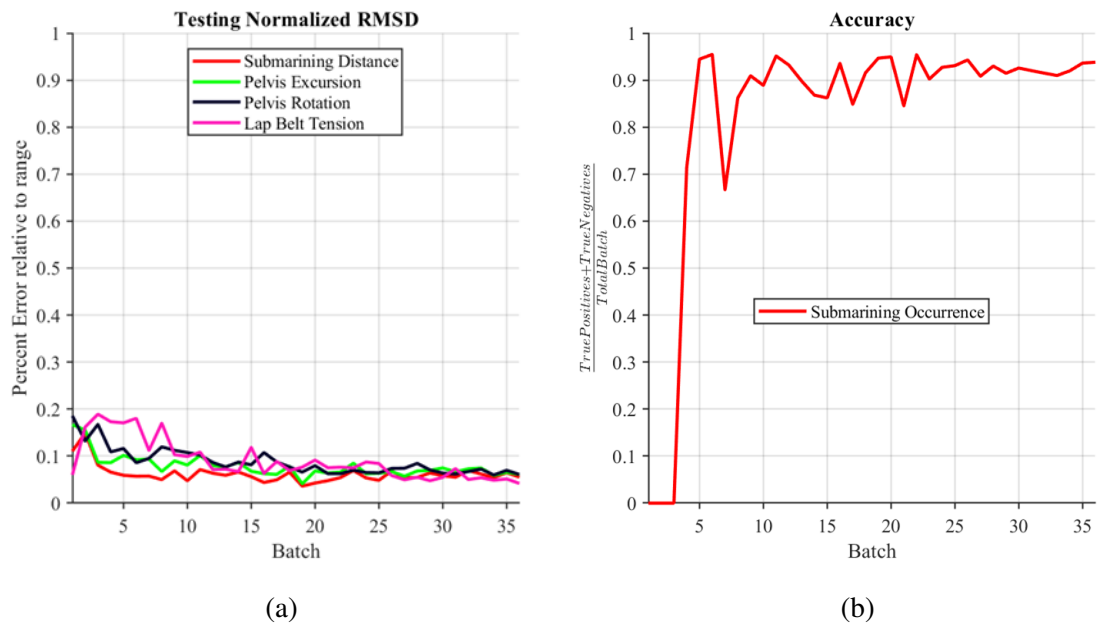


Figure 8.16: Metamodel error tracking. a) The progression of the normalized root mean square deviation (RMSD) of the four continuous output metrics. b) The progression of submarining prediction using accuracy. A value of 0 equates to 0% of the total dataset accurately predicted and a value of 1 equates to 100% of the total dataset accurately predicted. See Appendix H.1 for details on AU-ROC.

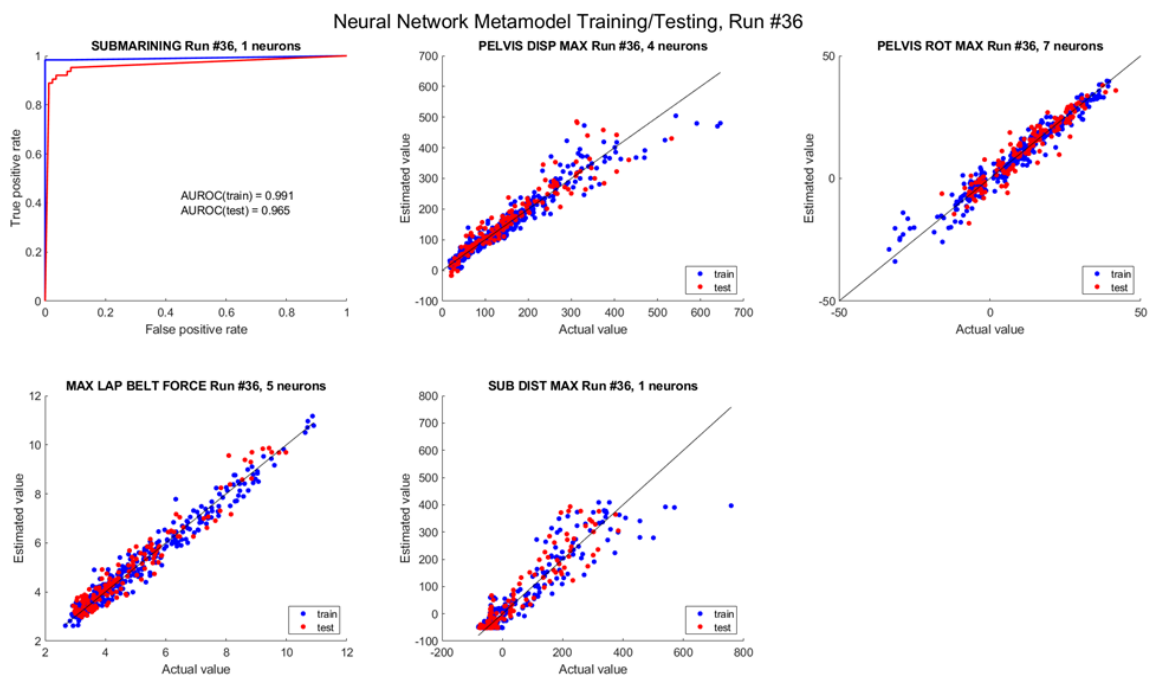


Figure 8.17: Predicted and actual values of the training and testing points for the output metrics. As the metamodel’s prediction of submarining occurrence was evaluated using the area under the receiver/operator curve (AUROC), the true and false positive rates are shown for this output.

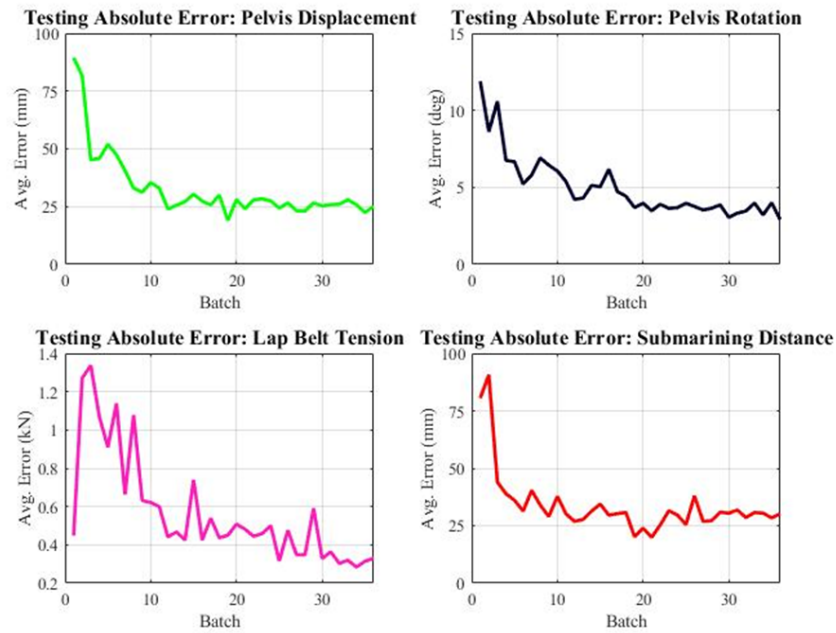


Figure 8.18: Metamodel error tracking, showing the progression of the absolute error of the four continuous output metrics.

8.4.3 Data Aggregation

Data aggregation was performed on the simulated results of the set of 480 frontal impact setups. This initial data analysis demonstrates the bounds of the results observed in the generated test sample (Table 8.5). Additionally, this analysis demonstrates the submarining rates across the two different postures (Table 8.6).

Table 8.5: Preliminary data aggregation: Non-submarining metrics.

Metric	Mean	Minimum	Maximum
Pelvis Displacement (mm)	154.85	18.00	645.70
Pelvis Rotation (deg)	9.96	-33.41	41.73
Lap Belt Tension (kN)	4.99	2.67	10.90

Table 8.6: Preliminary data aggregation: Submarining metrics.

Data Subset	Percent Submarined	Posture	Percent of Submarining
Total	37.5%	Upright	31.3%
		Recline	68.7%
Metric	Mean	Minimum	Maximum
Submarining Distance (mm)	71.06	-79.55	758.20

8.5 Discussion

This chapter described the development of the automated simulation cycle used to execute 36 batches of simulations, resulting in a total of 480 valid simulations used to develop, train, and test the NN metamodels. Further analysis was drawn from these models in Chapter 9.

While the evolution of the error showed a convergence at a low level (10%) for all output metrics, additional analysis was performed to test the model's predictions for another batch of simulations the metamodel had not been trained nor tested with. This analysis not only tested the NN metamodels with a new batch of (fifteen) simulations, but also revealed how the results of the model should be interpreted. These simulations were sampled and setup in the same manner as the previous batches.

The metamodels showed high sensitivity for all output metrics, where the magnitude of the predicted outputs correlated with the magnitude of the actual outputs (Table 8.7). In one of fifteen cases, the metamodel predicted submarining occurred when it was a non-submarining case (Simulation 4). The model's predictions for maximum lap belt tension were an average difference of 0.3 kN from the actual value (8.7% error relative to the range of outputs), with the maximum difference at 0.9 kN. Thus, the model's predicted magnitude of lap belt tension was generally close to the actual magnitude. This was also seen for maximum pelvis rotation, wherein the model's predictions were an average difference of 2.8° from the actual value (7.7% error relative to the range of outputs). The model predictions for pelvis forward displacement and submarining distance were an average distance of 37 mm and 49.6 mm from the actual values, respectively. Larger differences were seen at higher magnitudes of both outputs, which confirms the results of the plotted predictions from the final simulated dataset (Figure 8.17). In these cases, the model over-predicted the magnitudes of these metrics.

CHAPTER 8. QUANTIFYING EFFECTS OF FACTORS ON SUBMARINING: SIMULATIONS

Table 8.7: The NN metamodel’s predictions versus actual outcomes for the five output metrics for a new, unique batch of simulations. The green-shaded cells correspond to a difference between the NN’s predictions and the actual values below the average difference. The orange-shaded cells correspond to a difference above the average difference.

Simulation	Submarining			Pelvis Displacement			Pelvis Rotation			Lap Belt Tension			Submarining Distance		
	NN	Actual	Diff	NN	Actual	Diff	NN	Actual	Diff	NN	Actual	Diff	NN	Actual	Diff
1	0.0	0.0	0.0	78.8	55.6	23.2	19.1	17.3	1.8	4.0	3.8	0.2	24.8	-28.4	53.2
2	0.0	0.0	0.0	19.0	30.5	11.5	13.2	10.0	3.2	3.6	3.4	0.1	-47.2	-41.9	5.3
3	1.0	1.0	0.0	390.6	235.0	155.6	23.2	24.4	1.1	3.9	3.5	0.4	359.6	162.6	197.0
4	1.0	0.0	1.0	42.2	43.4	1.2	14.8	12.5	2.2	3.9	3.8	0.0	-6.5	-13.3	6.8
5	1.0	1.0	0.0	372.9	304.6	68.3	30.9	30.3	0.6	4.7	5.0	0.3	356.0	191.9	164.1
6	1.0	1.0	0.0	510.0	357.7	152.3	30.7	26.1	4.7	4.5	3.7	0.9	405.8	324.5	81.3
7	0.0	0.0	0.0	33.7	29.3	4.4	13.2	13.8	0.6	3.4	3.4	0.0	-40.1	-20.3	19.9
8	1.0	1.0	0.0	165.4	197.4	31.9	38.8	42.4	3.7	5.8	5.5	0.3	63.4	47.9	15.5
9	1.0	1.0	0.0	95.4	100.6	5.1	22.4	23.1	0.6	5.9	6.5	0.6	21.9	3.6	18.4
10	1.0	1.0	0.0	167.9	159.3	8.6	29.6	25.9	3.8	5.9	6.2	0.3	83.7	45.4	38.3
11	0.0	0.0	0.0	146.5	157.3	10.8	3.6	6.4	2.8	6.5	6.6	0.1	-51.4	-58.3	6.9
12	1.0	1.0	0.0	175.3	194.6	19.3	29.7	32.5	2.8	3.9	4.5	0.5	94.4	71.3	23.1
13	0.0	0.0	0.0	33.7	34.6	0.9	22.4	15.7	6.8	3.8	3.7	0.0	-13.8	-22.9	9.0
14	1.0	1.0	0.0	316.2	258.5	57.7	22.1	22.7	0.6	4.1	3.9	0.2	276.2	174.5	101.7
15	0.0	0.0	0.0	47.5	52.4	4.9	3.9	10.2	6.3	4.0	3.8	0.2	-47.2	-51.1	3.9
Ave Diff			0.1			37.0			2.8			0.3			49.6
% Diff (of range)			6.7%			11.3%			7.7%			8.7%			13.0%

8.6 Conclusions

The following conclusions were drawn from this chapter’s analysis:

1. The developed automation pipeline was an effective way of simulating large numbers of frontal impact simulations. Using this method, 480 full-body HBM frontal impact simulations were able to be run, downloaded, post-processed in parallel, in conjunction with the training and optimization of the NN metamodels.

CHAPTER 8. QUANTIFYING EFFECTS OF FACTORS ON SUBMARINING: SIMULATIONS

2. This dataset, with several stochastically sampled input parameters (i.e., impact pulse, lap belt angle, etc.), was proven sufficient to optimize the NN metamodels' prediction of several outputs (i.e., submarining occurrence, pelvis kinematics, etc.).
3. A sensitivity analysis was conducted using a unique batch of simulations the NN metamodel had not yet been trained or tested with. The magnitude of the metamodel's predictions were assessed relative to the actual magnitude from the simulations. This analysis showed the model exhibited excellent sensitivity across all metrics, but the model had larger error for relatively high magnitudes of pelvis displacement and submarining distance. In these cases, the model over-predicted the magnitude of the response. Additionally, the metamodel over-predicted submarining occurrence in one of fifteen cases.

Chapter 9

Quantifying Effects of Factors on Submarining: Analysis

9.1 Executive Summary

9.1.1 Relevance and Goal

A parametric study was designed to achieve the final goal of this dissertation, which was to quantify the relative effects of the intrinsic and extrinsic factors originally identified in the literature search results discussed in Chapter 2 on submarining occurrence and lap belt-pelvis interaction metrics. An automated simulation cycle was developed in Chapter 8 to setup and run several batches of unique simulations, where each batch was sampled to approximate the full design space. Each iteration was used in the development, training, and testing of a Neural Network (NN) metamodel, which served as a useful tool to draw predictions from far more simulations than could be simulated in a reasonable timeframe. In Chapter 8, the developed NN model showed both good predictability and sensitivity for all output metrics.

The goal of this chapter was to use this model to predict outcomes on a larger simulation dataset, which encompassed the full parameter space through a full-factorial design. This model's predictions were used to identify the following: 1) the dominating factors that affected submarining occurrence, and how submarining occurrence was affected by such factors (e.g., positive or negative correlations); 2) the applicability of current federal motor vehicle safety standards to a modern restraint system and a reclined seating posture; and 3) potential trade-offs in submarining and kinematic outcomes based on identified parameter effects.

9.1.2 Key Conclusions

The full list of conclusions can be found in Section 9.6. In summary, fore-aft lap belt angle and recline angle were identified as the dominating factors that affected submarining occurrence: a shallow lap belt angle, in combination with a reclined torso angle, increased the likelihood of submarining. Submarining risk was decreased for a steeper lap belt angle in both postures, but this risk was only substantially mitigated (20% risk) at the steepest level of fore-aft lap belt angle (87°) in the reclined posture.

The range of permitted lap belt angles by FMVSS 210 was shown to be insufficient to mitigate submarining risk in a reclined posture with a modern restraint system (equipped with dual lap belt pretensioners). To mitigate risk in a reclined seating posture, the lap belt anchorages needed to be positioned further forward relative to the occupant to allow for a steeper lap belt angle. Additionally, a 35° fore-aft lap belt angle (within FMVSS 210 anchorage specifications) showed an approximate 65% probability of submarining in an upright posture using this modern restraint system. This probability is likely to increase for a restraint system without lap belt pretensioners. Thus, the lower bound of this regulation should be increased to an approximate 45° angle, which showed a lower (20%) probability of submarining in the upright condition. Potential trade-offs from moving the lap belt anchorages further forward included increased pelvis forward displacement (from 63° to 75° in upright and 75° to 87° in recline) and increased lap belt tension (from 46° to 75° in both postures). Additionally, re-positioning lap belt anchorages may affect upper torso kinematics, which requires further study.

9.1.3 Contributions

The generated heatmaps from this analysis quantify how lap belt-pelvis interaction kinematic and kinetic outputs (including submarining occurrence) are affected by several intrinsic and extrinsic factors. This provides a wealth of data that can be utilized by the automotive safety industry of current limitations in vehicle restraint design and how current federal motor vehicle safety standards may need to adapt to improve pelvis restraint for a reclined seating posture.

9.1.4 Publication

Richardson, R., Forman, J., Gepner, B., Kerrigan, J. (2023). Quantifying the Effects of Intrinsic and Extrinsic Factors on Lap Belt-Pelvis Interaction and Submarining. *Traffic injury prevention*. (Planned).

9.2 Introduction

In Chapter 8, the parametric study was setup using the GHBMCM with several varied intrinsic and extrinsic factors, which were sampled to approximate the design space for a subset of 480 simulations. These simulations were used to develop, train, and test a Neural Network (NN) meta-model which predicted submarining occurrence and distance, pelvis kinematic and lap belt kinetic outputs based on these varied parameters. While a full-factorial simulation study was inefficient to execute due to the high computational cost, the metamodel could be used to interpolate for these missing datapoints, as it was trained at the discretized parameter levels. Thus, the metamodel was used to predict how the previously identified intrinsic and extrinsic factors (Chapter 2) affect lap belt-pelvis interaction and submarining occurrence for a full-factorial sample of simulations.

This model's predictions will be used to identify the following: 1) the dominating factors that affected submarining occurrence, and how submarining occurrence was affected by such factors (e.g., positive or negative correlations); 2) the applicability of current federal motor vehicle safety standards to a modern restraint system and a reclined seating posture; and 3) potential trade-offs in submarining and kinematic outcomes based on identified parameter effects.

9.3 Methodology

The developed NN metamodel was used to predict the outputs for a generated full-factorial sample using the discretized parameters from Chapter 8 (see Section 8.3.2), for a total of 14,580 simulations (three impact pulses \times five lap belt fore-aft angles \times three lap belt overhead angles \times two foot support contacts \times three belt/occupant friction levels \times three seat/occupant friction levels \times two recline angles \times three pelvis angles \times three pelvic-abdominal flesh stiffness levels).

9.3.1 Data Aggregation

As with the automated simulation dataset (Section 8.4.3), data aggregation was performed on the generated full-factorial dataset. This initial data analysis demonstrated the bounds of the results observed in the full-factorial sample, which was similar to those of the automated simulation dataset (Table 9.1). Additionally, this analysis demonstrated the submarining rates across the two different postures (Table 9.2). As with the simulated dataset, the majority of submarining occurred in a reclined posture.

Table 9.1: Preliminary data aggregation: Non-Submarining metrics.

Metric	Mean	Minimum	Maximum
Pelvis Displacement (mm)	159.73	0.00	634.29
Pelvis Rotation (deg)	8.87	-37.20	41.44
Lap Belt Tension (kN)	5.58	2.44	11.52

Table 9.2: Preliminary data aggregation: Submarining metrics.

Data Subset	Percent (predicted) Submarined	Posture	Percent of (Predicted) Submarining
Submarining Occurrence	32.2%	Upright	22.5%
		Recline	77.5%
Metric	Mean	Minimum	Maximum
Submarining Distance (mm)	26.35	-52.02	421.83

9.3.2 Clustering

K-means clustering is a method of separating observations into distinct groups, or clusters, by seeking to minimize the variance within clusters. This method was used to separate the simulations into distinct groups based on the different output metrics and determine the cutoff point between two extremes for continuous output metrics (e.g., a low versus high level of pelvis displacement).

First, the input parameters (Table 8.1) and output metrics (Table 8.3) were loaded into a MATLAB variable. The parameters were normalized so that each category had a minimum value of 0 and a maximum value of 1. The output values were then multiplied by 10 so that the algorithm would prioritize the output values during the clustering process. K-means clustering required the appropriate number of clusters to be determined in advance of the clustering process. Two clusters were used for the following metrics: submarining occurrence, maximum pelvis rotation, and maximum lap belt tension. Two clusters were chosen for submarining as it was a binary output. Two clusters were chosen for the continuous outputs as there was a smaller distribution for pelvis rotation and lap belt tension (relative to the other continuous parameters) (see Appendix I.1). For maximum forward pelvis displacement and maximum submarining distance, a third cluster was added to provide additional discretization to the data, as these outputs showed a wider range of responses. The following occurred from the clustering process: (1) each simulation was assigned a given cluster, (2) the cutoff output value between the clusters was determined, and (3) the average of each parameter for each cluster was recorded. The most influential parameters were identified using the average pa-

CHAPTER 9. QUANTIFYING EFFECTS OF FACTORS ON SUBMARINING: ANALYSIS

parameter values from each cluster. The greater the difference between the average parameter values across the two clusters, the larger of an affect that parameter has on the overall distance between the clusters.

As an example of the k-means clustering method, in the automated simulation dataset from Chapter 8 (480 simulations), fore-aft lap belt angle showed the largest effect on submarining occurrence, with the largest absolute distance (0.594) between cluster groups (Table 9.3). Additionally, recline angle and impact pulse showed substantial effects on submarining occurrence, with the absolute distance between cluster means (submarining versus non-submarining) above 0.1 (high relative to other parameters). Pelvis angle and occupant/seat friction showed a moderate effect, with the absolute distance between cluster means above 0.05. Overhead lap belt angle, occupant/belt friction, foot support, and pelvic-abdominal flesh stiffness all had negligible effects on submarining occurrence. The absolute distance between cluster means was contextualized by the illustrated effects in the plots (see below), where a noticeable effect was seen for parameters that had an absolute distance 0.05 between clusters.

Table 9.3: Influential parameter determination for submarining occurrence. The parameters in green showed an absolute distance greater than 0.1 between cluster means (negative versus positive outcome); the parameters in yellow showed an absolute distance greater than 0.05 between cluster means (negative versus positive outcome).

	Impact Pulse	Lap Belt Angle Fore-Aft	Overhead Lap Belt Angle	Foot Support	Belt Friction	Seat Friction	Recline Angle	Flesh Stiffness	Pelvis Angle
Cluster 1 Mean	0.364	0.741	0.485	0.485	0.498	0.543	0.386	0.495	0.520
Cluster 2 Mean	0.528	0.147	0.519	0.478	0.508	0.462	0.687	0.500	0.431
Absolute Distance	0.164	0.594	0.034	0.007	0.010	0.081	0.301	0.005	0.088
Rank	3	1	6	8	7	5	2	9	4

All input parameters were then plotted against each other for the given output. Again, an example is provided from the automated simulation dataset. Figure 9.1 shows the top three most influential parameters affecting submarining occurrence from the automated simulation dataset generated in Chapter 8. In the automated simulation dataset, the clustering for submarining occurrence did not require a cutoff value, as the simulations were clustered into a submarining and a non-

submarining group. In total, 37.7% of the simulated dataset resulted in submarining (Table 8.6). Submarining occurrence was most prevalent for a shallower lap belt angle and a reclined torso angle (Figure 9.1a). Additionally, submarining occurrence was more frequent at a higher impact pulse (Figure 9.1a). The K-means clustering analysis of the simulated dataset, which includes plots showing all input parameters relative to each other, in addition to the tables describing their ranked influence, are shown in Appendix I.2.

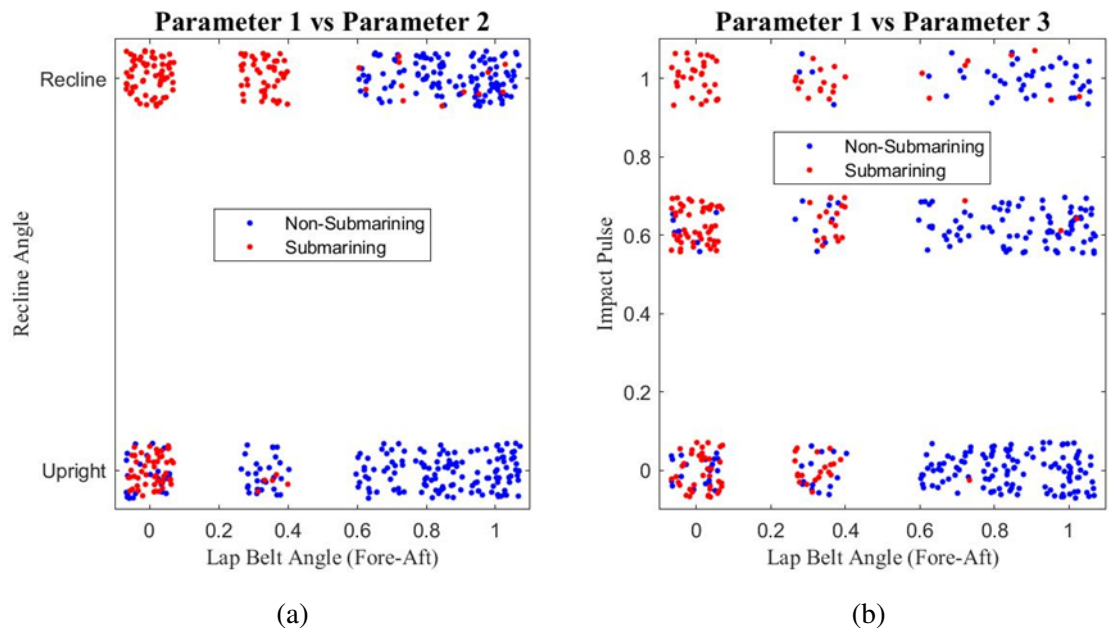


Figure 9.1: Selected submarining occurrence influential parameter plots (automated simulation dataset).

While clustering the automated simulation dataset was useful starting point in understanding the data, the parameters of the 480 simulations were biased towards the edges of the sample space as a result of the Simulated Annealing sampling algorithm, which maximizes the distance among points in the parameter space, thus oversampling at the bounds. The NN metamodel provided a solution, as it could predict submarining occurrence and other lap belt-pelvis interaction responses for a much larger dataset than can be simulated, such as a full-factorial design.

As with the automated simulation dataset, K-means clustering was used to cluster the sample of 14,580 simulations (full-factorial sample). This time, a different plotting strategy was used due to the much larger sample size: instead of plotting the outcome of each individual simulation, the predicted outcomes of all simulations in each subset were aggregated and reported as

a percentage of simulations that generated a poor outcome. This percentage corresponded to the relative “risk” or “probability” of a negative outcome for those given parameters.

For a given simulation, the NN predicted probability of that simulation resulting in submarining rather than a binary output as was seen in the automated simulations (Figure 9.1). Rather than always being either zero (no submarining) or one (submarining), the predicted submarining occurrence could take any value between zero and one. However, the NN generally had high confidence in the prediction, with 95.2% of the submarining predictions being below 0.05 or above 0.95. Four additional NN metamodels predicted maximum pelvis forward displacement and rotation, peak lap belt tension, and maximum submarining distance.

9.4 Results

9.4.1 Influential Parameter Ranking

As with the simulated dataset example shown above, the magnitude of influence the input parameters had on a given output was ranked based on the distance between cluster means (Table 9.4). In general, the parameter influence ranking derived from the generated full-factorial simulation sample mirrored that of the simulated dataset. The findings for each output metric are discussed in detail below. In brief, fore-aft lap belt angle, impact pulse, and occupant/seat friction had a large effect on all output metrics, resulting in an absolute distance greater than 0.1 between cluster means (negative versus positive outcome). Recline angle was also a highly influential parameter for all output metrics except lap belt tension. Pelvis angle had a substantial effect (0.1 absolute distance) on submarining occurrence and a moderate effect (0.05 absolute distance) on submarining distance but had negligible effects on all other output metrics. Additionally, foot support (presence or absence) had a substantial effect (0.1 absolute distance) on pelvis forward displacement and a moderate effect (0.05 absolute distance) on submarining distance and lap belt tension, but a negligible effect on all other output metrics. Pelvic-abdominal flesh stiffness, the overhead lap belt angle, and occupant/belt friction had only moderate effects on a few parameters (flesh stiffness on pelvis rotation; lap belt angle top on pelvis forward displacement; occupant/belt friction on submarining distance and pelvis forward displacement) but showed negligible effects otherwise. The tables showing the distances between cluster means for each output metric can be found in Appendix J.2.

CHAPTER 9. QUANTIFYING EFFECTS OF FACTORS ON SUBMARINING: ANALYSIS

Table 9.4: Rank of input parameter influence for the generated full-factorial simulation sample. The parameters in bold font had a substantial effect on the outcome: the parameters in green showed an absolute distance greater than 0.1 between cluster means (negative versus positive outcome); the parameters in yellow showed an absolute distance greater than 0.05 between cluster means (negative versus positive outcome).

Rank	Submarining Occurrence	Submarining Distance	Pelvis Forward Displacement	Pelvis Rotation	Lap Belt Tension
1	Lap Belt Angle Fore-Aft	Lap Belt Angle Fore-Aft	Recline Angle	Lap Belt Angle Fore-Aft	Impact Pulse
2	Recline Angle	Recline Angle	Impact Pulse	Occupant/Seat Friction	Lap Belt Angle Fore-Aft
3	Impact Pulse	Occupant/Seat Friction	Occupant/Seat Friction	Recline Angle	Occupant/Seat Friction
4	Pelvis Angle	Impact Pulse	Lap Belt Angle Fore-Aft	Impact Pulse	Foot Support
5	Occupant/Seat Friction	Occupant/Belt Friction	Foot Support	Flesh Stiffness	Overhead Lap Belt Angle
6	Occupant/Belt Friction	Foot Support	Occupant/Belt Friction	Occupant/Belt Friction	Recline Angle
7	Foot Support	Pelvis Angle	Overhead Lap Belt Angle	Foot Support	Flesh Stiffness
8	Flesh Stiffness	Overhead Lap Belt Angle	Pelvis Angle	Overhead Lap Belt Angle	Occupant/Belt Friction
9	Overhead Lap Belt Angle	Flesh Stiffness	Flesh Stiffness	Pelvis Angle	Pelvis Angle

The nature of the effect an input parameter had on a given output metric (e.g., positive, or negative) was inferred from the cluster plots. Selected plots are shown and discussed below for each output metric based on the cut-off magnitude determined through the k-means clustering algorithm. Additional plots generated using the k-means clustering algorithm are shown in Appendix J.2. Additionally, several unique cut-off points were established for the continuous output metrics based on distribution of the metamodels' predictions for these outputs and for thresholds of interest (Appendix J.1). These additional plots can be found in Appendix J.3.

9.4.2 Submarining Occurrence

The submarining occurrence cutoff value between the two clusters was a probability of 0.5, and 32.2% of the simulations clustered in the negative outcome group with predicted submarining. Fore-aft lap belt angle, recline angle, impact pulse, occupant/seat friction, and pelvis angle all had substantial effects on submarining occurrence, with a difference greater than 0.1 between cluster means (Table 9.4). The probability of submarining was higher for a shallow fore-aft lap belt angle across all other parameters. Submarining risk also increased at a reclined (50°) torso angle: at the shallowest fore-aft lap belt angle (35°), submarining probability was approximately 65% at an upright torso angle (25°) and 100% at a reclined torso angle (50°) (Figure 9.2a). Submarining risk also increased for a higher impact pulse: at the shallowest fore-aft lap belt angle (35°) submarining risk was approximately 60%, 80% and 97% for a 12g, 16g, and 35g pulse, respectively (Figure 9.2b). Increasing the level of friction between the HBM and the seat pan decreased submarining risk (Figure 9.2c). Finally, submarining occurrence was dependent on the HBM's initial pelvis angle, where a pelvis angle initially pitched 12° more rearward increased submarining likelihood relative a nominal and forward-pitched pelvis angle (Figure 9.2d). Foot support (presence or absence), occupant/belt friction, flesh stiffness, and the overhead lap belt angle had negligible effects on submarining occurrence (distance less than 0.02 between negative and positive outcome cluster groups).

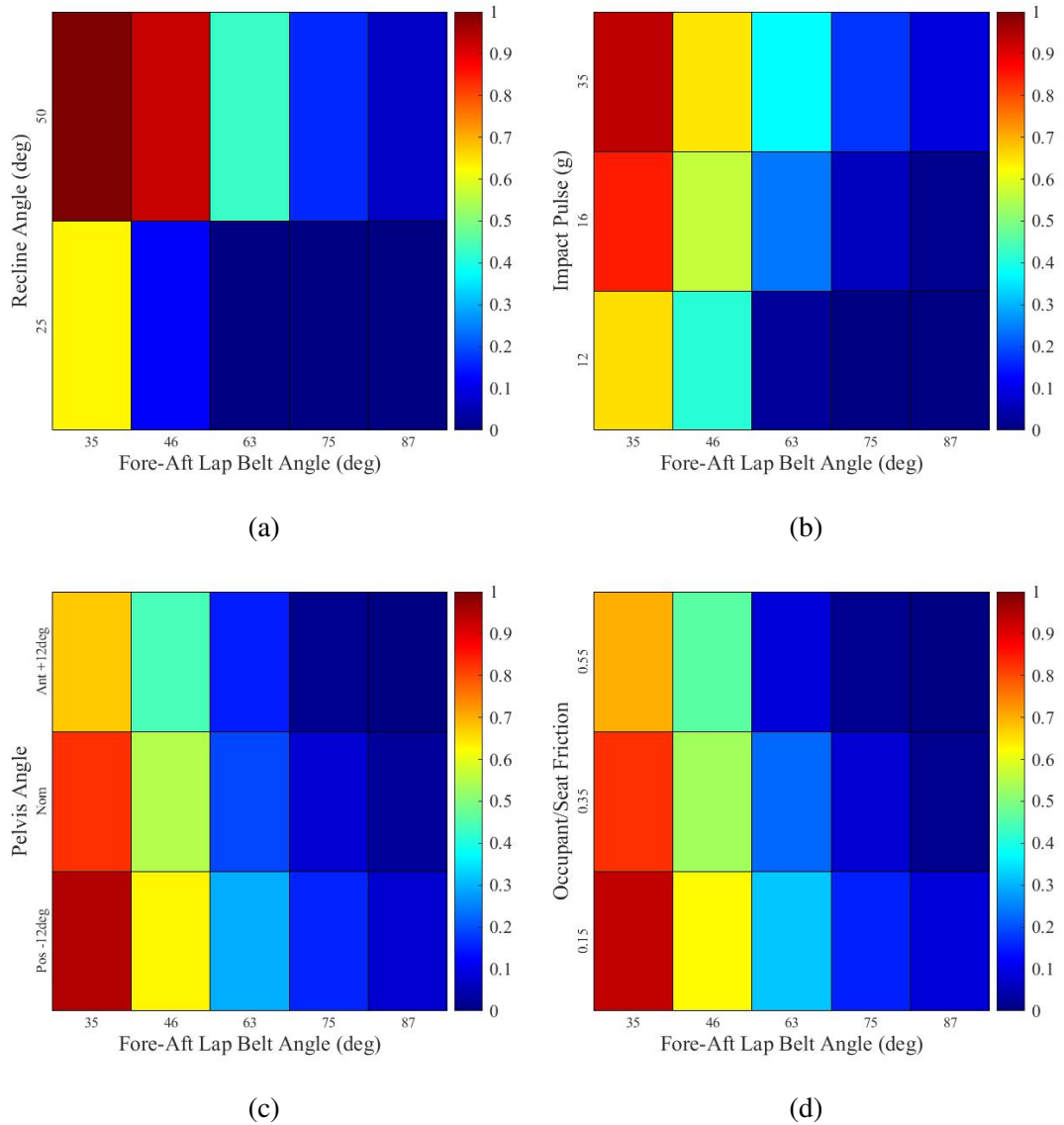


Figure 9.2: Selected submarining occurrence influential parameter plots (full-factorial sample). The color scale indicates the model’s predicted probability of submarining, based on the percentage of simulations that resulted in predicted submarining for given levels of those parameters (i.e., per square).

9.4.3 Maximum Submarining Distance

As mentioned in Section 9.3.2, three clusters were used when analyzing the submarining distance parameter, as this output showed a wide range with several outliers. The simulations in the lower two clusters were characterized as a negative outcome (higher submarining distance), while simulations in the top cluster was characterized as a positive outcome (lower submarining distance). This resulted in a cutoff value between the negative and positive outcome clusters of 75.1 mm, and 24.3% of the simulations clustered in the negative outcome cluster with a submarining distance exceeding 75.1 mm.

The maximum submarining distance metric was dependent on several of the input parameters, with seven of the nine parameters resulting in a distance greater than 0.05 between negative and positive outcome clusters (Table 9.2). As with the submarining occurrence output metric, flesh stiffness and the overhead lap belt angle had negligible effects on this parameter. However, unlike the submarining occurrence output metric, maximum submarining distance was also dependent on occupant/belt friction and foot support. Additionally, while maximum submarining distance was still dependent on pelvis angle, this input parameter had less influence (> 0.05 absolute distance) than it did for submarining occurrence (> 0.1 absolute distance).

The nature of the effects lap belt fore-aft angle, recline angle, occupant/seat friction, impact pulse, and pelvis angle had on maximum submarining distance correlated with the effects these input parameters had on submarining occurrence (Figure 9.3). A shallow fore-aft lap belt angle resulted in an increased probability of the model's maximum submarining distance exceeding 75.1 mm, which held across all other parameters. Additionally, a reclined torso angle (50°) (Figure 9.3a), lower occupant/seat friction (Figure 9.3b), higher impact pulse (Figure 9.3c), and pelvis initially pitched rearward (Figure 9.3e) all increased this probability. Additionally, a decreased occupant/belt friction (Figure 9.3d) and absence of foot support (Figure 9.3f) also increased the probability of the model's maximum submarining distance exceeding 75.1 mm.

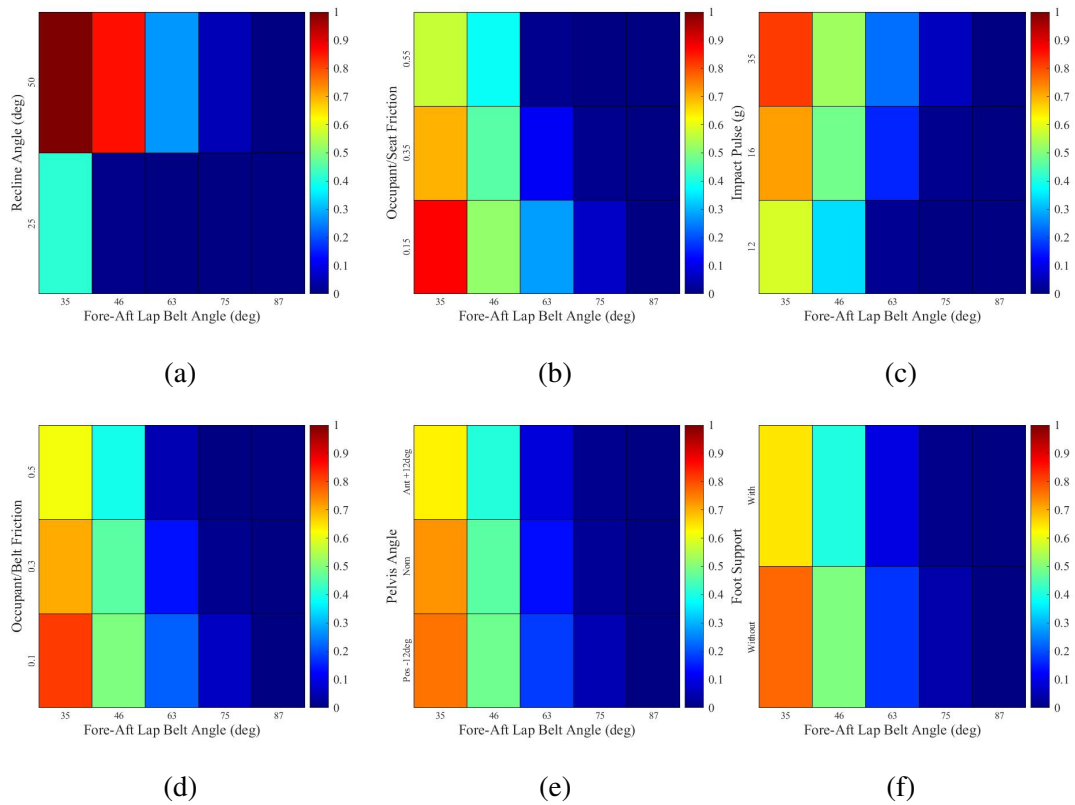


Figure 9.3: Selected submarining distance influential parameter plots (full-factorial sample). The color scale indicates the model’s predicted probability of the maximum submarining distance exceeding 75.1 mm, based on the percentage of simulations that were predicted to exceed this distance for given levels of those parameters (i.e., per square).

9.4.4 Maximum Pelvis Forward Displacement

As with maximum submarining distance, three clusters were used when analyzing pelvis forward displacement. This resulted in a cutoff value between the negative and positive outcome clusters of 137.8 mm, and 50.3% of the simulations clustered in the poor performing cluster with a submarining distance exceeding 137.8 mm.

As with maximum submarining distance, maximum pelvis forward displacement was dependent on seven of the nine input parameters; however, rather than pelvis angle, pelvis forward displacement was also dependent on the overhead lap belt angle (Table 9.4). While fore-aft lap belt angle was the most influential parameter affecting submarining occurrence and maximum submarining distance, the effect sizes of recline angle, impact pulse and occupant/seat friction preceded that of fore-aft lap belt angle. Foot support also had a greater effect (> 0.1 absolute distance) on maximum pelvis forward displacement than it did for maximum submarining distance (> 0.05 absolute distance).

As with maximum submarining distance, the probability of the model exhibiting a forward pelvis displacement that exceeded 137.8 mm was higher for a reclined torso angle (50°), higher impact pulse (Figure 9.4a), lower occupant/seat friction (Figure 9.4b), without a foot support (Figure 9.4d), and lower occupant/belt friction (Figure 9.4e). An interesting non-linear trend was seen for the different levels of fore-aft lap belt angle, where the risk was increased at the lower and upper bounds of this parameter (shallow and steep angle), but the risk was lower in the mid-range (Figure 9.4c). Overhead lap belt angle had an effect on maximum pelvis forward displacement, which was not seen for the other output metrics: for a larger overhead lap belt angle, indicating the lap belt anchorages positioned laterally more outward from the seat, the risk of the model exhibiting a pelvis displacement more than 136.5mm was increased (Figure 9.4f).

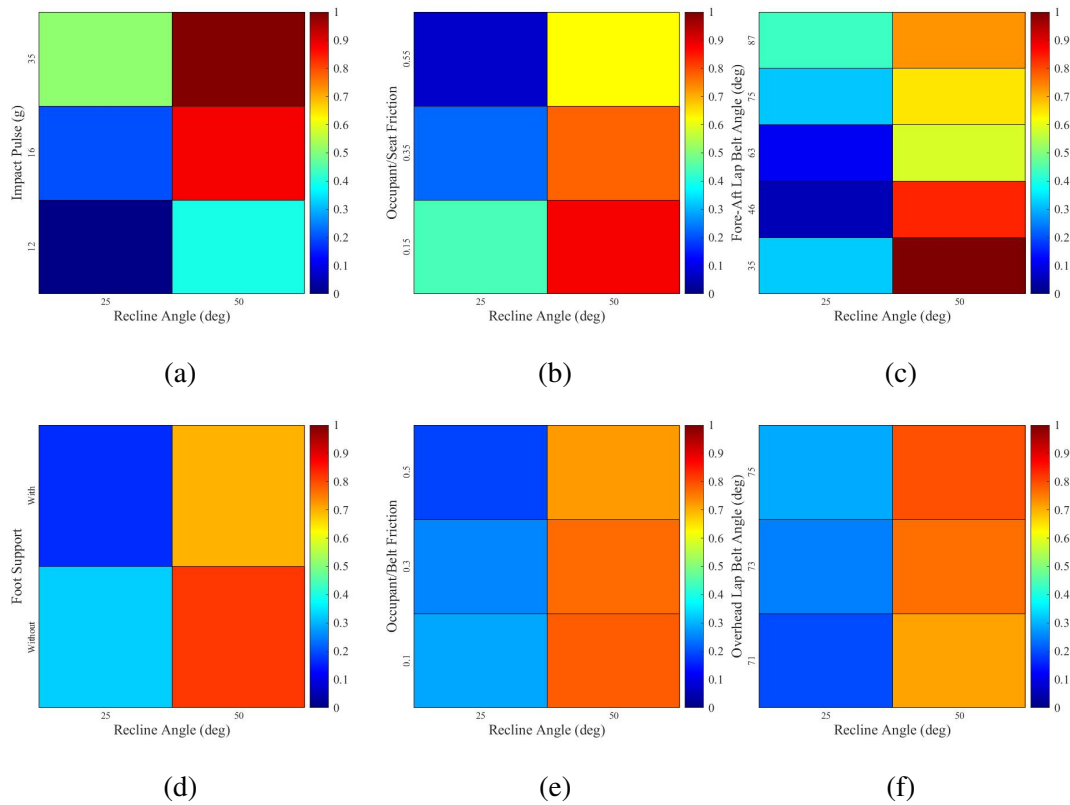


Figure 9.4: Selected pelvis forward displacement influential parameter plots (full-factorial sample). The color scale indicates the model’s predicted probability of the maximum forward pelvis displacement exceeding 137.8 mm, based on the percentage of simulations that were predicted to exceed this distance for given levels of those parameters (i.e., per square).

9.4.5 Maximum Pelvis Rotation (pitch)

The maximum pelvis rotation cutoff value between the negative and positive outcome clusters was 8.9° (rearward), and 49.7% of the simulations clustered in the negative outcome group with a pelvis rotation exceeding 8.9° (more rearward rotation). Fore-aft lap belt angle was the most influential parameter, with a shallow fore-aft lap belt angle increasing the likelihood of increased rearward pelvis rotation (greater than 8.9°) (Figure 9.5). The risk of the model exhibiting more rearward pelvis rotation was also increased for a lower occupant/seat friction (Figure 9.5a), reclined torso angle (50°deg) (Figure 9.5b), and higher impact pulse (Figure 9.5c). Though pelvic-abdominal flesh stiffness did not have as much of an effect as these other parameters, the risk of increased rearward pelvis rotation was increased for more compliant pelvic-abdominal flesh (50%) (Figure 9.5d).

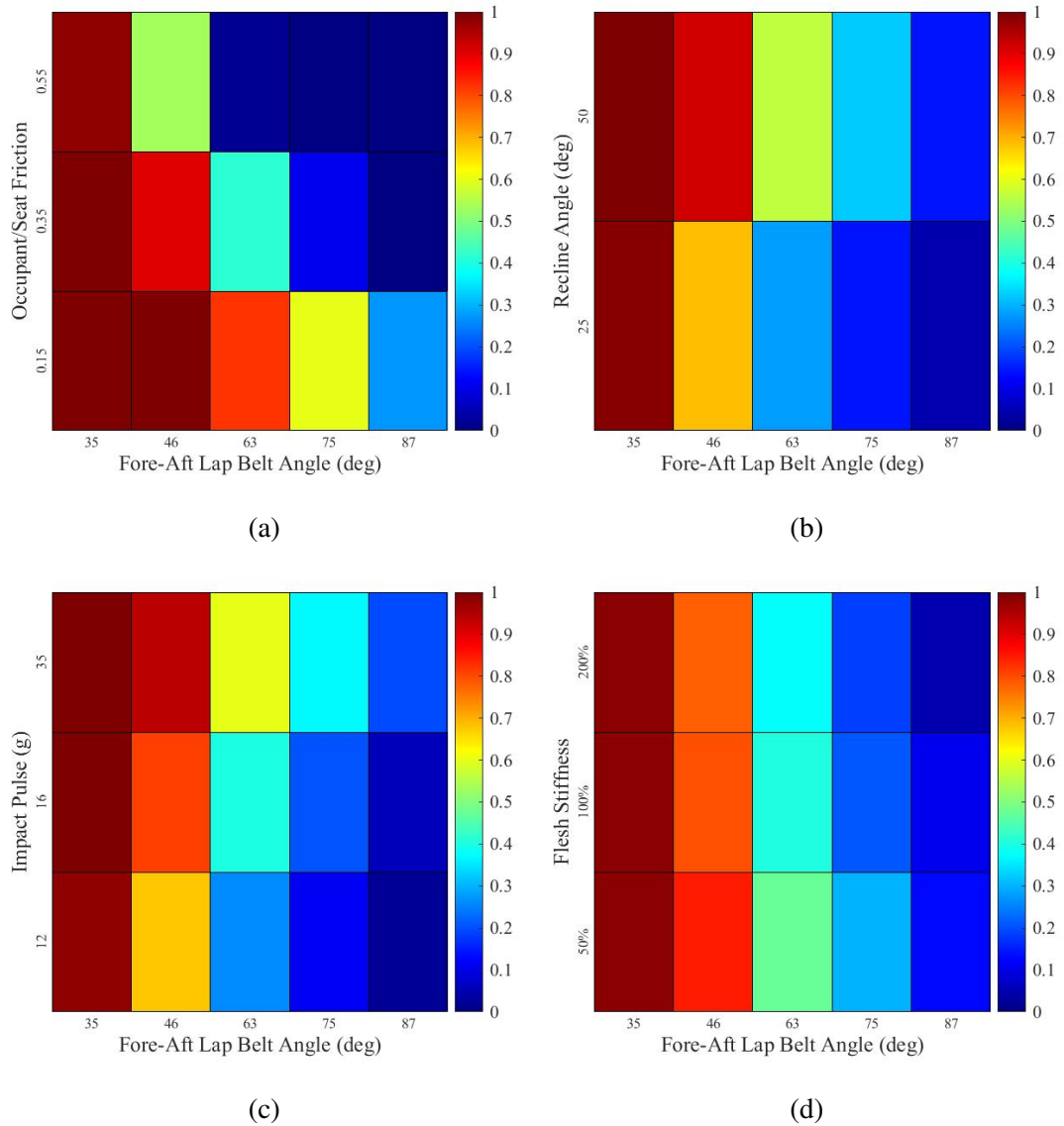


Figure 9.5: Selected pelvis rotation influential parameter plots (full-factorial sample). The color scale indicates the model’s predicted probability of the maximum pelvis rotation exceeding 8.9° (rearward), based on the percentage of simulations that were predicted to exceed this magnitude (more rearward rotation) for given levels of those parameters (i.e., per square).

9.4.6 Maximum Lap Belt Tension

The maximum lap belt tension cutoff value between the negative and positive outcome clusters was 6.2 kN, and 32.7% of the simulations clustered in the negative outcome group with the maximum lap belt tension exceeding 6.2 kN. Lap belt tension was primarily affected by impact pulse, where the higher impact pulse resulted in higher risk of the lap belt tension exceeding 6.2 kN (Table 9.4). As the 35g pulse was not a standard trapezoidal pulse (as were the 12g and 16g pulses) and also had a larger step size from 16g (versus 12g to 16g), the effect was not linear. The higher impact pulse (35g) resulted in substantially higher risk of the lap belt tension exceeding 6.2 kN (Figure 9.6). Fore-aft lap belt angle, occupant/seat friction, and foot support all affected lap belt tension, though the magnitude of their effect was dependent on the impact pulse. The risk of the lap belt tension exceeding 6.2 kN was approximately 0% at the 12g pulse across all parameters. This risk was increased at the 16g level based on the parameter value – a steeper lap belt angle (Figure 9.6a), lower level of occupant/seat friction (Figure 9.6b), and absence of foot support (Figure 9.6c) increased the risk above 20%. At the 35g level, the risk was substantially higher with a decreased sensitivity to these parameters. Variation in occupant/seat friction and foot support at the 35g level resulted in negligible change in risk, maintaining a probability of approximately 70% (Figure 9.6b and 9.6c). Less sensitivity was also seen at a fore-aft lap belt angle of 63° (nominal angle) and above (steeper angle), where 100% risk was maintained (Figure 9.6a). A similar “plateau” in this parameter’s effect was seen at the 16g level, for a fore-aft lap belt angle of 75° and above (steeper angle), maintaining approximately 45% risk.

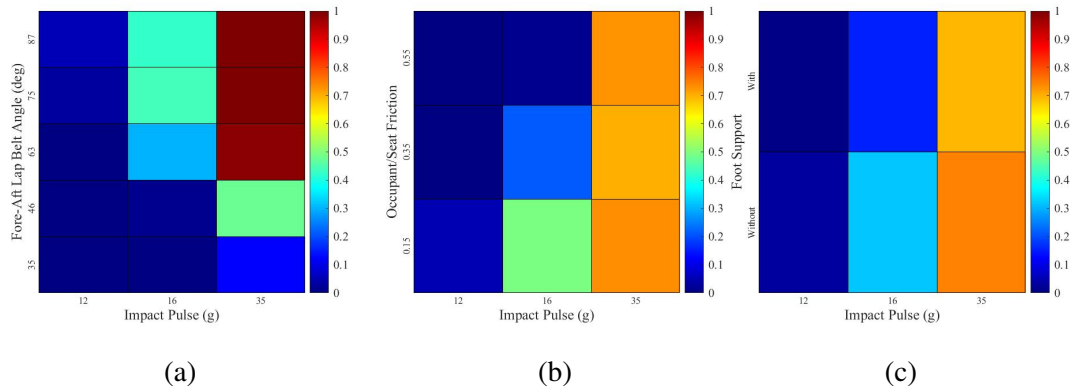


Figure 9.6: Selected lap belt tension influential parameter plots (full-factorial sample). The color scale indicates the model’s predicted probability of the maximum lap belt tension exceeding 6.2 kN, based on the percentage of simulations that were predicted to exceed this magnitude for given levels of those parameters (i.e., per square).

9.5 Discussion

The results from this chapter were used to infer the following: 1) the dominating factors that affect submarining occurrence, and how submarining occurrence is affected by such factors (e.g., positive or negative correlations); 2) the applicability of current federal motor vehicle safety standards to a modern restraint system and a reclined seating posture; and 3) potential trade-offs in submarining and kinematic outcomes based on identified parameter effects. First, a thought exercise was conducted to aid in the understanding of the metamodel’s predictions.

9.5.1 Exploring a Continuous Parameter Space: A Thought Exercise

The input parameters were discretized at 2-5 levels, which approximated the range between the upper and lower bounds of each parameter. However, to aid in the illustration of the overall trend (e.g., increasing or decreasing) of a particular output’s probability across a given parameter, continuously sampling between the parameter’s upper and lower bounds provides a better visualization due to the finer discretization of the range.

To provide a better visualization of how the influential parameters affect such outputs, a sample of 1,000,000 (1M) simulations was generated which homogeneously sampled between the upper and lower bounds of each parameter. The trained NN metamodel was then used to predict the outcomes of each simulation. It is important to note that the metamodel’s predictions were nei-

CHAPTER 9. QUANTIFYING EFFECTS OF FACTORS ON SUBMARINING: ANALYSIS

ther trained nor cross-validated for the datapoints that occurred between the discrete levels of each parameter. It is entirely possible that the trend between these levels is not discrete nor continuous – thus, the model’s predicted probability magnitudes between these levels are likely inaccurate and in order to draw accurate predictions, the model should be trained with continuous parameters. However, having drawn an assumption of linearity and continuity between data points allowed the resulting heatmap to serve as a better visual aid of the parameters’ effects on an outcome by illustrating the big picture trends.

K-means clustering was performed on the generated sample of 1M simulations. The influential parameters predominantly mirrored those of the full-factorial dataset using the discrete parameters (Table 9.5).

Table 9.5: Rank of input parameter influence for the generated 1M simulation sample with continuous input parameters (except for foot support). The parameters in bold font had a substantial effect on the outcome: the parameters in green showed an absolute distance greater than 0.1 between cluster means (negative versus positive outcome); the parameters in yellow showed an absolute distance greater than 0.05 between cluster means (negative versus positive outcome).

Rank	Submarining Occurrence	Submarining Distance	Pelvis Forward Displacement	Pelvis Rotation	Maximum Lap Belt Tension
1	Lap Belt Angle Fore-Aft	Lap Belt Angle Fore-Aft	Recline Angle	Lap Belt Angle Fore-Aft	Impact Pulse
2	Recline Angle	Recline Angle	Impact Speed	Occupant/Seat Friction	Lap Belt Angle Fore-Aft
3	Impact Pulse	Occupant/Seat Friction	Foot Support	Recline Angle	Occupant/Seat Friction
4	Occupant/Seat Friction	Impact Pulse	Occupant/Seat Friction	Impact Pulse	Foot Support
5	Pelvis Angle	Occupant/Belt Friction	Lap Belt Angle Fore-Aft	Flesh Stiffness	Overhead Lap Belt Angle
6	Foot Support	Pelvis Angle	Overhead Lap Belt Angle	Occupant/Belt Friction	Pelvis Angle
7	Occupant/Belt Friction	Foot Support	Occupant/Belt Friction	Overhead Lap Belt Angle	Recline Angle
8	Flesh Stiffness	Flesh Stiffness	Pelvis Angle	Foot Support	Occupant/Belt Friction
9	Overhead Lap Belt Angle	Overhead Lap Belt Angle	Flesh Stiffness	Pelvis Angle	Flesh Stiffness

CHAPTER 9. QUANTIFYING EFFECTS OF FACTORS ON SUBMARINING: ANALYSIS

For plotting purposes, the continuous parameters were divided into twenty bins which were uniformly distributed between the bounds. As with the full-factorial sample, the two dominant factors affecting submarining occurrence were fore-aft lap belt angle and recline angle (Figure 9.7). The interpretation of this plot relative to the full-factorial sample is shown in Figure 9.8. The resulting continuous plot showed a linear interpolation between the original discrete datapoints, allowing for a better visual of how these parameters affect submarining. While the sharpness and magnitude of the cutoff cannot be taken literally, this plot shows more clearly that for a reclined torso angle and shallow fore-aft lap belt angle (top left corner), there is a higher risk of submarining than for an upright torso angle (bottom left corner) or for a steeper fore-aft lap belt angle (top and bottom right corners) (Figure 9.8). Similarly, a steeper fore-aft lap belt angle is required to mitigate submarining in a reclined posture versus an upright posture, which is consistent with the full-factorial sample plot (Figure 9.2a). All generated heatmaps for this continuous sample can be found in Appendix K.

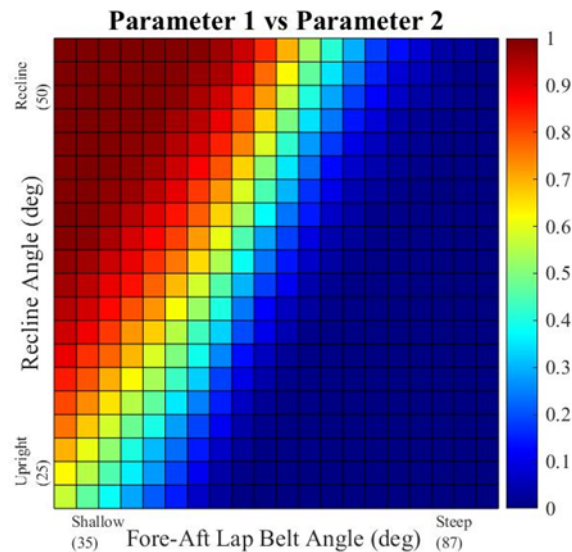


Figure 9.7: Selected submarining occurrence influential parameters plot (1M continuous sample). The color scale indicates the model's predicted probability of submarining, based on the percentage of simulations that resulted in predicted submarining for given levels of those parameters (i.e., per square).

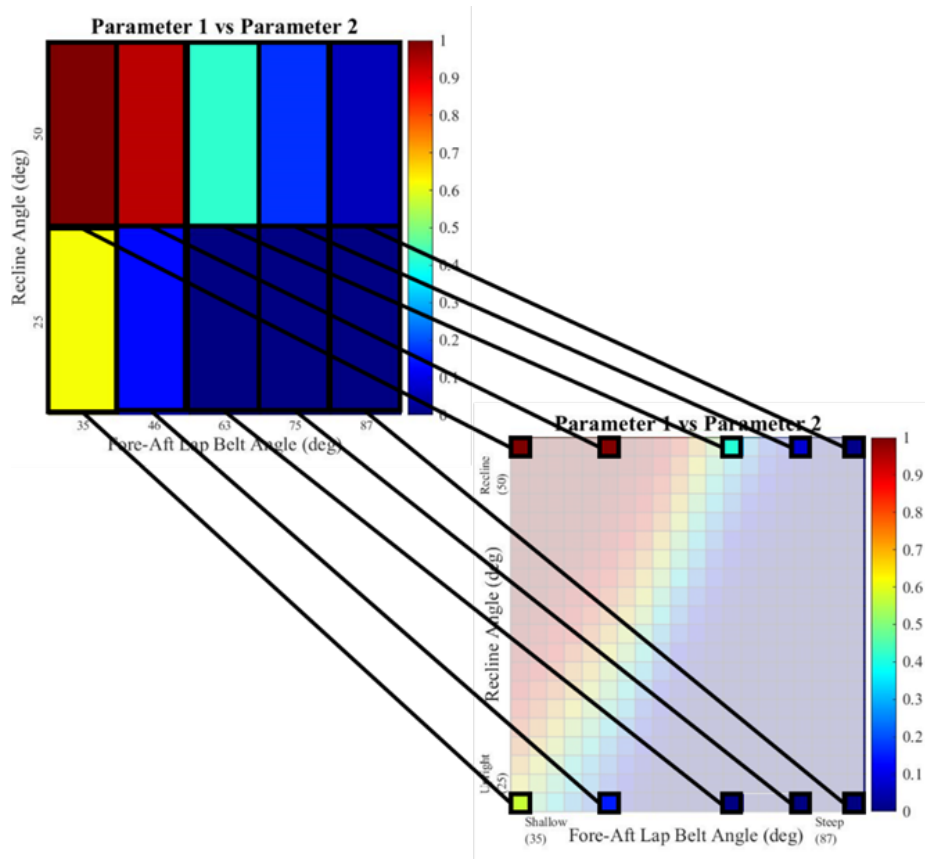


Figure 9.8: Aid in how to interpret the results of the continuous 1M sample plots relative to the discrete full-factorial sample plots. The probabilities were linearly interpolated between the discrete datapoints for which the metamodel was validated for, but the model’s predictions between these points were not validated. Thus, the continuous plots serve only as a gross overview of trends and exact magnitudes should not be extracted.

Continuous sampling provides a visual aid for nonlinear effects, such as the effect of fore-aft lap belt angle on maximum forward pelvis displacement (Figure 9.9). It is important to note that the cutoff values resulting from the k-means clustering were different between sample sets: for the full-factorial sample, this value was 137.8 mm and 50.3% of simulations clustered in the negative outcome group, whereas for the 1M sample, this value was 118.4mm and 51% of simulations clustered in the negative outcome group. However, understanding general trends (i.e., more pelvis displacement versus less pelvis displacement, depending on parameter value) still holds. Less pelvis displacement was seen at the mid-range level of fore-aft lap belt angle, which was at the shallower end (towards 35°) for the upright posture relative to the reclined posture. However,

for a shallower or steeper fore-aft lap belt angle (at the lower and upper bounds), the predicted displacement was higher. More discussion on how fore-aft lap belt angle and recline angle affect submarining occurrence and pelvis forward displacement is discussed below.

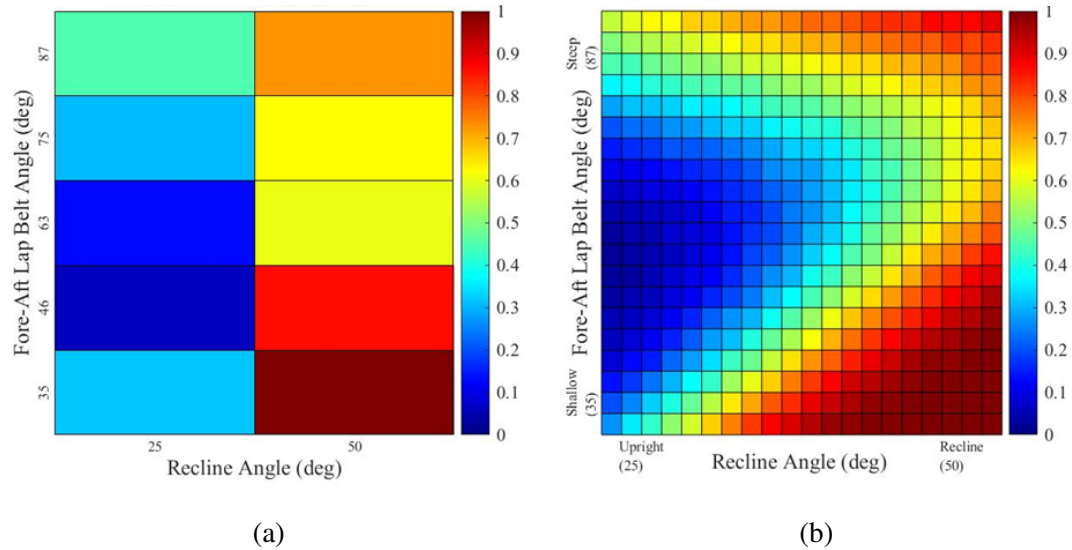


Figure 9.9: The effect of fore-aft lap belt angle and recline angle on maximum pelvis displacement. a) Full-factorial sample results, with discrete parameters. The color scale indicates the model’s predicted probability of the maximum pelvis displacement exceeding 136.5mm based on the percentage of simulations that were predicted to exceed this magnitude for given levels of those parameters (i.e., per square). b) 1M sample results, with continuous parameters. The color scale indicates the model’s predicted probability of the maximum pelvis displacement exceeding 118.4mm based on the percentage of simulations that were predicted to exceed this magnitude for given levels of those parameters (i.e., per square).

9.5.2 Dominating Factors Affecting Submarining Risk

The predominant factors found to affect submarining occurrence were fore-aft lap belt angle and recline angle. These two parameters were identified in the literature review and further confirmed in the experimental results of this dissertation as they are encompassed in the lap belt-pelvis angle metric. Indeed, for the simulated dataset, the cases that had an initial lap belt-pelvis angle $> 90^\circ$ (due to the lap belt angle and pelvis angle) were shown to have more submarining cases than those with a smaller lap belt-pelvis angle ($< 90^\circ$) (Figure 9.10). The larger lap belt-pelvis angle

increases the shear component of the lap belt force (see Figure 2.7) which promotes upward lap belt migration.

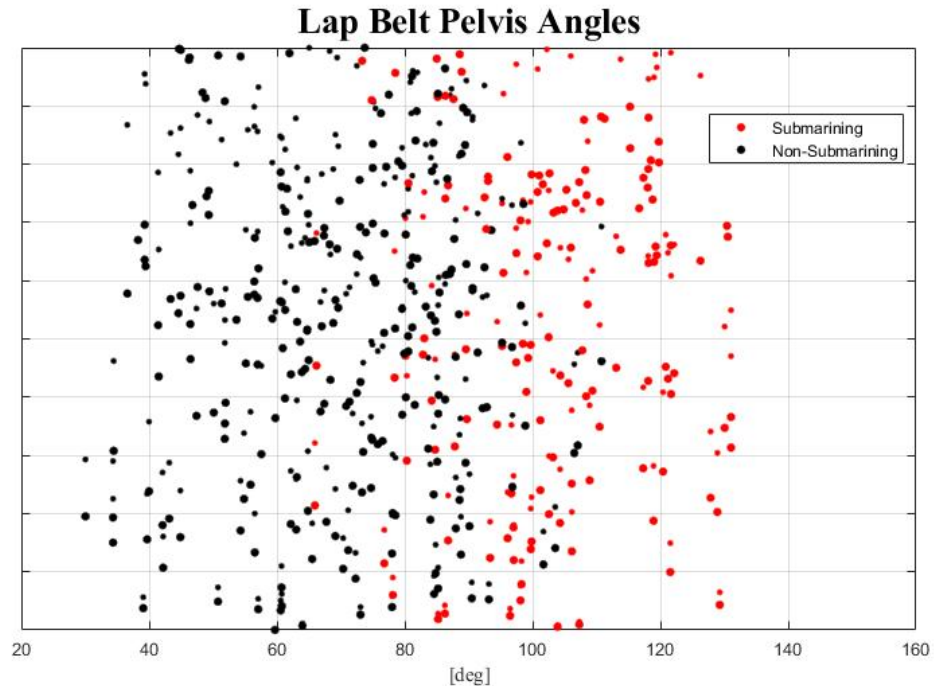


Figure 9.10: Initial lap belt-pelvis angles (see Figure 2.7) of the simulated dataset, divided by submarining outcome.

One possible explanation for why fore-aft lap belt angle and recline angle are most influential of dictating submarining is the effect these parameters have on initial lap belt placement, which was originally observed in the belt pull tests of Chapter 5: a reclined torso angle and more shallow lap belt angle will place the belt further rearward relative to the pelvis (Figure 5.7). A similar effect was seen in this case (Figure 9.11a). Additionally, the majority of these simulations submarined (Figure 9.11b).

To eliminate any potential bias caused from cases in which the lap belt was originally placed unfavorably relative to the pelvis – indicating “pre-submarining” – another analysis was performed on the simulated dataset (480 simulations) from Chapter 8. In Chapter 7, pre-submarining was classified as a simulation in which the lap belt bottom edge was over and behind the ASIS prior to the start of the simulation. This occurred for approximately 8% of the simulated dataset – eliminating these cases had no effect on influential parameter ranking resulting from k-means clustering.

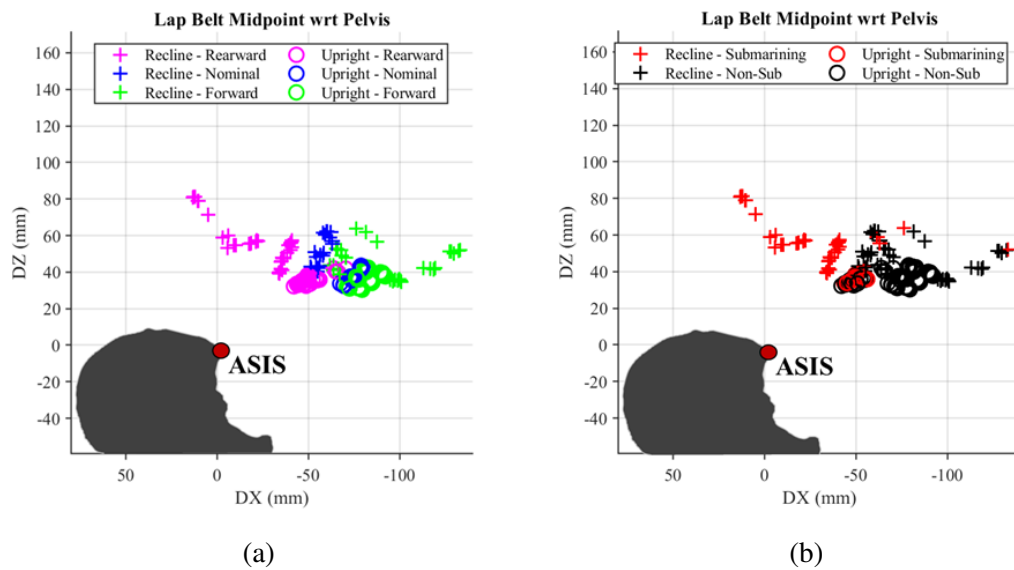


Figure 9.11: Lap belt placement relative to pelvis (global coordinate system): a) based on changing lap belt anchorage positions (e.g., rearward, nominal, forward) and torso recline angle. b) based on resulting submarining occurrence. The pelvis schematic is positioned to orient the viewer but is not to scale and the orientation varied based on recline angle and pelvis angle.

A second method of defining unfavorable initial lap belt placement was used, which was based on methods adapted from [71], which takes into account not just the global X-Z placement of the belt, but also the angle of the lap belt and the pelvis (Figure 9.12a). Using this method, 15% of the dataset was classified as having an initial lap belt placement that was unfavorable in mitigating submarining (Figure 9.12b).

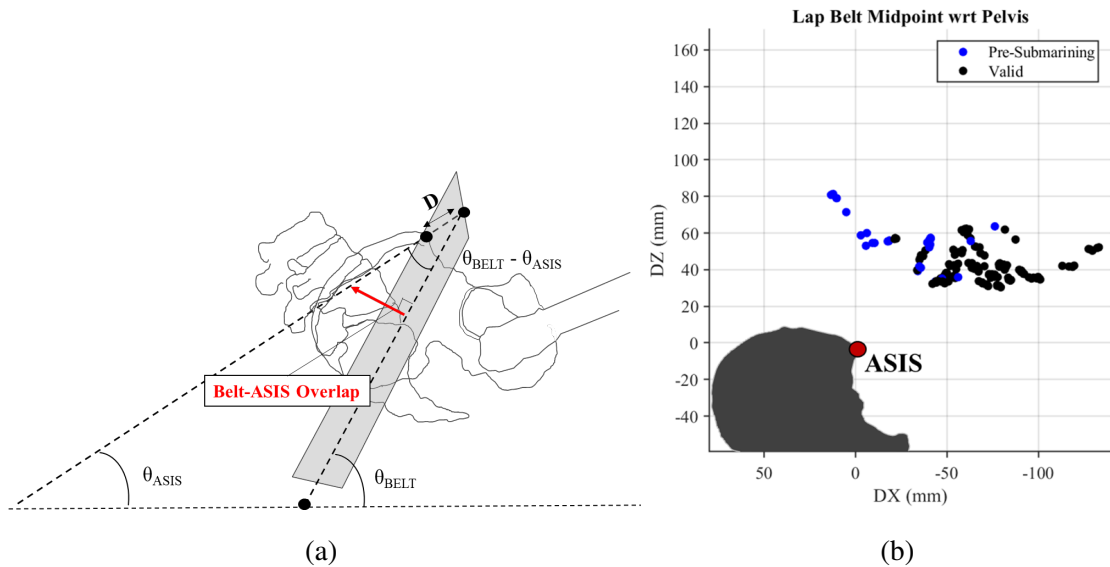


Figure 9.12: Identification of lap belts initially placed unfavorably relative to the pelvis: a) method of how these were identified (adapted from [71]); b) identified cases based on the method in a) looking at the lap belt midpoint wrt the ASIS. The pelvis schematic is positioned to orient the viewer but is not to scale and the orientation varied based on recline angle and pelvis angle.

However, eliminating these cases did not substantially change the resulting influential parameter ranking from the k-means clustering: fore-aft lap belt angle was still the dominating influential parameter, but impact pulse surpassed recline angle as the second-most influential parameter. Thus, even removing potential biases resulting from pre-submarining cases, or cases in which the lap belt was initially placed unfavorable as a result of the modifying lap belt angle or torso angle, did not affect the conclusions. These variables affect submarining occurrence for mechanical reasons aside from initial lap belt placement. This effect can best be understood with the free-body diagram originally generated in Chapter 2 (Figure 9.13). This shows that for a pelvis rotated more rearward (resulting from recline angle) and for a shallower lap belt angle (resulting from rearward anchorage positions), the “Belt Slip” force (lap belt force vector oriented more horizontal relative to the

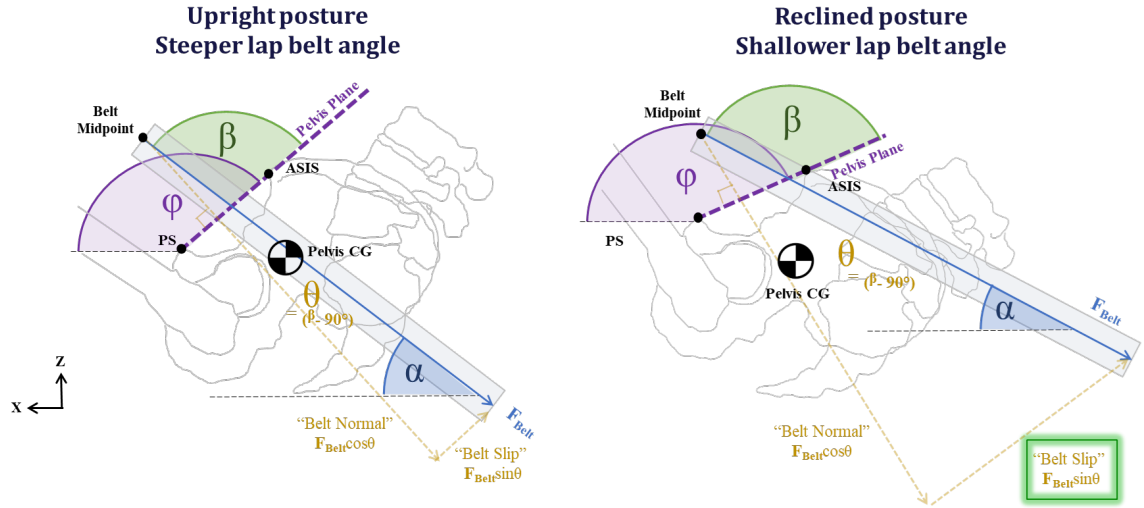


Figure 9.13: Free-body diagram of pelvis and increase in belt slip force resulting from an increase in lap belt-pelvis angle (due to reclined seating posture and shallow fore-aft lap belt angle).

pelvis plane) is increased relative to the “Belt Normal” force (lap belt force vector oriented normal to the pelvis plane), thus increasing the likelihood of submarining. It should also be noted that at a shallower lap belt angle and a reclined torso angle, the probability of a rearward pelvis rotation exceeding 8.9° was higher (Figure 9.5b). Thus, this “Belt Slip” force also dynamically increased during the impact in these cases as a result of an increased belt-pelvis angle (β).

9.5.3 Applicability of FMVSS 210

FMVSS 210 requires the lap belt anchorages to be installed such that the resulting lap belt angle is between $30\text{-}75^\circ$ in the sagittal plane [103]. An amendment of this standard was enforced in 1990, increasing the lower bound from 20° to 30° , in order to mitigate submarining [42]. However, this amendment took place prior to the advancement in restraint systems, which now incorporate pretensioning and load limiting technologies. Additionally, reclined seating postures, which are predicted to become more prevalent with the introduction of ADS [22], alter the initial lap belt-pelvis angle as the pelvis is rotated more rearward [29]. Thus, evaluating how the current FMVSS standard applies to a modern restraint system and to a reclined seating posture was necessary to understand whether the current standard is sufficient in mitigating submarining for these conditions, or whether further amendments may be required.

9.5.3.1 Modern restraint system

The restraint system used in this study was the same as that used in the dynamic reclined sled test experiments discussed in Chapter 3 and the matched simulations discussed in Chapter 4. This restraint incorporated dual lap belt pretensioners and a shoulder belt pretensioner and load limiter, with a seatback-integrated D-Ring and dual-locking tongue to prevent the webbing from translating through the buckle side. This restraint system had been shown to mitigate submarining in reclined sled tests with an anthropomorphic test device (ATD, or crash test dummy) relative to a restraint system that incorporated a single lap belt pretensioner or a standard D-Ring positioned at the B-pillar [46].

While the current FMVSS 210 standard was designed based off sled test experimental results conducted in traditional, upright and forward-facing seating postures, a 35° fore-aft lap belt angle (within the standard's 30-75° bounds) showed an approximate 65% probability of submarining occurrence in an upright posture (Figure 9.2a). Additionally, there was an approximate 35% the submarining distance would exceed 78mm at this posture and lap belt angle (Figure 9.3a). This probability would likely increase for a restraint system without pretensioners, as these mechanisms improve pelvis engagement and thus mitigate submarining risk [64]. Rear seat restraints typically have lap belt angles that are shallower than those of the front seat [107] and can be around the 30-35° level [108]. Additionally, while there is a growing prevalence of rear seat lap belt pretensioners, most vehicle rear seats do not incorporate pretensioners or load limiters [107, 109]. This finding highlights the increased risk of adverse lap belt-pelvis interaction and submarining in the rear seat condition. Indeed, abdominal injuries have been shown to be more prevalent for rear seat occupants relative to front seat occupants [69].

9.5.3.2 Reclined seating posture

The current FMVSS 210 standard proved insufficient to ensure submarining mitigation in a reclined seating posture: at a 35° fore-aft lap belt angle, submarining risk was 100% and only decreased by 10% at a 46° angle (Figure 9.2a). Not until the lap belt angle was at the upper bound of the FMVSS 210 standard (75°) did this risk decrease below 20% whereas in an upright posture, only a 46° angle was required to achieve a similarly low level of risk. Thus, to successfully mitigate submarining in a reclined seating posture, the lap belt anchorage points must be moved further forward relative to an upright posture. However, it is important to understand potential trade-offs resulting from lap belt anchorage re-positioning. These trade-offs are discussed below.

9.5.4 Trade-Offs Resulting from Varying Lap Belt Anchorage Position

The identified dominating parameters influencing submarining risk, lap belt angle and recline angle, offer an advantage from a design standpoint as seatback recline and lap belt anchorage position are controllable parameters (unlike impact pulse, for instance). The combination effect of recline angle and fore-aft lap belt angle indicate a more forward anchorage position (steeper lap belt angle) is required to mitigate submarining in the reclined posture. However, shifting these lap belt anchorages forward may affect other kinematic and injury outcomes. In particular, a more forward lap belt anchorage position increased pelvis displacement: the probability of the maximum pelvis forward displacement exceeding 137.8 mm increased from approximately 20% to 45% from a 63° to 87° fore-aft lap belt angle in the upright posture and approximately 60% to 75% for the same lap belt angles in recline (Figure 9.4c). Thus, the presence of a knee bolster may be required at steeper lap belt angles, particularly in reclined postures. Likewise, re-positioning the anchorages forward increases the lap belt tension magnitude: from a 46° to a 75° fore-aft lap belt angle, the probability of the maximum lap belt tension exceeding 6.2 kN increases from approximately 0% to 45% at the 16g impact pulse and from approximately 50% to 100% at the 35g impact pulse (Figure 9.6a). Pelvic fractures at the ASIS location occurred at a similar magnitude of lap belt tension in the reclined sled tests; however, the forward position of the lap belt anchorages results in engagement with the acetabulum and lower pelvis, of which the injury tolerance has yet to be identified. Additionally, moving the lap belt anchorages forward may result in trade-offs in injury and kinematic outcomes of the head, torso, and extremities. Further research is required to investigate such trade-offs.

9.6 Conclusions

The following conclusions were drawn from this chapter's analysis:

1. Fore-aft lap belt angle, impact pulse, and occupant/seat friction showed a large effect on all output metrics (submarining occurrence, submarining distance, pelvis forward displacement, pelvis rotation, and lap belt tension). Recline angle was a highly influential parameter for all output metrics except lap belt tension.
2. Pelvis angle had a substantial effect on submarining occurrence and a moderate effect on submarining distance but had negligible effects on all other output metrics. Foot support (presence or absence) had a substantial effect on pelvis forward displacement and a moderate

CHAPTER 9. QUANTIFYING EFFECTS OF FACTORS ON SUBMARINING: ANALYSIS

effect on submarining distance and lap belt tension, but a negligible effect on all other output metrics.

3. Pelvic-abdominal flesh stiffness, the overhead lap belt angle, and occupant/belt friction showed moderate effects on a few parameters (flesh stiffness on pelvis rotation; overhead lap belt angle on pelvis forward displacement; occupant/belt friction on submarining distance and pelvis forward displacement) but negligible effects otherwise.
4. Fore-aft lap belt angle and recline angle were identified as the dominating factors that affected submarining occurrence. This result was identified in the automated simulation dataset in addition to the NN metamodel's predictions for both a generated full-factorial simulation sample (approximately 15,000 simulations) and a generated 1M simulation dataset assuming continuous input parameters.
5. A shallower lap belt angle, in combination with a reclined torso angle, was linked to a higher likelihood of submarining. Submarining risk was decreased for a steeper lap belt angle in both postures, but this risk was only substantially mitigated at the steepest fore-aft lap belt angle (87°) in the reclined posture.
6. The range of permitted lap belt angles by FMVSS 210's specifications was shown to be insufficient in mitigating submarining risk in a reclined posture with a modern restraint system (equipped with dual lap belt pretensioners). For a reclined seating posture, the lap belt anchorages need to be positioned further forward relative to the occupant to reduce submarining risk.
7. Additionally, a 35° fore-aft lap belt angle (within FMVSS 210 regulation) shows a 65% probability of submarining in an upright posture using this modern restraint system. This probability is expected to increase for a restraint system without lap belt pretensioners. Thus, the lower bound of this regulation should be increased to an approximate 45° angle, which showed a lower (20%) probability of submarining in the upright condition.
8. Identified trade-offs from shifting the lap belt anchorages further forward included increased pelvis forward displacement (from 63° to 75° in upright and from 75° to 87° in recline) and increased lap belt tension (46° to 75° for both postures). Additionally, this shift may affect upper torso kinematics, which requires further study.

Chapter 10

Conclusions

10.1 Concluding Remarks

The goal of this dissertation was to evaluate how vehicle environment (extrinsic) and occupant-related (intrinsic) characteristics affect lap belt-pelvis kinematics and submarining occurrence using PMHS and computational HBMs (Figure 10.1).

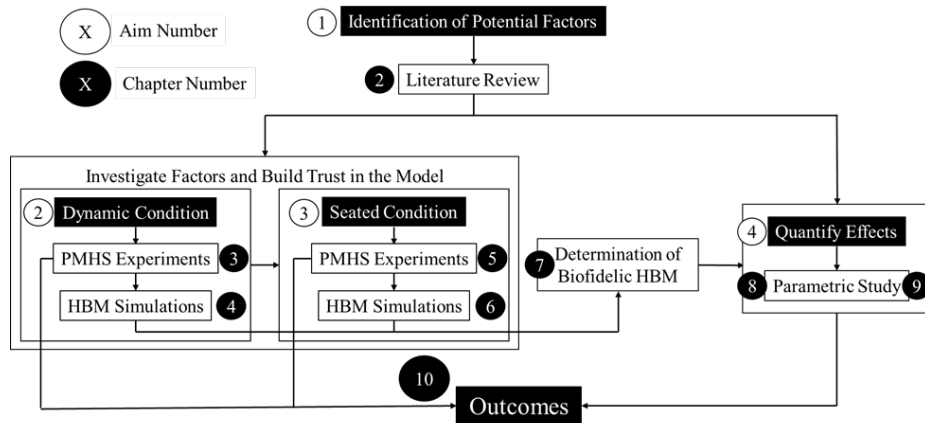


Figure 10.1: Overview of the dissertation.

To achieve this goal, a literature search, described in Chapter 2, identified several intrinsic and extrinsic factors from the literature that were proposed to affect lap belt-pelvis interaction and submarining occurrence. Several of these factors were identified from research conducted in 1970-1990, which guided the development and amendments of federal motor vehicle safety standards (FMVSS) in the early stages of restraint design. In particular, this research informed the lap belt

CHAPTER 10. CONCLUSIONS

anchorage position specifications in FMVSS 210, which requires lap belt anchorages to be installed such that the resulting lap belt angle is between 30° and 75° relative to the horizontal axis in the sagittal plane.

Advancements in restraint design, which took place after this phase of research, now incorporate pretensioning and load limiting technologies. These technologies were designed to improve occupant injury outcomes through more effective engagement with skeletal anatomy (for pretensioners) and yielding of this restraint force to prevent substantial load transfer to the occupant (for load limiters). As a result, these technologies have a substantially different effect on occupant kinematics than previous restraint systems. However, it's unknown how and to what degree the factors that were previously predicted to affect submarining for early restraint systems apply for restraint systems with this technology. Further, since this advancement in restraint system technologies, no mandates have been made to FMVSS 210's lap belt angle.

Additionally, the current phase-in of automated driving system (ADS) technologies predicts an increase in the prevalence of non-standard seating postures, including a reclined seating posture [22]. Thus, research was required to quantify the effects of the previously proposed factors on lap belt-pelvis interaction and submarining occurrence using a modern restraint system in addition to a reclined seating posture. A state-of-the-art computational HBM was used for this analysis. Chapters 3 through 7 built the foundation for this quantification.

As no experimental data existed to understand how a reclined seating posture affected lap belt-pelvis interaction and submarining occurrence, an innovative methodology was developed to investigate this through experimental sled tests using PMHS (Chapter 3). One subject that exhibited a relatively large lap belt-pelvis angle (indicating a shallow fore-aft lap belt angle, see Figure 2.7) submarined. This prompted the need for further experimental study to identify a submarining threshold through variation of this parameter. The GHBM HBM was shown to be the more suitable choice for detailed study of lap belt-pelvis interaction over the THUMS (Chapter 4).

Lap belt-pelvis angle was further investigated in belt pull experiments through systematic variation of lap belt and torso angle, which identified a submarining threshold (Chapter 5). Additionally, this parameter was found to affect the placement of the lap belt relative to the pelvis. The GHBM HBM ranked superior relative to the THUMS HBM, as the THUMS showed a downward lap belt migration relative to the pelvis at a steeper fore-aft lap belt angle, which was not seen in the PMHS (Chapter 6).

Further analysis was conducted to ensure the issues identified in the THUMS model were seen in other conditions relevant to the targeted parametric study (Chapter 7). This was confirmed:

CHAPTER 10. CONCLUSIONS

the THUMS model's external flesh - either the material stiffness or the sliding contact between the external flesh and the internal structures - was the primary cause of the identified issues related to lap belt-pelvis interaction.

This dissertation's final parametric study, in which the effects of extrinsic and intrinsic factors on lap belt-pelvis interaction and submarining would be quantified, was setup using the GHBMCM with several varied intrinsic and extrinsic factors (Chapter 8). These simulations were sampled to approximate the design space for a subset of 480 simulations and were used to develop, train, and test a Neural Network (NN) metamodel which predicted submarining occurrence and distance, pelvis kinematic and lap belt kinetic outputs based on these varied parameters.

As a full-factorial simulation study was inefficient to execute due to the high computational cost, the metamodel was used to interpolate for these missing datapoints as it was trained within the parameter bounds at the discretized levels. The metamodel predicted how these intrinsic and extrinsic factors, originally identified in Chapter 2, and further investigated in Chapters 3-6, affected submarining occurrence, submarining distance, pelvis displacement, pelvis rotation, and lap belt tension (Chapter 9).

From the NN metamodel's predictions, fore-aft lap belt angle and recline angle were identified as the dominating factors that affected submarining occurrence. A shallow lap belt angle, in combination with a reclined torso angle, was linked to a higher likelihood of submarining. Submarining risk was decreased for a steeper lap belt angle in both postures, however in the reclined posture this risk was only substantially mitigated at the steepest fore-aft lap belt angle (87°).

Additionally, the range of permitted lap belt angles by FMVSS 210 was shown to be insufficient in mitigating submarining risk in a reclined posture with a modern restraint system (equipped with dual lap belt pretensioners). For a reclined seating posture, the lap belt anchorages must be positioned further forward relative to the occupant to reduce submarining risk. Potential trade-offs resulting from moving the lap belt anchorages further forward included increased pelvis forward displacement (from 63° to 75° in upright and from 75° to 87° in recline) and increased lap belt tension (from 46° to 75° for both postures).

Additionally, a 35° fore-aft lap belt angle (within FMVSS 210 regulation) showed a 65% probability of submarining in an upright posture using this modern restraint system. This probability is expected to increase for a restraint system without lap belt pretensioners. Thus, the lower bound of the FMVSS 210 regulation should be increased to an approximate 45° angle, which showed a lower (20%) probability of submarining.

10.2 Future Research and Limitations

As with all research studies, this dissertation's conclusions should be interpreted based on the utilized tools and methods, and caution should be used when drawing conclusions beyond such tools and methods. Thus, this dissertation's conclusions are drawn with limitations resulting from the utilized HBM and its anthropometry and biofidelity as well as the boundary conditions. With additional data and research, the developed methodology can be used to deduce robust conclusions which will inform current and future restraint design.

10.2.1 HBM Biofidelity and Submarining Prediction

Two state-of-the-art mid-sized male HBMs, the GHBMC and the THUMS, were evaluated and compared relative to experimental PMHS data. Ultimately, the GHBMC was identified as having improved biofidelity over the THUMS model in both the reclined dynamic sled test and belt pull test environments, and thus was selected as the model to use for the final parametric study, wherein the effects of extrinsic and intrinsic factors on submarining were quantified.

Though the GHBMC was identified as the more suitable model over the THUMS, the GHBMC model still exhibited limitations. Thus, the conclusions drawn from the parametric study (Chapter 9) should be interpreted with caution as the HBM responses were not perfectly biofidelic. In particular, the GHBMC showed higher rearward pelvis rotation relative to the PMHS in the reclined dynamic sled test condition. Eliminating all other variables, a higher rearward pelvis rotation would increase the likelihood of submarining; however, neither HBM submarined in the reclined sled test condition described in Chapter 4 (despite testing with three different initial pelvis angles). Additionally, in the belt pull tests described in Chapter 6, the GHBMC (and the THUMS) required more pulling force to submarine at the same lap belt-pelvis angle as the tested obese PMHS since the PMHS had increased abdominal tissue depth. Evaluating the model's biofidelity relative to a PMHS of similar anthropometry (mid-sized male) would allow for a better one-to-one comparison in this condition and thus, a more thorough biofidelity evaluation.

This research highlighted biofidelity limitations of the THUMS model, which resulted from the model's sliding contact between the external flesh and the internal structures. This sliding contact resulted in issues with the collapsing of the lap belt elements, affecting lap belt loading, as well as issues in lap belt migration relative to the pelvis. Thus, this model's sliding contact was identified as a feature that needs to be addressed prior to using this model for detailed analysis of lap belt-pelvis interaction.

10.2.2 Alternative Boundary Conditions

The dynamic experiments and simulations, including those in the final parametric study, utilized a unique restraint system with a seatback-integrated D-Ring, dual lap belt pretensioners, a shoulder belt pretensioner and load limiter. This restraint system was developed by Autoliv Development AB (Vargarda, Sweden), and while it has been shown to mitigate submarining in dynamic sled test conditions using anthropomorphic test devices (ATDs, or crash test dummies), this restraint system is not installed in current vehicles and is still in development. Additionally, dual lap belt pretensioners and seatback-integrated D-Rings are still in the phase-in process in the current vehicle fleet. Thus, while it's likely that the trends associated with certain intrinsic and extrinsic parameters and submarining risk are similar between this restraint system and those installed in the current vehicle fleet, the simulations should be conducted using these current vehicle restraint systems to obtain data that can be directly interpreted as the state of risk in the current vehicle fleet.

Additionally, these simulations utilized a semi-rigid seat, composed of an aluminum seat pan and anti-submarining pan, each of which are independently articulated via springs tuned to match the stiffness of a real vehicle seat. Using a semi-rigid seat allows for better physical repeatability as well as easy computational replication of a physical test environment. However, performing additional experiments and/or simulations using a real vehicle seat would confirm all observed pelvis kinematics and submarining occurrence was not artificially affected by this semi-rigid seat.

10.2.3 Considerations for Occupants of Varying Anthropometry

Except for the belt pull experiments conducted in Chapter 5, this dissertation's research and resulting conclusions are based on kinematic and submarining outcomes of a mid-sized (50th percentile) male PMHS or HBM. This anthropometry was chosen as the current state-of-the-art mid-sized male HBMs have been developed and validated using several sources of experimental data with mid-sized male PMHS. Additional data is required to validate existing HBMs of other anthropometries, including the 95th percentile male and, more critically, the 5th percentile and 50th percentile female. Females have been shown to sustain more frequent and higher severity injuries in motor vehicle crashes, particularly of the lower extremity [11]. The higher prevalence of lower extremity injuries may be a result of increased pelvis forward displacement, which highlights the importance of understanding lap belt-pelvis interaction for females. Due to differences in local geometry of the lower abdomen and bony pelvis, it is inappropriate to scale this dissertation's conclusions to a female anthropometry. Instead, experimental data and simulations using a validated

CHAPTER 10. CONCLUSIONS

female HBM are required. Additionally, further research is required to understand submarining for the obese population, which has been shown to be more prone to adverse lap belt-pelvis interaction and submarining versus a population of normal BMI [16, 59].

10.2.4 Restraint Design Considerations

The conclusions of the parametric study, specifically those drawn from the NN meta-model's predictions, show that fore-aft lap belt angle and recline angle are the dominant parameters affecting submarining occurrence. This is highly useful from a restraint design standpoint: a thorough investigation of the threshold of increased risk resulting from the combination effect of increasing recline angle and decreasing fore-aft lap belt angle can directly inform how to position the lap belt anchorages (fore-aft) for a given seatback angle. It is difficult to infer this threshold from the NN metamodel's predictions of the full-factorial sample with discretized parameters (Figure 9.2a). Using the larger (1M) sample with continuous parameters shows an example of the threshold's trend and location (Figure 9.7); however, the NN metamodel must be trained and cross-validated with continuous input parameters to trust its predictions.

The conclusions drawn from the metamodel's validated predictions show that the lap belt anchorage points should be re-positioned further forward for a reclined occupant relative to an upright occupant. A reclined posture showed a higher risk of submarining for a nominal and a shallow fore-aft lap belt angle relative to an upright posture. However, it is important to investigate all potential trade-offs that may result from repositioning the anchorages further forward.

Two potential trade-offs of shifting the lap belt anchorages forward were identified from this analysis, including an increase in forward pelvis displacement at a more vertical fore-aft angle and a higher magnitude of lap belt tension. Inclusion of a knee bolster at a steeper fore-aft lap belt angle may aid in mitigating forward pelvis displacement and providing an alternative load path. At steeper lap belt angles, the lower bony pelvis and acetabulum are engaged, thus understanding injury thresholds at this region is an area of future research.

It is also critical to understand how varying these anchorage locations may alter upper torso kinematics and shoulder belt loading, as these kinematics were not analyzed into this dissertation. It is possible that, in addition to increased pelvis displacement, a steeper lap belt angle may increase forward displacement of the head and upper extremities, which could affect injury outcomes. Likewise, this may alter shoulder belt loading of the skeletal thorax and cervical spine, particularly as moving the lap belt anchorages fore-aft affected initial shoulder belt fit (Figure 8.12).

10.2.5 Other Considerations

While exploring how the parameter effects on submarining are modified based on different anthropometries and boundary conditions is critical to draw more robust conclusions from this research, an additional approach is suggested which can be implemented in the nearer future. Using both the GHMBC and THUMS HBMs in a parametric study, such as that described in Chapter 8, would identify whether parameters show similar effects across models of different formulations. Thus, parameters that affect submarining occurrence in both models are more robust relative to those that show model-dependency. This would eliminate possible artificial effects from using one model and the limitations of that model's biofidelity.

10.3 Contributions

The main contribution of this dissertation is the quantification of extrinsic or environment-related parameters and intrinsic or occupant-related parameters on submarining occurrence, the distance of submarining, pelvis displacement and rotation, and tension in the lap belt. The extrinsic parameters included impact pulse, fore-aft lap belt angle, overhead lap belt angle, presence or absence of foot support, lap belt-to-occupant friction, and seat pan-to-occupant friction. The intrinsic parameters included torso angle, pelvis angle, and pelvic-abdominal soft tissue compliance. The individual and relative effects of these parameters were quantified at 2-5 discrete levels. This provides the automotive safety community with a wealth of data to inform restraint system design for current and future vehicles. Specifically, this improves the automotive safety field's understanding of the fundamental characteristics that influence lap belt-pelvis interaction and submarining. This also identifies limitations of current safety standards (FMVSS 210) for a restraint system equipped with modern pretensioner and load-limiter technologies, and for a reclined seating posture. Finally, this quantification identifies consistencies and differences across different torso angles, providing guidance on potential vehicle environment modifications that need to be made to mitigate submarining in a reclined posture versus an upright posture.

In building up to this final quantification, several other contributions were made. This includes the first dataset of PMHS response to frontal-impact in a reclined environment, including a comprehensive evaluation of different computational models' abilities to capture the belt-pelvis interaction response in this posture. The execution of these tests provided the field with the first-ever understanding of how a reclined seating posture affects lap belt-pelvis interaction and submarining

CHAPTER 10. CONCLUSIONS

occurrence using PMHS. The matched simulations provided the biofidelity evaluation of two different HBMs in this condition, which identified important limitations in the models' formulations and thus, areas in which the models should be improved to increase biofidelity.

This dissertation includes a detailed investigation on the effect of lap belt-pelvis angle on lap belt-pelvis interaction and submarining occurrence for a PMHS in both an upright and reclined seating posture. This provides information on how each of these variables affects submarining, eliminating the complex and confounding factors of a dynamic sled test environment. Matched simulations were conducted using two different computational models for varying levels of flesh compliance. Again, this work identified key limitations in the models' formulations and thus, areas in which the models should be improved to increase biofidelity.

Novel load cell instrumentation was developed at the computational models' ASIS cross-sections, which permitted direct measurement of lap belt-to-pelvis loading. This instrumentation allowed for the comparison of the models' lap belt-pelvis interactions, quantified as ASIS load relative to lap belt tension, in several unique dynamic conditions.

An automation pipeline, originally developed by [90], was adapted for this application. This included automated seatbelt routing at several unique lap belt anchorage locations for different computational models in different postures. This automation cycle permitted the execution of several batches of simulations with iterative training and development of a Neural Network metamodel.

Overall, this research provides a fundamental contribution to the improvement of vehicle safety by providing an all-encompassing understanding of several factors that feed into the submarining problem and which factors should be prioritized to address this problem.

Chapter 11

Publications

11.1 Journal Articles

1. **Richardson, R.**, Forman, J., Gepner, B., Kerrigan, J. (2023). Quantifying the Effects of Intrinsic and Extrinsic Factors on Lap Belt-Pelvis Interaction and Submarining. Traffic injury prevention. (Planned).
2. **Richardson, R.**, Gepner, B., Kerrigan, J., Forman, J., (2023). Evaluation of Lap Belt-Pelvis Load Transfer in Frontal Impact Simulations. Traffic injury prevention. (Planned).
3. **Richardson, R.**, Gepner, B., Kerrigan, J. (2023). Evaluating the Effect of Recline Angle and Restraint Geometry on Lap Belt-Pelvis Interaction for Computational Human Body Models. Traffic injury prevention. (Planned).
4. **Richardson, R.**, Donlon, J. P., Forman, J., Gepner, B., Kerrigan, J. (2022). The Effect of Recline Angle and Restraint Geometry on Lap Belt-Pelvis Interaction for Automotive Occupants of High BMI. Annals of Biomedical Engineering. (Submitted).
5. Shin J, Donlon J-P, **Richardson R**, Gepner B, Forman J, Ostling M, Kerrigan J. (2022). Reclined Frontal Impact Sled Tests with the Hybrid-III 50th Percentile Male and the THOR-50M for Environment Validation. Traffic Injury Prevention. (Submitted)
6. **Richardson R**, Donlon J-P, Jayathirtha M, Forman J, Shaw G, Gepner B, Kerrigan J, Ostling M, Mroz K, Pipkorn B. (2020). Kinematic and Injury Response of Reclined PMHS in Frontal Impacts. Stapp Car Crash Journal, 64, 85-153.

CHAPTER 11. PUBLICATIONS

7. **Richardson R**, Jayathirtha M, Chastain K, Donlon J-P, Forman J, Gepner B, Ostling M, Mroz K, Shaw G, Pipkorn B, Kerrigan J. (2020) Thoracolumbar Spine Kinematics and Injuries in Frontal Impacts with Reclined Occupants. *Traffic Injury Prevention*. DOI: 10.1080/15389588.2020.183736
8. **Richardson RE**, McMurry TL, Gepner B, Kerrigan JR. (2018). Field data analysis of recreational off-highway vehicle crashes. *Traffic injury prevention*, 19(6), 623-628.
9. Donlon JP, **Richardson R**, Jayathirtha M, Forman J, Kerrigan J, Kent R, ... Scavnicky M. (2020). Kinematics of inboard-leaning occupants in frontal impacts. *Traffic injury prevention*, 21(4), 272-277.
10. Rawska K, Gepner B, Kulkarni S, Chastain K, Zhu J, **Richardson R**, ... Kerrigan JR. (2019). Submarining sensitivity across varied anthropometry in an autonomous driving system environment. *Traffic injury prevention*, 20(sup2), S123-S127.

11.2 Conference Proceedings

1. Gepner, B., **Richardson, R.**, Kerrigan, J., Forman, J., (2023). Modification of THOR Sacral Geometry to Improve Biofidelity in a Reclined Posture. *IRCOBI Short Communication*. (Planned).
2. Shin J, Donlon JP, **Richardson R**, Gepner B, Forman J, Ostling M, Kerrigan J. (2022). Biofidelity Evaluation of the Hybrid-III 50th Male and the THOR-50M in Reclined Frontal Impact Sled Tests. *Proceedings of the 2022 IRCOBI Conference*.
3. Moreau D, Donlon J-P, ... **Richardson R**, Gepner B, Forman J, Ostling M, Kerrigan J. (2021). A Methodology to Replicate Lap Belt Loading Conditions from a Sled Impact Test in a Non-Impact Dynamic Environment on Whole-Body Postmortem Human Subjects. *Proceeding of the 2021 IRCOBI Conference*, IRC-21-36 (261-287).
4. **Richardson R**, Jayathirtha M, Donlon JP, Forman JL, Gepner B, Ostling M, Mroz K, Pipkorn B, Kerrigan JR. (2020). Pelvis Kinematics and Injuries of Reclined Occupants in Frontal Impacts. *Proceedings of the 2020 IRCOBI Conference*, IRC-20-60 (499-515).
5. **Richardson R**, Donlon J-P, Chastain K, et al. (2019). Test methodology for evaluating the reclined seating environment with human surrogates. In *26th International Technical Conference on the Enhanced Safety of Vehicles (ESV)*, In press.

CHAPTER 11. PUBLICATIONS

6. Gepner BD, Draper D, Mroz K, **Richardson R**, Ostling M, Pipkorn B, ... Kerrigan JR. (2019). Comparison of Human Body Models in Frontal Crashes with Reclined Seatback. Proceedings of the 2019 IRCOBI Conference, IRC-19-44 (293-305).
7. Gepner B, Rawska K, **Richardson R**, Kulkarni S, Chastain K, Zhu J, ... Kerrigan J. (2019). Challenges for Occupant Safety in Highly Automated Vehicles across Various Anthropometries. In 26th International Technical Conference on the Enhanced Safety of Vehicles (ESV), In press.

Bibliography

- [1] Dieter Adomeit and Alfred Heger. Motion sequence criteria and design proposals for restraint devices in order to avoid unfavorable biomechanic conditions and submarining. *SAE Transactions*, pages 3150–3159, 1975.
- [2] YC Leung, C Tarriere, D Lestrelin, J Hureau, C Got, F Guillon, and A Patel. Submarining injuries of 3 pt. belted occupants in frontal collisions—description, mechanisms and protection. *SAE transactions*, pages 3521–3553, 1982.
- [3] Narayan Yoganandan, Frank A Pintar, and Matthew R Maltese. Biomechanics of abdominal injuries. *Critical Reviews in Biomedical Engineering*, 29(2), 2001.
- [4] Gerald S Poplin, Timothy L McMurry, Jason L Forman, Thomas Hartka, Gwansik Park, Greg Shaw, Jangho Shin, Hyung joo Kim, and Jeff Crandall. Nature and etiology of hollow-organ abdominal injuries in frontal crashes. *Accident Analysis & Prevention*, 78:51–57, 2015.
- [5] EERO Arajärvi, SEPPO Santavirta, and JORMA Tolonen. Abdominal injuries sustained in severe traffic accidents by seatbelt wearers. *The Journal of trauma*, 27(4):393–397, 1987.
- [6] Sophie Lamielle, Sophie Cuny, Jean-Yves Foret-Bruno, Philippe Petit, P Vezin, Jean-Pierre Verriest, and Herve Guillemot. Abdominal injury patterns in real frontal crashes: influence of crash conditions, occupant seat and restraint systems. In *Annual Proceedings/Association for the Advancement of Automotive Medicine*, volume 50, page 109. Association for the Advancement of Automotive Medicine, 2006.
- [7] M DeJeammes, R Biard, and Y Derrien. Factors influencing the estimation of submarining on the dummy. *SAE Transactions*, pages 3254–3267, 1981.

BIBLIOGRAPHY

- [8] YC Leung, C Tarriere, A Fayon, P Mairesse, and P Banzet. An anti-submarining scale determined from theoretical and experimental studies using three-dimensional geometrical definition of the lap-belt. *SAE Transactions*, 90:3232–3253, 1981.
- [9] Ali M Elhagediab and Stephen W Rouhana. Patterns of abdominal injury in frontal automotive crashes. In *The 16th International Technical Conference on the Enhanced Safety of Vehicles*, 1998.
- [10] Kathleen D Klinich, Carol AC Flannagan, Kristen Nicholson, Lawrence W Schneider, Jonathan Rupp, et al. Abdominal injury in motor-vehicle crashes. Technical report, University of Michigan, Ann Arbor, Transportation Research Institute, 2008.
- [11] Jason Forman, Gerald S Poplin, C Greg Shaw, Timothy L McMurry, Kristin Schmidt, Joseph Ash, and Cecilia Sunnevang. Automobile injury trends in the contemporary fleet: Belted occupants in frontal collisions. *Traffic injury prevention*, 20(6):607–612, 2019.
- [12] RS Jeffery and PL Cook. Seat belts and reclining seats. *Injury*, 22(5):416–417, 1991.
- [13] Jonathan D Rupp, Carl S Miller, Matthew P Reed, Nathaniel H Madura, Kathleen D Klinich, and Lawrence W Schneider. Characterization of knee-thigh-hip response in frontal impacts using biomechanical testing and computational simulations. *Stapp car crash journal*, 52:421, 2008.
- [14] Luise C Schaefer, Mirko Junge, Illés Vörös, Kaan Koçaslan, and Uwe Becker. Odds ratios for reclined seating positions in real-world crashes. *Accident Analysis & Prevention*, 161:106357, 2021.
- [15] Thomas Hartka, Mark Sochor, Kenadeed Hersi, Abigail Booker, and Gerald Poplin. Comparison of visual and ct 3d reconstructed abdominal seat belt sign locations. *Traffic Inj Prev*, 15(Suppl 1):S247, 2014.
- [16] Thomas R Hartka, Hannah M Carr, Brittany R Smith, Monica Melmer, and Mark R Sochor. Does obesity affect the position of seat belt loading in occupants involved in real-world motor vehicle collisions? *Traffic injury prevention*, 19(sup1):S70–S75, 2018.
- [17] Sharmila Dissanaikie, Robert Kaufman, Christopher D Mack, Charles Mock, and Eileen Bulger. The effect of reclined seats on mortality in motor vehicle collisions. *Journal of Trauma and Acute Care Surgery*, 64(3):614–619, 2008.

BIBLIOGRAPHY

- [18] Timothy L McMurry, Gerald S Poplin, Greg Shaw, and Matthew B Panzer. Crash safety concerns for out-of-position occupant postures: A look toward safety in highly automated vehicles. *Traffic injury prevention*, 19(6):582–587, 2018.
- [19] Christina G Rehm and Robert K Goldman. Seat belt and car seat in a reclined position: a dangerous combination. *Journal of Trauma and Acute Care Surgery*, 51(6):1189–1191, 2001.
- [20] Chandrashekhar K Thorbole. Dangers of seatback recline in a moving vehicle: how seatback recline increases the injury severity and shifts injury pattern. In *ASME International Mechanical Engineering Congress and Exposition*, volume 57380, page V003T03A056. American Society of Mechanical Engineers, 2015.
- [21] National Transportation Safety Board (NTSB). Performance of lap/shoulder belts in 167 motor vehicle crashes. 1(NTSB/SS-88/02), 1988.
- [22] SAE On-Road Automated Vehicle Standards Committee et al. Taxonomy and definitions for terms related to on-road motor vehicle automated driving systems. *SAE Standard J*, 3016:1–16, 2014.
- [23] Martin Östling and Annika Larsson. Occupant activities and sitting positions in automated vehicles in china and sweden. In *26th International Technical Conference on the Enhanced Safety of Vehicles (ESV)*, Eindhoven, Netherlands, pages 10–13, 2019.
- [24] Sofia Jorlöv, Katarina Bohman, and Annika Larsson. Seating positions and activities in highly automated cars—a qualitative study of future automated driving scenarios. In *International research conference on the biomechanics of impact*, pages 13–22, 2017.
- [25] Andreas Hagberg and Sandra Jodlovsky. Reclined seating positions for level 4 had vehicles: A comfort and safety approach, 2017.
- [26] D Viano. Introduction: Lap-shoulder belts: Some historical aspects. in: Seat belts: The development of an essential safety feature. *Publication of: Society of Automotive Engineers*, 2003.
- [27] Kenji Shigeta, Yuichi Kitagawa, and Tsuyoshi Yasuki. Development of next generation human fe model capable of organ injury prediction. *Proceedings of the 21st annual enhanced safety of vehicles*, pages 15–18, 2009.

BIBLIOGRAPHY

- [28] F Scott Gayzik, Daniel P Moreno, Nicholas A Vavalle, Ashley C Rhyne, and Joel D Stitzel. Development of a full human body finite element model for blunt injury prediction utilizing a multi-modality medical imaging protocol. In *12th International LS-DYNA User Conference*, pages 3–5, 2012.
- [29] Katarzyna Rawska, Bronislaw Gepner, Shubham Kulkarni, Kalle Chastain, Junjun Zhu, Rachel Richardson, Daniel Perez-Rapela, Jason Forman, and Jason R Kerrigan. Submarining sensitivity across varied anthropometry in an autonomous driving system environment. *Traffic injury prevention*, 20(sup2):S123–S127, 2019.
- [30] Katarzyna Rawska, Bronislaw Gepner, David Moreau, and Jason R Kerrigan. Submarining sensitivity across varied seat configurations in autonomous driving system environment. *Traffic injury prevention*, 21(sup1):S1–S6, 2020.
- [31] Katarzyna Rawska, Bronislaw Gepner, and Jason R Kerrigan. Effect of various restraint configurations on submarining occurrence across varied seat configurations in autonomous driving system environment. *Traffic injury prevention*, 22(sup1):S128–S133, 2021.
- [32] Kyle J Boyle, Matthew P Reed, Lauren W Zaseck, and Jingwen Hu. A human modelling study on occupant kinematics in highly reclined seats during frontal crashes. In *Proceedings of the International Research Conference on the Biomechanics of Impact, IRCOBI, Florence, Italy, 11th September-13th September. IRC-19-43*, 2019.
- [33] Jason Forman, Hongnan Lin, Bronislaw Gepner, Taotao Wu, et al. Occupant safety in automated vehicles-effect of seatback recline on occupant restraint. *International journal of automotive engineering*, 10(2):139–143, 2019.
- [34] BD Gepner, D Draper, K Mroz, R Richardson, M Ostling, B Pipkorn, JL Forman, and JR Kerrigan. Comparison of human body models in frontal crashes with reclined seatback. In *Proceedings of the International Research Conference on the Biomechanics of Impact, IRCOBI, Florence, Italy, 11th September-13th September. IRC-19-44*, 2019.
- [35] Bronislaw D Gepner, Hamed Joodaki, Zhaonan Sun, Mohan Jayathirtha, Taewung Kim, Jason L Forman, and Jason R Kerrigan. Performance of the obese ghbmc models in the sled and belt pull test conditions. In *IRCOBI Conference Proceedings*, 2018.

BIBLIOGRAPHY

- [36] Olivier Richard, Jérôme Uriot, Xavier Trosseille, and Marcin Sokolowski. Occupant restraint optimisation in frontal crash to mitigate the risk of submarining in out-of-position situation. In *Proceedings of IRCOBI Conference*, 2015.
- [37] Tomohiro Izumiyama, Norihiro Nishida, Hideyuki Iwanaga, Xian Chen, Junji Ohgi, Ryusuke Asahi, Shigeru Sugimoto, and Masanobu Fukushima. Identification of influential factors for seatbelt kinematics in a collision and analysis of their influence degree to the kinematics. In *IRCOBI conference*, pages 456–469, 2020.
- [38] Editors of Encyclopedia Britannica. pelvis. *Encyclopedia Britannica*, 2022.
- [39] Mathew Greenston, Rawson L. Wood, and Lars Reinhart. Clinical significance of the seat belt sign as evidence of a compromised occupant–seat belt relationship. *The Journal of Emergency Medicine*, 56(6):624–632, 2019.
- [40] Helen Harkreader, Mary Ann Hogan, and Marshelle Thobaben. *Fundamentals of Nursing: Caring and clinical judgment*. Saunders Elsevier, 2007.
- [41] National traffic and motor vehicle safety act. 15(1392), 1966.
- [42] Federal register: Rules and regulations. 55(83):17973–17975, 1990.
- [43] Thomas F MacLaughlin, LK Sullivan, and Christopher S O’Connor. *Rear seat submarining investigation*. National Highway Traffic Safety Administration, 1988.
- [44] Thomas F MacLaughlin, Lisa K Sullivan, and Christopher S O’Connor. Experimental investigation of rear seat submarining. *IIR Review*, 1(1), 1991.
- [45] HE Mueller and B Linn. Seat belt pretensioners. sae paper no. 980557. *Society of Automotive Engineers, Warrendale, PA*, 1998.
- [46] M Östling, C Sunnevång, C Svensson, and H Kock. Potential future seating positions and the impact on injury risks in a learning intelligent vehicle (liv)—how to avoid submarining in a reclined seating position in a frontal crash. *Proceedings of the VDI-Tagung Fahrzeugsicherheit, Berlin, Germany*, pages 28–29, 2017.
- [47] J-Y. Foret-Bruno, X. Trosseille, Jean-Yves Le Coz, F. Bendjellal, F. Bendjella, C. Steyer, T. Phalempin, D. Villeforceix, P. Dandres, and C. Got. Thoracic injury risk in frontal car

BIBLIOGRAPHY

- crashes with occupant restrained with belt load limiter. *SAE Transactions*, 107:2955–2975, 1998.
- [48] Zhaonan Sun. Material characterization and computational modeling of human subcutaneous adipose tissue. *Dissertation University of Virginia*, 2021.
- [49] Lawrence W Schneider. Development of anthropometrically based design specifications for an advanced adult anthropomorphic dummy family, volume 1. final report. Technical report, 1983.
- [50] Masami Iwamoto, Yoshikatsu Kisanuki, Isao Watanabe, Katsuya Furusu, Kazuo Miki, and Junji Hasegawa. Development of a finite element model of the total human model for safety (thums) and application to injury reconstruction. In *Proceedings of the international IRCOBI Conference*, pages 18–20, 2002.
- [51] Department of Transportation National Highway Traffic Safety Administration. Seat belt assembly anchorages. 571(210).
- [52] Jerome Uriot, Pascal Baudrit, Pascal Potier, Xavier Trosseille, et al. Investigations on the belt-to-pelvis interaction in case of submarining. *Stapp car crash journal*, 50:53, 2006.
- [53] Carole Luet, Xavier Trosseille, Pascal Drazétic, Pascal Potier, and Guy Vallancien. Kinematics and dynamics of the pelvis in the process of submarining using pmhs sled tests. *Stapp car crash journal*, 56:411, 2012.
- [54] John D Horsch and William E Hering. A kinematic analysis of lap-belt submarining for test dummies. *SAE transactions*, pages 1847–1854, 1989.
- [55] H Naseri, J Iraeus, and H Johansson. The effect of adipose tissue material properties on the lap belt-pelvis interaction: A global sensitivity analysis. *Journal of the Mechanical Behavior of Biomedical Materials*, 107:103739, 2020.
- [56] Raymond R McHenry and Kenneth N Naab. *Computer simulation of the crash victim: a validation study*. Society of Automotive Engineers Warrendale, PA, 1966.
- [57] Koji Mizuno, Wataru Hatano, Ryoichi Yoshida, Yutaka Nakajima, Yoshihiko Tanaka, Takamari Muroya, and Ryota Ishigaki. The geometrical relationship between the lap belt and occupants’ anterior superior iliac spine. In *26th International Technical Conference on the Enhanced Safety of Vehicles (ESV)*, Eindhoven, Netherlands, 2019.

BIBLIOGRAPHY

- [58] D DeRosa and JF Larssonneur. Seat belt improvements. *SAE transactions*, pages 1087–1098, 1984.
- [59] Matthew P Reed, Sheila M Ebert-Hamilton, and Jonathan D Rupp. Effects of obesity on seat belt fit. *Traffic injury prevention*, 13(4):364–372, 2012.
- [60] Matthew P Reed, Sheila M Ebert, and Jason J Hallman. Effects of driver characteristics on seat belt fit. *Stapp car crash journal*, 57(57):43–57, 2013.
- [61] Jason Forman, Francisco J Lopez-Valdes, David Lessley, Matthew Kindig, Richard Kent, and Ola Bostrom. The effect of obesity on the restraint of automobile occupants. In *Annals of Advances in Automotive Medicine/Annual Scientific Conference*, volume 53, page 25. Association for the Advancement of Automotive Medicine, 2009.
- [62] YC Leung, C Tarriere, A Fayon, P Mairesse, A Delmas, and P Banzet. A comparison between part 572 dummy and human subject in the problem of submarining. *SAE Transactions*, pages 3537–3556, 1979.
- [63] Stephen W Rouhana, David C Viano, Edward A Jedrzejczak, and Joseph D McCleary. Assessing submarining and abdominal injury risk in the hybrid iii family of dummies. *SAE transactions*, pages 1824–1846, 1989.
- [64] Yngve Håland and G Nilson. Seat belt pretensioners to avoid the risk of submarining—a study of lap-belt slippage factors. In *Proceedings: International Technical Conference on the Enhanced Safety of Vehicles*, volume 1993, pages 1060–1068. National Highway Traffic Safety Administration, 1993.
- [65] Kathleen D Klinich, Miriam A Manary, and Kathleen B Weber. Crash protection for child passengers: rationale for best practice. *The UMTRI Research Review*, 43(1):1, 2012.
- [66] Zhaonan Sun, Bronislaw D Gepner, Sang-Hyun Lee, Joshua Rigby, Patrick S Cottler, Jason J Hallman, and Jason R Kerrigan. Multidirectional mechanical properties and constitutive modeling of human adipose tissue under dynamic loading. *Acta Biomaterialia*, 129:188–198, 2021.
- [67] Hosein Naseri, Johan Iraeus, and Håkan Johansson. A numerical study on the safety belt-to-pelvis interaction. *International journal for numerical methods in biomedical engineering*, 38(4):e3572, 2022.

BIBLIOGRAPHY

- [68] Taewung Kim, Gwansik Park, Salvador Montesinos, Damien Subit, James Bolton, Brian Overby, Jason Forman, Jeff Crandall, and Hyungjoo Kim. Abdominal characterization test under lap belt loading. In *24th International Technical Conference on the Enhanced Safety of Vehicles (ESV) National Highway Traffic Safety Administration*, number 15-0312, 2015.
- [69] Stéphane Couturier, Jacques Faure, Ricardo Satué, Joaquim Huguet, and Julien Hordonneau. Procedure to assess submarining in frontal impact. In *20th International Conference on the Enhanced Safety of Vehicles*, pages 18–21, 2007.
- [70] Dieter Adomeit. Seat design—a significant factor for safety belt effectiveness. *SAE Transactions*, pages 3326–3337, 1979.
- [71] Keita Nakane, Masayoshi Nojiri, Ryo Maekawa, Makoto Esaki, Shigeyuki Suzuki, Yasushi Masuda, and Masahito Hitosugi. Analysis of abdominal injuries caused by the submarining phenomenon in the rear seat occupants. In *The 24th International Technical Conference on the Enhanced Safety of Vehicles*, 2015.
- [72] Jonathan D. Rupp, Carol A.C. Flannagan, Andrew J. Leslie, Carrie N. Hoff, Matthew P. Reed, and Rebecca M. Cunningham. Effects of bmi on the risk and frequency of ais 3+ injuries in motor-vehicle crashes. *Obesity*, 21(1):E88–E97, 2013.
- [73] Thomas M Rice and Motao Zhu. Driver obesity and the risk of fatal injury during traffic collisions. *Emergency Medicine Journal*, 31(1):9–12, 2014.
- [74] Greg Shaw, David Lessley, Joseph Ash, Salvador Acosta, Sara Heltzel, Patrick Riley, Taewung Kim, and Jeff Crandall. Pelvic restraint cushion sled test evaluation of pelvic forward motion. *Traffic injury prevention*, 19(3):250–255, 2018.
- [75] Stephen W Rouhana, Paul G Bedewi, Sundeep V Kankanala, Priya Prasad, Joseph J Zwolinski, Alex G Meduvsky, Jonathan D Rupp, Thomas A Jeffreys, and Lawrence W Schneider. Biomechanics of 4-point seat belt systems in frontal impacts. Technical report, SAE Technical Paper, 2003.
- [76] Jérôme Uriot, Pascal Potier, Pascal Baudrit, Xavier Trosseille, Philippe Petit, Olivier Richard, Sabine Compigne, Mitsutoshi Masuda, and Richard Douard. Reference pmhs sled tests to assess submarining. *Stapp car crash journal*, 59:203, 2015.

BIBLIOGRAPHY

- [77] Xavier Trosseille, Philippe Petit, Jérôme Uriot, Pascal Potier, Pascal Baudrit, Olivier Richard, Sabine Compigne, Mitsutoshi Masuda, and Richard Douard. Reference pmhs sled tests to assess submarining of the small female. *Stapp car crash journal*, 62:93–118, 2018.
- [78] Rachel Richardson, John Paul Donlon, Kalle Chastain, Greg Shaw, Jason Forman, Sara Sochor, Mohan Jayathirtha, Kevin Kopp, Brian Overby, Bronislaw Gepner, et al. Test methodology for evaluating the reclined seating environment with human surrogates. In *Proceedings of the 26th International Technical Conference on the Enhanced Safety of Vehicles, ESV, Eindhoven, Netherlands, 10th June–13th June, 2019*.
- [79] Gerald W Nyquist and Lawrence M Patrick. Lumbar and pelvic orientations of the vehicle seated volunteer. *SAE Transactions*, pages 2610–2621, 1976.
- [80] Matthew P Reed. Effects of recline on passenger posture and belt fit. Technical report, University of Michigan, Ann Arbor, Transportation Research Institute, 2018.
- [81] Rachel Richardson, John-Paul Donlon, Mohan Jayathirtha, Jason L Forman, Greg Shaw, Martin Östling, Krystoffer Mroz, and Bengt Pipkorn. Kinematic and injury response of reclined pmhs in frontal impacts. *Stapp car crash journal*, 64:83–153, 2020.
- [82] R Richardson, M Jayathirtha, JP Donlon, J Forman, B Gepner, M Ostling, K Mroz, B Pipkorn, and JR Kerrigan. Pelvis kinematics and injuries of reclined occupants in frontal impacts. In *Proceedings of the International Research Conference on the Biomechanics of Impact, IRCOBI. IRC-20-60, 2020*.
- [83] Patrick J Roache. *Verification and validation in computational science and engineering*, volume 895. Hermosa Albuquerque, NM, 1998.
- [84] Elemance LLC. *GHBMC, Global Human Body Models Consortium User Manual: Simplified Pedestrians*, 2020.
- [85] Daichi Kato, Yuko Nakahira, Noritoshi Atsumi, and Masami Iwamoto. Development of human-body model thums version 6 containing muscle controllers and application to injury analysis in frontal collision after brake deceleration. In *Proceedings of the International IRCOBI Conference. IRCOBI Council, Athens, Greece, 2018*.
- [86] David Moreau, John Paul Donlon, Aida Chebbi, Mohan Jayathirtha, Sara Sochor, Brian Overby, Rachel Richardson, Bronislaw Gepner, Jason Forman, Martin Östling, et al. A

BIBLIOGRAPHY

methodology to replicate lap belt loading conditions from a sled impact test in a non-impact dynamic environment on whole-body postmortem human subjects.

- [87] Monica LH Jones, S Ebert, Jingwen Hu, and Matthew P Reed. Effects of high levels of obesity on lap and shoulder belt paths. *International Research Council on Biomechanics of Injury (IRCOBI)*, pages 13–15, 2017.
- [88] Kemp B Doersch and William E Dozier. The seat belt syndrome: the seat belt sign, intestinal and mesenteric injuries. *The American Journal of Surgery*, 116(6):831–833, 1968.
- [89] Matthieu Lebarbé, Philippe Beillas, Tomas Janak, Yoann Lafon, Olivier Richard, and Philippe Petit. Geometrical and mechanical characterization of the abdominal fold of obese post mortem human subjects for use in human body modelling. *Stapp car crash journal*, 64:213–267, 2020.
- [90] Daniel Perez Rapela. *Methodology for the Evaluation of Human Response Variability to Intrinsic and Extrinsic Factors Including Uncertainties*. PhD thesis, Charlottesville, VA, 2020.
- [91] Matthew Miller. Large-scale parametric evaluation of child booster seats. Master’s thesis, Charlottesville, VA, 2021.
- [92] Warren N Hardy, Matthew J Mason, Craig D Foster, Chirag S Shah, James M Kopacz, King H Yang, Albert I King, Jennifer Bishop, Michael Bey, William Anderst, et al. A study of the response of the human cadaver head to impact. *Stapp car crash journal*, 51:17, 2007.
- [93] Jason L Forman, Francisco Lopez-Valdes, David J Lessley, Patrick Riley, Mark Sochor, Sara Heltzel, Joseph Ash, Rafal Perz, Richard W Kent, Thomas Seacrist, et al. Occupant kinematics and shoulder belt retention in far-side lateral and oblique collisions: a parametric study. *Stapp car crash journal*, 57:343, 2013.
- [94] Alope Prasad and Doug Weston. Nhtsa’s rear seat safety research. In *International Conference on Enhanced Safety of Vehicles (ESV)*, 2011.
- [95] James A Stimson, Edward G Carmines, and Richard A Zeller. Interpreting polynomial regression. *Sociological Methods & Research*, 6(4):515–524, 1978.
- [96] Arthur E Hoerl and Robert W Kennard. Ridge regression: applications to nonorthogonal problems. *Technometrics*, 12(1):69–82, 1970.

BIBLIOGRAPHY

- [97] Robert Tibshirani. Regression shrinkage and selection via the lasso. *Journal of the Royal Statistical Society: Series B (Methodological)*, 58(1):267–288, 1996.
- [98] Hamed Joodaki, Bronislaw Gepner, and Jason Kerrigan. Leveraging machine learning for predicting human body model response in restraint design simulations. *Computer Methods in Biomechanics and Biomedical Engineering*, 24(6):597–611, 2021.
- [99] Daniel Perez-Rapela, Jason L. Forman, Samuel H. Huddleston, and Jeff R. Crandall. Methodology for vehicle safety development and assessment accounting for occupant response variability to human and non-human factors. 24(4):384–399.
- [100] S. H. Huddleston and G. G. Brown. *Machine Learning. In J.J. Cochran, editor, INFORMS analytics body of knowledge*. John Wiley & Sons, 2019.
- [101] Gareth James, Daniela Witten, Trevor Hastie, and Robert Tibshirani. *An introduction to statistical learning*, volume 112. Springer, 2013.
- [102] Steve Lawrence, C Lee Giles, and Ah Chung Tsoi. What size neural network gives optimal generalization? convergence properties of backpropagation. Technical report, 1998.
- [103] National Highway Traffic Safety Administration et al. Federal motor vehicle safety standards; child restraint systems, child restraint anchorage systems. *Federal register*, 1999.
- [104] Bronislaw D Gepner, Daniel Perez-Rapela, Jason L Forman, Martin Ostling, Bengt Pipkorn, and Jason R Kerrigan. Evaluation of ghbmc, thums and safer human body models in frontal impacts in reclined postures.
- [105] Thomas J Santner, Brian J Williams, William I Notz, and Brian J Williams. *The design and analysis of computer experiments*, volume 1. Springer, 2003.
- [106] Luc Pronzato and Werner G Müller. Design of computer experiments: space filling and beyond. *Statistics and Computing*, 22(3):681–701, 2012.
- [107] Kathleen D Klinich and Carol AC Flannagan. Identifying priorities for improving rear seat occupant protection. Technical report, University of Michigan, Ann Arbor, Transportation Research Institute, 2009.

BIBLIOGRAPHY

- [108] Matthew P Reed, Sheila M Ebert-Hamilton, Kathleen D Klinich, Miriam A Manary, and Jonathan D Rupp. Effects of vehicle seat and belt geometry on belt fit for children with and without belt positioning booster seats. *Accident Analysis & Prevention*, 50:512–522, 2013.
- [109] Katarina Bohman and Rikard Fredriksson. Pretensioner loading to rear-seat occupants during static and dynamic testing. *Traffic injury prevention*, 15(sup1):S111–S118, 2014.

Appendix A

Automotive Restraint Timeline

This timeline was researched and organized based on the literature review presented in Chapter 2 and details the development and introduction of automotive restraints in the United States (U.S.) automotive fleet.

A.1 Timeline

- **1880s:** Belts securing to wagons (Viano et al., 2002)
- **1910-1930:** Belts in aviation; Belts securing to automobiles (Viano et al., 2002)
- **1930s:** Fatalities reach 15.6 per 100 million vehicle miles traveled. Automobile designers begin to consider safety issues
- **1940s:** Four-point safety belts for aviation with inertial locking (Alexander, 1940)
 - Founding fathers of crashworthiness in restraints: DeHaven and Stapp
 - * **1942:** “Structural provisions to reduce impact and distribute pressure could enhance survival and modify injury within wide limits in aircraft and automobile accidents” (DeHaven, 1942)
 - Showed leading cause of fatalities was ejection - prompted lap belt development
 - * **1950s:** Stapp established limits for human tolerance of deceleration (Viano, 102)
- **1949:** Nash was the first car company to install factory equipped lap belts (Viano, 2002)

APPENDIX A. AUTOMOTIVE RESTRAINT TIMELINE

- More than decade later, Ford and Chrysler gave the option (1955 in American made cars) (Viano, 2002)
- **1954:** SAE's belt committee was formed and issued initial recommendations and classifications (J4a 1955) which were dramatically updated in a later revision (J4a 1964).
 - **Type 1:** Lap Belt
 - **Type 2:** A Combination of Lap Belt and Upper Torso Restraint
 - **Type 2a:** Upper Torso Restraint to be used with Type 1 Belt
 - **Type 3:** Combination of Pelvic and Upper Torso Belt for Children Weighing \leq 50 lbs
 - Included webbing strength recommendations, hardware, etc.
- **1955:** Patent for lap-shoulder belt system for passenger safety in car crashes (Griswold and Dehaven, 1955)
- **1956:** National Safety Council publicly recommends use of safety belts (Wilson, 1979)
- **1959:** Full fleet of vehicles with lap-shoulder belts to study safety effectiveness (Andreasson and Backstrom, 2000)
- **1962:** Review of seat belt webbing for automotive restraints that included strength, elongation, abrasion, weather resistance, weave patterns, etc. (Neff, 1962)
- **1963:** Demonstrated essential characteristics of lap-shoulder belts for occupant restraint (preferred orientation and configuration) (Benedict, 1963)
 - *"Studies of racing car accidents suggest that the shoulder harness or upper torso restraint is of definite value and will give additional driver protection. A single upper torso strap should be used in all current production and sports cars. The occupant must be able to slide laterally from beneath the upper torso restraint in response to lateral forces from the opposite side of the car. The upper torso restraint should not be interconnected with the lap belt so that tightening one will cause the other to tighten; the lap belt can be snug and comfortable while the shoulder strap has to be looser to permit the use of the vehicle controls"*
- **Mid-1960s:** Five U.S. states passed laws requiring standard installation of front seat belts (Viano, 2002); first pretensioning device (spring) realized by Brown in 1965 (Brown, 1965)

APPENDIX A. AUTOMOTIVE RESTRAINT TIMELINE

- **1964 and 1967:** Comprehensive study on belt crash testing– found that lap-shoulder belts are convenient to put on, comfortable to wear with the inertia locking retractor, and gave a high degree of crash safety by virtually eliminating ejection and reducing impacts (Bohlin, 1964 and 1967)
 - These results were the turning point that started the phase-in of these belts
- **1964:** Summarized work by SAE in cooperation with National Bureau of Standards aimed at setting up minimum standards for seat belts for use in motor vehicles
- **1964:** Lap belts are required in most states (previously optional) (Viano, 2002)
- **1965:** President Johnson refers to the 1.6 million people who die on streets and highways as an “epidemic” of traffic fatalities (The White House, 1966)
- **1966:** National Traffic and Motor Vehicle Safety Act passed by Congress (Traffic and Motor Vehicle Safety Act, 1966)
 - First regulatory initiative in automotive safety
 - First step to require DOT to assemble a comprehensive body of regulations aimed at standardizing motor vehicle safety requirements
 - Directed the DOT to administer safety standards that are “practicable, shall meet the need for motor vehicle safety, and shall be stated in objective terms” (Traffic and Motor Vehicle Safety Act, 1966)
 - Incorporated general industry-wide standards set by the SAE (US Department of Commerce, 1967)
 - Lap belts federally required
- **1966:** Ralph Nader’s *Unsafe at Any Speed* becomes best seller
- **1967:** Department of Commerce evaluated the safety standards, pinpointing several major safety concerns, especially full frontal collision resulting in driver and front seat passenger impact with the steering column or dashboard (US Department of Commerce, 1967)
 - Recommended safety improvements for vehicle tires, headrests, and dashboards
- **1967:** NHTSA issues FMVSS 208 – mandates installation of restraint systems to protect vehicle occupants in collisions (Cutler, 1991; 32 FR 2408, 2415, 1967)

APPENDIX A. AUTOMOTIVE RESTRAINT TIMELINE

- One of the 19 original safety standards (Kratzke, 1995)
- Required lap shoulder belts (see below)
- Also included is FMVSS 209-210
- It is believed that FMVSS 210 had a standard for 20-75 deg lap belt angle at this time (following ECE)
- **1967-1968: Lap-shoulder belts – required in front seats** (Viano, 2002)
 - Took effect Jan 1, 1968
 - No specific design mandated
 - Weren't widely available until a federal law required them
 - Provide mitigation of interior impact
 - No crash testing requirements to evaluate the protection afforded to vehicle occupants (Kratzke, 1995)
 - U.S. Department of Transportation required lap-shoulder belts in front outboard seats as standard equipment after the clear demonstration of field effectiveness presented by Bohlin (1967); lap belts were required for all automobiles produced after Jan 1968
- **1970:** National Traffic Safety Administration renamed NHTSA (Bollier and Claybrook, 1986)
 - General Motors President Cole stated that airbags have greatest potential to increase safety and could replace seat belts (Cutler, 1991)
- **1970s:** Belt usage remained around 20% nationally – less than other countries with mandated seat belt laws (Wilson, 1979); interlock systems introduced for brief period (Hedlund, 1985)
- **1971:** Belts are required in multipurpose vehicles and trucks (Wilson, 1979)
- **1975:** First pyrotechnic pretensioner patent/demo (Schwanz, 1975)
 - Also, whiplash injuries were observed after the widespread use of lap-shoulder belts in the UK, which pointed to the concentration of loads on the neck with belt restraint in the absence of head contact (need for airbags) (Viano, 2002)
- **1977:** Secretary of Transportation Brock Adams amends FMVSS 208 to mandate passive restraint protection (airbags) in all passenger cars for the 1984 model year and larger wheelbase vehicles in the 1982 model year (42 FR 34,289-90, 1977)

APPENDIX A. AUTOMOTIVE RESTRAINT TIMELINE

- Airbags are required (to account for minimal seat belt usage – called “passive restraints” since occupants don’t have to physically put the safety measure into place like a seat belt) (Hedlund, 1985)
- Many opposed due to cost concerns but also concerns related to possible injuries of occupants out of position (Cutler, 1991)
- **1981:** NHTSA Rescinds FMVSS 208 requirements for passive restraints; passive restraints requirement suspended
- **1981:** Mercedes introduces pretensioners into front vehicle seats
- **1987:** Mercedes becomes industry leader in offering airbags as standard (Cutler, 1991)
- **1988:** Chrysler issues airbags – release crash data that reported 91 airbag deployments with no reported fatalities (Cutler, 1991)
- **1989-1995:** Airbags phase in (Cutler, 1991)
- **1980s:** Front seat lap-shoulder belts found to be 41+/- 4% in preventing fatality for front-seat occupants, 42 +/- 2% for drivers and 39 +/- 4% for right-front passengers (Evans 1986, 1991)
 - In frontal crashes, belts are 43% effective in preventing fatality; least effective in near-side crashes at 27%
 - Importantly, belts were effective in all crash modes ranging from 27-77%
- **1990:** Lap/shoulder belts required for rear outboard passengers
- **1990:** Notice of Proposed Rulemaking released to adopt a 30 deg minimum to FMVSS 210 (55 FR 17970, April 30, 1990)
 - The ECE regulation specifies a minimum lap belt angle of 30 degrees in front seats of passenger cars. Since the ECE 30 degree minimum (80 deg max) would enhance safety by reducing the risk of occupant submarining, the NPRM proposed to adopt a 30 degree minimum in Standard No. 210 – “specifically to improve belt fit and reduce the potential of occupant submarining”
 - * Those who supported: Chrysler, Volvo, Volkswagen, and BMW
 - * Those who opposed: Mitsubishi, Honda, Austin Rover, Fiat, Ford, Hino, GM, Toyota, Jaguar, Nissan, Mazda, and Subaru

APPENDIX A. AUTOMOTIVE RESTRAINT TIMELINE

- GM: “the interrelationship of factors that can contribute to occupant submarining in vehicle crashes is not fully understood”
 - NHTSA: “even though the interrelationship of these factors is not yet quantified, the available data show that increasing the minimum lap belt angle will decrease the likelihood of occupant submarining”
 - Rear Seat Submarining Investigation – MacLaughlin 1988
 - Previous data showed occupant excursion would increase as the belt angle approaches vertical – no data on this – so no harmonization with ECE
- **1991:** Driver airbag and belt combination provides an overall 47% effectiveness in preventing fatalities (Zador and Ciccone, 1991)
 - **1991:** President Bush signed into law the Intermodal Surface Transportation Efficiency Act which requires all passenger cars manufactured on or after Sept 1 1997 (1998 model year) have airbags
 - **1992:** Lap/shoulder belts required for rear outboard passengers in trucks and vans
 - **1998:** Lap/shoulder belts and airbags required for driver and right front passenger beginning in the 1998 model year of passenger cars (Sept. 1997) (Kratzke, 1995)
 - **1998:** Move to industry-wide application of pretensioners and load limiters
 - **1999:** Lap/shoulder belts and airbags required for driver and right front passenger beginning in the 1999 model year of light trucks and vans (Sept. 1998) (Kratzke, 1995)
 - **2005:** Lap/shoulder belts required in center rear seat (phase-in until 2007)

A.2 References for Timeline

Alexander, L. A. (1940). U.S. Patent No. 2,195,334. Washington, DC: U.S. Patent and Trademark Office.

Andréasson, R., Bäckström, C. G. (2000). The seat belt: Swedish Research and development for global automotive safety.

Benedict, J. F. (1963). Safe and unsafe upper torsion restraints for occupant protection in motor vehicles. In Proceedings: American Association for Automotive Medicine Annual Conference (Vol. 7, pp. 312-323). Association for the Advancement of Automotive Medicine.

APPENDIX A. AUTOMOTIVE RESTRAINT TIMELINE

Bohlin, N. I. (1964). Studies of three-point restraint harness systems in full-scale barrier crashes and sled runs (No. 640854). SAE Technical Paper.

Bohlin, N. I. (1967). A STATISTICAL ANALYSIS OF 28,000 ACCIDENT CASES WITH EMPHASIS ON OCCUPANT RESTRAINT VALUE. IN: SEAT BELTS: THE DEVELOPMENT OF AN ESSENTIAL SAFETY FEATURE. Publication of: Society of Automotive Engineers.

Bollier, D., Claybrook, J. (1986). Freedom from harm: the civilizing influence of health, safety and environmental regulation.

Brown, R. H. (1965). U.S. Patent No. 3,219,361. Washington, DC: U.S. Patent and Trademark Office.

Cutler, D. D. (1991). The continuing struggle for automotive safety. Seton Hall Legislative Journal, 15(2), 453-482.

DeHaven, H. (1942). Mechanical analysis of survival in falls from heights of fifty to one hundred and fifty feet. War medicine, 2, 586-596.

Evans, L. (1986). The effectiveness of safety belts in preventing fatalities. Accident Analysis Prevention, 18(3), 229-241.

Evans, L. (1991). Traffic safety and the driver. Science Serving Society.

Griswold, I. R. W., De, H. H. (1955). U.S. Patent No. 2,710,649. Washington, DC: U.S. Patent and Trademark Office.

Hedlund, J. (1985). Casualty reduction resulting from safety belt use laws. In effectiveness of safety belt use laws. A Multinational examination, Washington, DC. DOT HS-807-018.

Kratzke, S. R. (1995). Regulatory history of automatic crash protection in FMVSS 208. SAE transactions, 1497-1506.

Neff, R. J. (1962). Webbing for use in automobile seat belts. In Proceedings: American Association for Automotive Medicine Annual Conference (Vol. 6, pp. 133-138). Association for the Advancement of Automotive Medicine.

SAE J4a. Motor Vehicle Seat Belt Assemblies, Society of Automotive Engineers, Warrendale, PA 1955.

SAE J4b. Motor Vehicle Seat Belt Assemblies, Society of Automotive Engineers, Warrendale, PA 1964.

Shively, J. J. (1937). U.S. Patent No. 2,071,903. Washington, DC: U.S. Patent and Trademark Office.

APPENDIX A. AUTOMOTIVE RESTRAINT TIMELINE

The White House, "Remarks of the President at Signing of the Highway Safety Act and the Traffic Safety Act," press release, September 9, 1966, cited in National Traffic and Motor Vehicle Safety Act of 1966, Legislative History, vol. 1, p. 31, published by NHTSA in 1985.

Traffic and Motor Vehicle Safety Act, 15 U.S.C. § 1392 (1966).

US Department of Commerce. (Jan. 31, 1967). Report on the Development of the Initial Federal Motor Vehicle Safety Standards.

Viano, D. (2003). INTRODUCTION: LAP-SHOULDER BELTS: SOME HISTORICAL ASPECTS. IN: SEAT BELTS: THE DEVELOPMENT OF AN ESSENTIAL SAFETY FEATURE. Publication of: Society of Automotive Engineers.

Wilson, W. B. (1979). Occupant restraint legislation handbook: a guide for proponents. The Administration.

Zador, P. L., Ciccone, M. A. (1993). Automobile driver fatalities in frontal impacts: air bags compared with manual belts. American Journal of Public Health, 83(5), 661-666.

Appendix B

Reclined PMHS Frontal Impact Sled Test Experiments

B.1 Positioning Data

Table B.1: PMHS Position Data.

Measurement Point	Definition	X (mm)	Y (mm)	Z (mm)	SD X (mm)	SD Y (mm)	SD Z (mm)
Origin of Coordinate System	Seat edge right side	3196,7	-	461,7	-	-	-
Head Top	-	3472,0	-	1264,0	50,1	-	33,6
Head Origin Position	Midpoint btw L/R zygomatic processes	3512,5	-	1137,6	26,7	-	32,1
Head Angle (deg)	Midpoint btw L/R zygomatic process to midpoint btw eye orbits	33,6			2,6		
T1 Origin Position	Center of vertebral body	3467,3	-	996,3	23,1	-	15,1
T8 Origin Position	Center of vertebral body	3421,4	-	844,3	8,0	-	12,2
T11 Origin Position	Center of vertebral body	3374,2	-	787,5	4,4	-	15,9
L1 Origin Position	Center of vertebral body	3320,9	-	744,1	3,1	-	22,6
L3 Origin Position	Center of vertebral body	3255,0	-	701,7	14,0	-	5,9
Pelvis Origin Position	Midpoint btw L/R PSIS	3187,7	-	574,7	9,1	-	11,3
Pelvis Angle (deg)*	Angle of the vector from pubic symphysis to midpoint btw L/R ASIS with respect to the vertical	74,3			8,7		
Pelvis Angle (deg)*	Angle of the vector from midpoint btw L/R PSIS to midpoint btw L/R ASIS with respect to the horizontal	66,5			7,2		
Right Knee Position	Center lateral epicondyle	2658,7	-	750,9	19,9	-	28,2
Left Knee Position	Center lateral epicondyle	2660,2	-	754,1	7,0	-	28,6
Right Heel Position	-	2419,7	-	350,9	1,9	-	7,5
Left Heel Position	-	2418,8	-	351,2	5,4	-	12,5
Sternum	Midpoint btw L/R 4th rib insertion points	3299,3	-	928,8	20,8	-	15,5
HP Center btw R and L*	Midpoint btw L/R hip points	3078,0	-	642,7	1,4	-	3,3

*Data from S0531 was not included in the pelvis measurements

B.2 Pelvis and Sacrum Injuries

Subjects 1 and 3 exhibited pelvis fractures at the right iliac wing between the ASIS and AIIS landmarks B.1. The injuries were identified from post-test CT-scans and confirmed by autopsy. These injuries were coded using the Abbreviated Injury Scale (AIS) and were both coded as AIS-2 as the posterior arch and remainder of the pelvic wing remained intact.

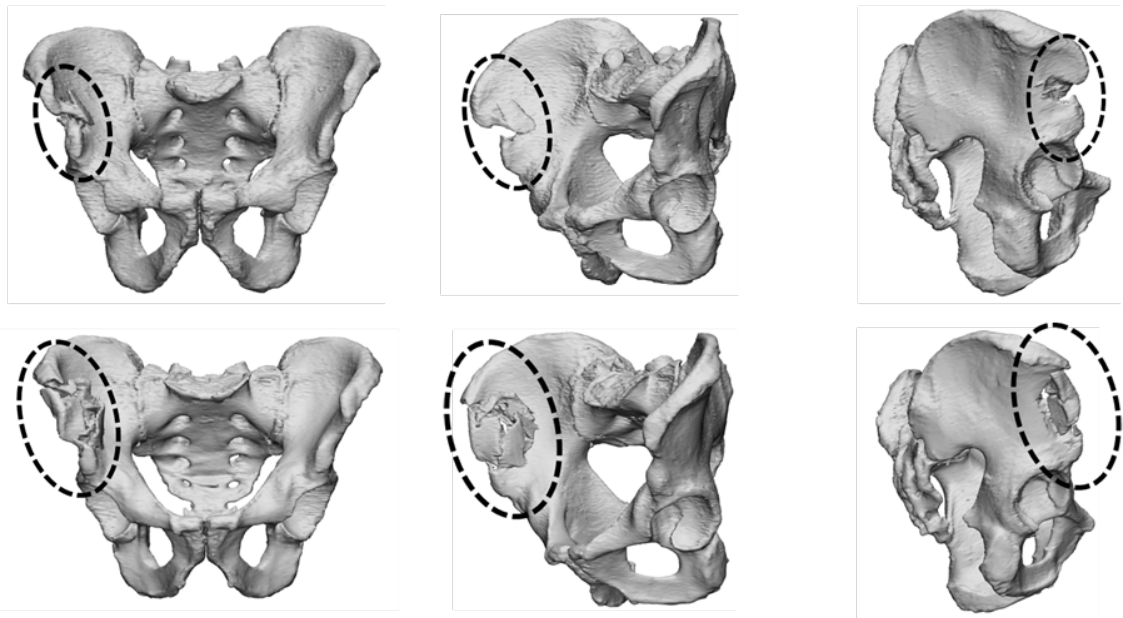


Figure B.1: Reconstructed pelvis CT-scans from Subject 1 (top row) and Subject 3 (bottom row), showing the fractures at the right iliac wing between the ASIS and AIIS landmarks in both of these subjects.

Timing of injury was identified by the strain gauge rosettes affixed to the lateral surface of the iliac wing between the ASIS and AIIS landmarks. The strain time history from gauges on the right iliac wing of Subject 1 indicated a sharp drop in strain beginning at approximately 60-65 ms due to the sensor being displaced from the fracture that happened at this time B.2. The lap-belt force at the time of fracture was 7.8 kN. Subject 3 exhibited fracture at approximately 53-58 ms (lap-belt force of 6.6 kN), which was indicated simultaneously with a peak in strain and drop in lap-belt force. Subjects 2 and 4, who did not sustain pelvis fractures had peak lap-belt forces of 4.6 kN and 8.3 kN. Subjects 1, 2, 3, and 5 all sustained injuries at the lower-level of the sacrum. Subject

APPENDIX B. RECLINED PMHS FRONTAL IMPACT SLED TEST EXPERIMENTS

1 exhibited a fracture at the S3-S4 level; Subject 2 exhibited a fracture at S5; Subject 3 exhibited a fracture at S4; and Subject 5 exhibited a fracture at S3.

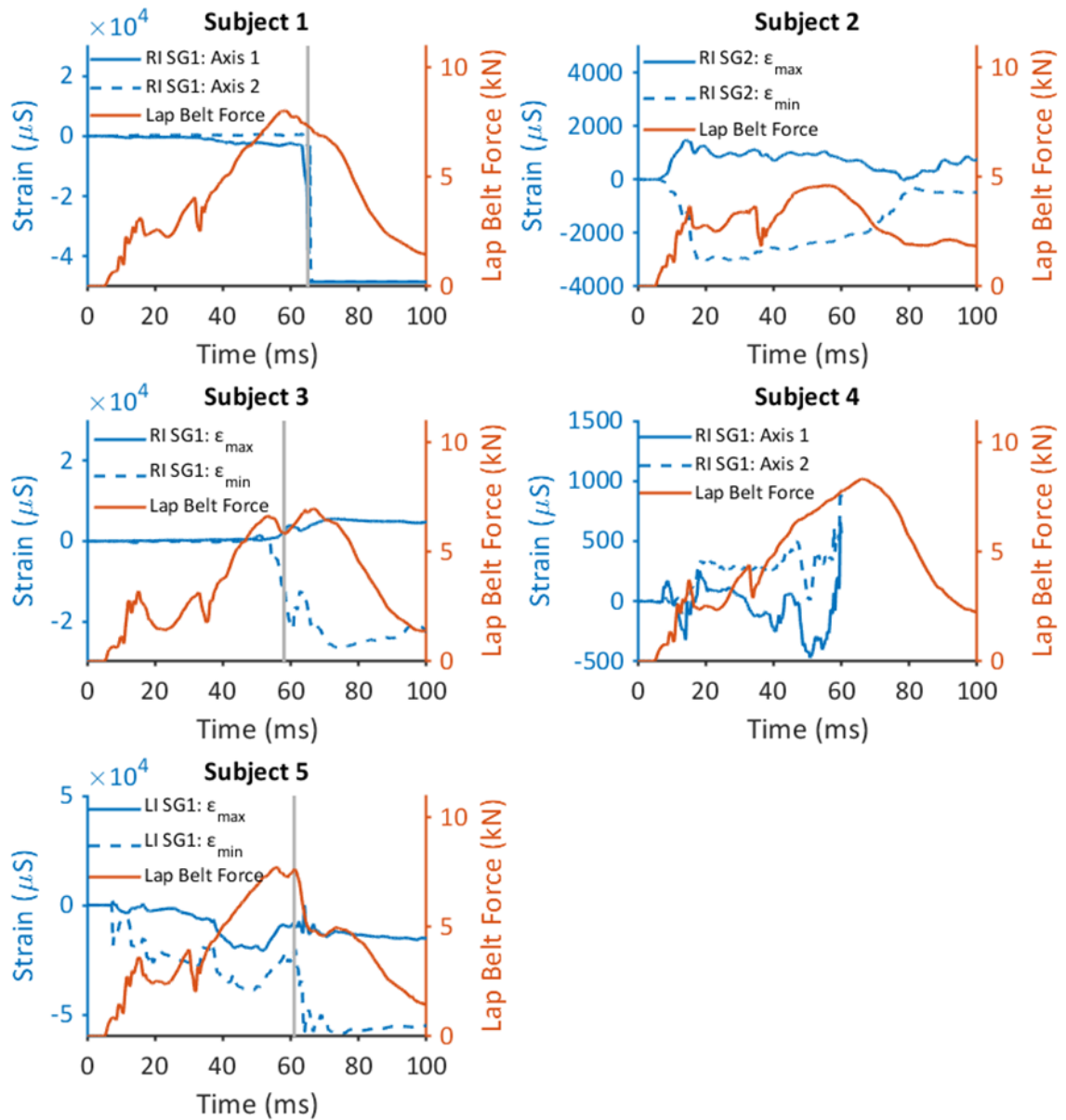


Figure B.2: Strain gauge signals (left axes) and outboard lap-belt forces (right axes) for all five subjects at either the lateral right iliac wing (“RI”) or left iliac wing (“LI”). For subjects 1 and 4, the third axis of the strain gauge rosette failed. Subject 4’s sensor detached at 60 ms.

Appendix C

Reclined HBM Frontal Impact Simulations

C.1 Positioning Data

APPENDIX C. RECLINED HBM FRONTAL IMPACT SIMULATIONS

Figure C.1: HBM position data relative to PMHS.

Coordinates in FE-Model global coordinate system	Definition	Tests (average)			THUMS Nominal dx (mm) dz (mm)	GHBMC Nominal dx (mm) dz (mm)	THUMS Amt12deg dx (mm) dz (mm)	GHBMC Amt12deg dx (mm) dz (mm)	THUMS Pos12deg dx (mm) dz (mm)	GHBMC Pos12deg dx (mm) dz (mm)	THUMS Avg. (deg)	GHBMC Avg. (deg)				
		X (mm)	Z (mm)	SD X Z (mm)												
Position	Definition	X (mm)	Z (mm)	SD X Z (mm)	dx (mm)	dz (mm)	dx (mm)	dz (mm)	dx (mm)	dz (mm)	Avg. (deg)	Avg. (deg)				
Buck LCS	Seat edge right side	3691.7	461.7	-	0.0	0.0	0.0	0.0	0.0	0.0	0.0	0.0				
Head	Midpoint btw. Zyg. Proc.	3512.5	1137.6	26.7	-8.2	27.8	-31.5	-3.1	-9.6	31.4	-27.9	-3.6	-10.1	17.3	-16.8	-14.0
T1	Center of vertebral body	3467.3	996.3	23.1	-9.4	-33.6	-7.2	-36.4	-5.6	-29.6	-10.0	-36.5	-14.0	-43.7	-12.5	-44.8
T8	Center of vertebral body	3421.4	844.3	8.0	-13.0	-24.0	-4.3	-20.7	-9.4	-20.0	-4.2	-22.1	-23.3	-32.0	-12.9	-28.0
T11	Center of vertebral body	3374.2	787.5	4.4	-15.9	-24.6	-10.7	-15.9	-11.9	-20.6	-6.0	-20.8	-25.9	-33.4	-19.4	-23.2
L1	Center of vertebral body	3320.9	744.1	3.1	-9.9	-15.9	-2.7	-9.8	-7.4	-9.2	-1.6	-8.4	-18.2	-27.0	-7.8	-21.6
L3	Center of vertebral body	3255.0	701.7	14.0	1.3	-10.1	4.9	0.7	-2.6	9.6	-0.5	18.7	-6.3	-22.1	5.9	-19.7
Pelvis Origin (PSIS)	Midpoint btw. L/R PSIS	3191.4	577.0	6.6	7.9	-1.4	-0.3	-9.8	15.9	24.7	7.9	13.5	-3.2	-24.1	-13.8	-31.3
Angle	Definition	Avg. (deg)	SD (deg)		Avg. (deg)		Avg. (deg)		Avg. (deg)		Avg. (deg)					
Nyquist	Pubic symphysis to midpoint btw L/R ASIS wrt the horizontal	165.2	5.2		161.6		162.7		149.6		150.7		173.6		174.7	

C.2 HBM Responses compared to PMHS Responses: Nominal Pelvis Angle

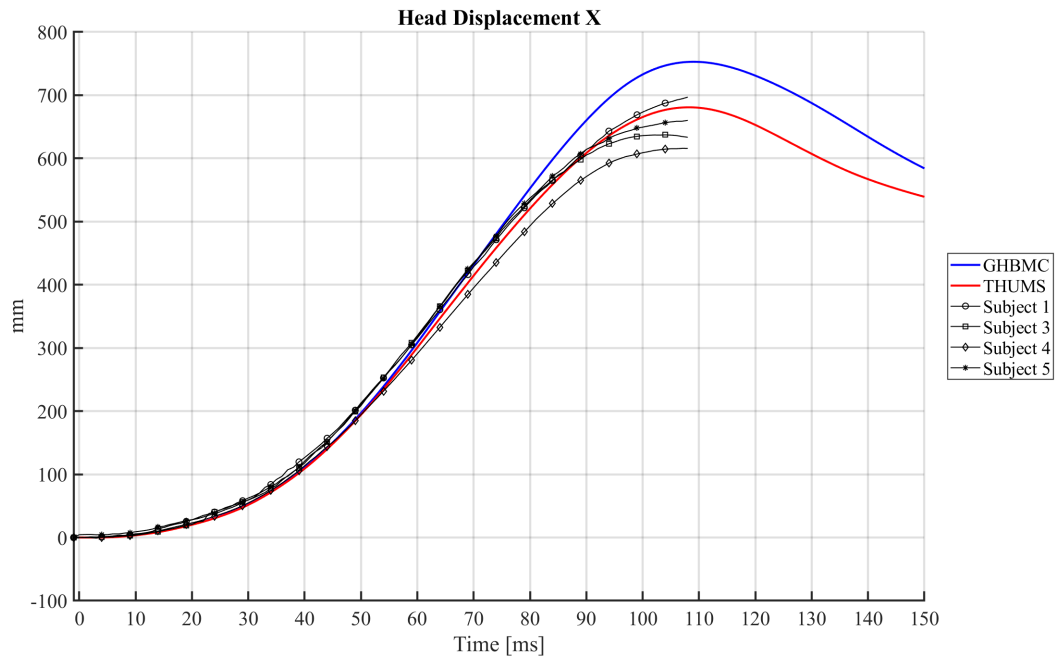


Figure C.2: Head X Displacement: HBMs (Nominal Pelvis Angle) vs. PMHS

APPENDIX C. RECLINED HBM FRONTAL IMPACT SIMULATIONS

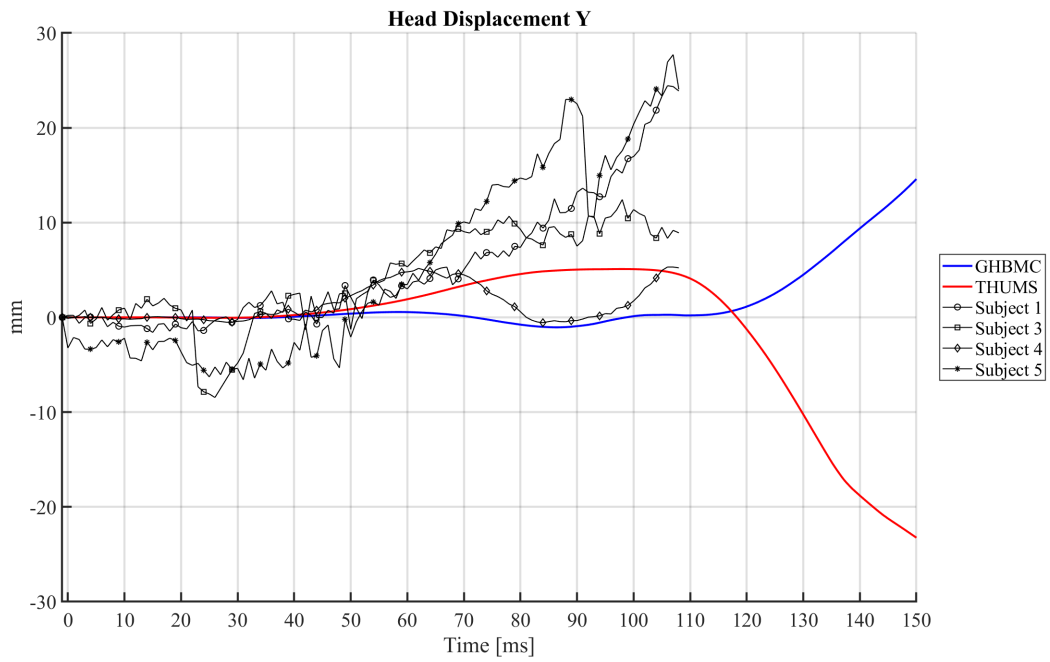


Figure C.3: Head Y Displacement: HBMs (Nominal Pelvis Angle) vs. PMHS

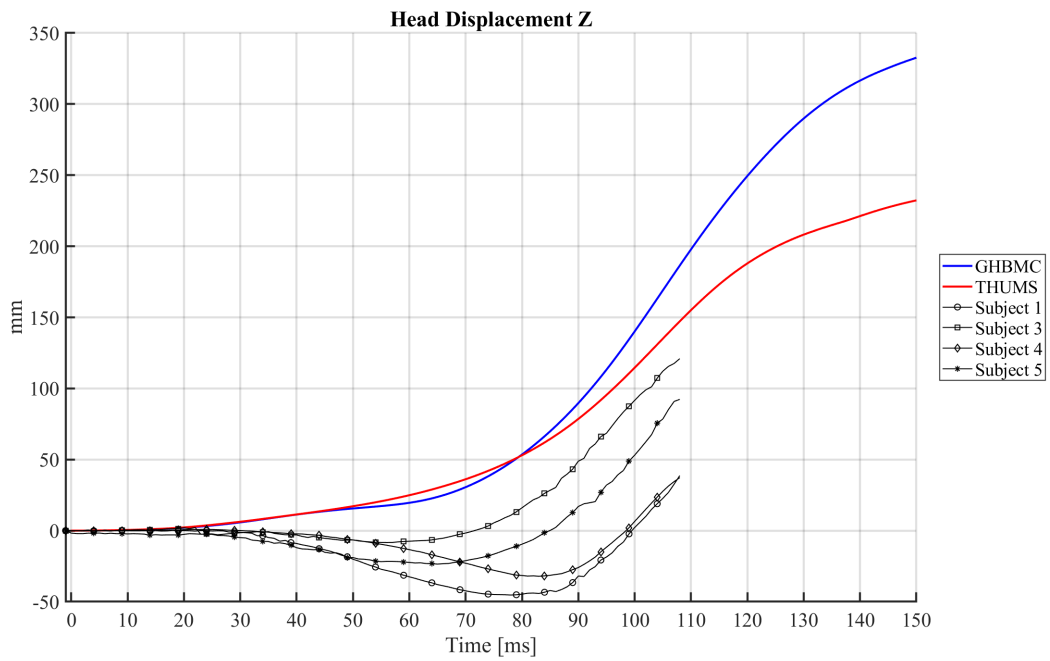


Figure C.4: Head Z Displacement: HBMs (Nominal Pelvis Angle) vs. PMHS

APPENDIX C. RECLINED HBM FRONTAL IMPACT SIMULATIONS

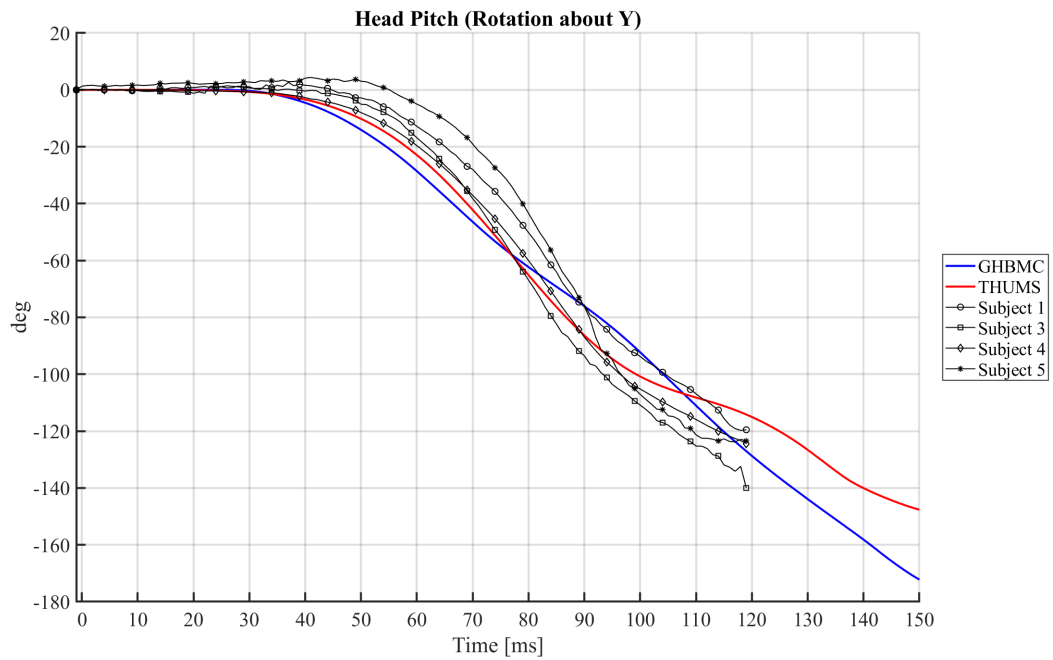


Figure C.5: Head Y Rotation: HBMs (Nominal Pelvis Angle) vs. PMHS

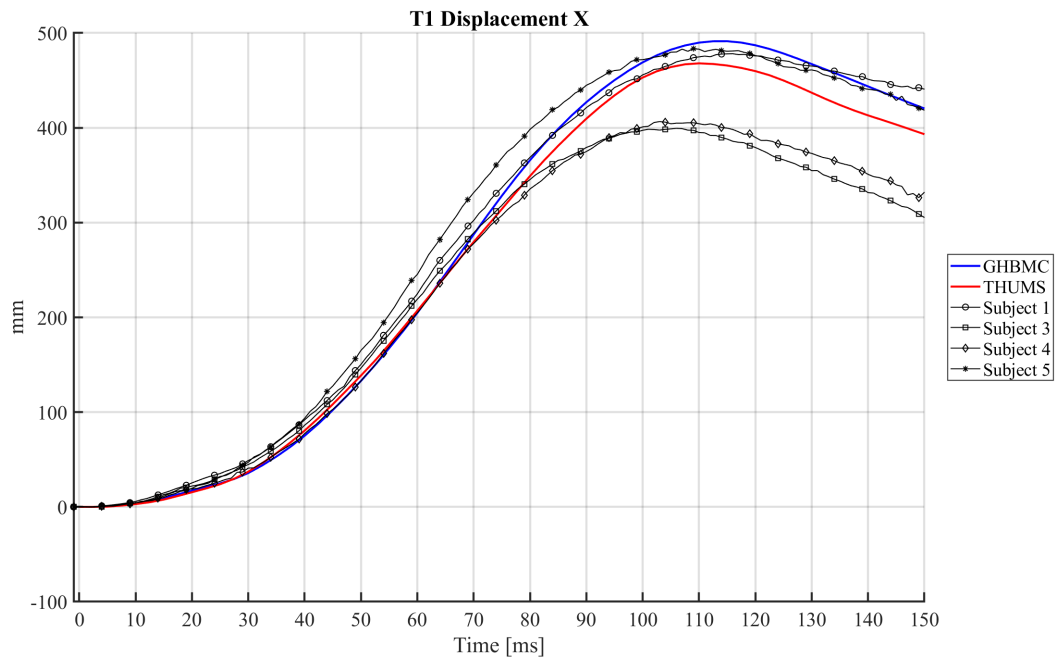


Figure C.6: T1 X Displacement: HBMs (Nominal Pelvis Angle) vs. PMHS

APPENDIX C. RECLINED HBM FRONTAL IMPACT SIMULATIONS

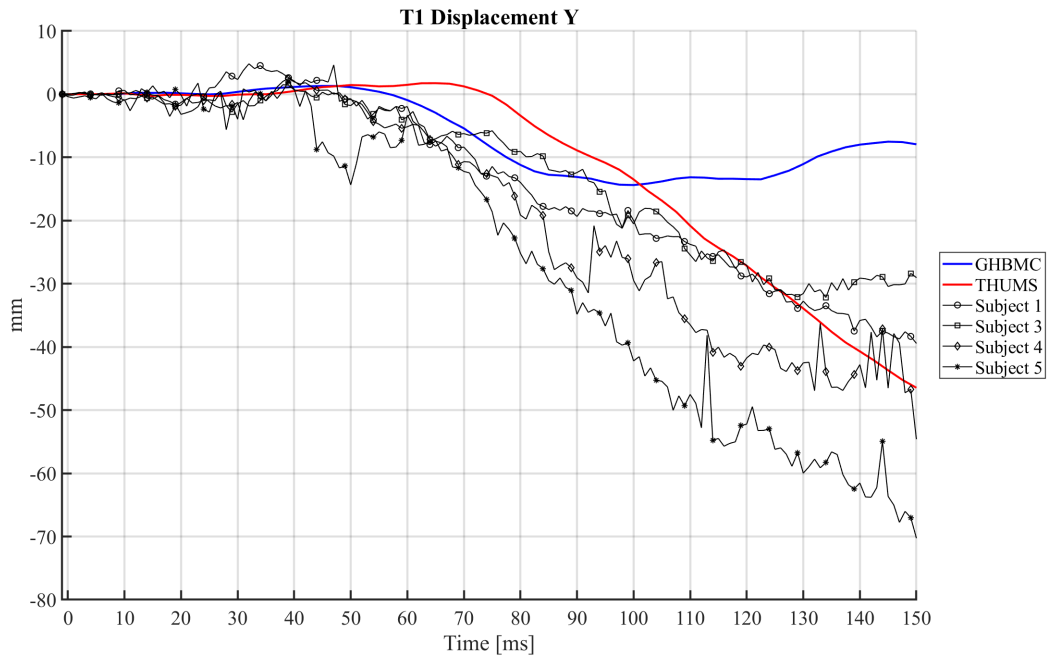


Figure C.7: T1 Y Displacement: HBMs (Nominal Pelvis Angle) vs. PMHS

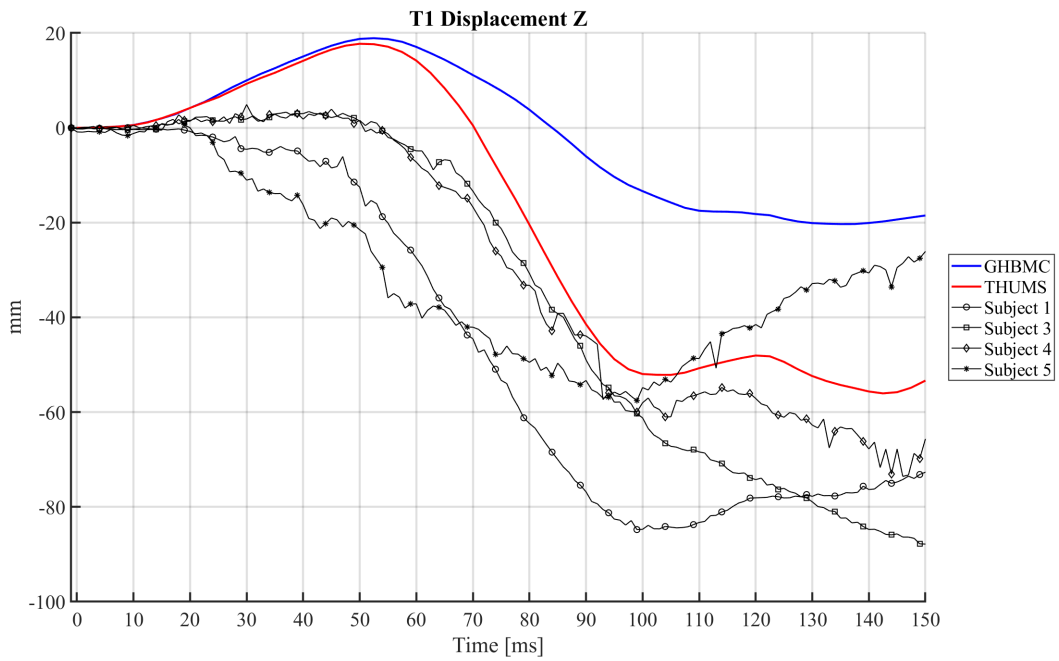


Figure C.8: T1 Z Displacement: HBMs (Nominal Pelvis Angle) vs. PMHS

APPENDIX C. RECLINED HBM FRONTAL IMPACT SIMULATIONS

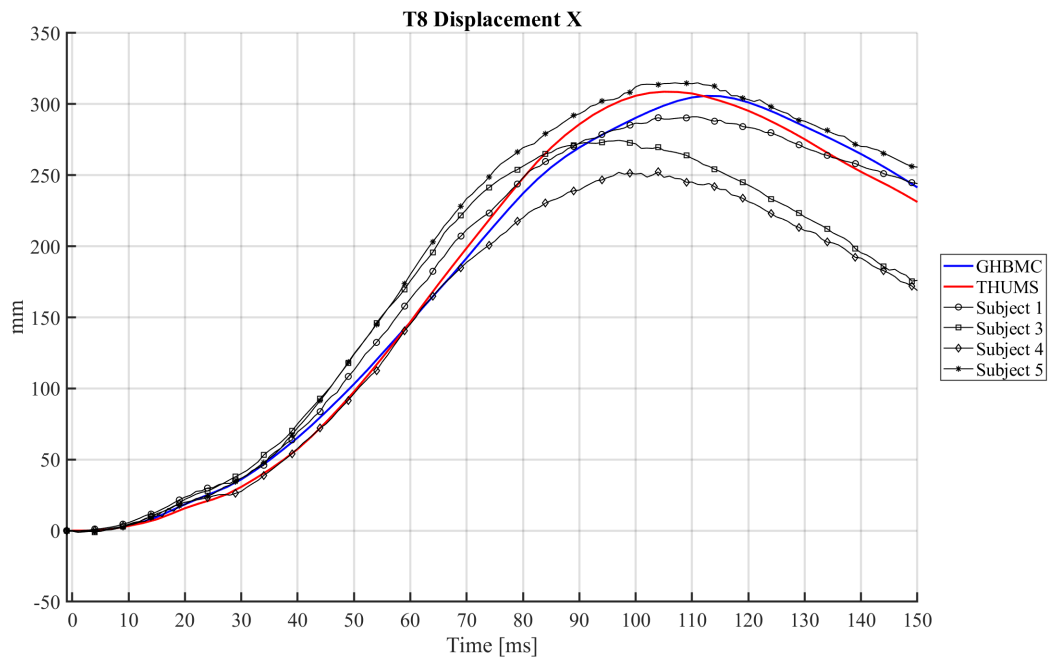


Figure C.9: T8 X Displacement: HBMs (Nominal Pelvis Angle) vs. PMHS

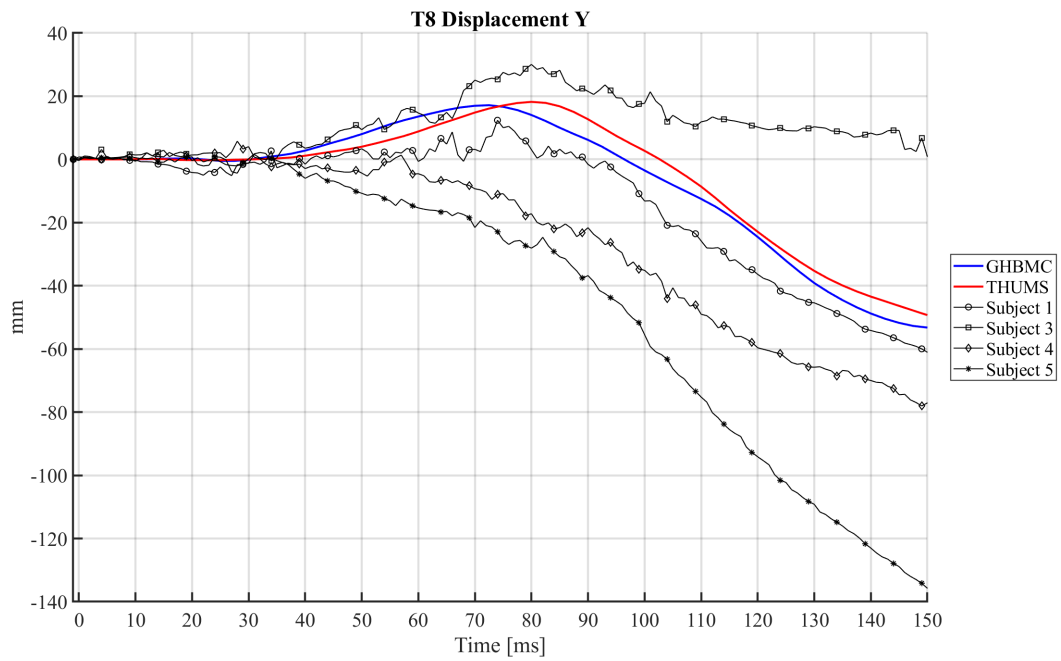


Figure C.10: T8 Y Displacement: HBMs (Nominal Pelvis Angle) vs. PMHS

APPENDIX C. RECLINED HBM FRONTAL IMPACT SIMULATIONS

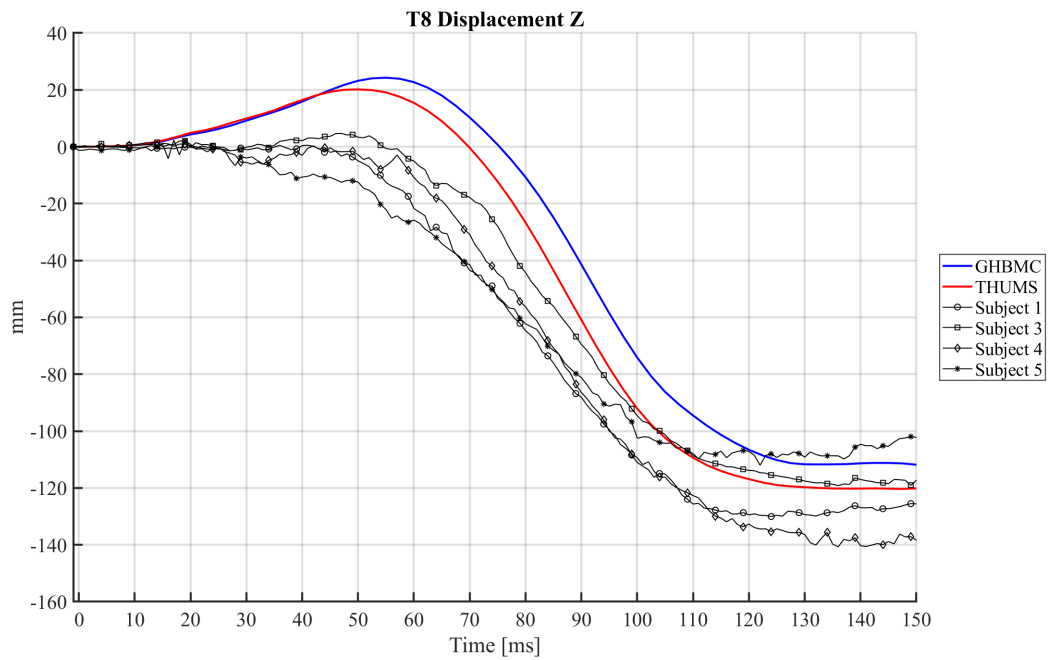


Figure C.11: T8 Z Displacement: HBMs (Nominal Pelvis Angle) vs. PMHS

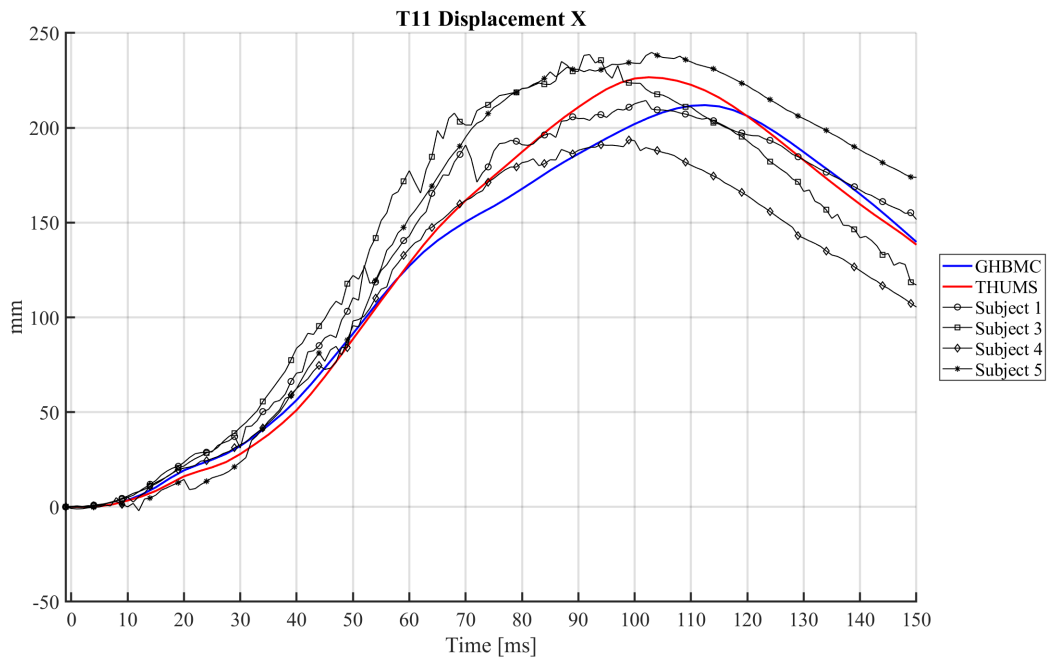


Figure C.12: T11 X Displacement: HBMs (Nominal Pelvis Angle) vs. PMHS

APPENDIX C. RECLINED HBM FRONTAL IMPACT SIMULATIONS

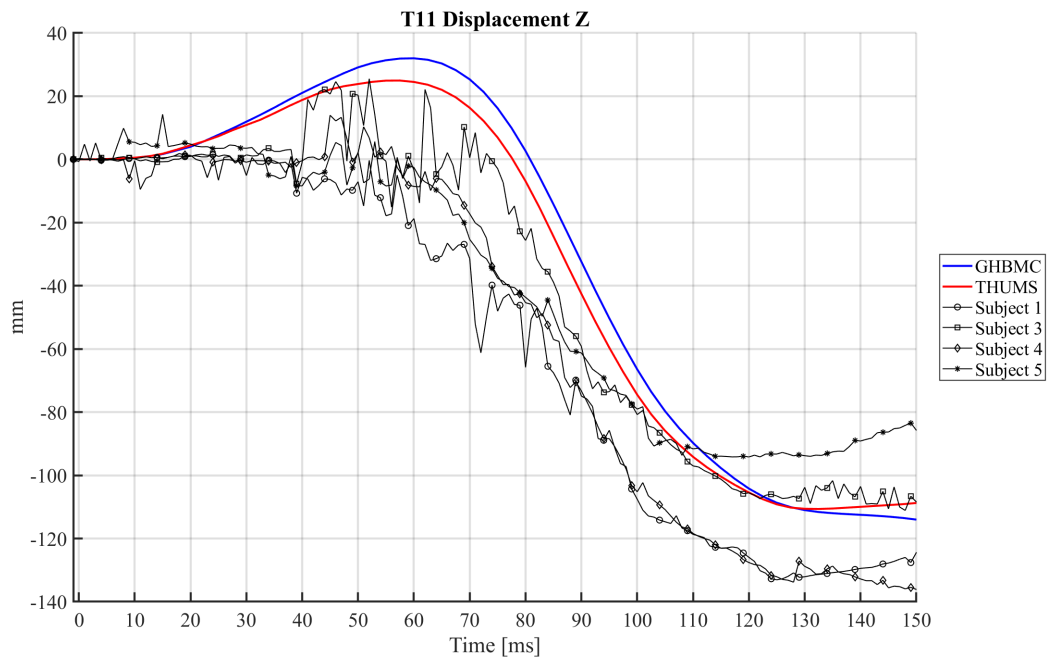


Figure C.13: T11 Z Displacement: HBMs (Nominal Pelvis Angle) vs. PMHS

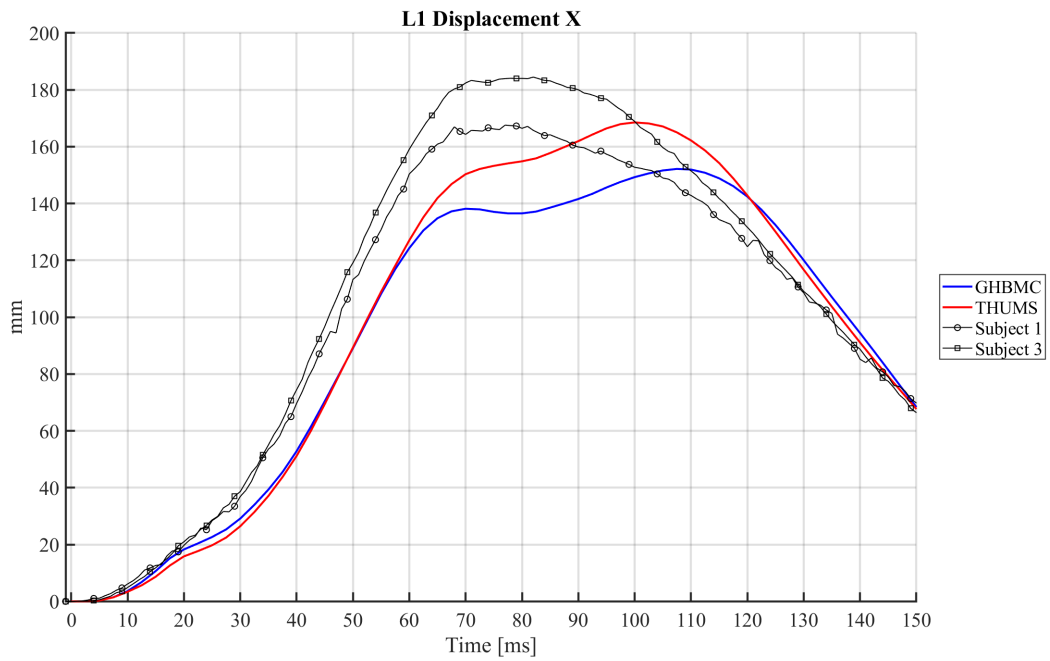


Figure C.14: L1 X Displacement: HBMs (Nominal Pelvis Angle) vs. PMHS

APPENDIX C. RECLINED HBM FRONTAL IMPACT SIMULATIONS

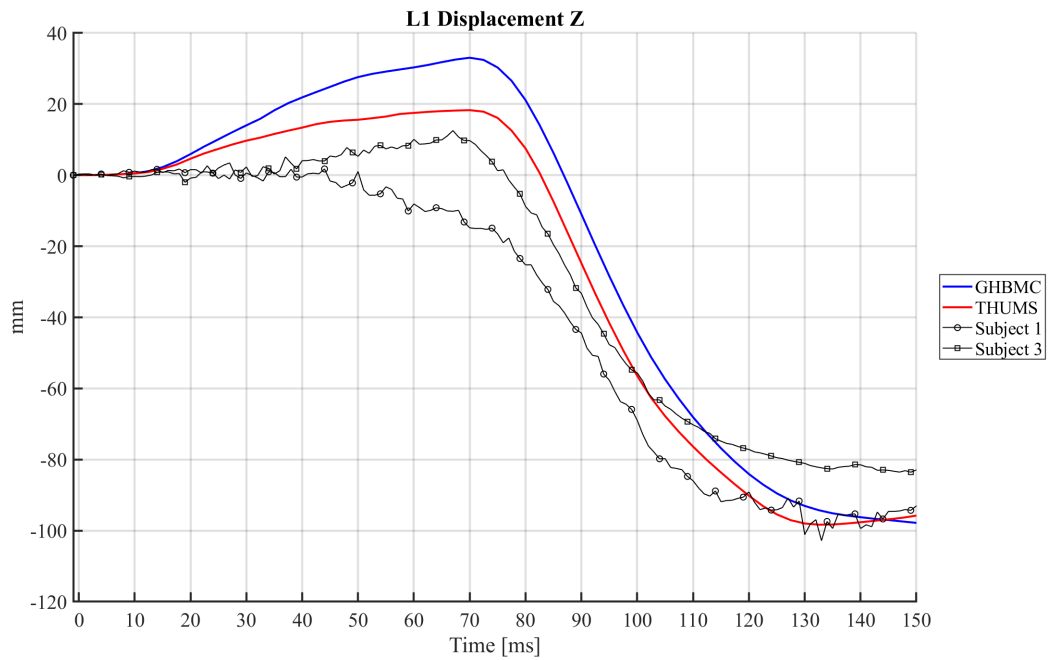


Figure C.15: L1 Z Displacement: HBMs (Nominal Pelvis Angle) vs. PMHS

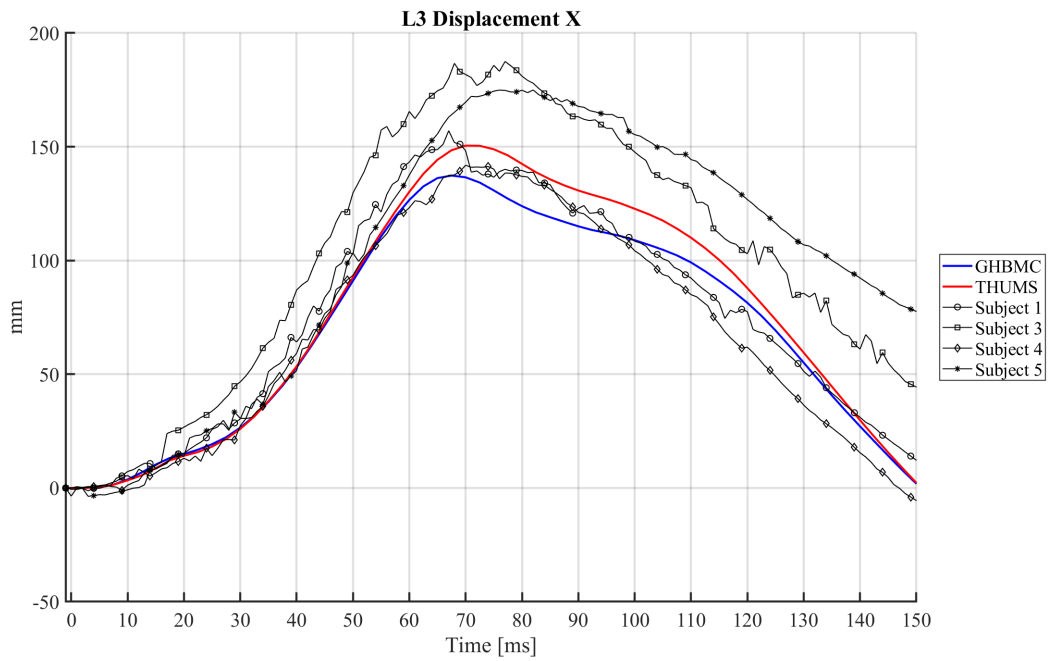


Figure C.16: L3 X Displacement: HBMs (Nominal Pelvis Angle) vs. PMHS

APPENDIX C. RECLINED HBM FRONTAL IMPACT SIMULATIONS

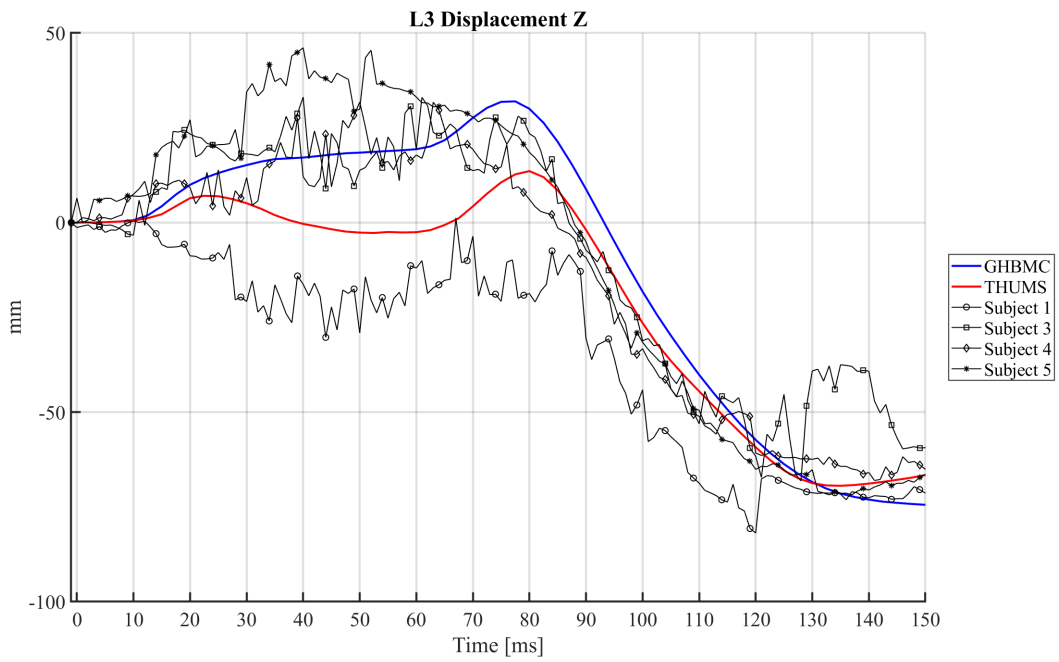


Figure C.17: L3 Z Displacement: HBMs (Nominal Pelvis Angle) vs. PMHS

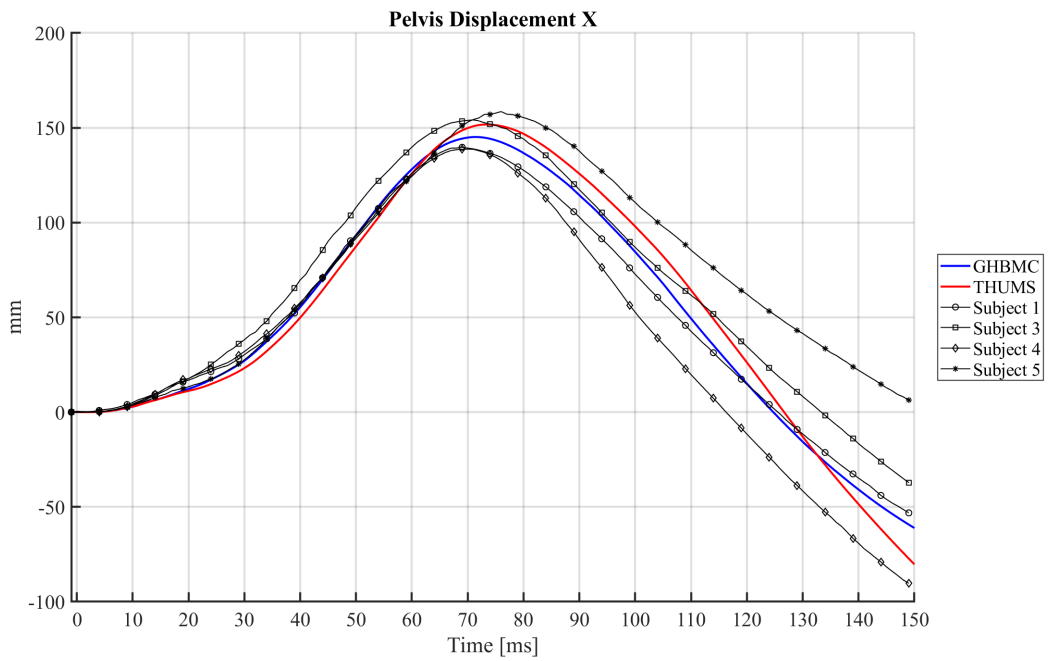


Figure C.18: Pelvis X Displacement: HBMs (Nominal Pelvis Angle) vs. PMHS

APPENDIX C. RECLINED HBM FRONTAL IMPACT SIMULATIONS

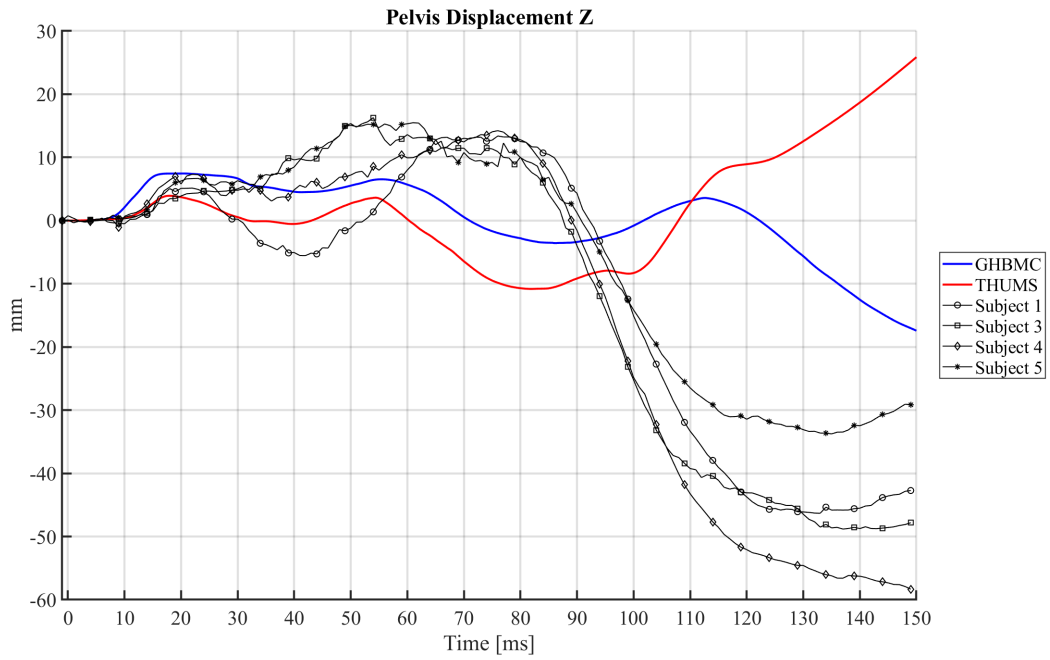


Figure C.19: Pelvis Z Displacement: HBMs (Nominal Pelvis Angle) vs. PMHS

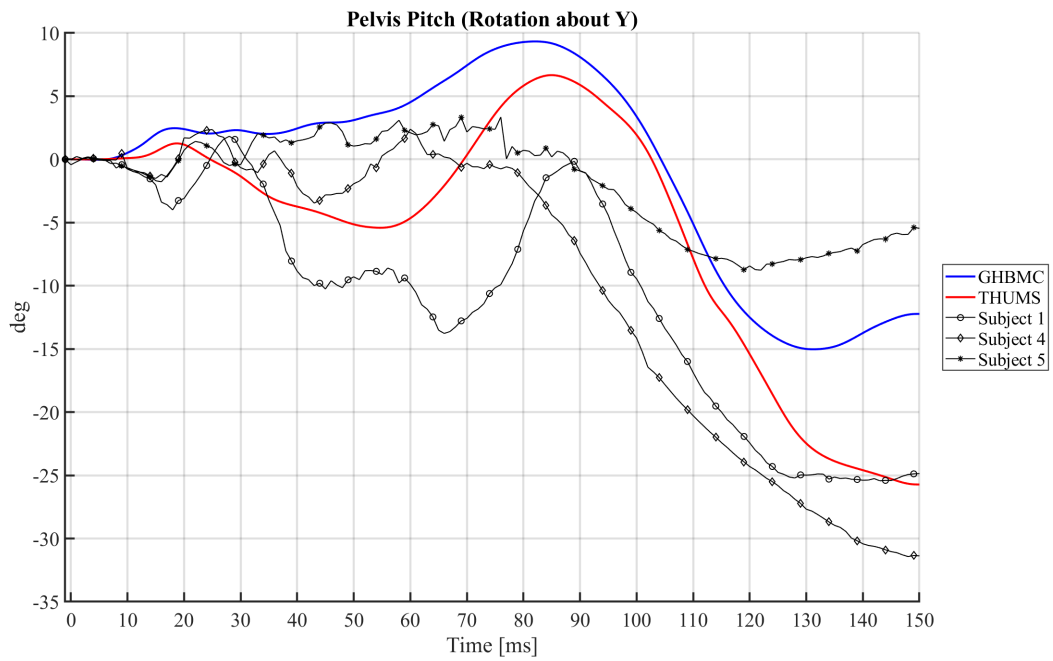


Figure C.20: Pelvis Y Rotation: HBMs (Nominal Pelvis Angle) vs. PMHS

APPENDIX C. RECLINED HBM FRONTAL IMPACT SIMULATIONS



Figure C.21: Lap Belt Resultant Displacement: HBMs (Nominal Pelvis Angle) vs. PMHS

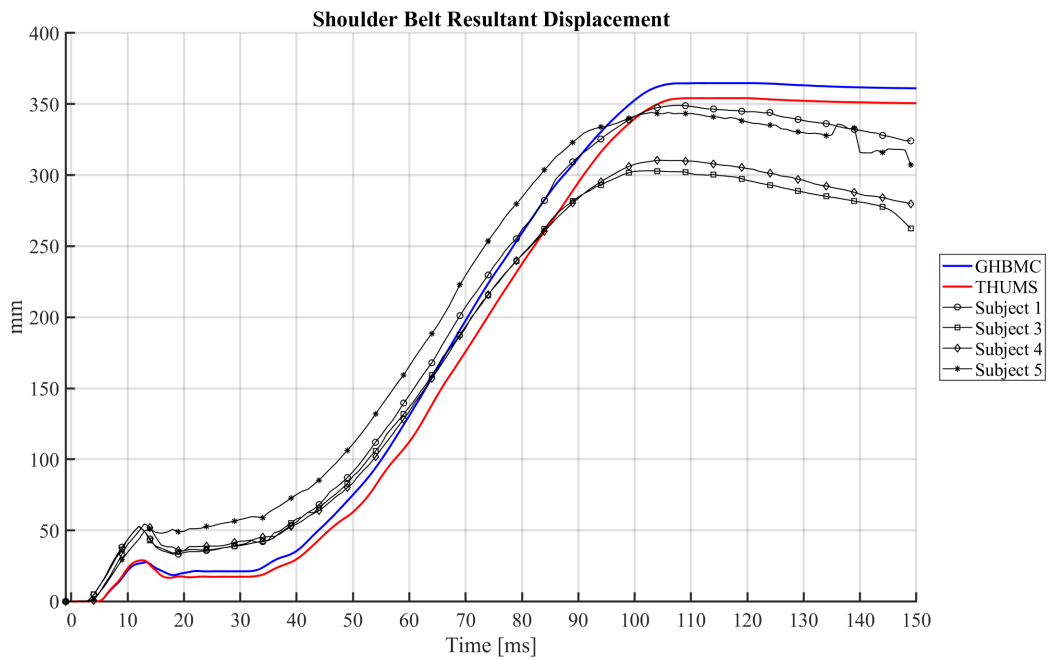


Figure C.22: Shoulder Belt Resultant Displacement: HBMs (Nominal Pelvis Angle) vs. PMHS

APPENDIX C. RECLINED HBM FRONTAL IMPACT SIMULATIONS

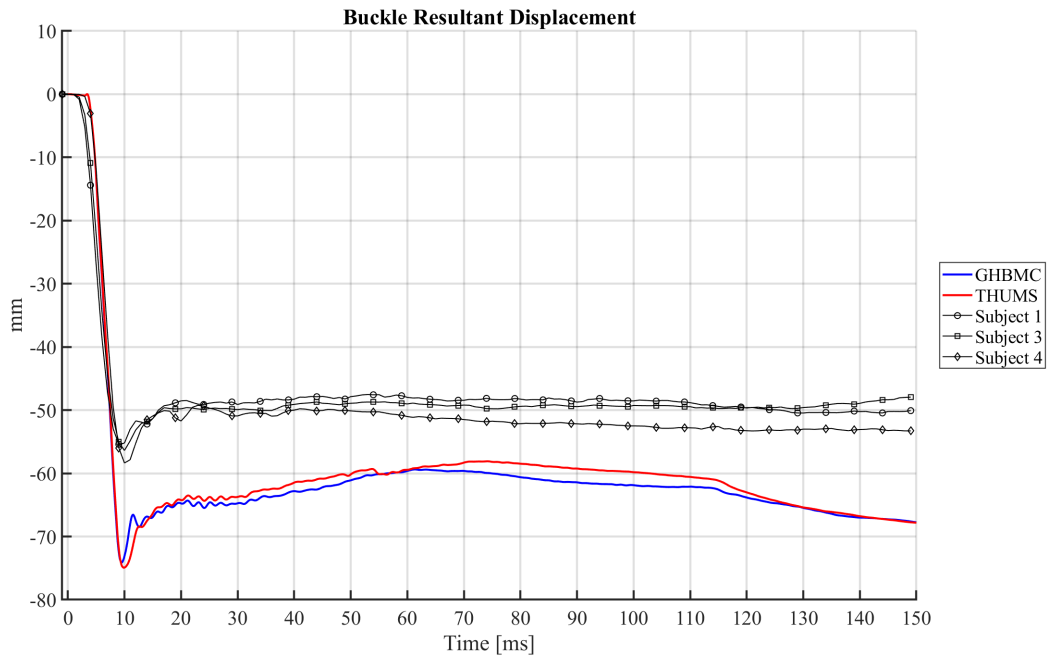


Figure C.23: Buckle Resultant Displacement: HBMs (Nominal Pelvis Angle) vs. PMHS

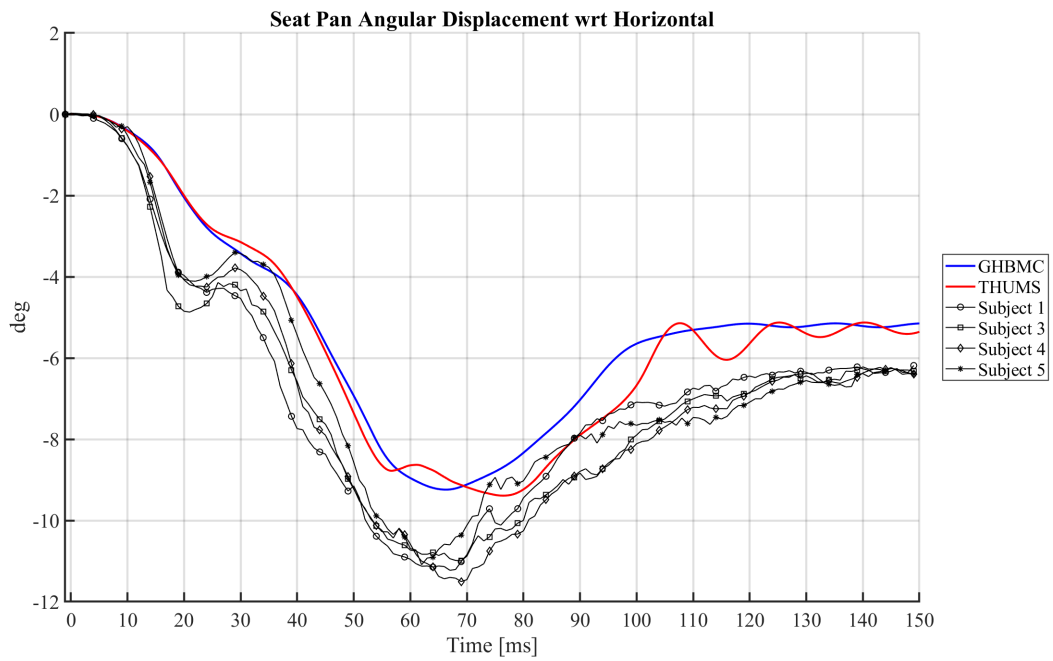


Figure C.24: Seat Pan Angular Displacement: HBMs (Nominal Pelvis Angle) vs. PMHS

APPENDIX C. RECLINED HBM FRONTAL IMPACT SIMULATIONS

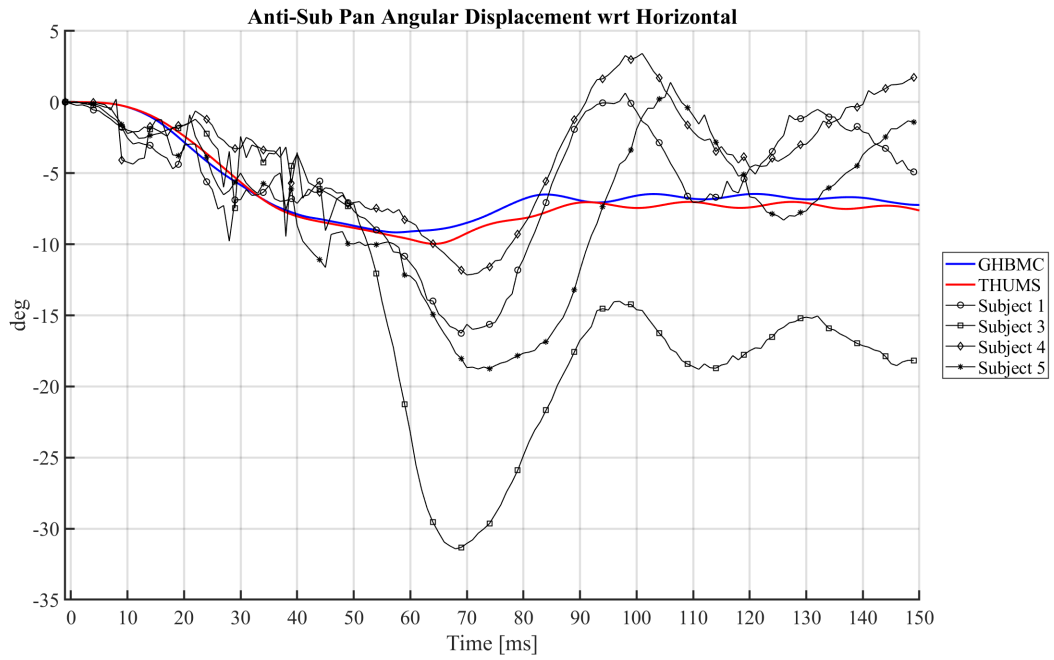


Figure C.25: Anti-Sub Pan Angular Displacement: HBMs (Nominal Pelvis Angle) vs. PMHS

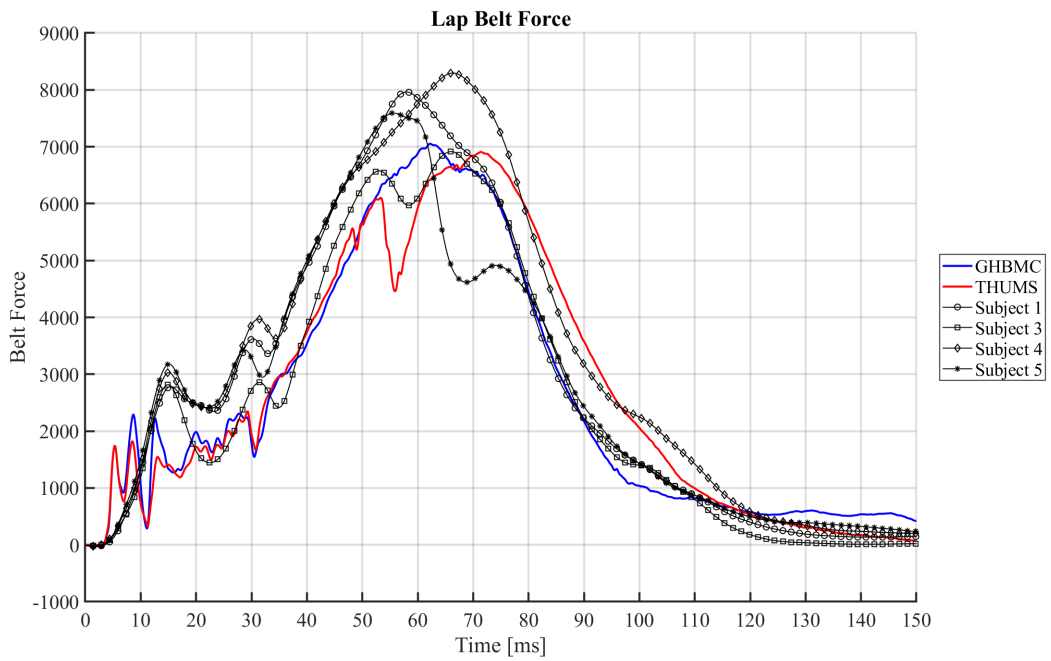


Figure C.26: Lap Belt Tension: HBMs (Nominal Pelvis Angle) vs. PMHS

APPENDIX C. RECLINED HBM FRONTAL IMPACT SIMULATIONS

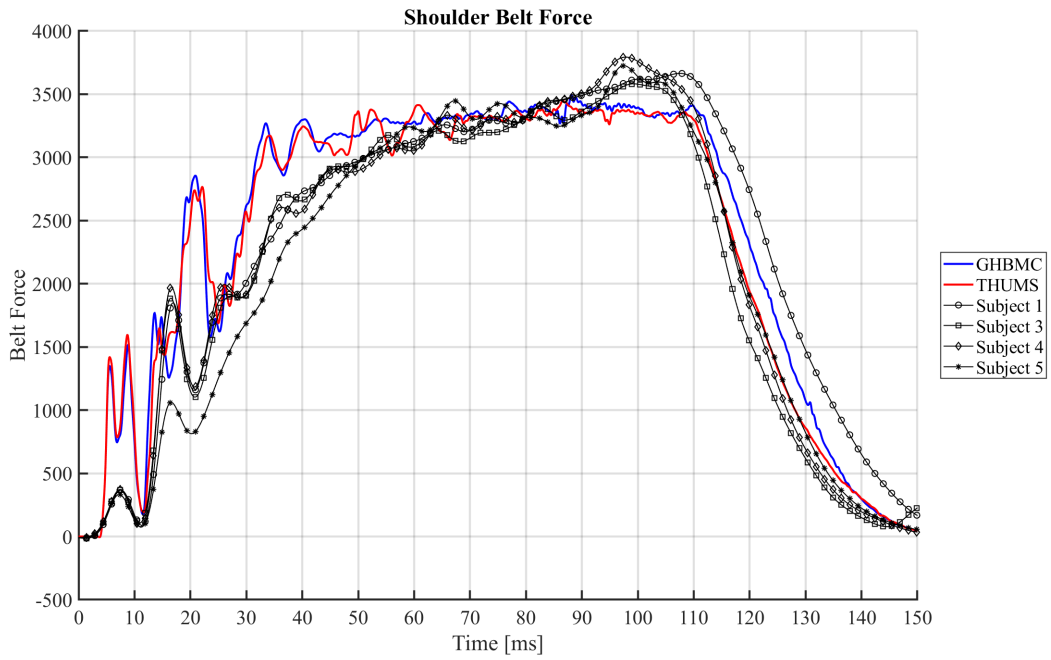


Figure C.27: Shoulder Belt Tension: HBMs (Nominal Pelvis Angle) vs. PMHS

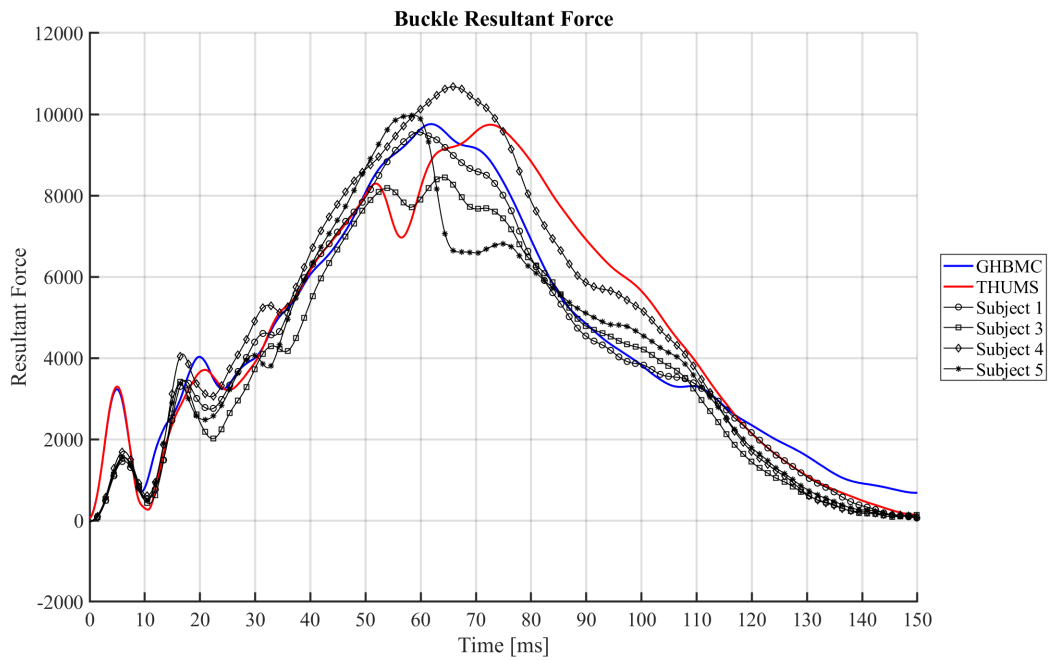


Figure C.28: Buckle Resultant Force: HBMs (Nominal Pelvis Angle) vs. PMHS

APPENDIX C. RECLINED HBM FRONTAL IMPACT SIMULATIONS

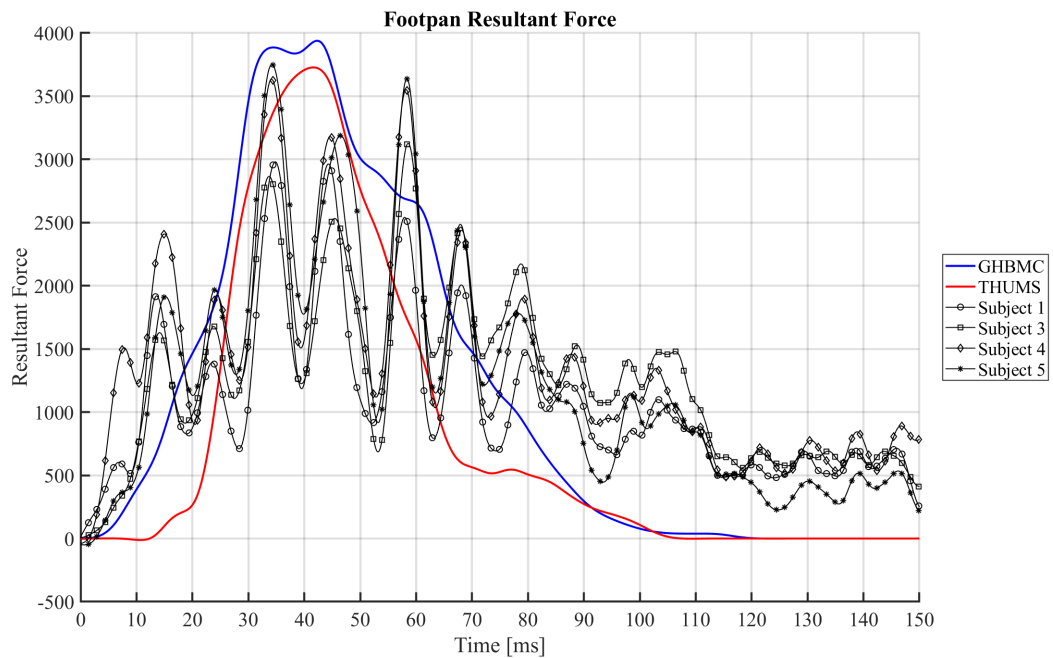


Figure C.29: Foot Pan Resultant Force: HBMs (Nominal Pelvis Angle) vs. PMHS

C.3 HBM Responses compared to PMHS Responses: 12° Posterior Pelvis Angle

APPENDIX C. RECLINED HBM FRONTAL IMPACT SIMULATIONS

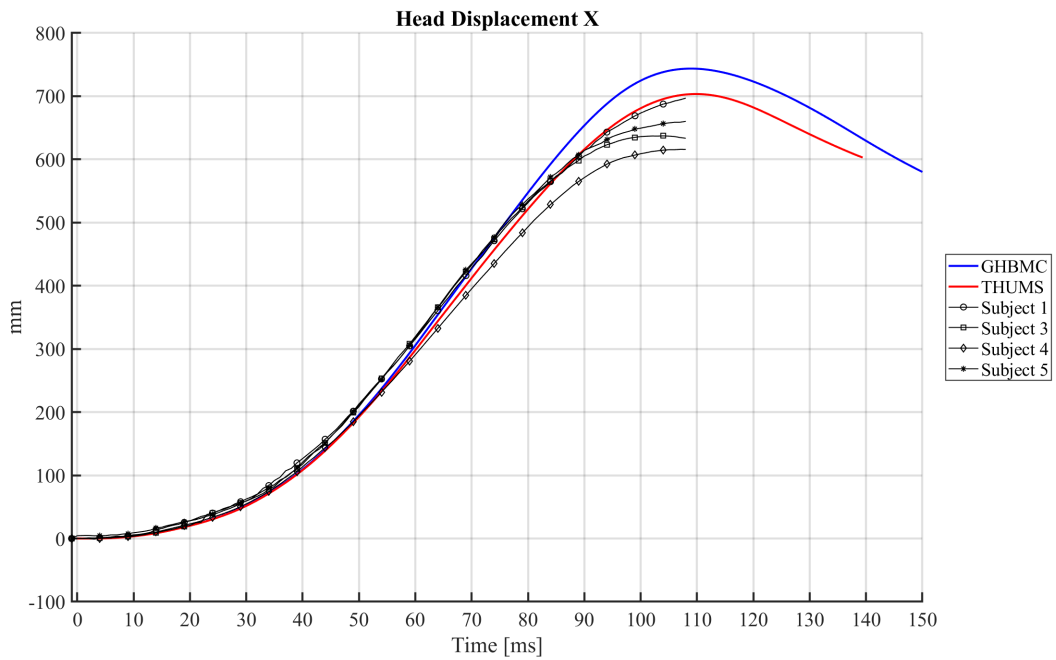


Figure C.30: Head X Displacement: HBMs (12°Posterior Pelvis Angle) vs. PMHS

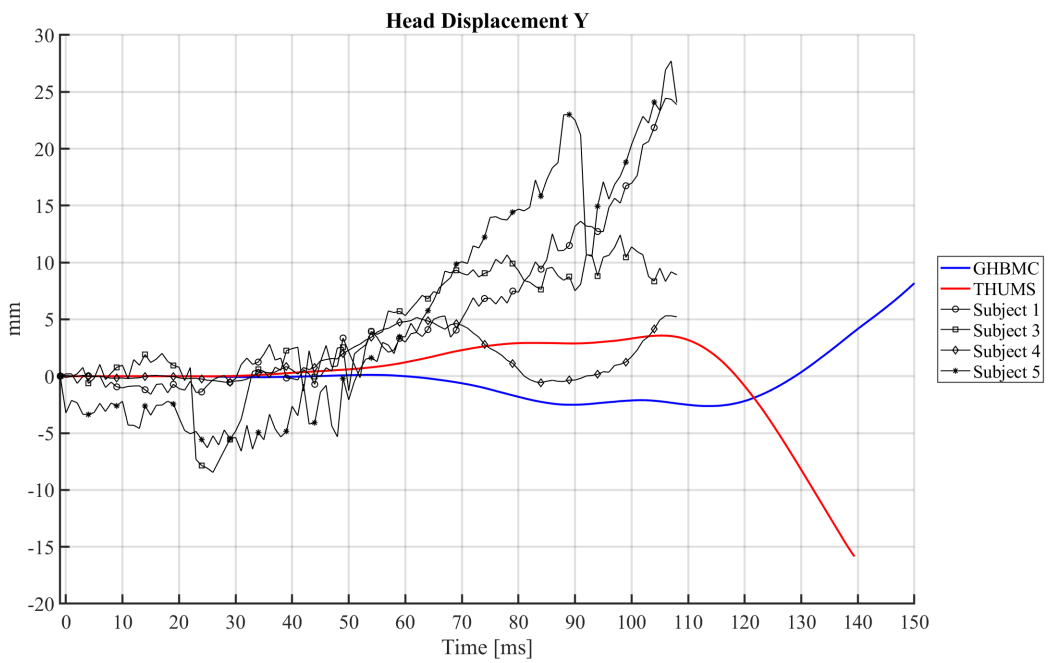


Figure C.31: Head Y Displacement: HBMs (12°Posterior Pelvis Angle) vs. PMHS

APPENDIX C. RECLINED HBM FRONTAL IMPACT SIMULATIONS

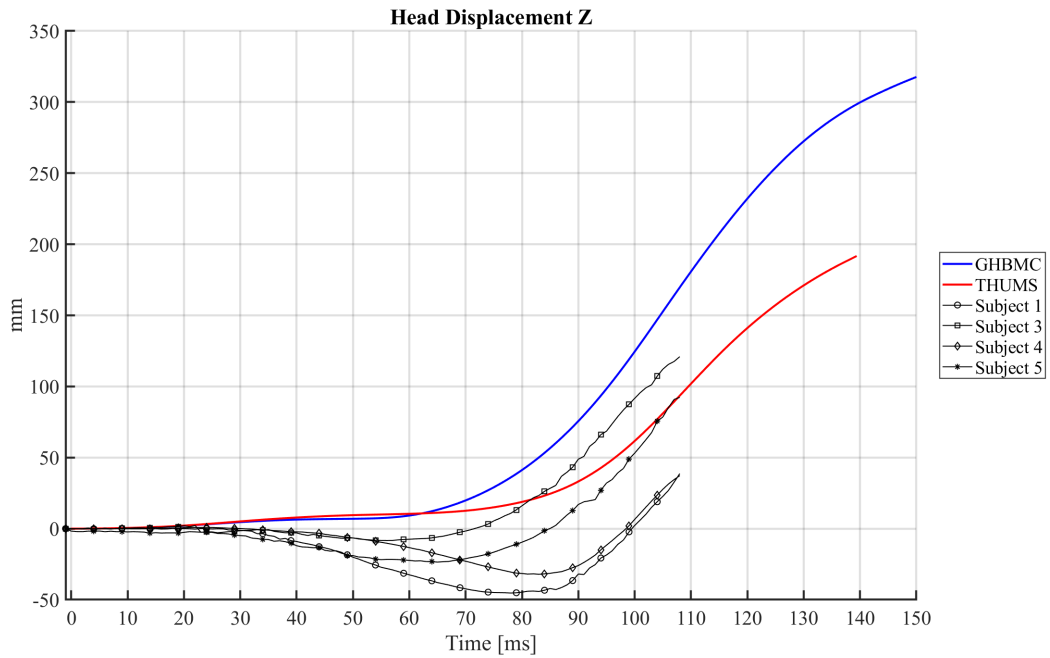


Figure C.32: Head Z Displacement: HBMs (12°Posterior Pelvis Angle) vs. PMHS

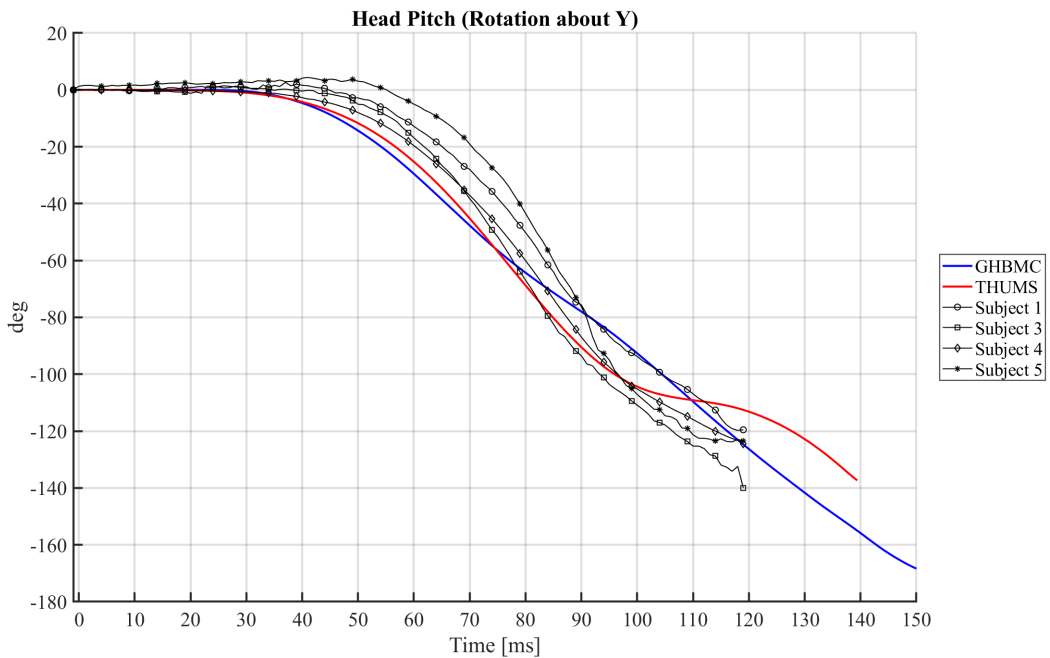


Figure C.33: Head Y Rotation: HBMs (12°Posterior Pelvis Angle) vs. PMHS

APPENDIX C. RECLINED HBM FRONTAL IMPACT SIMULATIONS

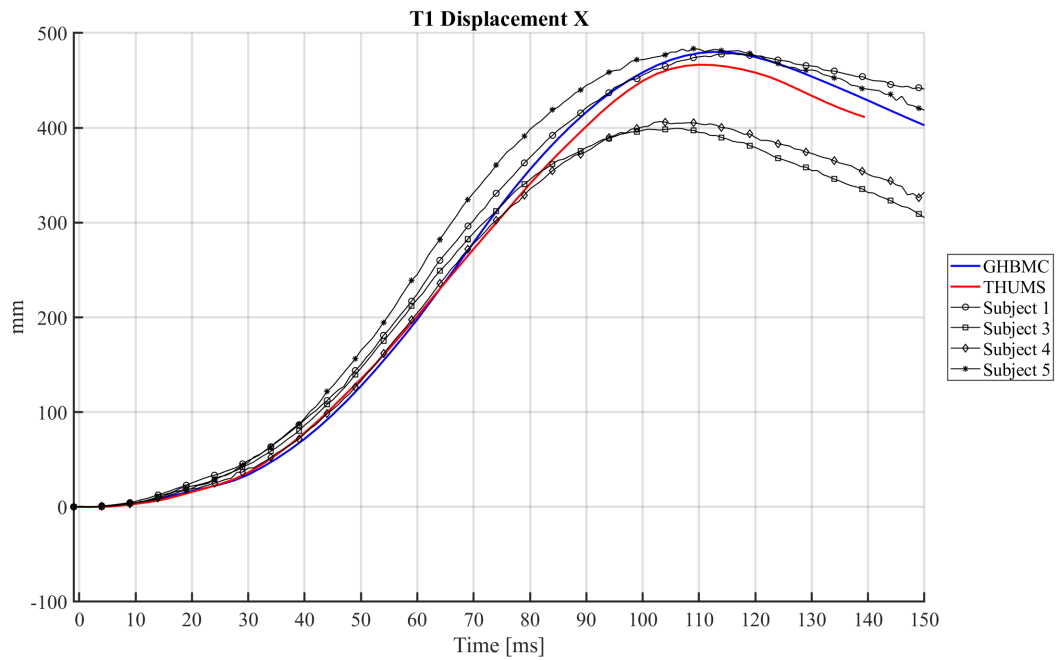


Figure C.34: T1 X Displacement: HBMs (12°Posterior Pelvis Angle) vs. PMHS

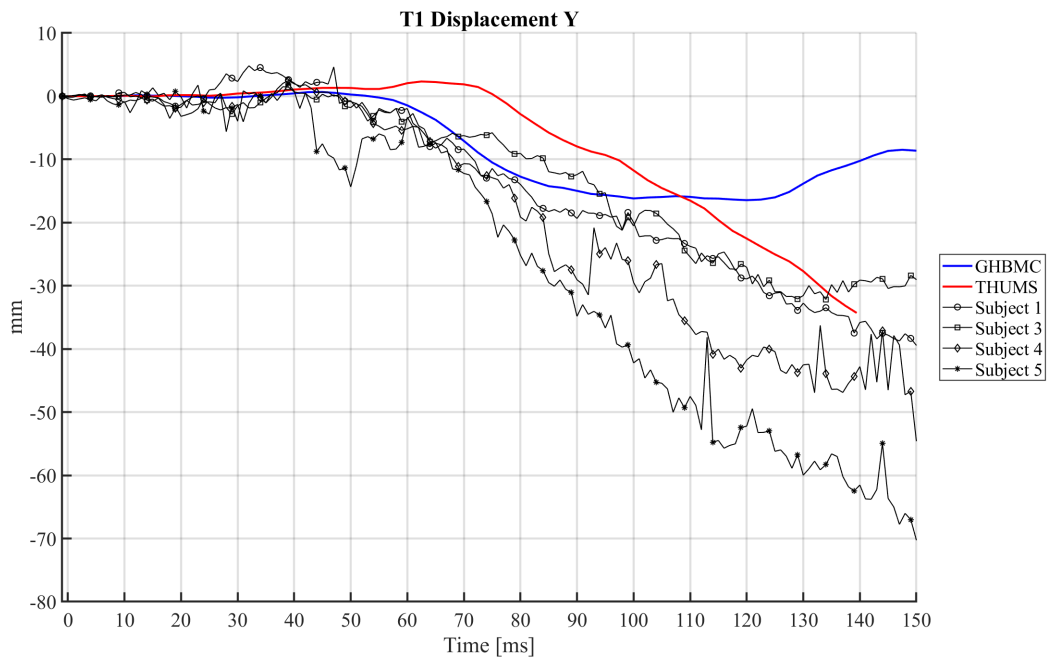


Figure C.35: T1 Y Displacement: HBMs (12°Posterior Pelvis Angle) vs. PMHS

APPENDIX C. RECLINED HBM FRONTAL IMPACT SIMULATIONS

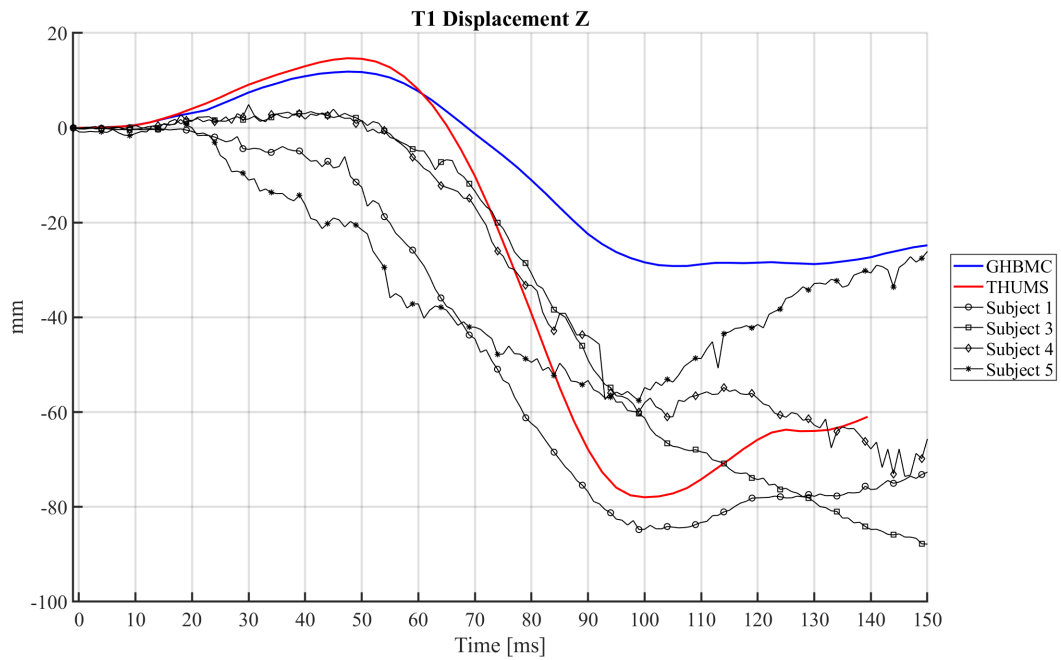


Figure C.36: T1 Z Displacement: HBMs (12°Posterior Pelvis Angle) vs. PMHS

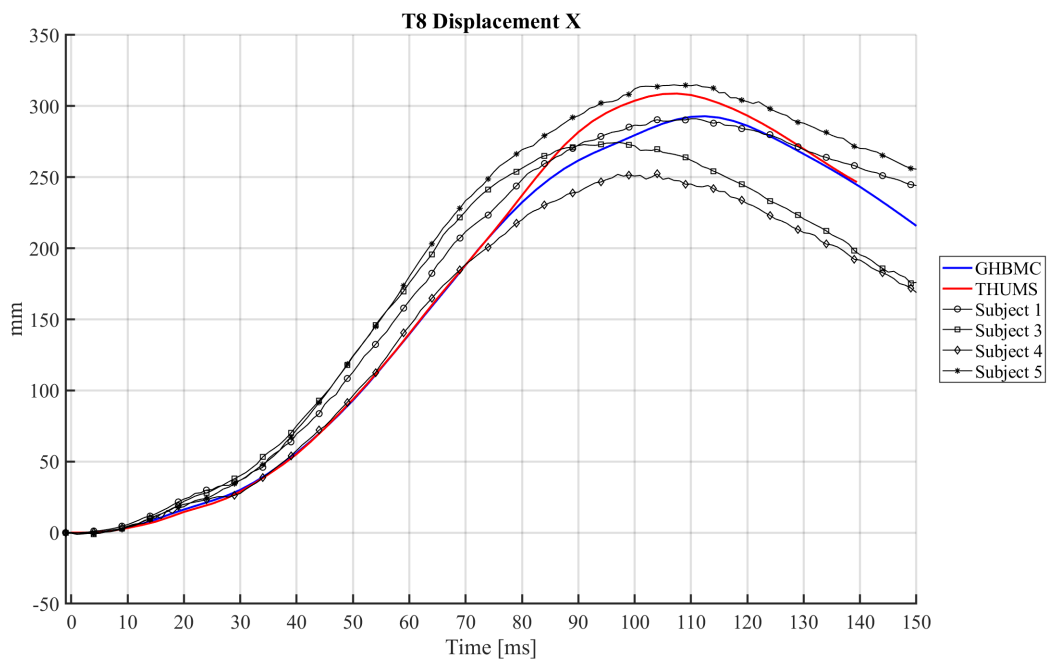


Figure C.37: T8 X Displacement: HBMs (12°Posterior Pelvis Angle) vs. PMHS

APPENDIX C. RECLINED HBM FRONTAL IMPACT SIMULATIONS

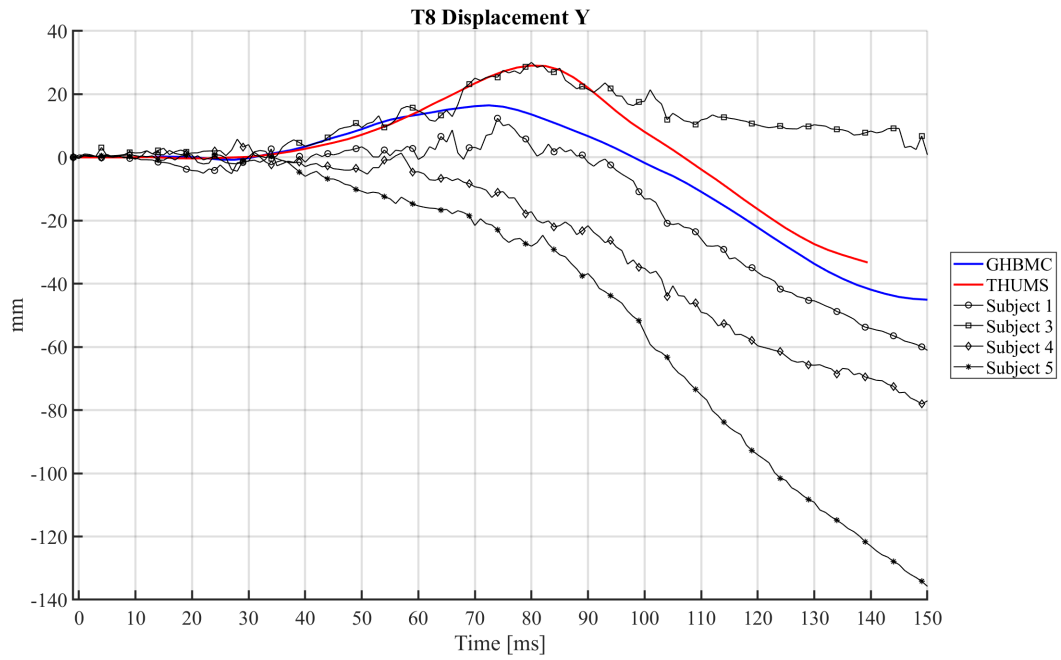


Figure C.38: T8 Y Displacement: HBMs (12°Posterior Pelvis Angle) vs. PMHS

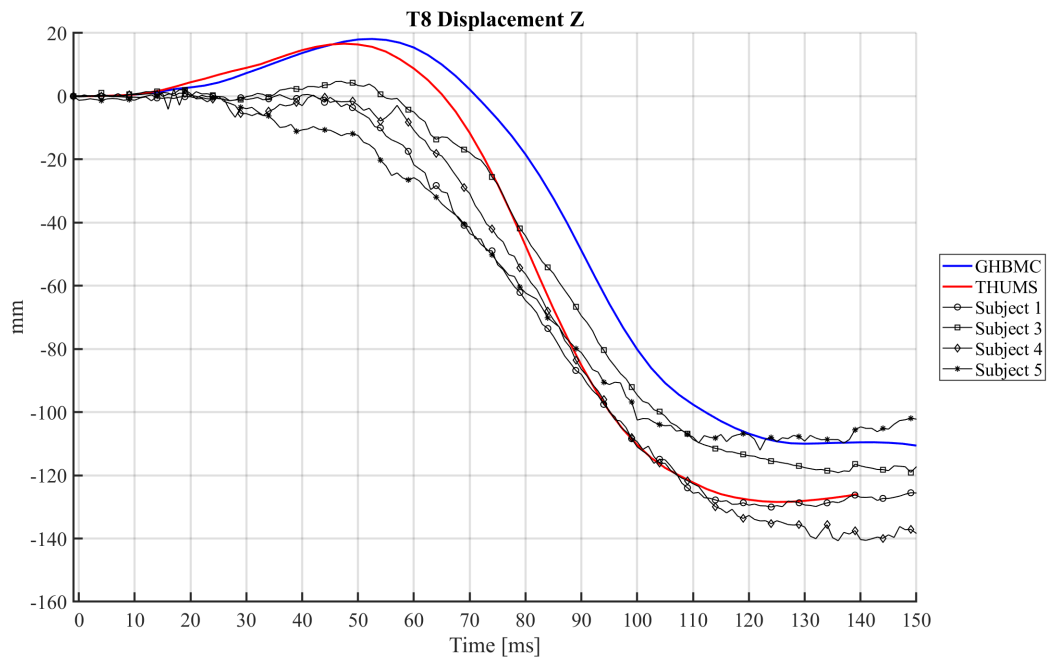


Figure C.39: T8 Z Displacement: HBMs (12°Posterior Pelvis Angle) vs. PMHS

APPENDIX C. RECLINED HBM FRONTAL IMPACT SIMULATIONS

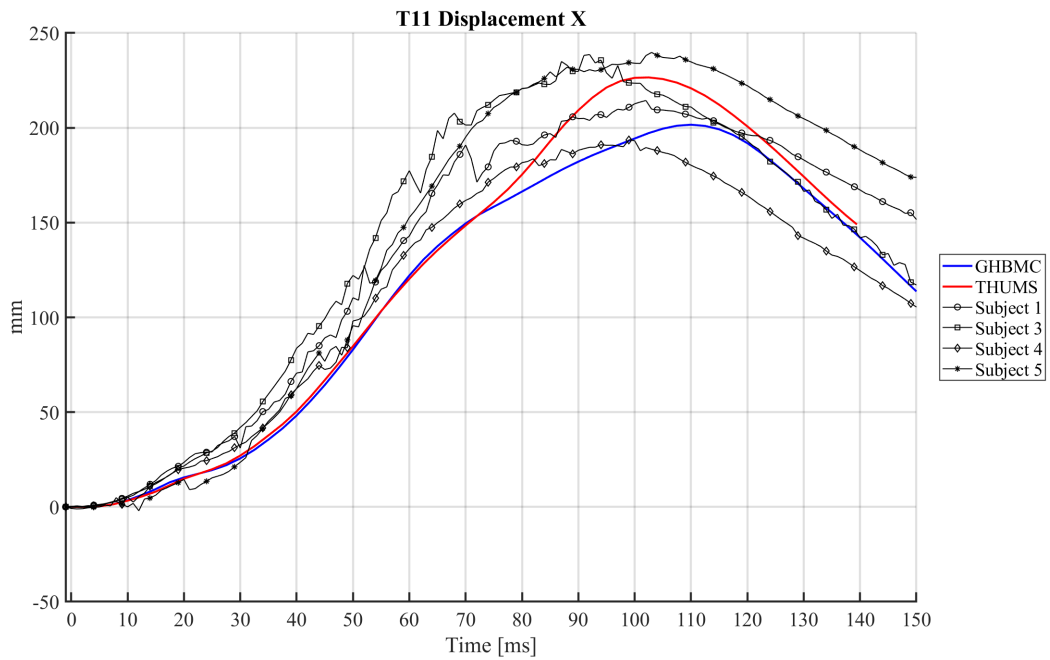


Figure C.40: T11 X Displacement: HBMs (12°Posterior Pelvis Angle) vs. PMHS

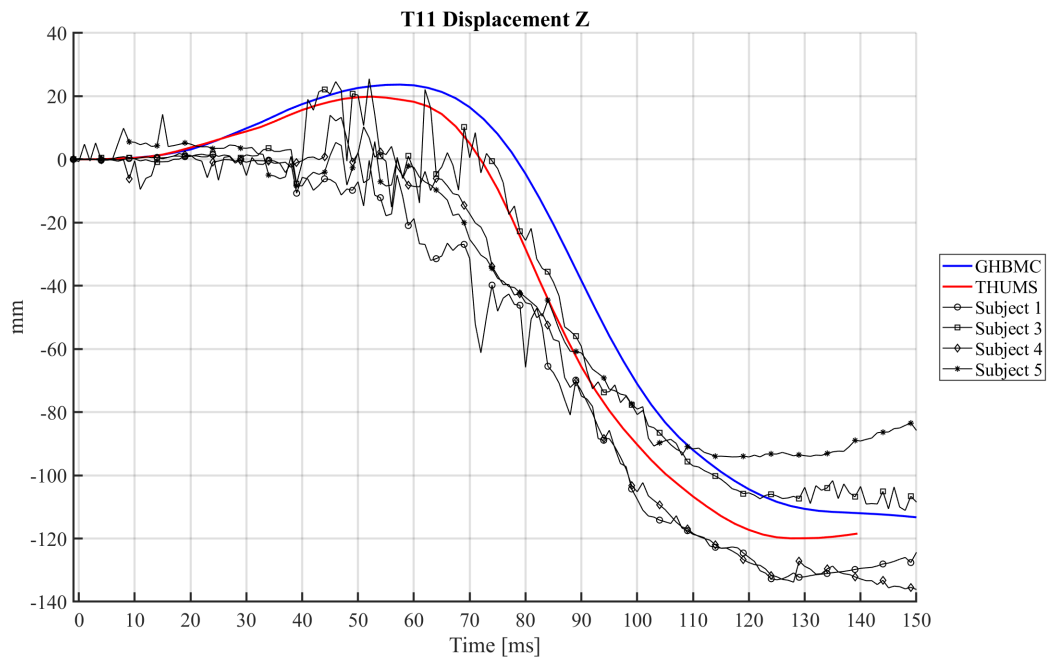


Figure C.41: T11 Z Displacement: HBMs (12°Posterior Pelvis Angle) vs. PMHS

APPENDIX C. RECLINED HBM FRONTAL IMPACT SIMULATIONS

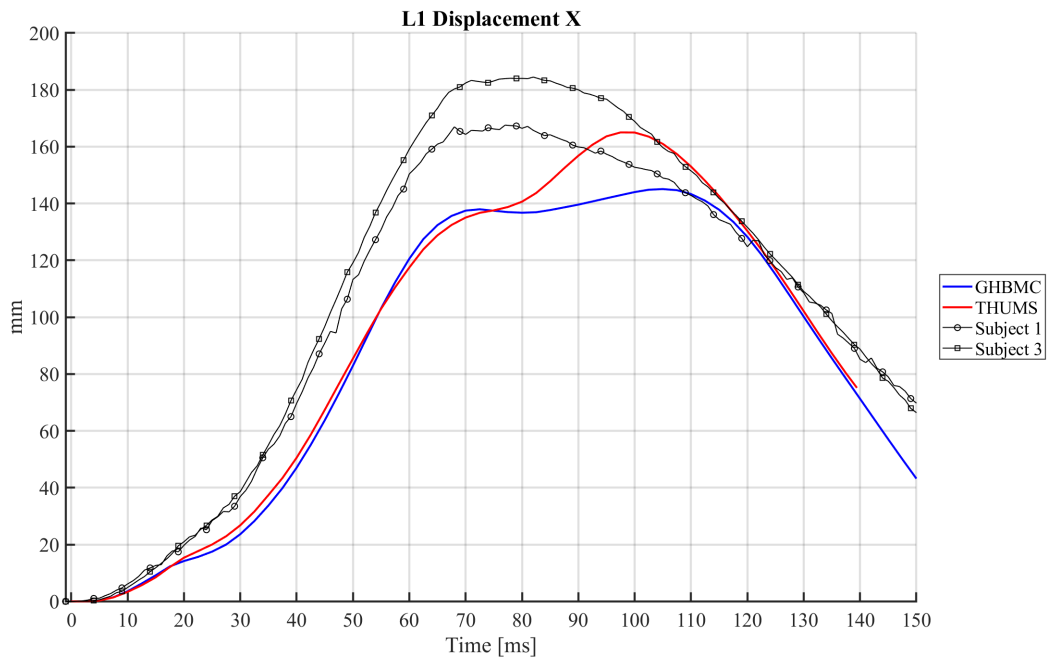


Figure C.42: L1 X Displacement: HBMs (12°Posterior Pelvis Angle) vs. PMHS

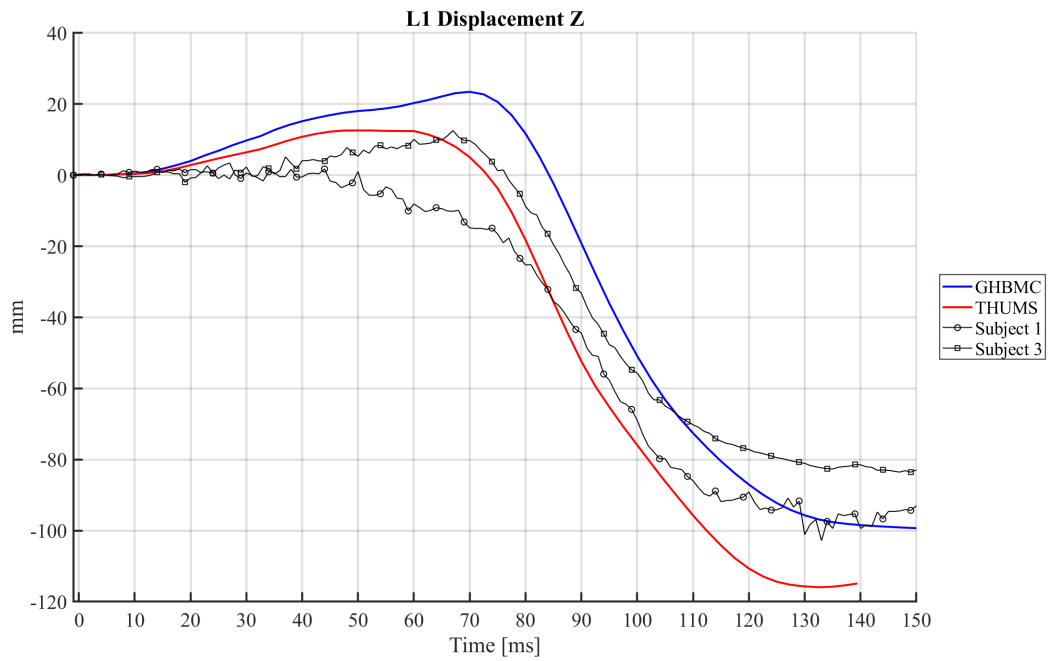


Figure C.43: L1 Z Displacement: HBMs (12°Posterior Pelvis Angle) vs. PMHS

APPENDIX C. RECLINED HBM FRONTAL IMPACT SIMULATIONS

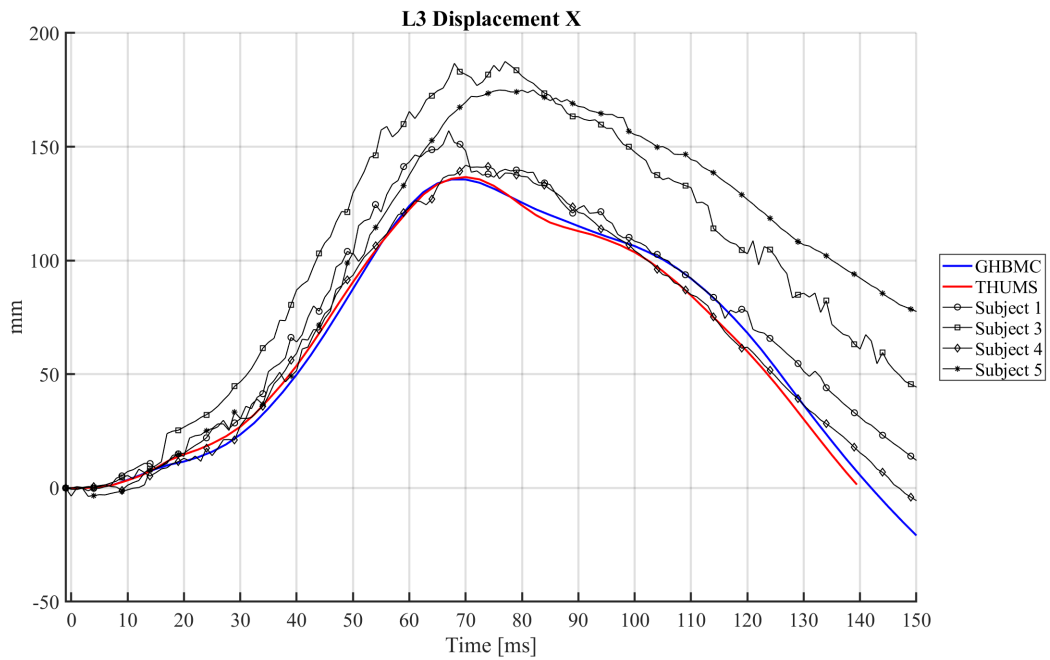


Figure C.44: L3 X Displacement: HBMs (12°Posterior Pelvis Angle) vs. PMHS

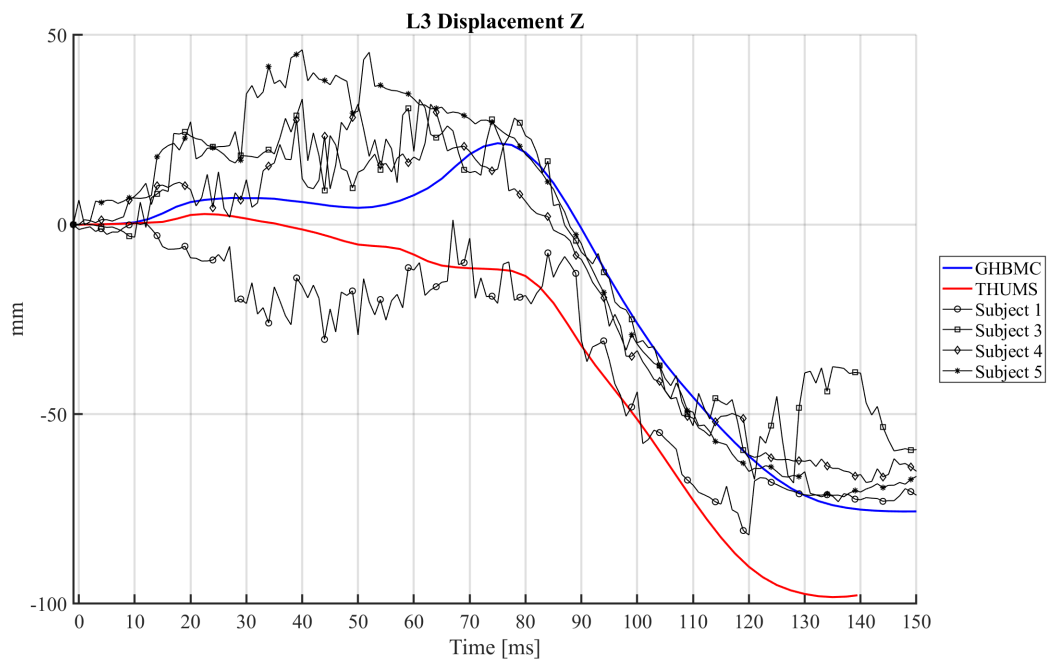


Figure C.45: L3 Z Displacement: HBMs (12°Posterior Pelvis Angle) vs. PMHS

APPENDIX C. RECLINED HBM FRONTAL IMPACT SIMULATIONS

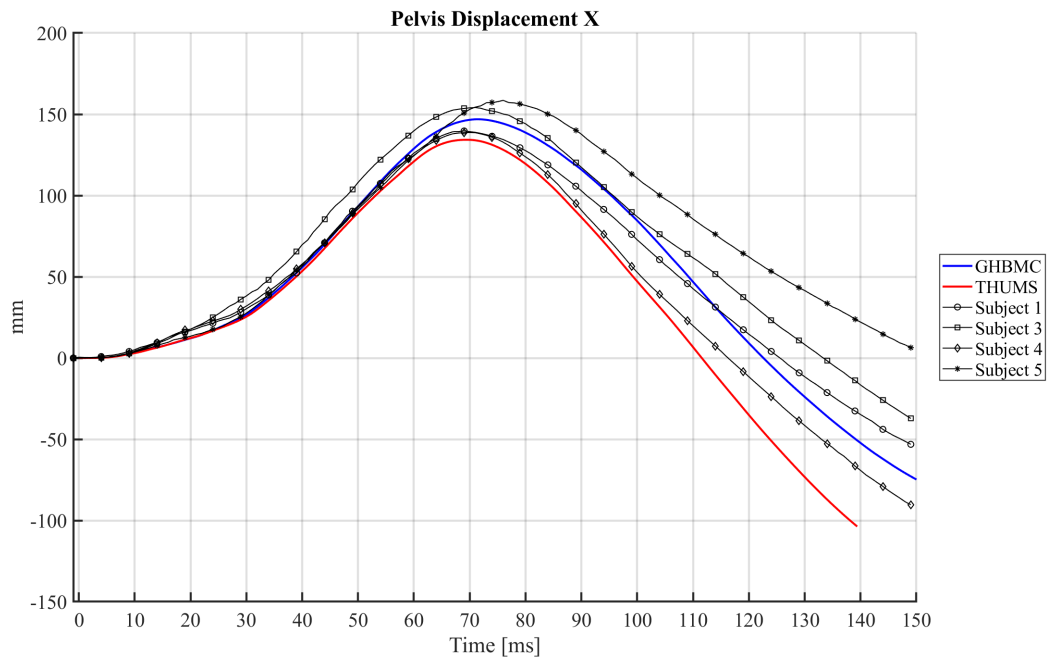


Figure C.46: Pelvis X Displacement: HBMs (12°Posterior Pelvis Angle) vs. PMHS

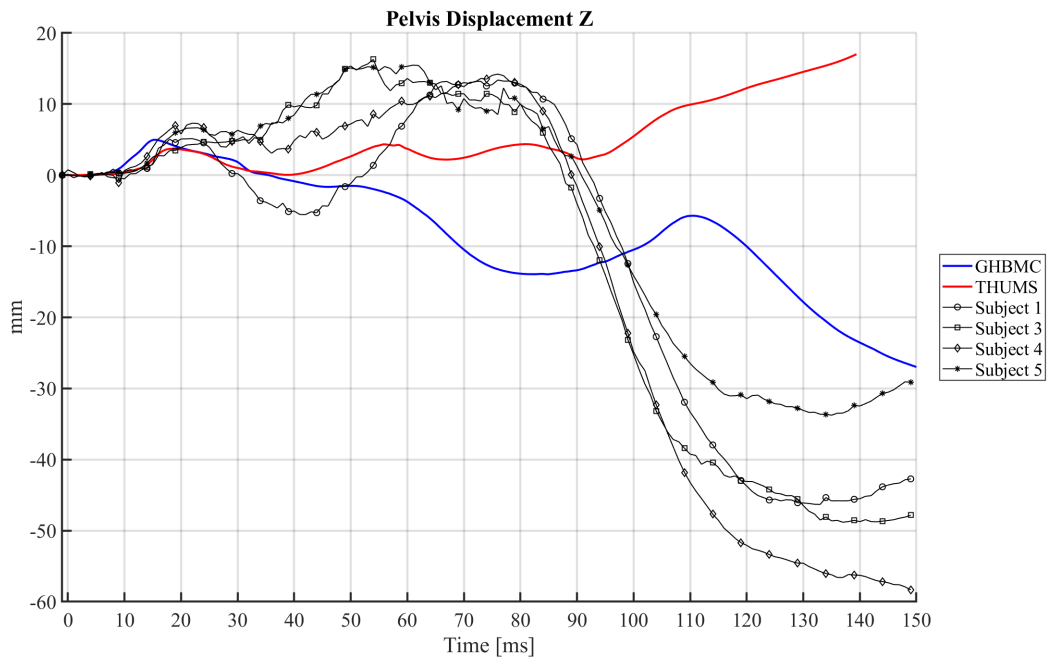


Figure C.47: Pelvis Z Displacement: HBMs (12°Posterior Pelvis Angle) vs. PMHS

APPENDIX C. RECLINED HBM FRONTAL IMPACT SIMULATIONS

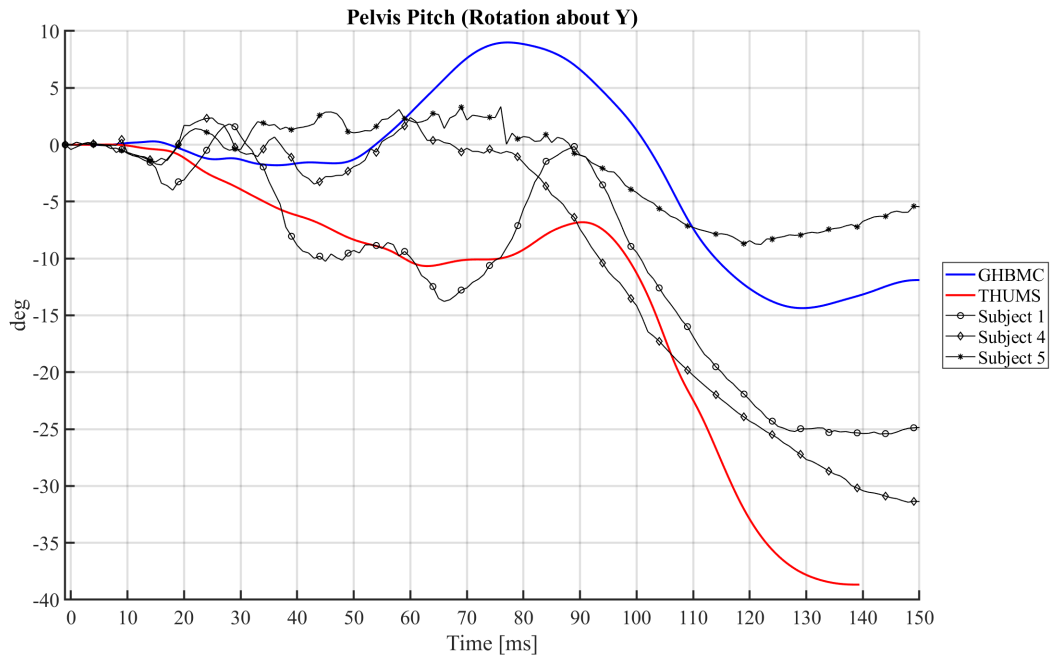


Figure C.48: Pelvis Y Rotation: HBMs (12°Posterior Pelvis Angle) vs. PMHS

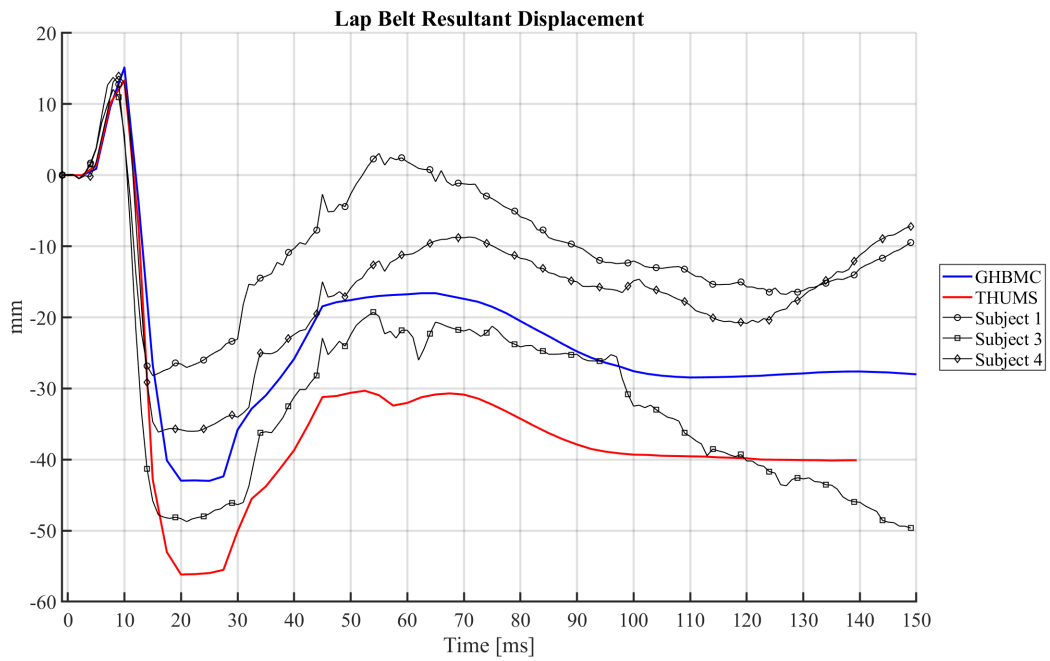


Figure C.49: Lap Belt Resultant Displacement: HBMs (12°Posterior Pelvis Angle) vs. PMHS

APPENDIX C. RECLINED HBM FRONTAL IMPACT SIMULATIONS

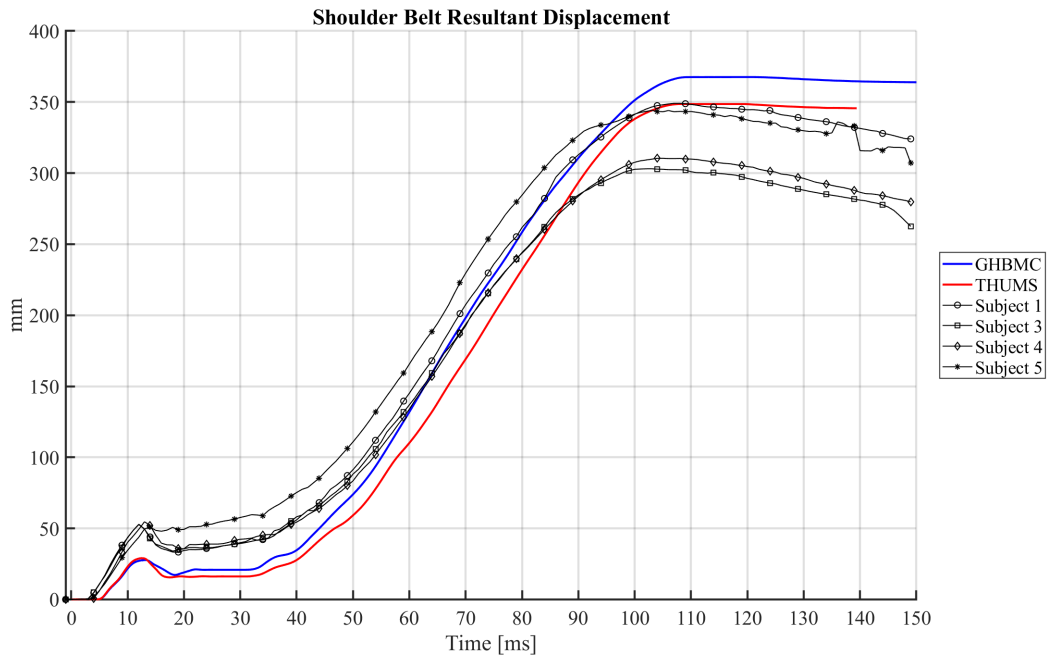


Figure C.50: Shoulder Belt Resultant Displacement: HBMs (12°Posterior Pelvis Angle) vs. PMHS

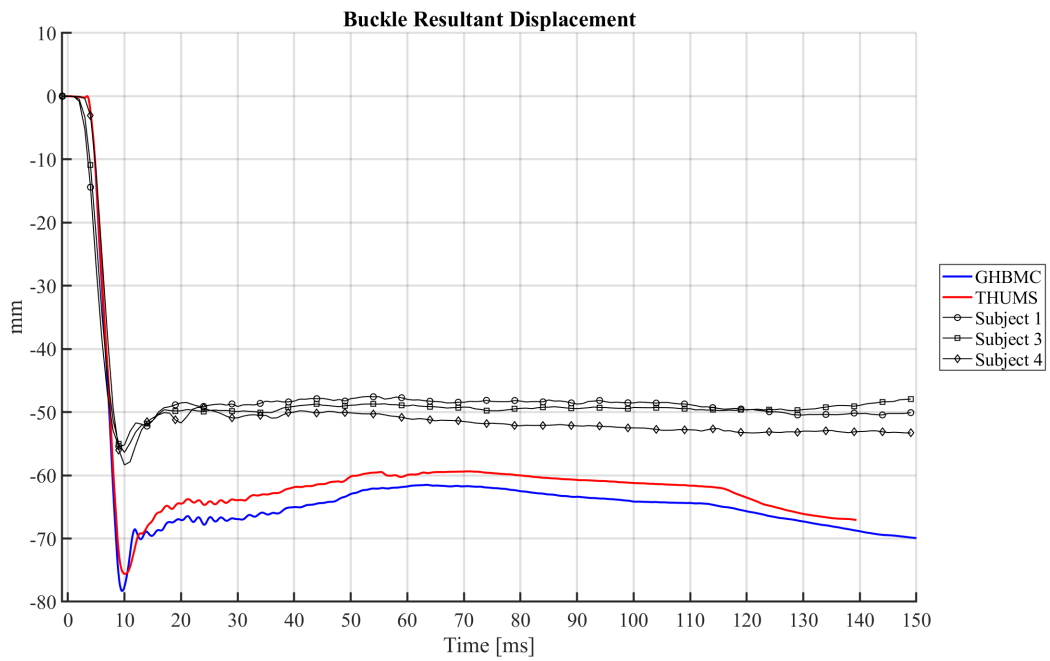


Figure C.51: Buckle Resultant Displacement: HBMs (12°Posterior Pelvis Angle) vs. PMHS

APPENDIX C. RECLINED HBM FRONTAL IMPACT SIMULATIONS

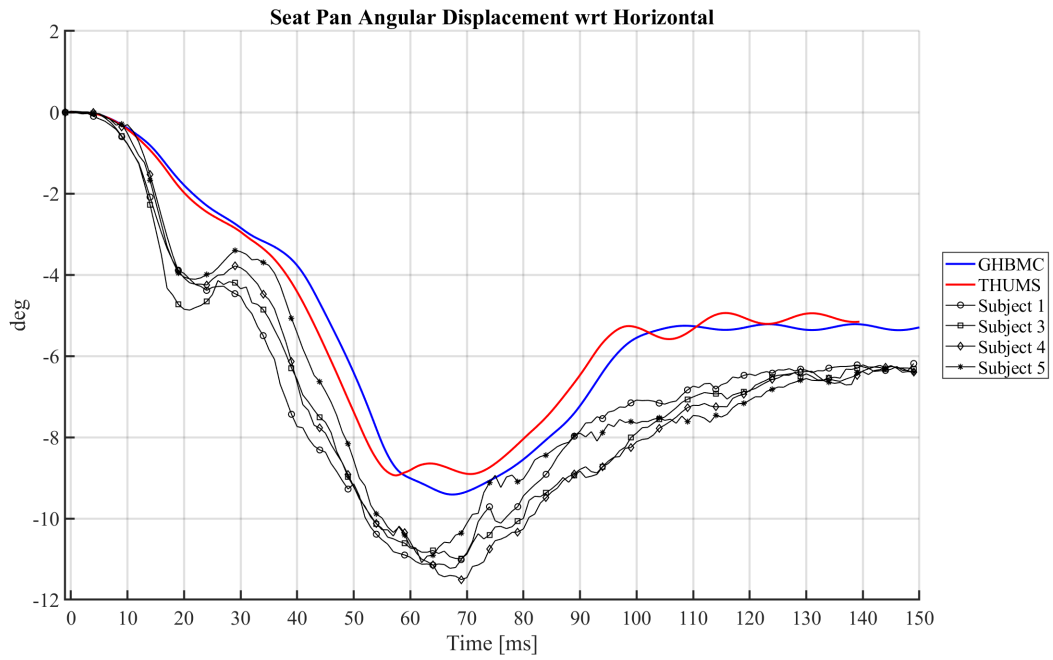


Figure C.52: Seat Pan Angular Displacement: HBMs (12°Posterior Pelvis Angle) vs. PMHS

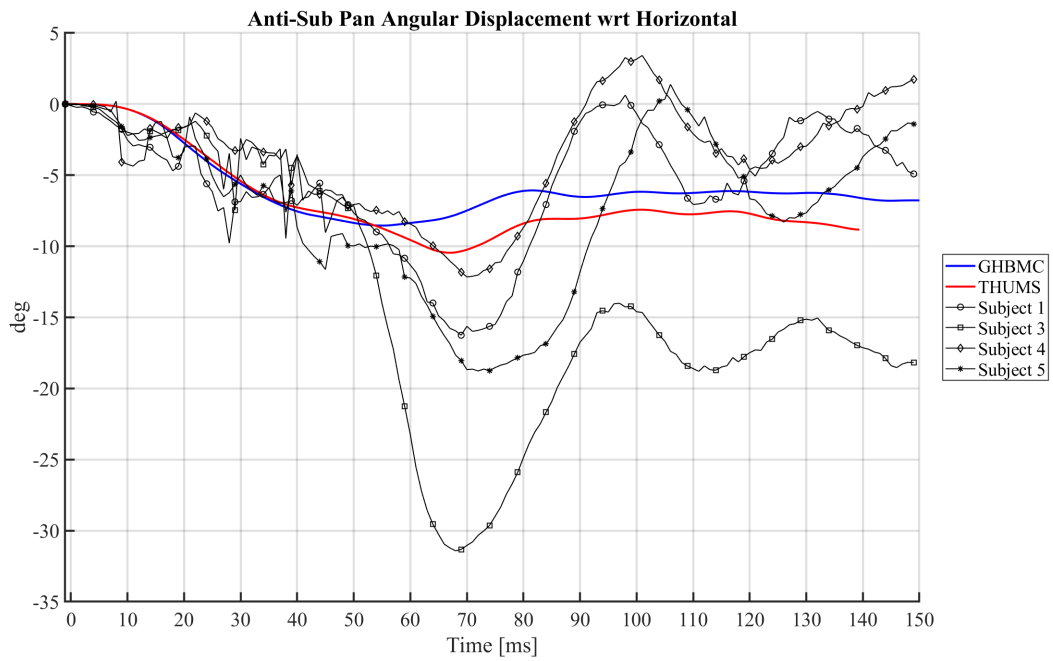


Figure C.53: Anti-Sub Pan Angular Displacement: HBMs (12°Posterior Pelvis Angle) vs. PMHS

APPENDIX C. RECLINED HBM FRONTAL IMPACT SIMULATIONS

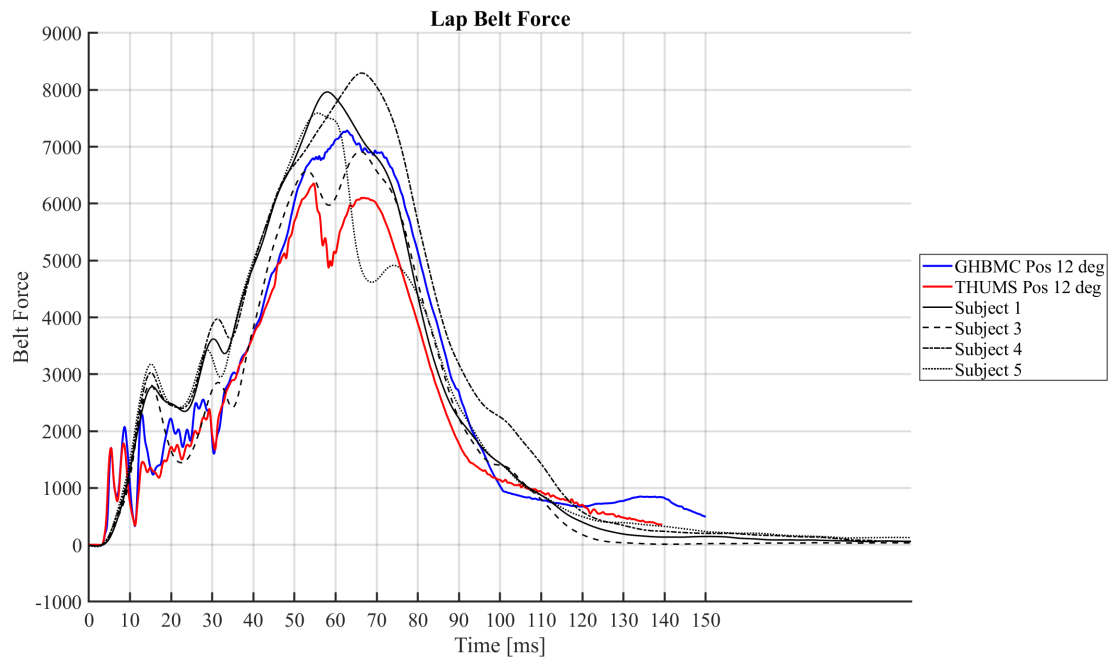


Figure C.54: Lap Belt Tension: HBMs (12°Posterior Pelvis Angle) vs. PMHS

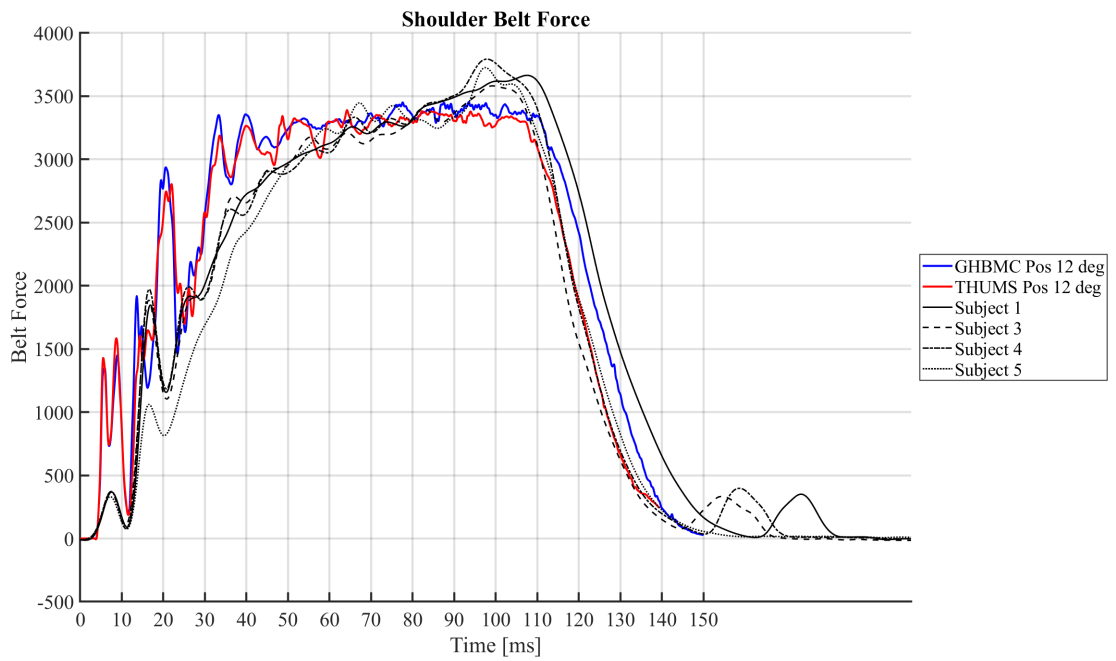


Figure C.55: Shoulder Belt Tension: HBMs (12°Posterior Pelvis Angle) vs. PMHS

APPENDIX C. RECLINED HBM FRONTAL IMPACT SIMULATIONS

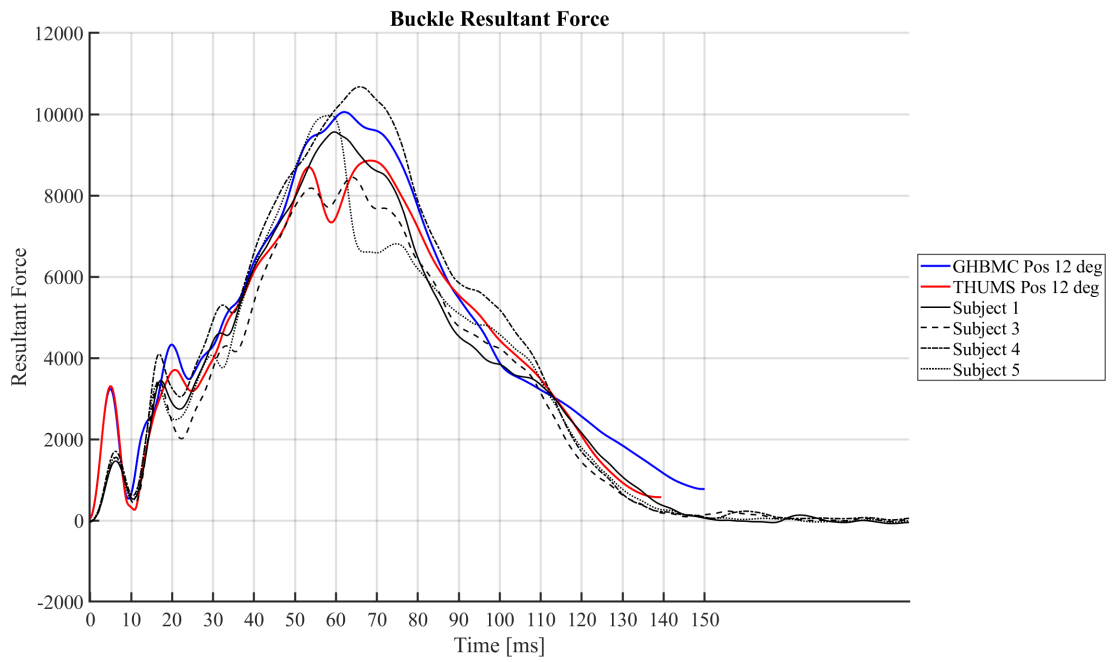


Figure C.56: Buckle Resultant Force: HBMs (12°Posterior Pelvis Angle) vs. PMHS

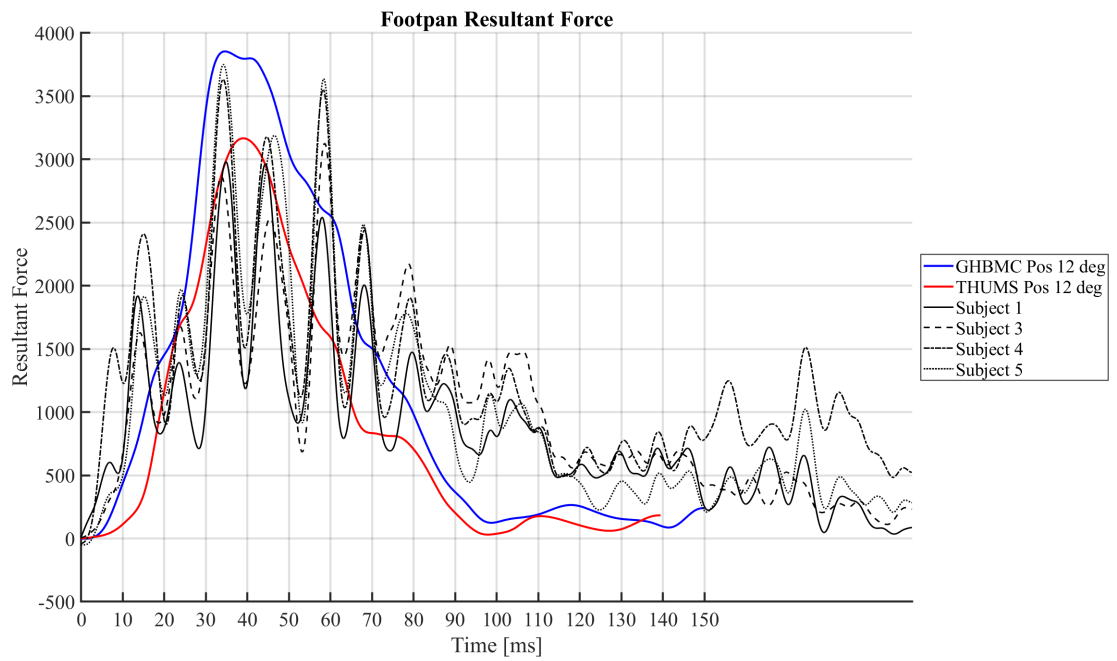


Figure C.57: Foot Pan Resultant Force: HBMs (12°Posterior Pelvis Angle) vs. PMHS

C.4 HBM Responses compared to PMHS Responses: 12° Anterior Pelvis Angle

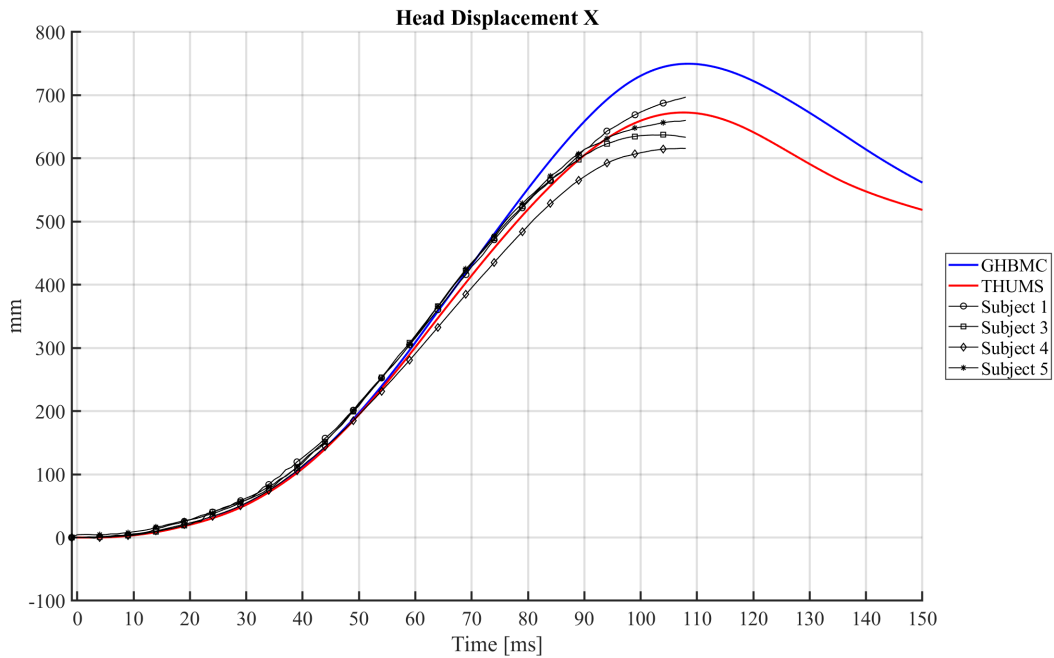


Figure C.58: Head X Displacement: HBMs (12° Anterior Pelvis Angle) vs. PMHS

APPENDIX C. RECLINED HBM FRONTAL IMPACT SIMULATIONS

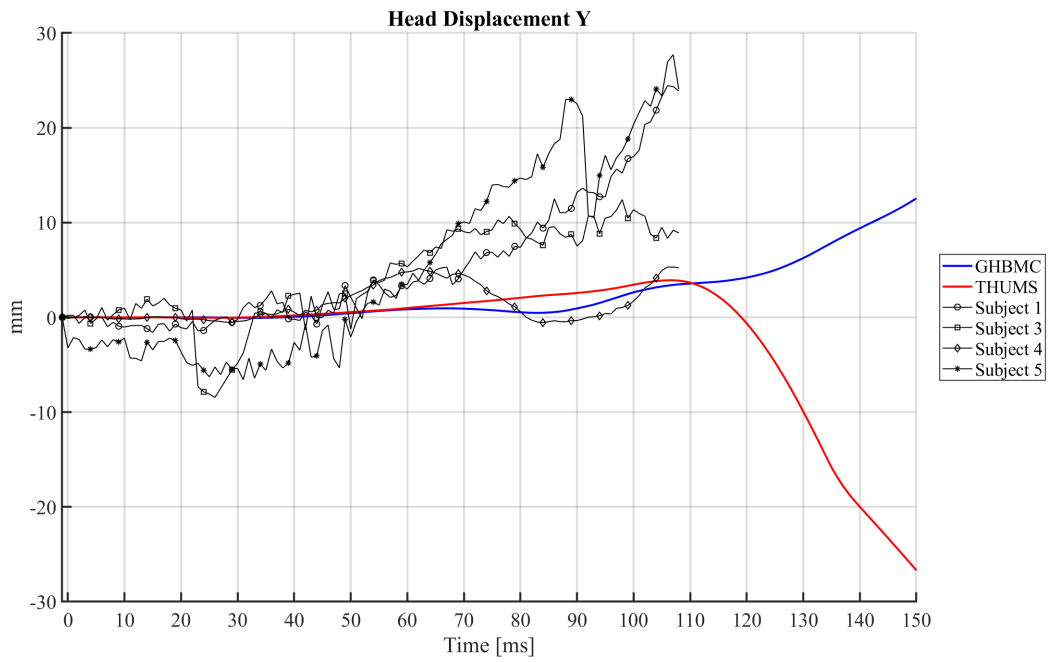


Figure C.59: Head Y Displacement: HBMs (12° Anterior Pelvis Angle) vs. PMHS

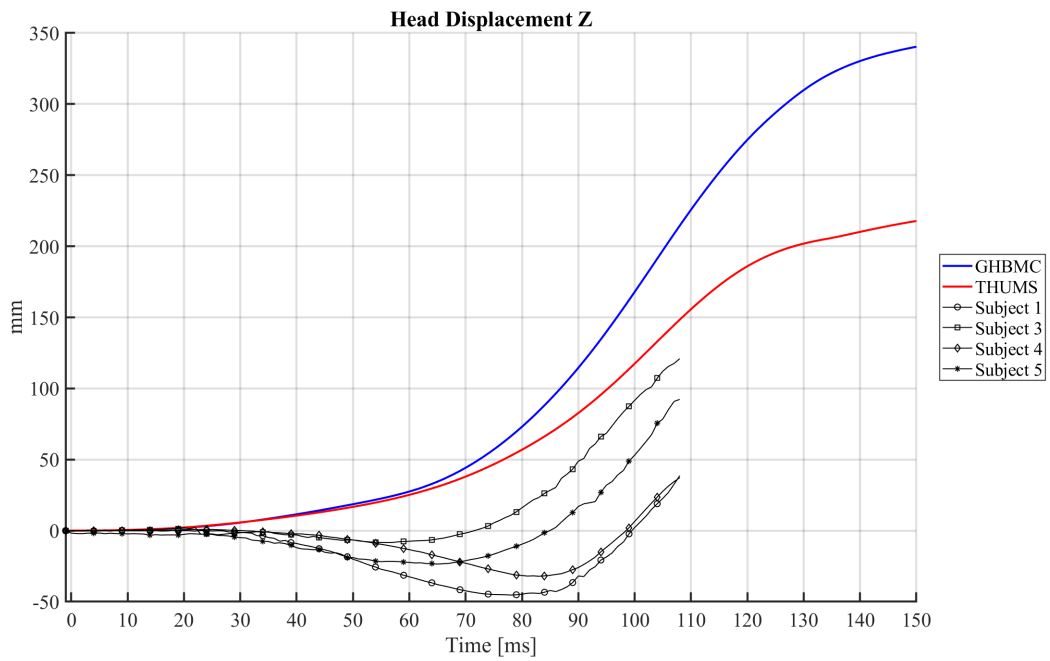


Figure C.60: Head Z Displacement: HBMs (12° Anterior Pelvis Angle) vs. PMHS

APPENDIX C. RECLINED HBM FRONTAL IMPACT SIMULATIONS

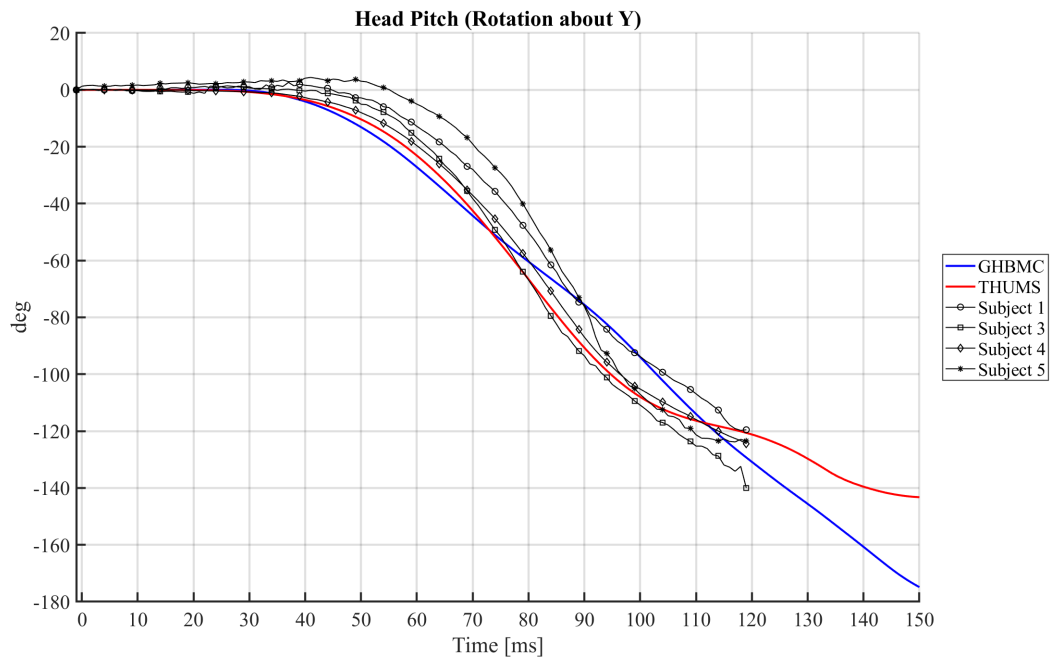


Figure C.61: Head Y Rotation: HBMs (12° Anterior Pelvis Angle) vs. PMHS

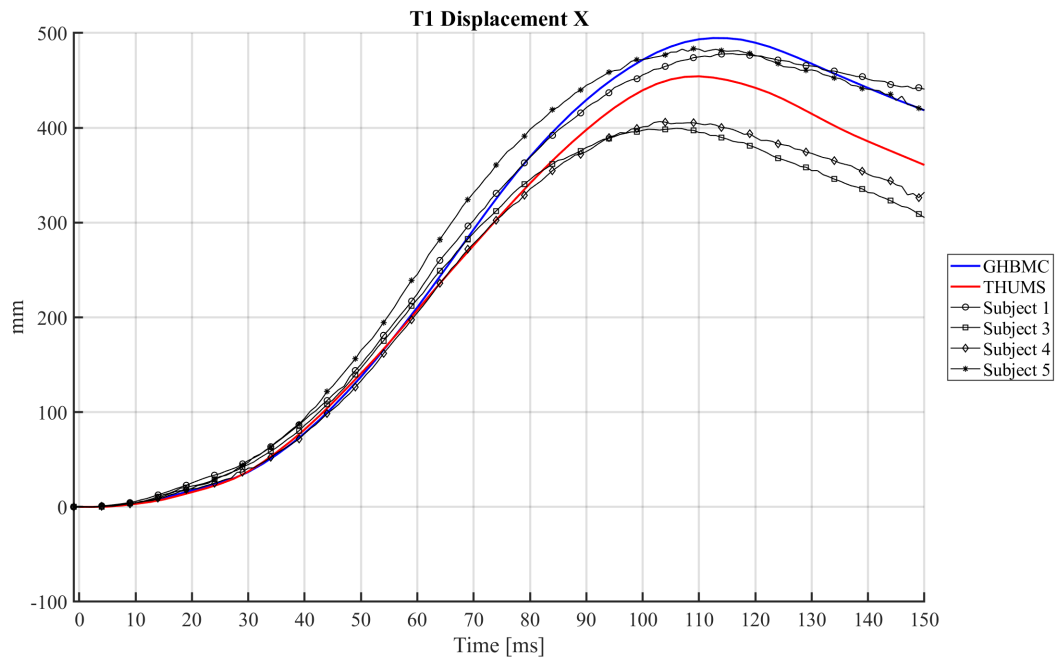


Figure C.62: T1 X Displacement: HBMs (12° Anterior Pelvis Angle) vs. PMHS

APPENDIX C. RECLINED HBM FRONTAL IMPACT SIMULATIONS

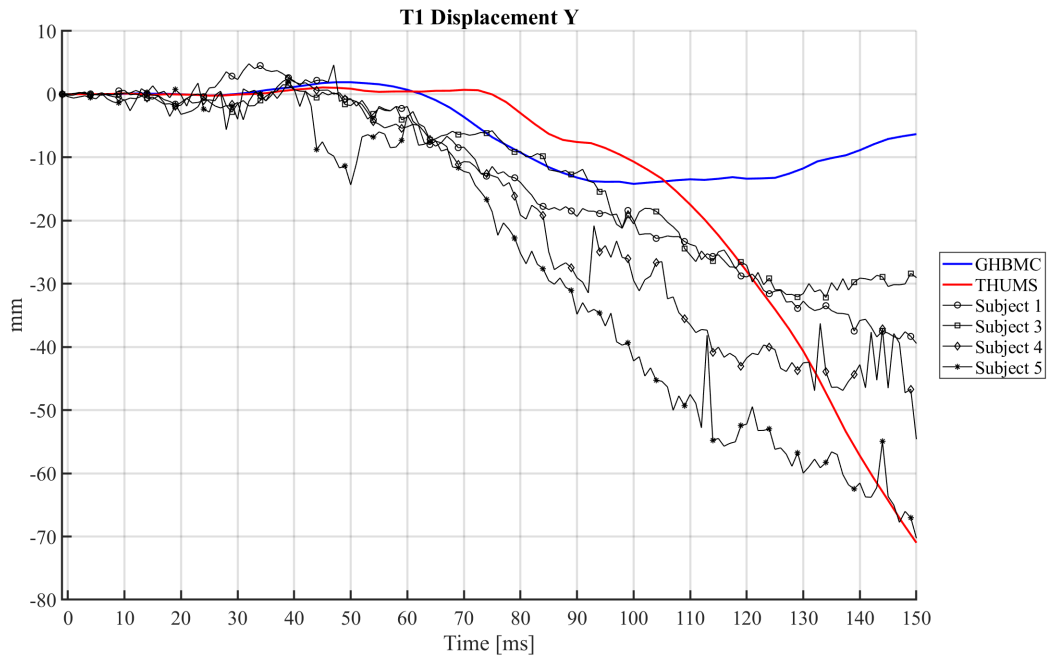


Figure C.63: T1 Y Displacement: HBMs (12° Anterior Pelvis Angle) vs. PMHS

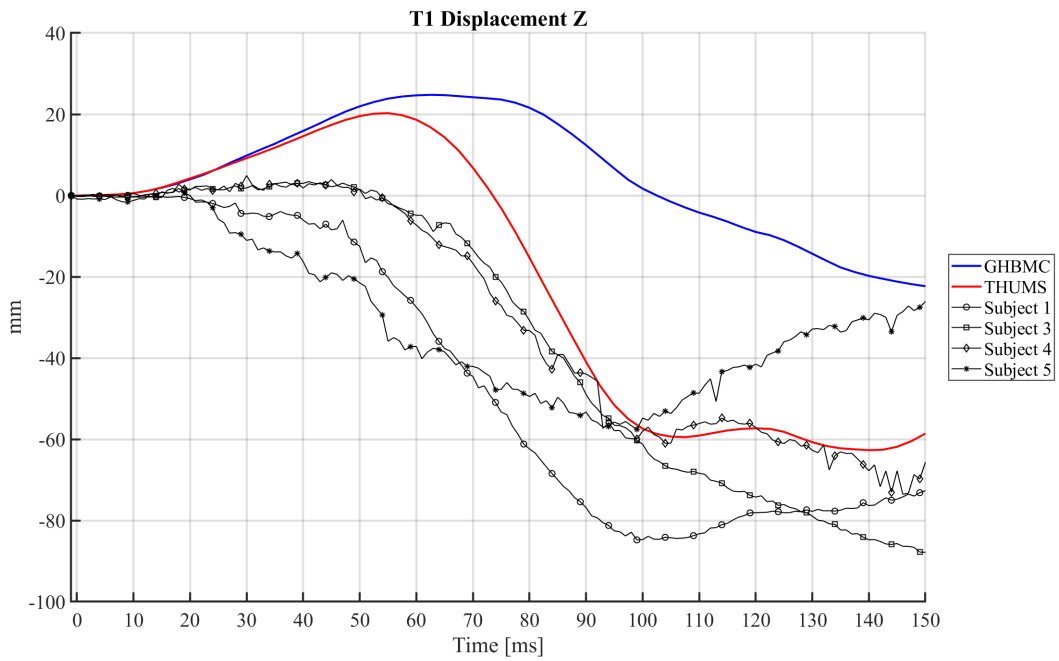


Figure C.64: T1 Z Displacement: HBMs (12° Anterior Pelvis Angle) vs. PMHS

APPENDIX C. RECLINED HBM FRONTAL IMPACT SIMULATIONS

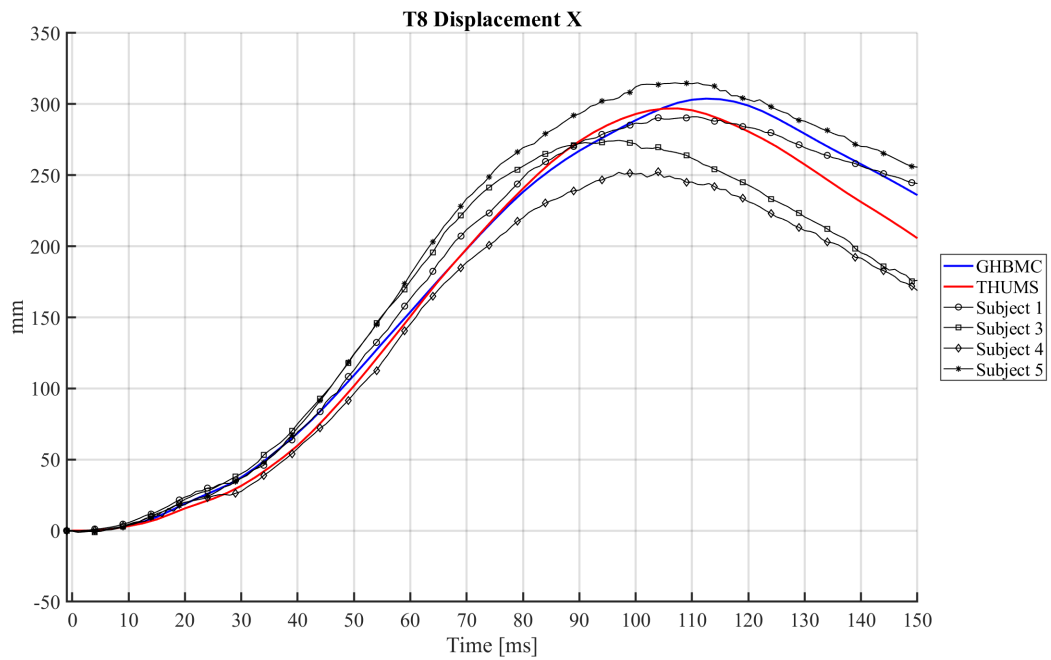


Figure C.65: T8 X Displacement: HBMs (12° Anterior Pelvis Angle) vs. PMHS

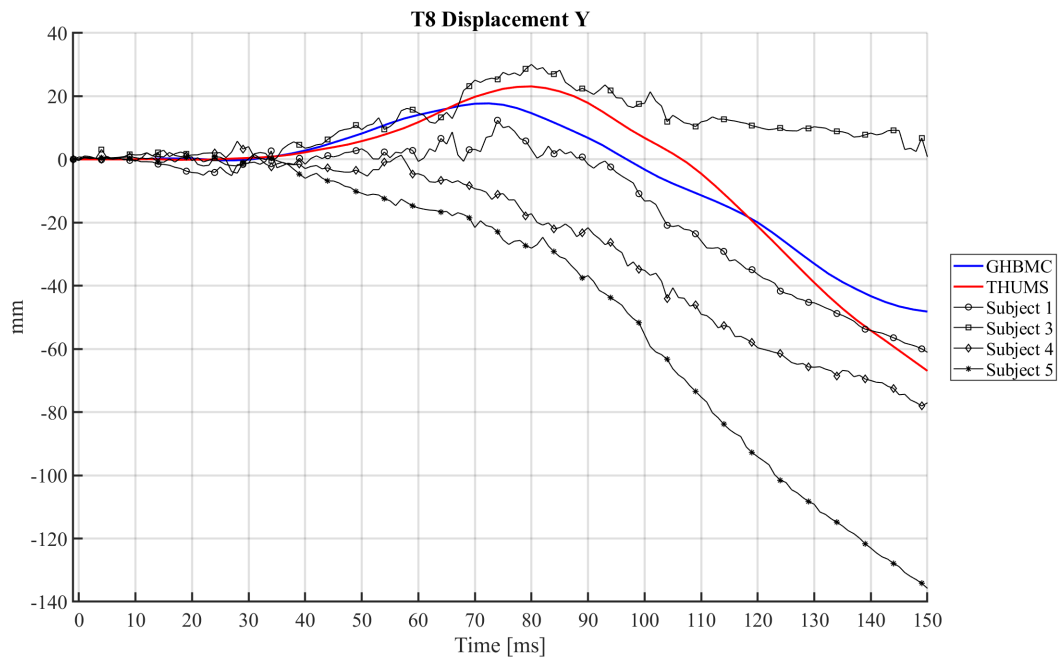


Figure C.66: T8 Y Displacement: HBMs (12° Anterior Pelvis Angle) vs. PMHS

APPENDIX C. RECLINED HBM FRONTAL IMPACT SIMULATIONS

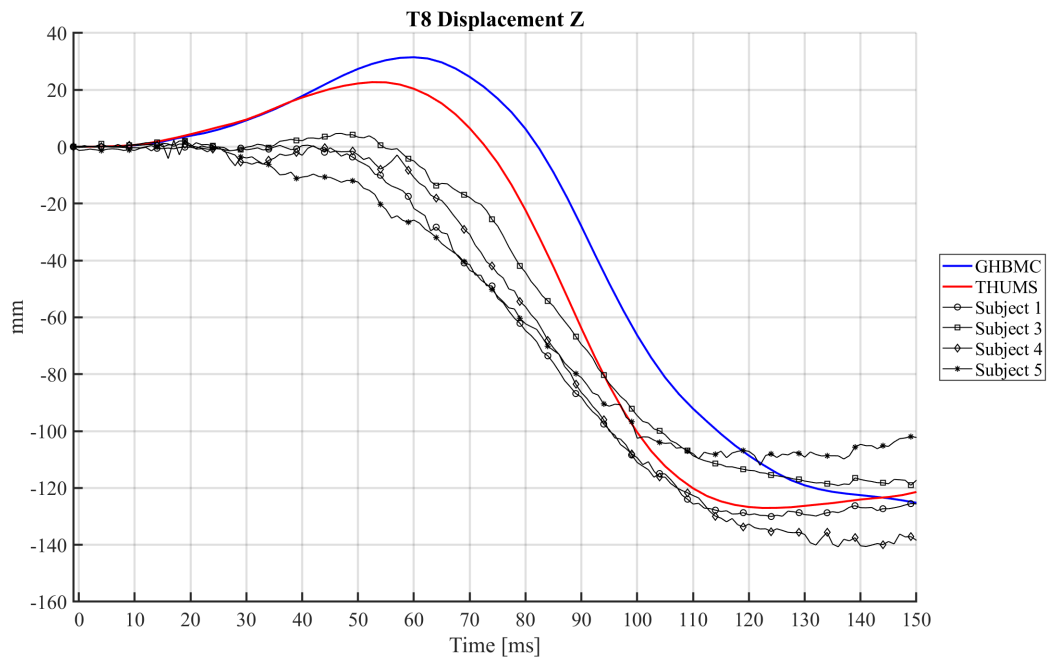


Figure C.67: T8 Z Displacement: HBMs (12° Anterior Pelvis Angle) vs. PMHS

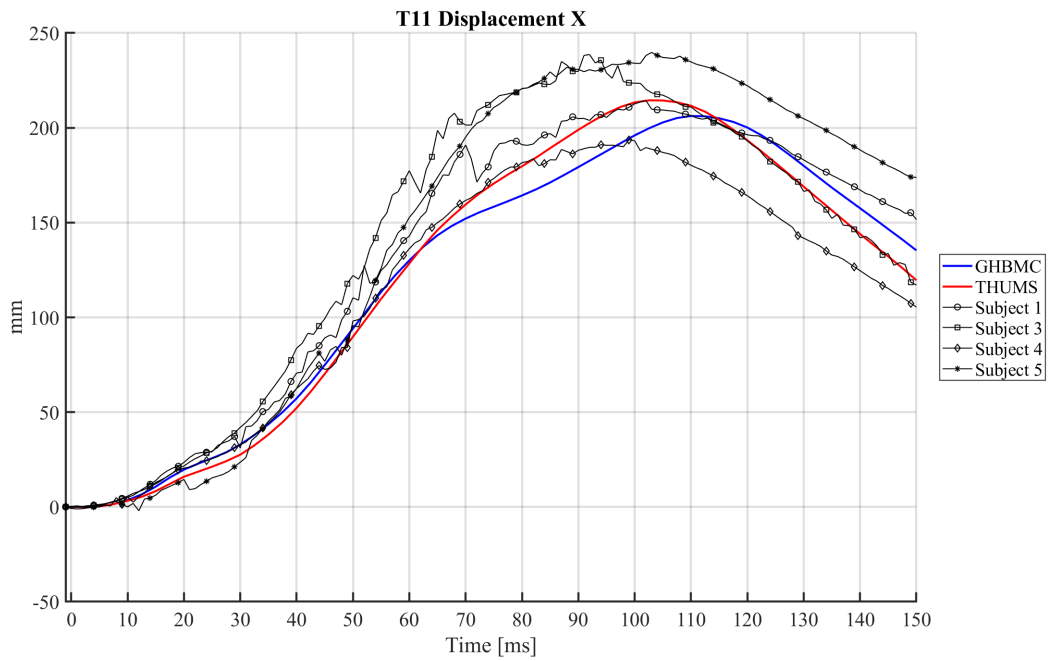


Figure C.68: T11 X Displacement: HBMs (12° Anterior Pelvis Angle) vs. PMHS

APPENDIX C. RECLINED HBM FRONTAL IMPACT SIMULATIONS

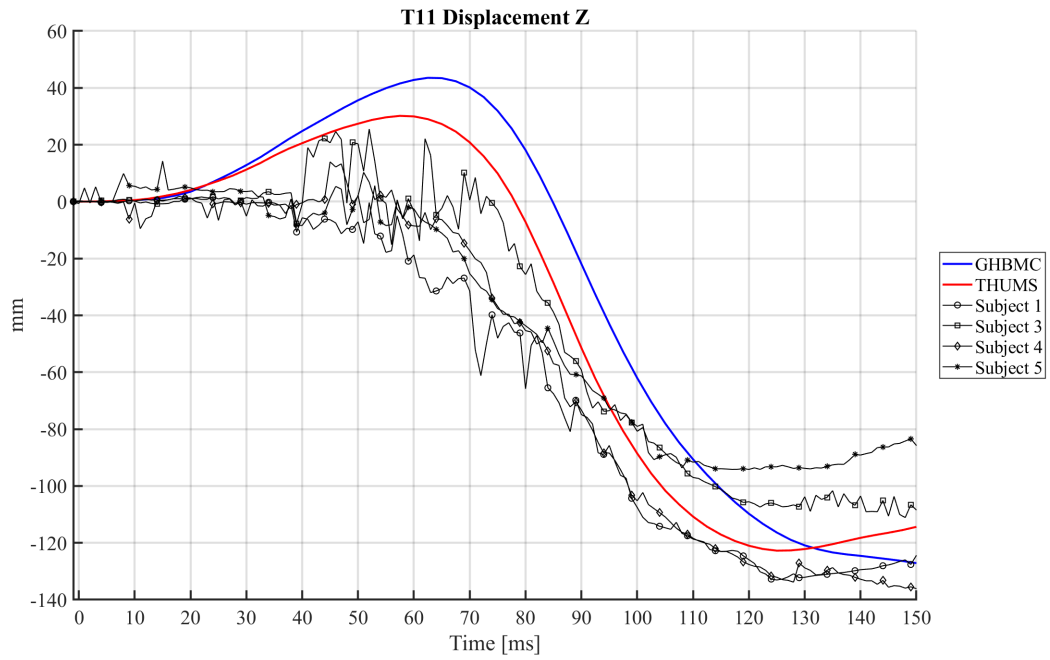


Figure C.69: T11 Z Displacement: HBMs (12° Anterior Pelvis Angle) vs. PMHS

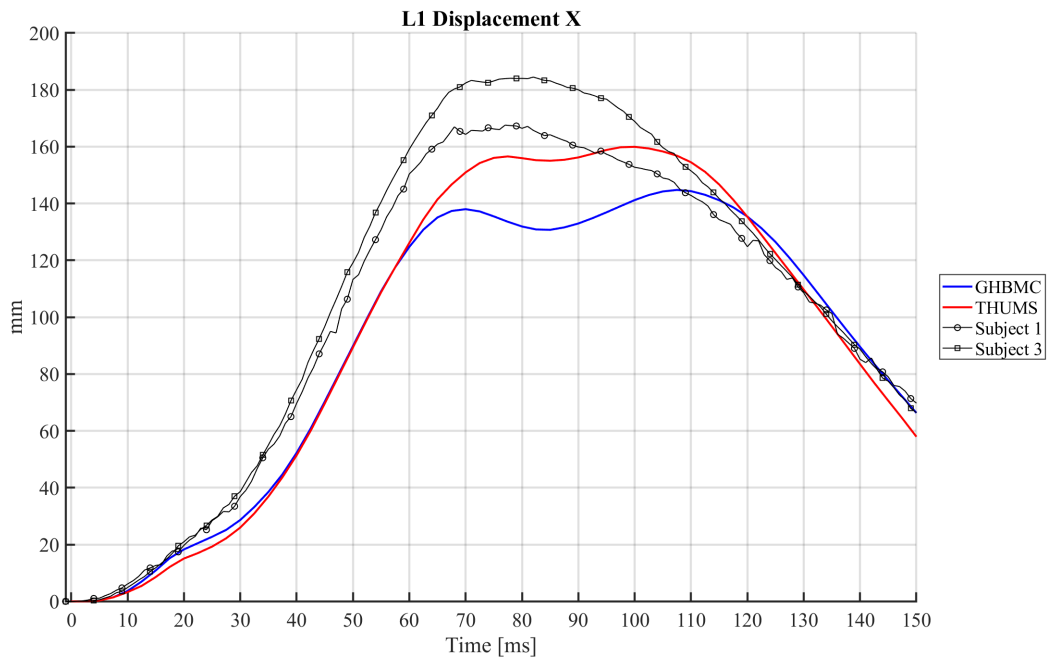


Figure C.70: L1 X Displacement: HBMs (12° Anterior Pelvis Angle) vs. PMHS

APPENDIX C. RECLINED HBM FRONTAL IMPACT SIMULATIONS

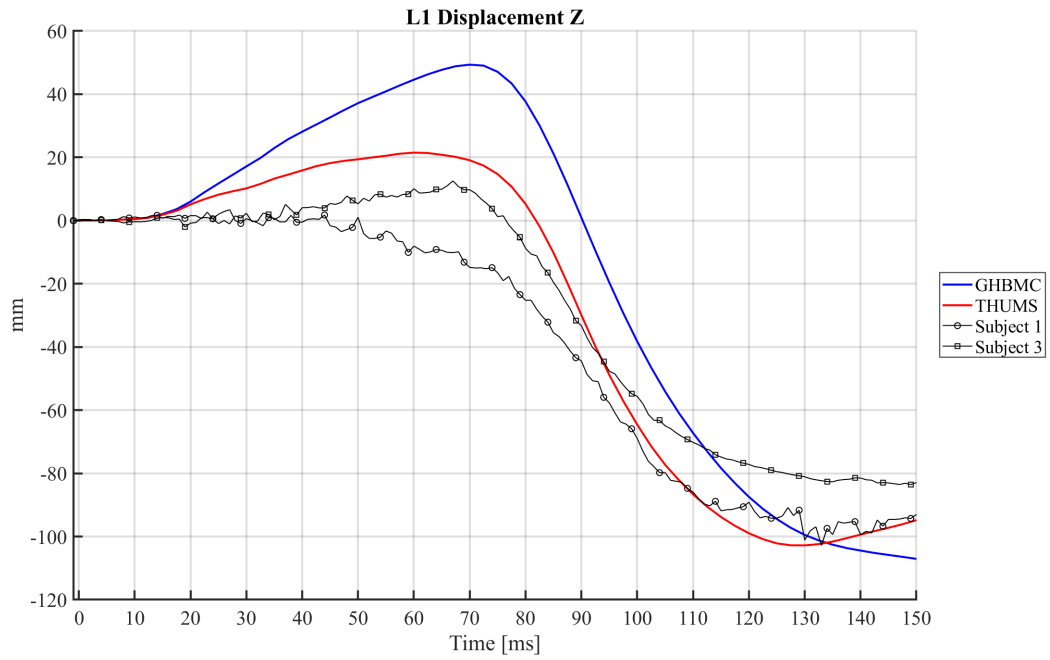


Figure C.71: L1 Z Displacement: HBMs (12° Anterior Pelvis Angle) vs. PMHS

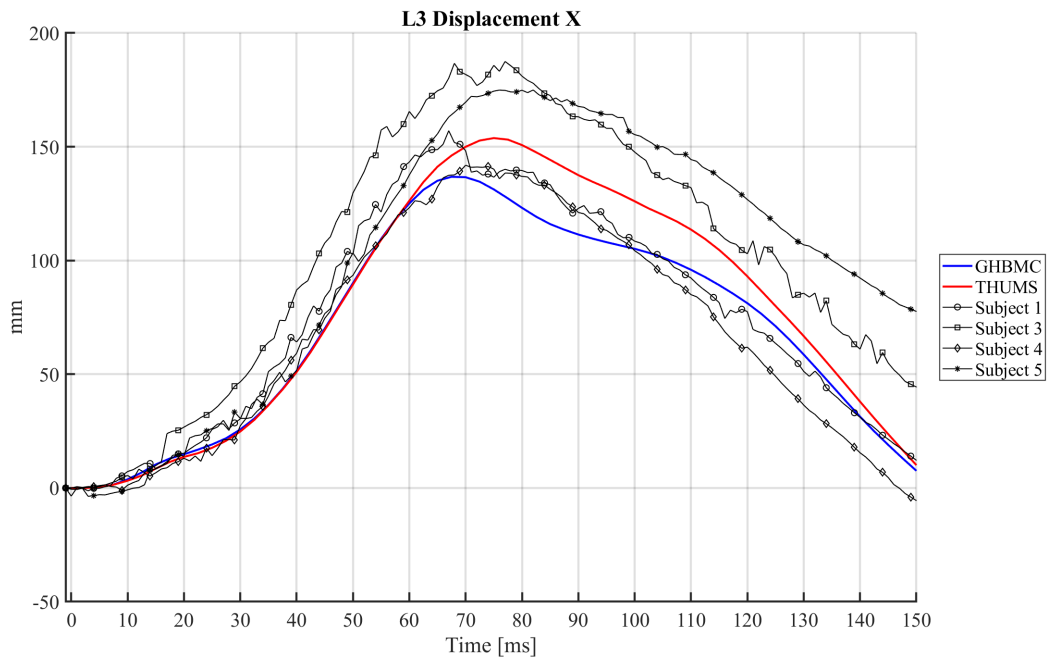


Figure C.72: L3 X Displacement: HBMs (12° Anterior Pelvis Angle) vs. PMHS

APPENDIX C. RECLINED HBM FRONTAL IMPACT SIMULATIONS

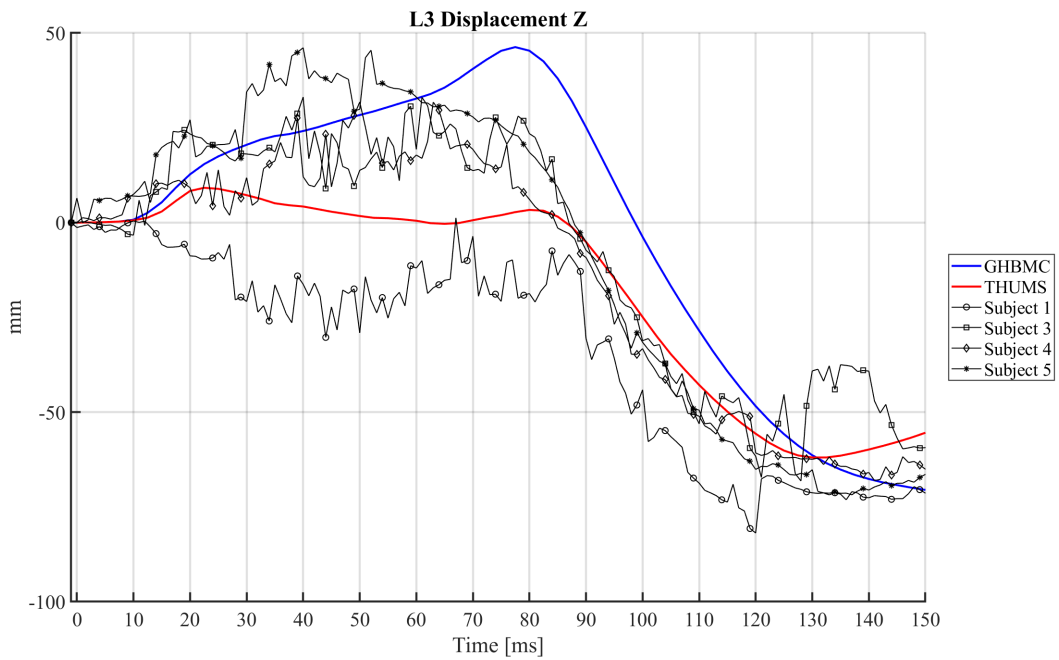


Figure C.73: L3 Z Displacement: HBMs (12° Anterior Pelvis Angle) vs. PMHS

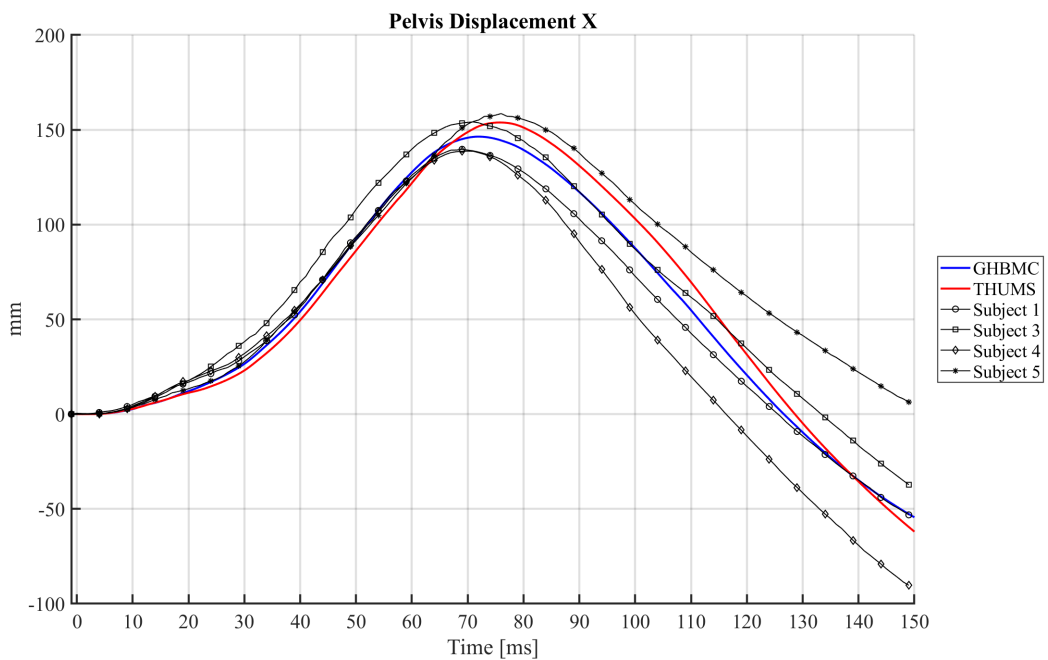


Figure C.74: Pelvis X Displacement: HBMs (12° Anterior Pelvis Angle) vs. PMHS

APPENDIX C. RECLINED HBM FRONTAL IMPACT SIMULATIONS

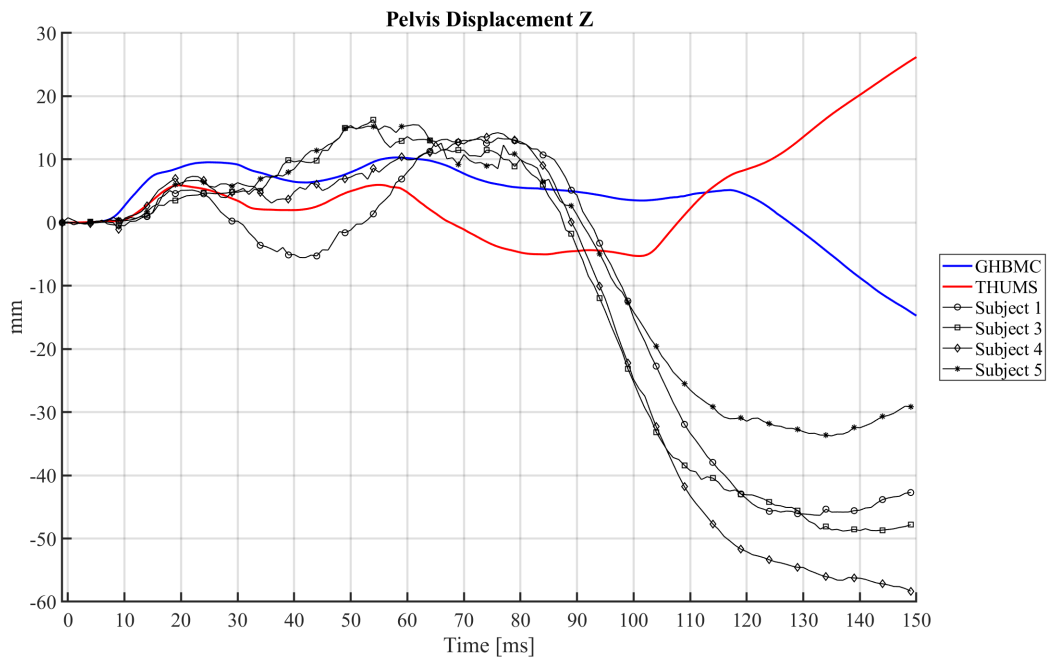


Figure C.75: Pelvis Z Displacement: HBMs (12° Anterior Pelvis Angle) vs. PMHS

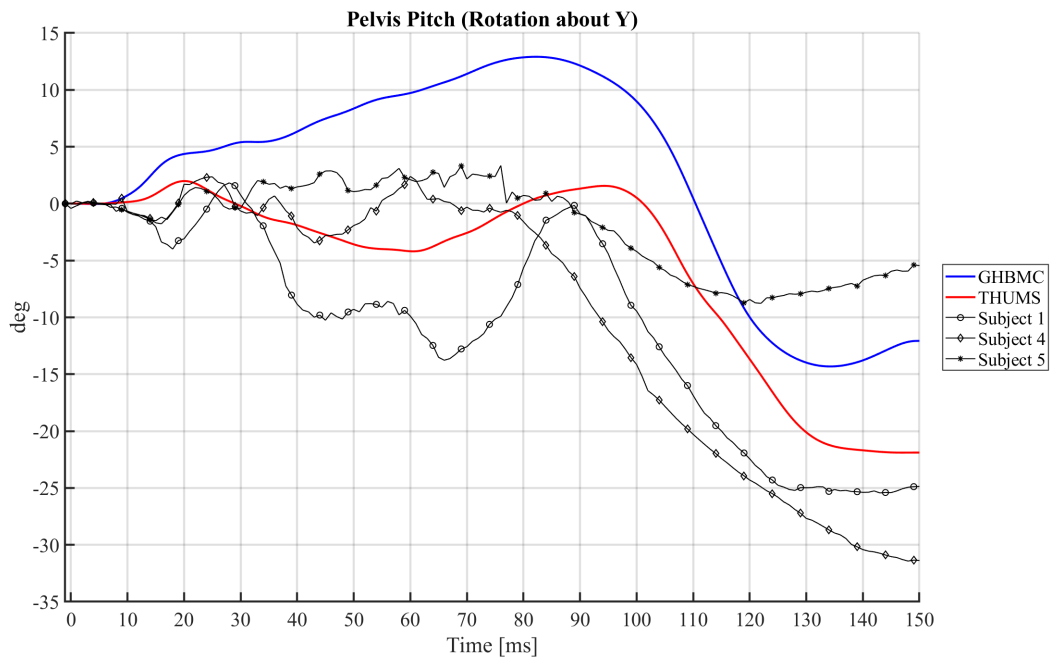


Figure C.76: Pelvis Y Rotation: HBMs (12° Anterior Pelvis Angle) vs. PMHS

APPENDIX C. RECLINED HBM FRONTAL IMPACT SIMULATIONS

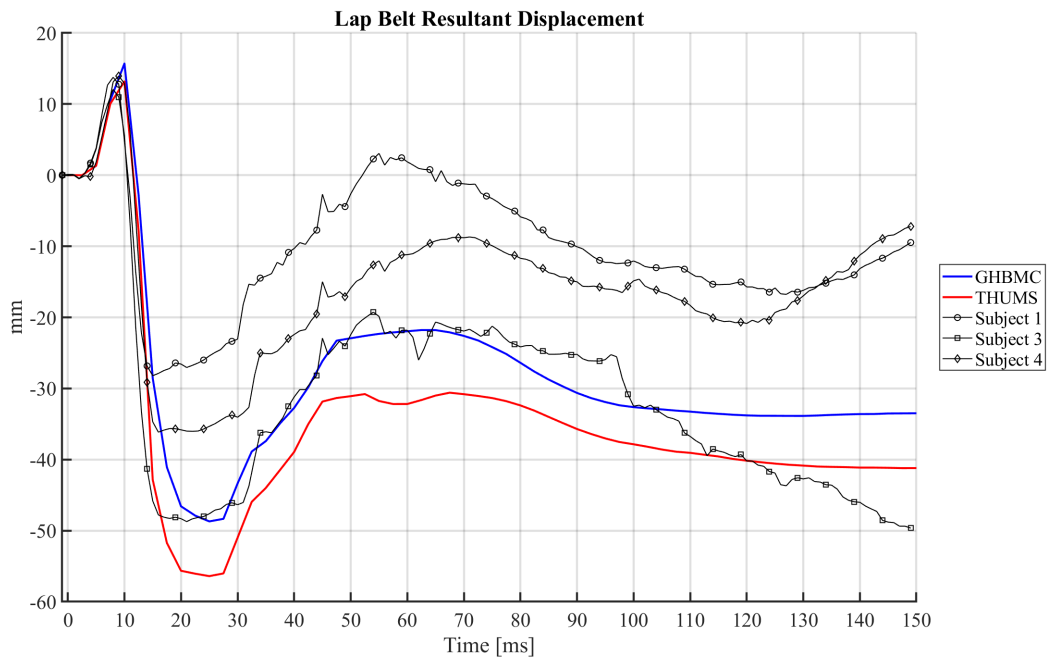


Figure C.77: Lap Belt Resultant Displacement: HBMs (12° Anterior Pelvis Angle) vs. PMHS

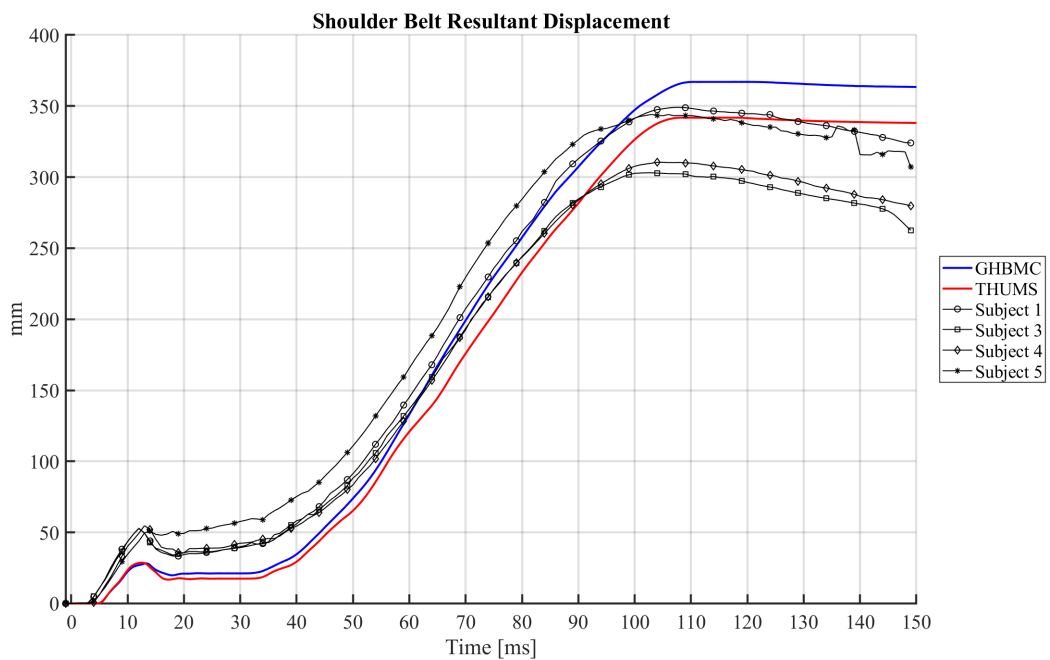


Figure C.78: Shoulder Belt Resultant Displacement: HBMs (12° Anterior Pelvis Angle) vs. PMHS

APPENDIX C. RECLINED HBM FRONTAL IMPACT SIMULATIONS

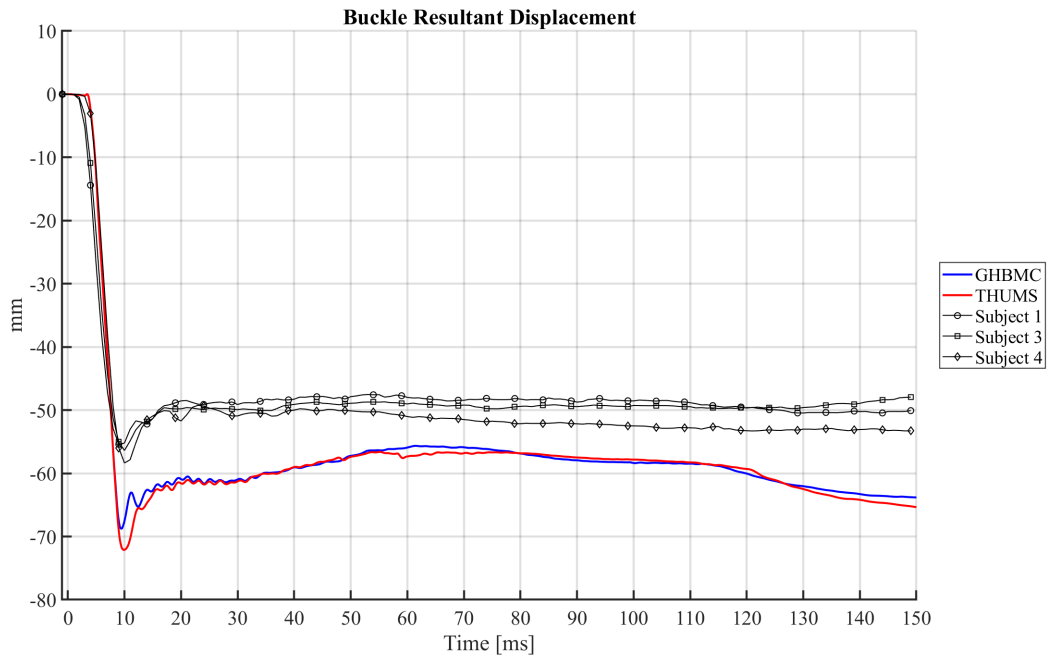


Figure C.79: Buckle Resultant Displacement: HBMs (12° Anterior Pelvis Angle) vs. PMHS

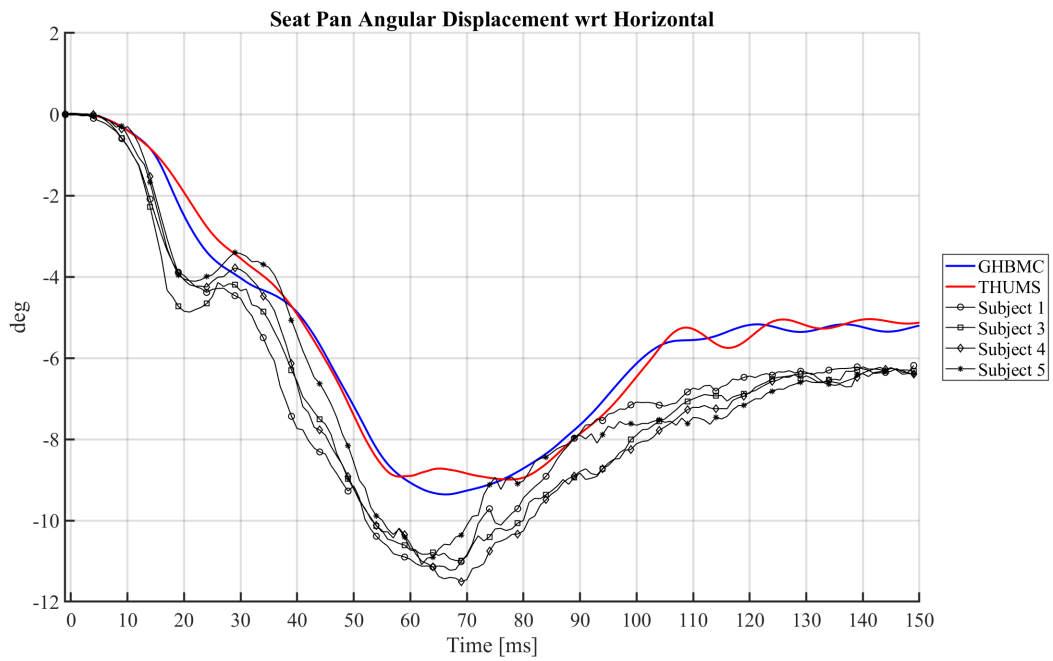


Figure C.80: Seat Pan Angular Displacement: HBMs (12° Anterior Pelvis Angle) vs. PMHS

APPENDIX C. RECLINED HBM FRONTAL IMPACT SIMULATIONS

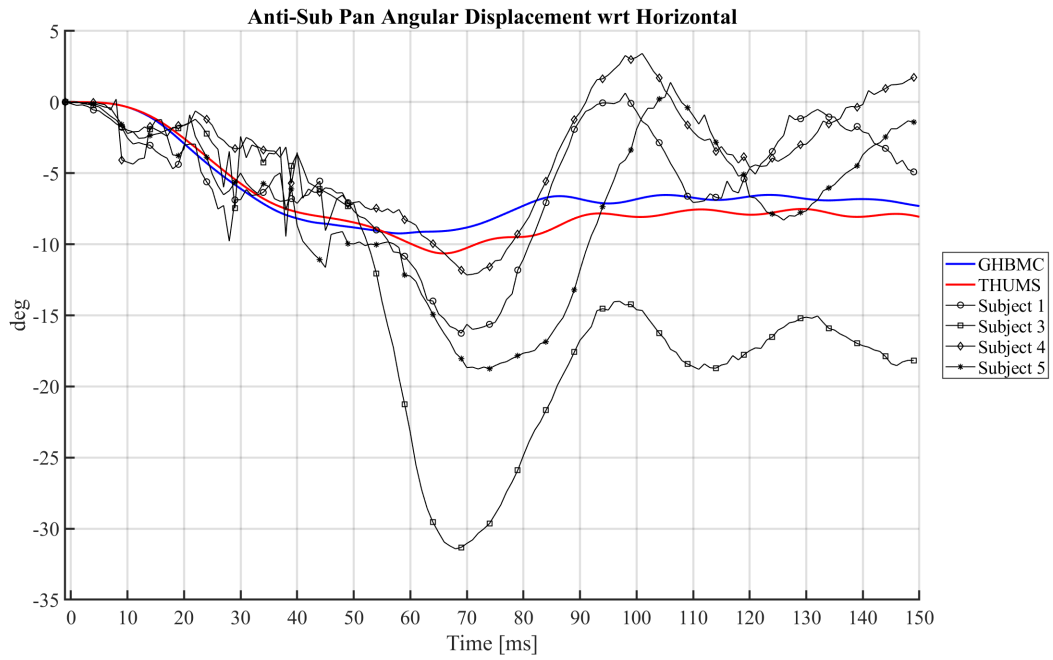


Figure C.81: Anti-Sub Pan Angular Displacement: HBMs (12° Anterior Pelvis Angle) vs. PMHS

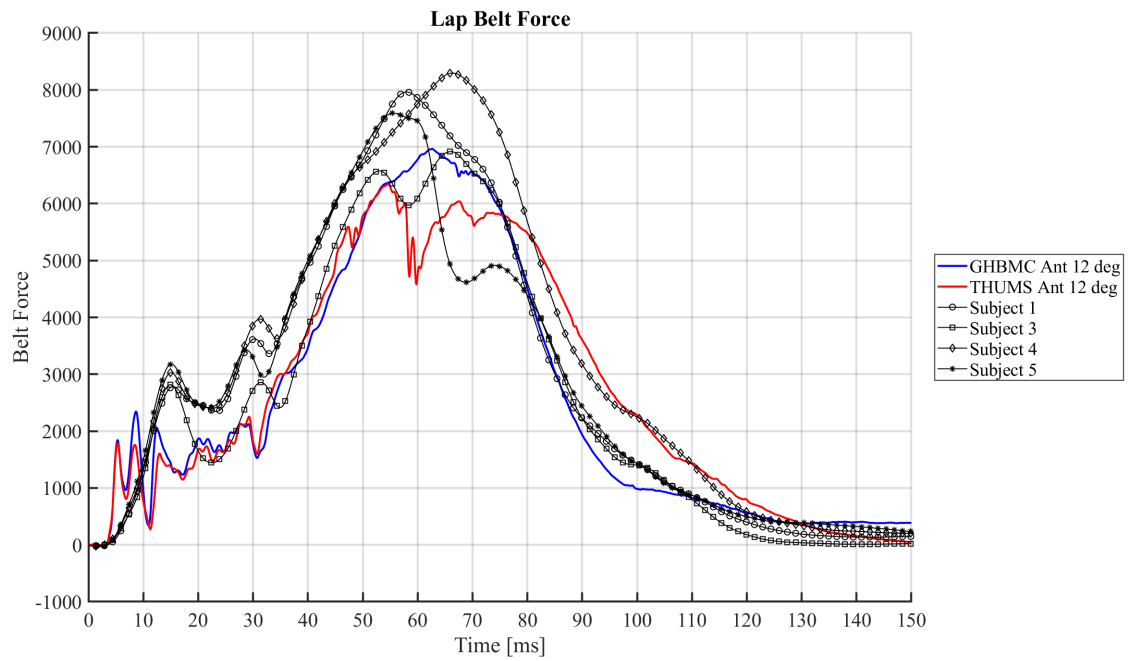


Figure C.82: Lap Belt Tension: HBMs (12° Anterior Pelvis Angle) vs. PMHS

APPENDIX C. RECLINED HBM FRONTAL IMPACT SIMULATIONS

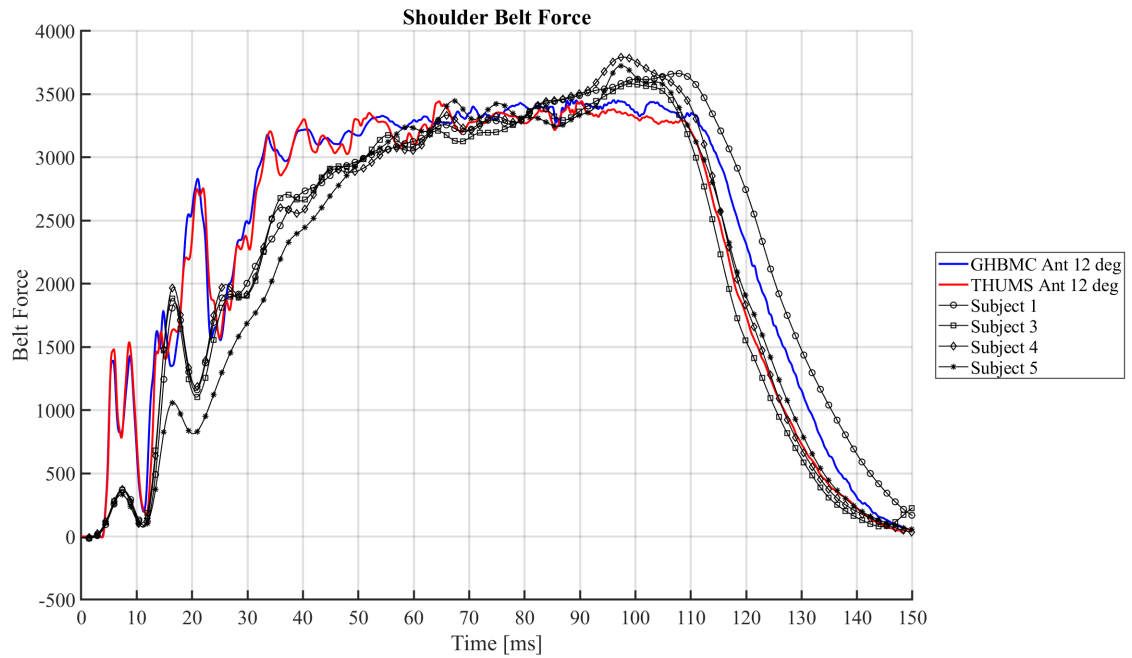


Figure C.83: Shoulder Belt Tension: HBMs (12° Anterior Pelvis Angle) vs. PMHS

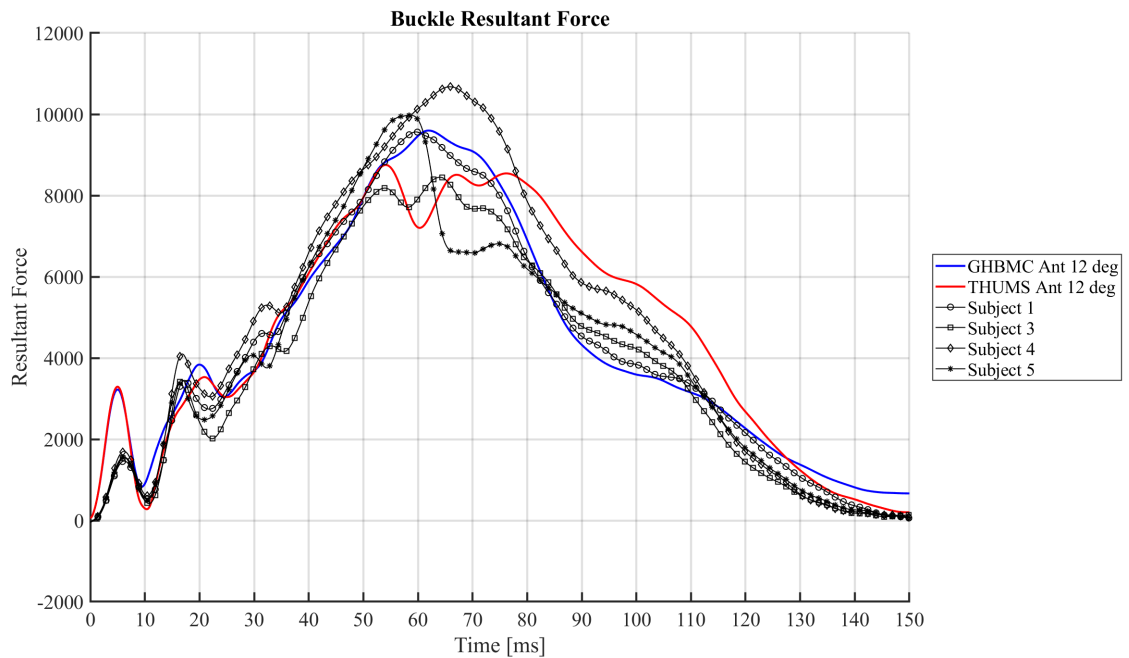


Figure C.84: Buckle Resultant Force: HBMs (12° Anterior Pelvis Angle) vs. PMHS

APPENDIX C. RECLINED HBM FRONTAL IMPACT SIMULATIONS

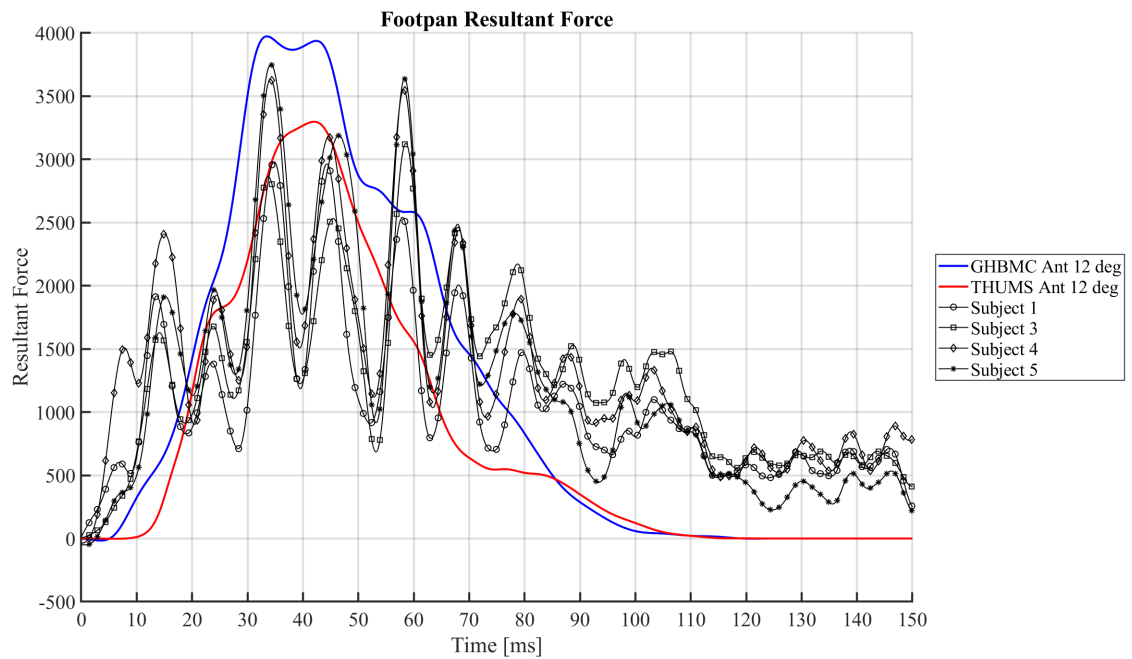


Figure C.85: Foot Pan Resultant Force: HBMs (12° Anterior Pelvis Angle) vs. PMHS

Appendix D

Belt Pull Experiments using PMHS

D.1 Lap Belt Anchorage Positions

Test	X position (mm)
D1589	-1920
D1591	-1832
D1592	-1917
D1594	-1753

Figure D.1: Lap Belt Anchorage Positions per Test wrt Global Reference Frame (see Figure 5.1).

Appendix E

Belt Pull Simulations

E.1 Soft Tissue Load Curve Changes

For the GHBMC model, the material load curves were scaled for the pelvic-abdominal flesh (*MAT_SIMPLIFIED_RUBBER/FOAM) Adipose tissue materials of 35% strain rate and 100% strain rate (see Figure 6.7a). These materials correspond to table IDs (TBIDs) 1999002 and 1999003, respectively. Each of these tables is comprised of different load curves, of which all ordinates were scaled by either 50% or 200% (e.g., E.1).

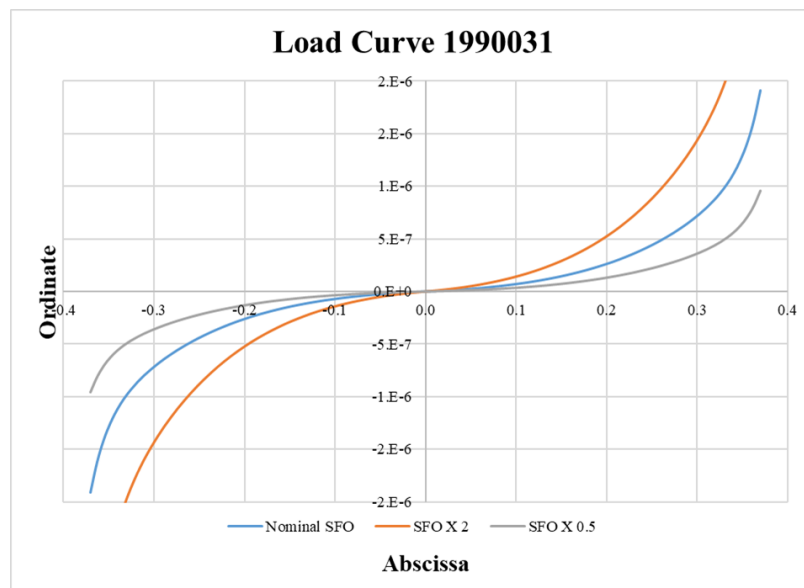


Figure E.1: Example of load curve scaling used for GHBMC.

Appendix F

Belt-ASIS Load Transfer Simulations

F.1 Verification load cases for ASIS cross-sections

Verification load cases were performed to ensure the full applied load was being captured. We did this by applying a concentrated load horizontally, then angled at $\pm 45^\circ$ (Figure F.1). The reaction load measured at the ASIS cross sections show that the full amount of applied load was measured by this method (Figure F.2).

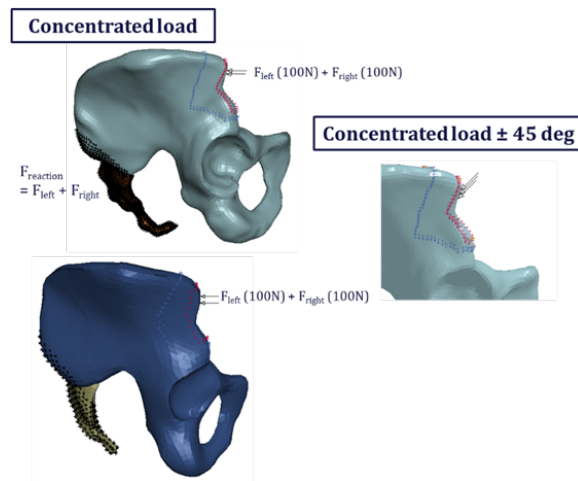


Figure F.1: Concentrated applied load shown for the GHBMC (top) and THUMS (bottom). 100N was applied at each iliac wing as a direct concentrated load as well as a concentrated load angled +45 deg then -45 deg from this nominal 0 deg.

APPENDIX F. BELT-ASIS LOAD TRANSFER SIMULATIONS

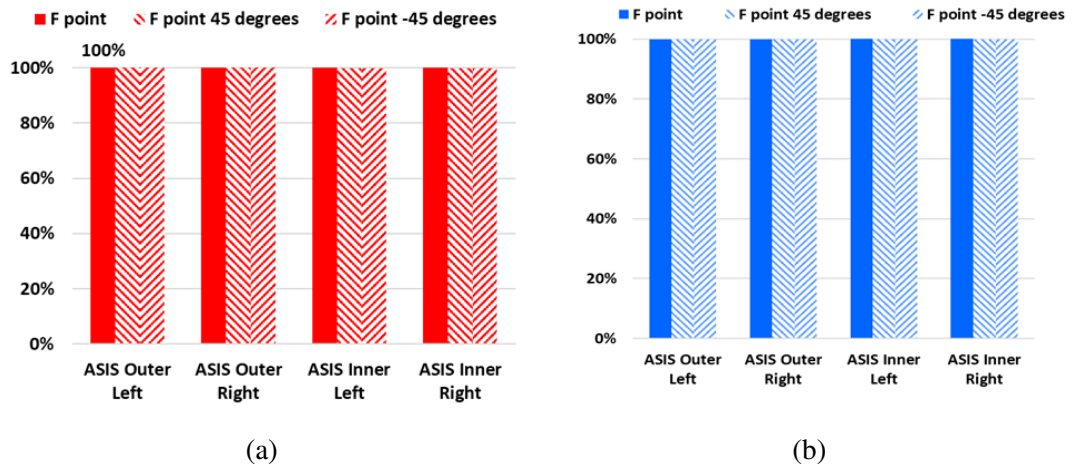


Figure F.2: The % measured load at the outer and inner ASIS cross sections (Left: GHBMC; Right: THUMS). The solid bar indicates the point load directed straight on the ASIS, the bar with the stripes angled down is the point load directed -45 deg downward, and the bar with the stripes angled up is the point load directed +45 deg upward.

F.2 Method to flag lap belt low on ASIS cases

A method to flag these cases was developed to detect the simulations in which the upper edge of the lap belt does not meet the AIIS. Figure F.3a shows a red area between the AIIS and ASIS nodes. If the upper edge of the belt (measured as the belt node that corresponded to the ASIS midpoint) did not translate further than 10 mm above (+Z) the AIIS node by 60 ms, or if the upper edge of the belt translated between 10-35 mm above (+Z) the AIIS node but did not move within 20 mm (+X) of the AIIS node by 60 ms, it was flagged as a “lap belt low on pelvis” case. The X-component was incorporated as there were many cases in which the upper edge of the belt was positioned further than 10 mm (+Z) relative to the AIIS, but was still located further anterior, toward the thighs, and did not move (Figure F.3b).

APPENDIX F. BELT-ASIS LOAD TRANSFER SIMULATIONS

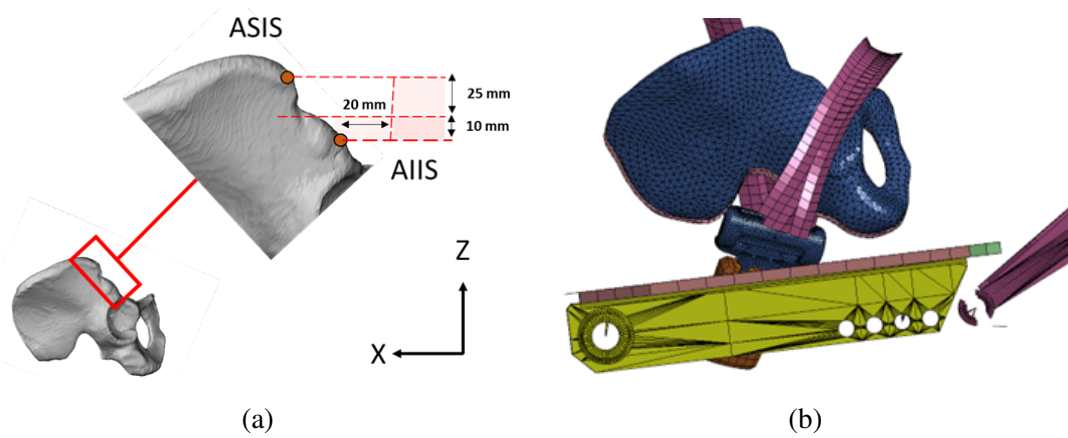


Figure F.3: a) Region showing where the “belt low” cases were flagged: If the upper edge of the belt did not pass further than 10 mm above (+Z) the AIIS, or if it passed between 10-35 mm above (+Z) the AIIS, but did not move within 20 mm (+X) the AIIS, the simulation was flagged. b) An image taken during a simulation wherein the belt was above 10 mm (+Z) the AIIS, but not within 20 mm (+X) – this image taken of the THUMS pelvis.

Appendix G

Pelvis Orientations of GHBMC Model

Table G.1: Pelvis orientations for the positioned model: 2 torso angles and 3 pelvis orientations.

Torso Angle	Pelvis Adjustment	Nyquist Angle (deg)
Recline	-12deg	144.5
	Nominal	156.5
	+12deg	168.5
Upright	-12deg	120.1
	Nominal	132.1
	+12deg	144.1

APPENDIX G. PELVIS ORIENTATIONS OF GHBMC MODEL

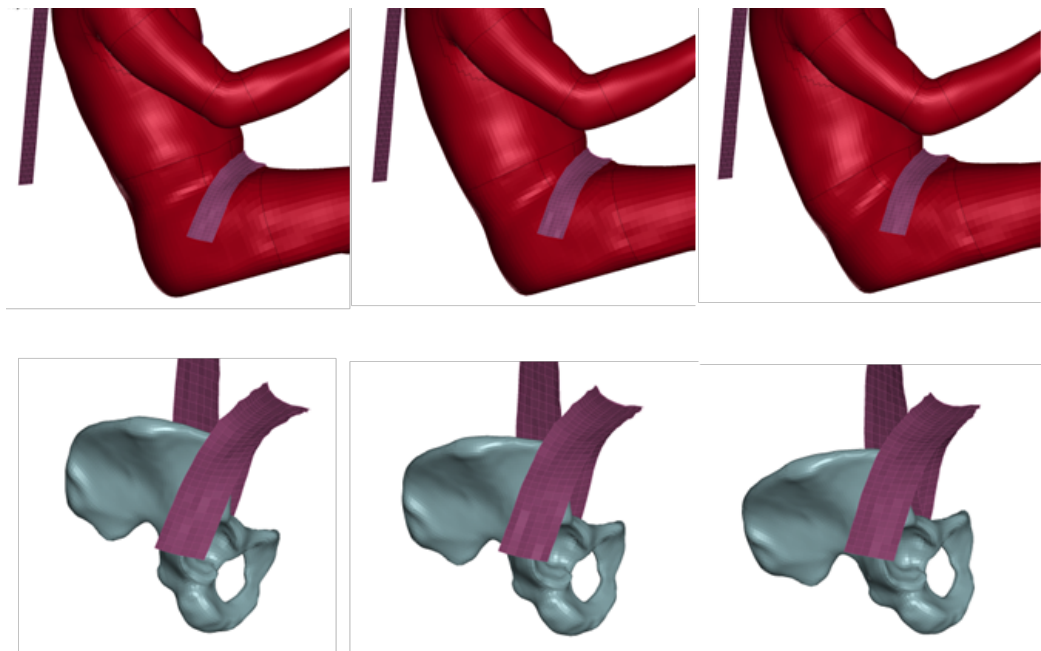


Figure G.1: Lap belt placement (no change in fore-aft or lateral anchorage position) for different pelvis angles in the upright condition. Left-right: anterior (+12°), nominal, and posterior angle (-12°).

Appendix H

Neural Network Metamodel Development

H.1 AU-ROC for Monitoring Error

In addition to accuracy, the area under receiver operator curve (AU-ROC) was used to monitor the metamodel's error in predicting submarining occurrence. The ROC curve showed the trade-off between the true positive rate (sensitivity; correctly identified cases) and the false positive rate (specificity; incorrectly identified cases), which shows the decrease in sensitivity results in an increase in specificity. Sensitivity measures the actual positives that are correctly identified, while specificity measures the proportion of actual negatives that are correctly identified. The higher the AU-ROC, the higher measure of separability the model has – i.e., the model can accurately distinguish between submarining (1's) and non-submarining (0's). The AU-ROC of a perfectly predictive model equals 1. If the AU-ROC is 0, it implies that the predictor is perfectly incorrect, meaning it predicts all 0's as 1's and all 1's as 0's. A model that makes random guesses has an AU-ROC score of 0.5. For example, if AU-ROC is 0.7, it means there is a 70% chance that the model will be able to distinguish between 0's and 1's (i.e., non-submarining vs. submarining).

H.2 Training and Testing Progression of Model Performance

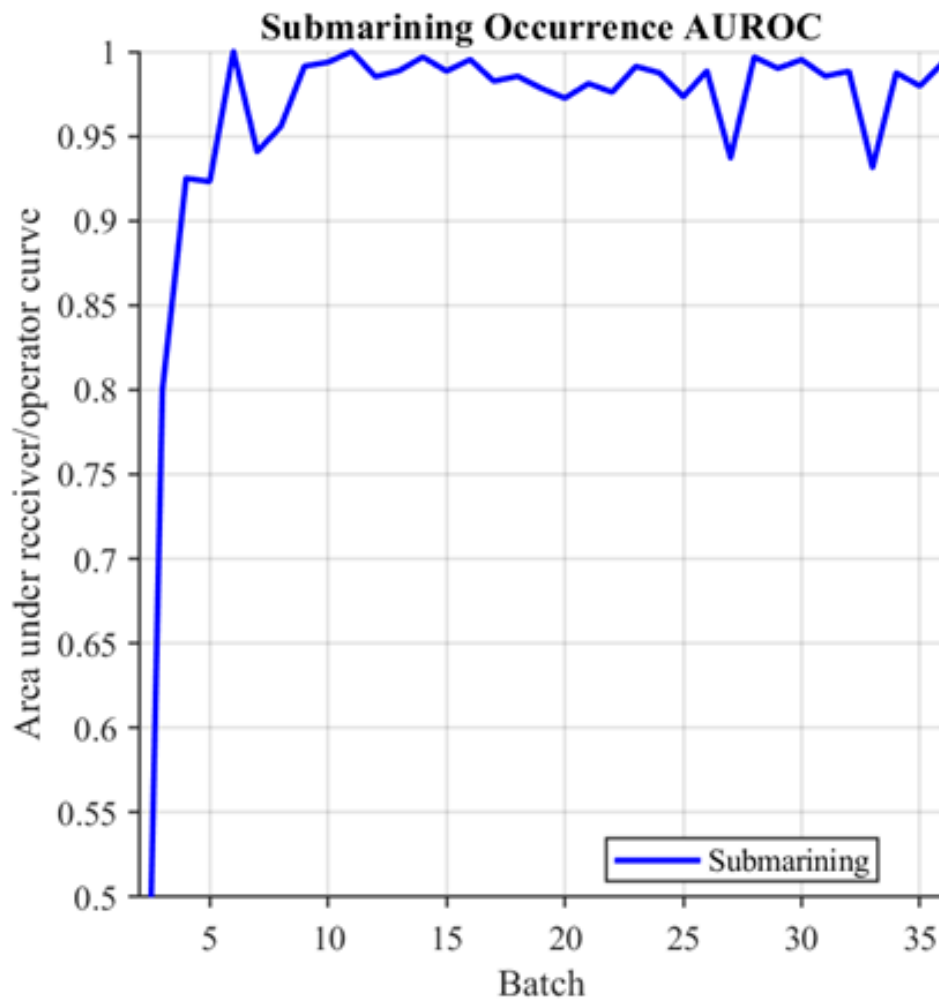


Figure H.1: The progression of submarining prediction using the area under the receiver/operator curve (AUROC). An AUROC value of 0.5 indicates no predictive capability, while an AUROC of 1 indicates perfect prediction.

APPENDIX H. NEURAL NETWORK METAMODEL DEVELOPMENT

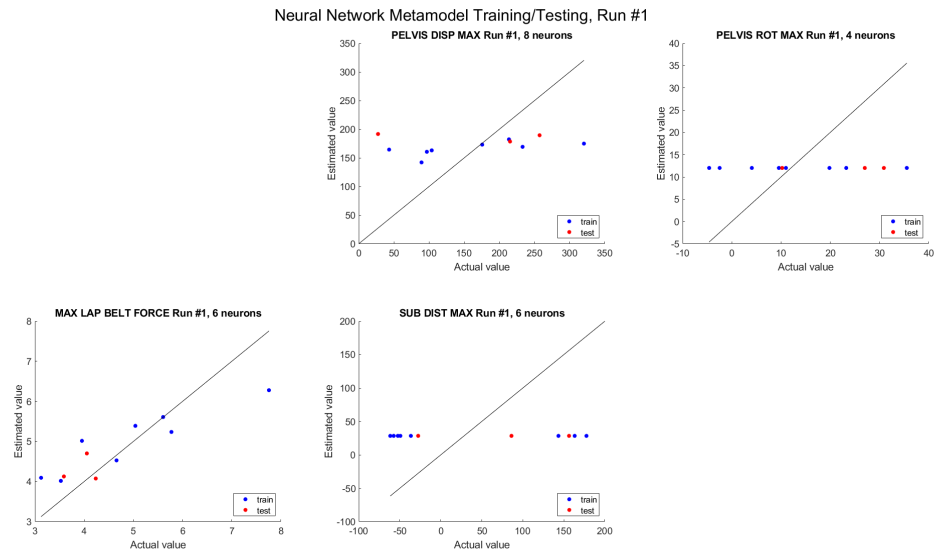


Figure H.2: Predicted and actual values of the training and testing points for the output metrics (Batch 1).

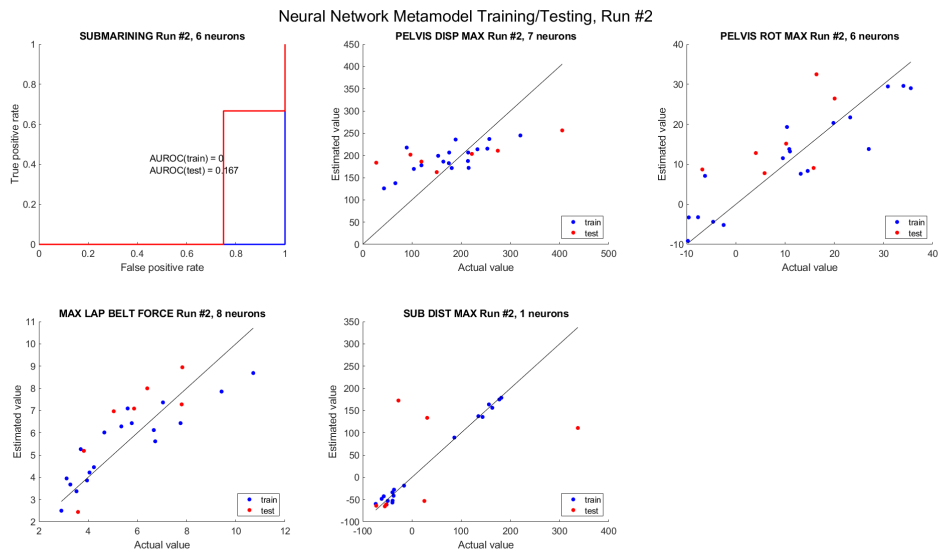


Figure H.3: Predicted and actual values of the training and testing points for the output metrics (Batch 2).

APPENDIX H. NEURAL NETWORK METAMODEL DEVELOPMENT

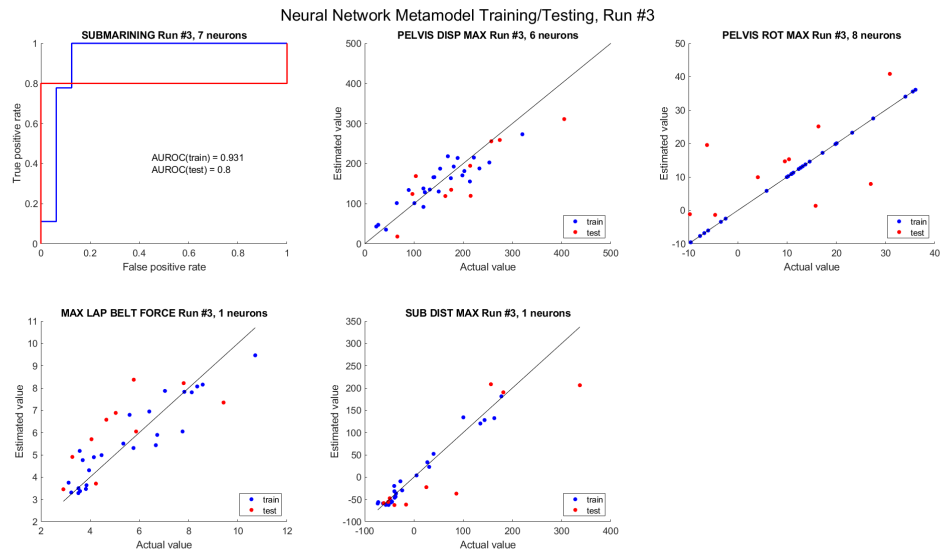


Figure H.4: Predicted and actual values of the training and testing points for the output metrics (Batch 3).

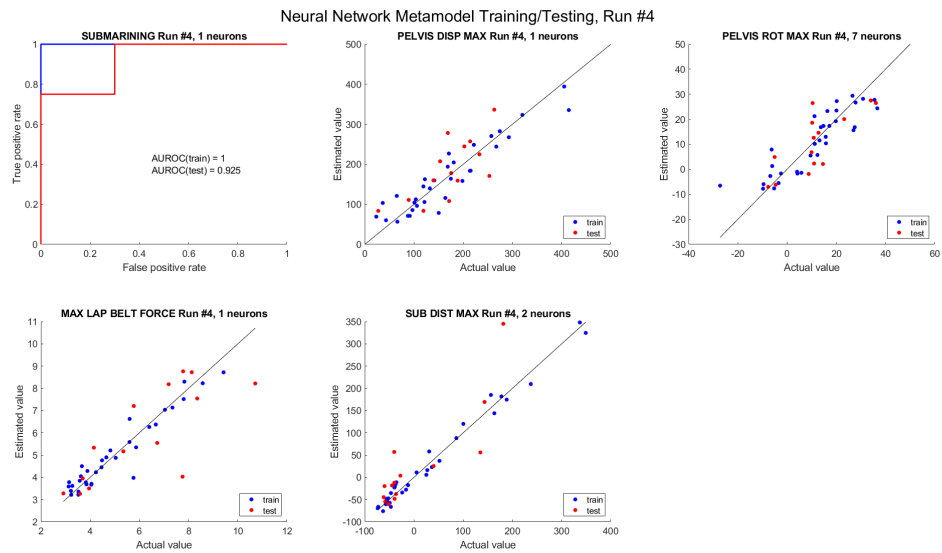


Figure H.5: Predicted and actual values of the training and testing points for the output metrics (Batch 4).

APPENDIX H. NEURAL NETWORK METAMODEL DEVELOPMENT

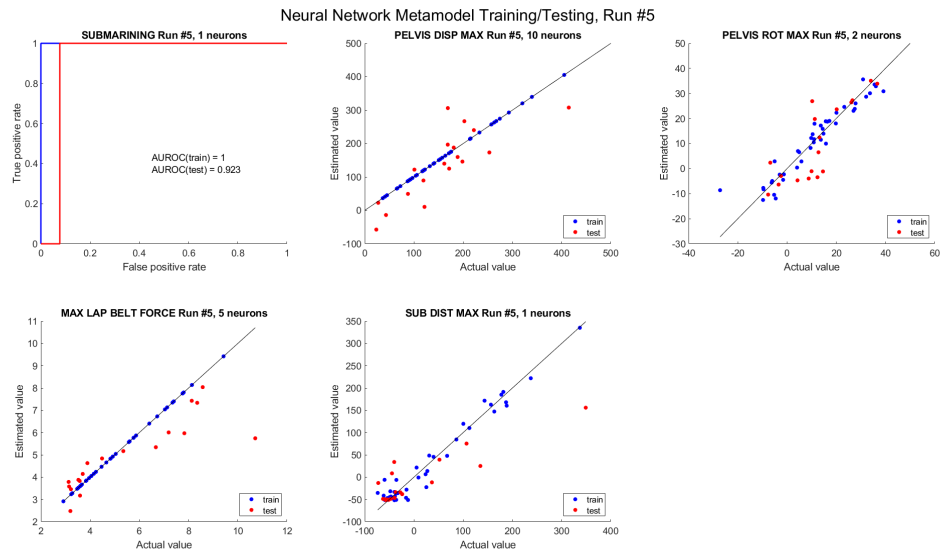


Figure H.6: Predicted and actual values of the training and testing points for the output metrics (Batch 5).

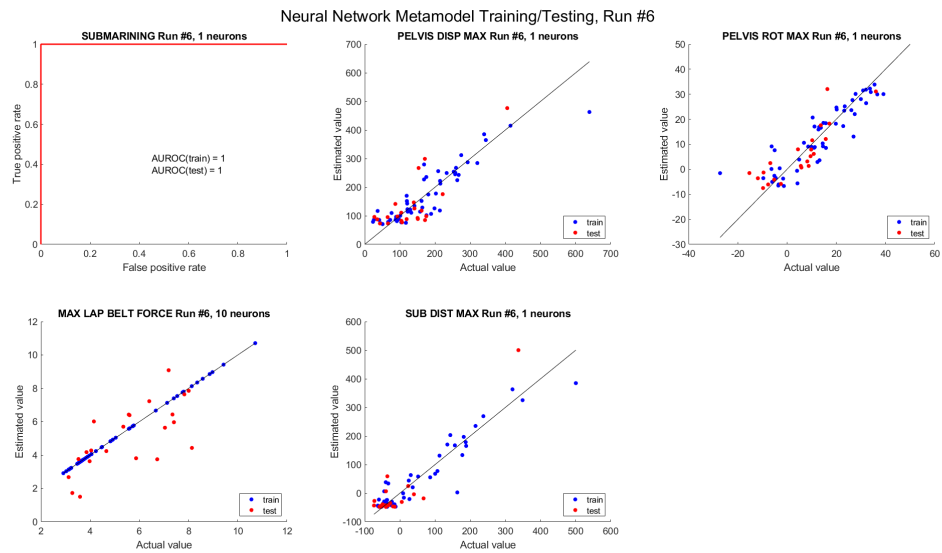


Figure H.7: Predicted and actual values of the training and testing points for the output metrics (Batch 6).

APPENDIX H. NEURAL NETWORK METAMODEL DEVELOPMENT

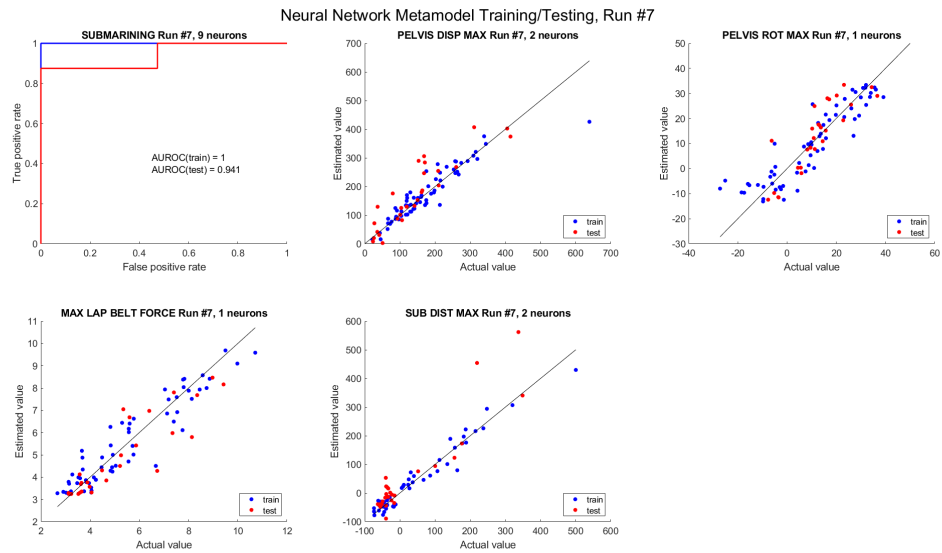


Figure H.8: Predicted and actual values of the training and testing points for the output metrics (Batch 7).

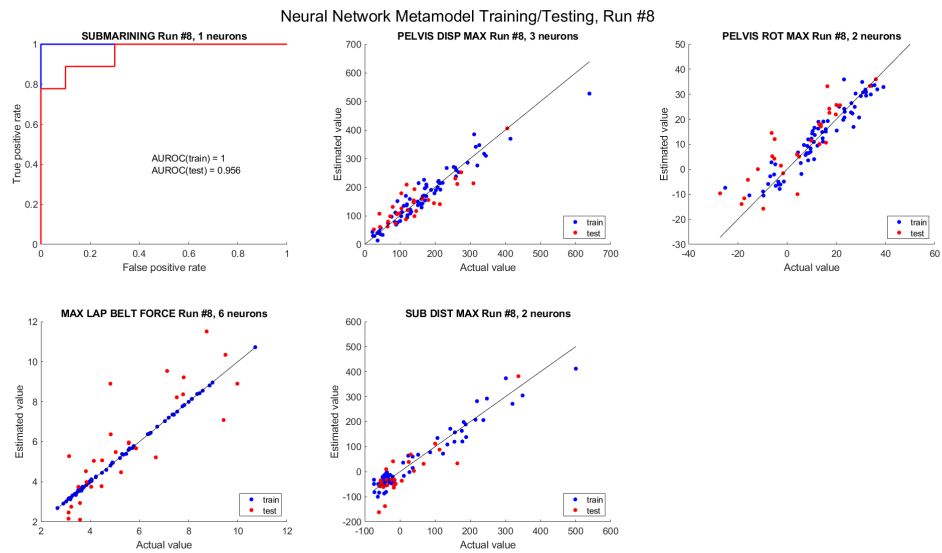


Figure H.9: Predicted and actual values of the training and testing points for the output metrics (Batch 8).

APPENDIX H. NEURAL NETWORK METAMODEL DEVELOPMENT

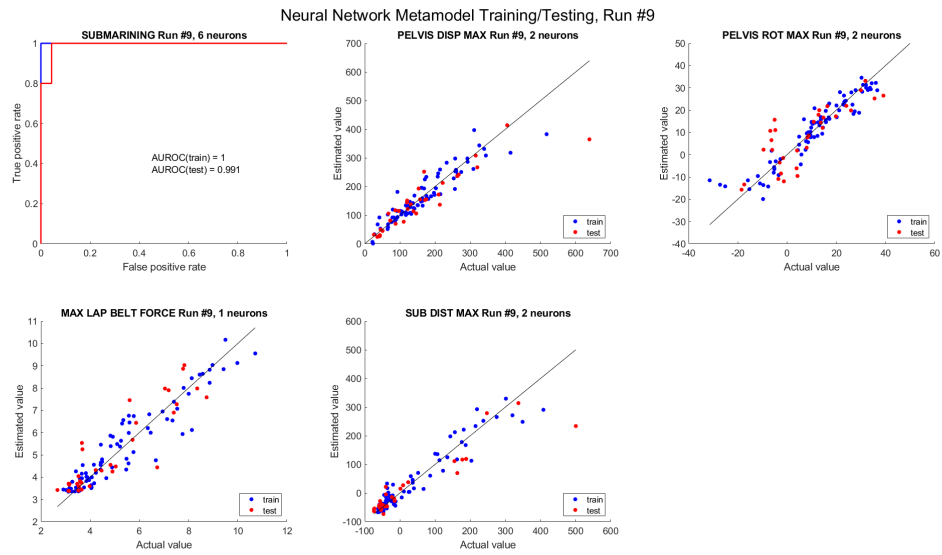


Figure H.10: Predicted and actual values of the training and testing points for the output metrics (Batch 9).

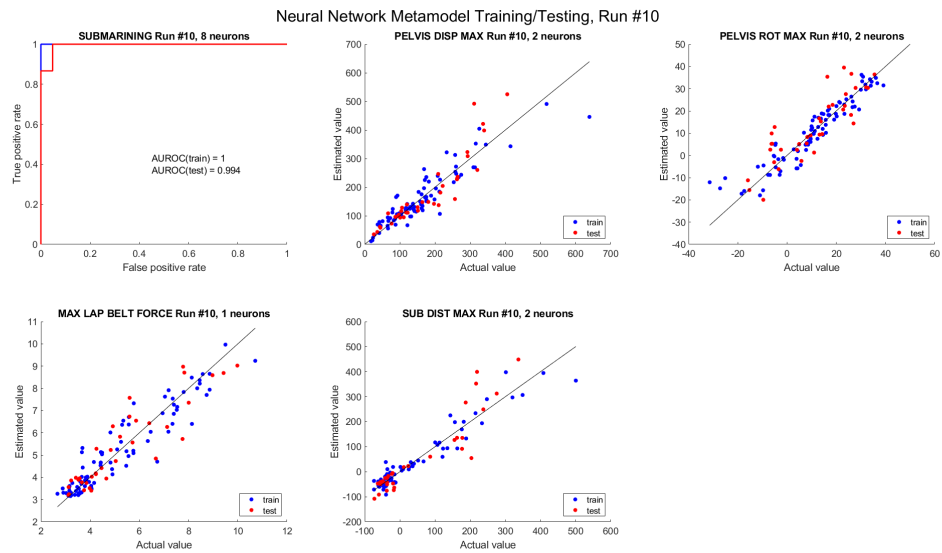


Figure H.11: Predicted and actual values of the training and testing points for the output metrics (Batch 10).

APPENDIX H. NEURAL NETWORK METAMODEL DEVELOPMENT

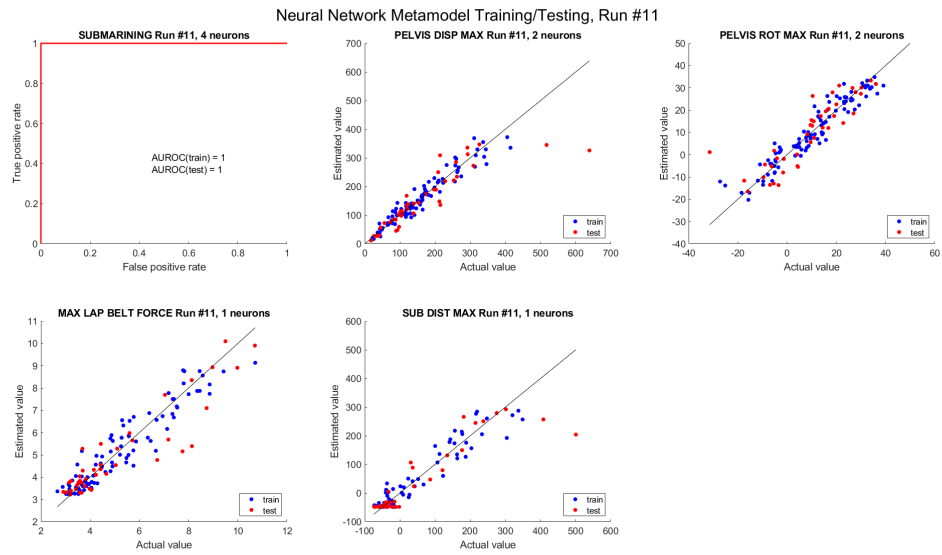


Figure H.12: Predicted and actual values of the training and testing points for the output metrics (Batch 11).

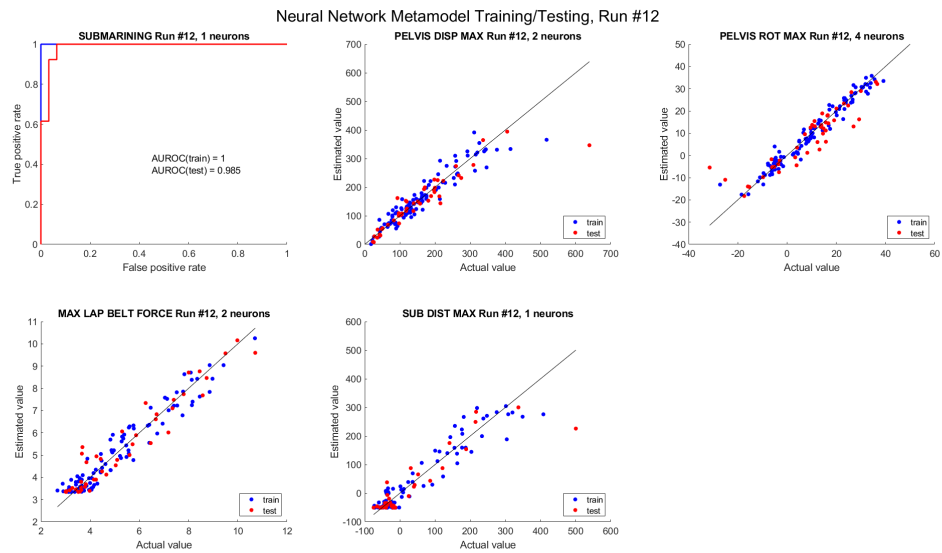


Figure H.13: Predicted and actual values of the training and testing points for the output metrics (Batch 12).

APPENDIX H. NEURAL NETWORK METAMODEL DEVELOPMENT

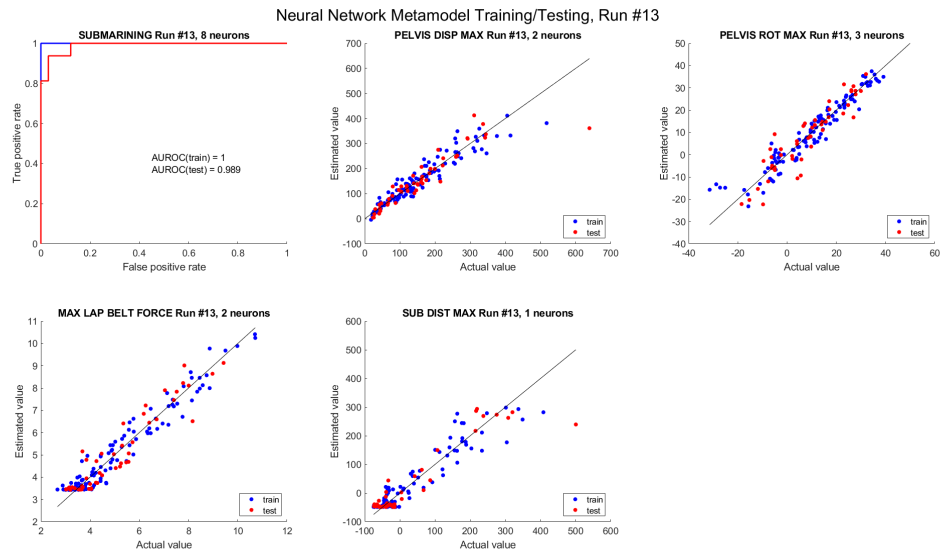


Figure H.14: Predicted and actual values of the training and testing points for the output metrics (Batch 13).

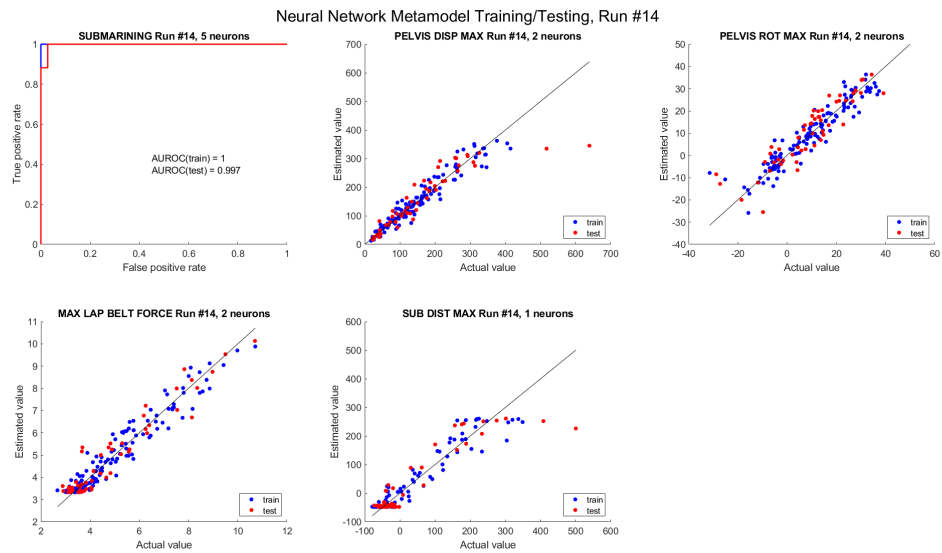


Figure H.15: Predicted and actual values of the training and testing points for the output metrics (Batch 14).

APPENDIX H. NEURAL NETWORK METAMODEL DEVELOPMENT

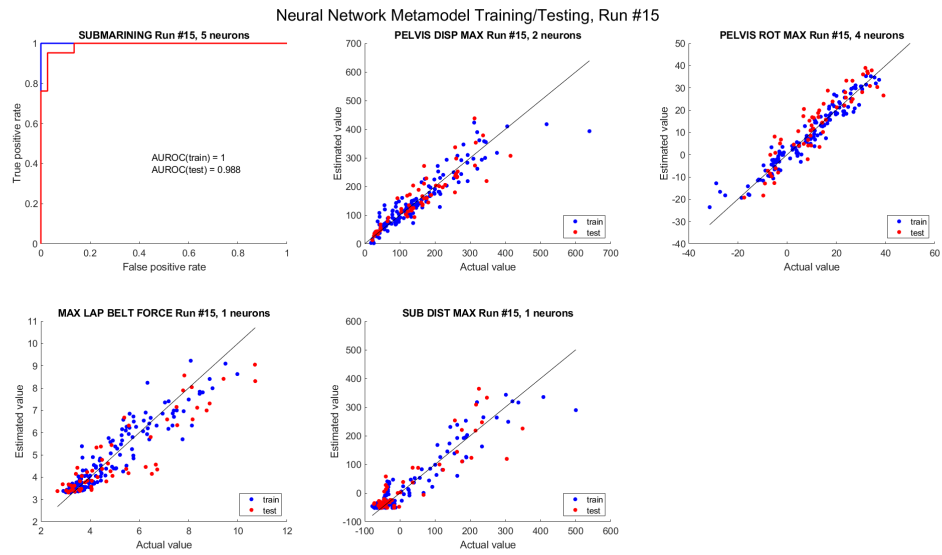


Figure H.16: Predicted and actual values of the training and testing points for the output metrics (Batch 15).

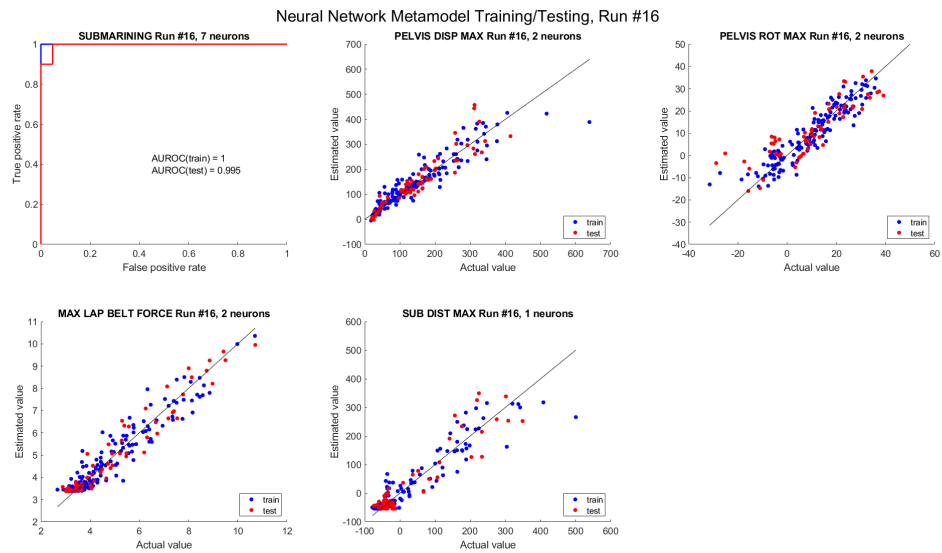


Figure H.17: Predicted and actual values of the training and testing points for the output metrics (Batch 16).

APPENDIX H. NEURAL NETWORK METAMODEL DEVELOPMENT

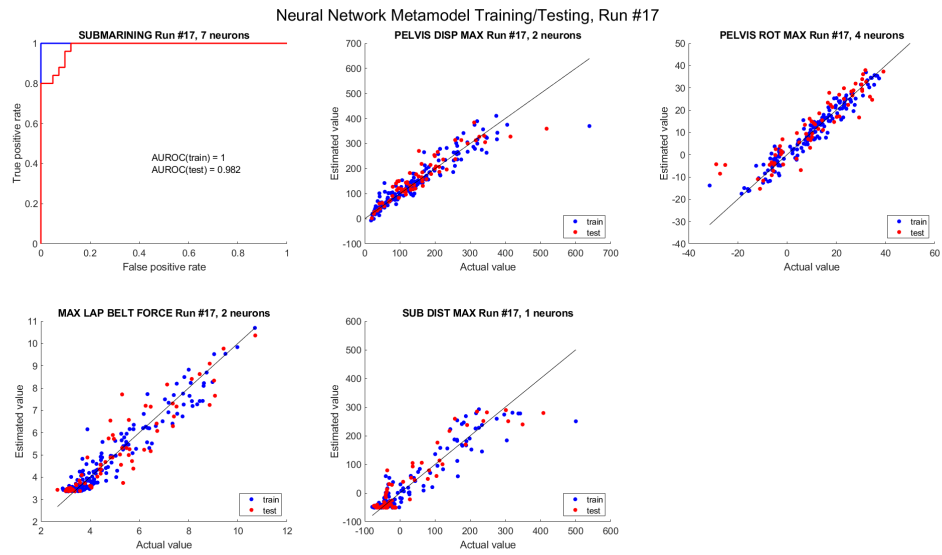


Figure H.18: Predicted and actual values of the training and testing points for the output metrics (Batch 17).

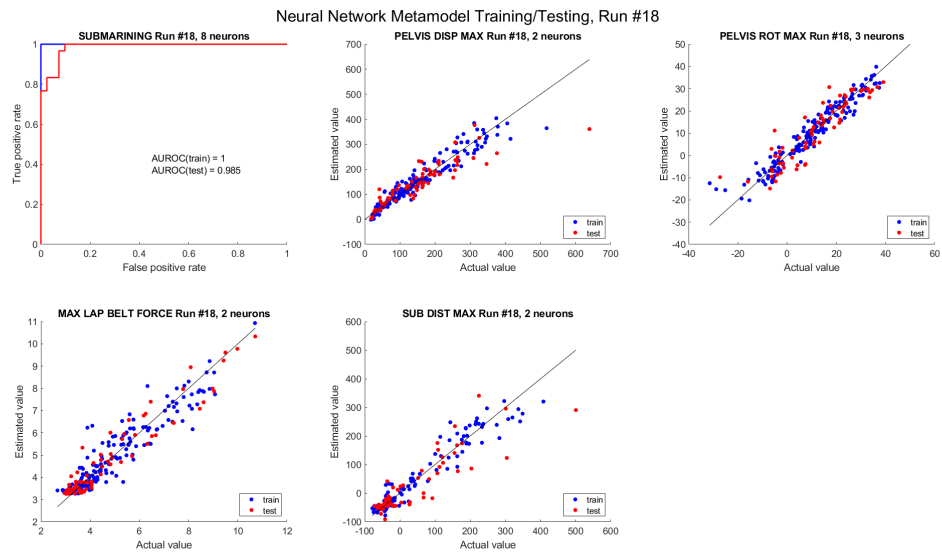


Figure H.19: Predicted and actual values of the training and testing points for the output metrics (Batch 18).

APPENDIX H. NEURAL NETWORK METAMODEL DEVELOPMENT

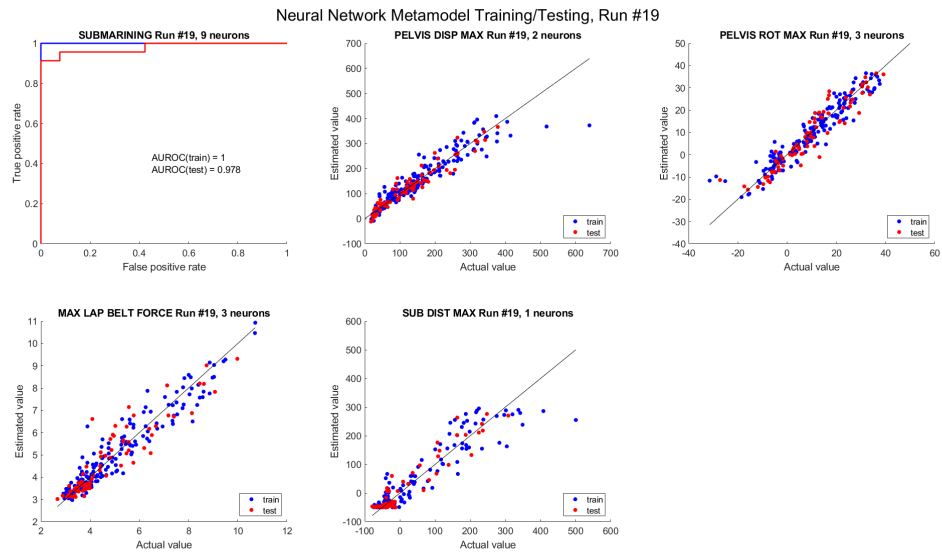


Figure H.20: Predicted and actual values of the training and testing points for the output metrics (Batch 19).

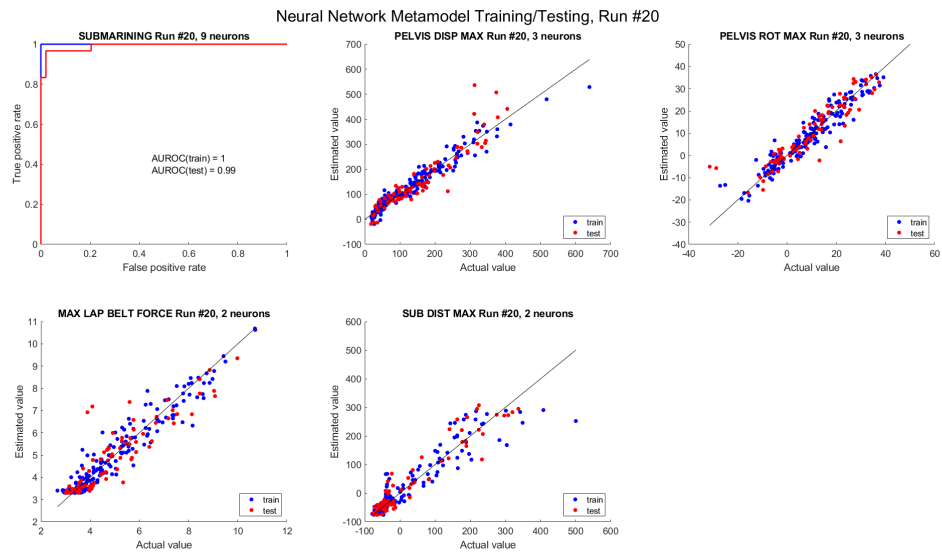


Figure H.21: Predicted and actual values of the training and testing points for the output metrics (Batch 20).

APPENDIX H. NEURAL NETWORK METAMODEL DEVELOPMENT

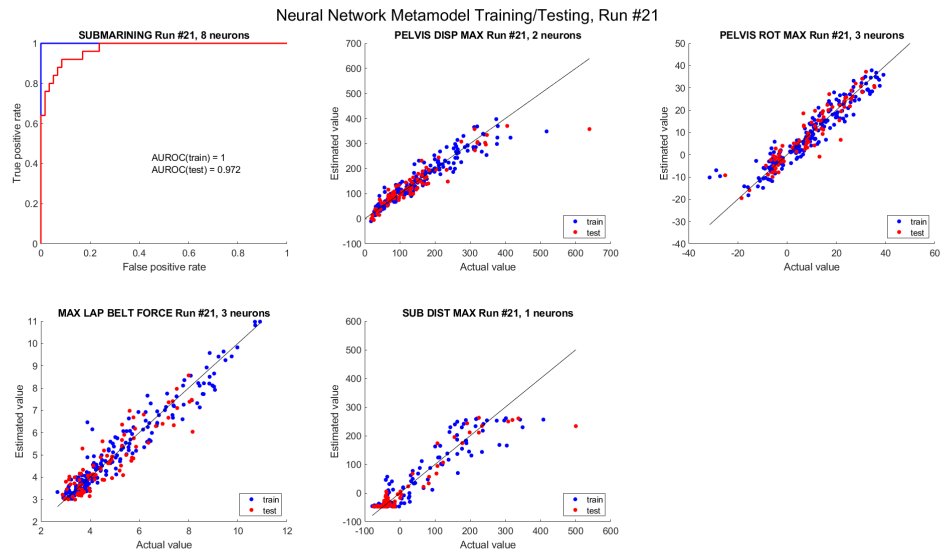


Figure H.22: Predicted and actual values of the training and testing points for the output metrics (Batch 21).

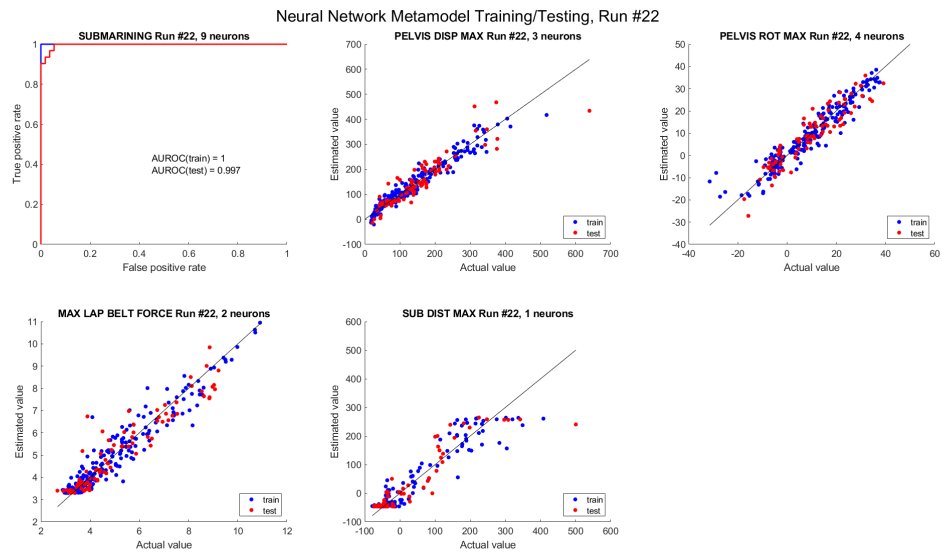


Figure H.23: Predicted and actual values of the training and testing points for the output metrics (Batch 22).

APPENDIX H. NEURAL NETWORK METAMODEL DEVELOPMENT

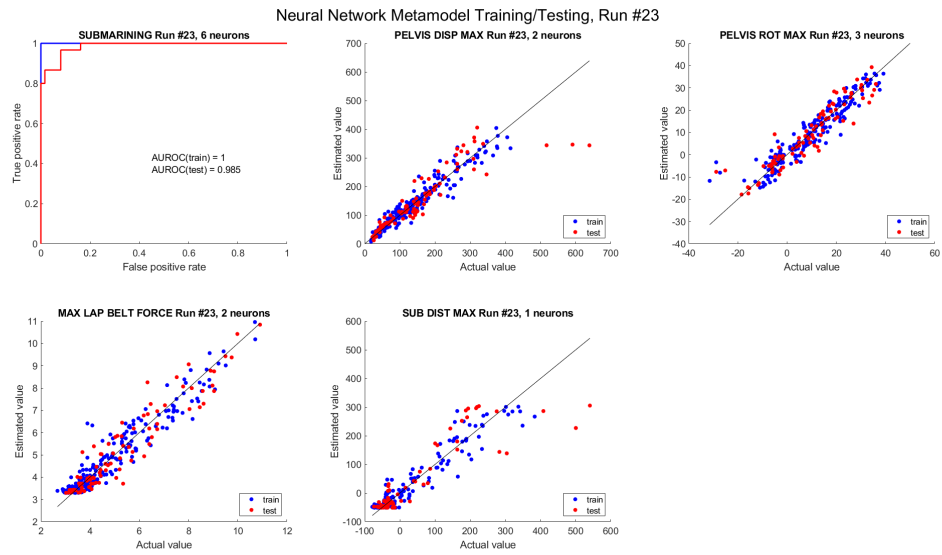


Figure H.24: Predicted and actual values of the training and testing points for the output metrics (Batch 23).

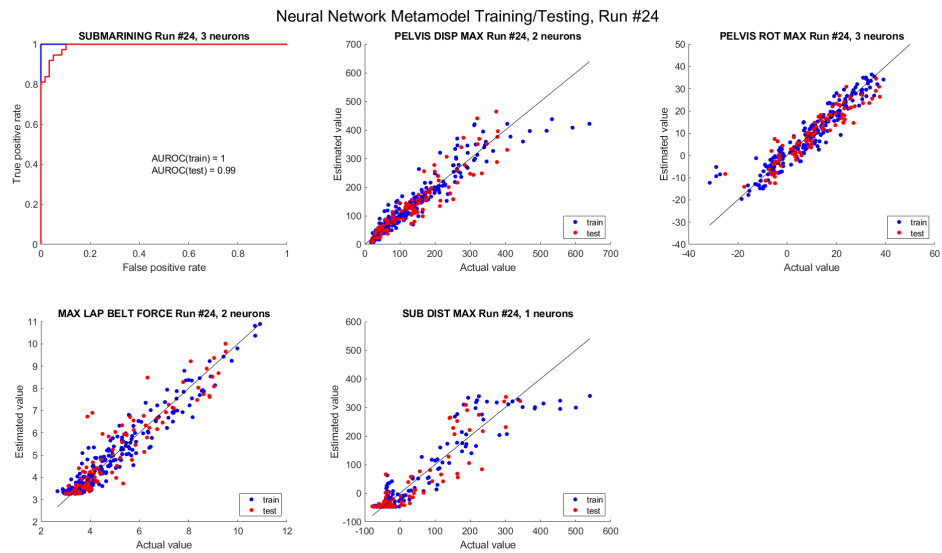


Figure H.25: Predicted and actual values of the training and testing points for the output metrics (Batch 24).

APPENDIX H. NEURAL NETWORK METAMODEL DEVELOPMENT

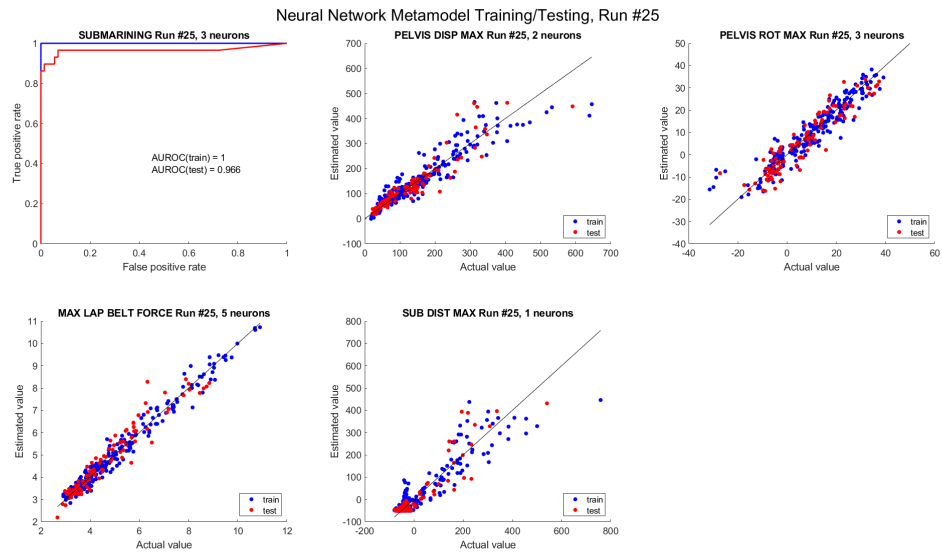


Figure H.26: Predicted and actual values of the training and testing points for the output metrics (Batch 25).

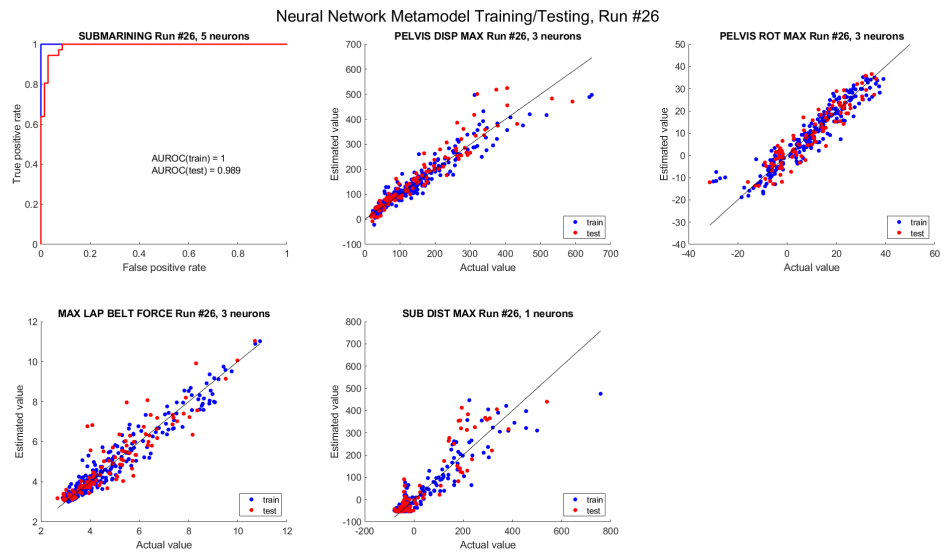


Figure H.27: Predicted and actual values of the training and testing points for the output metrics (Batch 26).

APPENDIX H. NEURAL NETWORK METAMODEL DEVELOPMENT

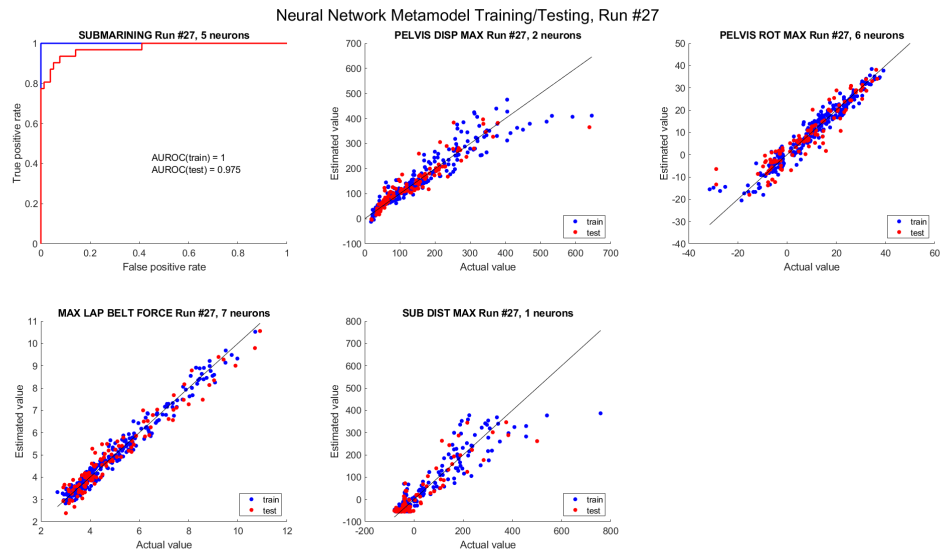


Figure H.28: Predicted and actual values of the training and testing points for the output metrics (Batch 27).

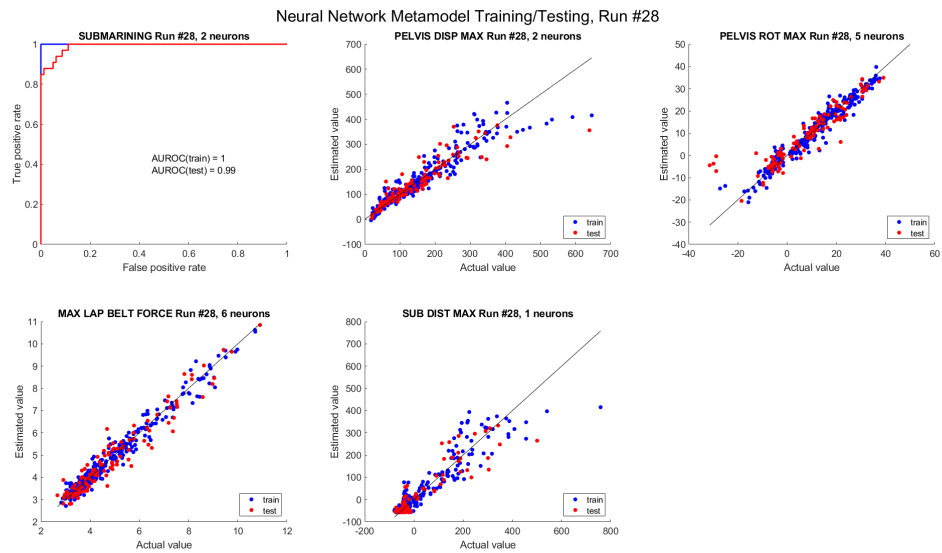


Figure H.29: Predicted and actual values of the training and testing points for the output metrics (Batch 28).

APPENDIX H. NEURAL NETWORK METAMODEL DEVELOPMENT

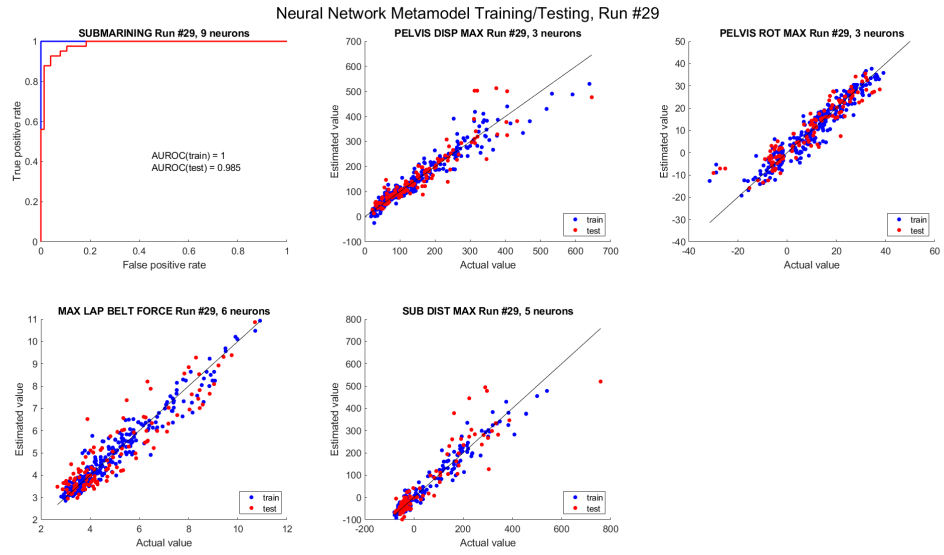


Figure H.30: Predicted and actual values of the training and testing points for the output metrics (Batch 29).

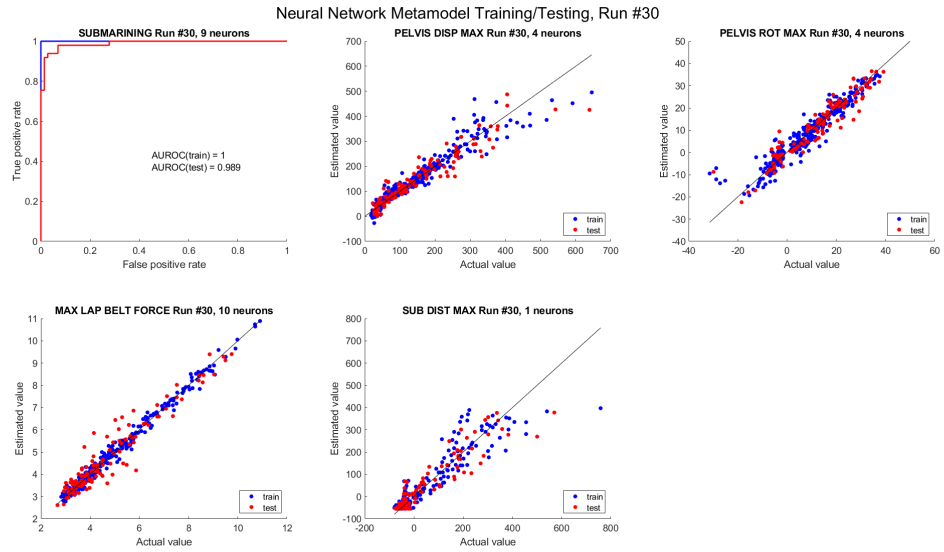


Figure H.31: Predicted and actual values of the training and testing points for the output metrics (Batch 30).

APPENDIX H. NEURAL NETWORK METAMODEL DEVELOPMENT

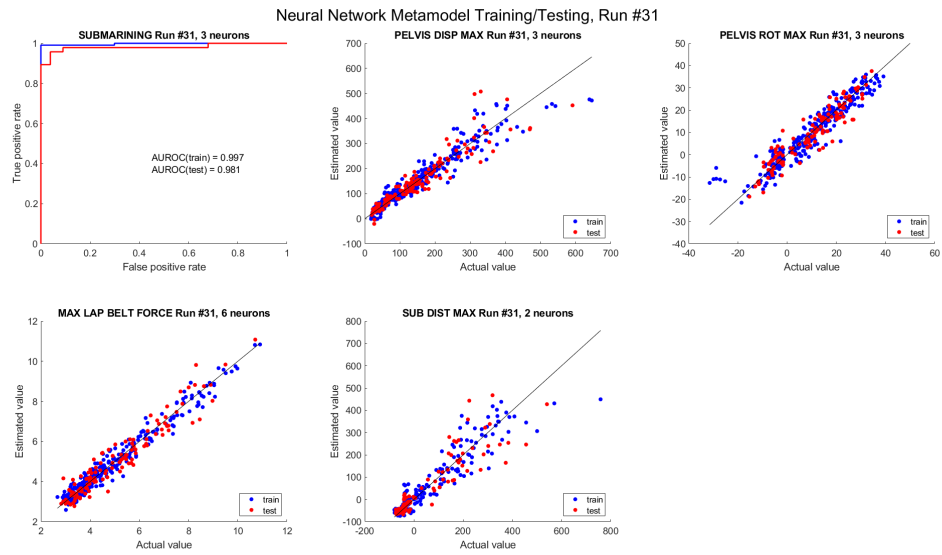


Figure H.32: Predicted and actual values of the training and testing points for the output metrics (Batch 31).

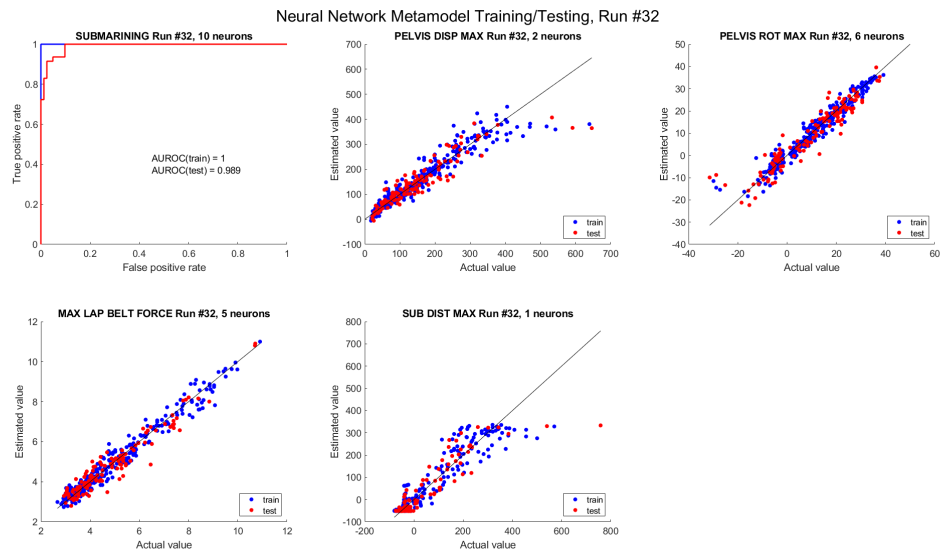


Figure H.33: Predicted and actual values of the training and testing points for the output metrics (Batch 32).

APPENDIX H. NEURAL NETWORK METAMODEL DEVELOPMENT

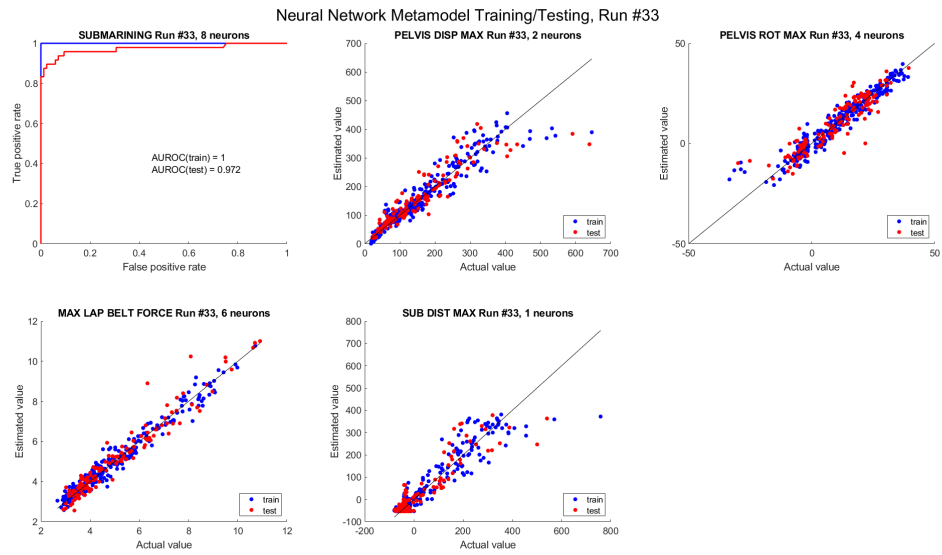


Figure H.34: Predicted and actual values of the training and testing points for the output metrics (Batch 33).

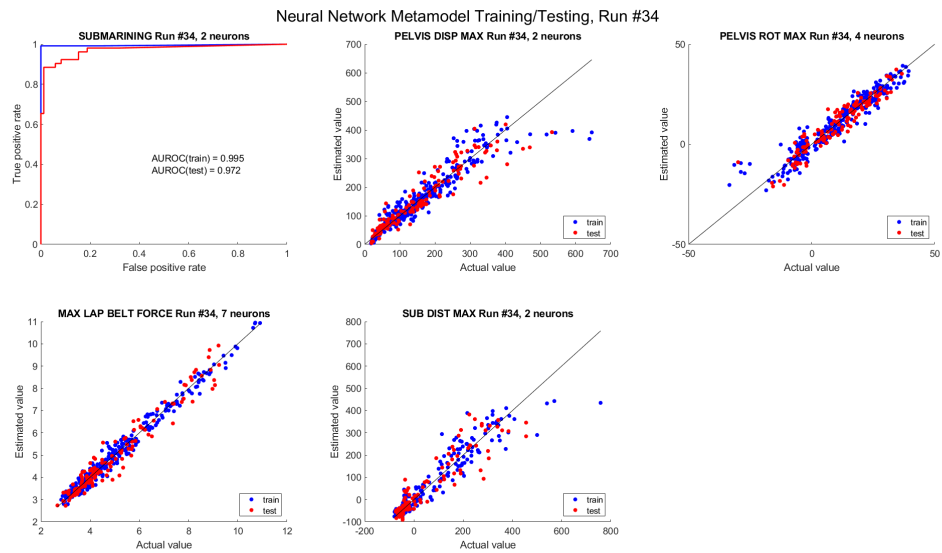


Figure H.35: Predicted and actual values of the training and testing points for the output metrics (Batch 34).

APPENDIX H. NEURAL NETWORK METAMODEL DEVELOPMENT

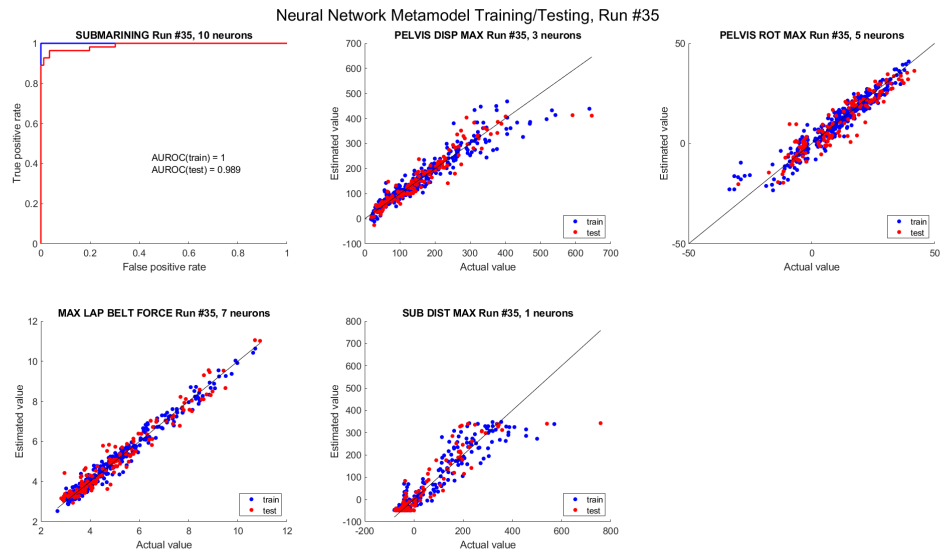


Figure H.36: Predicted and actual values of the training and testing points for the output metrics (Batch 35).

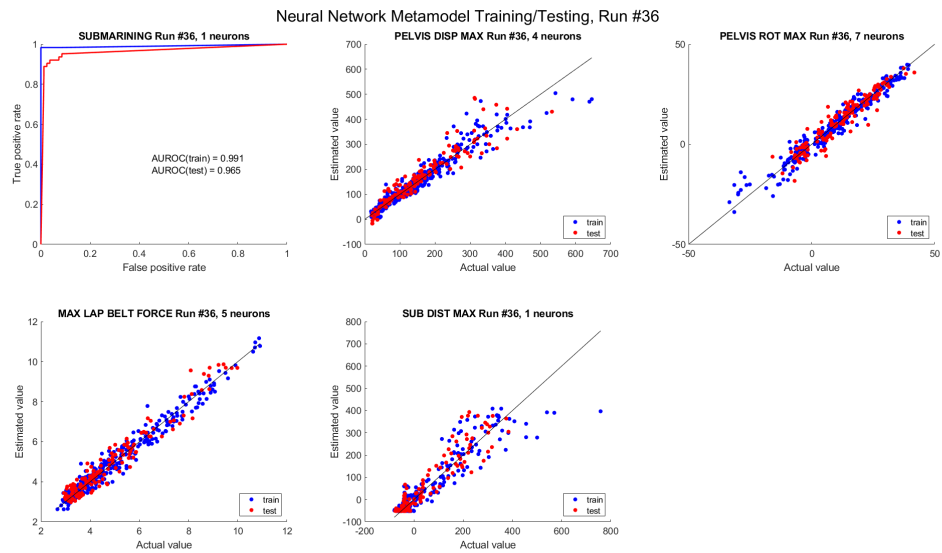


Figure H.37: Predicted and actual values of the training and testing points for the output metrics (Batch 36).

Appendix I

Analysis of Simulated Dataset

I.1 Distribution of Output Metrics

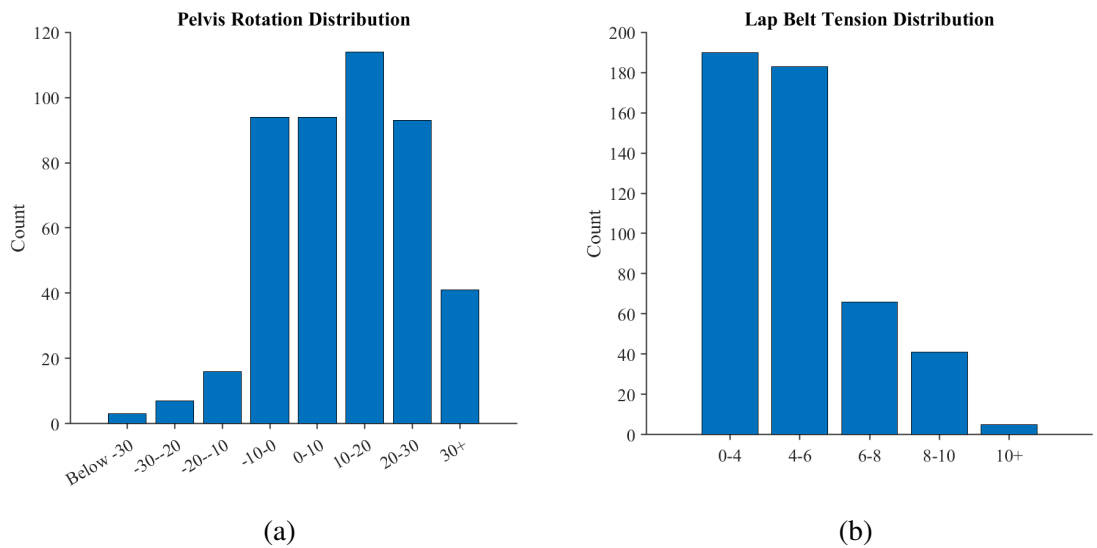


Figure I.1: The frequency of output metric magnitudes for the continuous output metrics for which two clusters were chosen in the k-means clustering analysis: a) Pelvis rotation; b) Lap belt tension

APPENDIX I. ANALYSIS OF SIMULATED DATASET

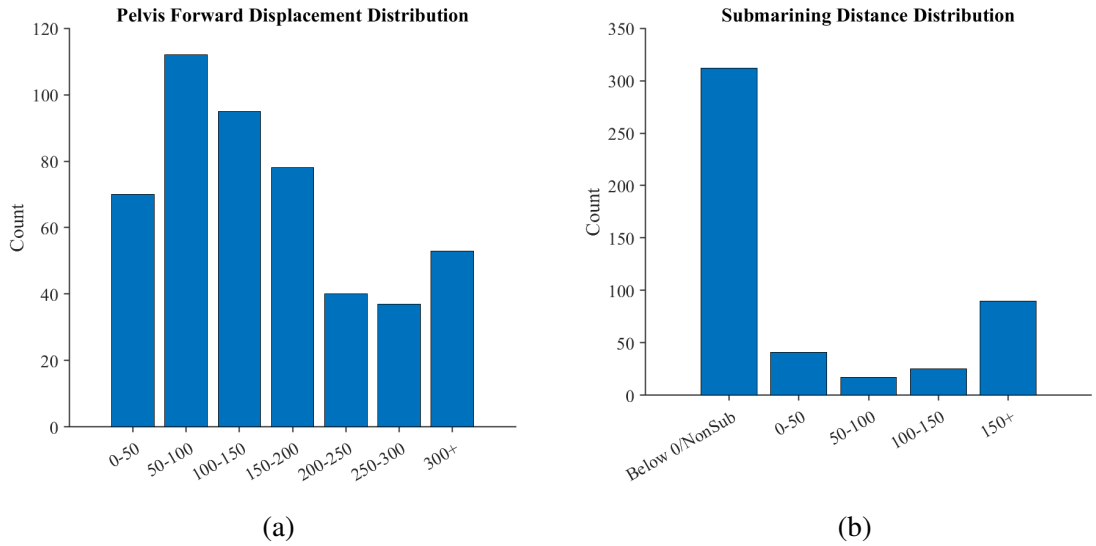


Figure I.2: The frequency of output metric magnitudes for the continuous output metrics for which three clusters were chosen in the k-means clustering analysis: a) Pelvis displacement; b) Submarining distance

I.2 K-Means Clustering Analysis

I.2.1 Submarining Occurrence

I.2.1.1 Influential Parameter Ranking

	Impact Pulse	Lap Belt Angle Fore-Aft	Lap Belt Angle Lateral	Foot Support	Belt Friction	Seat Friction	Recline Angle	Flesh Stiffness	Pelvis Angle
Cluster 1 Mean	0.364	0.741	0.485	0.485	0.498	0.543	0.386	0.495	0.520
Cluster 2 Mean	0.528	0.147	0.519	0.478	0.508	0.462	0.687	0.500	0.431
Absolute Distance	0.164	0.594	0.034	0.007	0.010	0.081	0.301	0.005	0.088
Rank	3	1	6	8	7	5	2	9	4

Figure I.3: Influential parameter determination for submarining occurrence. The parameters in green showed an absolute distance greater than 0.1 between cluster means (negative versus positive outcome); the parameters in yellow showed an absolute distance greater than 0.05 between cluster means (negative versus positive outcome).

I.2.1.2 Influential Parameter Plots

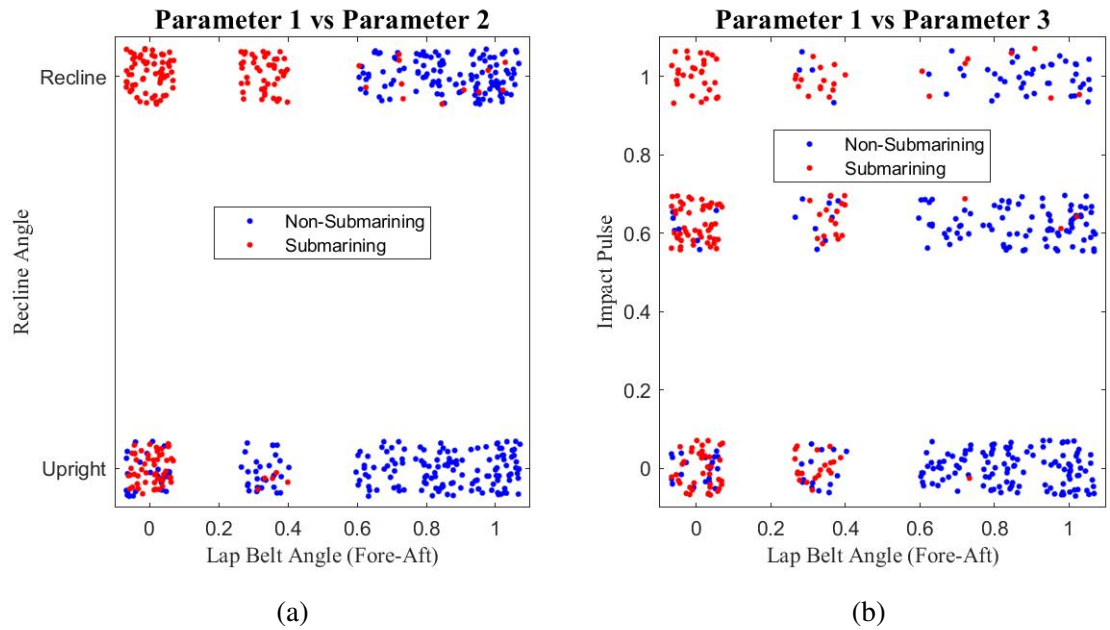


Figure I.4: Submarining occurrence influential parameter plots (automated simulation dataset): a) Parameter 1 vs Parameter 2, b) Parameter 1 vs Parameter 3.

APPENDIX I. ANALYSIS OF SIMULATED DATASET

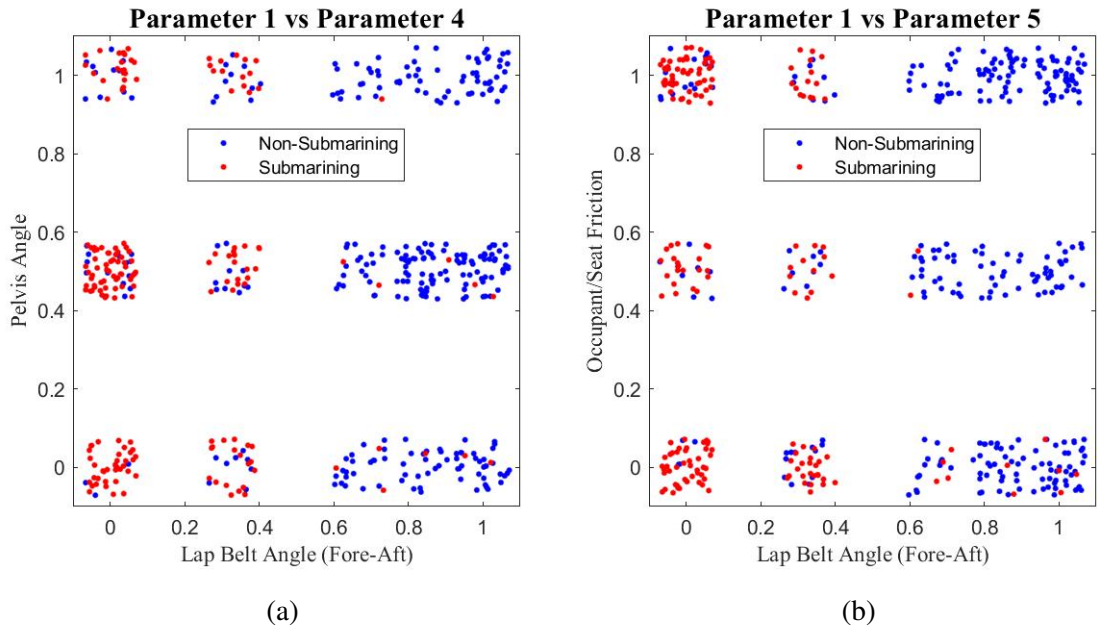


Figure I.5: Submarining occurrence influential parameter plots (automated simulation dataset): a) Parameter 1 vs Parameter 4, b) Parameter 1 vs Parameter 5.

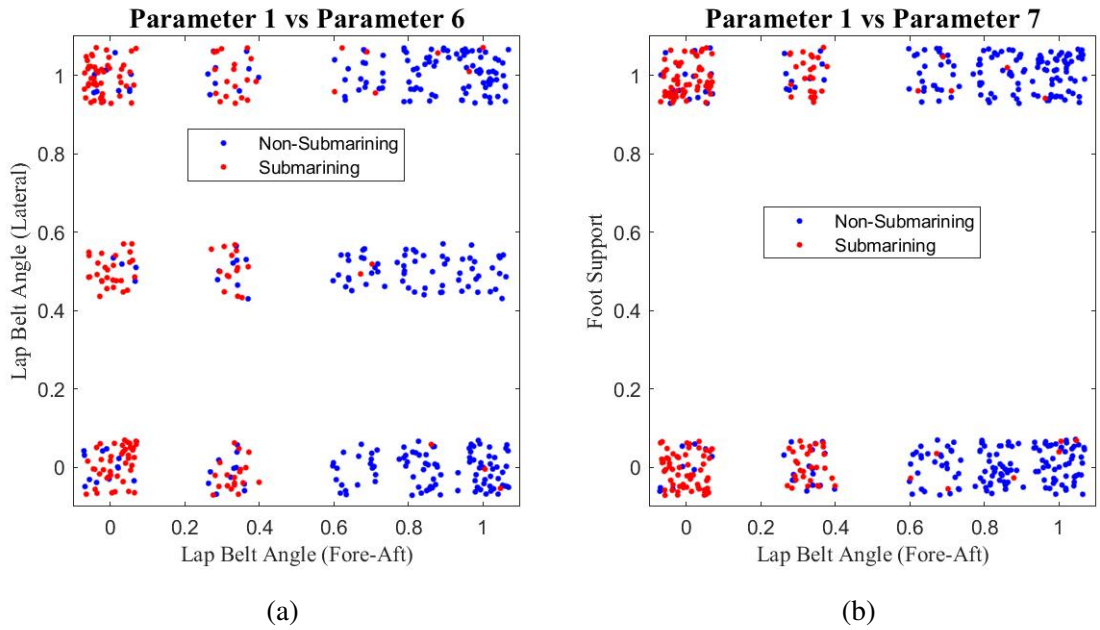


Figure I.6: Submarining occurrence influential parameter plots (automated simulation dataset): a) Parameter 1 vs Parameter 6, b) Parameter 1 vs Parameter 7.

APPENDIX I. ANALYSIS OF SIMULATED DATASET

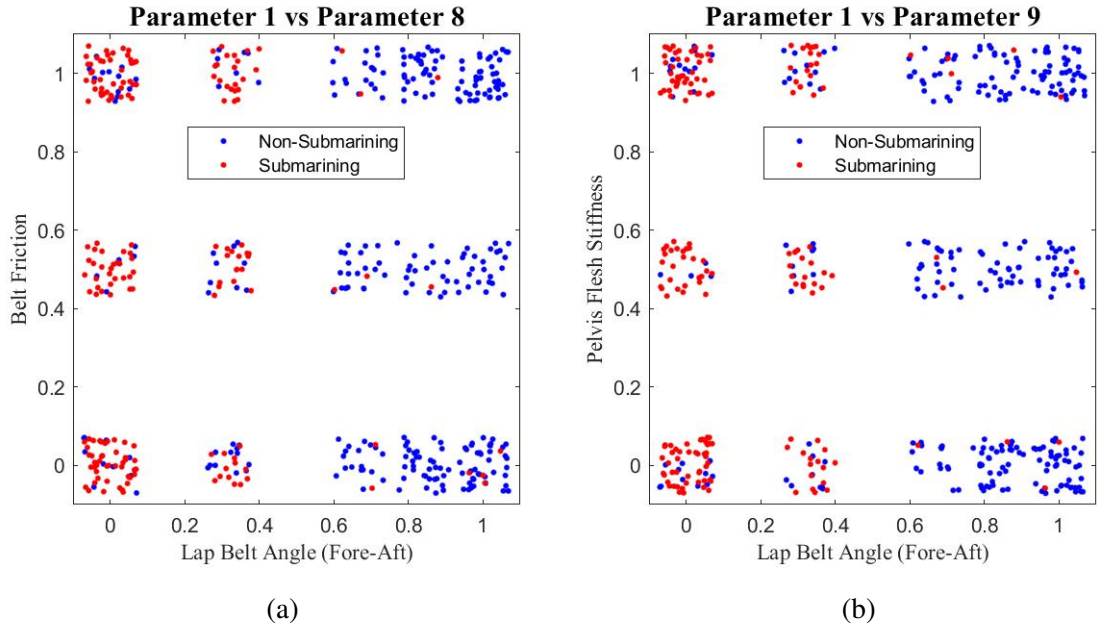


Figure I.7: Submarining occurrence influential parameter plots (automated simulation dataset): a) Parameter 1 vs Parameter 8, b) Parameter 2 vs Parameter 9.

I.2.2 Submarining Distance

I.2.2.1 Influential Parameter Ranking

	Impact Pulse	Lap Belt Angle Fore-Aft	Lap Belt Angle Lateral	Foot Support	Belt Friction	Seat Friction	Recline Angle	Flesh Stiffness	Pelvis Angle
Cluster 1 Mean	0.404	0.652	0.490	0.492	0.511	0.532	0.364	0.494	0.494
Cluster 2 Mean	0.436	0.151	0.506	0.465	0.558	0.512	0.849	0.483	0.471
Cluster 3 Mean	0.603	0.085	0.551	0.436	0.295	0.333	0.974	0.551	0.449
Absolute Distance (Clusters 1 and Averaged 2 and 3)	0.115	0.534	0.038	0.041	0.085	0.109	0.548	0.022	0.035
Rank	3	2	7	6	5	4	1	9	8

Figure I.8: Influential parameter determination for submarining distance. The parameters in green showed an absolute distance greater than 0.1 between cluster means (negative versus positive outcome); the parameters in yellow showed an absolute distance greater than 0.05 between cluster means (negative versus positive outcome).

I.2.2.2 Influential Parameter Plots

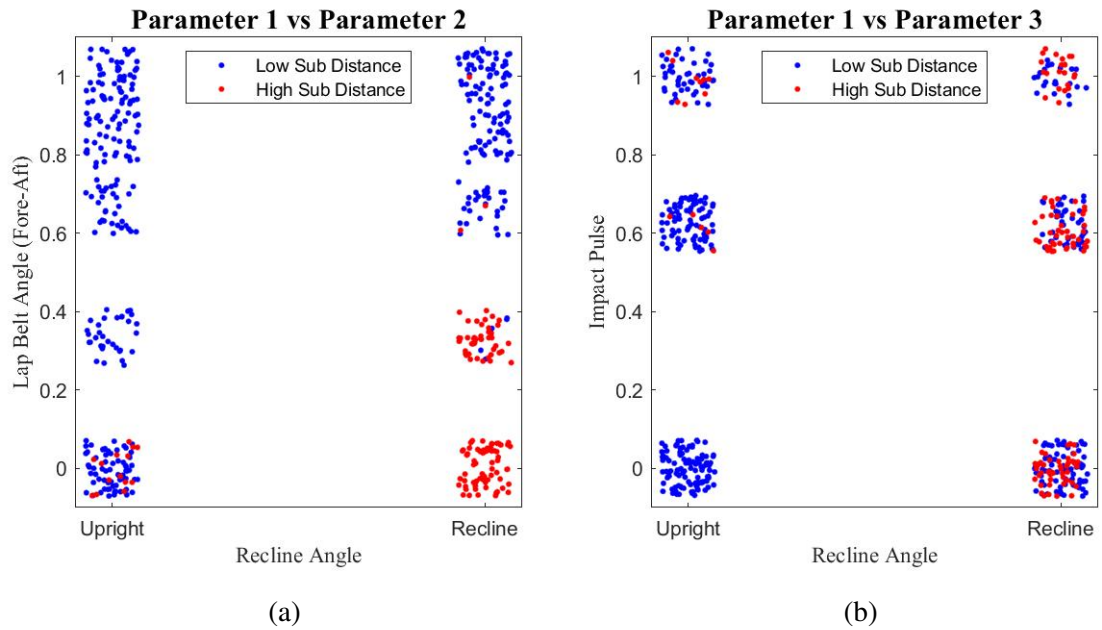


Figure I.9: Submarining distance influential parameter plots (automated simulation dataset): a) Parameter 1 vs Parameter 2, b) Parameter 1 vs Parameter 3.

APPENDIX I. ANALYSIS OF SIMULATED DATASET

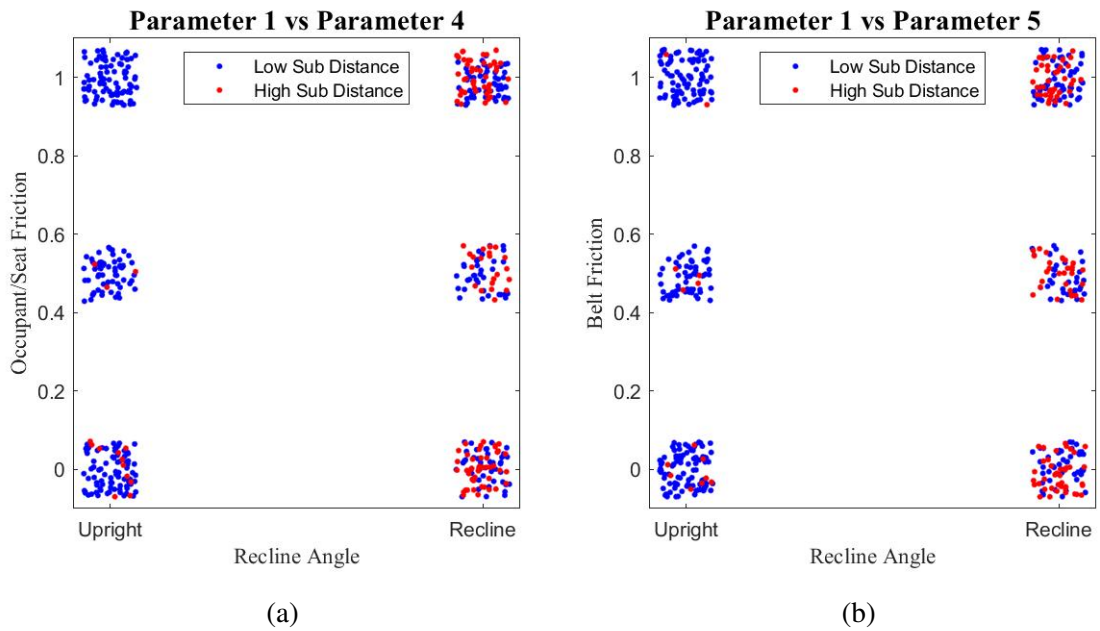


Figure I.10: Submarining distance influential parameter plots (automated simulation dataset): a) Parameter 1 vs Parameter 4, b) Parameter 1 vs Parameter 5.

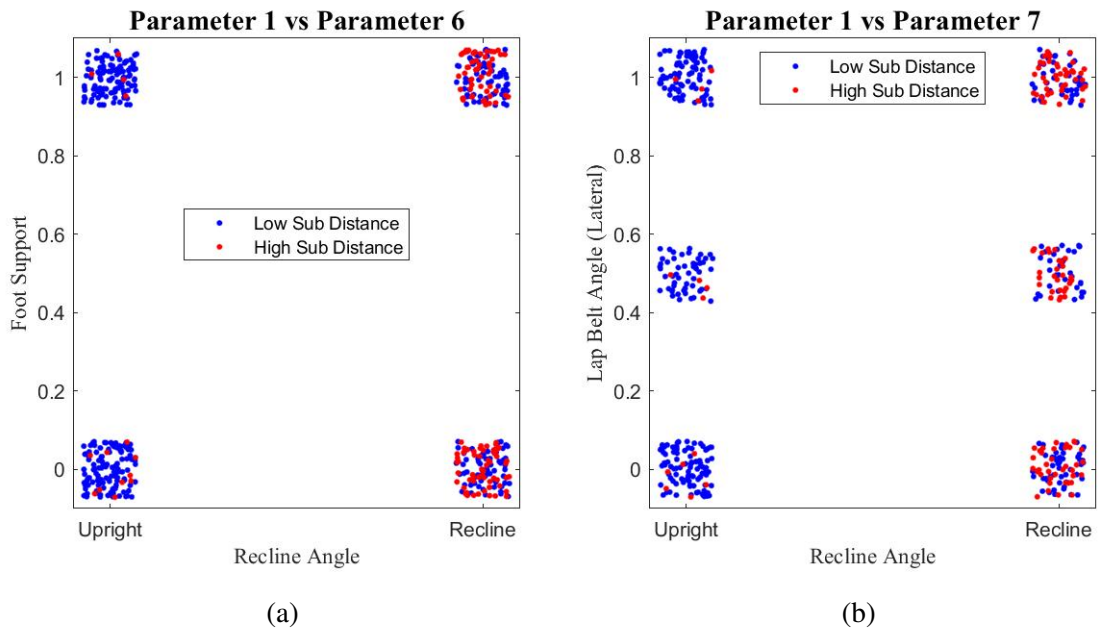


Figure I.11: Submarining distance influential parameter plots (automated simulation dataset): a) Parameter 1 vs Parameter 6, b) Parameter 1 vs Parameter 7.

APPENDIX I. ANALYSIS OF SIMULATED DATASET

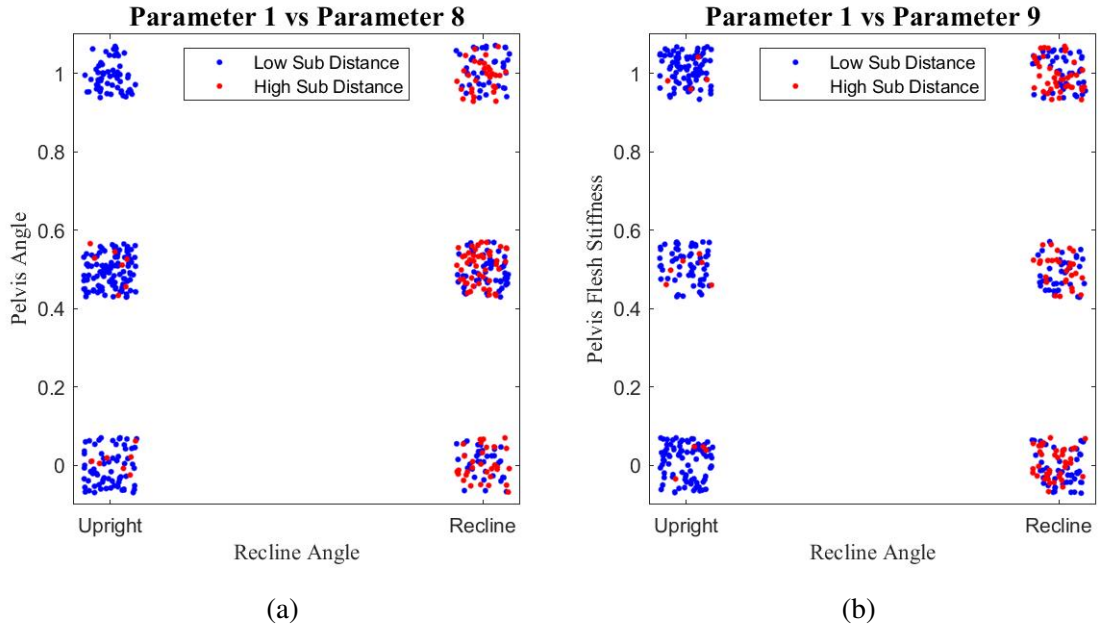


Figure I.12: Submarining distance influential parameter plots (automated simulation dataset): a) Parameter 1 vs Parameter 8, b) Parameter 2 vs Parameter 9.

I.2.3 Pelvis Forward Displacement

I.2.3.1 Influential Parameter Ranking

The cutoff value identified from the k-means clustering was 138.8 mm, in which 48.9% of simulations clustered in the negative outcome (higher pelvis displacement) group.

	Impact Pulse	Lap Belt Angle Fore-Aft	Lap Belt Angle Lateral	Foot Support	Belt Friction	Seat Friction	Recline Angle	Flesh Stiffness	Pelvis Angle
Cluster 1 Mean	0.268	0.559	0.471	0.527	0.492	0.622	0.249	0.506	0.486
Cluster 2 Mean	0.567	0.579	0.494	0.461	0.551	0.449	0.685	0.483	0.494
Cluster 3 Mean	0.641	0.180	0.613	0.371	0.403	0.258	0.952	0.500	0.468
Absolute Distance (Clusters 1 and Averaged 2 and 3)	0.336	0.180	0.082	0.111	0.015	0.269	0.570	0.015	0.005
Rank	2	4	6	5	7	3	1	8	9

Figure I.13: Influential parameter determination for pelvis forward displacement. The parameters in green showed an absolute distance greater than 0.1 between cluster means (negative versus positive outcome); the parameters in yellow showed an absolute distance greater than 0.05 between cluster means (negative versus positive outcome).

I.2.3.2 Influential Parameter Plots

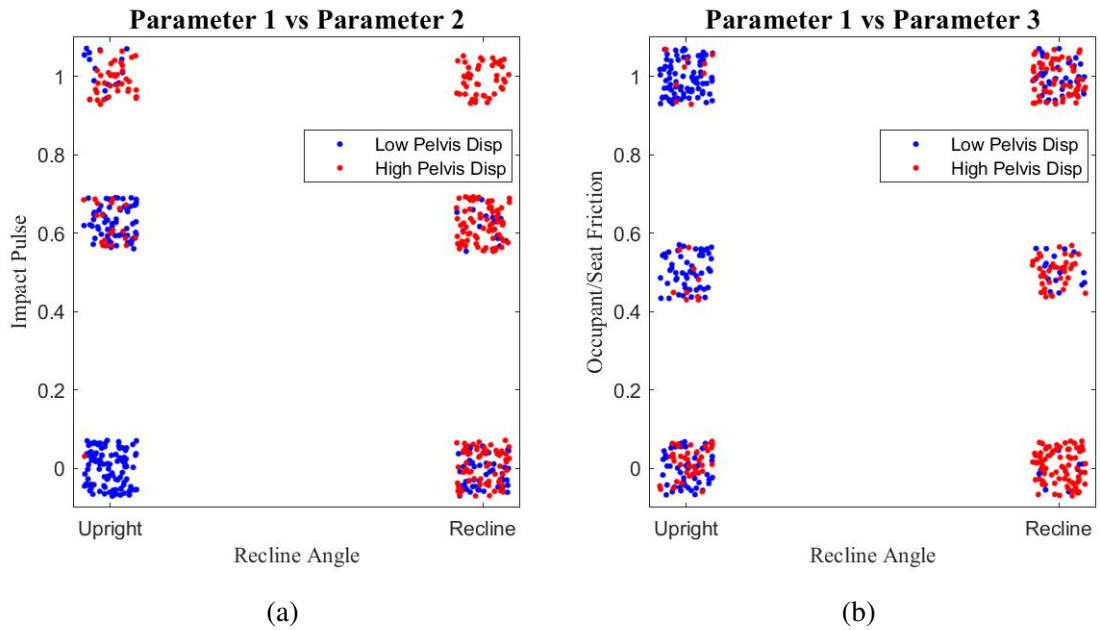


Figure I.14: Pelvis forward displacement influential parameter plots (automated simulation dataset):
a) Parameter 1 vs Parameter 2, b) Parameter 1 vs Parameter 3.

APPENDIX I. ANALYSIS OF SIMULATED DATASET

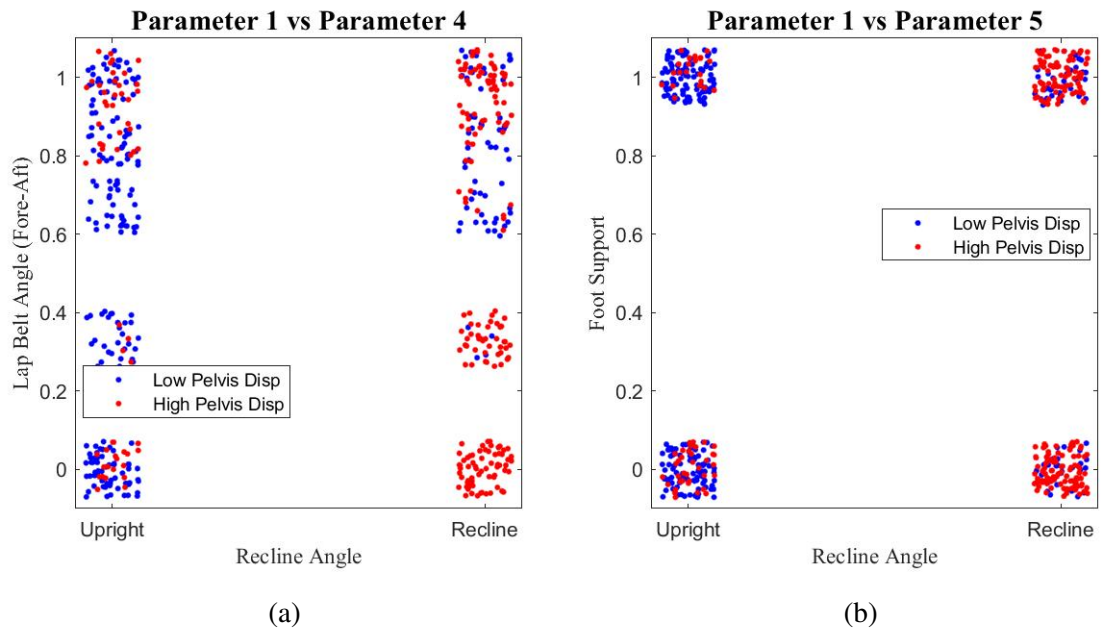


Figure I.15: Pelvis forward displacement influential parameter plots (automated simulation dataset):
a) Parameter 1 vs Parameter 4, b) Parameter 1 vs Parameter 5.

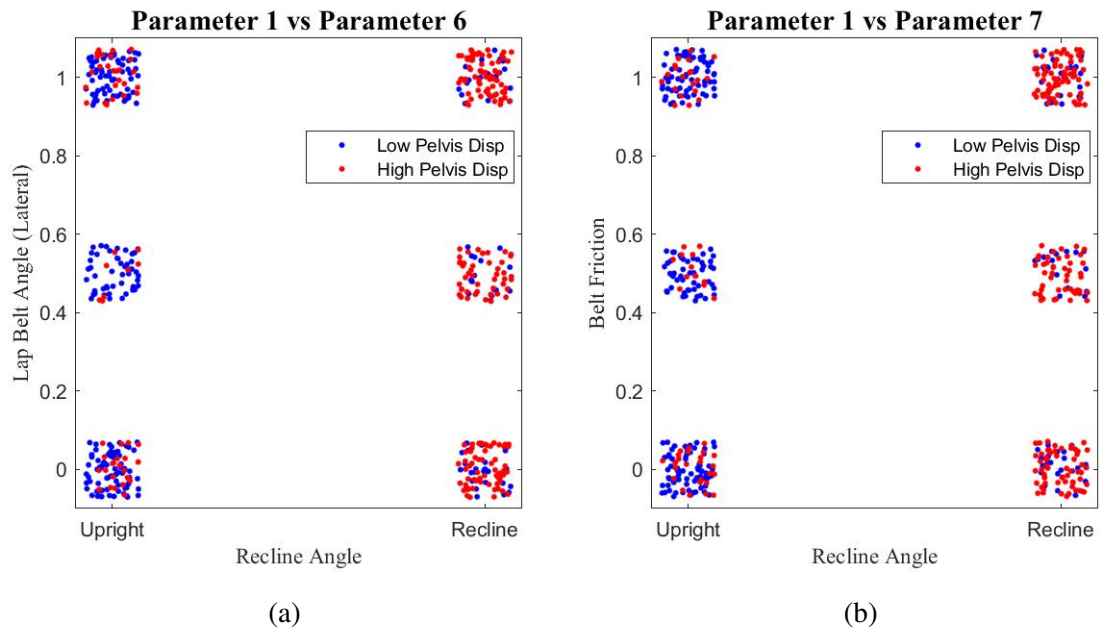


Figure I.16: Pelvis forward displacement influential parameter plots (automated simulation dataset):
a) Parameter 1 vs Parameter 6, b) Parameter 1 vs Parameter 7.

APPENDIX I. ANALYSIS OF SIMULATED DATASET

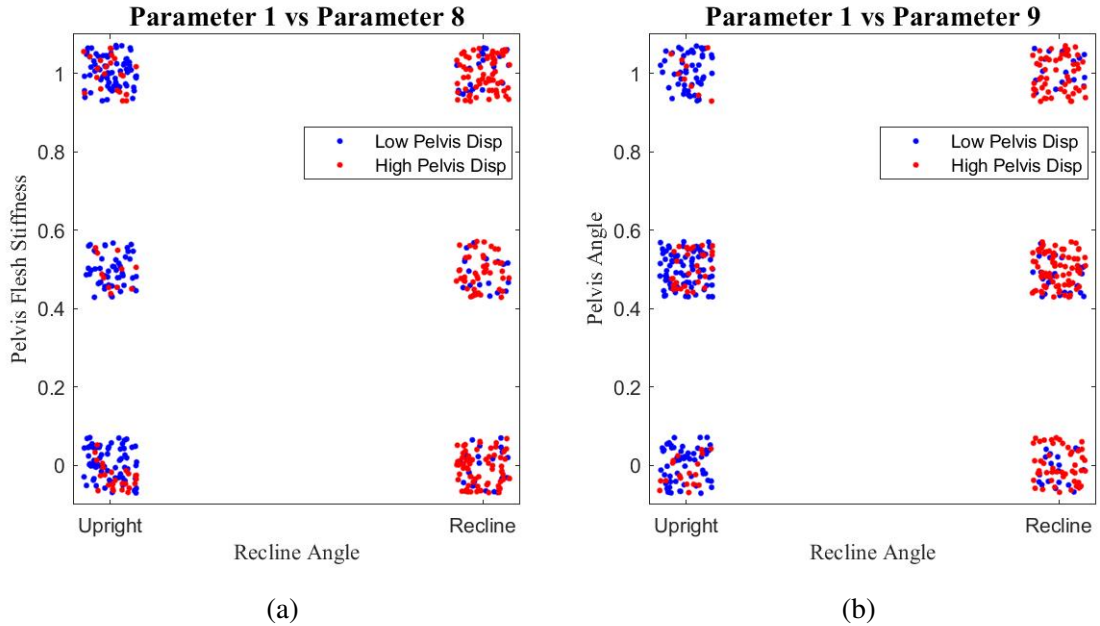


Figure I.17: Pelvis forward displacement influential parameter plots (automated simulation dataset): a) Parameter 1 vs Parameter 8, b) Parameter 2 vs Parameter 9.

I.2.4 Pelvis Rotation

I.2.4.1 Influential Parameter Ranking

The cutoff value identified from the k-means clustering was 9.2° (rearward), in which 52.2% of simulations clustered in the negative outcome (larger rearward pelvis rotation) group.

	Impact Pulse	Lap Belt Angle Fore-Aft	Lap Belt Angle Lateral	Foot Support	Belt Friction	Seat Friction	Recline Angle	Flesh Stiffness	Pelvis Angle
Cluster 1 Mean	0.356	0.842	0.496	0.473	0.509	0.624	0.434	0.531	0.498
Cluster 2 Mean	0.486	0.235	0.500	0.490	0.496	0.415	0.556	0.467	0.477
Absolute Distance	0.130	0.607	0.004	0.017	0.013	0.209	0.122	0.064	0.021
Rank	3	1	9	7	8	2	4	5	6

Figure I.18: Influential parameter determination for pelvis rotation. The parameters in green showed an absolute distance greater than 0.1 between cluster means (negative versus positive outcome); the parameters in yellow showed an absolute distance greater than 0.05 between cluster means (negative versus positive outcome).

I.2.4.2 Influential Parameter Plots

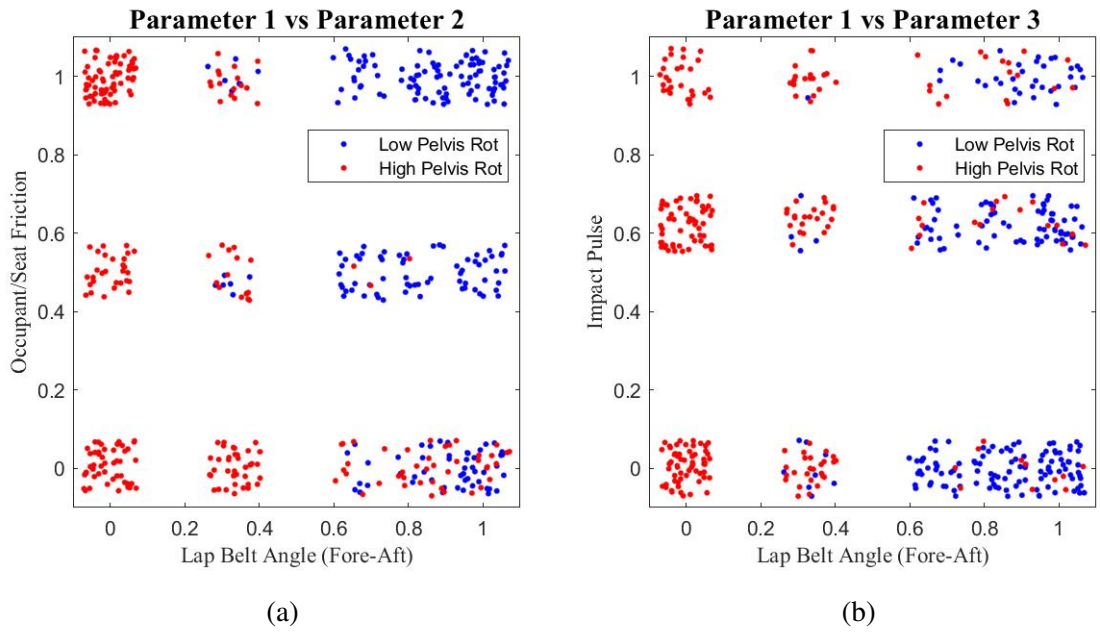


Figure I.19: Pelvis rotation influential parameter plots (automated simulation dataset): a) Parameter 1 vs Parameter 2, b) Parameter 1 vs Parameter 3.

APPENDIX I. ANALYSIS OF SIMULATED DATASET

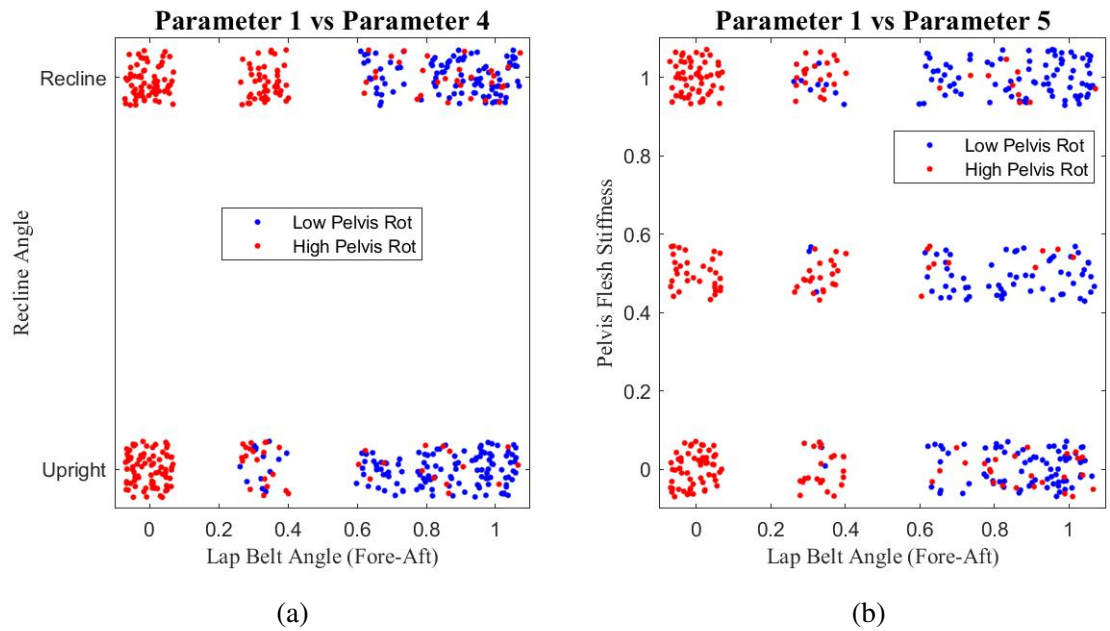


Figure I.20: Pelvis rotation influential parameter plots (automated simulation dataset): a) Parameter 1 vs Parameter 4, b) Parameter 1 vs Parameter 5.

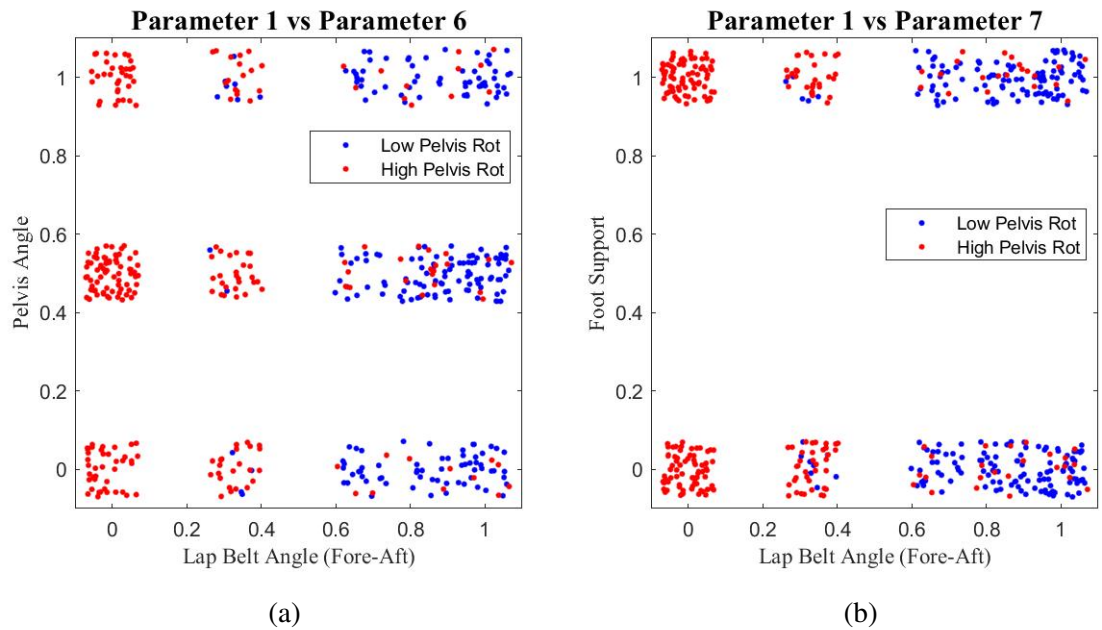


Figure I.21: Pelvis rotation influential parameter plots (automated simulation dataset): a) Parameter 1 vs Parameter 6, b) Parameter 1 vs Parameter 7.

APPENDIX I. ANALYSIS OF SIMULATED DATASET

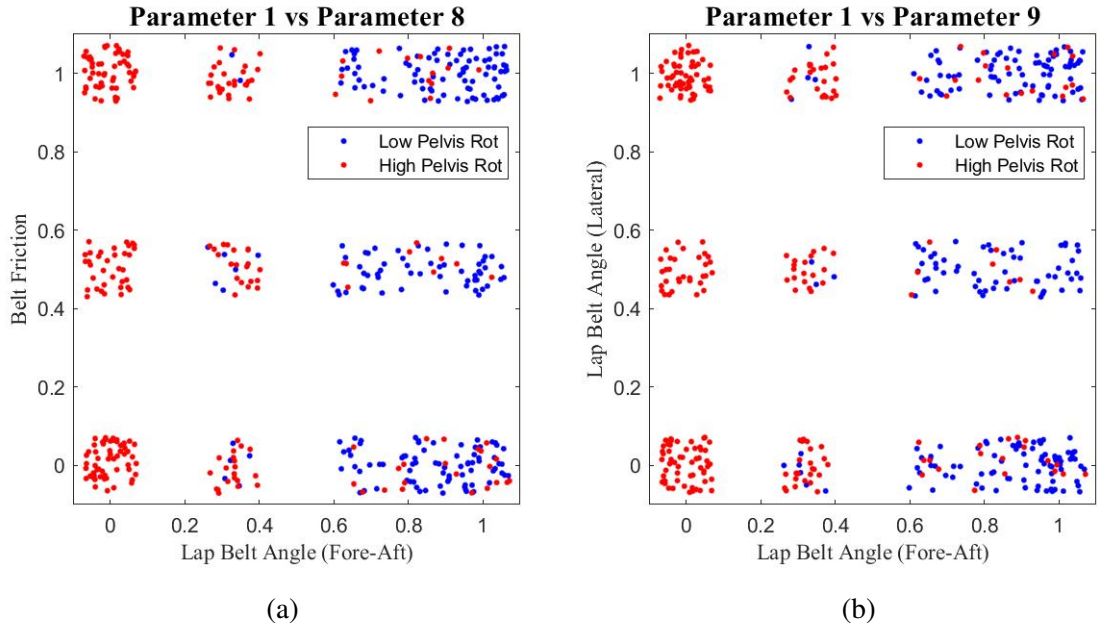


Figure I.22: Pelvis rotation influential parameter plots (automated simulation dataset): a) Parameter 1 vs Parameter 8, b) Parameter 2 vs Parameter 9.

I.2.5 Lap Belt Tension

I.2.5.1 Influential Parameter Ranking

The cutoff value identified from the k-means clustering was 5.9 kN, in which 23.5% of simulations clustered in the negative outcome (higher lap belt tension) group.

	Impact Pulse	Lap Belt Angle Fore-Aft	Lap Belt Angle Lateral	Foot Support	Belt Friction	Seat Friction	Recline Angle	Flesh Stiffness	Pelvis Angle
Cluster 1 Mean	0.314	0.433	0.501	0.518	0.493	0.567	0.499	0.497	0.485
Cluster 2 Mean	0.788	0.796	0.487	0.368	0.531	0.333	0.500	0.496	0.491
Absolute Distance	0.474	0.363	0.015	0.149	0.037	0.234	0.001	0.002	0.006
Rank	1	2	6	4	5	3	9	8	7

Figure I.23: Influential parameter determination for lap belt tension. The parameters in green showed an absolute distance greater than 0.1 between cluster means (negative versus positive outcome); the parameters in yellow showed an absolute distance greater than 0.05 between cluster means (negative versus positive outcome).

I.2.5.2 Influential Parameter Plots

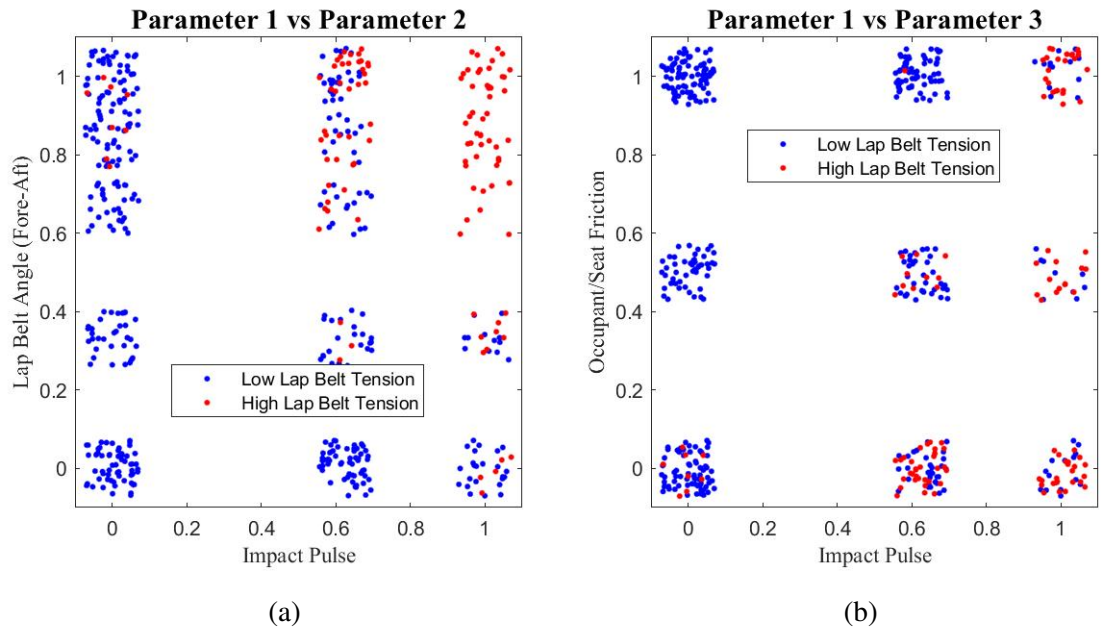


Figure I.24: Lap belt tension influential parameter plots (automated simulation dataset): a) Parameter 1 vs Parameter 2, b) Parameter 1 vs Parameter 3.

APPENDIX I. ANALYSIS OF SIMULATED DATASET

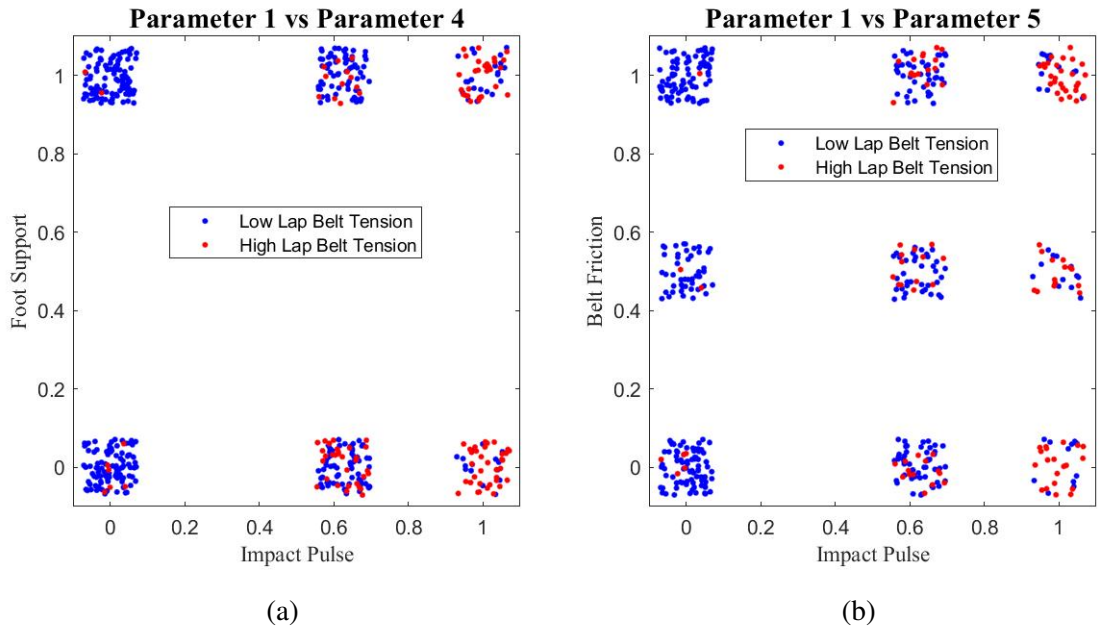


Figure I.25: Lap belt tension influential parameter plots (automated simulation dataset): a) Parameter 1 vs Parameter 4, b) Parameter 1 vs Parameter 5.

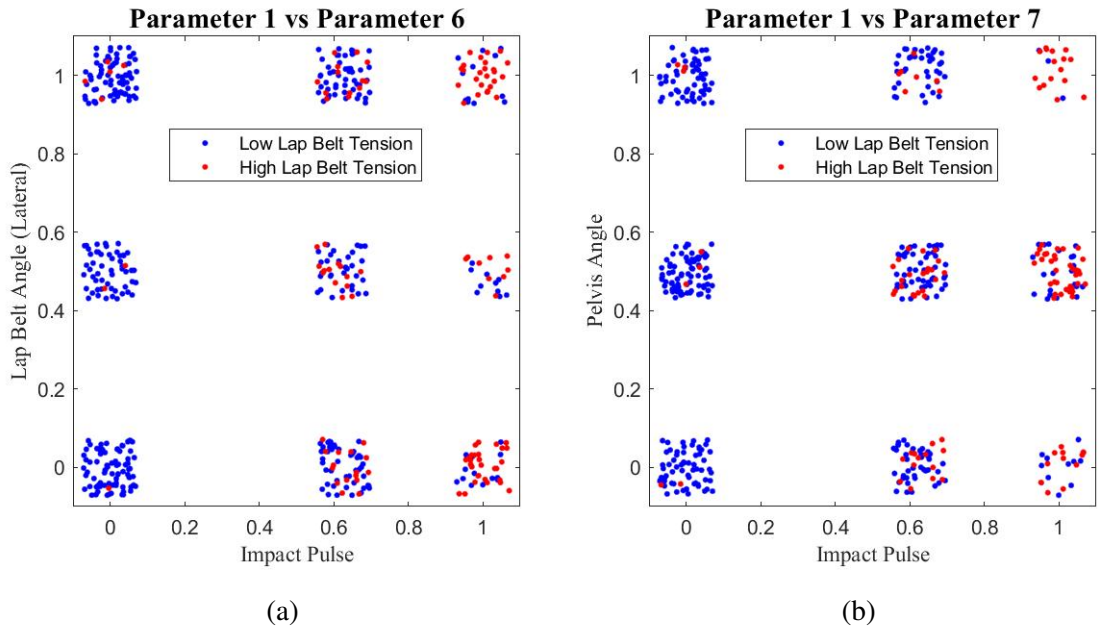


Figure I.26: Lap belt tension influential parameter plots (automated simulation dataset): a) Parameter 1 vs Parameter 6, b) Parameter 1 vs Parameter 7.

APPENDIX I. ANALYSIS OF SIMULATED DATASET

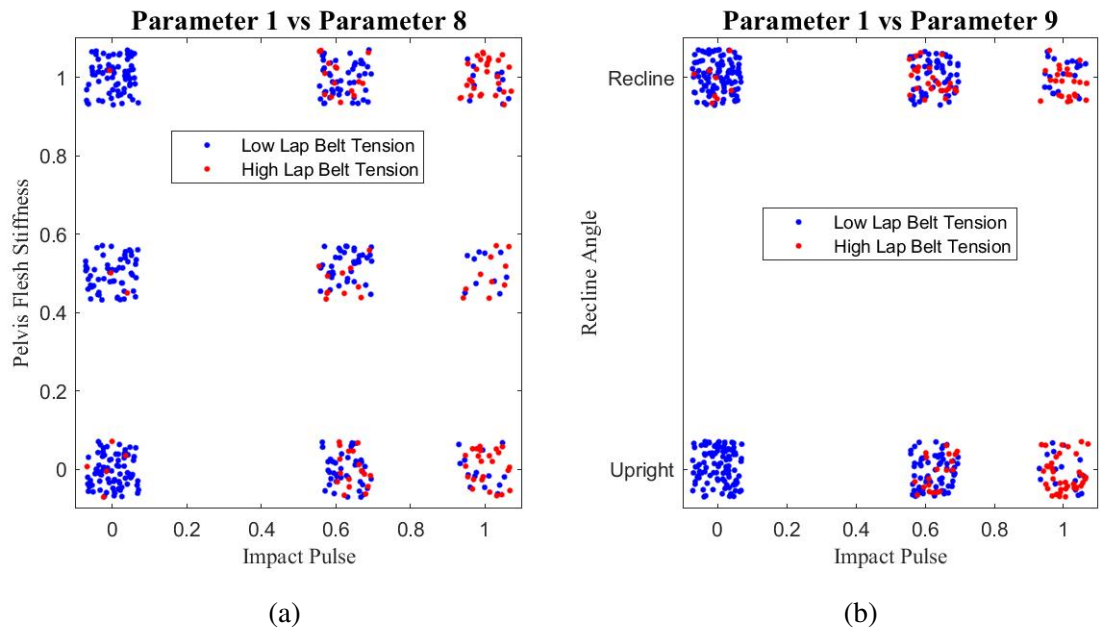


Figure I.27: Lap belt tension influential parameter plots (automated simulation dataset): a) Parameter 1 vs Parameter 8, b) Parameter 2 vs Parameter 9.

Appendix J

Analysis of Full-Factorial Generated Dataset

J.1 Distribution of Output Metrics

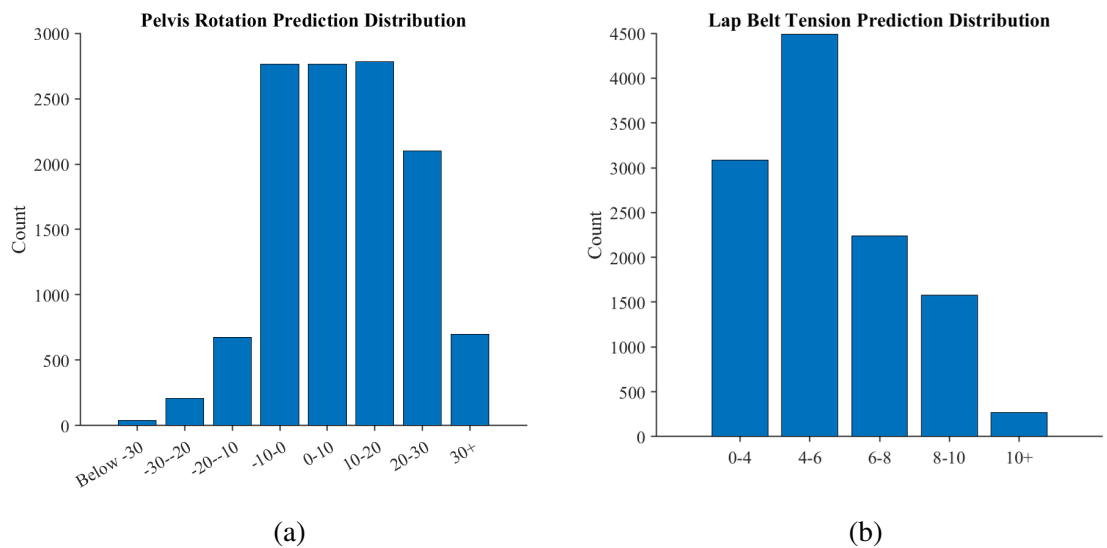


Figure J.1: The frequency of output metric magnitudes for the continuous output metrics for which two clusters were chosen in the k-means clustering analysis: a) Pelvis rotation; b) Lap belt tension

APPENDIX J. ANALYSIS OF FULL-FACTORIAL GENERATED DATASET

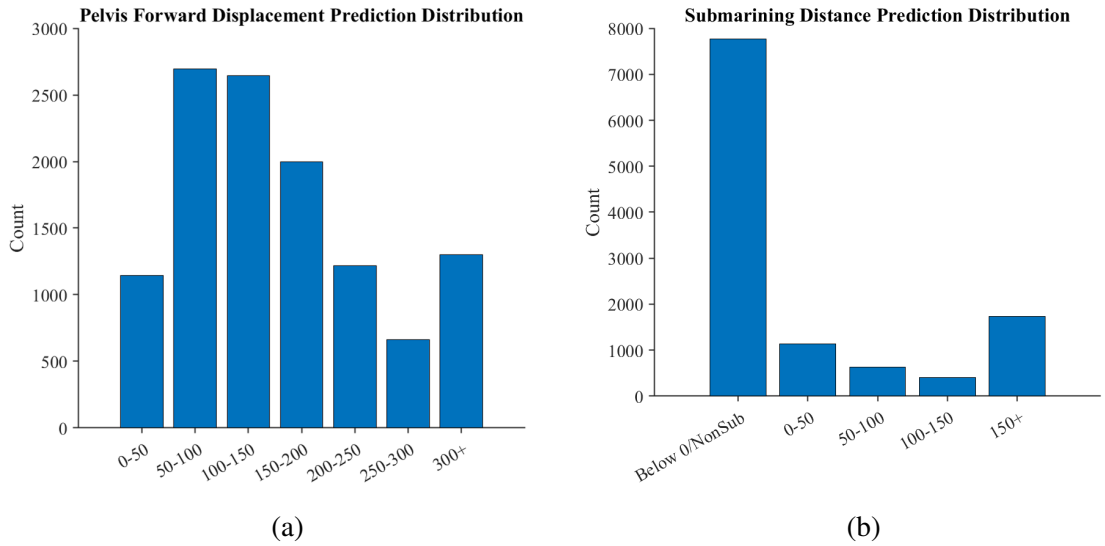


Figure J.2: The frequency of output metric magnitudes for the continuous output metrics for which three clusters were chosen in the k-means clustering analysis: a) Pelvis displacement; b) Submarining distance

J.2 K-Means Clustering Analysis

J.2.1 Submarining Occurrence

J.2.1.1 Influential Parameter Ranking

The cutoff value identified from the k-means clustering was a probability of 0.5, in which 33.3% of simulations clustered in the negative outcome (submarining) group.

	Impact Pulse	Lap Belt Angle Fore-Aft	Lap Belt Angle Lateral	Foot Support	Belt Friction	Seat Friction	Recline Angle	Flesh Stiffness	Pelvis Angle
Cluster 1 Mean	0.488	0.728	0.502	0.503	0.511	0.548	0.364	0.500	0.548
Cluster 2 Mean	0.662	0.257	0.512	0.484	0.492	0.426	0.782	0.513	0.420
Absolute Distance	0.174	0.471	0.009	0.019	0.019	0.122	0.418	0.013	0.127
Rank	3	1	9	7	6	5	2	8	4

Figure J.3: Influential parameter determination for submarining occurrence. The parameters in green showed an absolute distance greater than 0.1 between cluster means (negative versus positive outcome); the parameters in yellow showed an absolute distance greater than 0.05 between cluster means (negative versus positive outcome).

J.2.1.2 Influential Parameter Plots

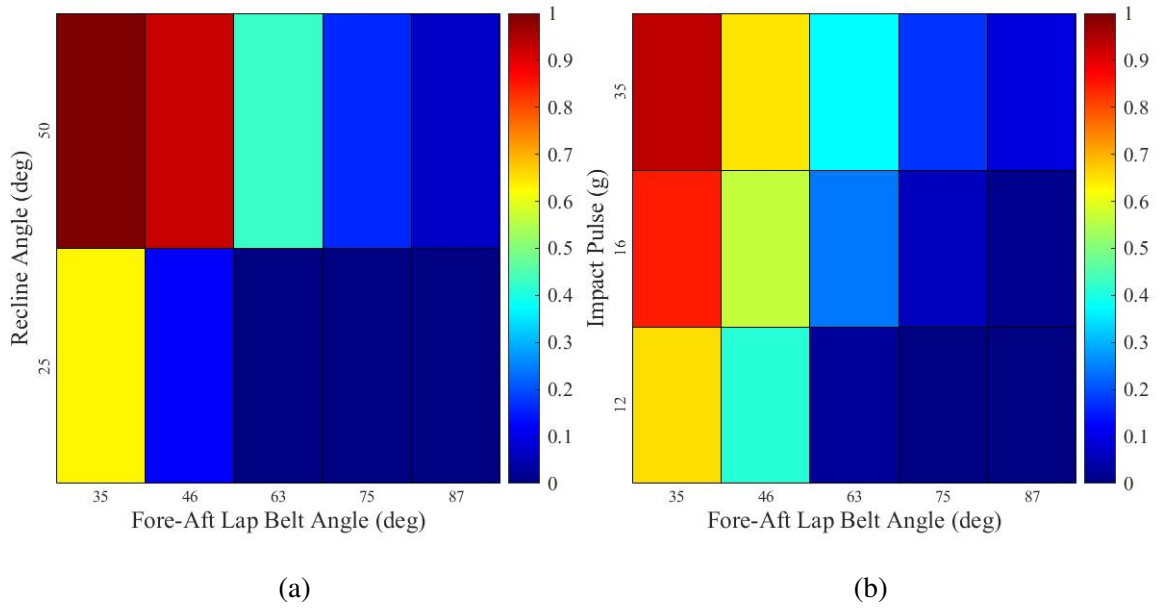


Figure J.4: Submarining occurrence influential parameter plots (generated full-factorial dataset): a) Parameter 1 vs Parameter 2, b) Parameter 1 vs Parameter 3.

APPENDIX J. ANALYSIS OF FULL-FACTORIAL GENERATED DATASET

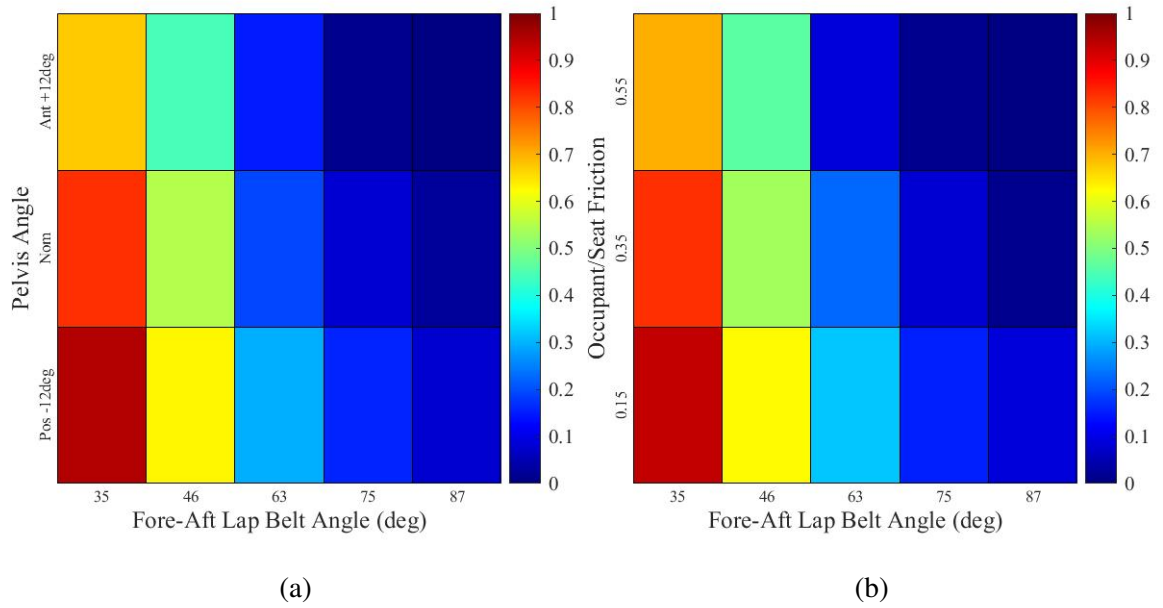


Figure J.5: Submerging occurrence influential parameter plots (generated full-factorial dataset): a) Parameter 1 vs Parameter 4, b) Parameter 1 vs Parameter 5.

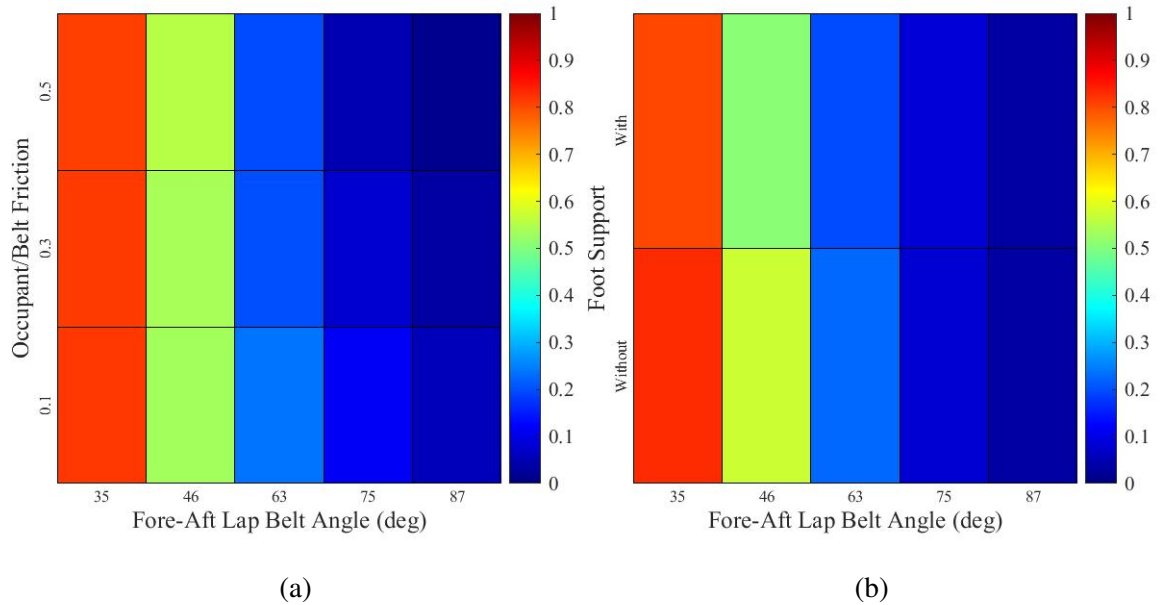


Figure J.6: Submerging occurrence influential parameter plots (generated full-factorial dataset): a) Parameter 1 vs Parameter 6, b) Parameter 1 vs Parameter 7.

APPENDIX J. ANALYSIS OF FULL-FACTORIAL GENERATED DATASET

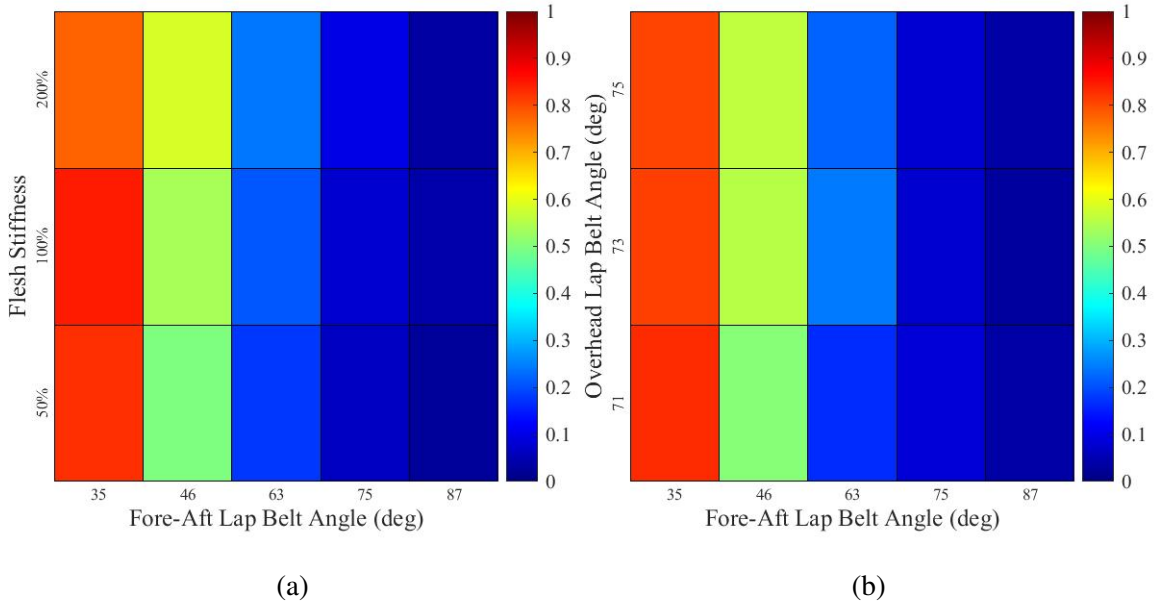


Figure J.7: Submarining occurrence influential parameter plots (generated full-factorial dataset): a) Parameter 1 vs Parameter 8, b) Parameter 2 vs Parameter 9.

J.2.2 Submarining Distance

The cutoff value identified from the k-means clustering was a probability of the maximum submarining distance exceeding 75.1 mm, in which 24.3% of simulations clustered in the negative outcome (increased submarining distance) group.

	Impact Pulse	Lap Belt Angle Fore-Aft	Lap Belt Angle Lateral	Foot Support	Belt Friction	Seat Friction	Recline Angle	Flesh Stiffness	Pelvis Angle
Cluster 1 Mean	0.513	0.701	0.503	0.517	0.528	0.541	0.384	0.505	0.521
Cluster 2 Mean	0.617	0.299	0.520	0.439	0.439	0.439	0.723	0.507	0.472
Cluster 3 Mean	0.666	0.085	0.501	0.441	0.436	0.382	0.990	0.496	0.448
Absolute Distance (Clusters 1 and Averaged 2 and 3)	0.128	0.509	0.007	0.077	0.091	0.130	0.473	0.004	0.061
Rank	4	1	8	6	5	3	2	9	7

Figure J.8: Influential parameter determination for submarining distance. The parameters in green showed an absolute distance greater than 0.1 between cluster means (negative versus positive outcome); the parameters in yellow showed an absolute distance greater than 0.05 between cluster means (negative versus positive outcome).

J.2.2.1 Influential Parameter Plots

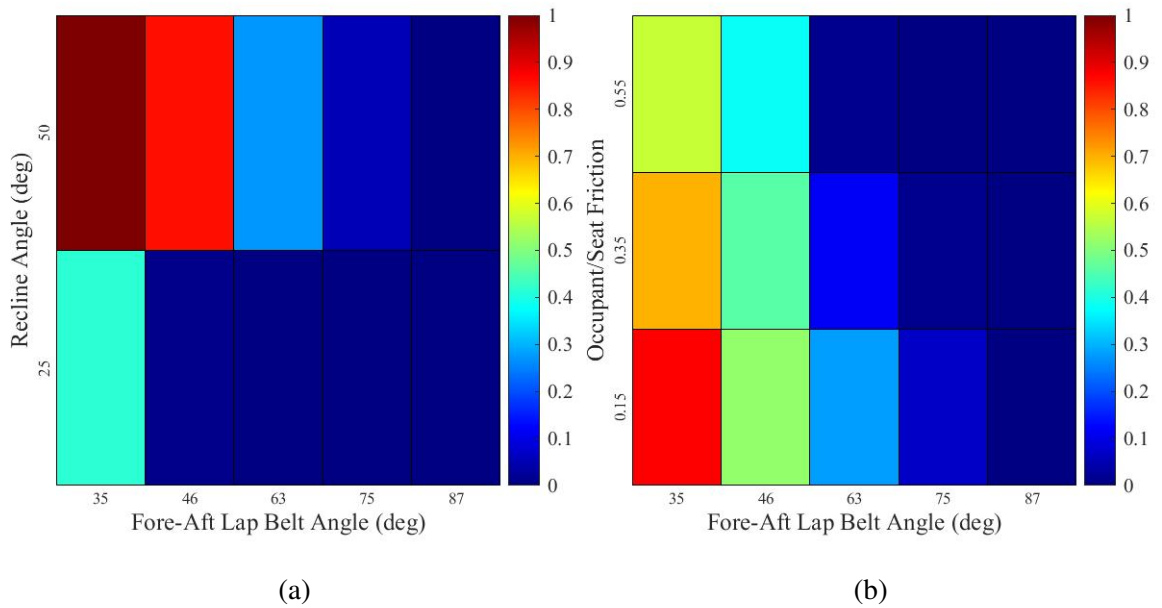


Figure J.9: Submarining distance influential parameter plots (generated full-factorial dataset): a) Parameter 1 vs Parameter 2, b) Parameter 1 vs Parameter 3.

APPENDIX J. ANALYSIS OF FULL-FACTORIAL GENERATED DATASET

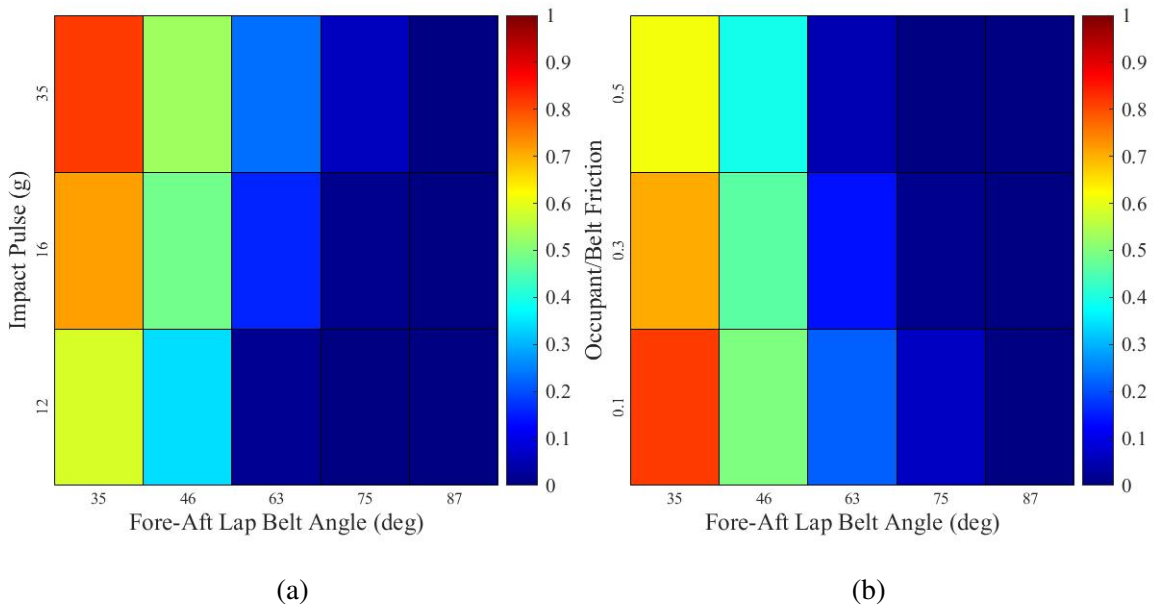


Figure J.10: Submarining distance influential parameter plots (generated full-factorial dataset): a) Parameter 1 vs Parameter 4, b) Parameter 1 vs Parameter 5.

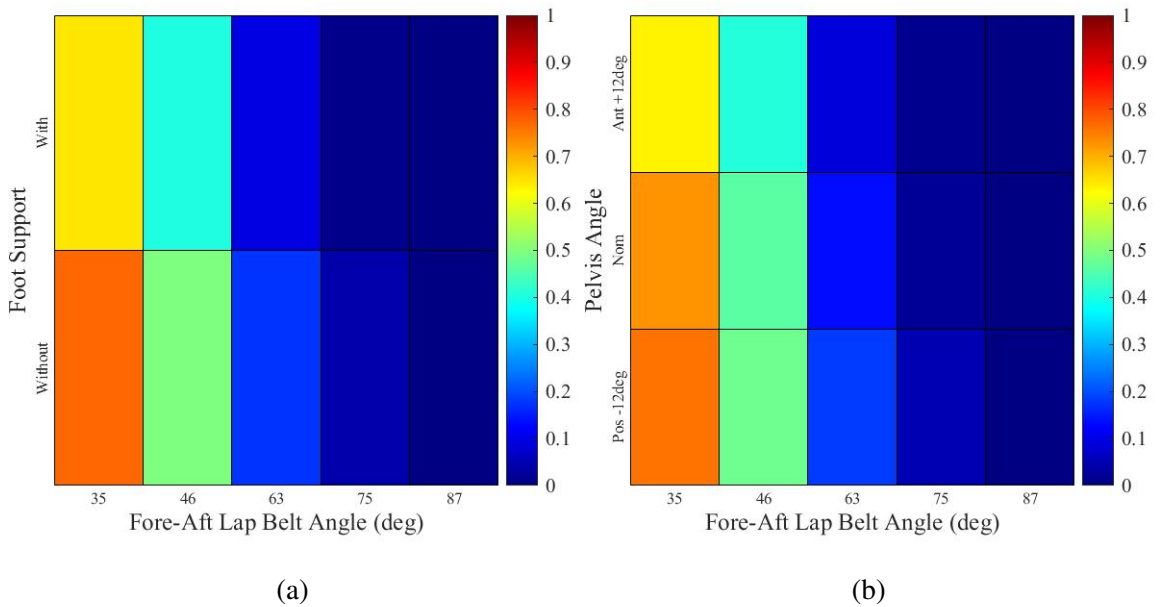


Figure J.11: Submarining distance influential parameter plots (generated full-factorial dataset): a) Parameter 1 vs Parameter 6, b) Parameter 1 vs Parameter 7.

APPENDIX J. ANALYSIS OF FULL-FACTORIAL GENERATED DATASET

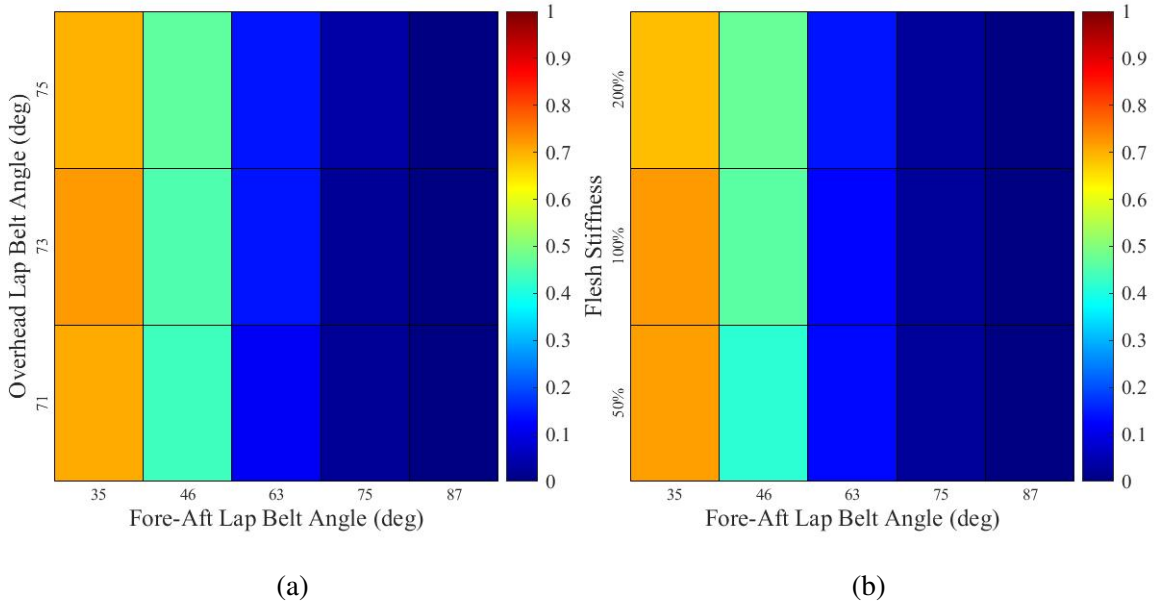


Figure J.12: Submerging distance influential parameter plots (generated full-factorial dataset): a) Parameter 1 vs Parameter 8, b) Parameter 2 vs Parameter 9.

J.2.3 Pelvis Forward Displacement

The cutoff value identified from the k-means clustering was a probability of the maximum forward pelvis displacement exceeding 137.8 mm, in which 50.3% of simulations clustered in the negative outcome (increased pelvis displacement) group.

	Impact Pulse	Lap Belt Angle Fore-Aft	Lap Belt Angle Lateral	Foot Support	Belt Friction	Seat Friction	Recline Angle	Flesh Stiffness	Pelvis Angle
Cluster 1 Mean	0.360	0.598	0.476	0.569	0.529	0.612	0.245	0.495	0.517
Cluster 2 Mean	0.720	0.670	0.537	0.434	0.504	0.432	0.689	0.505	0.510
Cluster 3 Mean	0.762	0.162	0.527	0.399	0.409	0.321	0.967	0.541	0.448
Absolute Distance (Clusters 1 and Averaged 2 and 3)	0.381	0.182	0.056	0.153	0.073	0.235	0.583	0.029	0.038
Rank	2	4	7	5	6	3	1	9	8

Figure J.13: Influential parameter determination for pelvis forward displacement. The parameters in green showed an absolute distance greater than 0.1 between cluster means (negative versus positive outcome); the parameters in yellow showed an absolute distance greater than 0.05 between cluster means (negative versus positive outcome).

J.2.3.1 Influential Parameter Plots

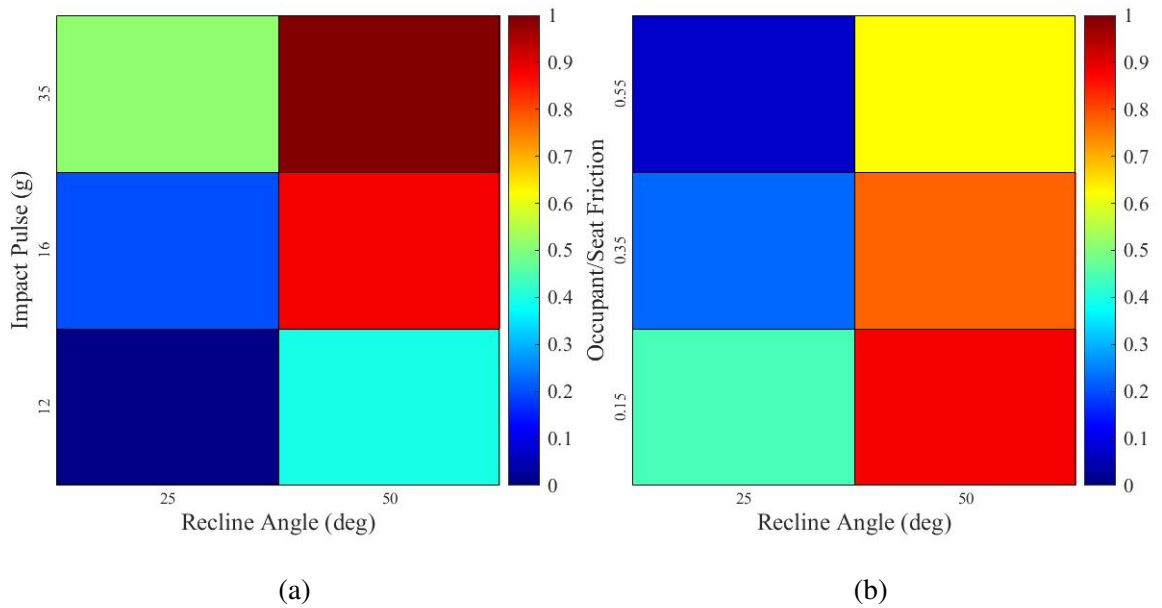


Figure J.14: Pelvis displacement influential parameter plots (generated full-factorial dataset): a) Parameter 1 vs Parameter 2, b) Parameter 1 vs Parameter 3.

APPENDIX J. ANALYSIS OF FULL-FACTORIAL GENERATED DATASET

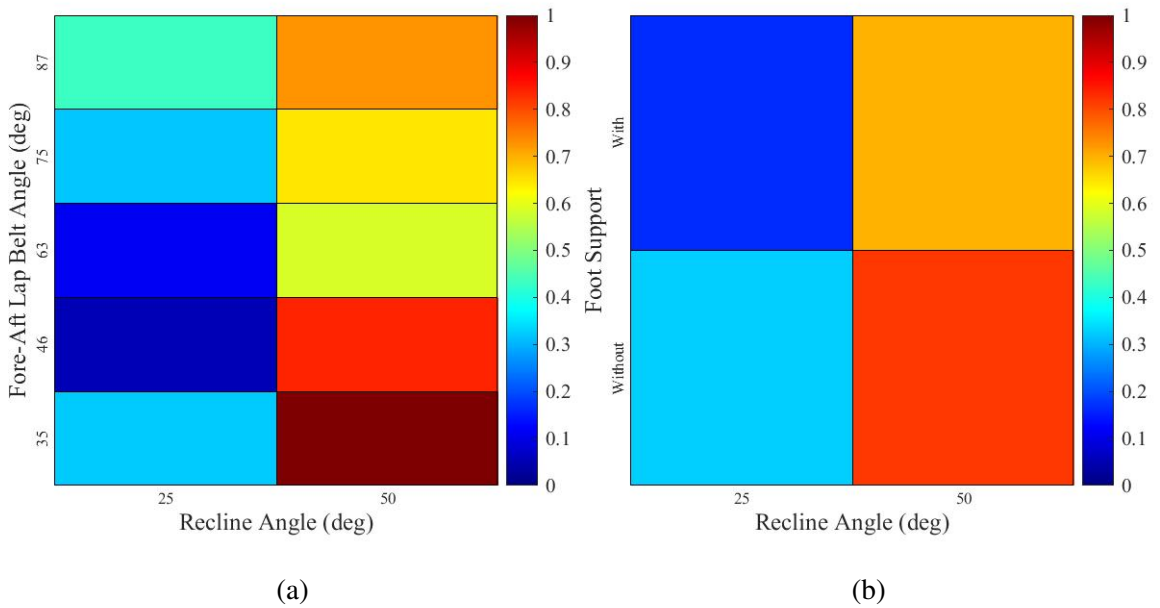


Figure J.15: Pelvis displacement influential parameter plots (generated full-factorial dataset): a) Parameter 1 vs Parameter 4, b) Parameter 1 vs Parameter 5.

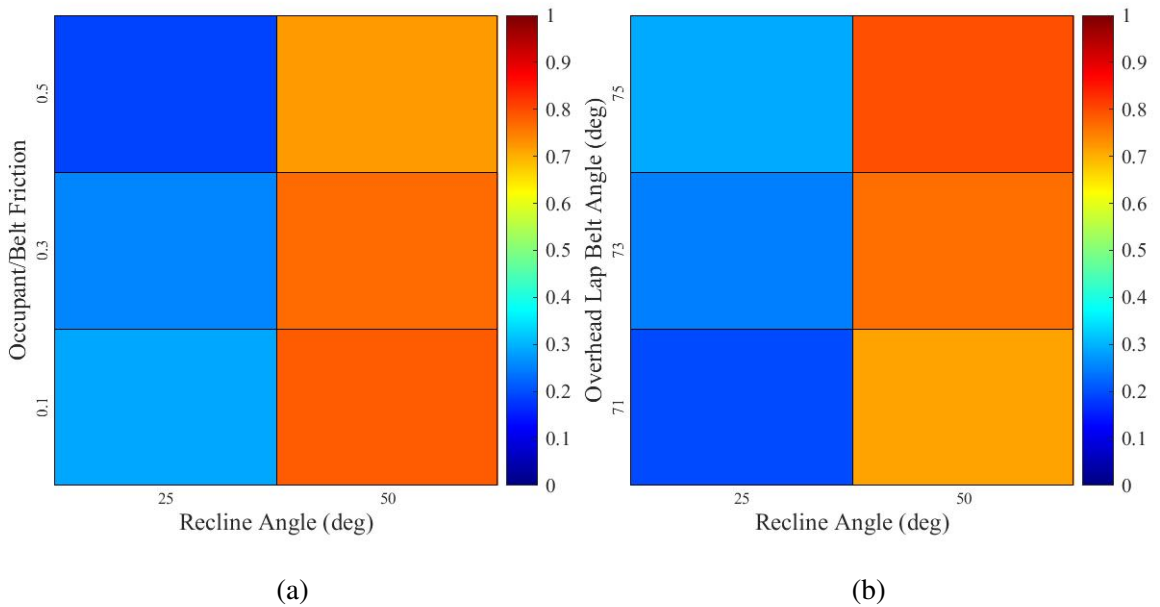


Figure J.16: Pelvis displacement influential parameter plots (generated full-factorial dataset): a) Parameter 1 vs Parameter 6, b) Parameter 1 vs Parameter 7.

APPENDIX J. ANALYSIS OF FULL-FACTORIAL GENERATED DATASET

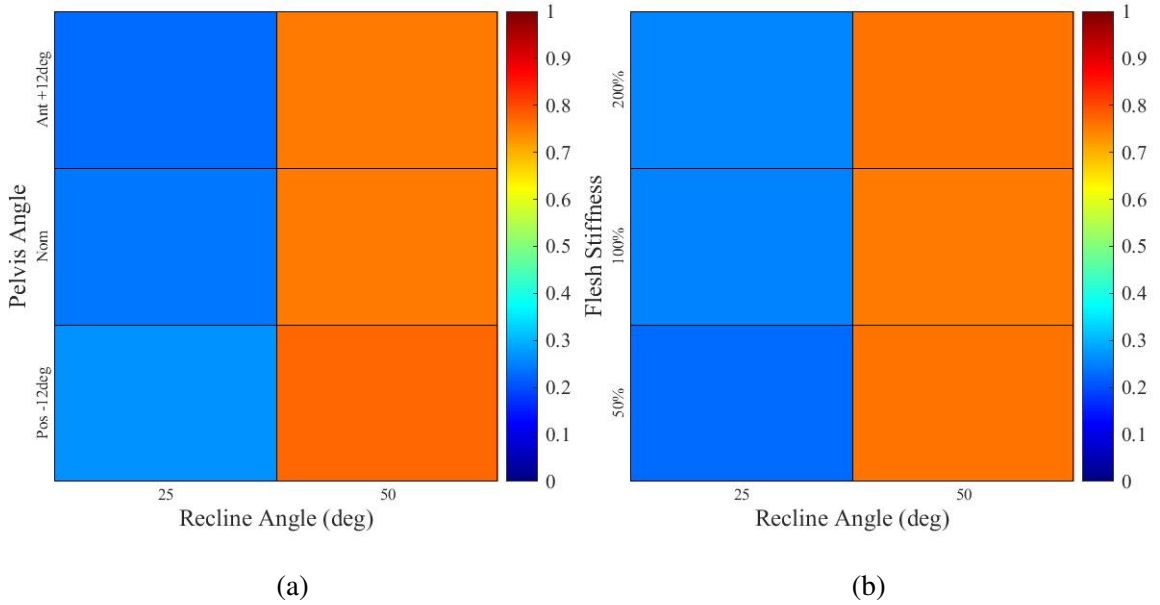


Figure J.17: Pelvis displacement influential parameter plots (generated full-factorial dataset): a) Parameter 1 vs Parameter 8, b) Parameter 2 vs Parameter 9.

J.2.4 Pelvis Rotation (Pitch)

The cutoff value identified from the k-means clustering was a probability of the maximum rearward pelvis rotation exceeding 8.9°, in which 50.6% of simulations clustered in the negative outcome (increased rearward pelvis rotation) group.

	Impact Pulse	Lap Belt Angle Fore-Aft	Lap Belt Angle Lateral	Foot Support	Belt Friction	Seat Friction	Recline Angle	Flesh Stiffness	Pelvis Angle
Cluster 1 Mean	0.475	0.813	0.500	0.486	0.516	0.651	0.418	0.533	0.509
Cluster 2 Mean	0.615	0.334	0.511	0.507	0.493	0.367	0.586	0.476	0.502
Absolute Distance	0.139	0.479	0.011	0.021	0.023	0.284	0.168	0.057	0.006
Rank	4	1	8	7	6	2	3	5	9

Figure J.18: Influential parameter determination for pelvis rotation. The parameters in green showed an absolute distance greater than 0.1 between cluster means (negative versus positive outcome); the parameters in yellow showed an absolute distance greater than 0.05 between cluster means (negative versus positive outcome).

J.2.4.1 Influential Parameter Plots

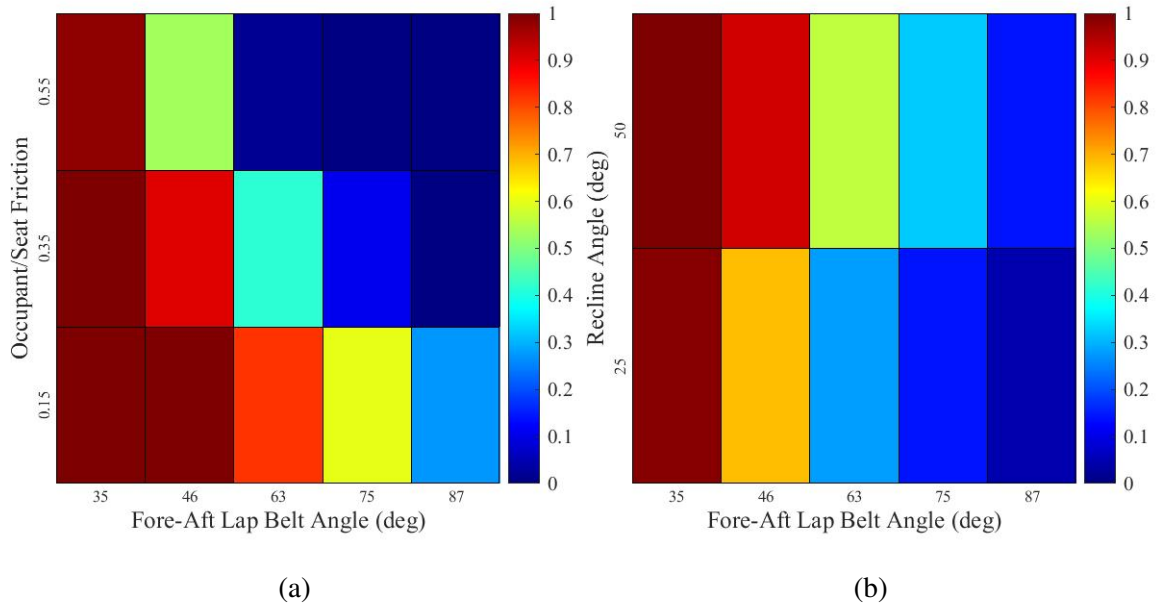


Figure J.19: Pelvis rotation influential parameter plots (generated full-factorial dataset): a) Parameter 1 vs Parameter 2, b) Parameter 1 vs Parameter 3.

APPENDIX J. ANALYSIS OF FULL-FACTORIAL GENERATED DATASET

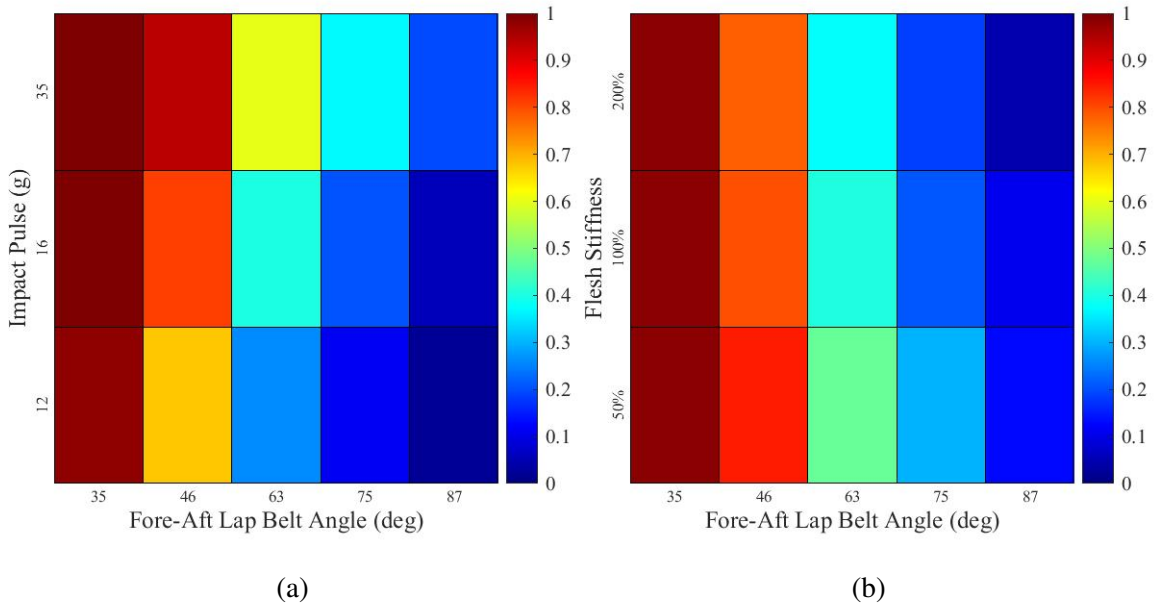


Figure J.20: Pelvis rotation influential parameter plots (generated full-factorial dataset): a) Parameter 1 vs Parameter 4, b) Parameter 1 vs Parameter 5.

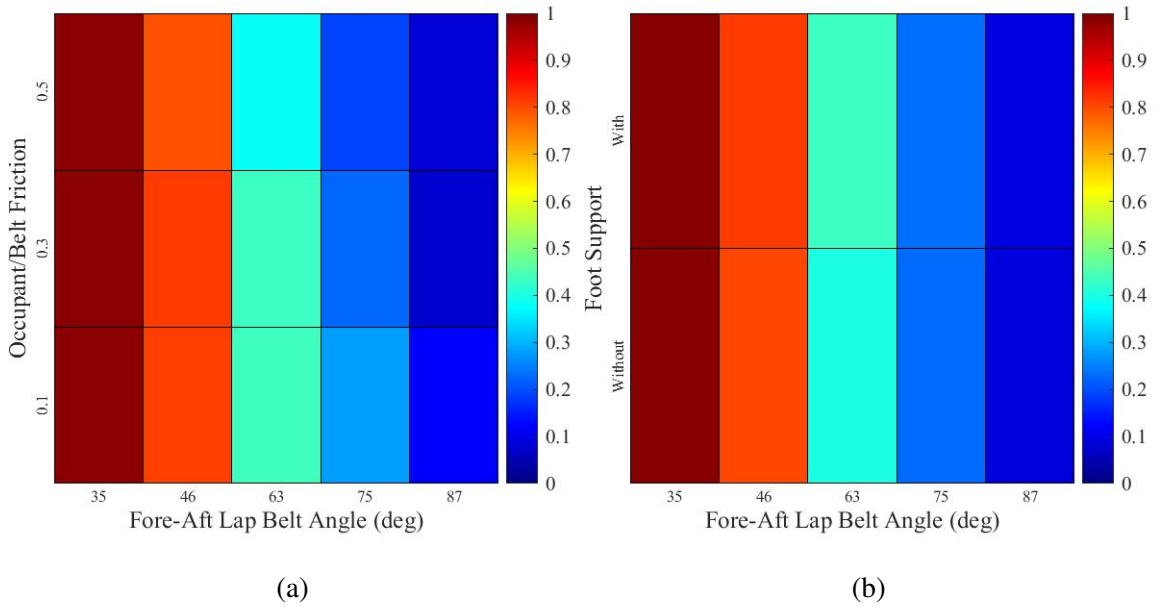


Figure J.21: Pelvis rotation influential parameter plots (generated full-factorial dataset): a) Parameter 1 vs Parameter 6, b) Parameter 1 vs Parameter 7.

APPENDIX J. ANALYSIS OF FULL-FACTORIAL GENERATED DATASET

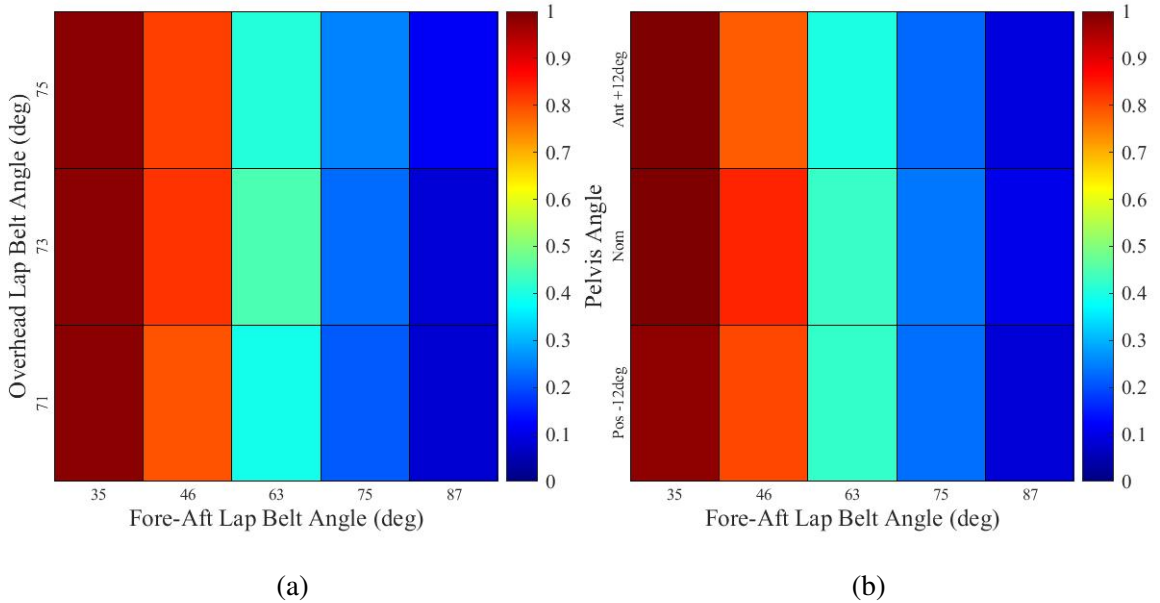


Figure J.22: Pelvis rotation influential parameter plots (generated full-factorial dataset): a) Parameter 1 vs Parameter 8, b) Parameter 2 vs Parameter 9.

J.2.5 Lap Belt Tension

The cutoff value identified from the k-means clustering was a probability of the maximum lap belt tension exceeding 5.9 kN, in which 50.6% of simulations clustered in the negative outcome (increased rearward pelvis rotation) group.

	Impact Pulse	Lap Belt Angle Fore-Aft	Lap Belt Angle Lateral	Foot Support	Belt Friction	Seat Friction	Recline Angle	Flesh Stiffness	Pelvis Angle
Cluster 1 Mean	0.377	0.475	0.488	0.527	0.506	0.551	0.507	0.501	0.507
Cluster 2 Mean	0.893	0.770	0.541	0.435	0.502	0.419	0.494	0.512	0.503
Absolute Distance	0.516	0.295	0.053	0.091	0.004	0.132	0.013	0.011	0.004
Rank	1	2	5	4	8	3	6	7	9

Figure J.23: Influential parameter determination for lap belt tension. The parameters in green showed an absolute distance greater than 0.1 between cluster means (negative versus positive outcome); the parameters in yellow showed an absolute distance greater than 0.05 between cluster means (negative versus positive outcome).

J.2.5.1 Influential Parameter Plots

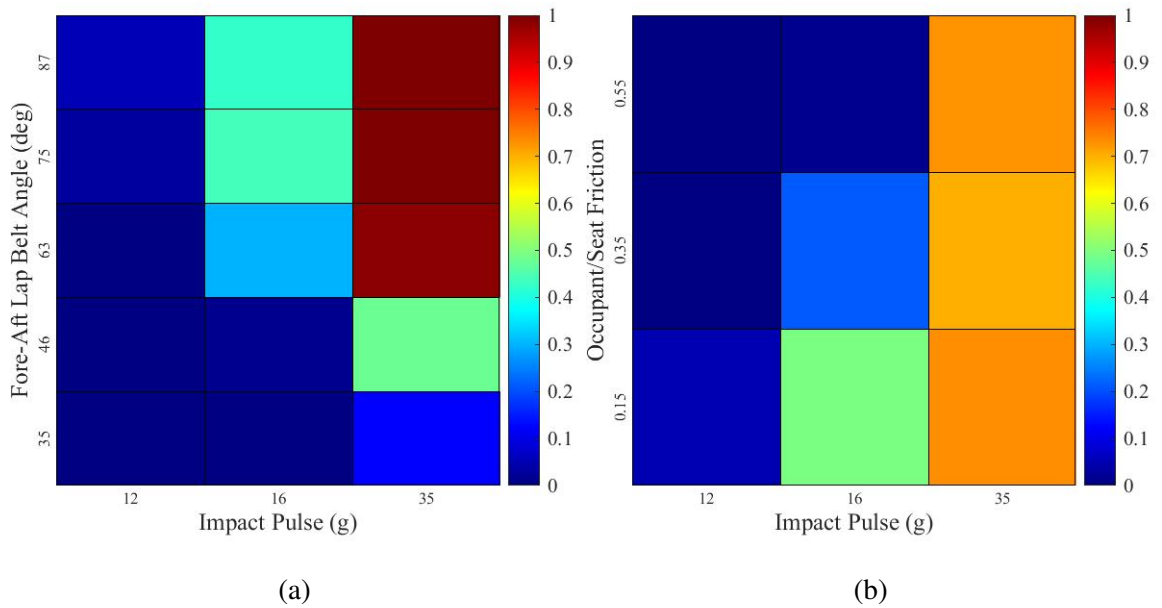


Figure J.24: Lap belt tension influential parameter plots (generated full-factorial dataset): a) Parameter 1 vs Parameter 2, b) Parameter 1 vs Parameter 3.

APPENDIX J. ANALYSIS OF FULL-FACTORIAL GENERATED DATASET

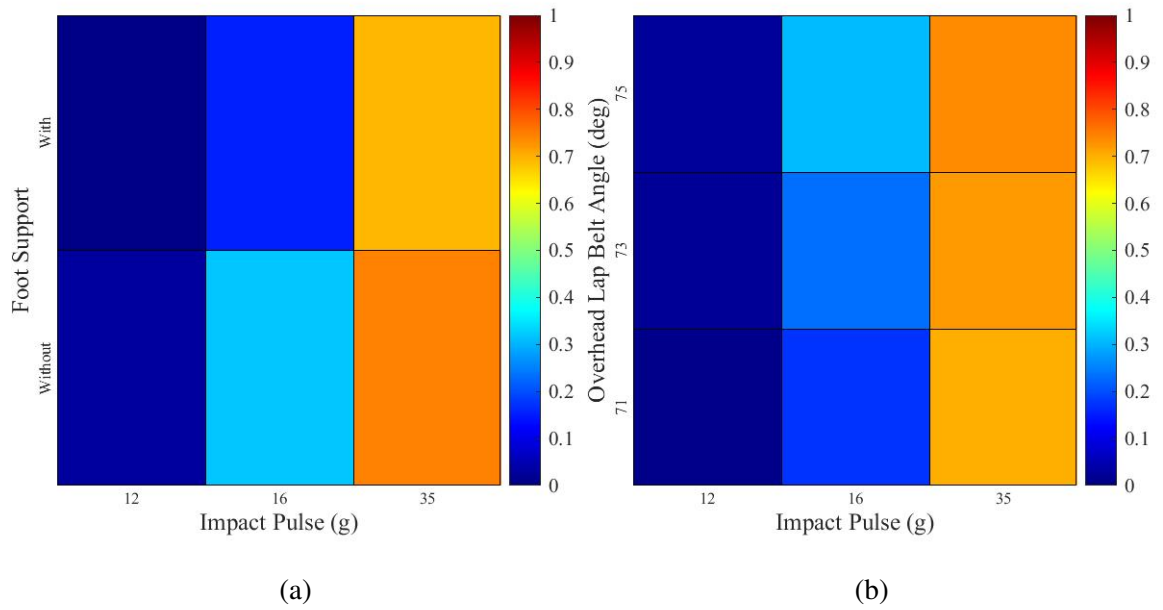


Figure J.25: Lap belt tension influential parameter plots (generated full-factorial dataset): a) Parameter 1 vs Parameter 4, b) Parameter 1 vs Parameter 5.

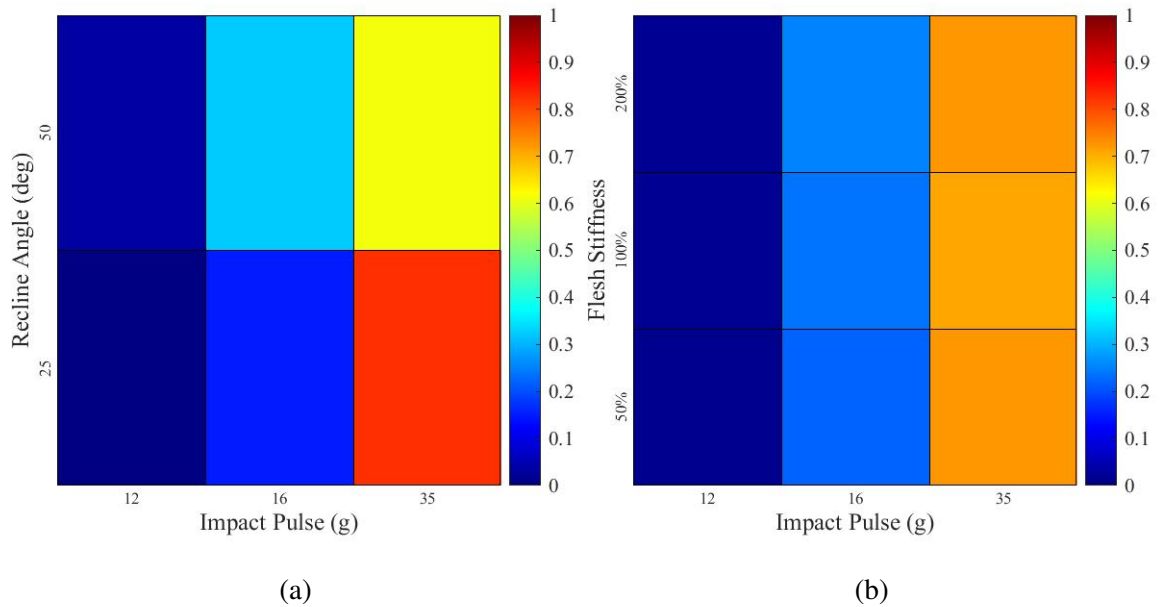


Figure J.26: Lap belt tension influential parameter plots (generated full-factorial dataset): a) Parameter 1 vs Parameter 6, b) Parameter 1 vs Parameter 7.

APPENDIX J. ANALYSIS OF FULL-FACTORIAL GENERATED DATASET

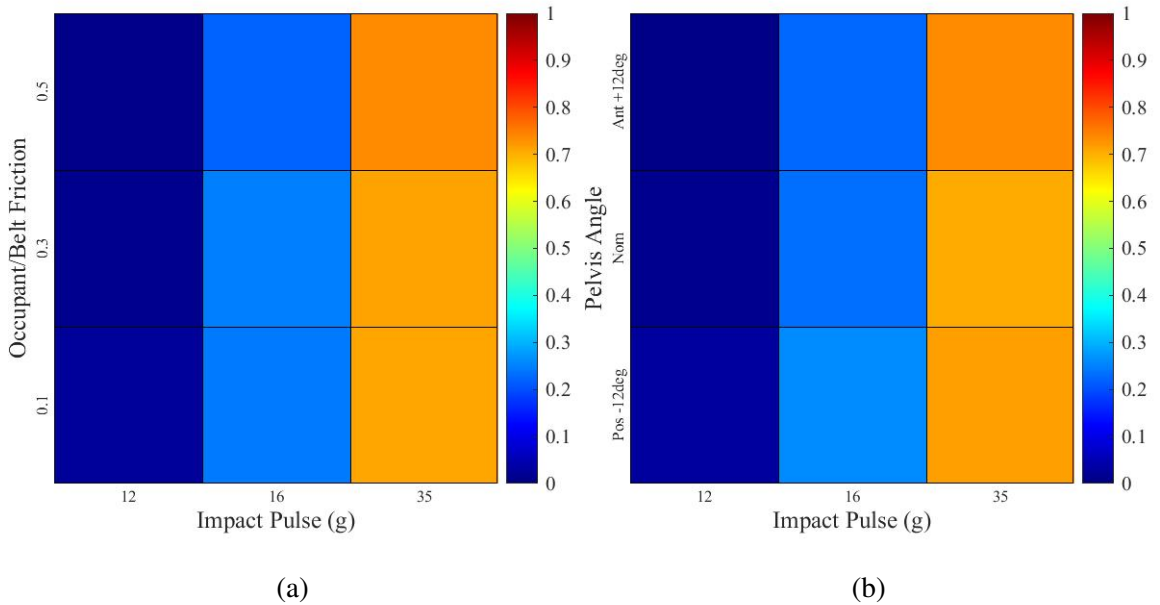


Figure J.27: Lap belt tension influential parameter plots (generated full-factorial dataset): a) Parameter 1 vs Parameter 8, b) Parameter 2 vs Parameter 9.

J.3 Additional Cut-Off Values for Continuous Output Metrics

To investigate the influence of parameters on regions of interest, different cut-off values were established for each of the continuous output metrics based on the metamodel's prediction distributions for that metric (see Section J.1). These figures are plotted below.

J.3.1 Pelvis Forward Displacement

Three cut-off values were established for this metric: 100, 200, and 300 mm. These plots are shown for each parameter in order of influence (see Table 9.1).

APPENDIX J. ANALYSIS OF FULL-FACTORIAL GENERATED DATASET

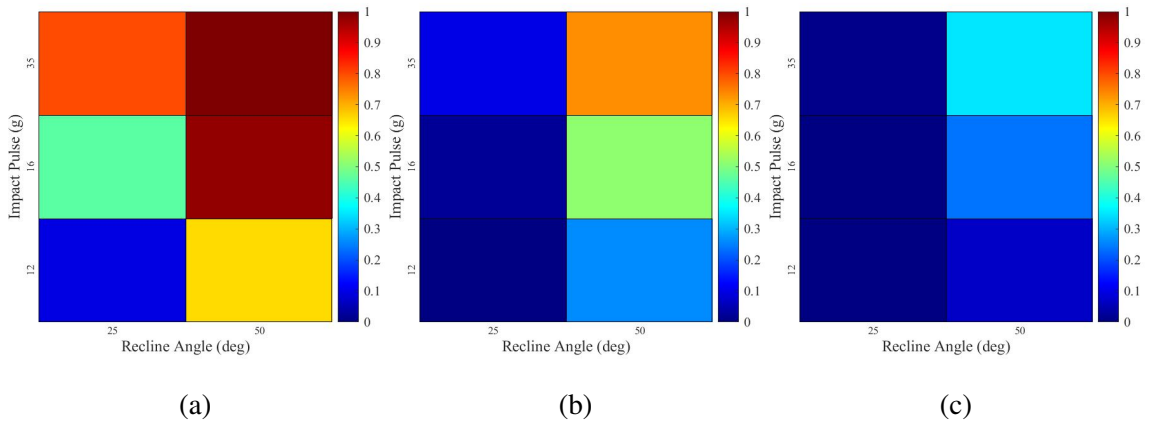


Figure J.28: Influence of recline angle and impact pulse on the risk of the maximum pelvis displacement exceeding: a) 100 mm, b) 200 mm, c) 300 mm.

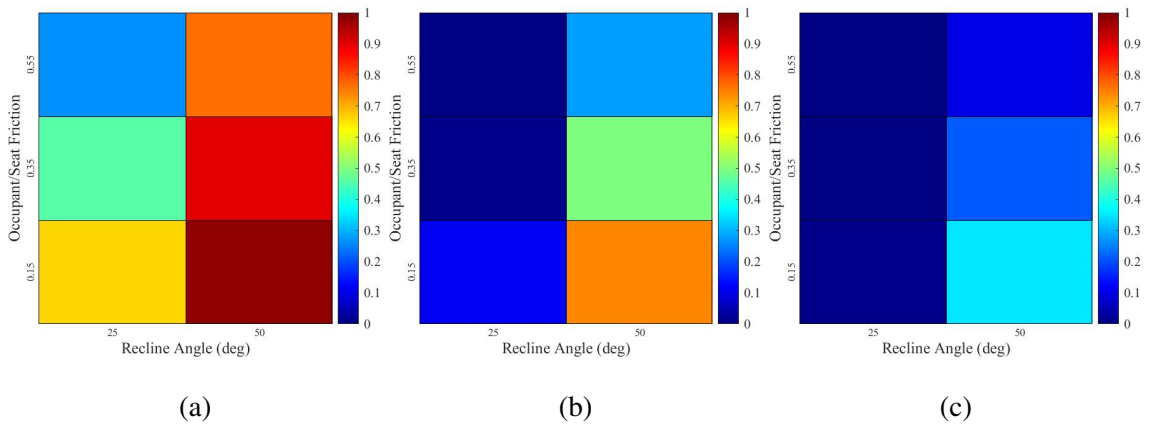


Figure J.29: Influence of recline angle and occupant/seat friction on the risk of the maximum pelvis displacement exceeding: a) 100 mm, b) 200 mm, c) 300 mm.

APPENDIX J. ANALYSIS OF FULL-FACTORIAL GENERATED DATASET

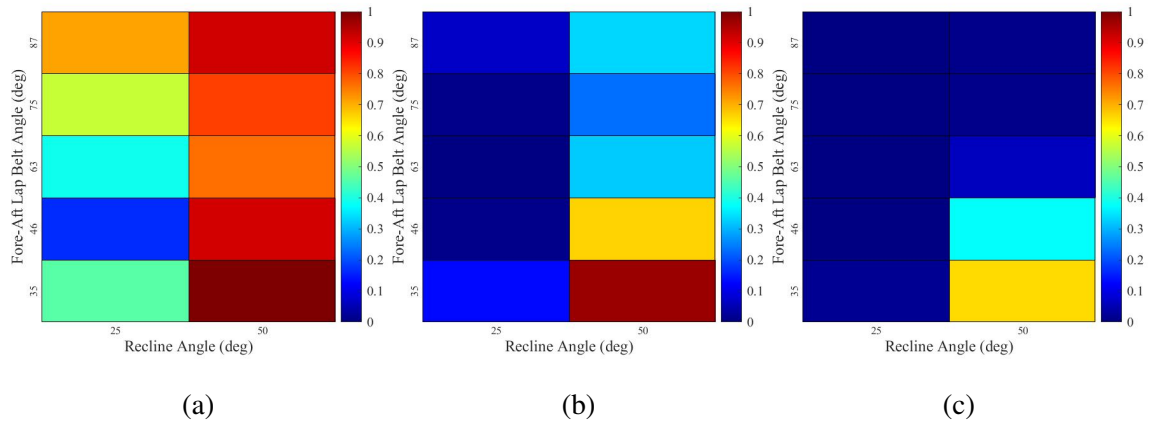


Figure J.30: Influence of recline angle and fore-aft lap belt angle on the risk of the maximum pelvis displacement exceeding: a) 100 mm, b) 200 mm, c) 300 mm.

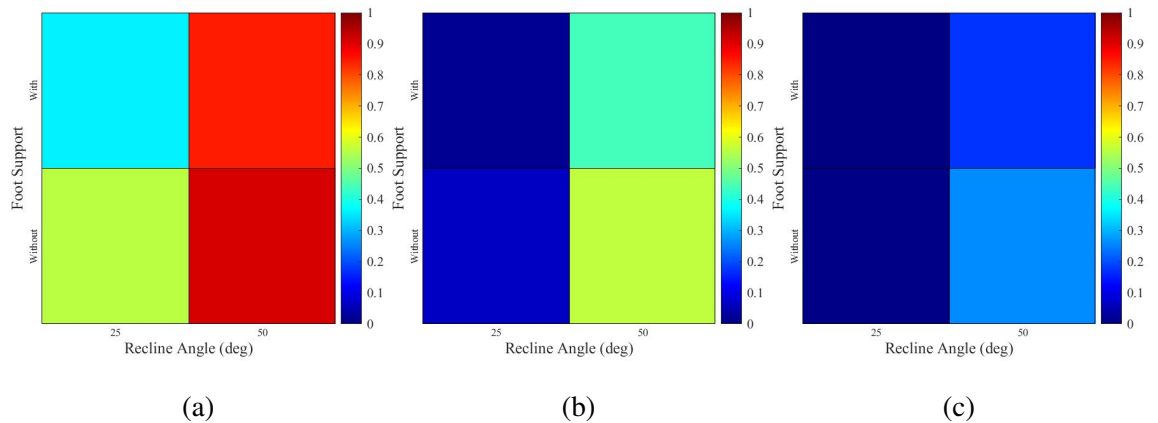


Figure J.31: Influence of recline angle and foot support on the risk of the maximum pelvis displacement exceeding: a) 100 mm, b) 200 mm, c) 300 mm.

APPENDIX J. ANALYSIS OF FULL-FACTORIAL GENERATED DATASET

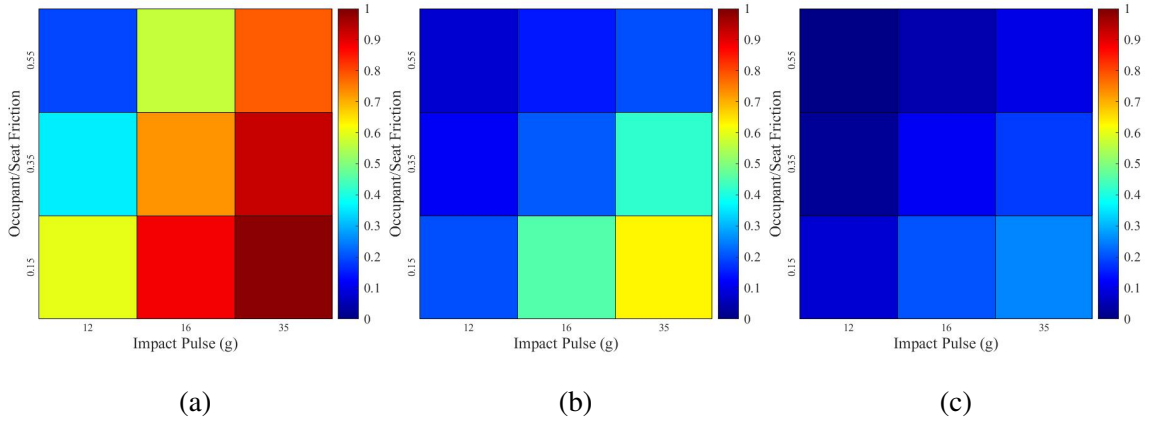


Figure J.32: Influence of impact pulse and occupant/seat friction on the risk of the maximum pelvis displacement exceeding: a) 100 mm, b) 200 mm, c) 300 mm.

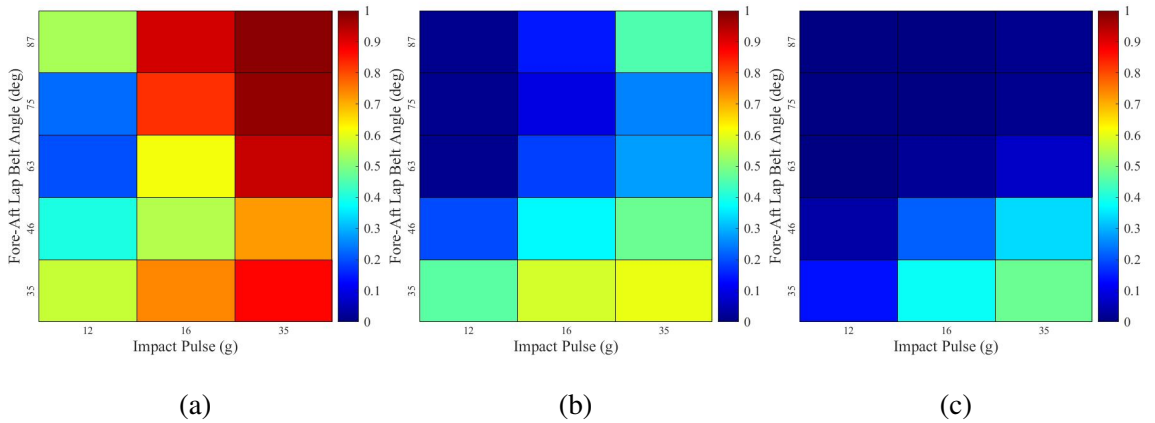


Figure J.33: Influence of impact pulse and fore-aft lap belt angle on the risk of the maximum pelvis displacement exceeding: a) 100 mm, b) 200 mm, c) 300 mm.

APPENDIX J. ANALYSIS OF FULL-FACTORIAL GENERATED DATASET

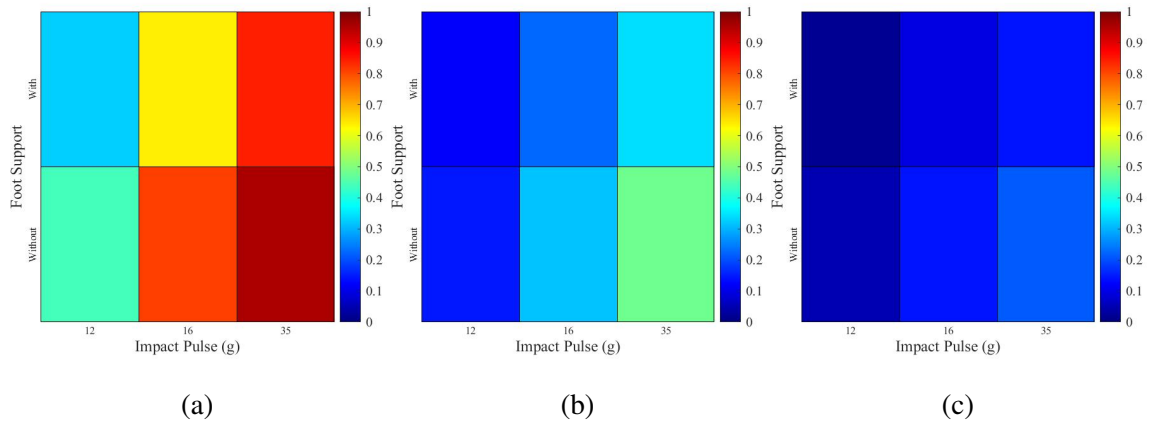


Figure J.34: Influence of impact pulse and foot support on the risk of the maximum pelvis displacement exceeding: a) 100 mm, b) 200 mm, c) 300 mm.

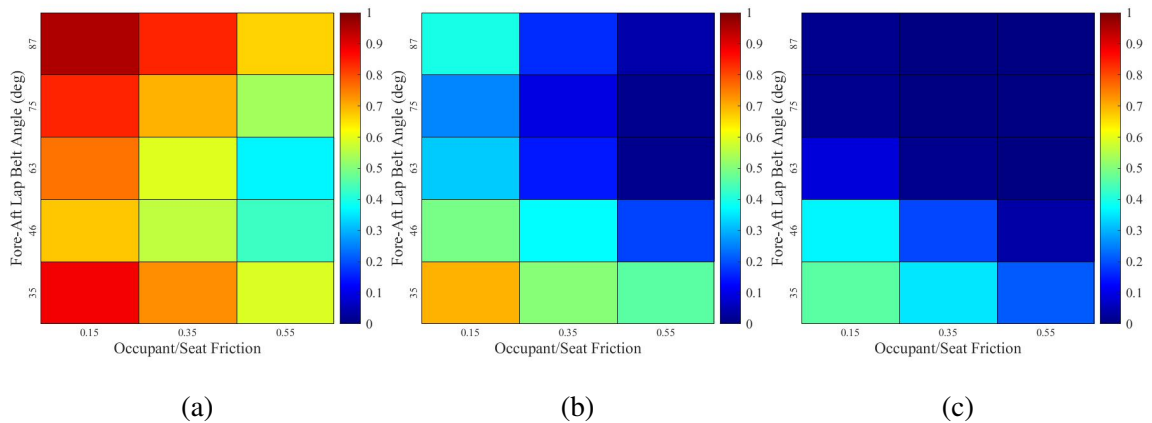


Figure J.35: Influence of occupant/seat friction and fore-aft lap belt angle on the risk of the maximum pelvis displacement exceeding: a) 100 mm, b) 200 mm, c) 300 mm.

APPENDIX J. ANALYSIS OF FULL-FACTORIAL GENERATED DATASET

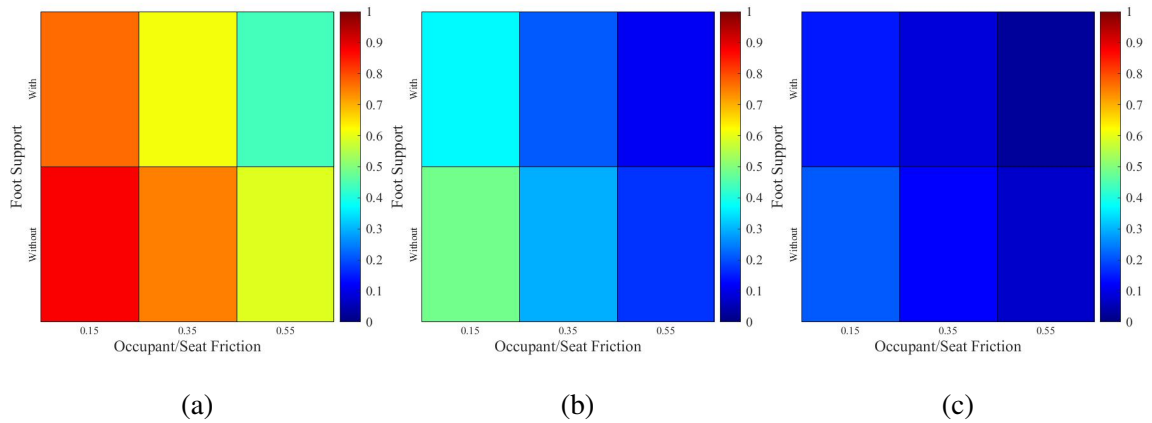


Figure J.36: Influence of occupant/seat friction and foot support on the risk of the maximum pelvis displacement exceeding: a) 100 mm, b) 200 mm, c) 300 mm.

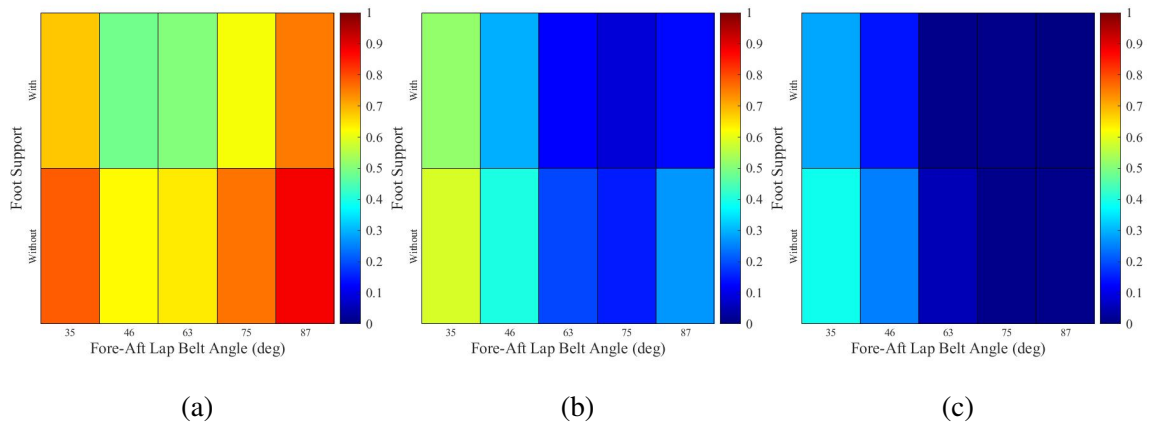


Figure J.37: Influence of fore-aft lap belt angle and foot support on the risk of the maximum pelvis displacement exceeding: a) 100 mm, b) 200 mm, c) 300 mm.

J.3.2 Pelvis Rotation

Three cut-off values were established for this metric: 0, 10, and 20 degrees. These plots are shown for each parameter in order of influence (see Table 9.1).

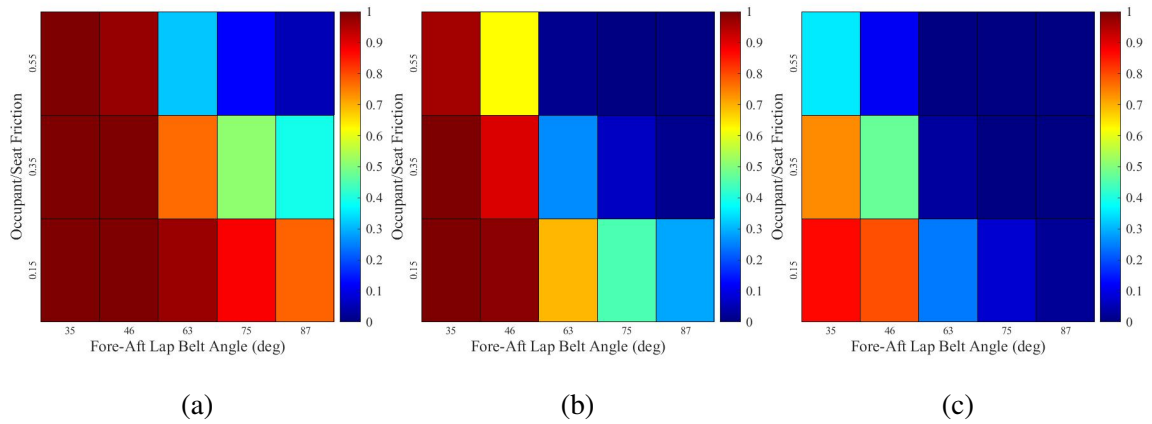


Figure J.38: Influence of fore-aft lap belt angle and occupant/seat friction on the risk of the maximum rearward pelvis rotation exceeding: a) 0°, b) 10°, c) 20°.

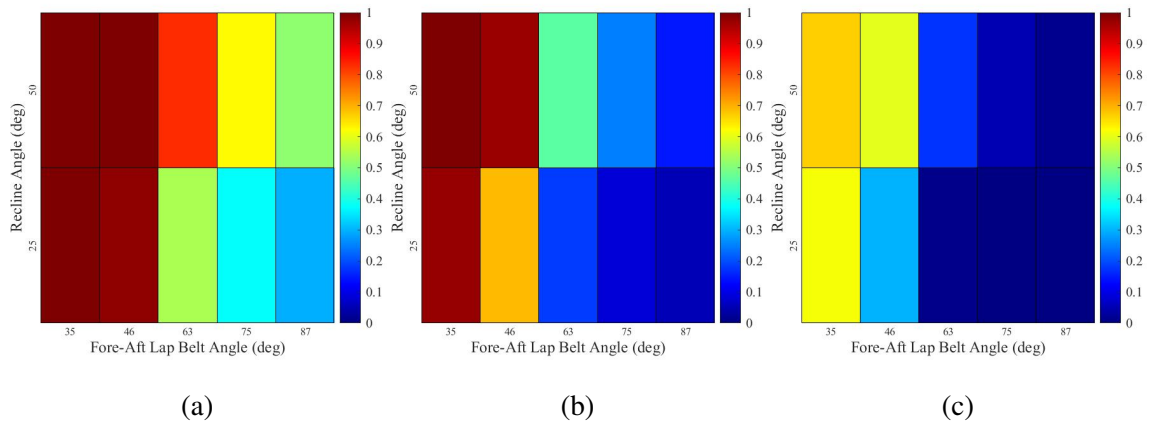


Figure J.39: Influence of fore-aft lap belt angle and recline angle on the risk of the maximum rearward pelvis rotation exceeding: a) 0°, b) 10°, c) 20°.

APPENDIX J. ANALYSIS OF FULL-FACTORIAL GENERATED DATASET

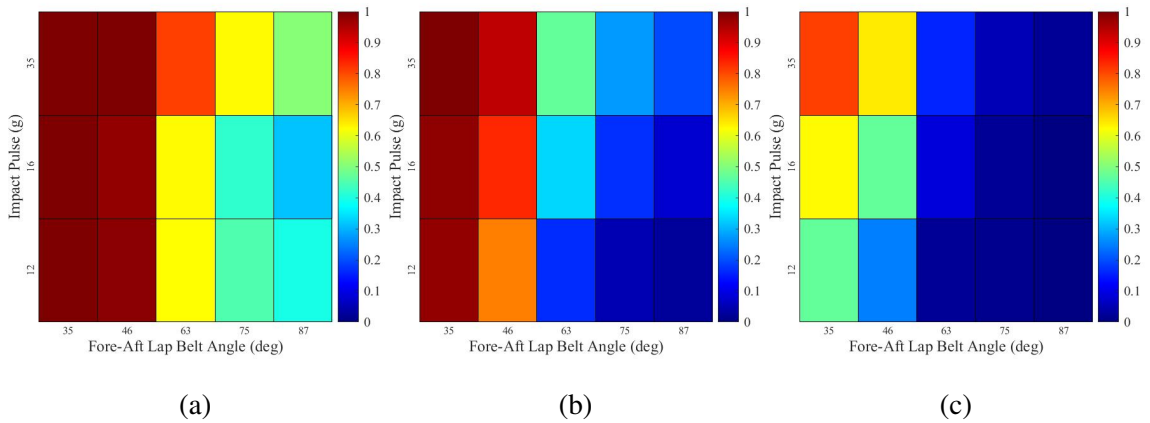


Figure J.40: Influence of fore-aft lap belt angle and impact pulse on the risk of the maximum rearward pelvis rotation exceeding: a) 0°, b) 10°, c) 20°.

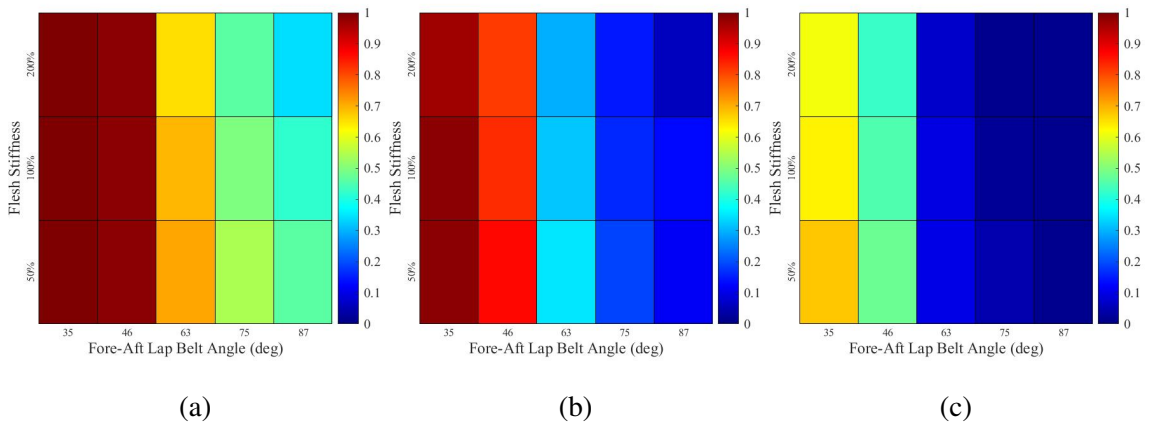


Figure J.41: Influence of fore-aft lap belt angle and flesh stiffness on the risk of the maximum rearward pelvis rotation exceeding: a) 0°, b) 10°, c) 20°.

APPENDIX J. ANALYSIS OF FULL-FACTORIAL GENERATED DATASET

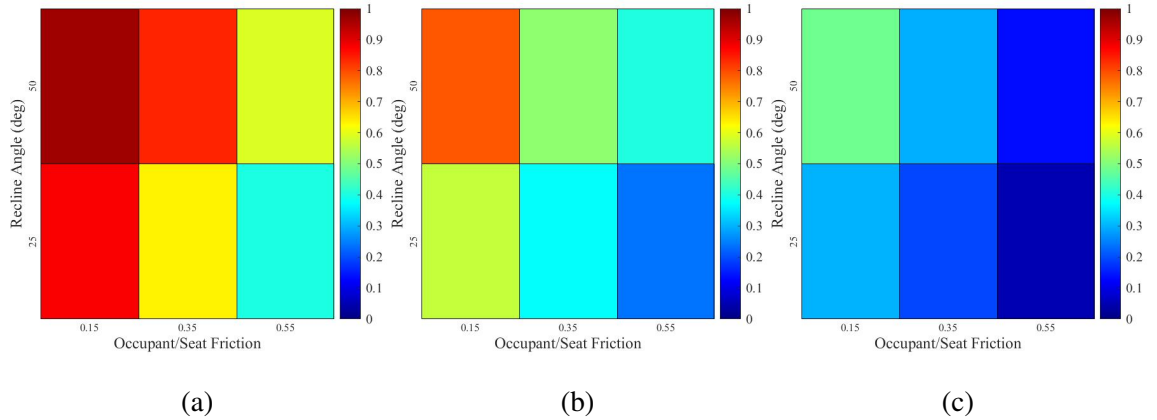


Figure J.42: Influence of occupant/seat friction and recline angle on the risk of the maximum rearward pelvis rotation exceeding: a) 0°, b) 10°, c) 20°.

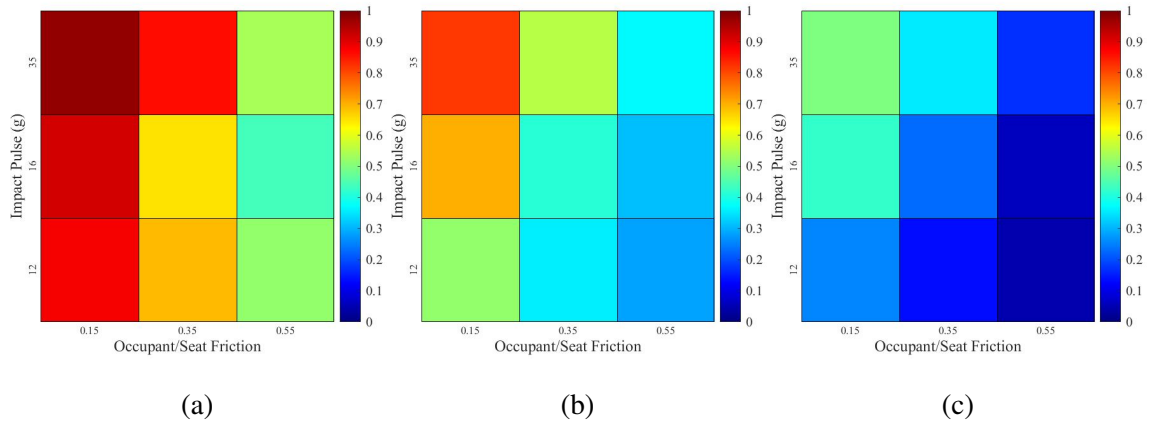


Figure J.43: Influence of occupant/seat friction and impact pulse on the risk of the maximum rearward pelvis rotation exceeding: a) 0°, b) 10°, c) 20°.

APPENDIX J. ANALYSIS OF FULL-FACTORIAL GENERATED DATASET

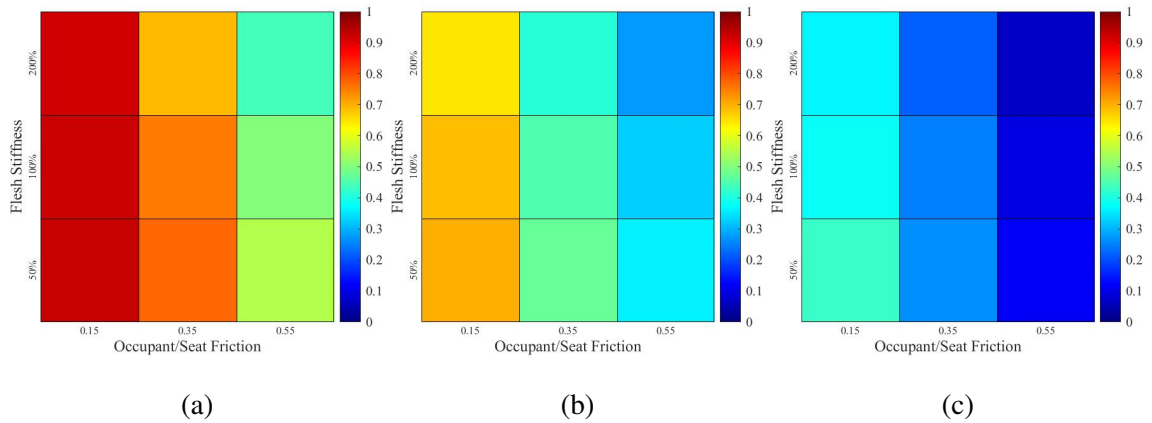


Figure J.44: Influence of recline angle and flesh stiffness on the risk of the maximum rearward pelvis rotation exceeding: a) 0°, b) 10°, c) 20°.

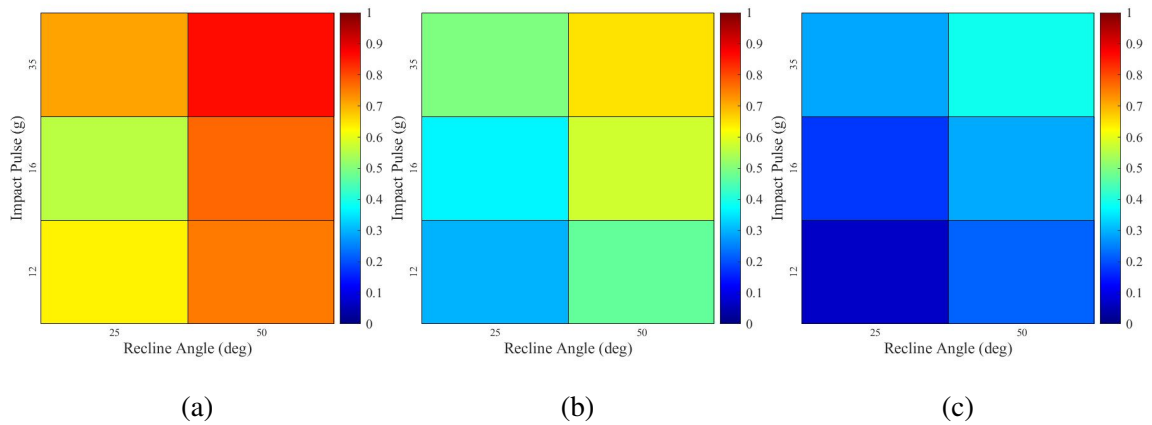


Figure J.45: Influence of recline angle and impact pulse on the risk of the maximum rearward pelvis rotation exceeding: a) 0°, b) 10°, c) 20°.

APPENDIX J. ANALYSIS OF FULL-FACTORIAL GENERATED DATASET

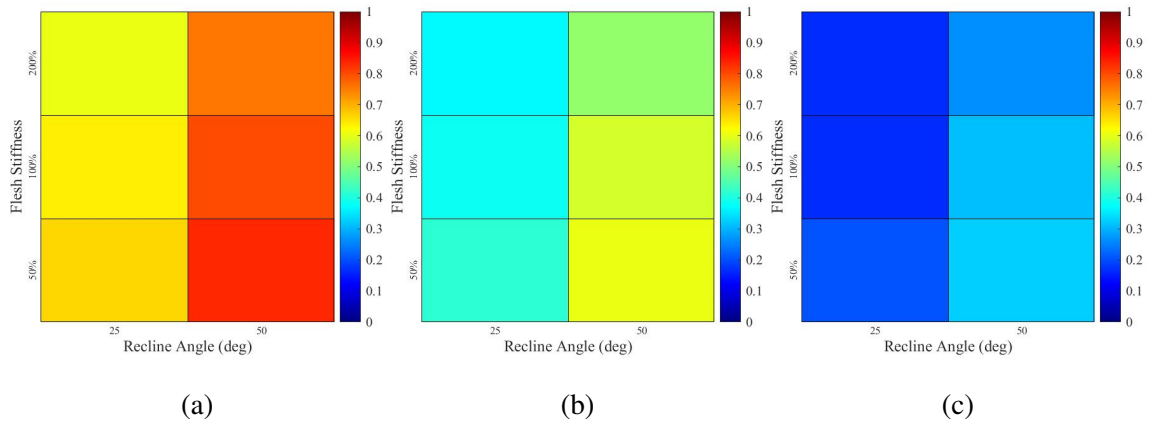


Figure J.46: Influence of recline angle and flesh stiffness on the risk of the maximum rearward pelvis rotation exceeding: a) 0°, b) 10°, c) 20°.

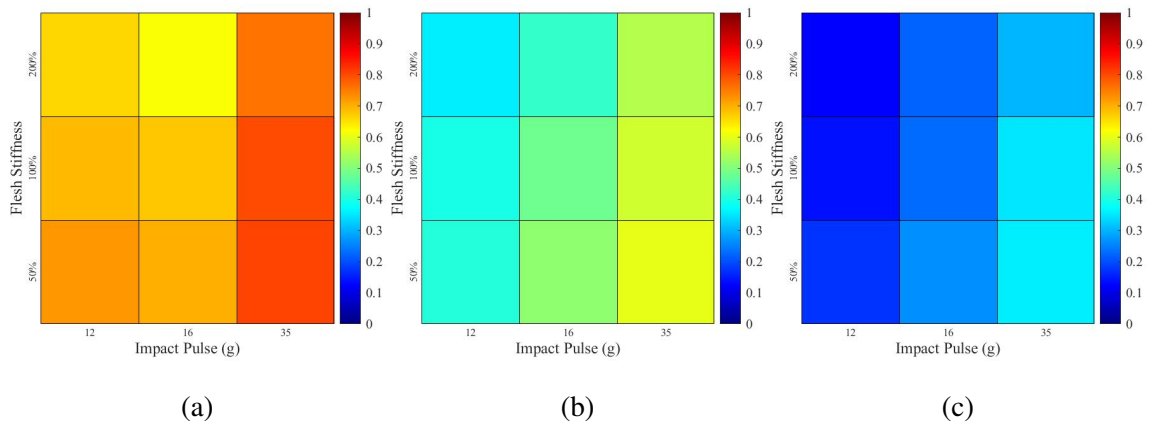


Figure J.47: Influence of impact pulse and flesh stiffness on the risk of the maximum rearward pelvis rotation exceeding: a) 0°, b) 10°, c) 20°.

J.3.3 Submarining Distance

Three cut-off values were established for this metric: 0, 50, and 150 mm. These plots are shown for each parameter in order of influence (see Table 9.1).

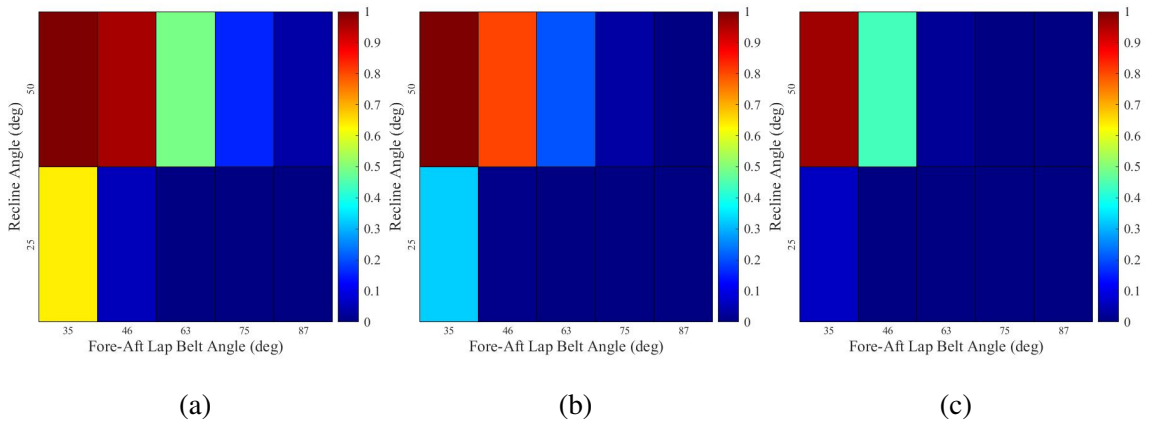


Figure J.48: Influence of fore-aft lap belt angle and recline angle on the risk of the maximum submarining distance exceeding: a) 0 mm, b) 50 mm, c) 150 mm.

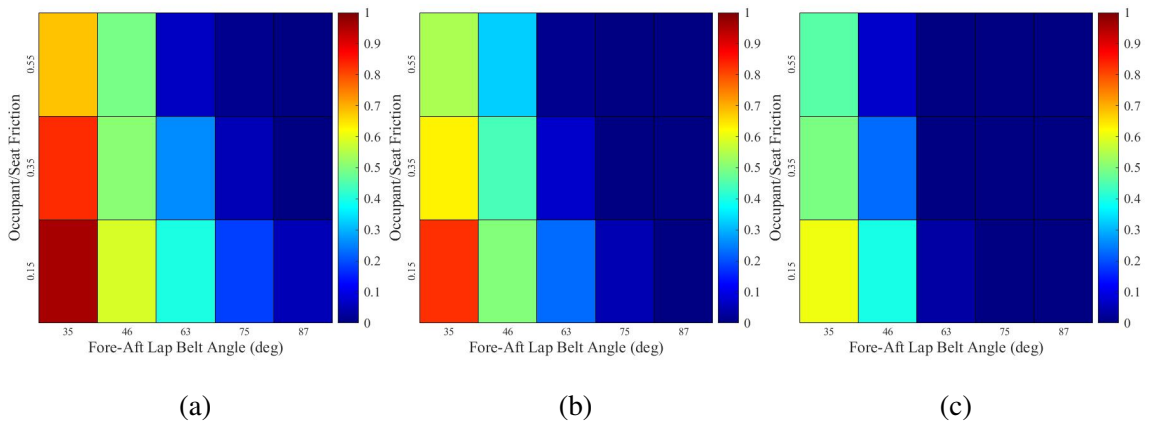


Figure J.49: Influence of fore-aft lap belt angle and occupant/seat friction on the risk of the maximum submarining distance exceeding: a) 0 mm, b) 50 mm, c) 150 mm.

APPENDIX J. ANALYSIS OF FULL-FACTORIAL GENERATED DATASET

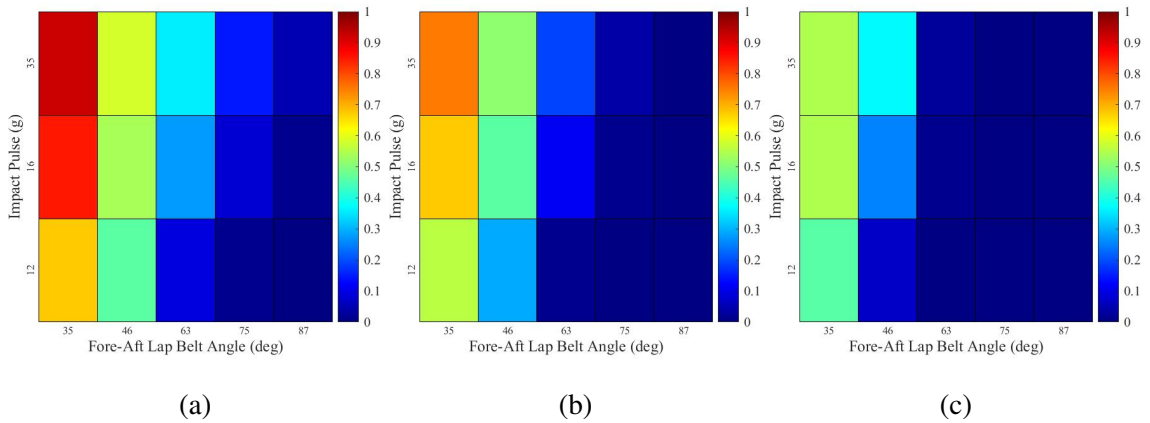


Figure J.50: Influence of fore-aft lap belt angle and impact pulse on the risk of the maximum submarining distance exceeding: a) 0 mm, b) 50 mm, c) 150 mm.

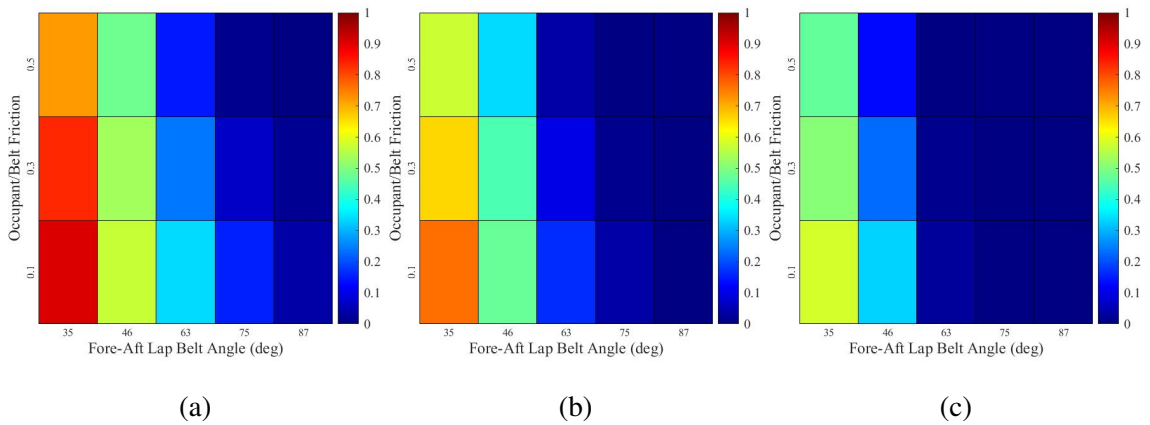


Figure J.51: Influence of fore-aft lap belt angle and occupant/belt friction on the risk of the maximum submarining distance exceeding: a) 0 mm, b) 50 mm, c) 150 mm.

APPENDIX J. ANALYSIS OF FULL-FACTORIAL GENERATED DATASET

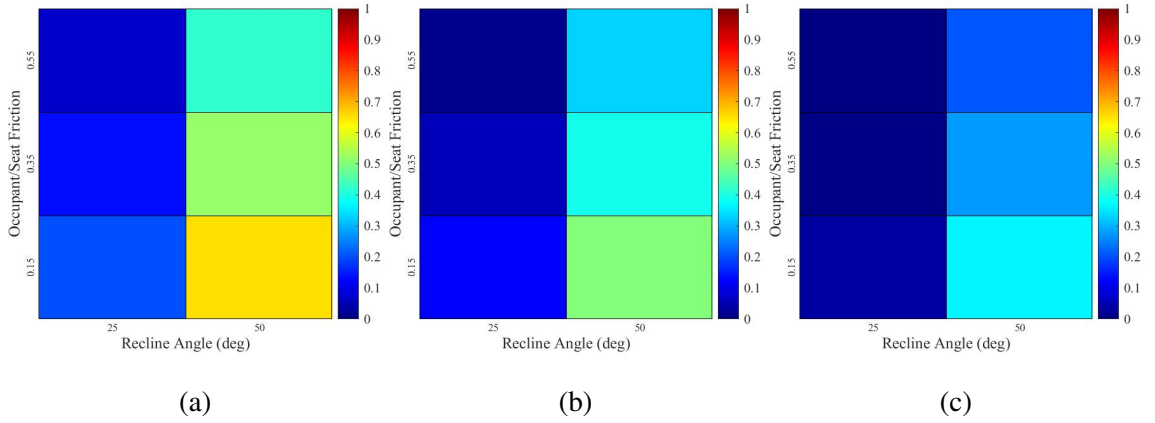


Figure J.52: Influence of recline angle and occupant/seat friction on the risk of the maximum submarining distance exceeding: a) 0 mm, b) 50 mm, c) 150 mm.

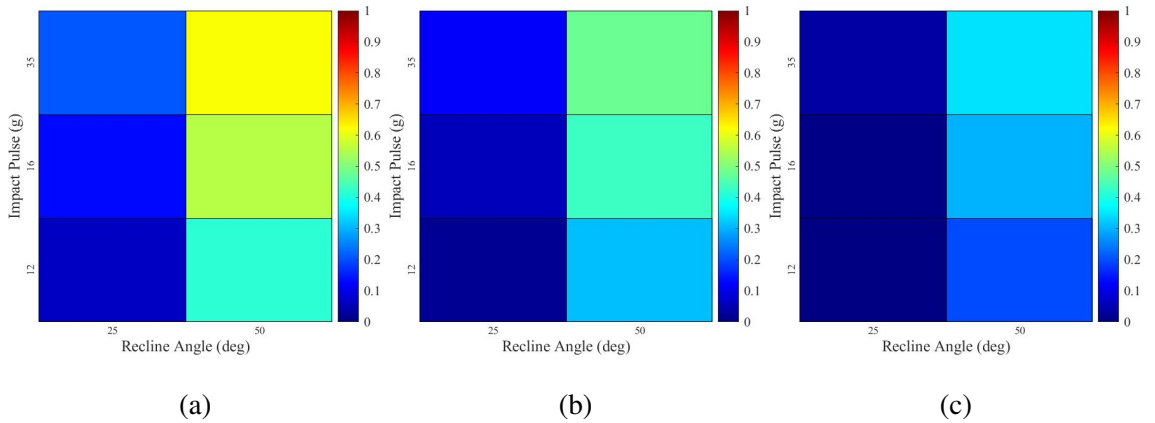


Figure J.53: Influence of recline angle and impact pulse on the risk of the maximum submarining distance exceeding: a) 0 mm, b) 50 mm, c) 150 mm.

APPENDIX J. ANALYSIS OF FULL-FACTORIAL GENERATED DATASET

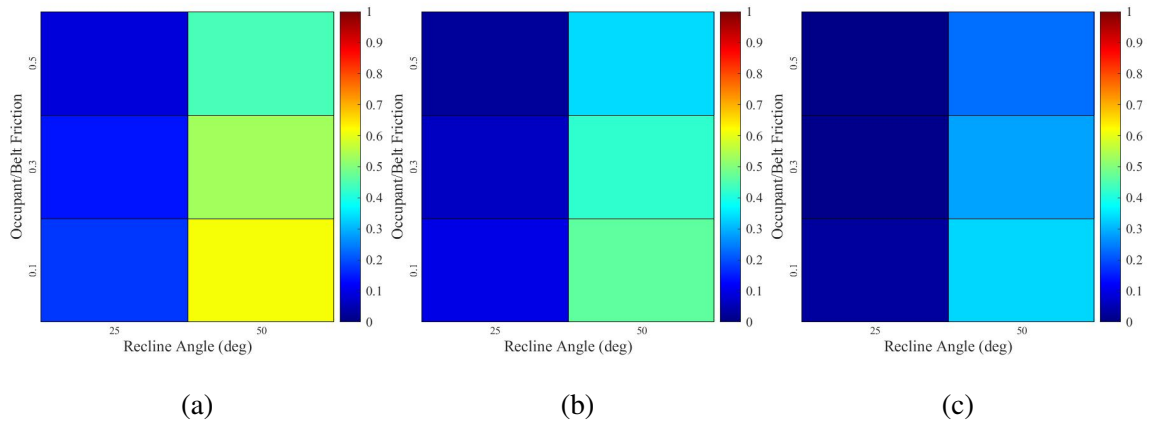


Figure J.54: Influence of recline angle and occupant/belt friction on the risk of the maximum submaring distance exceeding: a) 0 mm, b) 50 mm, c) 150 mm.

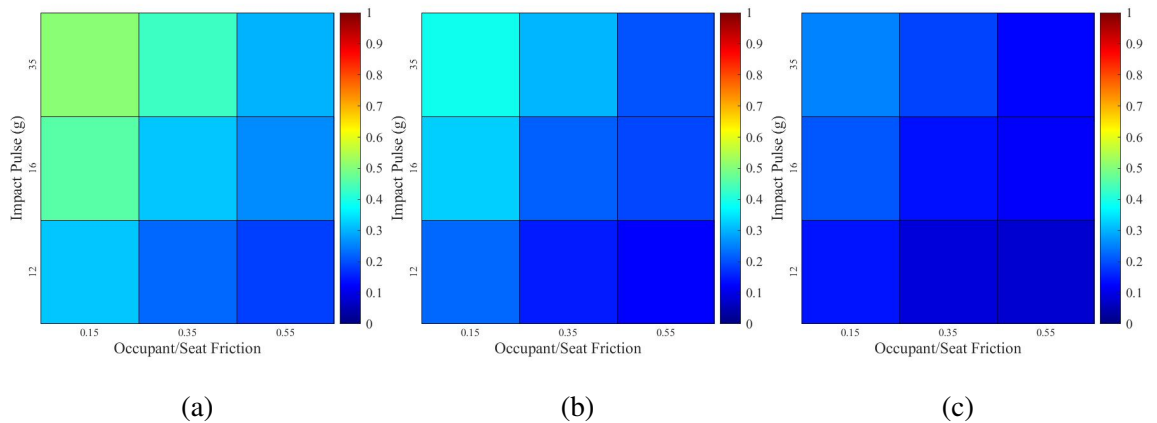


Figure J.55: Influence of occupant/seat friction and impact pulse on the risk of the maximum submaring distance exceeding: a) 0 mm, b) 50 mm, c) 150 mm.

APPENDIX J. ANALYSIS OF FULL-FACTORIAL GENERATED DATASET

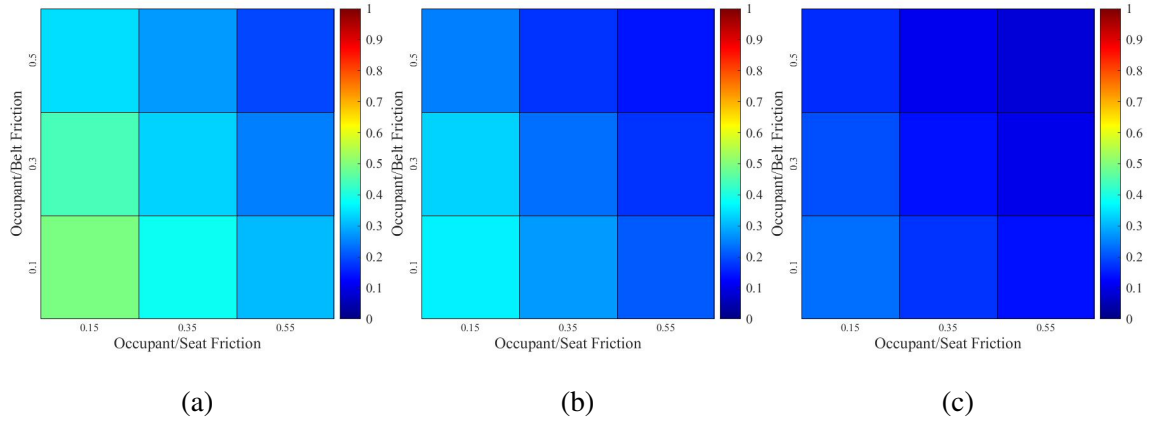


Figure J.56: Influence of occupant/seat friction and occupant/belt friction on the risk of the maximum submarining distance exceeding: a) 0 mm, b) 50 mm, c) 150 mm.

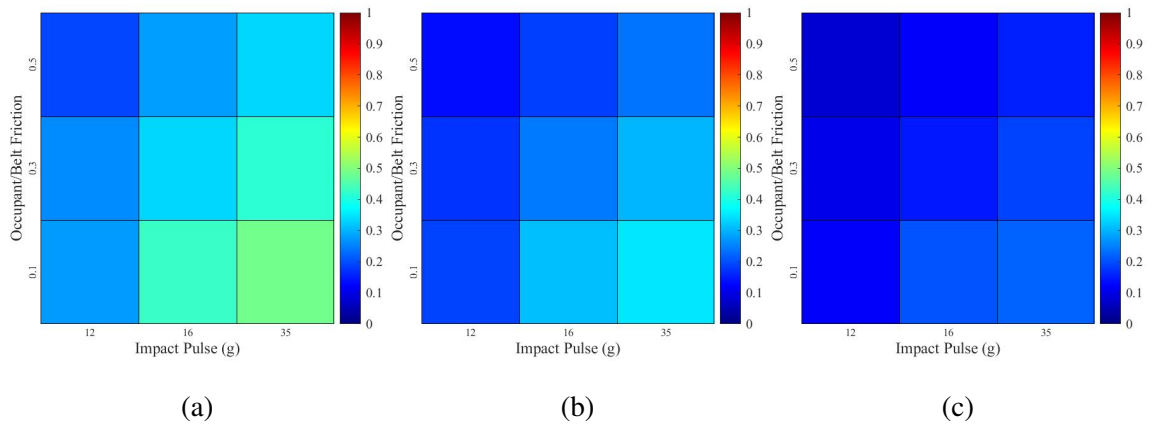


Figure J.57: Influence of impact pulse and occupant/belt friction on the risk of the maximum submarining distance exceeding: a) 0 mm, b) 50 mm, c) 150 mm.

J.3.4 Lap Belt Tension

Three cut-off values were established for this metric: 4, 6, and 8 kN. These plots are shown for each parameter in order of influence (see Table 9.1).

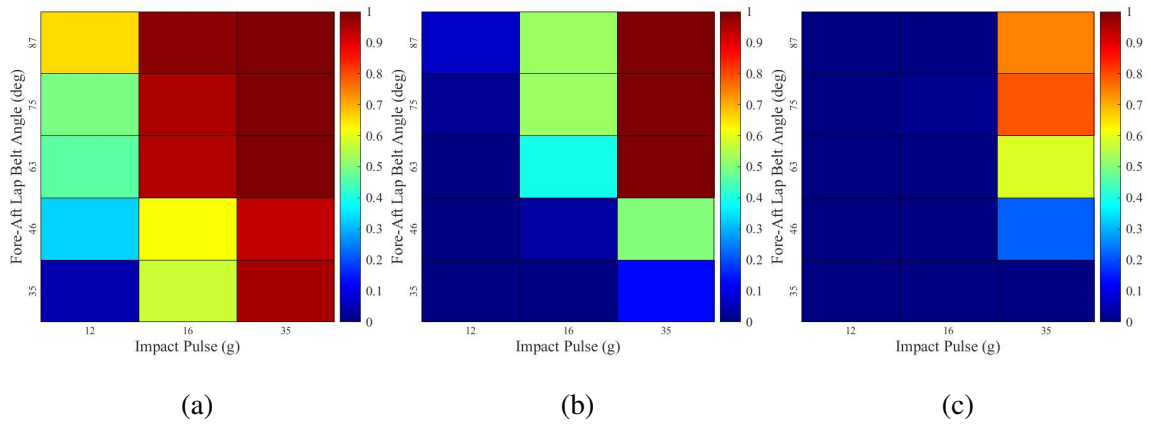


Figure J.58: Influence of impact pulse and fore-aft lap belt angle on the risk of the maximum lap belt tension exceeding: a) 4 kN, a) 6 kN, c) 8 kN.

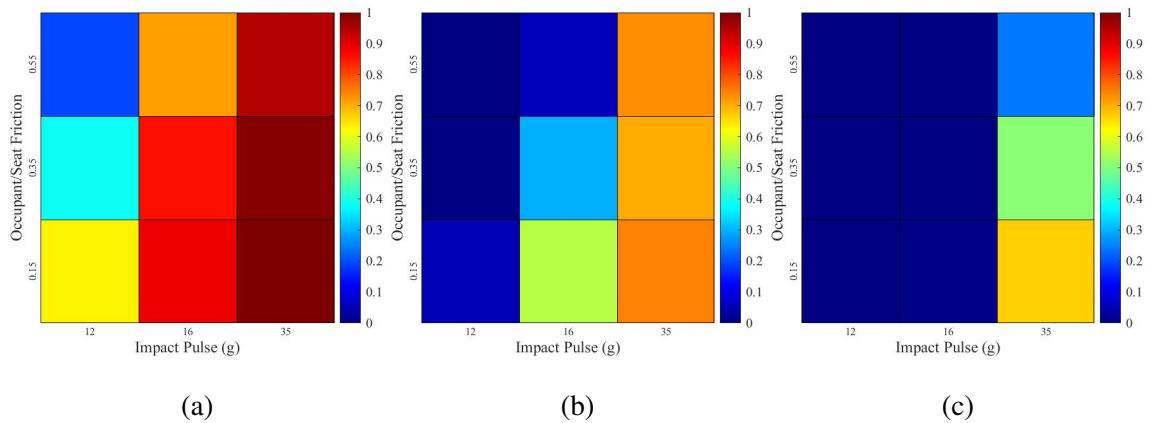


Figure J.59: Influence of impact pulse and occupant/seat friction on the risk of the maximum lap belt tension exceeding: a) 4 kN, a) 6 kN, c) 8 kN.

APPENDIX J. ANALYSIS OF FULL-FACTORIAL GENERATED DATASET

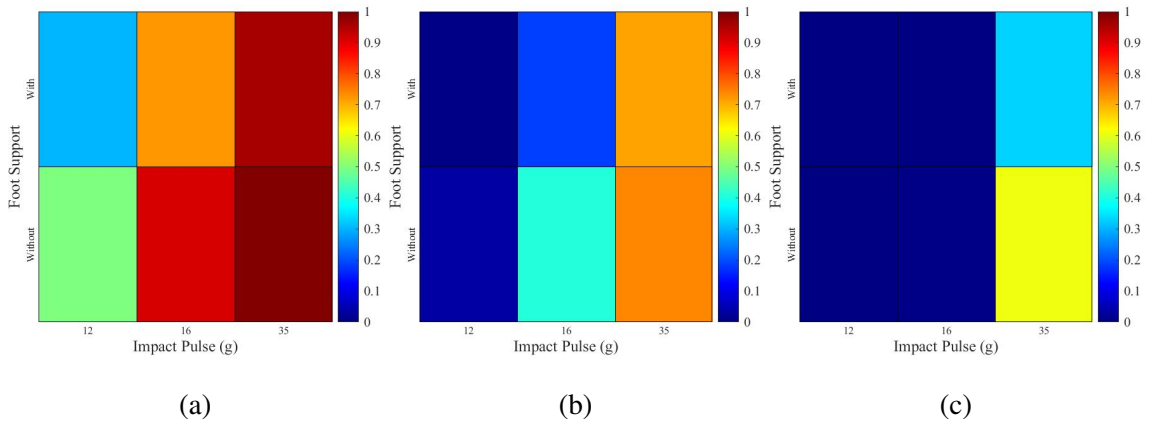


Figure J.60: Influence of impact pulse and foot support on the risk of the maximum lap belt tension exceeding: a) 4 kN, a) 6 kN, c) 8 kN.

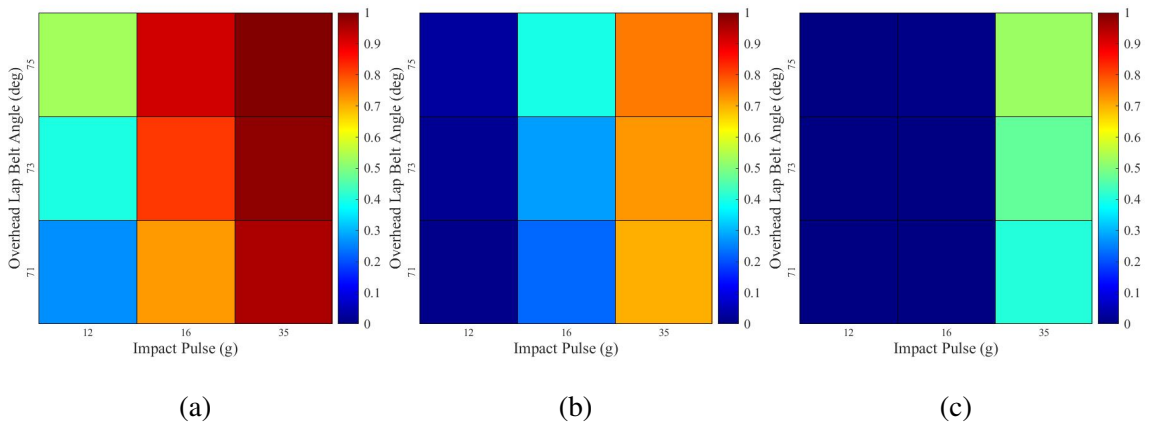


Figure J.61: Influence of impact pulse and overhead lap belt angle on the risk of the maximum lap belt tension exceeding: a) 4 kN, a) 6 kN, c) 8 kN.

APPENDIX J. ANALYSIS OF FULL-FACTORIAL GENERATED DATASET

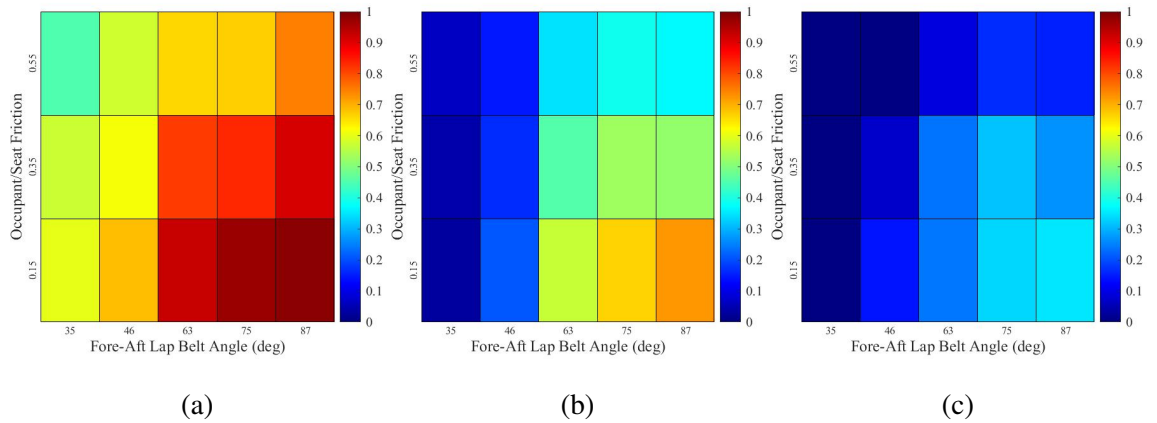


Figure J.62: Influence of fore-aft lap belt angle and occupant/seat friction on the risk of the maximum lap belt tension exceeding: a) 4 kN, a) 6 kN, c) 8 kN.

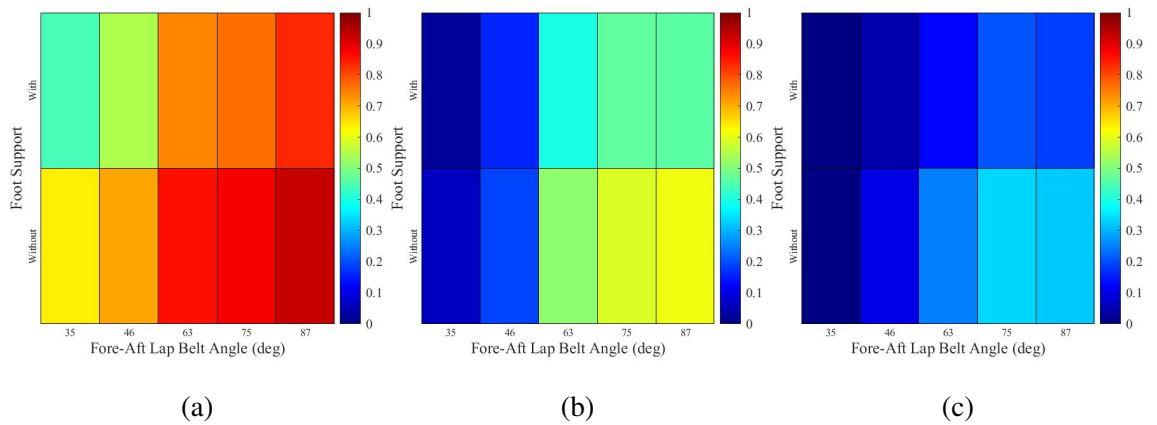


Figure J.63: Influence of fore-aft lap belt angle and foot support on the risk of the maximum lap belt tension exceeding: a) 4 kN, a) 6 kN, c) 8 kN.

APPENDIX J. ANALYSIS OF FULL-FACTORIAL GENERATED DATASET

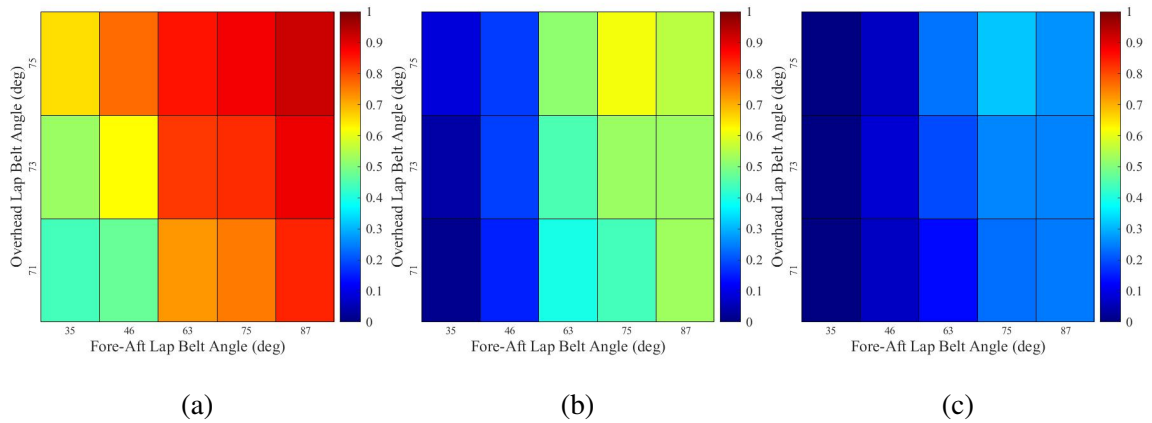


Figure J.64: Influence of fore-aft lap belt angle and overhead lap belt angle on the risk of the maximum lap belt tension exceeding: a) 4 kN, a) 6 kN, c) 8 kN.

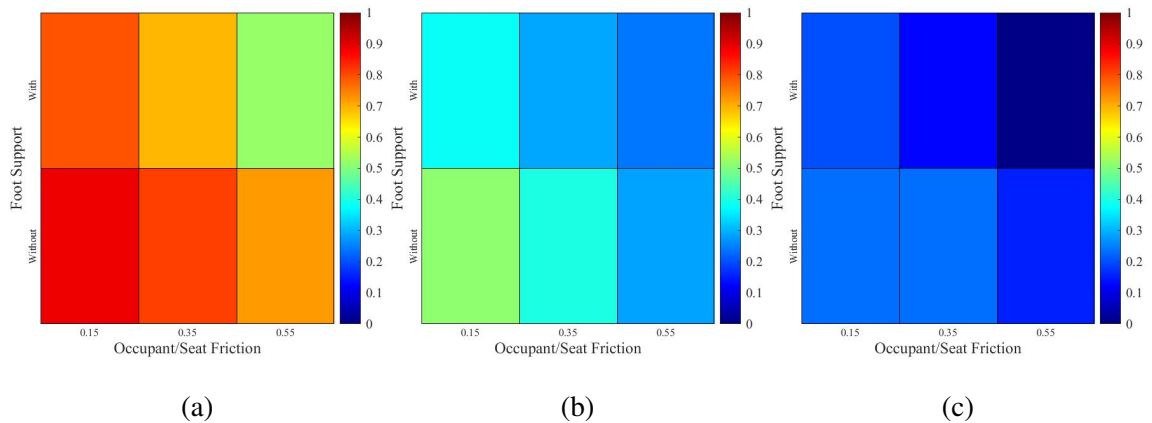


Figure J.65: Influence of occupant/seat friction and foot support on the risk of the maximum lap belt tension exceeding: a) 4 kN, a) 6 kN, c) 8 kN.

APPENDIX J. ANALYSIS OF FULL-FACTORIAL GENERATED DATASET

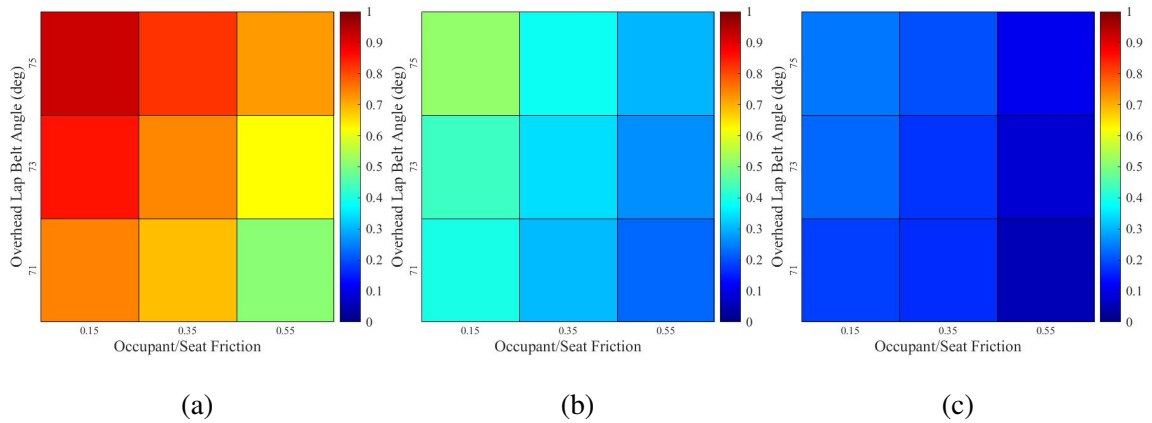


Figure J.66: Influence of occupant/seat friction and overhead lap belt angle on the risk of the maximum lap belt tension exceeding: a) 4 kN, a) 6 kN, c) 8 kN.

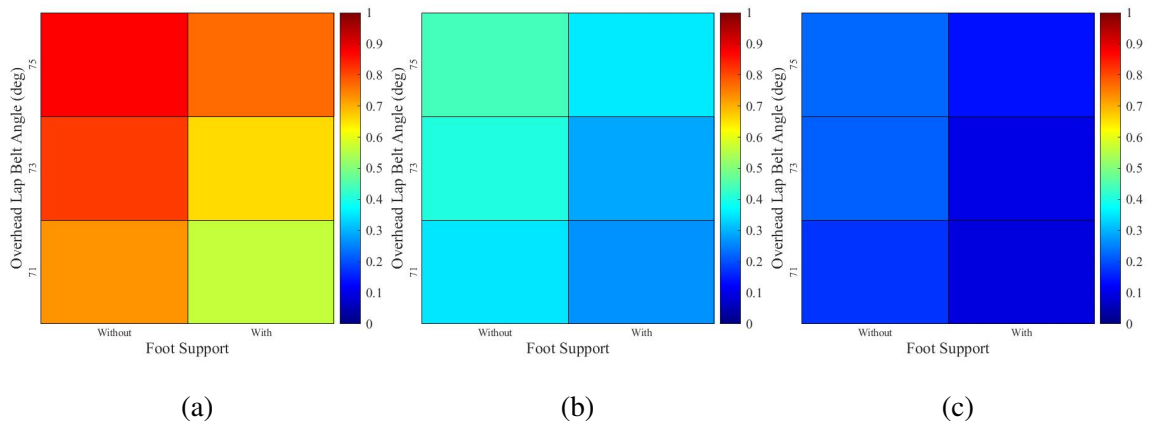


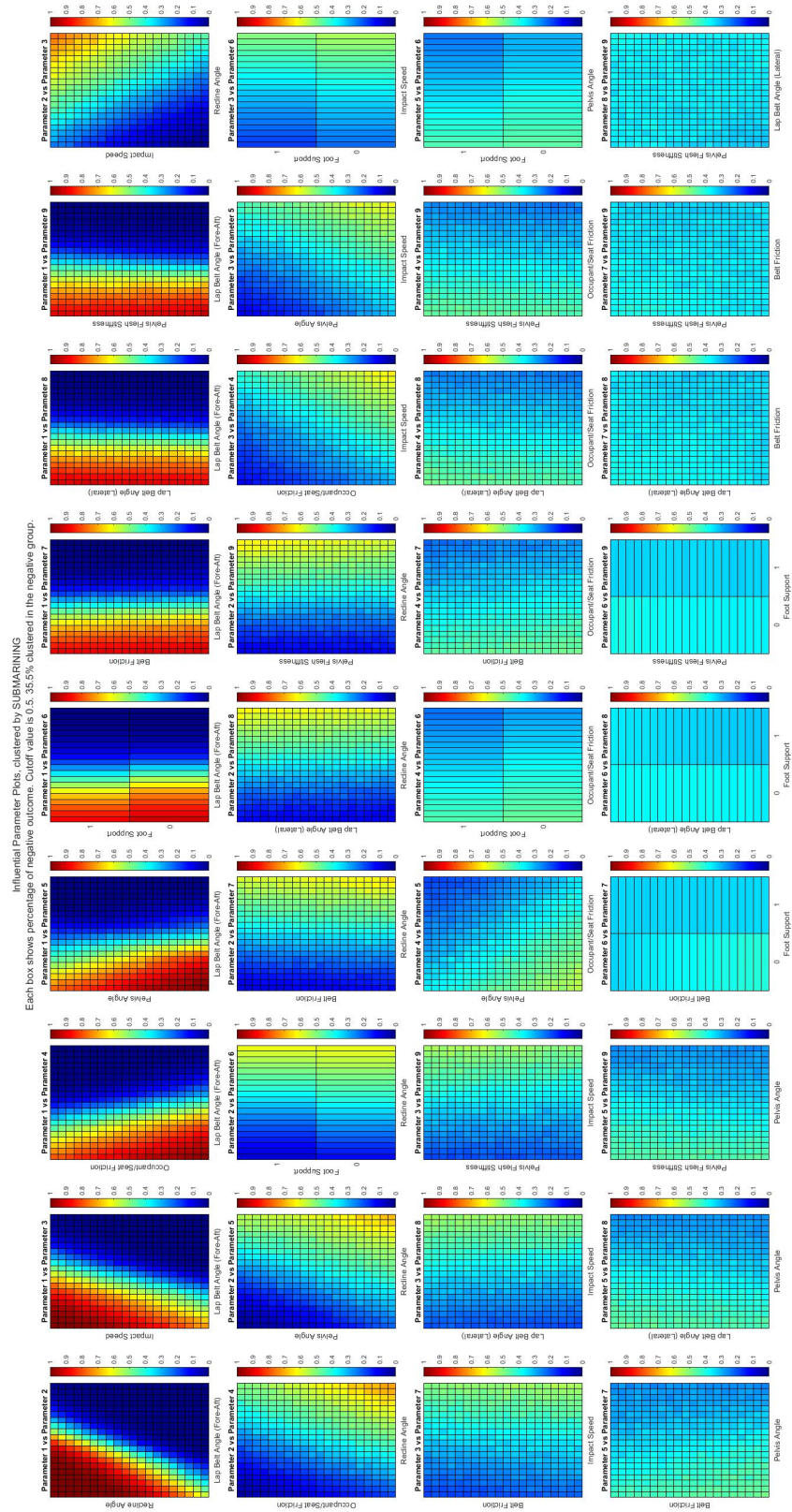
Figure J.67: Influence of foot support and overhead lap belt angle on the risk of the maximum lap belt tension exceeding: a) 4 kN, a) 6 kN, c) 8 kN.

Appendix K

1M Generated Dataset (Continuous Sampling)

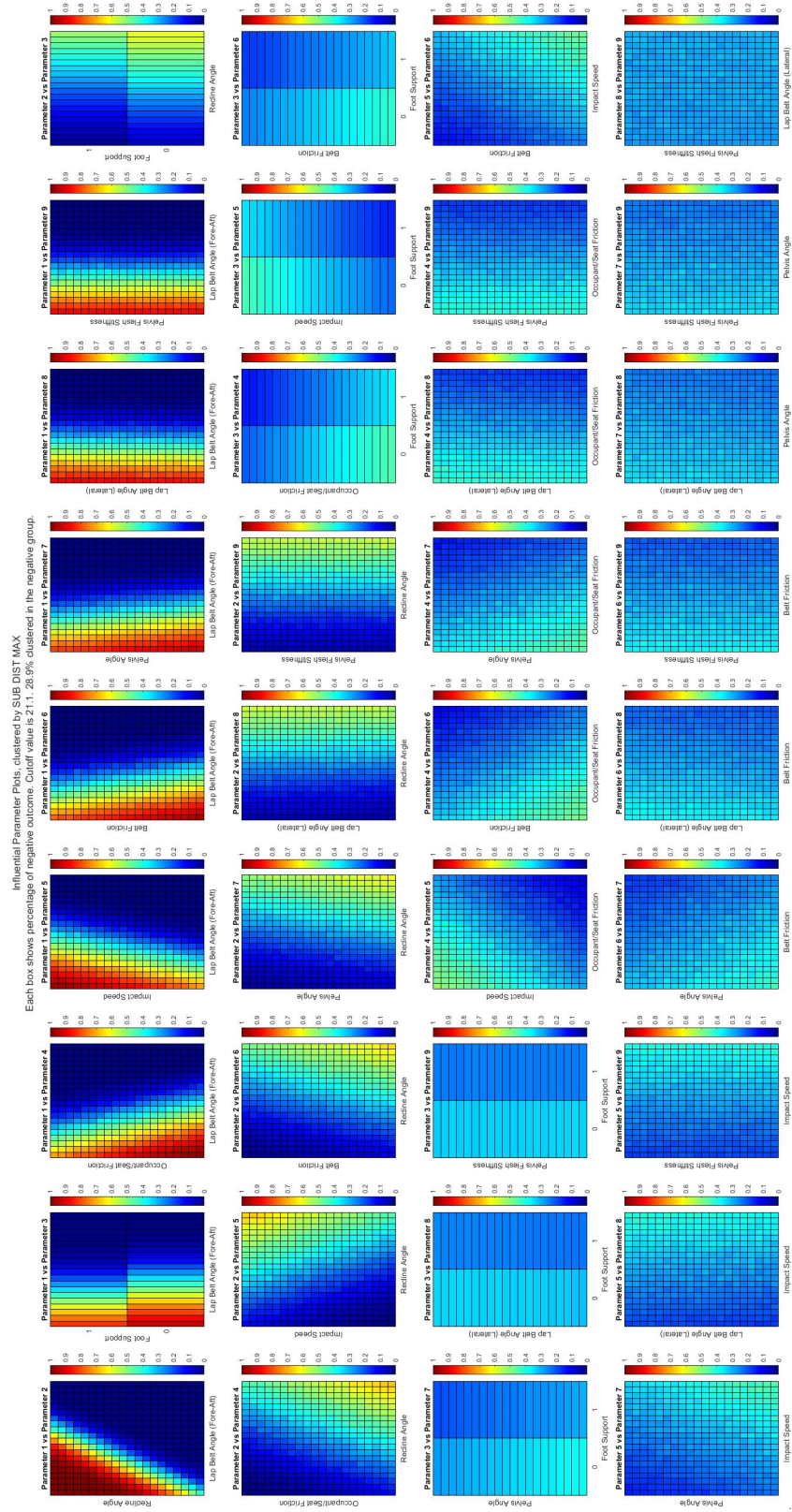
APPENDIX K. 1M GENERATED DATASET (CONTINUOUS SAMPLING)

Figure K.1: Submarining Heatmaps.



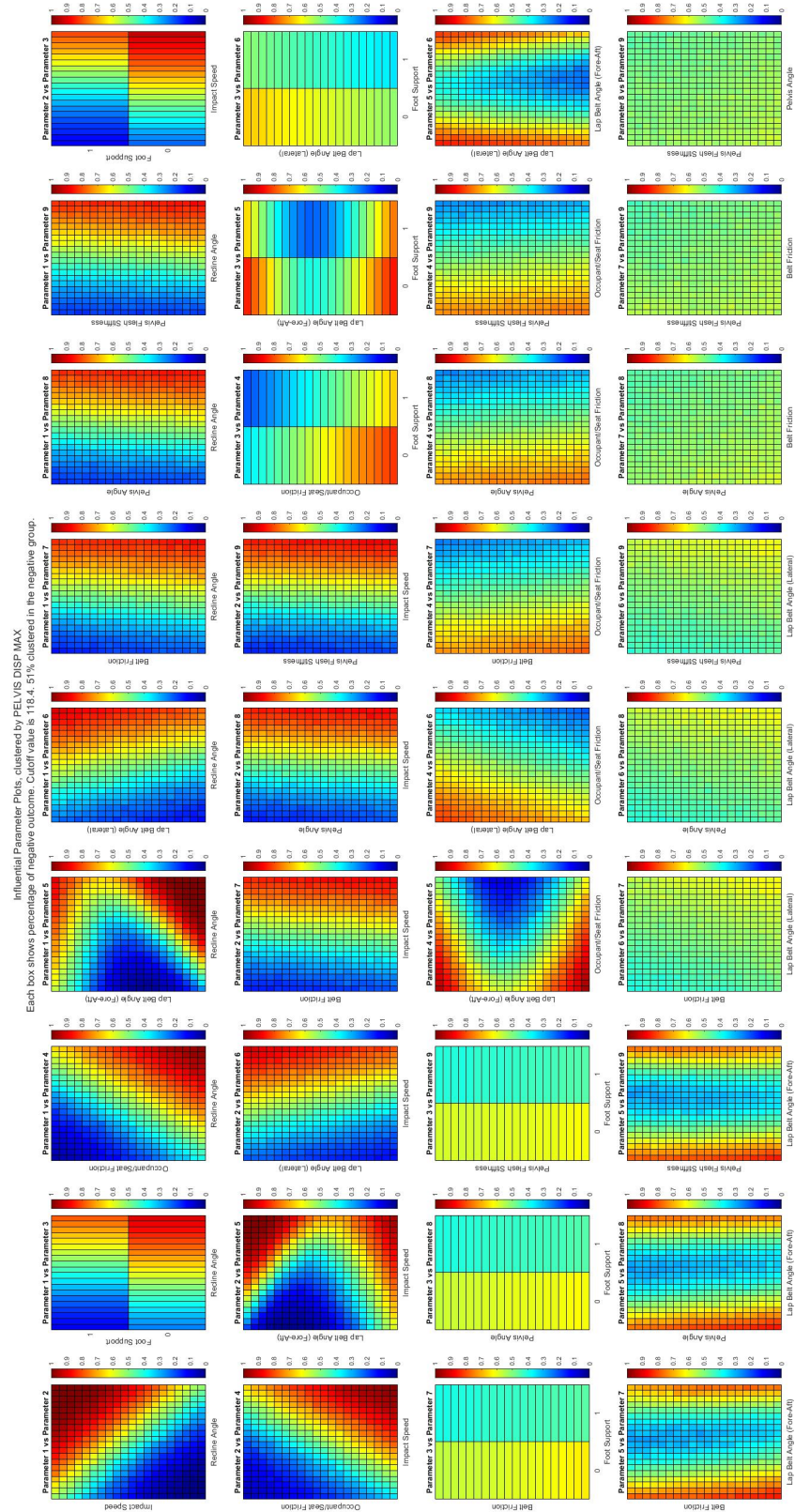
APPENDIX K. 1M GENERATED DATASET (CONTINUOUS SAMPLING)

Figure K.2: Submarining Distance Heatmaps.



APPENDIX K. IM GENERATED DATASET (CONTINUOUS SAMPLING)

Figure K.3: Pelvis Forward Displacement Heatmaps.



APPENDIX K. 1M GENERATED DATASET (CONTINUOUS SAMPLING)

Figure K.4: Pelvis Rotation Heatmaps.

